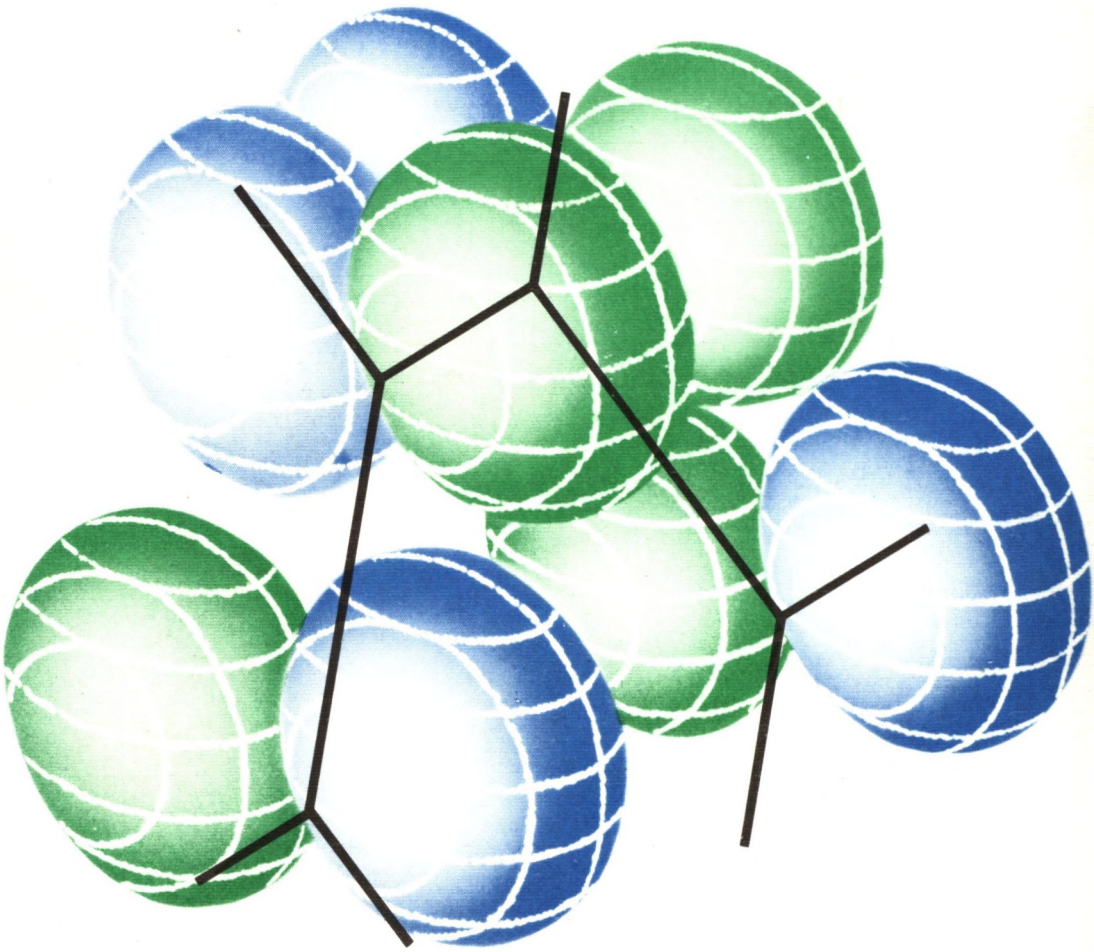
UNDERSTANDING CHEMICAL REACTIVITY

APPLIED QUANTUM CHEMISTRY

GÁBOR NÁRAY-SZABÓ • PÉTER R. SURJÁN • JÁNOS G. ÁNGYÁN



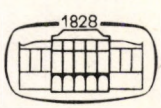
AKADÉMIAI KIADÓ, BUDAPEST

APPLIED QUANTUM CHEMISTRY

APPLIED QUANTUM CHEMISTRY

GÁBOR NÁRAY-SZABÓ
PÉTER R. SURJÁN
JÁNOS G. ÁNGYÁN

Scientific Information Department,
CHINOIN Pharmaceutical and Chemical Works,
Budapest, Hungary



AKADÉMIAI KIADÓ, BUDAPEST 1987

This book is published by D. Reidel Publishing Company
as Vol. 1 in the series "Understanding Chemical Reactivity."

Revised by ISTVÁN MAYER

ISBN 963 05 4201 3

© Akadémiai Kiadó, Budapest 1987

Joint edition published by
Akadémiai Kiadó, Budapest, Hungary
and
D. Reidel Publishing Company, Dordrecht, Holland

Printed in Hungary

CONTENTS

PREFACE VII

LIST OF ACRONYMS IX

LIST OF SYMBOLS XI

1. MODELS AND METHODS OF QUANTUM CHEMISTRY 1
   1.1 Principles of quantum chemistry 1
   1.2 Basic physical models in quantum chemistry 6
      1.2.1 Atoms and molecules 6
      1.2.2 The Born–Oppenheimer model 13
      1.2.3 One-electron functions and configuration interaction 17
      1.2.4 Independent particle models 21
      1.2.5 The LCAO model: link to chemistry 35
      1.2.6 Separability of electron groups 52
      1.2.7 The valence bond picture 55
   1.3 Computational methods 58
      1.3.1 *Ab initio* methods 58
      1.3.2 Semiempirical methods 77
      1.3.3 Qualitative methods in quantum chemistry 92
   1.4 The framework of localized molecular orbitals 109
      1.4.1 *A posteriori* localization criteria 115
      1.4.2 *A priori* localized MOs 119
   1.5 Representation of environmental effects in quantum chemical calculations 130

2. THE CHEMICAL BOND 143
   2.1 Definitions and origin of bonding 143
   2.2 Sigma bonds 149
   2.3 Pi bonds 153
   2.4 Lone pairs 157
   2.5 Three-centre bonds 159
   2.6 Aromaticity 161
   2.7 Metal–metal bonds 168
   2.8 Transition metal complexes 174
   2.9 The hydrogen bond 184
   2.10 Electron donor–acceptor complexes 190
   2.11 Van der Waals molecules 193

3. MOLECULAR STRUCTURE 197
3.1 Geometry 197
3.2 Conformation 205
3.3 Molecular vibrations 214
3.4 Electric properties 222
3.4.1 Charge distribution 222
3.4.2 Electron density and electric field at the nuclei 243
3.4.3 Molecules in electrostatic field 249
3.5 Magnetic properties 257
3.5.1 Magnetic moments and susceptibilities 257
3.5.2 Free radicals in magnetic field 261
3.5.3 Electron-mediated coupling between nuclear spins 270
3.5.4 Magnetic field at the nuclei 276
3.6 Excited and ionized electronic states 281
3.6.1 Single configurational description of electronic states and spectroscopic methods 282
3.6.2 Ionized states 287
3.6.3 Molecular excited states 310
3.7 Interaction of molecules with electromagnetic radiation 333
3.7.1 Vibrational transition probabilities 337
3.7.2 Electronic transition probabilities 343
3.7.3 Chiroptical phenomena 355

4. CHEMICAL REACTIONS 370
4.1 Chemical equilibria 370
4.2 Molecular collisions 377
4.3 Reaction paths 384
4.4 Reactivity of molecules 393
4.4.1 Reaction potential maps 394
4.4.2 Reactivity indices 400
4.5 Conservation of orbital symmetry 408
4.6 Environmental effects 415
4.7 Catalysis 424

APPENDIX 428
A.1 Energetics in the world of molecules 428
A.2 Physical constants and conversion factors 431

REFERENCES 433

SELECTED RECENT REFERENCES 464

SUBJECT INDEX 479

PREFACE

This book is based on an earlier version: "*Alkalmazott kvantumkémia*" *(Applied Quantum Chemistry)* published in Hungarian in 1979 by Műszaki Könyvkiadó (Budapest). One of its main goals is to show that basic principles and equations of quantum mechanics can be applied to a vast variety of problems concerning molecular structure and chemical reactions. Since we discuss a very large number of examples and applications, not only quantum chemists but structural chemists, spectroscopists, theoretical organic chemists and biochemists may find the book useful as a general overview of the practical aspects of theoretical chemistry. We hope that graduate students can use the book also with success.

A more or less deductive treatment is given: starting from the numerically accurate solutions of the Schrödinger equation we approach gradually to more general, qualitative concepts. While such concepts can rarely be deduced exactly from the basic equations of quantum chemistry they play an outstanding role in understanding nature; therefore we discussed them with special care. We had to reconcile the physicist's and chemist's ways of thinking which is by no means simple. Therefore, we had to make some compromises, especially by avoiding more detailed analyses and making the text sometimes extremely terse. This was imperative since the extent of the book is limited. However, we cited numerous papers and books from the relevant literature. These may help the interested reader to pick up more information on a specific topic. A further compromise is that Part One, dealing with methods of quantum chemistry, cannot be considered as a didactic introduction—this can be found in numerous textbooks. It is rather an overview for those who have some experience in methods of quantum mechanics.

It is our pleasure to express our gratitude to Dr. I. Mayer (Budapest) who took the trouble to read the manuscript very thoroughly. His suggestions and corrections allowed us to improve the final version considerably. We are grateful to those friends who made comments on some specific parts of the work: Profs E. Kőrös (Budapest), P. Mezey (Saskatoon), J. Tomasi (Pisa) and N. Trinajstić (Zagreb)

The authors

LIST OF ACRONYMS

AO	atomic orbital
APSG	antisymmetrized product of strongly orthogonal geminals
CD	circular dichroism
CEPA	coupled electron-pair approximation
CHF	coupled Hartree-Fock
CI	configuration interaction
CNDO	complete neglect of differential overlap
DODS	different orbitals for different spins
DZ	double zeta
EHF	extended Hartree–Fock
EHT	extended Hückel theory
ESCA	electron spectroscopy for chemical analysis
ESR	electron spin resonance
FEMO	free electron molecular orbital
FPT	finite perturbation theory
FSGO	floating spherical Gaussian orbital
GTO	Gaussian-type orbital
GVB	generalized valence bond
HF	Hartree–Fock
HFR	Hartree–Fock–Roothaan
HYO	hybrid orbital
IEPA	independent electron pair approximation
INDO	intermediate neglect of differential overlap
IR	infrared
LCAO	linear combination of atomic orbitals
LMO	localized molecular orbital
LP	lone pair
MBPT	many-body perturbation theory
MCSCF	multi-configuration self-consistent field
MINDO	modified intermediate neglect of differential overlap
MO	molecular orbital
MORD	magnetic optical rotatory dispersion
NBMO	non-bonding molecular orbital
NMR	nuclear magnetic resonance

NQR	nuclear quadrupole resonance
ORD	optical rotatory dispersion
PCILO	perturbative configuration interaction with localized orbitals
PMO	perturbative molecular orbital
PNO	pair natural orbital
PPP	Pariser–Parr–Pople
PT	perturbation theory
PUHF	projected unrestricted Hartree–Fock
REPE	resonance energy per electron
RHF	restricted Hartree–Fock
RPA	random-phase approximation
RSPT	Rayleigh–Schrödinger perturbation theory
SCF	self-consistent field
SCRF	self-consistent reaction field
SD	single-double
SLMO	strictly localized molecular orbital
STO	Slater-type orbital
TDHF	time-dependent Hartree–Fock
UCHF	uncoupled Hartree–Fock
UHF	unrestricted Hartree–Fock
UPS	ultraviolet photoelectron spectroscopy
UV	ultraviolet
VB	valence bond
VIS	visible light spectroscopy
VSEPR	valence-shell electron-pair repulsion
XPS	X-ray photoelectron spectroscopy
ZDO	zero differential overlap

LIST OF SYMBOLS

indices

A, B	nuclei
i, j, k, l	electrons, bonds, orbitals
m, n	electronic states
α, β, γ	vector components
$\mu, \nu, \ldots$	basis functions

operators

$\hat{\mathbf{A}}$	antisymmetrizer
$\hat{\mathbf{F}}$	Fockian
$\hat{\mathbf{H}}$	Hamiltonian
$\hat{\mathbf{L}}$	orbital moment
$\hat{\mathbf{p}}$	electron momentum
$\hat{\mathbf{P}}$	total momentum
$\mathbf{r}$	electron position
$\mathbf{R}$	nuclear position
$\hat{\mathbf{s}}$	electron spin
$\hat{\mathbf{S}}$	total spin
$\hat{\mathbf{T}}$	kinetic energy
$\hat{\mathbf{V}}$	potential energy
Δ	Laplace operator
∇	gradient operator
$\hat{\rho}$	charge density

measurable quantities

a_0	Bohr radius
A	mass number of nucleus, hyperfine coupling constant
c	velocity of light
C	quadrupole polarizability
D	dissociation energy

e	electronic charge
E	energy, electron affinity
f	force constant, oscillatory strength, partition function
$\mathbf{F}$	force, electric field, electric field gradient
h	Planck's constant
$\hbar$	$h/2\,\pi$
H	reaction enthalpy, magnetic field component
$\mathbf{H}$	magnetic field
I	ionization energy
J	nuclear-nuclear spin-spin coupling constant
k	force constant, rate constant
K	equilibrium constant
m	mass of electron
n	refraction index
p	momentum
Q	normal coordinate, nuclear quadrupole moment, spherical tensor multipole moment, charge
r	spherical coordinate
$\mathbf{r}$	electronic position
R	interatomic distance, octupole polarizability
$\mathbf{R}$	nuclear position
T	nuclear kinetic energy, Coulomb interaction tensor
V	potential energy
$\mathbf{x}$	foursome of coordinates (3 spatial + 1 spin)
x	Cartesian coordinate
y	Cartesian coordinate
z	Cartesian coordinate
Z	nuclear charge
α	polarizability, bond angle
$\bar{\alpha}$	mean polarizability
β	first hyperpolarizability
β_B	Bohr magneton
γ	second hyperpolarizability, gyromagnetic coefficient
$\boldsymbol{\gamma}$	first-order density matrix
$\boldsymbol{\Gamma}$	second-order density matrix
δ	Mössbauer isomeric shift, NMR chemical shift
ε	relative permittivity (dielectric constant), molar extinction coefficient
η	polarizability anisotropy, asymmetry parameter
ϑ	spherical coordinate, bond angle
Θ	quadrupole moment, molar ellipticity, spherical coordinate
λ	wave length
μ	dipole moment, reduced mass

μ^{m}	magnetic dipole moment
ν	wave number
ν_Q	nuclear quadrupole coupling
$\xi^{(l)}$	l-th order multipole moment (according to Buckingham)
ρ	charge density
ρ_s	spin density
σ	spin coordinate, NMR shielding constant
τ	dihedral angle
φ	spherical coordinate
Φ	hexadecapole moment, spherical coordinate
χ	diamagnetic susceptibility
Ω	octupole moment

other notations

B	bond order
c	molecular orbital coefficient
f	free valence number
$F_{\mu\nu}$	Fock-matrix
$\mathbf{H}$	Hessian matrix
$\mathbf{I}$	unit matrix
l	localizability
$\mathcal{N}$	number of electrons
$P_{\mu\nu}$	bond order, density matrix element
q	atomic charge
Q	gross atomic population
R	covalent radius
$\mathbf{S}$	overlap matrix
$\mathbf{U}$	unitary matrix
v	valence number
Y_{lm}	spherical harmonics
α	Coulomb integral; spin function
β	resonance integral; spin function
ζ	orbital exponent
η	tail of localized orbital
φ	one-electron spin orbital
ϕ	configuration, one-determinantal wave function
Φ	wave function
σ, λ	bond polarity
Ψ	stationary state wave function
ψ	molecular orbital
χ	atomic orbital, electronegativity

special symbols

$\in$	element of
$\langle\ \rangle$	expectation value
$\langle\ \vert\ \rangle$	binary product
$\{\ \}$	set of elements
$(\ \vert\ )$	two-centre electron repulsion integral in (11|22) convention
$\sum^{\text{occ}}$	summation over occupied orbitals
$\times$	vector product
$+$	adjoint

1. MODELS AND METHODS OF QUANTUM CHEMISTRY

1.1 PRINCIPLES OF QUANTUM CHEMISTRY

Introductory remarks. In the first part of this book we intend to give a short review of the most important aspects of quantum chemistry. This discipline is the theoretical basis of molecular chemistry dealing with structure, properties and interaction of molecules. The basic principles are offered by *quantum mechanics.* It is to be stressed that, though the physical laws for the whole of chemistry are completely known [327], quantum chemistry cannot be viewed as applied mathematics. It is a general feature of most of the present-day theoretical physics that it struggles with solving "well-known" equations, while earlier attention was paid mainly to the *discovery of laws* and the corresponding equations, rather than to the question of *how to solve* these equations for different systems. Due to the complexity of basic quantum mechanical equations, the straightforward application of mathematics alone cannot help us in searching for the appropriate solutions. Approximations have to be introduced which are based on physical considerations by constructing simplified models of the phenomena under study. High-speed computers provide an important tool if the aim is to calculate a given property of a given system quantitatively. However, it is to be emphasized that if we wish to compare different systems qualitatively and to find the nature of a given phenomenon in the form of a relatively simple law, the use of computers is much less significant. In this case the main goal is to find the relevant physical model on which the properties of the system in question can be studied explicitly. Moreover, even computers do not solve the problem of finding accurate solutions for complicated systems; here again appropriate models which help us in introducing acceptable approximations are important.

The methodological part of the present book is organized as follows. In the present Section we briefly summarize those parts of quantum mechanics which are essential for the further development. This is to be considered just as a recapitulation since the reader is supposed to be, familiar with elementary quantum mechanics. In Section 1.2 we outline the hierarchy of physical (chemical) models which are often used in quantum chemistry. Section 1.3 reviews the most important computational schemes the emphasis being placed on the chemical and physical significance rather than on technical details. In Section 1.4 we discuss localized molecular orbitals, an efficient conceptual tool in bridging the gap between classical and quantum chemistry. Finally, Section 1.5 deals with the interactions between molecules and their environment.

Principles of quantum mechanics. To gain insight into most molecular phenomenon only a very simple and primitive extract of the whole complicated quantum theory is

necessary. Measurement theory, axiomatic presentation and quantum logic, etc. are not important with respect to practical quantum chemistry. In addition, whenever the interaction of a molecule with an electromagnetic field is considered, a semiclassical treatment is sufficient: only the molecule is discussed quantum mechanically while the field is usually described by classical electrodynamics. In other words, the (very small) effects due to the quantization of the electromagnetic field are neglected.* The importance of relativistic effects is also restricted. These are to be considered only in the study of the inner shell structure of heavy ($Z > 40$) atoms. The detailed discussion of relativistic effects is beyond the scope of this book; for some references see, for example, [476, 864a, 891, 1147]. There are, however, some typical relativistic phenomena such as spin–spin or spin–orbit coupling (*cf.* Sections 3.4 and 3.5) where the basic formulas are derived relativistically. Once we have these formulas we may use the nonrelativistic wave function to calculate the corresponding molecular properties, without introducing significant loss of accuracy.

Let us now recall the most important features of molecular quantum theory which are assumed to be known. A more detailed, but still simple, treatment is found for example in the excellent elementary textbook by Zahradník and Polák [1449], see also [7a].

Molecules consist of electrons and nuclei which are considered as points. They are characterized by their mass, charge and their intrinsic angular momentum, the *spin*. The charges give rise to the Coulomb potential which is the only primary interaction considered in the theory of isolated molecules. The electronic charge is $-e$, the charge of a nucleus with atomic number Z is $+Ze$. The spin of an electron may be $\pm\frac{\hbar}{2}$ corresponding to the "spin up" and "spin down" states, α and β, respectively.

The physical state of a molecule is represented** by the wave function, $\Phi(\mathbf{x}, t)$, which depends on the spatial and spin coordinates of all particles and on the time (t). The space of all coordinates (dynamical variables) is called *configuration space*, a point in this space is denoted by $\mathbf{x}$. The Φ has some special mathematical properties which are characteristic of the elements of an (abstract) Hilbert space which is usually represented by the so-called L_2 function space. This is the space of the square-integrable functions, for which the integral $\int \Phi^* \Phi \, d\mathbf{x}$ is finite. In addition, it is assumed that Φ is differentiable and regular. The above conditions are valid only for bound states and there are cases when $\Phi \notin L_2$, *e.g.* for the translation of free atoms or molecules the system is described by a non square-integrable plane-wave function. The overall motion of atoms and molecules is of interest in scattering theory; in quantum chemistry attention is paid to the internal degrees of freedom (electronic structure and relative motion of nuclei).

* Recently, efforts have been made to treat optical absorption of molecules and related phenomena *via* quantum electrodynamics [1131].

** For other representations of quantum theory see *e.g.* Refs [829] and [830].

According to the probability interpretation, the wave function $\Phi(\mathbf{x}, t)$ is considered as a probability amplitude: $\Phi^*(\mathbf{x}, t)\Phi(\mathbf{x}, t)$ is interpreted as the probability density for finding the system in the point $\mathbf{x}$ of the configuration space at time t.

Physical quantities are represented by Hermitian operators over the Hilbert space. Expectation values of a given physical quantity corresponding to operator $\hat{A}$, are given by the expression

$$\langle \hat{A} \rangle = \frac{\int \Phi^* \hat{A} \Phi \, d\mathbf{x}}{\int \Phi^* \Phi \, d\mathbf{x}} \equiv \frac{\langle \Phi | \hat{A} | \Phi \rangle}{\langle \Phi | \Phi \rangle}. \tag{1.1}$$

The operator of the energy is called the *Hamiltonian*. Neglecting the weak magnetic (spin–spin, spin–orbit) interactions one obtains the nonrelativistic molecular Hamiltonian, $\hat{H}$, which has the simple form analogous to that in classical mechanics

$$\hat{H} = \hat{T} + \hat{V} \tag{1.2}$$

where $\hat{T}$ is the sum of the kinetic energy operators of all particles and $\hat{V}$ is the operator of the potential energy. For an isolated molecule we can write in the usual coordinate representation*

$$\hat{V} = \sum_{i<k} \frac{Q_i Q_k}{|\mathbf{r}_i - \mathbf{r}_k|} \tag{1.3}$$

and

$$\hat{T} = -\frac{\hbar^2}{2} \sum_i \frac{\Delta_i}{m_i} \tag{1.4}$$

where Q_i is the charge of particle i, $\mathbf{r}_i$ and $\mathbf{r}_k$ are the position vectors of particles i and k, m_i is the mass of particle i and Δ_i is the Laplace operator corresponding to the coordinates of particle i. In the presence of an external field the operator $\hat{V}$ in Eq. (1.3) has to be modified appropriately.

The time evolution of the state is given by the *Schrödinger equation*

$$i\hbar \frac{\partial \Phi}{\partial t} = \hat{H} \Phi . \tag{1.5}$$

Stationary states of the molecule, Ψ_n, can be obtained from the time-independent Schrödinger equation

$$\hat{H} \Psi_n = E_n \Psi_n . \tag{1.6}$$

The n-th eigenvalue of $\hat{H}$, E_n is the energy of the molecule in eigenstate Ψ_n. If the spectrum is discrete, $n = 0, 1, 2, \ldots$ (the explicit consideration of continuous spectra is

* Some effort has been made recently to formulate quantum chemistry in momentum space (momentum representation) [284a, 720, 720a, 721, 722, 926, 928, 988, 1030, 1275, 1275a, 1407].

needed rarely in quantum chemistry). The states are usually labelled in order of ascending energy. The lowest energy state, $n=0$, is said to be the ground state while others are called excited states.

In quantum chemistry we are mostly interested in solving Eq. (1.6) (for the time-dependent phenomena see *e.g.* [828]). The bound state solutions can be made unique (up to an irrelevant phase factor) by the following boundary and normalization conditions

$$\Psi_n(\pm\infty)=0 \tag{1.7a}$$

$$\langle\Psi_n|\Psi_n\rangle\equiv\int\Psi_n^*(\mathbf{x})\Psi_n(\mathbf{x})\,d\mathbf{x}=1 \tag{1.7b}$$

This means that the wave function must vanish asymptotically with increasing (at least one of the) spatial variables, *cf.* Eq. (1.7a). The Eq. (1.7b) is consistent with the probability interpretation. The fulfillment of Eq. (1.7a) is necessary to ensure square integrability of Ψ_n.

The Hamiltonian of Eqs (1.2–4) is spin independent. Thus the main role of spin (as a quantum number) is to ensure the antisymmetry of the wave function of polyelectronic systems according to the *Pauli principle.** This states that Ψ_n must be antisymmetric with respect to the interchange of the independent electronic coordinates

$$\Psi_n(\mathbf{x}_1,\mathbf{x}_2,\ldots\mathbf{x}_i,\ldots\mathbf{x}_j,\ldots\mathbf{x}_m)=-\Psi_n(\mathbf{x}_1,\mathbf{x}_2,\ldots\mathbf{x}_j,\ldots\mathbf{x}_i,\ldots\mathbf{x}_m) \tag{1.8}$$

where $\mathbf{x}_i$ stands for the quadruple of coordinates of electron i (three spatial and one spin)**.

The Pauli principle can also be formulated pictorially. The proper antisymmetry of the wave function involves that electrons with parallel spin avoid each other, a "Fermi hole" is formed around them. The wave function Ψ_n would vanish if $\mathbf{x}_i$ were equal to $\mathbf{x}_j$ in Eq. (1.8). This means that all the spatial and spin coordinates of two electrons cannot be equal, *i.e.* only electrons with opposite spins can occupy the same orbital.

The eigenvectors of the Hamiltonian are also eigenvectors of all operators commuting with $\hat{H}$($\hat{S}^2$, $\hat{S}_z$ and symmetry operators of the molecule). If we are constructing approximate wave functions this is a requirement in judging their validity. Other quantum chemical theorems (for example virial and hypervirial theorems [201], Hellmann–Feynman theorem [387, 545]) have a similar importance. Besides the label referring to the energy it is customary to indicate the eigenvalue of the operators commuting with $\hat{H}$ as additional sub- or superscripts on the wave function. For

* The absence of the spin variables in the Hamiltonian permits us to develop the so-called spin-free quantum chemistry, where the spin variables are not explicitly mentioned at all. The Pauli principle is fulfilled by subjecting the wave function (depending in this case only on spatial variables) to specific complicated permutational symmetry requirements. For details see for example [1072] pp. 229–266 and references therein, and [878].

** More generally, the Pauli principle requires that, with respect to the corresponding permutation, the wave function must be symmetric or antisymmetric if the spin of the particles (in units of $\hbar$) is integral or half-integral respectively.

example ${}^1\Psi_n$ (${}^3\Psi_n$) refers to the n-th singlet (triplet) excited state, indicating the eigenvalue of $\hat{\mathbf{S}}^2$. (More precisely, if the eigenvalue of $\hat{\mathbf{S}}^2$ is $S(S+1)$, the multiplicity m of the state ${}^m\Psi_n$ is $m=2S+1$.)

As far as the Hamiltonian $\hat{\mathrm{H}}$ is a real operator the stationary states Ψ_n can always be chosen as real functions. This will be utilized throughout this book assuming the wave function to be real and writing Ψ instead of Ψ^* in most cases. Note that complex wave functions are necessary in the presence of an external magnetic field, in certain cases of orbital degeneracy for finding the appropriate symmetry of the wave function, and in studying time-dependent phenomena.

The Schrödinger equation (1.6) can be deduced from the *variation principle* which states that the exact ground state wave function has the lowest energy (lowest expectation value of $\hat{\mathrm{H}}$). Mathematically, for an arbitrary but normalized function Ψ, the variation principle is expressed as

$$\langle \Psi | \hat{\mathrm{H}} | \Psi \rangle \geq E_0 \tag{1.9}$$

where E_0 is the exact ground state energy. Equality in (1.9) holds if and only if Ψ is the exact ground state wave function. The variation principle is often applied in searching for good approximate wave functions. If one specifies a class of functions possessing some free parameters, the best approximation within this class can be obtained by minimizing the energy with respect to the free parameters. This is the most important approximate method used in quantum chemistry.

Another important tool for obtaining approximate eigenvectors and eigenvalues is the perturbation theory (PT). It is applicable if the solutions for a simpler model Hamiltonian $\hat{\mathrm{H}}^0$, differing only slightly from $\hat{\mathrm{H}}$, are already known. Perturbation theory provides the solution of $\hat{\mathrm{H}}$ as a power series expansion in terms of the eigenvectors and eigenvalues of $\hat{\mathrm{H}}^0$. Among different formulations [824, 825, 826], the Rayleigh–Schrödinger PT is the most important one which is presented in almost all standard textbooks (see for example [759] and [1449]).

Atomic units. Many formulae used in atomic and molecular physics contain the universal constants e, m, and $\hbar$ (the charge and mass of electrons and Planck's constant divided by 2π, respectively). By an appropriate choice of the units of physical quantities one can make the values of the above quantities equal to unity:

$$e=1; \quad m=1; \quad \text{and} \quad \hbar=1.$$

By this choice the unit of length is the so-called Bohr radius (or Bohr), denoted by a_0:

$$a_0=\hbar^2/me^2=0.529\,10^{-10}\,\mathrm{m},$$

while the atomic unit of energy (called hartree or rydberg, Ry) is

$$e^2/a_0=4.3598\,10^{-18}\,\mathrm{J}.$$

The velocity of light in atomic units has the value $c\approx 137$ a.u.

For a comparison of different units of energy, see the nomogram of Table A1. In the appendix the conversion factors of some other physical quantities can also be found (Table A2).

The use of atomic units has two advantages. First, the expressions become simpler, since one may avoid the explicit use of the universal constants e, m and $\hbar$. Secondly, if the results of calculations are expressed in atomic units, they are independent of the actual values of these universal constants which are determined experimentally and may be changed occasionally when the measurement techniques become finer. For this reason, further on in this book, we will use atomic units if the contrary is not stated.

1.2 BASIC PHYSICAL MODELS IN QUANTUM CHEMISTRY

1.2.1 ATOMS AND MOLECULES

The atom [94, 759]. It has been mentioned that molecules consist of electrons and nuclei. This view is not consistent with the chemical way of thinking, where molecules are considered as composed of *atoms*. It is therefore important to talk about individual atoms before starting to develop the general theory of molecules. We will not go into details, this would be beyond the scope of the present book. Only the most important features which contribute to the theory of molecules are summarized.

The concept of the atom (= indivisible particle) was introduced in philosophy rather than in experimental physics and through many centuries nobody knew exactly whether atoms existed or not. In the modern context the term "atom" refers to a divisible particle which consists of one nucleus with a charge of $+Z$ and of one or more electrons. If the number of electrons is just Z the atom is neutral, otherwise we talk about (positive or negative) *ions*. The nuclear charge, Z, is called in other words the *atomic number*.

The atoms strongly interact with their surroundings, which leads to the formation of crystals and molecules. There are only a few kinds of atoms, namely those of rare gases, which usually interact weakly with each other and with other kinds of atoms. So, one can ask why we are talking about individual atoms at all, and why we do not consider different molecules as the primary entities. The reason is that, from the chemical point of view, there are fewer kinds of atoms compared to an enormous number of different molecules, thus the concept of atoms is essential in systematizing chemistry. The point here is that it is possible to consider atoms as elementary building blocks of molecules. Moreover, from the physical point of view, the atoms preserve some of their basic properties even if they form a molecule. Thus the chemical formula contains much information about the molecule. In other words: *the same atoms in different molecules behave similarly.*

The simplest atom is hydrogen, H, with $Z=1$. Its Schrödinger equation can be solved exactly and this system serves as the usual basis for testing different levels of

quantum theory. Within the approximations discussed in the previous Section, and assuming the proton being fixed at the origin, the Schrödinger equation reads

$$\left(-\frac{1}{2}\Delta-\frac{1}{r}\right)\Psi(r,\vartheta,\varphi)=E\Psi(r,\vartheta,\varphi) \tag{1.10}$$

where r, ϑ and φ are the spherical coordinates.

The solution is

$$E_n=-\frac{1}{2n^2} \tag{1.11}$$

$$\Psi_{nlm}=R_{nl}(r)Y_{lm}(\vartheta,\varphi) \tag{1.12}$$

with

$$l=0,1,\ldots,n-1 \tag{1.13a}$$

$$|m|\leq l \tag{1.13b}$$

and

$$R_{nl}(r)=\mathcal{N}\left(\frac{2r}{n}\right)^l e^{-r/n}L_{n+l}^{2l+1}\left(\frac{2r}{n}\right). \tag{1.14}$$

Y_{lm} denotes the spherical harmonics, L_i^k are the so-called associated Laguerre polynomials and $\mathcal{N}$ is a normalization constant. The solutions Eq. (1.12) are usually referred to as *hydrogenic functions*. Note that Ψ_{nlm} is a product of radial (R_{nl}) and angular (Y_{lm}) parts. This feature is a consequence of the spherical symmetry of Eq. (1.10). Explicit formulae for L_{n+l}^{2l+1}, Y_{lm} and the radial part of the hydrogenic wave function $R_{nl}(r)$ are presented for some low-lying states in Table 1.1.

The indices n, l, m are called *principal*, *azimuthal* and *magnetic quantum numbers*, respectively. Due to the high symmetry of the H atom the energy depends only on n. Solutions, belonging to the same n but different l and m, are *degenerate*. The degenerate energy levels split if the atom is put into external electric or magnetic fields. These are the *Stark* and *Zeeman effects*, respectively.

The spherical harmonics Y_{lm} are complex functions of ϑ and φ, but the degeneracy in m permits to take the appropriate linear combinations of functions with the same n and l to form real orbitals (see Table 1.1). The orbitals corresponding to $l=0, 1, 2, \ldots$ are called $s, p, d, \ldots$ functions, respectively. Their graphic representation is depicted in Fig. 1.1. In the ground state of the hydrogen atom the electron is ascribed to the $1s$ orbital while in excited states it occupies higher ($2s$, $2p$, $3d$, etc.) levels.

Two mathematical properties of the orbitals in Eq. (1.12) are worth mentioning. First, these functions form an infinite orthonormal set in the space of square integrable functions. Second, they still *do not* represent a complete set in this space. This is related to the fact that the exponent in Eq. (1.14) depends on the principal quantum number n; if we had a state-independent exponent the corresponding set would be complete in the

TABLE 1.1

Associated Laguerre polynominals $L_{n+l}^{2l+1}(\rho)$, radial parts of hydrogenic functions, $R_{nl}(r)$, and normalized spherical harmonics $Y_{lm}(\vartheta, \varphi)$ in complex and real representations for some quantum numbers n, l and m. The ρ stands for $2r/n$. The symbols (x), (y), etc. in parentheses at the values of the magnetic quantum number m refer to the real representation of spherical harmonics

	n	l	m	$L_{n+l}^{2l+1}(\rho)$	$R_{nl}(r)$	$Y_{lm}(\vartheta, \varphi)$ Complex	$Y_{lm}(\vartheta, \varphi)$ Real
s	1	0	0	-1	$2e^{-r}$	$1/\sqrt{4\pi}$	$1/\sqrt{4\pi}$
s	2	0	0	$-4+2\rho$	$1/\sqrt{8}(2-r)e^{-r/2}$	$1/\sqrt{4\pi}$	$1/\sqrt{4\pi}$
	2	1	-1 (x)			$\sqrt{3/8\pi}\sin\vartheta e^{-i\varphi}$	$\sqrt{3/4\pi}\sin\vartheta\cos\varphi$
p	2	1	0 (y)	-6	$\frac{1}{\sqrt{24}}re^{-r/2}$	$\sqrt{3/8\pi}\cos\vartheta$	$\sqrt{3/4\pi}\sin\vartheta\sin\varphi$
	2	1	$+1$ (z)			$\sqrt{3/8}\sin\vartheta e^{+i\varphi}$	$\sqrt{3/4\pi}\cos\vartheta$
s	3	0	0	$-18+18\rho-\rho^3$	$(27-18r+2r^2)e^{-r/3}$	$1/\sqrt{4\pi}$	$1/\sqrt{4\pi}$
	3	1	-1 (x)				
p	3	1	0 (y)	$-96+24\rho$	$\frac{4}{\sqrt{2\times 27}}(6r-r^2)e^{-r/3}$	The same as for $2p$	The same as for $2p$
	3	1	$+1$ (z)				
	3	2	-2 (z^2)			$\frac{1}{2}\sqrt{15/8\pi}\sin^2\vartheta e^{-2i\varphi}$	$\sqrt{5/16\pi}(1-3\cos^2\vartheta)$
	3	2	-1 (xz)			$\sqrt{15/8\pi}\sin\vartheta\cos\vartheta e^{-i\varphi}$	$\sqrt{15/4\pi}\sin\vartheta\cos\vartheta\cos\varphi$
d	3	2	0 (yz)	-120	$\frac{4}{\sqrt{10\times 27}}r^2e^{-r/3}$	$\sqrt{5/4\pi}\left(\frac{3}{2}\cos^2\vartheta-\frac{1}{2}\right)$	$\sqrt{15/4\pi}\sin\vartheta\cos\vartheta\sin\varphi$
	3	2	$+1$ (x^2-y^2)			$\sqrt{15/8\pi}\sin\vartheta\cos\vartheta e^{+i\varphi}$	$\sqrt{15/16\pi}\sin^2\vartheta\cos 2\varphi$
	3	2	$+2$ (xy)			$\frac{1}{2}\sqrt{15/8\pi}\sin^2\vartheta e^{+2i\varphi}$	$\sqrt{15/16\pi}\sin^2\vartheta\sin 2\varphi$

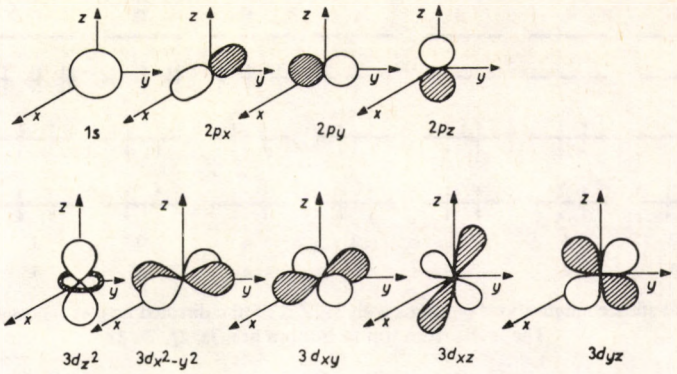


Fig. 1.1 Schematic view of hydrogenic 1*s*, 2*p* and 3*d* orbitals

L_2 space. The presence of the $1/n$ factor in the exponential indicates that the hydrogenic orbitals are the more diffuse the larger is the principal quantum number.

The hydrogenic orbitals are of central importance in studying the electronic structure of other atoms. As a matter of fact, the nature of all atoms can be qualitatively understood by introducing the following model.

(i) Consider the hydrogenic functions Ψ_{nml} with the restrictions of Eqs (1.13a, b). Suppose that their overall mathematical form does not change if we treat a many-electron atom instead of H.

(ii) The energy levels, however, do not correspond exactly to the hydrogenic solution since the degeneracy of the *s*, *p*, *d* and further orbitals is removed by the presence of the "new" electrons or, more precisely, by the electrostatic interaction between them. Based on experimental findings the following energy spectrum is assumed:

$$\varepsilon_{1s} \ll \varepsilon_{2s} < \varepsilon_{2p} \ll \varepsilon_{3s} < \varepsilon_{3p} \ll \varepsilon_{4s} < \varepsilon_{3d} < \varepsilon_{4p} \ldots . \tag{1.15}$$

For a qualitative understanding it is not necessary to specify the numerical relations which evidently are not the same for all atoms. The validity of Eq. (1.15) is supported by the effectiveness of the model.

(iii) Electronic structures of the many-electron atoms are then obtained by assigning electrons to *hydrogenic* orbitals in the order of increasing energy as in Eq. (1.15). This is the so-called "*Aufbau*" *principle*. According to the Pauli principle, no more than two electrons with opposite spins may be put to each orbital.

(iv) The degeneracy of the energy levels with respect to the magnetic quantum number applies also to the many-electron atom. The degeneracy is split only if the atom is placed in a magnetic field. Thus, following Eqs (1.13a, b), we may have at most two electrons on nondegenerate *s*-type levels, at most six ones on threefold degenerate *p*

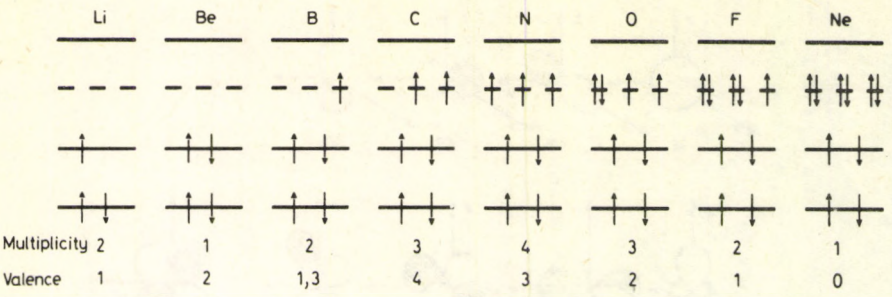


Fig. 1.2 Ground-state configurations of atoms with $3 \leq Z \leq 10$ (the directed arrows represent electron spins). The levels from top to bottom are: 3*s*, 2*p*, 2*s*, 1*s*

levels, ten electrons on the fivefold degenerate *d* levels, etc. The distribution of electrons between orbitals is called *configuration.*

(v) Hund's rules are applied to distribute electrons among degenerate levels. These state that *(i)* the configurations with maximum multiplicity are preferred, and *(ii)* among different states of equal multiplicity, the state with greatest angular momentum has the lowest energy.

Let us note that we do not specify here the wave function of a many-electron atom as this differs essentially from a many-electron wave function built up by hydrogenic wave functions. The latter can be considered only as a qualitative, pictorial representation of the electronic structure of multielectronic atoms. A more precise meaning of the description of this kind will be given in Sections 1.2.3 and 1.2.4 discussing one-electron orbitals.

Let us now discuss the electronic structure of some neutral atoms. We have already treated the hydrogen atom whose configuration is $1s^1$. The superscript means that we have just one electron on the 1*s* level. The configuration of He is $1s^2$. For a third electron the 2*s* orbital has to be considered. Its energy is much higher than that of the 1*s* orbital; this confirms the relative stability of He which is a noble-gas atom.

The model of the eight first-row atoms, Li to Ne, is obtained by filling the $n=2$ shell, *i.e.* considering the 2*s*, and the three 2*p*-type hydrogenic orbitals. Since the energy difference between the 2*s* and 2*p* levels is not too large, a more or less continuous change in the properties of atoms going from Li to Ne can be observed. Figure 1.2 shows the ground-state configurations of these atoms. As lithium has a configuration $1s^2 2s^1$, it chemically resembles hydrogen. We can understand this if we realize that $\varepsilon_{1s} \ll \varepsilon_{2s}$; therefore the 1*s*-electrons are little influenced by chemical processes, which affect almost exclusively the 2*s* valence shell. Thus a qualitative model of Li is obtained by treating its single 2*s*-electron in the field of a screened nucleus with a charge of $Z-2=1$. This model is similar to the H atom; the only difference is in the form of the 2*s* orbital. Such valence-electron pictures will, in connection with molecules, be discussed in Section 1.2.6.

In Be ($Z=4$), the $2s$ level is completely filled. Though this atom is very similar to He in the above valence-electron scheme, it is not as stable and inactive as the latter, since the difference between $2s$ and $2p$ energies is small; thus the Be atom can easily be in an excited configuration. The B atom is the first where the $2p$ level is partly filled. Carbon has two $2p$ electrons with parallel spins (*cf.* Hund's rule) therefore its ground state is a triplet. Similarly, N has three $2p$ electrons all having the same spin, the multiplicity is 4 (quartet state). Going further in the O, F and Ne series, one, two and three electrons sequentially compensate the spins: the $2p$ shell becomes completely filled in Ne. Since $\varepsilon_{3s} \gg \varepsilon_{2p}$ (see Eq. (1.15)), Ne is also a noble gas atom.

Figure 1.2 shows also the valence numbers of atoms. Except Be and C this number equals the number of electrons with unpaired spins, *i.e.* the multiplicity minus one. This feature will be discussed later (*cf.* Section 1.2.5). Here we note only that the exceptions are usually ascribed to the role of some low-lying excited states in bonding. The same holds for the B atom with valence number 3, indicated also in Fig. 1.2.

Similar considerations as those above can be adopted to describe the electronic structure of atoms with larger atomic numbers. Owing to the periodicity of the valence shell configurations the arrangement of atoms in the periodic system can be qualitatively understood by this simple approach [759]. This is one of the greatest successes of quantum theory in chemistry. Let us emphasize again that we did not use exact quantum mechanical methods; this would be both extremely complicated and unnecessary for an understanding of the phenomena. As we shall see later, hydrogenic orbitals preserve their central importance also in constructing molecular wave functions.

The molecule. From the physical point of view free atoms are stable objects: their energy as obtained by the Schrödinger equation (1.5) is always negative, disregarding the translational motion of the atom as a whole. Nevertheless, one cannot observe free atoms except in some special cases such as the noble gases or when using emission spectroscopy. The reason is that atoms strongly interact with each other. This interaction can be either repulsive or attractive, the latter being responsible for the formation of molecules and crystals. In other words, except with rare gases, free atoms are not stable in the chemical sense since they form *molecules* with somewhat lower energies than the sum of the energies of the constituent atoms. The term 'molecule' refers to the (microscopic) building blocks of chemical compounds; the properties of a molecule are determined by the nature and geometrical arrangement of atoms. The former defines the empirical formula while the latter determines the structural formula of the molecule. The stability of the molecule is measured by the binding (atomization) energy, E_b, which is defined as

$$E_b = E_{\text{tot}} - \sum_i E_i \tag{1.16}$$

where E_{tot} is the total energy of the molecule and E_i is the total energy of the i'th atom.

The sum of atomic energies, as well as E_{tot}, are very large numbers in absolute values, compared to their difference E_b (see Table A1 in Appendix). However, chemists are interested just in the value of the binding energy (*cf.* heats of formation); the total energy is chemically irrelevant. The problem of calculating "small differences of large numbers" is a general characteristic of quantum chemistry which causes that very accurate computations are necessary. The required accuracy is about 10^{-3} a.u. (2.6 kJ/mol) whereas the total energy, for example, of a medium-size molecule can be several hundreds of atomic units. This means that quantum chemical computations should be relevant up to 6–8 decimal figures or more.

From a purely mathematical point of view, crystals and polymers (extended systems) can be considered as very large molecules which are sometimes of macroscopic size. It is quite natural that the treatment of such systems needs different physical models and approximations than that of molecules; their discussion is out of the scope of this book (for a recent review on the electronic structure of polymers, see [686]).

The specific features of molecule formation, that is, the nature of the chemical bond will be discussed in Part 2. Here we emphasize only the following points:

(i) Similar to the theory of atoms, the existence and properties of molecules can be understood only in the framework of quantum physics. Even a rough qualitative understanding is impossible on the basis of classical mechanics.

(ii) In many cases it can be assumed that molecules of a given system (in contrast to its atoms) do not interact with each other. This is the *isolated molecule approach.* Even if there is some attraction or repulsion between two molecules, typical values of interaction energies are less by about an order of magnitude than intramolecular binding energies (*cf.* Fig. A1 in Appendix). As a consequence, environmental effects on molecules (solvation, *etc.*) can usually be taken into account as relatively small perturbations (see Section 1.5). In studying chemical reactions, we may be interested in the interaction of two (or more) molecules which are close to each other. In such a case the interaction is large and the system of the two molecules can be considered as a whole, forming a "supermolecule".

(iii) The number and nature of the constituent atoms of a molecule determine the empirical chemical formula, but they do not determine the structure unequivocally. Many isomers have the same empirical formula but are considered as quite different molecules. It must be emphasized that the Hamiltonian in Eq. (1.2), being completely determined by the number and quality of the nuclei and by the number of electrons, corresponds to the empirical formula and not to a specific isomeric structure. Stationary states of the total molecular Hamiltonian are therefore, in general, superpositions of several wave functions describing different chemical structures. One can thus conclude that molecules, defined in the chemical sense, *do not correspond to a stationary state of their Hamiltonian* [757, 1439]. However, if the isomers are separated by a sufficiently high and wide potential barrier (see in the next Section), they can be considered as quasistationary states, the lifetime of which may be extremely large. For

this, the *Born–Oppenheimer model* is of practical and conceptual importance where the positions of the nuclei (*i.e.*, the steric arrangement of atoms) can be *a priori* fixed, thus one deals with just one of the isomers from the very beginning. This model will be discussed in the next Section.

1.2.2 THE BORN–OPPENHEIMER MODEL

Characteristics of the motion of electrons and nuclei in a molecule are not identical. The mass of a proton is 1836-times larger than that of an electron, thus the nuclear masses are by three or four orders-of-magnitude larger than the electronic mass. This permits us to introduce a very important model for molecular (as well as for crystalline) systems.

On the basis of simple classical arguments one expects that the motion of electrons will be much faster than that of the nuclei, because of the much larger mass of the latter. Thus the time-scales of the two motions can be separated. The slow nuclei see only an averaged potential of the electrons, or at most some fluctuations around this average. As for the fast electrons, they can follow immediately (=adiabatically) any change in the positions of the nuclei. Accordingly, in the so-called *adiabatic approximation* [728] one solves separate Schrödinger equations for the nuclear and electronic wave functions, though some coupling between the two motions is accounted for. (Note that the term "adiabatic" has nothing to do with adiabacity in the thermodynamical sense.)

A further simplification can be made by neglecting any effects which are due to the motion of the nuclei when writing down the electronic Schrödinger equation. This fixed nuclei model is usually referred to as the Born–Oppenheimer approximation [129].

The full separation of the equation for the electrons and that for the nuclei is done as follows. The total molecular Hamiltonian is $\hat{H}=\hat{T}_n+\hat{T}_e+\hat{V}$, where $\hat{T}_n$ is the kinetic energy operator of nuclei, $\hat{T}_e$ is that of electrons. In the Born–Oppenheimer approximation one assumes that, in studying the motion of electrons, the nuclei can be considered as being fixed. That is, in writing down the *electronic* Schrödinger equation one drops the kinetic energy operator of the nuclei, provided that the coordinate system is chosen in such a way that the centre of mass of the molecule is of zero velocity. Then the Hamiltonian for the electrons becomes:

$$\hat{H}=-\frac{1}{2}\sum_{i=1}^{n}\Delta_i-\sum_{i=1}^{n}\sum_{A=1}^{m}\frac{Z_A}{|\mathbf{R}_A-\mathbf{r}_i|}+\sum_{i<j}\frac{1}{|\mathbf{r}_i-\mathbf{r}_j|} \tag{1.17}$$

where the indices i, j, and A run over the electrons and nuclei, respectively, n and m are the number of electrons and nuclei, respectively.

The Hamiltonian in Eq. (1.17) is called the *Born–Oppenheimer electronic Hamiltonian*, its eigenfunctions are the *Born–Oppenheimer electronic states*. In the Born–Oppenheimer formalism the nuclear coordinates are handled as parameters of the Hamiltonian and the wave function, and the position vectors of electrons, $\mathbf{r}_i$, together

with their spin coordinates, represent the dynamical variables of the system. While the total number of electrons and nuclei together with the atomic numbers of the latter define the total Hamiltonian of Eq. (1.1) completely, in order to define the Born–Oppenheimer electronic Hamiltonian of Eq. (1.17), the position vectors of the nuclei $\mathbf{R}_A (A = 1, 2, \ldots m)$ should also be specified. The time independent electronic Schrödinger equation has the form

$$\hat{H}\Psi = E_e(\mathbf{R}_1, \mathbf{R}_2, \ldots \mathbf{R}_m)\Psi \tag{1.18}$$

where E_e is the so-called electronic energy of the system and we mentioned that it depends on the nuclear coordinates parametrically. In the Born–Oppenheimer model the total energy of the molecule, E, is obtained from the electronic energy E_e by adding a term E_{nucl} which represents the nuclear–nuclear repulsion:

$$E = E_e + E_{\text{nucl}}; \qquad E_{\text{nucl}} = \sum_{A<B}^{m} \frac{Z_A Z_B}{|\mathbf{R}_A - \mathbf{R}_B|}. \tag{1.19a}$$

It is clear that similar to E_e, the total energy E also depends parametrically on the nuclear coordinates. In other words, E is not simply a scalar, but it is a vector–scalar functional $E(\mathbf{R}_A)$ with the domain of a $3m$ dimensional* vector space. Therefore, $E(\mathbf{R}_A)$ is called the *potential hypersurface*. This plays the role of the potential energy for the nuclei in the Born–Oppenheimer approximation, thus the Schrödinger equation for the nuclear motion becomes:

$$[\hat{T}_n + E(\mathbf{R}_1, \mathbf{R}_2, \ldots \mathbf{R}_m)]\Phi_i(\mathbf{R}_1, \mathbf{R}_2, \ldots \mathbf{R}_m) = \varepsilon_i \Phi_i(\mathbf{R}_1, \mathbf{R}_2, \ldots \mathbf{R}_m). \tag{1.19b}$$

Pictorially speaking, the point representing the position of the nuclei in the $3m-6$ dimensional configuration space moves on the hypersurface $E(\mathbf{R}_A)$ like a ball on a mountain, trying to reach the low energy regions. Thus the structure of the hypersurface is of considerable importance in the theory of molecular conformations and chemical reactions.

The Born–Oppenheimer approximation corresponds to the following approach. One first approximates the total molecular wave function $\Psi(\mathbf{x}_1, \mathbf{x}_2, \ldots \mathbf{x}_n, \mathbf{X}_1, \mathbf{X}_2, \ldots \mathbf{X}_m)$ depending on both the electronic and nuclear spatial and spin variables as a product $\Psi = \Psi_n \Psi_e$ where the nuclear wave function $\Psi_n = \Psi_n(\mathbf{X}_1, \mathbf{X}_2, \ldots \mathbf{X}_m)$ depends only on the nuclear variables while the electronic wave function $\Psi_e = \Psi_e(\mathbf{x}_1, \mathbf{x}_2, \ldots \mathbf{x}_n)$ depends on the electronic spatial and spin coordinates as dynamical variables and on the nuclear (space) coordinates as parameters. Then one substitutes this product wave function $\Psi = \Psi_n \Psi_e$ into the Schrödinger equation (1.6) [note that $\hat{H}$ in Eq. (1.6) is the total Hamiltonian]; utilizing Eqs (1.3), (1.4), and (1.17) one finds that Eqs (1.18),

* More precisely, disregarding the 3 translational and 3 rotational degrees of freedom of the whole molecule, one has $3m-6$ independent internal coordinates determining the dimension of the vector space $\{\mathbf{R}_A\}$. This space is called the *configuration space*.

(1.19) and (1.19a) would be fulfilled if one dropped the relatively small terms containing the derivatives of Ψ_e with respect to the nuclear coordinates.

A chemical process is said to be *adiabatic* (not to be confused with the adiabatic approximation mentioned above), if the system moves on one and the same hypersurface during the process. There exist non-adiabatic reactions as well, involving transitions from one potential hypersurface to another [1019], usually when the two surfaces come close to each other.

The critical (stationary) points of the potential hypersurface where the gradients of the energy vanish are particularly significant. Some important types of critical points on one and two dimensional energy surfaces are illustrated in Figs 1.3 and 1.4. The absolute minimum (Fig. 1.3 *a*) corresponds to the most stable nuclear configuration (geometry) of the molecule. Maxima (Fig. 1.4 *b*) are in general not important. Saddle points (Fig. 1.4 *c*) are linked with (hypothetical) transition states. Shallow local minima may represent metastable states (reaction intermediates).

For larger molecules one can usually find a great number of minima describing stable nuclear configurations. They correspond either to different conformations of the same molecule, or to different isomers. The former is the case if the overall topology of the molecule is the same in the configurations compared, while for different isomers the whole arrangement of atoms is different.

It often happens that there exist more than one minimum with the same energy; this is the situation for example with optical enantiomers. In such a case, depending on the height and width of the barrier separating the two minima in the potential hypersurface, the total wave function is either a superposition of the two structures corresponding to the two minima, or the molecule can be more or less stabilized in one of the configurations. An example for the latter is the resolution of *l* and *d* optical enantiomers, while in the former situation there is a continuous tunnelling between the two limiting structures (as in the umbrella inversion of the NH_3 molecule).

As can be seen from Figs 1.3 and 1.4, different points on the energy hypersurface can be characterized by the corresponding derivatives $\partial E/\partial q$ with respect to each, given nuclear coordinate q. For example, all $\partial E/\partial q = 0$ in critical points. Such derivatives, in principle, can be evaluated through the Hellmann–Feynman theorem [387, 545]:

$$-F_0 = \left(\frac{\partial E}{\partial q}\right)_{q=q_0} = \langle \Psi | \left(\frac{\partial \hat{H}}{\partial q}\right)_{q=q_0} | \Psi \rangle \tag{1.20}$$

where both $\hat{H}$ and Ψ depend on q parametrically. The Hellmann–Feynman theorem states that the derivatives of the wave function, $\partial \Psi/\partial q$, need not be known to obtain the derivative of the total energy, $\partial E/\partial q$ at a given point $q = q_0$. If the Hamiltonian in Eq. (1.20) contains also the nuclear repulsion term of Eq. (1.18), the quantity F_0 is called the Hellmann–Feynman force since it gives the classical force $\mathbf{F}_0 = -(\nabla E)_{q_0}$ on the nuclei at the configuration q_0 in the Born–Oppenheimer approximation. The statement of the Hellmann–Feynman theorem is rather surprising, but it holds exactly as far as the wave function Ψ is an exact eigenstate of the Hamiltonian $\hat{H}$.

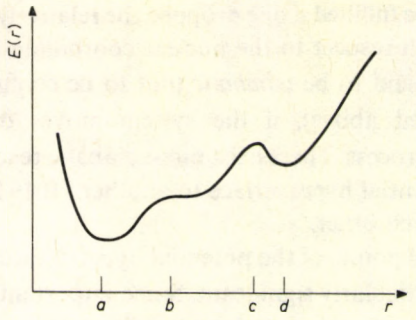


Fig. 1.3 One dimensional energy "surface" $E(r)$ *a:* absolute minimum, *b:* inflection point, *c:* maximum, *d:* local minimum

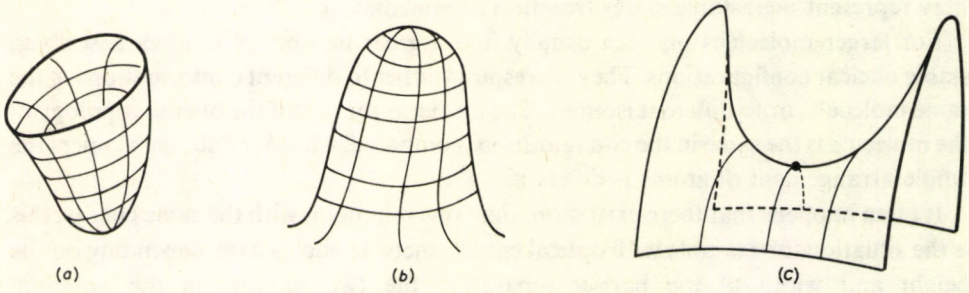


Fig. 1.4 Critical points on a two-dimensional energy surface

There is an important physical significance of the Hellmann–Feynman theorem. Namely, by substituting the Born–Oppenheimer electronic Hamiltonian of Eq. (1.17) augmented with the nuclear repulsion term of Eq. (1.19a) into Eq. (1.20), and evaluating the derivatives of the Hamiltonian, one finds:

$$\mathbf{F}_A = Z_A \int \rho(\mathbf{r}) \frac{\mathbf{r}-\mathbf{R}_A}{|\mathbf{r}-\mathbf{R}_A|^3} \, d^3\mathbf{r} - Z_A \sum_{B(\neq A)} Z_B \frac{\mathbf{R}_A-\mathbf{R}_B}{|\mathbf{R}_A-\mathbf{R}_B|^3} \tag{1.20a}$$

where $\rho(\mathbf{r})$ is the electron density defined by the relation (*cf.* Section 1.2.3):

$$\rho(\mathbf{r}) = \left\langle \Psi \left| \sum_{i=1}^{n} \delta(\mathbf{r}-\mathbf{r}_i) \right| \Psi \right\rangle . \tag{1.20b}$$

That is, if one knew the exact density $\rho(\mathbf{r})$, the quantum mechanical forces acting on nuclei could be evaluated by the above formula, which is simply the classical electrostatic force acting on the given nucleus A due to the other nuclei and the charge distribution of the electronic cloud.

It must be emphasized that approximate wave functions may violate the Hellmann–Feynman theorem which is thus a necessary (but not sufficient) criterion for the

accuracy of the wave function. Note that wave functions commonly used in practical quantum chemistry usually do not obey this criterion. If using such an approximate wave function, the forces are to be calculated by the following formula:

$$F'_0 = F_0 - \left\langle \frac{\partial \Psi}{\partial q} | \hat{H} | \Psi \right\rangle - \left\langle \Psi | \hat{H} | \frac{\partial \Psi}{\partial q} \right\rangle \tag{1.21}$$

where F_0 is the Hellmann–Feynman force and the two latter terms together are called *wave function forces* [1134].

Within the Born–Oppenheimer framework the most important nuclear configurations (in other words: geometries) correspond to *minima* in the potential energy hypersurface, for which

$$\frac{\partial E}{\partial \mathbf{R}_A} = 0, \qquad \frac{\partial^2 E}{\partial \mathbf{R}_A \partial \mathbf{R}_B} > 0 \tag{1.22}$$

holds for all nuclei A, B. (A distinction between minima, maxima and saddle points can be made by checking the second derivatives.) We say that the nuclei are in an equilibrium position* and the corresponding geometry is said to be *optimized.* For computational procedures determining optimal geometries see Section 3.1.

The Born–Oppenheimer approximation represents the most important and most frequently used model in nonrelativistic quantum chemistry. For most chemically relevant cases its accuracy is completely satisfactory (see *e.g.* p. 86 in Ref. [1449]; one usually does not go beyond the Born–Oppenheimer approximation in studying electronic structure. As we will see, in quantum chemistry one usually applies further approximations which bring much larger errors into the theory. If very fine details of electronic properties are necessary, or if we study nuclear motions, we can, in principle, take into account adiabatic [1449] or even non-adiabatic corrections. Further on in this book, we always remain in the framework of the Born–Oppenheimer model unless the contrary is stated.

1.2.3 ONE-ELECTRON FUNCTIONS AND CONFIGURATION INTERACTION

The Born–Oppenheimer model represents a remarkable simplification in determining electronic states. Analytical solutions of the Schrödinger equation, however, can be obtained even in this approximation only for one-electron systems (*e.g.*, H atom, H_2^+ ion [69, 1429]). In the chemically more interesting many-electron cases one has to develop numerical methods, which, in principle, can approximate the exact Born–Oppenheimer wave function to any desired accuracy. In this Section we introduce a general tool for obtaining such numerical solutions, namely the configuration

* Strictly speaking, in a real situation nuclei oscillate around the equilibrium geometry due to the quantum mechanical zero point vibration, and to the thermal effects leading to excited vibrational states.

interaction method. To reach this goal, we should first discuss the concept of one- and many-electron wave functions.

The wave function Ψ of an n-electron system in the Born–Oppenheimer model depends on the electronic coordinates as dynamical variables:

$$\Psi = \Psi(\mathbf{x}_1, \mathbf{x}_2, \ldots \mathbf{x}_n) \tag{1.23}$$

where $\mathbf{x}_i$ represents the foursome of (three spatial and one spin) coordinates of electron i ($\mathbf{x}_i = \{x_i, y_i, z_i, \sigma_i\}$). We may say that Ψ is an n-electron function. Accordingly, $\varphi(\mathbf{x})$ is said to be a one-electron function if it depends only on a single quartet of coordinates $\mathbf{x} = \{x, y, z, \sigma\}$ where x, y and z are the Cartesian coordinates and σ is the spin coordinate.

Let us now consider a complete set of arbitrary one-electron functions

$$\varphi_i(\mathbf{x}), \qquad i = 1, 2, 3, \ldots \tag{1.24}$$

and let us assume that the set $\{\varphi_i\}$ is orthonormal, that is

$$\langle \varphi_i | \varphi_k \rangle = \delta_{ik} . \tag{1.25}$$

The one-electron functions φ_i are often called *spinorbitals*, referring to their explicit dependence on both the spatial and spin coordinates. The orthogonality requirement Eq. (1.25) for the spinorbitals is introduced only for the sake of simplicity, since the whole theory can be developed also for non-orthogonal one-electron functions. In the latter case, however, the resulting formulae would be too complicated.

By means of the spinorbitals φ_i, a particular n-electron state Φ_K can be formed by distributing the electrons among n selected spinorbitals; i.e., each electron i is assigned to a given spinorbital φ_{K_i}:

$$\Phi_K = \hat{\mathrm{A}}[\varphi_{K_1}(\mathbf{x}_1)\varphi_{K_2}(\mathbf{x}_2) \ldots \varphi_{K_n}(\mathbf{x}_n)] \tag{1.26}$$

where $\hat{\mathrm{A}}$ is the so-called antisymmetrizer. This is a notation for an operator which has the effect of making the simple Hartree-product wave function $\varphi_{K_1}(\mathbf{x}_1)\varphi_{K_2}(\mathbf{x}_2) \ldots \varphi_{K_n}(\mathbf{x}_n)$ to be antisymmetric in the variables $\mathbf{x}_i$ (see also later). The Φ_K of Eq. (1.26) may be interpreted as a function obtained by putting one electron on spinorbital φ_{K_1}, another one onto φ_{K_2}, etc. That is, the orbitals $\varphi_{K_1}, \varphi_{K_2}, \ldots \varphi_{K_n}$ are occupied, while others ($\varphi_l, l \notin \{K_i\}$) are empty or unoccupied. A set of the occupied spinorbitals is called a *configuration* (we have already used this expression in a qualitative context in Section 1.2.1). The index K in Eq. (1.26) labels the configurations.

The importance of introducing one-electron functions is, in part, to offer a pictorial representation of the distribution of electrons in a given configuration by assigning each electron to a given spinorbital φ_i. As for the physical reality of this picture, it depends on the choice of one-electron functions (*cf.* Sections 1.2.4 and 1.2.7). (We note that, departing from this picture, another important possibility for constructing many-electron wave functions is the explicit use of relative electron coordinates $(\mathbf{r}_i - \mathbf{r}_j)$ in the wave function which are obviously absent in Eq. (1.26) [617, 729]. Such methods are

not considered in this book, since they are applicable practically only for very small systems.) The set of n-electron states constructed from one-electron orbitals *via* Eq. (1.26) permits us to find the exact wave function in the following manner.

Due to the completeness of the set $\{\varphi_i\}$ of the one-electron functions the set of all possible n-electron configurations Φ_K, $K=1, 2, 3, \ldots$ constructed from them forms also a complete orthonormal set. In terms of this, any n-electron function, thus also the exact wave function Ψ, can be expanded:

$$\Psi = \sum_{L=1}^{\infty} C_L \Phi_L \tag{1.27}$$

where the C_L coefficients can be obtained formally as $C_L = \langle \Phi_L | \Psi \rangle$. By substituting the series in Eq. (1.27) into the Schrödinger equation, $\hat{\mathrm{H}}\Psi = E\Psi$, then multiplying by Φ_K and integrating by utilizing the orthonormality of the set $\{\Phi_L\}$, i.e. that $\langle \Phi_K | \Phi_L \rangle = \delta_{KL}$ holds, we get the so-called *secular equation*

$$\sum_L \langle \Phi_K | \hat{\mathrm{H}} | \Phi_L \rangle C_L = E C_K \tag{1.28}$$

(*cf.* matrix representation of quantum mechanics [759, 1449]). The off-diagonal matrix elements of the Hamiltonian, $\langle \Phi_K | \hat{\mathrm{H}} | \Phi_L \rangle$, $K \neq L$, describe the "interaction" between configurations K and L. Therefore the above technique is called the configuration interaction (CI) method [1449], and the matrix having the elements $\mathrm{H}_{KL} = \langle \Phi_K | \hat{\mathrm{H}} | \Phi_L \rangle$ is the CI matrix.

Let us now discuss the antisymmetrizer $\hat{\mathrm{A}}$ introduced in Eq. (1.26). As we have mentioned, its role is simply to ensure that each configuration Φ_K, thus the exact wave function as well, be antisymmetric in the variables $\mathbf{x}_i$ to satisfy in the Pauli principle. Let us at first study the effect of $\hat{\mathrm{A}}$ on a two-electron system. The simple Hartree-product wave function

$$\varphi_i(\mathbf{x}_1)\varphi_j(\mathbf{x}_2) \tag{1.29}$$

is neither symmetric nor antisymmetric, but the following normalized linear combination

$$\Phi = \frac{1}{\sqrt{2}} [\varphi_i(\mathbf{x}_1)\varphi_j(\mathbf{x}_2) - \varphi_i(\mathbf{x}_2)\varphi_j(\mathbf{x}_1)] \tag{1.30}$$

is properly antisymmetric in $\mathbf{x}_1$ and $\mathbf{x}_2$. Now, Eq. (1.30) can be written as a determinant:

$$\Phi = \frac{1}{\sqrt{2}} \begin{vmatrix} \varphi_i(\mathbf{x}_1) & \varphi_j(\mathbf{x}_1) \\ \varphi_i(\mathbf{x}_2) & \varphi_j(\mathbf{x}_2) \end{vmatrix}. \tag{1.31}$$

Similarly, in the n-electron case instead of a simple Hartree-product $\varphi_{K_1}\varphi_{K_2}\ldots\varphi_{K_n}$ one should have the following determinant:

$$\Phi_K = \frac{1}{\sqrt{n!}} \begin{vmatrix} \varphi_{K_1}(\mathbf{x}_1) & \varphi_{K_2}(\mathbf{x}_1) & \dots & \varphi_{K_n}(\mathbf{x}_1) \\ \varphi_{K_1}(\mathbf{x}_2) & \varphi_{K_2}(\mathbf{x}_2) & \dots & \varphi_{K_n}(\mathbf{x}_2) \\ \vdots & & & \\ \varphi_{K_1}(\mathbf{x}_n) & \varphi_{K_2}(\mathbf{x}_n) & \dots & \varphi_{K_n}(\mathbf{x}_n) \end{vmatrix} \tag{1.32}$$

where the factor $1/\sqrt{n!}$ arises from normalization. The above determinantal wave functions are called *Slater-determinants*. Equation (1.32) is often written in short-hand notation as

$$\Phi_K = \frac{1}{\sqrt{n!}} |\varphi_{K_1} \varphi_{K_2} \dots \varphi_{K_n}| . \tag{1.33}$$

The expectation value of an arbitrary operator by the many-electron wave function Ψ can easily be obtained by using the CI series Eq. (1.27). For the energy for example one has

$$E = \langle \Psi | \hat{\mathrm{H}} | \Psi \rangle = \sum_{K,L} C_K C_L H_{KL} \tag{1.34}$$

where $H_{KL} = \langle \Phi_K | \hat{\mathrm{H}} | \Phi_L \rangle$ is the matrix element of $\hat{\mathrm{H}}$ over the Slater-determinants Φ_K and Φ_L. The rules for calculating matrix elements of one- and two-electron operators between determinantal wave functions are called *Slater* (or sometimes Slater–Condon) *rules* (not to be confused with the Slater rules for atomic orbital exponents, *cf.* Section 1.2.5). For the relevant formulae, see [819, 1286].

The energy expression can also be given by means of the density matrices [819], without considering the wave function explicitly as

$$E = \int \hat{h}^1 \gamma(\mathbf{x}, \mathbf{x}') \, d\mathbf{x} + \int \hat{h}^{12} \Gamma(\mathbf{x}_1, \mathbf{x}_2, \mathbf{x}'_1 \mathbf{x}'_2) \, d\mathbf{x}_1 \, d\mathbf{x}_2 \tag{1.35}$$

where $\gamma(\mathbf{x}, \mathbf{x}')$ is the first order (or one-particle) *density matrix*, defined by

$$\gamma(\mathbf{x}, \mathbf{x}') = n \int \Psi(\mathbf{x}, \mathbf{x}_2, \dots \mathbf{x}_n) \Psi(\mathbf{x}', \mathbf{x}_2, \dots \mathbf{x}_n) \, d\mathbf{x}_2 \dots d\mathbf{x}_n; \tag{1.36}$$

while $\Gamma(\mathbf{x}_1 \mathbf{x}_2, \mathbf{x}'_1 \mathbf{x}'_2)$ is the second order (or two-particle) density matrix

$$\Gamma(\mathbf{x}_1, \mathbf{x}_2, \mathbf{x}'_1, \mathbf{x}'_2) = \binom{n}{2} \int \Psi(\mathbf{x}_1, \mathbf{x}_2, \mathbf{x}_3, \dots \mathbf{x}_n) \Psi(\mathbf{x}'_1, \mathbf{x}'_2, \mathbf{x}_3, \dots \mathbf{x}_n) \, d\mathbf{x}_3 \dots d\mathbf{x}_n \tag{1.37}$$

and $\hat{h}^1$ and $\hat{h}^{12}$ are the one- and two-electron parts of the Hamiltonian $\hat{\mathrm{H}}$. The notations used in Eq. (1.35) are to be understood as the operators $\hat{h}^1$ and $\hat{h}^{12}$ act on the primed coordinates, and after this the integration is to be performed by setting $\mathbf{x}' = \mathbf{x}$ and $\mathbf{x}'_i = \mathbf{x}_i$.

The density matrices are useful in studying the convergence properties of the CI expansion Eq. (1.27). Let us express the first order density matrix $\gamma(\mathbf{x}, \mathbf{x}')$ in terms of one-electron functions:

$$\gamma(\mathbf{x}, \mathbf{x}') = \sum_{kl} \gamma_{kl} \varphi_k(\mathbf{x}) \varphi_l(\mathbf{x}') \tag{1.38}$$

where γ_{kl} is the representant of $\gamma(\mathbf{x}, \mathbf{x}')$ in the space $\{\varphi_i\}$. The matrix γ is generally not diagonal in indices k and l. By considering a unitary transformation of one-electron spinorbitals, it can be brought into a diagonal form. It is easy to show that the total many-electron wave function Ψ is invariant—up to a phase factor—under such transformations provided that the set of configurations is complete. The transformed one-electron functions are called natural spinorbitals; it was shown that in some sense they provide the best convergence properties for the CI expansion series of Eq. (1.27). Since the exact density matrix $\gamma(\mathbf{x}, \mathbf{x}')$ is not known before solving the Schrödinger equation, natural orbitals can only be constructed *a posteriori*. There are, however, some methods for constructing approximate natural orbitals directly; see Section 1.3.2.

Most quantum chemical methods approximate the wave function in terms of the series (1.27). Of course, since no infinite number of configurations can be taken into account in actual computations, the crucial point is the choice of the one-electron functions $\{\varphi_i\}$ which can be done by means of further physical and/or chemical arguments. The aim is to find one-electron functions which enable us to approximate the exact wave function as closely as possible by only a limited number of configurations. The most important possibility is discussed in the next Section. Actual procedures for performing CI calculations will be treated in Section 1.3.1.

1.2.4 INDEPENDENT PARTICLE MODELS

General formulation. To achieve satisfactory convergence properties in the configuration expansion Eq. (1.27), one has to select carefully the one-electron spinorbitals $\{\varphi_i\}$. Moreover, it is important which are the appropriate one-electron functions most suitable to derive the many-electron wave function by a *single* determinant only. A physically acceptable possibility is the so-called independent particle picture also called the one-electron or Hartree–Fock approximation [820, 821]. This model will be discussed in the present Section.

As a first approximation one may assume that each electron of a molecule moves in the field of the nuclei and in some average field of all the other electrons, *i.e.* the motion of a given electron is independent of the actual position of the other electrons. This assumption can be considered as a physical model, and is quite justified if the interaction between electrons is not too strong. This condition is generally not fulfilled very well for molecular systems, but we will see later that there are some physical properties for which reasonable approximate values can be obtained by the above model for most molecules. Moreover, the importance of the one-electron picture is stressed by its power in interpreting atomic and molecular wave functions. For example, the concept of the shell structure of atoms (*cf.* Section 1.2.1), is based conceptually on that picture.

The average interaction potential for electrons can be formulated as follows. The Born–Oppenheimer Hamiltonian may be written as

$$\hat{H} = \sum_i \hat{H}_i^1 + \sum_{i<j} \hat{H}_{ij}^2 \tag{1.39}$$

where $\hat{H}_i^1$ stands for the one-electron part of $\hat{H}$ depending on the coordinates of electron i, while $\hat{H}_{ij}^2 = 1/r_{ij}$ contains the relative electron coordinates $r_{ij} = |\mathbf{r}_i - \mathbf{r}_j|$, so $\sum_{i<j} \hat{H}_{ij}^2$ is a sum of two-electron operators. The averaging of electronic interactions means that, instead of handling the $\hat{H}_{ij}^2$ term explicitly, it is approximately replaced by a sum of effective interactions $\hat{V}_i^{av}$ each representing the average effect of the cloud of the other $n-1$ electrons on the i-th one. Mathematically:

$$\sum_{i<j} \hat{H}_{ij}^2 \approx \sum_i \hat{V}_i^{av}. \tag{1.40}$$

The form of $\hat{V}_i^{av}$ is to be determined by further considerations. Using the simplification in Eq. (1.40), the Hamiltonian of Eq. (1.39) becomes a sum of (pseudo-) one-electron operators; thus the Schrödinger equation transforms approximately to:

$$\sum_i (\hat{H}_i^1 + \hat{V}_i^{av}) \Psi(\mathbf{x}_1, \mathbf{x}_2, \ldots \mathbf{x}_n) = E\Psi(\mathbf{x}_1, \mathbf{x}_2, \ldots \mathbf{x}_n). \tag{1.41}$$

Eq. (1.41) suggests that Ψ can be written as a single Slater determinant (antisymmetrized product) in the form of Eq. (1.37), permitting us to separate Eq. (1.41) in the variables of the different electrons. (The simple Hartree-product form, which is also consistent with Eq. (1.41), would violate the Pauli principle.) The separated equations become:

$$(\hat{H}_i^1 + \hat{V}_i^{av}) \varphi_i(\mathbf{x}) = \varepsilon_i \varphi_i(\mathbf{x}) \tag{1.42}$$

where ε_i is the i'th eigenvalue of the effective one-particle operator $\hat{H}_i^1 + \hat{V}_i^{av}$. The mathematical meaning of the one-electron approximation is to take the many-electron wave function as a single determinant (antisymmetrized product) of one-electron spinorbitals the latter being solutions of Eq. (1.42). In other words, the configuration interaction series Eq. (1.27) is truncated to one term only, which will be denoted by Φ_0. This is clearly a drastic approximation but if we determine the spinorbitals in an optimal manner, the single determinant HF wave function Φ_0 often yields a satisfactory result. Furthermore, as within the HF scheme each electron is assigned to a separate spinorbital, this approximation permits us to study various molecular effects in terms of one-electron contributions. This greatly facilitates understanding and interpretation of the results.

Let us turn now to the problem of determining the effective interaction operators $\hat{V}_i^{av}$. The guide here is the variational principle (see Section 1.1) which suggests that one should choose the orthonormalized one-electron orbitals φ_i occupied in Φ_0 in such a way that the approximate energy $E = \langle \Phi_0 | \hat{H} | \Phi_0 \rangle$ be minimal. Such Φ_0 is called the optimum determinant—the zero subscript refers to the ground state. The actual form of $\hat{V}_i^{av}$ can be determined most easily by means of the *Brillouin theorem* [775]:

$$\langle \Phi_{i\to j^*} | \hat{H} | \Phi_0 \rangle = 0 \tag{1.43}$$

where $\Phi_{i\to j^*}$ is any "singly excited" Slater-determinant which is obtained from Φ_0 by replacing the spinorbital φ_i by an arbitrary unoccupied spinorbital φ_{j^*} which has to be orthogonal to all orbitals occupied in Φ_0. The Brillouin theorem means that Φ_0 does not interact with the singly excited configurations. As it can be proven easily [880, 882], Eq. (1.43) is valid if and only if Φ_0 is an optimum determinant in the above sense. Thus, the Brillouin theorem is completely equivalent to the variational principle applied for the independent particle model.

Substituting the Hamiltonian into Eq. (1.43), and expanding Φ_0 and $\Phi_{i\to j^*}$ *via* the Slater rules one obtains:

$$\langle \varphi_{j^*} | \hat{F} | \varphi_i \rangle = 0 \tag{1.44}$$

where $\hat{F}$ is the so-called Fock operator or Fockian which is defined as follows

$$\hat{F}\varphi_i(\mathbf{x}_1) = \hat{H}_i^1 \varphi_i(\mathbf{x}_1) + \sum_k^{\text{occ}} \int \varphi_k(\mathbf{x}_2) \frac{\varphi_k(\mathbf{x}_2)\varphi_i(\mathbf{x}_1) - \varphi_i(\mathbf{x}_2)\varphi_k(\mathbf{x}_1)}{r_{12}} \mathrm{d}\mathbf{x}_2 \tag{1.45}$$

here the summation index k runs over all spinorbitals which are occupied in Φ_0. Eq. (1.44) is sometimes called the *local Brillouin* theorem; it states that the matrix elements of the Fockian between occupied and unoccupied orbitals are zero. Since the unoccupied orbital φ_{j^*} is arbitrary but orthogonal to the optimum occupied orbitals, Eq. (1.44) can be fulfilled if the occupied orbitals satisfy the following equations*:

$$\hat{F}\varphi_i = \sum_k^{\text{occ}} \varepsilon_{ik} \varphi_k \,. \tag{1.46}$$

These are the Hartree–Fock equations; their solutions are the optimum HF spinorbitals. Let us discuss now some of the most important features of the HF equations.

(i) Owing to the properties of determinants, the one-determinantal many-electron wave function is invariant with respect to unitary transformations** among the set $\{\varphi_i\}$. For a more detailed discussion of such transformations, see Section 1.4. Making use of the particular transformation bringing the matrix ε_{ik} of Eq. (1.46) to a diagonal form, the HF equations get the form of Eq. (1.42):

$$\hat{F}\varphi_i = \varepsilon_i \varphi_i \,. \tag{1.47}$$

* This can be seen easily by multiplying Eq. (1.46) by φ_{j^*}. One can also prove that Eqs (1.46) are not only sufficient but also necessary conditions for the fulfillment of Eq. (1.44).

** A transformation with matrix $\mathbf{U}$ is said to be unitary if $\mathbf{U}\mathbf{U}^+ = \mathbf{I}$ where $\mathbf{I}$ is the unit matrix and the superscript "+" refers to the adjoint of the matrix.

The HF equations in this form are referred to as canonical HF equations. The resulting HF orbitals are called canonical orbitals and they are eigenfunctions of the Fockian $\hat{F}$.

(ii) The Fock operator in Eq. (1.45) depends on the orbitals which are being searched for; thus the HF equations are nonlinear. For this reason Eqs (1.47) are usually called pseudo-eigenvalue equations: the operator in the left-hand side depends on its own eigenfunctions. The solutions of Eqs (1.46) or (1.47) can be obtained in an iterative manner: some initial guess is used to construct the first approximation of the Fockian, the HF equations are then solved for obtaining new orbitals. These are used to build the new Fockian and the whole procedure is repeated until convergence is reached, that is, the orbitals obtained by solving the equations do not differ appreciably from those which were used in constructing the equations themselves.

(iii) Physically, the Fockian $\hat{F}$ depends on the orbitals φ_i as a consequence of averaging the interelectronic interactions in the HF scheme. By comparing Eqs (1.42) and (1.47) we find that $\hat{F} = \hat{H}_i^1 + \hat{V}_i^{av}$, thus the averaged interaction operator is defined by

$$\hat{V}_i^{av}\varphi_i(\mathbf{x}_1) = \sum_k^{occ} \int \varphi_k(\mathbf{x}_2) \frac{\varphi_k(\mathbf{x}_2)\varphi_i(\mathbf{x}_1) - \varphi_i(\mathbf{x}_2)\Phi_k(\mathbf{x}_1)}{r_{12}} d\mathbf{x}_2 . \tag{1.48}$$

As noted above, the solutions φ_i should be consistent with the average field they are producing, and simultaneously with that from which they are obtained. Therefore, the HF model is often referred to as the self-consistent field (SCF) method.

(iv) The convergency of the usual SCF procedure is by no means guaranteed. According to numerical experience, it converges in most cases, but often some dumping techniques [930, 1227] have to be applied to avoid oscillations. There are cases when intrinsic divergence occurs [1305], and, very accidentally, it may happen that the SCF procedure converges spontaneously to an "excited" state instead of the optimum, that is, SCF (ground state) orbitals. Converging of the SCF procedure to excited states may also be useful in some cases, for example, when the so-called "hole states" are of interest; *cf.* ionization processes (Section 3).

Energy expression. The HF electronic energy, $E = \langle \Phi_0 | \hat{H} | \Phi_0 \rangle$, can be calculated by expanding this matrix element using the Slater rules. The result is:

$$E = \sum_i^{occ} H_{ii}^1 + \sum_{i,j}^{occ} [(\varphi_i\varphi_i|\varphi_j\varphi_j) - (\varphi_i\varphi_j|\varphi_i\varphi_j)] \tag{1.49}$$

where $H_{ii}^1 = \langle \varphi_i | \hat{H}_i^1 | \varphi_i \rangle$ and we have introduced the following short-hand notation*:

$$(\varphi_i\varphi_j|\varphi_k\varphi_l) = \iint \varphi_i(\mathbf{x}_1)\varphi_j(\mathbf{x}_1) r_{12}^{-1} \varphi_k(\mathbf{x}_2)\varphi_l(\mathbf{x}_2)\, d\mathbf{x}_1\, d\mathbf{x}_2 . \tag{1.50}$$

* Referring to the order of indices, this notation is called the (11|22) convention. Some authors prefer to use the [12|12] convention where $[ij|kl] = (ik|jl)$. The notations $\langle ij|kl\rangle = [ij|kl]$ and $\langle ij\|kl\rangle = [ij|kl] - [ij|lk]$ are also sometimes used.

The different terms in Eq. (1.49) can be physically interpreted as follows. The H^1_{ii} contains the kinetic energy of electron i and the nuclear-electron attraction energies. The $(\varphi_i\varphi_i|\varphi_j\varphi_j)$ integrals are usually called Coulomb integrals, they describe the classical electrostatic repulsion between electrons on spinorbitals φ_i and φ_j. The last terms of type $(\varphi_i\varphi_j|\varphi_i\varphi_j)$ have no classical analogues; they are called exchange integrals and originate from the determinantal nature (antisymmetry requirement) of the many-electron wave function. The presence of the exchange integrals in Eq. (1.49) decreases the value of the resulting electronic energy since these integrals are usually positive numbers and enter Eq. (1.49) with a negative sign. We note that it is often the total energy E_{tot} which is needed. Besides the electronic energy this includes also the classical electrostatic repulsion energy $E_n = \sum_{A<B} Z_A Z_B / R_{AB}$ of the nuclei: $E_{tot} = E + E_n$.

Formulation for non-orthogonal HF orbitals. The mathematical properties of determinants permit to introduce not only a unitary but also any general nonsingular transformation among the occupied HF orbitals. Such transformations influence only the normalization of the Slater-determinant (*cf.* also Section 1.4). If using a nonunitary transformation, however, the transformed orbitals will not be orthogonal to each other any more, but, since the transformation is carried out only within the subspace of occupied orbitals, they still remain orthogonal to the unoccupied orbitals (assuming that the latter were taken orthogonal to the original occupied ones). As can be seen easily, the Brillouin theorem (1.43), the local Brillouin theorem (1.44), and therefore the general HF equations (1.46) remain valid if using non-orthogonal orbitals. In other words, non-orthogonal HF orbitals can be considered as the most general solutions of the HF equations (1.46). The canonical HF equations (1.47) cannot be used in the non-orthogonal case, because their solutions (the canonical spinorbitals) are eigenfunctions of the Hermitian operator $\hat{F}$, and, as such, are necessarily orthogonal to each other in all non-degenerate cases. One has to realize, however, that Eq. (1.45) defining the Fockian in terms of orthogonal one-electron orbitals is not applicable in the non-orthogonal case. Similarly, the energy expression Eq. (1.49) was obtained by means of the Slater rules [1286] and is valid only for orthogonal orbitals. We shall not discuss here the construction of the Fockian in the non-orthogonal case, and note only that the appropriate energy formula can be derived by the general Löwdin-rules [817, 819]. The relevant expression reads:

$$E = \sum_{i,k}^{occ} T_{ik} H^1_{ik} + \sum_{ijkl}^{occ} (T_{ij} T_{kl} - T_{ik} T_{jl}) (\varphi_i\varphi_j|\varphi_k\varphi_l) \tag{1.51}$$

where $\mathbf{T}$ is the inverse of the overlap matrix of the spinorbitals:

$$\mathbf{T} = \mathbf{S}^{-1} \tag{1.52a}$$

$$S_{ij} = \langle \varphi_i | \varphi_j \rangle . \tag{1.52b}$$

The considerable degree of freedom in chosing one-electron HF spinorbitals corresponding to the same many-electron determinantal wave function calls our

attention to the limited physical significance of the one-electron orbitals themselves. Only the subspace of the occupied HF orbitals, called the occupied subspace, has a general physical significance at the HF level.

Further on, if the contrary is not stressed, we will work with orthogonal spinorbitals.

Physical significance of one-electron energies. The eigenvalues ε_i of the Fockian can be expressed in terms of canonical spinorbitals φ_i, using Eq. (1.45) and the notation (1.50) as

$$\varepsilon_i = \langle \varphi_i | \hat{\mathrm{F}} | \varphi_i \rangle = H_{ii}^1 + \sum_k^{\mathrm{occ}} [(\varphi_i \varphi_i | \varphi_k \varphi_k) - (\varphi_i \varphi_k | \varphi_i \varphi_k)] , \tag{1.53}$$

The eigenvalue ε_i is interpreted as the effective energy of the i-th electron assigned to the canonical spinorbital φ_i. In the HF approximation ε_i is equal to the energy needed for removing an electron from the orbital φ_i, *i.e.* to the ionization potential. This follows from the Koopmans theorem [735] which states that for the canonical orbitals the energy of the resulting ion, $E - \varepsilon_i$, is optimal (*i.e.*, stationary with respect to the variation of the canonical orbital φ_i under question), as far as the subspace of the occupied orbitals is considered only.

The restricted HF method. The solution of the HF equations in their general forms of Eqs (1.46) or (1.47) is extremely complicated since no restrictions are applied for the form of spinorbitals $\{\varphi_i(\mathbf{x})\}$. Moreover, the approximate wave function should be the eigenfunction of all operators commuting with the Hamiltonian, as it is required by quantum mechanics. Thus, Φ_0 must also be a symmetry- and spin-eigenfunction. This requirement would be generally not fulfilled if one solved the unrestricted HF equations (1.46) or (1.47).

In order to achieve Φ_0 be an eigenfunction of the $\mathbf{S}^2$ and $\mathbf{S}_z$ operators, the simplest possibility is to introduce the following restrictions:

(i) the spinorbitals are taken as products of spatial and spin parts:

$$\varphi_i(\mathbf{x}) = \psi_i(\mathbf{r})\sigma_i \tag{1.54}$$

where $\psi_i(\mathbf{r})$ is the spatial orbital and σ_i is the spin function the latter being either α or β;

(ii) every spatial orbital gives rise to two spinorbitals: $\psi_i(\mathbf{r})\alpha$ and $\psi_i(\mathbf{r})\beta$, which are either both occupied or both empty. That is, identical (spatial) orbitals for different spins are used. In other words, the many-electron wave function is built up from spatial orbitals, each filled by two electrons with opposite spins. Obviously, this can be done for molecules containing an even number of electrons; accordingly, this method is preferably applied to *closed shell systems.*

Referring to the above restrictions *(i)* and *(ii)*, one usually speaks about the restricted Hartree–Fock (RHF) method.

To obtain the RHF equations from the general forms of Eq. (1.46) or Eq. (1.47) we have to use the spinorbitals of form Eq. (1.54) and perform the integrations over spin functions. For the canonical case one gets:

$$\hat{F}\psi_i = \varepsilon_i \psi_i \tag{1.55}$$

where $\hat{F}$ is now defined over the spatial orbitals as

$$\hat{F} = \hat{H}^1 + \sum_k^{occ} (2\hat{J}_k - \hat{K}_k) \tag{1.56}$$

with

$$\hat{H}^1 = -\frac{1}{2}\Delta - \sum_A Z_A/|\mathbf{r} - \mathbf{R}_A|\,; \tag{1.57}$$

$$\hat{J}_k \psi_i(\mathbf{r}_1) = \psi_i(\mathbf{r}_1) \int \psi_k(\mathbf{r}_2)\psi_k(\mathbf{r}_2) r_{12}^{-1}\, dV_2 \tag{1.58}$$

and

$$\hat{K}_k \psi_i(\mathbf{r}_1) = \psi_k(\mathbf{r}_1) \int \psi_k(\mathbf{r}_2)\psi_i(\mathbf{r}_2) r_{12}^{-1}\, dV_2 \tag{1.59}$$

where $dV_2 = dx_2\, dy_2\, dz_2$ is the volume element. The operator $\hat{H}^1$ is sometimes called the core Hamiltonian. The $\hat{J}_k$ is the Coulomb-, $\hat{K}_k$ is the exchange operator corresponding now to the spatial orbital ψ_k. The summation index k in Eq. (1.56) runs over all (doubly) occupied orbitals. Similarly, the total energy of the molecule in the RHF method, is obtained from Eq. (1.49) by integrating over the spin variables and adding the nuclear repulsion energy E_n:

$$E_{tot} = E_n + 2\sum_i^{occ} H_{ii} + 2\sum_{i,j}^{occ} (ii|jj) - \sum_{i,j}^{occ} (ij|ij) \tag{1.60}$$

where $H_{ii} = \langle \psi_i | \hat{H}_i^1 | \psi_i \rangle$ and $(ij|kl)$ is a notation analogous to that in Eq. (1.50), but for the spatial orbitals ψ_i:

$$(ij|kl) = \iint \psi_i(\mathbf{r}_1)\psi_j(\mathbf{r}_1) r_{12}^{-1} \psi_k(\mathbf{r}_2)\psi_l(\mathbf{r}_2)\, dV_1\, dV_2\,. \tag{1.61}$$

The terms of Eq. (1.60) have the same physical meaning as those of Eq. (1.49).

It may be useful to rewrite the expression for the total energy, Eq. (1.60), in terms of the one-electron orbital energies ε_i. From Eqs (1.56–59) we have

$$\varepsilon_i = \langle \psi_i | F | \psi_i \rangle = H_{ii} + \sum_k^{occ} [2(ii|kk) - (ik|ik)]\,. \tag{1.62}$$

This equation is the specialization of Eq. (1.53) to the RHF case. By comparing Eq. (1.62) with Eq. (1.60), we obtain:

$$E_{\text{tot}} = 2\sum_{i}^{\text{occ}} \varepsilon_i - 2\sum_{ik}^{\text{occ}} (ii|kk) + \sum_{ik}^{\text{occ}} (ik|ik) + E_n \,. \tag{1.63}$$

The significance of the terms in (1.63) are as follows. Since ε_i can be considered as the effective energy of an electron on the RHF orbital ψ_i, the first term gives the sum of effective energies of all electrons (note that there are two electrons on the spatial orbital ψ_i). The effective energy ε_i for a given electron contains its total interaction both with the nuclei and with all the other electrons. As a consequence, the sum $2\sum_i \varepsilon_i$ contains the electron–electron repulsion twice. In fact, this interaction between each pair of electrons is taken into account twice, being counted for both electrons when the sum $2\sum_i \varepsilon_i$ is formed, not only for the independent pairs. For this reason one should subtract the electronic repulsion energy (both the Coulomb and the exchange terms) from the sum, which is expressed by the second and third terms in Eq. (1.63). Finally, in the last term the nuclear repulsion energy is added.

A useful alternative expression for the total energy can be obtained by substituting Eq. (1.62) into Eq. (1.63):

$$E_{\text{tot}} = E_n + \sum_{i}^{\text{occ}} (\varepsilon_i + H_{ii}) \,.$$

Obviously, the computation of E_{tot} *via* the above equation is more economic since no two-electron integrals appear.

As we will see in Section 1.3.2, there are some simple approximate methods of quantum chemistry which make use of only the sum of orbital energies for estimating the total energy E_{tot}. These are the (Hückel-type) methods which do not account for electrostatic interactions explicitly. Therefore, some effort has been made to analyze how the simple formula

$$E \approx 2\sum_{i}^{\text{occ}} \varepsilon_i \tag{1.64}$$

could be used in approximating the energy. It is expected that this would be an acceptable approximation since the electron-electron repulsion and the nuclear-nuclear repulsion (*i.e.*, the two terms omitted in (1.63) as compared to (1.64)) roughly cancel each other because they enter into Eq. (1.63) with opposite signs and are of similar magnitude. On the basis of a more sophisticated approximation by Politzer [1113], Ruedenberg has shown [1204] that for achieving a better accuracy Eq. (1.64) should be replaced by

$$E \approx k\sum_{i}^{\text{occ}} \varepsilon_i \tag{1.65}$$

where $k=3$. It was found empirically that an even better approximation arises if using $k=3.1$ [1204]. Similar possibilities were investigated by several authors (see *e.g.* [687, 1256, 1257] and it turned out that, though high accuracy can be achieved in some cases, the generality of such types of approximations is not wide enough to allow the use of Eq. (1.65) or similar formulae in strict numerical computations. The same holds for other approaches deriving approximate energy formulae [31, 864, 1113, 1118]; their use is certainly conceptual rather than computational.

The RHF orbitals ψ_i are said to be *molecular orbitals* (MO) or *atomic orbitals* (AO), referring to the system under study. The existence of the RHF AOs is the mathematical hint behind the qualitative picture used in discussing the electronic structure of atoms in Section 1.2.1.

The RHF model provides a relatively simple and pictorial tool in molecular electronic structure studies. Certainly, this method in its LCAO version (see Section 1.2.5) is the basis of most quantum chemical calculations. As we have mentioned, the RHF wave function is automatically an eigenfunction of the $\hat{\mathbf{S}}^2$ and $\hat{\mathbf{S}}_z$ operators; its energy is the "best" (*i.e.* the lowest) one which can be obtained by a single determinant built of doubly occupied spatial orbitals. The antisymmetry of the RHF wave function ensures that electrons with parallel spin avoid each other, since if they had the same spatial and spin-coordinates the wave function would become zero. This is the so-called *Fermi hole*. The Fermi hole means that the sum of exchange terms in the energy expressions Eqs (1.49), (1.60) is of negative sign, because the average distance among electrons of parallel spins is larger than would be the case without antisymmetrization; this leads to a smaller overall (positive) electronic repulsion energy. The Fermi hole can also be visualized by means of the physical interpretation of the density matrices introduced in Eqs (1.36) and (1.37). The diagonal elements of the second order density matrix, $\Gamma(\mathbf{x}_1\mathbf{x}_2)=\Gamma(\mathbf{x}_1,\mathbf{x}_1,\mathbf{x}_2,\mathbf{x}_2)$ give the probability of finding an electron at $\mathbf{r}_1$ with spin σ_1 and another one at $\mathbf{r}_2$ with spin σ_2; here $\mathbf{x}_1=\{\mathbf{r}_1,\sigma_1\}$ and $\mathbf{x}_2=\{\mathbf{r}_2,\sigma_2\}$. Now, due to the antisymmetry of the second order density matrix (reflecting that of the total wave function) one has $\Gamma(\mathbf{x},\mathbf{x})=0$. At the same time, for the given $\mathbf{x}=\{\mathbf{r},\sigma\}$ the diagonal element $\gamma(\mathbf{x})=\gamma(\mathbf{x},\mathbf{x})$ of the first order density matrix, which gives the probability of finding an electron at the space point $\mathbf{r}$ with spin σ (multiplied by the total number of the electrons) does not in general vanish. This means, that the probability of finding two electrons with parallel spins at the same point in space is zero, even if there is a considerable electron density at the given point. So, the antisymmetry introduces some effective correlation in the motion of electrons of parallel spins.

Another correlation in the motion of electrons is represented by the so-called *Coulomb hole*. The Coulomb repulsion ensures that electrons cannot get close to each other even if they are of opposite spin. This can also be imagined by considering a "hole" around each electron. Due to the averaged account of electron repulsion, however, the Coulomb hole is neglected in the HF theory. In other words, the correlation between the motion of electrons with opposite spins is not accounted for. This shortcoming has the consequence that the RHF energy of polyelectronic systems

is always higher than the exact lowest eigenvalue of the Born–Oppenheimer Hamiltonian. This is trivial from the variational point of view but it can also be interpreted pictorially: the absence of the Coulomb hole has the consequence that the "averaged distance" between electrons is slightly underestimated at the RHF level, leading to an overestimated (positive) electron repulsion energy, and, as a consequence, a higher total energy.

As proposed by Löwdin [822], the correlation energy is defined just as the difference of the exact nonrelativistic Born–Oppenheimer energy and $E_{\mathrm{RHF}} = \langle \Phi_0 | \hat{\mathrm{H}} | \Phi_0 \rangle$:

$$E_{\mathrm{corr}} = E_{\mathrm{exact}} - E_{\mathrm{RHF}} \,. \tag{1.66}$$

The correlation energy is always negative. This energy accounts for the part of electron correlation which is due to the Coulomb repulsion, but not for that connected to the Fermi hole.

The role of electron correlation will be discussed in Section 1.3.1 where some methods of calculating E_{corr} are also mentioned. Here we stress only that E_{corr} is usually less by about two orders of magnitude than E_{RHF}, *i.e.* the HF method accounts for $\approx 99\%$ of the exact energy. However, the chemically interesting energy differences (*e.g.* binding energies, barriers to internal rotations, isomerisation energies, etc.) are also small and comparable with E_{corr} (*cf.* Table A1 in the Appendix). Thus, the neglect of correlation effects is never justified by assuming that $E_{\mathrm{exact}} \approx E_{\mathrm{RHF}}$, but, only by supposing that the correlation energy *does not change* too much in the chemical process under consideration. This statement, that is, the "conservation of the correlation energy", is a condition for the applicability of the RHF model to quantitative studies.

The UHF method. The importance of the correlation energy in certain chemical processes motivates the search for models taking into account correlation effects. For this, there are some possibilities even in the framework of the one-particle model by maintaining the feature of assigning each electron to one orbital. In such methods one relaxes some freedoms which are frozen at the RHF level.

The most severe restriction in the RHF theory is the condition of double occupancy. One can get a deeper energy by allowing the use of different orbitals for different spins (DODS methods). In deriving the relevant orbital equations, the two sets of orbitals $\{\psi_i^\alpha\}$ and $\{\psi_i^\beta\}$ are varied independently (here α and β refers to the spin states). Reflecting this fact, the DODS method is also called (spin-) unrestricted HF (UHF) method if one does not drop the one-determinantal approximation. The UHF equations are rather similar to the RHF ones except that in the UHF case one has two sets of orbital equations, one for ψ_i^α and another for ψ_i^β [1121]:

$$\hat{\mathrm{F}}^\alpha \psi_i^\alpha = \varepsilon_i^\alpha \psi_i^\alpha \tag{1.67a}$$

$$\hat{\mathrm{F}}^\beta \psi_i^\beta = \varepsilon_i^\beta \psi_i^\beta \tag{1.67b}$$

where

$$\hat{\mathrm{F}}^\alpha = \hat{\mathrm{H}}^1 + \sum_k^{\mathrm{occ}} \hat{\mathrm{J}}_k - \sum_k^{(\alpha)} \hat{\mathrm{K}}_k \tag{1.68a}$$

$$\hat{F}^{\beta} = \hat{H}^1 + \sum_k^{occ} \hat{J}_k - \sum_k^{(\beta)} \hat{K}_k . \tag{1.68b}$$

Here the summations for the Coulomb operators run over *all* occupied orbitals, while for the exchange operators only over the orbitals with spin α or β, as indicated by the symbols $\sum^{(\alpha)}$ or $\sum^{(\beta)}$, respectively. Since the Coulomb repulsion is insensitive to the spins, the two sets of equations (1.68a) and (1.68b) are coupled through the Coulomb integrals.

The splitting of orbitals for different spins permits us to consider the Coulomb hole to some extent. In this manner some part of the correlation energy, in principle, can be accounted for. However, for many closed shell systems one cannot find UHF solutions which differ from the RHF ones [882]. Anyway, the importance of the UHF wave function is underlined by the following facts:

(i) The RHF method leads to the so-called "dissociation catastrophe'": the RHF wave function cannot describe, even qualitatively, chemical processes where one of the bonds is broken or the atoms dissociate. This feature clearly follows from the restriction of double occupancy since in the dissociation limit, for a diatomic molecule AB, say, one has to put one electron on atom A, the other one on atom B, thus the 'doubly filled orbitals' restriction cannot be maintained. On the other hand, the DODS wave function provides a correct dissociation limit. Consequently, dissociation processes within the independent particle model are to be treated by the UHF (or by some even better) method.

(ii) The RHF method is unambiguous only for closed shell systems. In an open shell molecule containing an odd number of electrons the number of electrons with spins α and β is not equal. Thus the environment of the α and β electrons is not symmetric making the condition of double occupancy somewhat arbitrary. Therefore, open shell systems such as free radicals are usually treated by the UHF method.

Unfortunately, a very important shortcoming of the UHF wave function is that it is not an eigenfunction of the $\hat{S}^2$ operator. Thus, one cannot speak about the (spin) multiplicity of the UHF wave function, but in fact, it is a mixture of components with different multiplicities. This formal shortcoming can lead to serious problems, for example in some cases the UHF wave function represents a worse approximation than the RHF one [882] if properties other than energy are considered, though $E_{UHF} < E_{RHF}$ remains valid.

The extended HF method and the "symmetry dilemma". To overcome the above difficulty, one can project out from the UHF wave function that component which is of desired multiplicity, thus obtaining an eigenfunction of the operator $\hat{S}^2$ [821]. This spin-projected wave function is no longer a single determinant, but a linear combination of a great number of determinants. The linear combination coefficients are called the Sanibel coefficients.

To be consistent with the variational principle, one should vary the projected DODS determinant as the trial function and to derive in this manner the relevant orbital equations [882]. This procedure is the spin-projected extended Hartree–Fock (EHF) method. Due to the complicated form of the orbital equations, computations with the EHF method are expensive. This limits its use to special problems where it works extremely well [882, 888]. Instead of solving the complicated EHF equations, it is possible to solve the standard UHF equations and *then* to select the component of desired multiplicity, or simply to eliminate some components which are not of interest. This procedure, though it is not consistent from the variational point of view, is often used in studying magnetic phenomena (see Section 3.5) where the multiplicity of the wave function is of crucial importance.

The UHF wave function, which is not an eigenfunction of the operator $\hat{S}^2$, represents an example for Löwdin's general symmetry dilemma [821, 823] which is explained as follows.

Though the exact wave function is automatically an eigenfunction of all operators commuting with the Hamiltonian, an approximate wave function may violate this requirement if it is not forced to fulfil it. However, a restriction for obeying an eigenfunction requirement decreases the flexibility of a variational wave function which may result in a worse (higher) energy. Now, one has the dilemma whether to use the wave function with better energy or that of correct symmetry. To solve this problem, one has to use the general form of the wave function without any restrictions, then to project out the relevant components of correct symmetry, and optimize the variational parameters for the projected wave function.

In the following, if the opposite is not stated, we will work with the RHF method. We note that the short-hand term 'HF method' usually refers to the RHF one. Note also that the EHF wave function can be considered as a special type of multi-configuration SCF (MC–SCF) wave function which will be mentioned in Section 1.3.2 discussing correlation methods.

Description of electronic excited states. The Fock operator $\hat{F}$ has usually more eigenfunctions than the number of occupied orbitals of the molecule (the latter is just the half of the number of electrons in the closed shell RHF case). The occupied orbitals are selected by using the *Aufbau* principle: the MOs with lowest orbital energies are filled if one considers the ground state. The unoccupied eigenfunctions are called *virtual orbitals*. The use of the vacant virtual MOs allows us to treat electronic excitations at the HF level.

Let us consider a situation when we have N occupied and M empty MOs. In principle, M can be any positive integer and even infinite. In the molecular ground state the N lowest energy MOs are occupied by $2N$ electrons. The excited states of the molecule can be described by means of the "excited determinants" which are obtained by replacing one or more *spinorbitals* of the ground state determinant by other spinorbitals which are empty in the ground state. For instance, if the ground state RHF wave function of a four-electron system has the form

$$\Phi_0 = \frac{1}{\sqrt{4!}} \begin{vmatrix} \psi_1(r_1)\alpha(\sigma_1) & \psi_1(r_1)\beta(\sigma_1) & \psi_2(r_1)\alpha(\sigma_1) & \psi_2(r_1)\beta(\sigma_1) \\ \psi_1(r_2)\alpha(\sigma_2) & \psi_1(r_2)\beta(\sigma_2) & \psi_2(r_2)\alpha(\sigma_2) & \psi_2(r_2)\beta(\sigma_2) \\ \psi_1(r_3)\alpha(\sigma_3) & \psi_1(r_3)\beta(\sigma_3) & \psi_2(r_3)\alpha(\sigma_3) & \psi_2(r_3)\beta(\sigma_3) \\ \psi_1(r_4)\alpha(\sigma_4) & \psi_1(r_4)\beta(\sigma_4) & \psi_2(r_4)\alpha(\sigma_4) & \psi_2(r_4)\beta(\sigma_4) \end{vmatrix}$$

$$= \hat{A} \mid \psi_{1\alpha}\psi_{1\beta}\psi_{2\alpha}\psi_{2\beta} \mid \tag{1.69}$$

then an example for a singly excited determinant is:

$$\Phi_{2\alpha \to k^*\alpha} = \frac{1}{\sqrt{4!}} \begin{vmatrix} \psi_1(r_1)\alpha(\sigma_1) & \psi_1(r_1)\beta(\sigma_1) & \psi_{k^*}(r_1)\alpha(\sigma_1) & \psi_2(r_1)\beta(\sigma_1) \\ \psi_1(r_2)\alpha(\sigma_2) & \psi_1(r_2)\beta(\sigma_2) & \psi_{k^*}(r_2)\alpha(\sigma_2) & \psi_2(r_2)\beta(\sigma_2) \\ \psi_1(r_3)\alpha(\sigma_3) & \psi_1(r_3)\beta(\sigma_3) & \psi_{k^*}(r_3)\alpha(\sigma_3) & \psi_2(r_3)\beta(\sigma_3) \\ \psi_1(r_4)\alpha(\sigma_4) & \psi_1(r_4)\beta(\sigma_4) & \psi_{k^*}(r_4)\alpha(\sigma_4) & \psi_2(r_4)\beta(\sigma_4) \end{vmatrix}$$

$$= \hat{A} \mid \psi_{1\alpha}\psi_{1\beta}\psi_{k^*\alpha}\psi_{2\beta} \mid . \tag{1.70}$$

The physical picture behind this substitution is clearly that we excite an electron from MO ψ_2 to ψ_{k^*} (the asterisk refers to the virtual level). For this excitation, due to the doubly filled character of MO ψ_2, Eq. (1.70) does not represent the only possibility. The excited determinant in Eq. (1.70) corresponds to the transition $\psi_{2\alpha} \to \psi_{k^*\alpha}$ which is illustrated by Fig. 1.5 *b* where the "spin up" and "spin down" functions α and β are symbolized by arrows $\uparrow$ and $\downarrow$, respectively. Figure 1.5 *a* depicts the ground state configuration while Fig. 1.5 *c–e* show the other possibilities arising in the $i \to k^*$ excitation. The states *d* and *e* describe degenerate pure triplet states, while states *b* and *c* are not eigenfunctions of $\hat{S}^2$, but are 1 : 1 mixtures of a singlet and a triplet. States with pure spin multiplicities can be formed by appropriate linear combinations (spin adaptation):

$${}^1\Phi_{i \to k^*} = \frac{1}{\sqrt{2}} [\Phi_{i\alpha \to k^*\alpha} - \Phi_{i\beta \to k^*\beta}] \tag{1.71}$$

$${}^3\Phi_{i \to k^*} = \frac{1}{\sqrt{2}} [\Phi_{i\alpha \to k^*\alpha} + \Phi_{i\beta \to k^*\beta}] \tag{1.72}$$

where the left superscripts indicate the spin multiplicity. That is, these wave functions consist of two determinants as a consequence of the spin-adaptation. The triplet state, Eq. (1.72) has also the same energy as that indicated in Fig. 1.5 *d* or *e*, while the singlet state of Eq. (1.71) is, in general, of different energy. The three degenerate states are different components of the same triplet belonging to different S_z eigenvalues. By evaluating the matrix elements of the Hamiltonian one finds that the energy changes

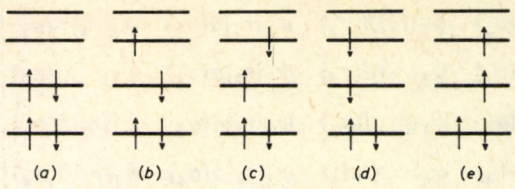


Fig. 1.5 Schematic view of ground- and singly-excited configurations.
(a): Ground state, *(b)*, *(c)*: siglet and triplet excited states; *(d)*, *(e)*: degenerate triplet states

corresponding to the singlet–singlet and singlet–triplet excitations are:

$$^1\Delta E = \langle {}^1\Phi_{i\to k^*} \mid \hat{H} \mid {}^1\Phi_{i\to k^*}\rangle - \langle \Phi_0 \mid \hat{H} \mid \Phi_0\rangle$$

$$= \varepsilon_{k^*} - \varepsilon_i - (ii \mid k^*k^*) + 2(ik^* \mid ik^*) \tag{1.73}$$

$$^3\Delta E = \langle {}^3\Phi_{i\to k^*} \mid \hat{H} \mid {}^3\Phi_{i\to k^*}\rangle - \langle \Phi_0 \mid \hat{H} \mid \Phi_0\rangle = \varepsilon_{k^*} - \varepsilon_i - (ii \mid k^*k^*) \tag{1.74}$$

where ε_i and ε_{k^*} are the orbital energies* of the occupied and virtual MOs, respectively. Since the exchange integral $(ik^* \mid ik^*)$ is positive, the singlet–triplet excitation energy, Eq. (1.74), is smaller than the singlet–singlet one in Eq. (1.73). As will be discussed in Section 3.6, low lying excited states can be approximately described by these singly excited configurations (determinants) or their linear combinations. In studying higher states or searching for more accurate descriptions, one should also deal with double, triple, etc. excitations.

In contrast to the ground state one-determinantal wave function, the above description of the electronic excitation is not invariant with respect to unitary transformations of the occupied (or virtual) MOs. Using different sets of MOs spanning the same occupied subspace, one can obtain quite different excitation energies and it is not easy to decide *a priori* what kind of unitary transformations are to be considered for obtaining the most reliable result. Here the use of the canonical orbitals is of prime importance since they are usually symmetry-adapted ensuring that the excited state wave function is also an eigenfunction of the symmetry operators commuting with the Hamiltonian. Canonical MOs, however, are delocalized usually over the whole molecule allowing us to describe global excitations. Certain unitary transformations performed within the occupied and virtual subspaces (*cf.* Section 1.4) may lead to localized molecular orbitals suitable for describing excitations which are of local character.

It may be noted also that the use of virtual orbitals and their energies, as obtained from the ground state calculation, represent a poor description of electronically excited states. The reason is that an electron placed on a virtual level can see the field of *all* electrons filling the occupied levels in the ground state, and does not see the hole which

* Energies of virtual orbitals can be interpreted as approximations to the *electron affinities* of the molecule.

occurs when an electron is excited. This is corrected in part by the terms $(ii \mid k^*k^*)$ and $(ik^* \mid ik^*)$ in Eqs (1.73) and (1.74) for the excitation energies: this integral must be subtracted from the difference of the one-electron energies $\varepsilon_{k^*} - \varepsilon_i$. The deficiencies in the form of virtual orbitals, however, cannot be corrected in this manner. For this reason, the above simple picture of one-electron excitations does not lead to very good results for calculating electronic transitions as compared to experiments (see also Section 3.6).

Once the spectrum of the Fockian has been obtained, the reliability of the HF method for the system actually studied can be judged by the following qualitative considerations. As a matter of fact, whenever the energy gap between the highest occupied and lowest virtual levels is small, breakdown of the RHF approximation is expected. For an extreme example, let us consider the case when the highest occupied and the lowest virtual MOs are (nearly) degenerate: it is clear that there is no reason to select one of these two degenerate orbitals and to place two electrons on it, leaving the other empty. In such a case, the HF model is unrealistic and it is not appropriate even as a starting point for further calculations. On the other hand, if the gap were infinitely large, the HF wave function would be essentially an eigenfunction of the Hamiltonian. As a rule of thumb, one can say that the greater the gap between the highest occupied and the lowest empty level, the better is the Hartee–Fock approximation.

1.2.5 THE LCAO MODEL: LINK TO CHEMISTRY

Expansion of molecular orbitals. The HF equations given in the previous section represent a system of coupled integro-differential equations, the Coulomb and exchange operators being integral operators, while the kinetic energy in $\hat{H}^{(1)}$ is a differential operator. Due to the large number of independent variables, analytical solution of these integro-differential equations is hopeless, and even the numerical solution is cumbersome. The latter is possible only if the number of electrons is small and the system possesses a high symmetry, as in a single atom or a diatomic [755] molecule. In dealing with more complicated systems the only possibility is to use a *Fourier expansion* for the molecular orbitals as

$$\psi_i = \sum_{\mu=1}^{N} c_{i\mu}\chi_\mu \tag{1.75}$$

and determine the $c_{i\mu}$ coefficients variationally. In Eq. (1.75) N is the number of basis functions. If N were infinite and the set $\{\chi_\mu\}$ were complete, Eq. (1.75) would introduce no further approximation into the theory. In this case, by substituting the expansion (1.75) into the canonical HF equations (1.55) we obtain the following matrix equation

$$\sum_\nu F_{\mu\nu}c_{i\nu} = \varepsilon_i \sum_\nu S_{\mu\nu}c_{i\nu} \tag{1.76}$$

with

$$F_{\mu\nu} = \langle \chi_\mu \mid \hat{F} \mid \chi_\nu \rangle \tag{1.77}$$

and

$$S_{\mu\nu} = \langle \chi_\mu \mid \chi_\nu \rangle . \tag{1.78}$$

The matrix **S** with the elements $S_{\mu\nu}$ is called the overlap (or metric) matrix. If the set $\{\chi_\mu\}$ were orthogonal, **S** would be diagonal but generally this is not required.

In the real case, when the set $\{\chi_\mu\}_{\mu=1}^{N}$ is incomplete, the above derivation of Eq. (1.76) does not warrant that the MOs in Eq. (1.75), constructed with the coefficients $c_{i\mu}$ obtained from the solution of Eq. (1.76), minimize the energy functional in the sense of the variational principle in the given truncated basis. However, it can be shown [881, 1189] that even if using a finite basis set, Eq. (1.76) provides the best $c_{i\mu}$'s making the energy stationary. The Eq. (1.76) is the set of Hartree–Fock–Roothaan (HFR) equations.

Using Eqs (1.55–59), the matrix elements of the Fockian can be written as

$$F_{\mu\nu} = H_{\mu\nu} + \sum_{\lambda\sigma} P_{\lambda\sigma}[(\chi_\mu\chi_\nu \mid \chi_\lambda\chi_\sigma) - \frac{1}{2}(\chi_\mu\chi_\lambda \mid \chi_\nu\chi_\sigma)] \tag{1.79}$$

where $H_{\mu\nu}$ is the matrix element of the core Hamiltonian:

$$H_{\mu\nu} = \langle \chi_\mu \mid \hat{H}^1 \mid \chi_\nu \rangle \tag{1.80}$$

and

$$P_{\mu\nu} = 2 \sum_{i}^{\text{occ}} c_{i\mu} c_{i\nu} . \tag{1.81}$$

The matrix **P** having the elements $P_{\mu\nu}$ is usually called the *density matrix*. The origin of this term lies in the physical interpretation of $P_{\mu\nu}$. The electron density $\rho(\mathbf{r})$ of a closed shell molecule at the space point **r** in the HF approximation is given by [819]:

$$\rho(\mathbf{r}) = 2 \sum_{i}^{\text{occ}} \psi_i(\mathbf{r})\psi_i(\mathbf{r}) = 2 \sum_{i}^{\text{occ}} \sum_{\mu\nu} c_{i\mu} c_{i\nu} \chi_\mu(\mathbf{r})\chi_\nu(\mathbf{r}) = \sum_{\mu\nu} P_{\mu\nu} \chi_\mu(\mathbf{r})\chi_\nu(\mathbf{r}). \tag{1.82}$$

The electron density is "diagonal" in index i referring to MOs, but not in indices μ and ν referring to basis orbitals. This means that the electron density $\rho(\mathbf{r})$ appears as the sum of MO contributions. The expansion coefficients at the $\chi_\mu(\mathbf{r})\chi_\nu(\mathbf{r})$ overlap densities in $\rho(\mathbf{r})$ are the density matrix elements $P_{\mu\nu}$. There is a close connection between the "first order density matrix" $\gamma(\mathbf{x}, \mathbf{x}')$ and the "density matrix" **P** having some important mathematical properties which are not discussed here; see *e.g.* [819].

The HFR orbitals of form (1.75) are suitable one-electron functions for an actual CI procedure (*cf.* Section 1.2.3). Thus, in principle, an exact solution of the Schrödinger equation can be obtained within a given basis set, *via* a HFR + CI calculation (basis limit). For an impressive example see ref. [1228], where such solution for the water molecule is presented (see also [66, 515, 1228]).

The accuracy of the HFR (or basis limit) calculations compared with the HF (or exact nonrelativistic) scheme depends on the quality (size and adequacy) of the basis set. As follows from the variational principle, larger basis sets provide better (lower) energy which, as the basis becomes larger and larger, and approaches a complete one, converges to the so-called "HF limit", *i.e.* the value which would be obtained by solving the original integro-differential HF equations exactly. This consideration does not mean that all physical quantities converge monotonically to their HF limit since, until the convergence is not closely approached, a better energy does not necessarily correspond to a better wave function. Moreover, even the energy can converge very slowly as one extends the basis set $\{\chi_\mu\}$, thus the selection of the suitable basis orbitals is a question of crucial importance in actual HF calculations.

Significance of atomic orbitals. In determining the suitable form of the basis orbitals, the best guide is chemical intuition. Molecules are composed of atoms, and in studying the electronic structure of molecules one has to use as much information about the constituent atoms as possible. The selection of the basis orbitals represents a more or less empirical element even in a strict "*ab initio*" *(vide infra)* theory. This explains the success of the idea that the MOs are best expanded as *linear combinations of atomic orbitals* (LCAO), where the atomic orbitals (AOs) are one-electron functions of the atoms which the molecule is built from. (If a basis orbital χ_μ represents an AO of atom A, one says that χ_μ is centred on A and uses the notation $\mu \in$ A.) For example, a simple but surprisingly efficient description of the H_2 molecule is to consider its single MO as the linear combination of the two 1s AOs of the two hydrogen atoms denoted by A and B:

$$\psi(\mathbf{r}) = \frac{1}{\sqrt{2(1+S)}}[\chi_{1sA}(\mathbf{r}) + \chi_{1sB}(\mathbf{r})]. \tag{1.83}$$

The factor $1/\sqrt{2(1+S)}$ ensures that ψ be normalized. Here $S = \langle \chi_{1sA} | \chi_{1sB} \rangle$ is the overlap integral of the AOs of atoms A and B. The equal weight of the AOs belonging to the two atoms is required by symmetry. (For a detailed analysis of the H_2 molecule see Section 2.2.2.)

The actual representations of AOs will be discussed later. Now we note only that the basis orbitals are not necessarily solutions of the atomic HF problems.

Doubly occupied, singly occupied and virtual AOs can be equally well used in the LCAO method. In principle, one can consider all virtual orbitals of every atom in constructing the LCAO basis set. One could argue in this case, that as the number of basis functions belonging to an atom goes to infinity, the total basis set becomes redundant since one has a nearly complete basis on each atom. This latter conclusion is, however, generally not true because most sets of AOs are not complete even if their size were infinite (*cf.* the hydrogen orbitals in Section 1.2.1). Due to the incompleteness of individual atomic basis sets, the actual danger of constructing redundant molecular bases is very small, and appears only because of the limited numerical accuracy of the

computations. Later some cases will be mentioned, where there is some chance that the basis set becomes approximately linearly dependent* (see Section 1.3.1).

One disadvantage of using polycentric AO basis sets is that, in constructing the matrix elements of the Fockian through Eq. (1.79), one has to evaluate a large number of two-, three- and even four-centre two-electron integrals of the type $(\chi_\mu\chi_\nu|\chi_\lambda\chi_\sigma)$. (This integral is said to be a p-centre one if the AOs χ_μ, χ_ν, χ_λ and χ_σ belong to p different atoms.) The computation of such integrals is difficult and time-consuming, and was considered formerly as the bottleneck of quantum chemistry. Thus, attempts were made to construct molecular basis sets by using AOs centred on one and the same atom. This is the so-called one-centre expansion or united atom treatment [107]. It turned out that, except for some special cases, the advantage of bypassing the polycentric integrals is lost due to the much worse quality of the resulting molecular basis if the same number of basis orbitals is used. The one-centre orbitals can hardly mimic an AO on a different centre. The few exceptional cases are those where the opposite is true: *e.g.* for first row hydrides such as CH_4, the large atomic basis set on the heavy atom can simulate the role of 1*s* AOs on hydrogens. For this reason, the one-centre expansions are rarely applied and most HFR calculations use a polycentric LCAO basis.

Mathematical form of atomic orbitals. Since the AOs are one-electron functions, the most "accurate" choice is to take them as the HF orbitals of individual atoms. However, the numerical solution of the RHF equations is rather laborious even for atoms, and the resulting HF orbitals are too complicated to handle as basis orbitals in molecular calculations. On the other hand, as we have already mentioned in Section 1.2.1, hydrogen orbitals are suitable for a qualitative understanding of the electronic structure of other atoms as well. Therefore, constructing the LCAO basis set, it is a reasonable simplification to use hydrogen functions on each atom. Moreover, even the hydrogenic orbitals are somewhat complicated; their use would cause difficulties in evaluating the polycentric integrals over AOs. As was suggested by Slater [1285] with the aim of studying different atomic properties, one can construct some functions χ^{SL}_{nlm} reflecting the most important properties of hydrogenic AOs corresponding to the quantum numbers, n, l, and m:

$$\chi^{SL}_{nlm} = \mathcal{N} r^{n-1} e^{-\zeta_n r} Y_{l,m}(\vartheta, \varphi) \tag{1.84}$$

where $\mathcal{N}$ is a normalization constant, Y_{lm} is the spherical harmonics (*cf.* Section 1.2.1), r, ϑ and φ are spherical coordinates, and ζ is the orbital exponent. The χ^{SL}_{nlm} in Eq. (1.84) are called *Slater-functions* or *Slater-type orbitals* (STOs). Note that the hydrogen functions are linear combinations of STOs. Values for orbital exponents can be obtained either by considering them as nonlinear variational parameters, or by setting some "empirical" values in order to approximate the AO optimally. Such

* A basis set is said to be *linearly dependent* if one of the basis functions can be expressed as linear combination of the others. Otherwise the basis is *linearly independent*. In case of linear dependency the superfluous function may be dropped, this is why one speaks about *redundant* basis sets.

TABLE 1.2

Slater exponents for atoms Li to Kr
The n^* is an effective principal quantum number used in Eq. (1.84)

Z	Atom	2s, 2p, $n^*=2$	3s, 3p, $n^*=3$	3d, $n^*=3$	4s, 4p $n^*=3.7$
3	Li	0.650			
4	Be	0.975			
5	B	1.300			
6	C	1.625			
7	N	1.950			
8	O	2.275			
9	F	2.600			
10	Ne	2.925			
11	Na	3.425	0.733		
12	Mg	3.925	0.950		
13	Al	4.425	1.167		
14	Si	4.925	1.383		
15	P	5.425	1.600		
16	S	5.925	1.817		
17	Cl	6.425	2.033		
18	Ar	6.925	2.250		
19	K	7.425	2.583		0.595
20	Ca	7.925	2.917		0.770
21	Sc	8.425	3.250	1.000	0.811
22	Ti	8.925	3.583	1.217	0.851
23	V	9.425	3.917	1.433	0.892
24	Cr	9.925	4.250	1.867	0.797
25	Mn	10.425	4.583	1.867	0.973
26	Fe	10.925	4.917	2.083	1.014
27	Co	11.425	5.250	2.300	1.054
28	Ni	11.925	5.583	2.517	1.095
29	Cu	12.425	5.917	2.950	1.000
30	Zn	12.925	6.250	2.950	1.176
31	Ga	13.425	6.583	3.283	1.351
32	Ge	13.925	6.917	3.617	1.527
33	As	14.425	7.250	3.950	1.703
34	Sc	14.925	7.583	4.283	1.878
35	Br	15.425	7.917	4.617	2.054
36	Kr	15.925	8.250	4.950	2.230

empirical values were given for example, by Slater [1285] and others [166a, 230a]. In the former case, the exponents are varied until the total electronic energy of the system becomes minimal. In this manner we obtain non-transferable optimized orbital exponents. The empirical Slater-exponents are listed for some atoms in Table 1.2. Like the hydrogenic orbitals, the STOs behave correctly at the $r \to 0$ (*i.e.*, they have *cusps*) and $r \to \infty$ limits. The 1*s* STO ($n=1, l=0$) with $\zeta_1 = 1.0$ is exactly the same as the hydrogenic

1*s* function. The essential difference between STOs and hydrogen AOs is that the former have no nodal surfaces and, as a consequence, do not form an orthogonal set (see Figure 1.6).

Using Slater-type orbitals, only a minor part of the integrals appearing in the HFR problem can be evaluated without difficulties. There are some two-electron integrals (most of three and four-centre ones) for which neither exact analytical formulae nor efficient numerical techniques exist (for some possibilities, see *e.g.* [477, 478, 1337a, 1363]. Evaluation of such integrals over STOs is laborious *(vide infra)*. Therefore, instead of STOs, following Boys' idea [137], modern quantum chemical methods usually employ the so-called Gaussian-type orbitals (GTOs) having the form

$$\chi^{G}_{uvw} = \mathcal{N} x^u y^v z^w e^{-\zeta_n r^2}. \tag{1.85}$$

The Gaussian nature of the radial part (*i.e.*, the presence of r^2 in the exponent) makes the calculation of polycentric integrals much easier. The price we have to pay for this is that GTOs do not behave correctly at the $r \to \infty$ and $r \to 0$ limits. As for the $r \to \infty$ asymptotics, they vanish too quickly, and at $r = 0$ they are too flat. The main shortcomings of GTOs are shown in Fig. 1.6. A failure is illustrated by the absence of cusps at $r = 0$: analytical asymptotic solutions of the Schrödinger equation for atoms in the $r \to 0$ limit require that the first derivative of AOs with *s* symmetry at $r = 0$ be different from zero, but this condition is not fulfilled when using GTOs. These shortcomings mean that, to achieve the same quality of the basis set, one should use a larger number of GTOs than STOs [182].

Some further details on the properties of molecular basis sets will be reviewed in Section 1.3.1, discussing *ab initio* methods.

The LCAO model as a link to chemistry. Neither the Born–Oppenheimer nor the one-electron models, nor the Hartree–Fock–Roothaan equations themselves take into

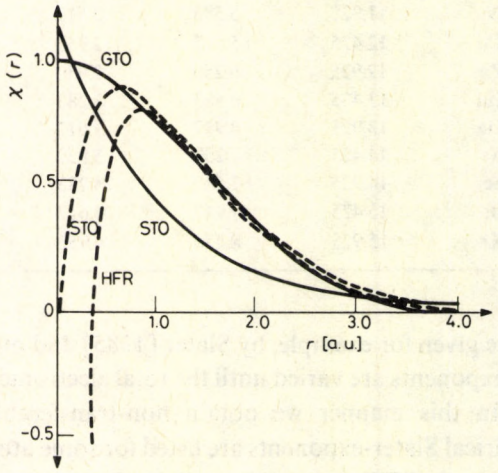


Fig. 1.6 Radial parts of some atomic orbitals. Solid line: STO and GTO for the 1*s* AO of hydrogen; dashed line: STO and single-zeta HFR 2*s* AOs of carbon (the latter is taken from Ref. [231]

consideration that molecules are formed by atoms. The LCAO expansion represents the basic reference to chemistry in the present-day quantum chemical methods. Due to the use of atomic orbitals, in principle, all molecular properties can be related to atomic contributions or interatomic interactions. This is very important for making chemically relevant interpretations, on one hand, and for developing approximate and/or semiempirical MO theories by incorporating atomic data into molecular calculations, on the other hand (*cf.* Section 1.3.2). Further on we shall discuss the interpretative value of using LCAO basis sets.

The atomic charge. Electron distribution in molecules plays an important role in analyzing and interpreting chemical processes. This distribution can be characterized by the charge density function $\rho(\mathbf{r})$, [*cf.* Eq. (1.82) and Section 3.4.1] which obeys the following relation

$$\int \rho(\mathbf{r})\, \mathrm{d}^3\mathbf{r} = n \tag{1.86}$$

where n is the total number of electrons in the molecule. Pictorially speaking, those volume elements containing many electrons have a large $\rho(\mathbf{r})$ while small $\rho(\mathbf{r})$-s indicate regions which are poor in electrons. Thus the information contained in $\rho(\mathbf{r})$ is very useful in making predictions, for example, on charge-controlled chemical reactions, see Section 4.4. (A more general significance of the charge density has already been discussed in connection with the Hellmann–Feynman theorem, see Section 1.2.2. For a more detailed discussion on charge distribution in molecules we refer to Section 3.4.1.)

However, we are usually interested not directly in the density $\rho(\mathbf{r})$ in different spatial regions, but in the influence of different *atoms* in a molecule on some chemical properties. Experience shows that there are electron-attracting atoms, which are surrounded by a region where $\rho(\mathbf{r})$ is large, while others are situated in a region of the molecule with relatively small ρ compared to that in the free atoms. For example, the charge density around oxygen or fluorine atoms is usually large while in regions near hydrogens $\rho(\mathbf{r})$ is often relatively low. It is also very important that there are (either systematic or specific) deviations in the above "property" of atoms: *e.g.*, oxygen attracts electrons in almost all molecules but the extent of this attraction depends on many factors and it is characteristic for the molecule in question. Intuitively, one can speak about atoms which are positive or negative in the given molecule. To be more specific, one has to define the charge (q_A) of the atom A in a molecule.

Obviously, the sum of all atomic charges should be equal to the total charge of the molecule. It is clear that q_A consists of two parts: one is simply the nuclear charge Z_A, the other is due to the electrons.

It is to be noted that the atomic charge q_A is not a physical quantity in the sense that it is not directly measurable. There is a tendency to eliminate such quantities from the theory, but we feel that, in order to make practically useful interpretations and to develop effective models, we need to use "non-observable" but conceptually important quantities like the atomic charge, even if there is some ambiguity in their definition [301].

The conceptually simplest and most pictorial definition for q_A is to divide the whole space into domains each containing just one atom [1115]. If we denote the domain containing atom A by V_A, the atomic charge can be defined as

$$q_A = Z_A - \int_{V_A} \rho(\mathbf{r})\, d^3\mathbf{r}. \tag{1.87}$$

This definition has the unfortunate property that the quantity q_A strongly depends on the particular choice for the shape of the regions V_A which is especially ambiguous for molecules with low symmetry. (One possibility is to define an appropriate partition of the space. It is based on analyzing the topological structure of the electron density $\rho(\mathbf{r})$ [47]). Furthermore, the evaluation of integrals in Eq. (1.87) is rather laborious. Therefore, most quantum chemical programs adopt different definitions for q_A among which Mulliken's [950] is of extreme importance.

Substitution of the LCAO expansion of $\rho(\mathbf{r})$, Eq. (1.82), into (1.86) yields

$$\sum_{\mu,\nu} P_{\mu\nu} \int \chi_\mu(\mathbf{r})\chi_\nu(\mathbf{r})\, d^3\mathbf{r} = \sum_{\mu,\nu} P_{\mu\nu} S_{\mu\nu} = \sum_{\mu} (\mathbf{PS})_{\mu\mu} = n. \tag{1.88}$$

The sum of the diagonal elements of the **PS** matrix gives just the total number of electrons. Thus, the **PS** matrix is interpreted as the LCAO representation of the charge density $\rho(\mathbf{r})$, and Eq. (1.88) can be further written as

$$n = \sum_{A} \sum_{\mu \in A} (\mathbf{PS})_{\mu\mu} = \sum_{A} Q_A. \tag{1.89}$$

(Let us remember that the label A runs over all atoms, and the symbol $\mu \in A$ means that μ is an orbital centred on atom A.) In this partition Q_A can be interpreted as the gross electron population on atom A, and the resulting Mulliken atomic charges are defined as

$$q_A = Z_A - Q_A = Z_A - \sum_{\mu \in A} (\mathbf{PS})_{\mu\mu}. \tag{1.90}$$

It was observed that the Mulliken populations Q_A, thus the atomic charges q_A in Eq. (1.90) as well, strongly depend on the particular choice for the basis set. Therefore the results of different calculations of q_A can be compared only if they are computed exactly by the same basis. Moreover, it is to be noted that the multipole moments of the point-charge system of Mulliken charges q_A do not agree with those calculated as expectation values of multipole moment operators. Atomic charge definitions reproducing at least the dipole moment of the molecule have also been proposed [656, 818, 1351].

In contrast to the previous definition, the derivation of the Mulliken charge is inherently based on the use of LCAO basis sets, i.e. on the fact that we assign each basis orbital to a particular atom. Anyway, as has been shown recently [886, 884] as far as the LCAO expansion is adopted, the Mulliken charges represent not only one of the

many possibilities for defining q_A, but they have a privileged importance within the LCAO framework.

Energy partitioning. The LCAO concept permits us to break down the total molecular energy Eq. (1.60) in terms of atomic contributions and interatomic interactions. This partition, similarly to the definition of atomic charges, is not completely unique. One possibility was proposed by Clementi [223]. Substituting the LCAO expansion of MOs (Eq. 1.75) into Eq. (1.60), and introducing the density matrix **P**, Eq. (1.81), the energy expression becomes:

$$E=\sum_{A<B}\frac{Z_A Z_B}{R_{AB}}+\sum_{\mu\nu}P_{\mu\nu}H_{\mu\nu}+\frac{1}{2}\sum_{\mu\nu\lambda\sigma}P_{\mu\nu}P_{\lambda\sigma}\left[(\mu\nu|\lambda\sigma)-\frac{1}{2}(\mu\lambda|\nu\sigma)\right]. \tag{1.91}$$

The first term (nuclear repulsion) is a two-centre contribution. Partition of indices μ, ν, λ and σ leads to the following relation

$$E=\sum_{A}E_A+\sum_{AB}E_{AB}+\sum_{ABC}E_{ABC}+\sum_{ABCD}E_{ABCD} \tag{1.92}$$

where E_A contains those terms of Eq. (1.91) which refer to atom A, E_{AB} collects all possible two-centre contributions, etc. Since the integrals $(\mu\nu|\lambda\sigma)$ possess at most four different centres, E_{ABCD} represents the possible highest order term in the energy partition Eq. (1.91). The magnitudes of different terms in Eq. (1.91) are generally the smaller, the larger is the number of centres. The analysis of different terms permits one to draw useful information on the role of atoms and atomic interactions in chemical bonding.

Another energy partitioning scheme has been proposed recently by Mayer [886], who has shown that the total Hartree–Fock energy can be written in the LCAO model as

$$E=\sum_{A}(E_A+\delta E_A)+\sum_{AB}(E_{AB}+\delta E_{AB}) \tag{1.93}$$

where E_A is the actual energy of the atom A in the molecule, E_{AB} is the pairwise interaction energy between atoms A and B, and $\delta E_A(\delta E_{AB})$ represent "nonphysical" one-(two-) centre correction terms. The terms E_{AB} contain the two-centre electrostatic and overlap interactions. The appearance of the nonphysical terms is a consequence of the incompleteness of the monoatomic basis set: these terms arise due to the (arte)fact that the description of an atom in a molecule is "better" than that of a free atom since in a molecule one works with a larger basis set. In other words, orbitals centred on other atoms improve the description of the atom in question; such artefact effects are usually referred to as *basis set extension errors* (BSSE). The most important features of Mayer's energy partitioning are that (*i*) only one- and two-centre physical terms appear containing no three and four centre integrals, (*ii*) BSSE terms can be decoupled explicitly. We do not present here the actual expressions for the different terms in Eq. (1.93) for which the reader is referred to [886].

Bond orders and valence. Energy partition schemes are very useful in the sense that they permit us to study atomic interactions energetically. As will be outlined in Part 2, chemical bonds are mostly two-centre in nature (*cf.* Lewis-structures). The "strength" of such a chemical bond, however, is reflected only implicitly by the corresponding two-centre energy term, E_{AB}. For another mathematical representation, the concept of bond order was introduced [254].

Let us assume first that the LCAO basis is orthonormalized, *i.e.* $S_{\mu\nu}=\delta_{\mu\nu}$. Furthermore, let us introduce a model where only one orbital per atom is considered (such models will be examined in Section 1.3.2). Then, the bond order between atoms A and B is defined by the off-diagonal element of the density matrix [254]:

$$p_{AB}=P_{\mu\nu}; \qquad \mu\in A, \quad \nu\in B. \tag{1.94}$$

The value of p_{AB} characterizes the bond strength, or, more precisely, the single or multiple character of the chemical bond* between A and B. It has been observed that an approximately linear relationship exists between p_{AB} and the experimental bond distance r_{AB}, if atom A and B are first neighbours (*cf.* Section 3.1).

Whenever one considers more than one AO on one atom, the simple bond order definition (Eq. 1.94) cannot be maintained. For such a case, if the AO basis is orthogonal, Wiberg has proposed [1418] an index characterizing the AB bond order:

$$W_{AB}=\sum_{\mu\in A}\sum_{\mu\in B}(P_{\mu\nu})^2. \tag{1.95}$$

One can see that the Wiberg indices are necessarily positive numbers. A larger W_{AB} indicates a stronger bond.

Sophisticated quantum chemical HF methods as well as the extended Hückel method (*cf.* Section 1.3.2) work within nonorthogonal (overlapping) AO basis sets. In such a case neither Wiberg indices nor simple bond orders of Eq. (1.94) can serve as appropriate measures of the chemical bond strength. As indicated by Eq. (1.88), the quantity

$$p^{ov}_{\mu\nu}=P_{\mu\nu}S_{\mu\nu} \tag{1.96}$$

can be associated with the "population" between orbitals μ and ν, since by summing over all μ and ν we obtain just the total number of the electrons. The $p^{ov}_{\mu\nu}$ is called the *overlap population* and in some sense it can be considered as a measure of binding between μ and ν. If μ and ν refer to orbitals belonging to different atoms, a larger positive $P_{\mu\nu}S_{\mu\nu}$ indicates that there is a contribution to the chemical binding between the two atoms, while negative (zero) overlap population refers to an antibonding

* Considering *e.g.* a dissociation process of a diatomic molecule AB, the bond order p_{AB} is not affected by the bond length r_{AB}, while the strength of the bond decreases rapidly with increasing bond length. However, it is well known that at the equilibrium positions of the nuclei a greater bond oder involves a shorter bond length and a "stronger" bond.

(nonbonding) contribution. The populations can be assigned to atoms in the following manner. The quantity

$$p_{AB}^{ov} = \sum_{\mu \in A} \sum_{\nu \in B} P_{\mu\nu} S_{\mu\nu}$$

is referred to as the overlap population between atoms A and B, and it characterizes the binding between these two atoms. The *net atomic population* on A is obtained as $\sum_{\mu \in A} P_{\mu\mu}$ while the *gross atomic populations* are defined by adding the half of all overlap populations:

$$Q_A = \sum_{\mu \in A} P_{\mu\mu} + \frac{1}{2} \sum_{B(\neq A)} p_{AB}^{ov}$$

which is readily shown to be equal to Q_A of Eqs (1.89–90). That is, when calculating the gross population Q_A and Q_B, the overlap population p_{AB}^{ov} is shared by atoms A and B in an equal weight. This is, together with the definition of the atomic charge in Eq. (1.90), the so-called *population analysis* developed by Mulliken [950].

Generalizations of the concept of the interatomic bond order to the general multiorbital and nonorthogonal case were proposed by Kutzelnigg [749] and recently by Mayer [884]. According to this latter definition [884] the "bond order" between atoms A and B in a closed shell molecule can be calculated as

$$b_{AB} = \sum_{\mu \in A} \sum_{\nu \in B} (\mathbf{PS})_{\mu\nu} (\mathbf{PS})_{\nu\mu} \tag{1.97}$$

which obviously reduces to the Wiberg index W_{AB} in the special case of $S_{\mu\nu} = \delta_{\mu\nu}$. The quantity b_{AB} was proven to be a significant characteristic of the binding situation [884, 885, 887, 889].

By means of Eq. (1.97) one can define the valence (v_A) of atom A in a closed shell molecule as the sum of all bond orders [884]:

$$v_A = \sum_{B(\neq A)} b_{AB} . \tag{1.98}$$

The above quantities b_{AB} and v_A reflect the classical chemical picture appropriately (see Table 1.3). The use of Eqs (1.97) and (1.98) permits us to extract atomic properties even from nondescriptive sophisticated quantum chemical HF calculations, provided that they work within an LCAO basis set [29].

Generalizations for open shell systems. The above definitions of atomic properties were given in the special case of RHF MOs describing a closed shell electron configuration. In an open shell system one preferably adopts the UHF scheme where the density function for electrons with spins α and β is given by, *cf.* Eq. (1.82):

$$\rho^{\alpha}(\mathbf{r}) = \sum_{i=1}^{n_\alpha} \psi_i^{\alpha}(\mathbf{r}) \psi_i^{\alpha}(\mathbf{r}) = \sum_{\mu\nu} P_{\mu\nu}^{\alpha} \chi_\mu(\mathbf{r}) \chi_\nu(\mathbf{r}) \tag{1.99}$$

$$\rho^{\beta}(\mathbf{r}) = \sum_{i=1}^{n_\beta} \psi_i^{\beta}(\mathbf{r})\psi_i^{\beta}(\mathbf{r}) = \sum_{\mu\nu} P_{\mu\nu}^{\beta}\chi_\mu(\mathbf{r})\chi_\nu(\mathbf{r}) \tag{1.100}$$

where ψ_i^{α}, ψ_i^{β} are the UHF MOs, n_α and n_β are the total number of electrons with spin α and β, respectively, and the density matrices $\mathbf{P}^{\alpha}$ and $\mathbf{P}^{\beta}$ are defined by

$$P_{\mu\nu}^{\alpha} = \sum_{i=1}^{n_\alpha} c_{\mu i}^{\alpha} c_{\nu i}^{\alpha} \tag{1.101}$$

$$P_{\mu\nu}^{\beta} = \sum_{i=1}^{n_\beta} c_{\mu i}^{\beta} c_{\nu i}^{\beta} . \tag{1.102}$$

The $c_{\mu i}$-s being the UHF LCAO coefficients. By comparing with Eq. (1.81) it is clear that the total spinless density matrix is given by the sum

$$P_{\mu\nu} = P_{\mu\nu}^{\alpha} + P_{\mu\nu}^{\beta} \tag{1.103}$$

whereas the so-called *spin density matrix* $\mathbf{P}^s$, corresponding to the *spin density* $\rho^{\alpha}(\mathbf{r}) - \rho^{\beta}(\mathbf{r})$, is just the difference of $\mathbf{P}^{\alpha}$ and $\mathbf{P}^{\beta}$:

$$P_{\mu\nu}^{s} = P_{\mu\nu}^{\alpha} - P_{\mu\nu}^{\beta} . \tag{1.104}$$

The sign of $\mathbf{P}^s$ becomes unambiguous if we choose, for example, $n_\alpha > n_\beta$. (Note that Eqs (1.99)–(1.104) are adequate formulae for any finite basis expansion of the MOs, not only in the strict LCAO framework.)

Equation (1.103) can be used for obtaining the total atomic charge defined in Eq. (1.89), the total overlap population in Eq. (1.96) and the bond orders in Eq. (1.97) for an

TABLE 1.3

Mayer's bond orders (b_{AB}), total (v_A^{tot}) and free- (f_A) valence indices for some molecules as computed by the ab initio HFR STO-3G method (the values are taken from Ref. [884])

Molecule	Bond	b_{AB}	Atom	Classical valence	v_A^{tot}	f_A
C_2H_6	C—C	1.01	C	4	3.97	0.0
	C—H	0.98	H	1	1.00	0.0
C_2H_4	C=C	2.01	C	4	3.97	0.0
	C—H	0.98	H	1	1.00	0.0
CH_3 radical	C—H	0.98	C	4	3.96	1.02
			H	1	1.00	0.01
H_2O	O—H	0.95	O	2	1.91	0.0
			H	1	0.97	0.0
HCN	H—C	0.97	H	1	0.98	0.0
	C≡N	2.99	C	4	3.96	0.0
			N	3	3.00	0.0
CN radical	C≡N	2.80	C	4	3.81	1.00
			N	3	3.09	0.29

open shell system by substituting everywhere the total spinless density matrix. As for the generalization of the valence index defined in Eq. (1.98), one has to distinguish between the total (v_a^{tot}) and free (f_a) valence of an atom. For instance, in the methyl radical CH_3 the total valence of the carbon atom is four, while the free valence is equal to unity according to the chemical picture. The relevant formulae read [884]:

$$v_A^{tot} = 2 \sum_{\mu \in A} (\mathbf{PS})_{\mu\mu} - \sum_{\mu,\nu \in A} (\mathbf{PS})_{\mu\nu}(\mathbf{PS})_{\nu\mu} \tag{1.105}$$

$$f_A = v_A^{tot} - v_A \tag{1.106}$$

where v_A is the sum of the bond orders, Eq. (1.98), as calculated by Eq. (1.97) using the spinless density matrix. One can prove that in the closed shell case v_A^{tot} reduces to v_A, thus the free valence indices are automatically equal to zero. Some examples for numerical v_A^{tot} and f_A values are given in Table 1.3.

The above equations provide a similar tool in interpreting UHF calculations as Eqs (1.97)–(1.98) do in the closed shell RHF case. Here again, the importance of the LCAO model should be stressed as this permits us to assign orbital properties to different atoms in a molecule.

Core and valence shell orbitals. Different kinds of AOs may have quite different roles in interpreting LCAO wave functions. Orbitals corresponding to the outermost, partly filled shell of an atom form its valence shell. The valence shell of the first-row atoms is composed of the $2s$, $2p_x$, $2p_y$, and $2p_z$ AOs, while that of the second row atoms includes the corresponding AOs with $n = 3$. The valence shell orbitals play a predominant role in forming chemical bonds.

Orbitals corresponding to lower principal quantum numbers than that of the valence shell, are called inner shell or core orbitals and can be considered as being doubly occupied in the valence states of atoms. Such core orbitals are the 1s AOs for first row atoms, the $2s$ and $2p$ AOs for second row atoms, etc. The influence of inner shell orbitals on chemical properties is usually of secondary importance.

σ and π atomic orbitals. Molecular symmetry can provide another approach to classifying atomic orbitals. It is to be emphasized that this classification does not originate from inherent properties of individual atoms, but is connected with the specific bonding situation of the atoms in a given molecule. The valence AOs of a diatomic molecule AB are shown in Fig. 1.7. It is supposed that the valence shell is formed of s and p AOs. It is convenient to choose the coordinate system in such a way that the bond AB lies along the x axis. Then, by definition, the s and p_x orbitals, which are invariant with respect to the rotation around the x axis, are said to be σ type AOs, while the p_y and p_z functions perpendicular to the AB bond axis are π-type orbitals. This concept can be obviously generalized to polyatomic linear molecules.

A similar distinction can be made in planar molecules. If the molecule lies in the xy plane, the s, p_x and p_y AOs are σ functions while the p_z orbitals, perpendicular to the molecular plane, are the π orbitals. This situation is illustrated in Fig. 1.8. Here the σ-

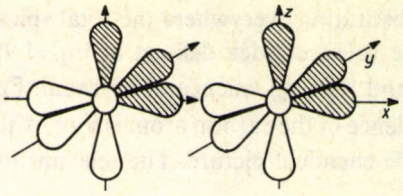


Fig. 1.7 The s and p type valence orbitals in a diatomic molecule AB

type AOs are symmetric, the π-ones are antisymmetric with respect to a reflection in the molecular plane.

The above nomenclature can also be maintained for quasiplanar and quasilinear cases as far as the identification of the AOs in plane, out-of-plane, etc. is possible.

Hybridization. The use of $1s$, $2s$, $2p$, ... etc. AOs is not the only possibility of constructing LCAO basis sets. From a purely mathematical point of view, one can consider any unitary transformation* mixing the orbitals on the same atom. Such a transformation is called a hybridization transformation and the resulting "mixed" AOs are the hybrid orbitals (HYOs). The physical and/or chemical meaning of hybridization is that, under similar circumstances, the atomic orbitals appear in certain wave functions in well defined and more-or-less transferable combinations. (This is more pronounced in the so-called minimal basis (see Section 1.3), where each inner and valence shell orbital is represented by a single function. We limit here the discussion of hybridization to the minimal basis level.)

A well known example is the hybridization on the tetracoordinated carbon atom. For example, in methane (CH_4) there are two electrons on the $1s_C$ core orbital, and there are four on the carbon valence shell; one electron on each of the $2s$, $2p_x$, $2p_y$ and $2p_z$ AOs**. These latter four electrons, together with the $1s$ AOs of the four hydrogens,

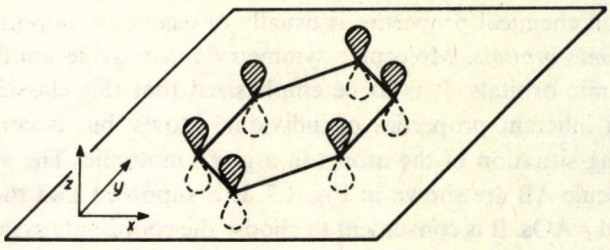


Fig. 1.8 π-type $2p_z$ AOs in a planar molecule (benzene)

* Or, more generally, any nonsingular linear transformation.

** Note that this hypothetical electron configuration corresponds to an excited state of the C atom with a multiplicity of 5, since the ground state configuration is $(1s)^2\ (2s)^2\ (2p)^2$ (*cf.* Section 1.2.1).

form the four C—H bonds of the molecule. These bonds are completely equivalent: they have equal lengths, strengths, etc., thus there is no reason to assign the 2*s* electron to one of them and the three 2*p* ones to the remaining three. Instead, the bonding situation can be more properly represented if we consider the four equivalent hybrids $h_i = 1, 2, 3, 4$, resulting from a unitary transformation within the valence shell:

$$h_1 = \frac{1}{2}[\chi_{2s} + \chi_{2p_x} + \chi_{2p_y} + \chi_{2p_z}] \qquad h_3 = \frac{1}{2}[\chi_{2s} - \chi_{2p_x} + \chi_{2p_y} - \chi_{2p_z}]$$

$$h_2 = \frac{1}{2}[\chi_{2s} + \chi_{2p_x} - \chi_{2p_y} - \chi_{2p_z}] \qquad h_4 = \frac{1}{2}[\chi_{2s} - \chi_{2p_x} - \chi_{2p_y} + \chi_{2p_z}] \qquad (1.107)$$

where we assumed that the hydrogens are arranged in a tetrahedral geometry as illustrated in Fig. 1.9. The HYOs h_1 to h_4 are the so-called standard sp^3 tetrahedral hybrids. The square of the coefficient of the 2*s* AO, $\lambda_s = 0.25$, is called the *s-character* of the HYO, while the sum of squares of the 2*p* coefficients $\lambda_p = 0.75$ is its *p-character*. Since the HYOs in Eq. (1.107) are normalized*, $\lambda_s + \lambda_p = 1$.

The *p*-type orbitals have different orientations, therefore the direction of a HYO is determined by the relative weight of the p_x, p_y and p_z AOs according to the vector addition rule. The HYOS in Eq. (1.107) are oriented along the CH bond axes (*cf.* Fig. 1.9). If we choose the coordinate system in another way, maintaining however the symmetrical tetrahedral arrangement, we have to change the coefficients of the individual *p*-type AOs appropriately, but the resulting *p*-character will not be changed.

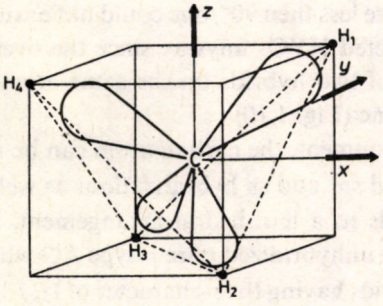


Fig. 1.9 Tetrahedral arrangement of H atoms around the central C atom in methane. The edges of the cube (solid lines) define the *x*, *y*, *z* coordinate axes. The four equivalent sp^3 valence shell hybrids on the C atom are directed towards the hydrogens H1–H4

The transformation matrix in Eq. (1.107) is unitary which means that, the four valence AOs being orthonormal*, the resulting HYOs also form an orthonormal set. It is important to realize that the orthogonality of the valence shell hybrids can be

* Due to the orthogonality of the spherical harmonics, the four original valence shell AOs are mutually orthogonal, independently of the choice of their radial parts.

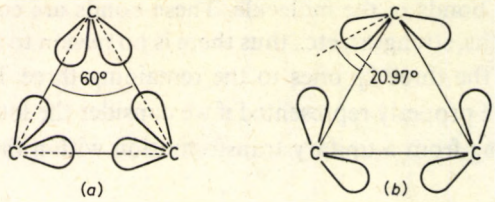


Fig. 1.10 Hybridization in cyclopropane
(a): non-orthogonal bond-directed hybrids; *(b):* orthogonalized HYOs

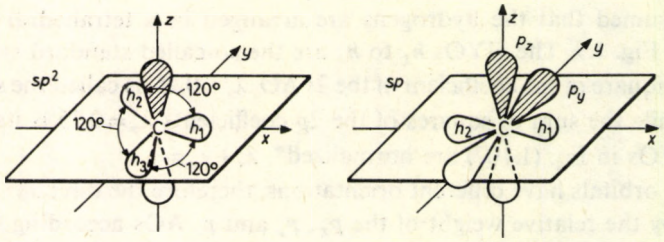


Fig. 1.11 The sp^2 and sp hybridization on a C atom

incompatible with the bond-direction requirement in some cases: the tetrahedral case is a specific situation where the bond directed HYOs are just orthogonal to each other. If one of the bond angles were less then 90°, one could not ensure the orthogonality of the corresponding bond-directed HYOs anyway since the overlaps between both the 2*s* and the 2*p* components of two hybrids on the same atom are positive. Such a case occurs *e.g.* in cyclopropane (Fig. 1.10).

Depending on its environment, the carbon atom can be not only in an sp^3 "hybrid state": there exist standard sp^2 and sp hybridizations as well (Fig. 1.11). While the sp^3 hybridization corresponds to a tetrahedral arrangement, in the sp^2 case one has a planar geometry with one unhybridized pure *p*-type AO which is perpendicular to the plane of the three sp^2 hybrids having the *s*-character of $1/\sqrt{3}$. The typical bond angle in the plane is 120°. In the case of the sp hybridization, the characteristic bond angle is 180° (linear arrangement), and two AOs are left as unhybridized *p*-type orbitals. The standard *s*-character of the sp hybrids is $1/\sqrt{2}$.

First row atoms, which have more electrons than carbon does, can also be described in terms of sp^3, sp^2, etc. hybridization. An interesting difference is that some of the resulting HYOs are doubly occupied and do not correspond to a two-centre chemical bond. Such hybrids are called lone pairs (LPs, *cf.* Section 2.4). There is one LP on nitrogen, two on oxygen, and three on fluorine. Accordingly, the valence of N, O and F atoms is usually 3, 2 and 1, respectively (see Fig. 1.12).

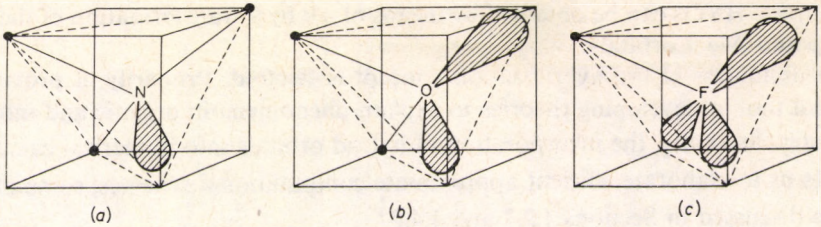


Fig. 1.12 The sp^3 hybrids on N,O and F atoms

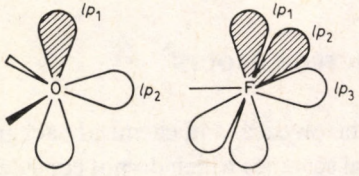


Fig. 1.13 "spectroscopic" lone pairs on O and F atoms.
The O_{lp_1} and F_{lp_1}, F_{lp_2} hybrids are pure 2_p orbitals ($\lambda_s = 0$, $\lambda_p = 1$)

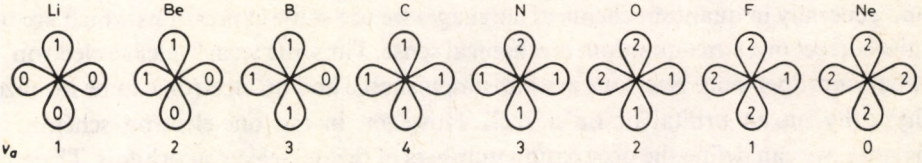


Fig. 1.14 Schematic view of valence shell hybrids of first-row atoms. Each loop indicates a hybrid orbital. The figures inside the HYOs are the occupation numbers

If we have more than one LP there is some ambiguity in specifying them. In Fig. 1.12 we depict the tetrahedral arrangements; another possibility is shown in Fig. 1.13 (*cf.* also Section 1.4).

Atoms, which are poor in electrons relative to carbon, possess completely empty HYOs as well. The valence shell hybridization of atoms from Li to Ne is illustrated schematically in Fig. 1.14. The electronic structure of Li, Be, B and C can be described by filling 1, 2, 3 and 4 HYOs with a single electron, respectively. Accordingly, these atoms can form 1, 2, 3 and 4 single bonds. For N, O, F and Ne we have 1, 2, 3 and 4 doubly occupied LPs allowing us to form 3, 2, 1 and zero single bonds, respectively. As may be seen, the usual atomic valence is equal to the number of singly occupied HYOs.

Usually one considers hybridization transformations which affect only the valence shell. For first- and second-row atoms this involves a four-by-four transformation since the valence shell consists of one *s* and three *p* orbitals. The 3*d* AOs lie much higher in energy than the 3*s*, 3*p* levels, thus their inclusion into the valence shell of second row atoms is not usually necessary. However, there are cases when the bonding situation can be described only by considering 3*d* orbitals, too [889]. In such a case the

appropriate HYOs can be obtained by means of a 9 by 9 transformation of the one *s*, three *p* and five *d* orbitals.

The usefulness of the hybridization concept is twofold. Primarily, it provides an essential tool in developing theories to explain phenomena in organic and inorganic chemistry. Secondly, the incorporation of hybrid orbitals into numerical calculation permits us to elaborate efficient approximate computational schemes; some of them will be discussed in Sections 1.2.7 and 1.4.2.

Some further problems of hybridization not discussed here, can be found in the literature (see *e.g.* [101, 299, 300, 351, 401, 657, 854, 859, 863, 1070, 1107, 1108, 1163]).

1.2.6 SEPARABILITY OF ELECTRON GROUPS

In this section we outline the physical and chemical background of quantum chemical theories and computational schemes which do not consider all electrons of a molecule explicitly. This requires some classification of electrons. We shall discuss here the distinction between core- and valence electrons, and the so-called sigma-pi separation.

Before going into details there is one point to be emphasized. Throughout this book, (and generally in quantum chemical language) we use some expressions which are not quite correct in a strict quantum mechanical sense. Thus, the term "valence electron" is rather improper since electrons are indistinguishable and no electron can be localized physically on an orbital or on a shell. However, in the one-electron scheme, for instance, we can define the occupation numbers of the one-electron orbitals. There are no "core-" and "valence-electrons", but we can state that there are always two electrons on the 1*s* orbital of heavy atoms. This is the "physical" hint behind the underlying discussion. This means also that there is a one-to-one correspondence between electrons and spin-orbitals in the independent particle model, so the above non-rigorous terminology cannot cause any misunderstanding.

We note also that the distinction between the core and the valence shell, as well as the σ–π separation, can be generalized to levels of approximation more sophisticated than the HF model.

All valence-electron schemes. The limited role of inner shell electrons in chemistry has already been mentioned. This feature can be formulated in several ways. One can say, for example that the bonding situation in a molecule can be described merely by appropriate valence shell hybrids without mixing the core orbitals, or, a completely filled inner shell is chemically rather inactive (*cf.* chemical periodicity). The less phenomenological statement is to say that the core AOs are of very low energy relative to the valence orbitals, and usual chemical processes can hardly stimulate a virtual core $\rightarrow$valence electronic excitation which would make the role of core orbitals important (see Table A1 in Appendix). There are, however, exceptions where the behaviour of core electrons reflects chemically important effects (*cf.* X-ray spectroscopy or ESCA, Section 3.6.2).

Anyway, a physically acceptable model for most of chemistry arises if one considers only valence electrons explicitly. In such a theory the inner shells are considered as rigid (independent of chemical changes), influencing only the $H_{\mu\nu}$ one-electron part of the Fockian, Eq. (1.79). In other words, in an all-electron method the matrix element of the one-electron Hamiltonian, containing kinetic energy and nuclear-electron attraction parts, is

$$H_{\mu\nu} = -\frac{1}{2}\Delta_{\mu\nu} - \sum_{A} Z_A \langle \chi_\mu | \, | \mathbf{r} - \mathbf{R}_A | \, ^{-1} | \chi_\nu \rangle \tag{1.108}$$

while in a valence electron scheme, instead of $H_{\mu\nu}$ one has:

$$H^c_{\mu\nu} = -\frac{1}{2}\Delta_{\mu\nu} + V_{\mu\nu} \tag{1.109}$$

where $V_{\mu\nu}$ is the matrix element of an effective interaction potential containing nuclear-electron attraction and valence-core electron repulsion. The "c" superscript refers to the term "core". In Eq. (1.108) the indices μ and ν run over all the AOs while the core indices do not appear in Eq. (1.109); so, the dimension of the matrix $\mathbf{H}^c$ is less by the number of core orbitals than that of $\mathbf{H}$. That is, the size of the problem for the molecule in question is reduced. The $V_{\mu\nu}$ is called *pseudopotential* and it is usually taken in the following form:

$$V_{\mu\nu} = -\sum_{A} (Z_A - n^c_A) \langle \chi_\mu | \, | \mathbf{r} - \mathbf{R}_A | \, ^{-1} | \chi_\nu \rangle + V^{nc}_{\mu\nu} \tag{1.110}$$

where n^c_A is the number of core electrons on atom A. The sum in Eq. (1.110) represents the Coulombic nuclear-electron attraction screened by the core electrons, while V^{nc} means the "noncoulombic" part of the pseudopotential. The V^{nc} should contain electrostatic effects connected to the deviation from the pointlike distribution, as well as orthogonality and nonlocal exchange effects. If one has an explicit functional form for V^{nc}, the use of Eq. (1.110) permits us to perform SCF calculations for the valence shell while the effect of the core is taken into account *via* the pseudopotential. Many different formulae have been proposed for V^{nc} [208, 427, 457, 662, 1097, 1216, 1406] which were derived from different physical or quantum chemical considerations [953]. It is also possible to take into account correlation effects between core- and valence electrons with the pseudopotential formalism [642].

The use of pseudopotentials in the HFR scheme can lead to a significant saving of computational time, especially if heavy atoms are also present in the molecule, since the ratio between the number of core and valence electrons increases with the atomic number. It should be noted, however, that there are some cases where even the core orbitals become chemically significant and then the pseudopotential approach cannot be justified. Therefore, sophisticated standard quantum chemical SCF programs do not [530], or only optionally [104], involve the pseudopotential approximation.

An even simpler model arises if we consider only the coulombic part of $V_{\mu\nu}$. In this case the inner shell electrons can be viewed as being compressed into the nuclei: we

define the core charge as

$$Z_A^c = Z_A - n_A^c . \tag{1.111}$$

Then the core Hamiltonian simplifies to:

$$H_{\mu\nu}^c = -\frac{1}{2}\Delta_{\mu\nu} - \sum_A Z_A^c \langle \chi_\mu | r_A^{-1} | \chi_\nu \rangle . \tag{1.112}$$

The neglect of the $V_{\mu\nu}^{nc}$ noncoulombic part of the pseudopotential represents a basis for the semiempirical all-valence electron schemes [1121] which will be discussed in Section 1.3.2. As Eq. (1.112) suggests, in this approach one need not deal even with a pseudopotential explicitly: the only thing to do is to substract the number of core electrons n_A^c from Z_A, according to Eq. (1.111). For instance, the core charges of the C, N, O, and F nuclei are 4, 5, 6 and 7, respectively. Accordingly, the basis does not contain 1*s*-like functions, but only valence orbitals.

This drastic simplification, of course, does not provide a sufficiently accurate model from the numerical point of view, but it does reflect many chemical trends in a qualitatively correct manner.

σ–π separation. In certain types of molecules, even the valence electrons can be further grouped by distinguishing between σ and π electrons.

As a matter of fact, in planar unsaturated compounds, the molecular symmetry enforces that each canonical MO be either symmetric or antisymmetric with respect to reflection in the molecular plane. Consistent with the nomenclature for AOs, the MOs symmetric with respect to the molecular plane are expanded over symmetric AOs, and they are said to be σ type molecular orbitals while antisymmetric MOs are π-type orbitals. The π type MOs consist of only p_Z AOs; the mixing between σ and π orbitals is symmetry forbidden. The antisymmetric nature of the π-type MOs means that the π electrons have a zero probability density in the molecular plane. This implies that in a certain sense they are not so strongly bonded to the molecule as the sigma electrons which have maximum density in the molecular plane. Thus, the π electrons are most easily excitable in an unsaturated planar molecule. In such a case it is a physically acceptable model to handle only the π electrons explicitly while the σ electrons are considered as a rigid core having only an electrostatic influence on the π electron system. Mathematically, the *σ–π separation* means that the total wave function of the molecule is assumed to be an antisymmetrized product of separate σ and π many-electron wave functions which depend only on the space and spin coordinates of σ and π electrons, respectively. A π electron theory arises if we take the σ wave function to be rigid and try to describe any change in the electronic structure of the molecule by considering the changes only of the π part of the wave function. It is obvious that only those changes in the electronic structure which do not significantly affect the σ core can be accounted for by a π-electron theory. The molecular geometry, for example, cannot be calculated at the π electron level since in this respect the σ bonds play a determining role. There exist some methods, however, in which only the π electrons are treated at

the quantum chemical level, while the effects of the σ core on the molecular geometry are taken into account in an empirical way [688, 689, 812]. Moreover, correlation has been observed between bond lengths and π bond orders (see Section 3.1).

The possibility of separating the σ and π electron systems is, in principle, not restricted to the HF model. One can also take into account the electronic correlation among the π electrons or among the σ electrons as well, but by neglecting the correlation between σ and π electrons.

Some π electron methods will be reviewed in Section 1.3.2. For details of π electron theories, the reader is referred to the literature [260, 517, 1219, 1313].

The separability of electrons in space. According to the chemical way of thinking, not only core- and valence- or σ and π electrons can be separated, but one speaks often about electrons of different chemical groups in a molecule, such as a methyl- or hydroxyl-group. The quantum chemical theory of such a separation is still under development; there exists no widely accepted method for introducing this type of separation *a priori*. Most of such approaches are based on using localized MOs; some aspects of this problem will be shortly discussed in Section 1.4.

1.2.7 THE VALENCE BOND PICTURE

The Heitler–London wave function. The Hartree–Fock method discussed so far is not the only possible model for qualitative explanations and for getting first approximations to the exact wave function. Indeed, the first success of "quantum chemistry" in 1927, the first qualitative physical explanation of the chemical bond based on a semi-quantitative quantum mechanical description of the H_2 molecule by Heitler and London [542], was achieved by a quite different treatment.

Let us consider a simple model where we have one orbital on each atom in H_2, χ_A and χ_B. Heitler and London proposed to apply the following approximate wave function for the molecule

$$\Psi_{HL} = \mathcal{N}[\chi_A(1)\chi_B(2) + \chi_B(1)\chi_A(2)]\Xi \tag{1.113a}$$

where $\mathcal{N}$ is a normalization factor and Ξ is a proper singlet spin function antisymmetric in the variables of electrons 1 and 2:

$$\Xi = \alpha(1)\beta(2) - \alpha(2)\beta(1). \tag{1.113b}$$

Since the spatial part in Eq. (1.113a) is symmetric, Ψ_{HL} is properly antisymmetric. This wave function does not correspond to a single determinant of one-electron functions. The first term in Eq. (1.113a) describes a situation where one of the electrons, carrying label 1, is assigned to atom A while electron 2 is assigned to atom B. The second term, describing the situation with interchanged electrons, appears quite naturally as electrons are indistinguishable. Both products are called *covalent terms* of the wave function. The Ψ_{HL} is called a Heitler–London wave function and it describes the

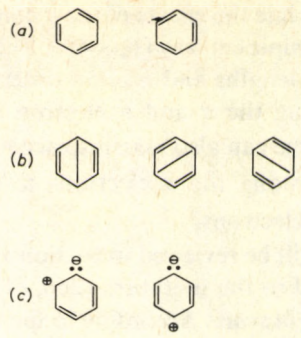


Fig. 1.15 Some of the independent VB structures for π electrons in benzene. *(a):* Kekulé structures; *(b):* Dewar structures; *(c):* ionic structures

electronic structure of the H_2 molecule in a qualitatively correct manner [542]. We can say that the Coulomb hole, that is the correlation between electrons 1 and 2, is accounted for since the two electrons possessing opposite spins cannot be found at the same atom simultaneously. However, in reality one cannot exclude the possibility that both electrons are instantenously located on the same atom; due to the absence of such ionic configurations the Heitler–London wave function does not represent the exact solution even for a finite basis. It can be improved by permitting an admixture of the two *ionic terms*, $\chi_A(1)\chi_A(2)$ and $\chi_B(1)\chi_B(2)$, to Ψ_{HL}:

$$\Psi = \mathcal{N}'[\chi_A(1)\chi_B(2) + \chi_B(1)\chi_A(2) + \lambda\{\chi_A(1)\chi_A(2) + \chi_B(1)\chi_B(2)\}]\Xi \tag{1.114}$$

where $\mathcal{N}'$ is a normalization constant and the mixing coefficient λ has to be determined variationally. The first ionic term, $\chi_A(1)\chi_A(2)$ represents the situation when both electrons are at atom A (A^-B^+ ionic structure), while $\chi_B(1)\chi_B(2)$ corresponds to the opposite case A^+B^-. The two ionic terms enter Eq. (1.114) with the same weight due to symmetry.

VB Structures. Eq. (1.114) describes the "valence bond" (VB) wave function of a symmetric two electron–two orbital system. In a polyatomic molecule possessing many electrons and AOs, one should split the whole system into several "two electron–two orbital" subsystems for which the above scheme works (for lone pairs, "two electron–one orbital" subsystems should be considered). These subsystems, in some sense, correspond to the two-centre chemical bonds of the molecule. Besides the "chemically reasonable" structures, one has to consider *all* linearly independent structures (spin functions) as well. For example, the π-electron system of benzene can be represented as shown in Fig. 1.15. Chemical intuition suggests that the two Kekulé structures *(a)* will be of dominating importance while the Dewar structures *(b)* contribute to a less significant (but not negligible) extent. The role of ionic structures is of smaller importance.

Once all possible VB structures of a molecule have been found, the total many-electron wave function can be constructed as follows. Let ϕ_K denote a particular VB

structure, which is an antisymmetrized and spin-coupled product of some selected singly and doubly occupied AOs, participating in the given structure. The total many-electron wave function is then written as

$$\Psi_{VB} = \sum_K C_K \phi_K \tag{1.115}$$

where K runs over all the posble independent VB structures. The coefficients C_K can be determined variationally. This involves the solution of the corresponding secular equation *(see below)*.

To describe the binding situation appropriately, one usually works with hybridized AOs. An essential difference to the case discussed in Section 1.2.3 is that the VB structures are not orthogonal to each other*, *i.e.*:

$$S_{KL} = \langle \phi_K | \phi_L \rangle \neq \delta_{KL}. \tag{1.116}$$

This feature produces serious computational difficulties in evaluating the $H_{KL} = \langle \phi_K | \hat{H} | \phi_L \rangle$ integrals (matrix elements) appearing in the secular equation

$$\sum_L (H_{KL} - ES_{KL}) C_L = 0 \tag{1.117}$$

which is the generalization of Eq. (1.28) to the non-orthogonal case.

Comparison of VB and MO schemes. As we have mentioned above, the first attempts in quantum chemistry were made within the VB scheme [255, 542, 1070]. Later, due to the above computational difficulties, the LCAO MO picture came to the front. For this reason in the present book we will discuss almost exclusively the MO model with the exception of the present paragraph. However, it is to be noted that there is some renaissance in the use of the VB model [438, 750, 781, 857, 1277], especially if a qualitative picture is needed [374, 510, 698]. As a matter of fact, one can argue that the VB method is more "chemical" in some sense since it deals with one- and two-centre structures, and chemistry suggests that intramolecular interactions are essentially two-centre in nature. We note, however, in this respect that there are some possibilities even in the MO picture to consider two-centre bonds and their interactions, namely the use of localized MOs which will be discussed in Section 1.4.

In order to gain some insight into the similarities and differences of MO and VB schemes, it is worthwhile to write down the simple MO wave function of the H_2 molecule:

$$\Psi_{MO} = \frac{1}{2} | \psi(1)\alpha(1) \quad \psi(2)\alpha(2) | \tag{1.118}$$

* Neither the spatial, nor the spinfunctions corresponding to different structures are orthogonal, the latter representing the more serious difficulty. As to the non-orthogonality of the atomic basis orbitals, an efficient procedure was used by Norbeck and McWeeny in connection with the VB method [1026].

where ψ is the LCAO MO: $\psi = \frac{1}{\sqrt{2}}(\chi_A + \chi_B)$. Substituting ψ into Eq. (1.118) we get:

$$\Psi_{MO} = \mathcal{N}[\chi_A(1)\chi_A(2) + \chi_A(1)\chi_B(2) + \chi_B(1)\chi_A(2) + \chi_B(1)\chi_B(2)] \cdot \Xi. \tag{1.119}$$

By comparing this expression with Eq. (1.99) we find that the ionic and covalent terms appear with an equal weight ($\lambda = 1$). This may be related to the fact that the MO model does not take into account correlation effects: the probability distribution of the two electrons is independent of each other. Thus the MO wave function exaggerates the weights of the ionic terms, for which both electrons are located on the same atom. In a real situation, the Coulomb hole makes the weight of ionic terms smaller: $\lambda < 1$. At the same time for the Heitler–London wave function one has no ionic terms, that is, $\lambda = 0$, *cf.* Eqs (1.113) and (1.114); thus one says that Ψ_{MO} is uncorrelated, while Ψ_{HL} is "overcorrelated".

It should be emphasized that exact wave functions within a given finite LCAO basis can be obtained in both (MO + CI or VB) schemes. The series expansions of the wave function in Eqs (1.27) and (1.115) over determinants and VB structures, respectively, converge to the same "basis limit". It seems that, at the present stage of computational quantum chemistry, the "cost/performance" ratio is smaller for the MO method.

1.3 COMPUTATIONAL METHODS

This section is devoted to a brief survey of the computational methods most frequently used in present day quantum chemistry. First we discuss current *ab initio* SCF procedures. Secondly some methods for taking into account electron correlation are reviewed. Then, among standard semiempirical methods, π-electron and all-valence electron models will be discussed at the SCF and Hückel-type levels. Finally, we will mention some qualitative MO models useful in an understanding of various molecular phenomena.

The aim of this survey is to gain a general insight into the jungle of different quantum chemical procedures calling the reader's attention to the use and limitations (fields of application) of the methods discussed. For this purpose it is necessary to explain the basic physical and mathematical ideas behind the different computational methods to some extent.

1.3.1 AB INITIO METHODS

The term '*ab initio*' refers to the specific feature that this class of computational schemes does not use empirical parameters except the fundamental physical constants e, m, h (and c). That is, within this model, all necessary quantities are computed accurately from the very beginning. More precisely, we define a set of basis functions over which

the molecular orbitals can be expanded. (The choice of this basis set, of course, requires some intuition and experience.) Within the basis specified, the Hartree–Fock–Roothaan SCF equations* (1.79) are solved exactly; in particular, no approximation in evaluating the integrals appearing in the Fock matrix (see Eq. 1.79) is allowed. In practice this means that, even if numerical integral evaluation methods have to be used, the accuracy of the computed integrals should be at least 8 decimal digits. Similarly, SCF cycles (*cf.* Section 1.2.4) should be repeated until self-consistency is achieved up to ca. 10^{-5} a.u. (≈ 0.06 kcal/mol ≈ 0.26 kJ/mol) or better in the total energy. If the aim is to go beyond the HF scheme, the SCF calculation can be followed by some CI calculation to account for correlation effects. As for the latter, it is usually hopeless to perform a "full CI" calculation (*i.e.* to consider all possible configurations), especially when using large basis sets *(see below)*. The *ab initio* framework in this context requires the specification of a model accounting for electron correlation (*cf.* electron pair methods): this may be approximate but the results obtained should be accurate within the given model.

Some commonly used basis sets, a few problems in performing the SCF procedure and the most important standard methods of calculating electron correlation will be discussed below. For a more detailed, but easy-to-understand review, the reader is referred to the excellent short monograph by Čársky and Urban [182]. Some other books and review articles are given by Refs [953, 1230] and [1231]. Very useful bibliographies of *ab initio* molecular wave functions are collected by Richards *et al.* [1171–1173] and Ohno and Morokuma [1035].

Basis sets

Most *ab initio* methods work within an LCAO basis set. For atoms or diatomics, the use of a basis set consisting of Slater-type AOs (Eq. 1.84) is preferable since STOs $\chi^{SL}(\mathbf{r})$ possess correct $r \to \infty$ and $r \to 0$ asymptotics (exponential decay and cusp condition; see Section 1.2.5). For molecules containing three or more atoms, three- and four centre integrals appear in the expression (1.79) of the Fockian. The evaluation of such integrals over STOs, though possible in principle [477, 478, 648, 1226, 1266, 1309, 1337a, 1363] is rather laborious and cannot be managed in routine calculations for larger molecules. Multicentre integrals, however, can easily be evaluated over Gaussian-type orbitals (GTOs), which are of the form of Eq. (1.85); (see also Section 1.2.5). This represents a great advantage, since for polyatomic molecules an enormous number of integrals has to be computed (approximately $N^4/8$, where N is the number of basis orbitals). Therefore, present standard *ab initio* programs construct the LCAO basis set in terms of GTOs. Since the STOs, except the above computational difficulties, are more suitable as basis functions, Gaussian basis sets are often constructed considering the following guidelines [535, 614, 1044, 1164]. (1) An appropriate STO basis is determined for free atoms (or, for diatomics in certain cases), for which all

* We discuss here the RHF model applicable for closed shell system; the same holds, however, for the UHF and other *ab initio* methods as well.

integrals are managable. (2) Atomic STOs are approximately expanded in terms of several GTOs as

$$\chi^{SL} \approx \sum_{\nu=1}^{n} k_\nu \chi_\nu^G . \tag{1.120}$$

The coefficients k_ν are determined by a least-square fit procedure. (3) The molecular basis set is constructed as the direct product of atomic basis functions of Eq. (1.120). Such molecular bases are referred to as STO-nG, where n is the number of pure gaussians (the so-called primitives) in the above expansion. Usually $3 \leq n \leq 6$. Six primitive gaussians give a reasonably accurate representation of a Slater orbital (see *e.g.* [182], p. 28). Most commonly the cheaper STO-3G and STO-4G bases are used.

The exponent of the STO-nG orbitals (1.120) can be optimized for molecules*, instead of adopting the original Slater values. Though fully optimized exponents are not strictly transferable, standard sets of exponents are available [529] which are suitable for calculating most common molecules.

The STO-nG basis sets are typical examples of an extremely important concept in *ab initio* quantum chemistry: *contraction of basis functions* [229, 346, 1244, 1263, 1339, 1417]. In larger basis sets containing a number of primitive gaussians with different exponents but of the same symmetry, the optimized HFR atomic orbitals often contain the primitives in more or less transferable combinations. Therefore, these combinations can be kept fixed in building the AO in a molecular computations with a minor loss of flexibility, *i.e.*, they need not be reoptimized. This allows a significant saving in computation time since in the molecular HFR problem the rigid contraction of the primitives is considered as a single basis function, thus reducing the number of integrals to be manipulated during the SCF procedure. Of course, the number of integrals to be evaluated cannot be reduced in this way. Such basis sets are called contracted basis sets. Note that contracted sets never contain STOs as primitives, since in this case the integral evaluation time would increase more than we could save by the contraction of the orbitals in the SCF cycles.

We have discussed so far the form of basis functions for *ab initio* calculations. As for the size of basis sets, the following levels can be distinguished:

(1) *Subminimal basis:* one basis function per two electrons. No variational freedom appears in the HFR equations, since each basis function is doubly filled (there are no virtual orbitals). Consequently, the HFR equations need not be solved: one has just to calculate the energy. Such subminimal basis is used in Frost's "Floating spherical Gaussian orbital" (FSGO) method [414]. Here primitive gaussians are used which are not necessarily centred on atoms, but their positions are considered as nonlinear variational parameters and optimized directly in each calculation. The exponents are

* For inner shell orbitals, the optimization can be performed for free atoms. Exponents of valence shell orbitals are preferably optimized directly for molecules.

also optimized. The conceptual advantage of this oversimplified basis set lies in assigning each basis function to an inner shell, bonding or lone electron pair, respectively, according to the classical chemical picture. The disadvantages are that (i) the optimization of the centres and exponents of the primitives is rather expensive for larger systems; (ii) bonding orbitals of π symmetry cannot be represented effectively by a single gaussian; (iii) even the fully optimized basis is inadequate in most cases for reproducing experimental data with sufficient accuracy; and (iv) no excitation process can be described by this basis due to the absence of virtual MOs.

(2) *Minimal basis sets:* one basis function per two inner shell electrons + one for each atomic valence orbital. For first row atoms, for example, the minimal basis consists of the $1s$, $2s$, $2p_x$, $2p_y$, and $2p_z$ orbitals. For hydrogen atoms only the $1s$ AOs are considered. Clearly, such a basis set for a rare gas atom is not flexible at all since one has the same number of orbitals and electron pairs, as in the case of the subminimal basis. For other atoms of a molecule, however, some flexibility is ensured and such minimal basis sets are commonly used in doing *ab initio* calculations for larger molecules. With hydrocarbons *e.g.*, the number of electrons and basis orbitals is just the same in the valence shell, thus the number of occupied valence and virtual MOs is also equal. Note also that for studying *free* atoms the minimal basis provides no flexibility, because the mixing of orbitals corresponding to the same valence shell is symmetry forbidden in that case. Thus, the minimal basis can account only for the distortion of the electronic structure of atoms when participating in a molecule.

(3) *Double zeta and extended bases:* two functions for each AO of the minimal basis (DZ basis). The flexibility of the basis significantly increases as compared to the previous case. Since the flexibility is much more important for the valence shell than for the chemically less active inner shells, it is customary to treat the latter at the minimal level and to use the double zeta (DZ) quality only in the valence shell (split-valence shell basis, *vide infra*). Similarly, one can speak about triple zeta (TZ), etc. basis sets, which are called extended sets. The general feature of the double and triple zeta basis sets is that they provide a better quantitative description of the individual atoms of the molecule due to their increased flexibility. Double zeta calculations can be performed routinely for molecules of medium size, while due to the much larger number of basis functions, extended basis sets are generally used only for relatively small molecules containing a few atoms.

(4) *Polarization functions:* orbitals with higher azimuthal quantum number. The use of more and more basis functions for the inner shell and valence orbitals leads to a better and better description of atomic electronic states. The increased flexibility of the DZ and extended basis sets in the valence shell permits us to take into account the distortion of the AOs. The symmetry of these basis functions, however, is the same as that of the minimal basis (*e.g.*, s and *p* for first row atoms). Therefore, such basis sets can hardly describe those changes in the atomic structure which are due to the lower symmetry molecular environment [1000], *i.e.*, the polarization of an atom in a molecule. It is clear, for example that the polarization of the electron cloud in a

hydrogen atom towards the atom to which the hydrogen is attached, cannot be accounted for by spherically symmetric *s*-type basis functions, and *p*-type AOs are needed for this purpose [347]. For atoms K to Ne *d*-type orbitals are necessary to describe similar effects. Generally, orbitals of higher azimuthal quantum number than those involved in the valence shell of the free atoms are called *polarization functions.* The inclusion of polarization functions provides a further type of extended basis set. Owing to the different symmetry of the polarization functions, a polarized basis set cannot be substituted by turning to a more flexible valence shell basis.

Since polarization functions describe typically interatomic effects, and do not affect the SCF energy of free atoms, their exponents cannot be optimized by calculations on free atoms. Standardized values, based on optimization studies on small molecules, are available (see Ref. [182] and references therein).

It should be noted that if, in a molecular computation, the valence shell orbitals are not flexible enough, polarization functions improve the description of the valence shells, which is clearly an artefact. Polarization functions may therefore be included only in basis sets of DZ (or better) quality.

(5) *Basis sets with diffuse orbitals* [348, 518]. In certain applications it is necessary to include functions with very small exponents into the basis set. These functions are said to be diffuse, since they are expanded far beyond the valence region. Diffuse functions are inevitable if treating states where an electron is only weakly bound to the atom or molecule. Such states arise in negatively charged species, in certain (Rydberg) electronic excitations, transition metal compounds, etc. Diffuse functions cannot be substituted by polarization functions, since they describe quite different effects.

(6) "*Beyond LCAO*" *bases: bond functions and floating orbitals.* We have already commented on the one-centre expansion of MOs in Section 1.2.5. Here we discuss the non-LCAO sets in another context. The LCAO basis was introduced to account for atomic properties many of which are conserved also in the molecule. However, especially to account for typical molecular effects such as polarization, one may use molecular basis sets, where the basis functions are not necessarily centred on nuclei. It has therefore been proposed [1133] that, in order to increase the flexibility of the basis, instead of using polarization functions, GTOs can be placed at interatomic positions to ensure a better description of chemical bonds and lone pairs. Such off-centred orbitals are called bond functions. The advantage of using bond functions instead of polarization functions lies in reducing the amount of computation, since a smaller number of orbitals can be used to account for the same effect. Positions and exponents of bond functions should be optimized for the molecule, but these nonlinear variational parameters were found to be fairly transferable [990, 991, 1211] between similar bonds. Locating bond functions at the midpoint of the bonds represent also a reasonable choice [899]. The application of bond functions can also be combined with the use of polarization functions; this is especially advantageous for studying potential surfaces [1440a, b].

If off-centred functions are used also for representing the valence shell, we speak about a floating basis. The simplest floating basis is the subminimal FSGO one discussed above. More sophisticated versions [210, 993, 1255] of the floating basis model use additional gaussians and new variational freedoms appear. As a consequence, the reliability of the model is significantly improved, but, unfortunately, as the number of nonlinear parameters to be optimized increases, the computational costs soon become prohibitive. The nonlinear variational parameters of the floating model cannot be estimated on the basis of atomic calculations. Therefore, quantum chemists, at present, prefer LCAO basis sets to floating ones.

In the following we discuss the most popular basis sets which are usually built in the standard *ab initio* programs, so that the users need not worry about the selection of exponents and contraction coefficients. We have already mentioned the STO-*n*G minimal basis set. Among split-valence gaussian basis sets, the most widely used are the 4-31G and 6-31G sets, developed by Pople and coworkers [328, 527, 532], where the *k*-*nm*G means that k primitive gaussians are contracted for representing an inner shell AO, and $n+m$ primitives for the valence AOs are contracted to two functions containing n and m orbitals, respectively. Accordingly, these basis sets are of double zeta quality in the valence shell ("split valence" basis). When passing from 4-31G to 6-31G, due to the better description of the inner shell AOs, considerable lowering of the energy is observed, but the energy differences (which are usually of actual interest only) and equilibrium molecular geometries do not alter strongly [527]. This, of course, reflects the restricted chemical significance of the inner shells. Therefore, the 4-31G basis is more often used since it is economical due to the smaller number of the primitives. Among split valence basis sets, 4-21G proposed by Pulay *et al.* [1136] is worth mentioning, which is even less expensive but still sufficiently flexible for calculating molecular geometries. Pople's 3-21G basis is also quite economic. Polarization functions can also be added to *k*-*nm*G basis sets, the resulting sets are denoted as, for example 4-31G* or 4-31G**. One asterisk indicates the d orbitals on heavy (first and second-row) atoms, while the second asterisk denotes that the p functions on hydrogens are also considered.

A general criterion in constructing molecular basis sets is that they should be balanced as the different atoms are compared: in order to avoid artefacts in the results, one has to use similarly good or poor basis sets on each atom, but the basis must not be improved only on one atom or only on a part of the atoms in the molecule. The symmetry of the molecule should also be reflected by the symmetry of the basis set: such a distorted, bad basis would appear, for example, if one used a minimal AO basis on one of the oxygens with a DZ basis on the other oxygen of the O_2 molecule. In a polyatomic molecule, even if there is no spatial symmetry, an unbalanced basis set can lead to serious failures, such as qualitatively wrong charge distributions. Experience has shown that the standard basis sets (minimal, DZ, polarization functions, split shell with or without polarization functions) provide sufficiently balanced descriptions. Nonetheless, it should be noted that the requirement of using "balanced" basis sets is a

characteristic consequence of the very incomplete nature of the bases: if the expansion were complete, a polyatomic molecule could be described even by situating all basis orbitals on one of the atoms. Usual basis sets are very far from this quality, however.

In performing actual *ab initio* calculations, the choice of the basis set should depend on what kind of physical parameters are to be computed (Table 1.4). Since the evaluation and manipulation of the two-electron integrals $(\mu\nu|\lambda\sigma)$ requires computation times roughly proportional* to N^4 (N is the number of basis functions), the size of the basis usually kept as small as possible, while preserving the reliability of the results. In other words, some compromise must be made between the accuracy and the cost of computations. In connection with this problem, there is one point to be emphasized. It is very rarely the case that quantum chemical calculations give results in exact quantitative agreement with experimental data (provided that the latter are indeed accurate). This can be expected only for very large basis sets and often only if correlation effects are properly accounted for; sometimes even relativistic corrections are needed. Obviously, such accurate wave functions can be obtained only for small molecules. However, semiquantitative agreement can often be achieved with manageable computations. In such a case it is very important to pay attention to the qualitative aspects of the results which are surely reliable. In addition, they can contain information of the same, or greater, practical importance as the numerical data themselves. For example, in comparing a theoretical and an experimental UV excitation spectrum, the aim of the computation is usually not to *predict* the position and intensity of the UV bands (this can easily be measured), but rather to assign the various bands to different electronic transitions. Another instance is represented by two stable conformers of a molecule differing only by a few kJ/mol in energy. It is almost hopeless to decide by quantum chemical computations which conformer is the more stable: different basis sets may yield different answers. However, even experimental data concerning this question may be uncertain and the only chemically meaningful statement is to establish that there exist two conformers which are about of equal energy, and to determine of what type they are.

Let us finally remark on a problem which can arise when using large basis sets. If the basis contains many orbitals of the same symmetry on one centre, there is some danger that the basis set becomes approximately linearly dependent (see the footnote on p. 37). This can be controlled easily by checking the smallest eigenvalue of the overlap matrix which tends to zero in the case of linear dependency.

The SCF procedure. Once the basis set had been defined and the integrals were evaluated, the next step was to choose an initial guess $\mathbf{P}^0$ of the density matrix $\mathbf{P}$, in order to be able to construct the first Fockian *via* Eq. (1.64). The matrix $\mathbf{P}^0$ is usually chosen in one of the following ways:

* More precisely, the time requirement of *ab initio* SCF programs is mainly determined by the number of independent two-electron integrals, which is given by $p=q(q+1)/2$ where $q=N(N+1)/2$. This can be easily seen by counting those $(\mu\nu|\lambda\sigma)$ integrals which are equal due to symmetry: $(\mu\nu|\lambda\sigma)=(\mu\nu|\sigma\lambda)=(\nu\mu|\sigma\lambda)=(\nu\mu|\sigma\lambda)=(\sigma\lambda|\mu\nu)=\ldots$, etc. Asymptotically, for sufficiently large N one has $p\sim N^4/8$.

TABLE 1.4

The reliability of different LCAO basis sets in *ab initio* calculations. N represents the number of contracted basis orbitals for ethane. The computation time is roughly proportional to the number of independent two-electron integrals, P. Typical errors are given relative to the experiments

Basis set	N	P	Bond lengths	Bond angles	Rotational barriers	Inversion barriers	Dipole moments	Force constants	Reaction energies
Minimal STO-3G	16	9 316	3 pm error	3–4° error	Good for ethane-like molecules; inappropriate if vicinal lone pairs are present	Improper	Qualitatively good	Poor	Poor
Split valence 4–21G 4–31G 6–31G	30	108 345	2 pm error	2–4° error		Poor	Somewhat large	Good	Qualitatively good
Polarized 4–31G* 4–31G**	40 58	336 610 1 464 616	1 pm error	1–2° error	Good	Good	Good	Good	~10 kJ/mol error

(1) A simplified model Hamiltonian is defined which does not contain explicitly any electron-electron interaction (see the extended Hückel method in Section 1.3.2). This Hamiltonian is diagonalized and the eigenvectors are used for building $\mathbf{P}^0$ by using Eq. (1.66).

(2) *A priori* constructed, approximate, strictly localized MOs (see Section 1.4.2) can also be used in constructing the initial approximation $\mathbf{P}^0$ [783, 784].

(3) One can apply density matrices obtained for similar systems, *e.g.* related (isoelectronic) molecules, the same molecule calculated at some (slightly) different geometry or in smaller basis set, etc. In split valence shell calculations results of an STO-3G calculation are often utilized to form $\mathbf{P}^0$ by appropriate techniques.

Among the above possibilities, the technically simplest is (1). Usually it works fairly well, but sometimes represents a quite inappropriate initial guess: $\mathbf{P}^0$ and the true SCF density matrix $\mathbf{P}$ can be considerably different. In such a case there is a danger that the SCF procedure fails to converge. Method (2) is certainly more laborious but the corresponding $\mathbf{P}^0$ includes some important effects of electron repulsion, and the SCF procedure usually converges quickly. (There are, however, some cases observed at the CNDO/2 level of approximation, where starting with $\mathbf{P}^0$ obtained by (2) requires more iterations until self-consistency is reached, than with that by (1) [1324].) For large basis sets, the most reasonable choice is perhaps (3).

Having obtained the initial density matrix $\mathbf{P}^0$, the SCF iteration is made according to the following scheme:

$$\mathbf{P}^0 \rightarrow \mathbf{F} \rightarrow \mathbf{C}_k \rightarrow \mathbf{P} \qquad (1.121)$$

where $\mathbf{F}$ is the Fockian defined in Eq. (1.79), and the vectors $\mathbf{C}_k$ are the eigenvectors of the Fockian over which the new density matrix is built up. The iterations are to be repeated until convergence is reached, that is, until the largest deviation between the elements of density matrices obtained in the n'th and $n+1$'th iterations is less than a given treshold (*e.g.* 10^{-4}). Often the deviation of the energy is quite simply checked, for which the threshold should be smaller (*e.g.* 10^{-5} a.u. or less), since the energy is a quadratic quantity and is less sensitive to the quality of the wave function. The expression of the total energy in the LCAO representation can be obtained by substituting the expansion of MOs, Eq. (1.75), into the Hartree–Fock energy formula (1.60), and introducing the Fockian (1.79) and the density matrix (1.81):

$$E = E_n + \frac{1}{2}\sum_{\mu\nu}(H_{\mu\nu} + F_{\mu\nu})P_{\mu\nu} \qquad (1.122)$$

where $H_{\mu\nu}$ is the core Hamiltonian as defined by Eq. (1.80).

In order to reduce the computer time of the SCF procedure [1382], attempts can be made (*i*) to make the individual iteration cycles faster, and (*ii*) to reduce the necessary number of cycles. As for (*i*), the crucial step is the construction of the Fock matrix since

for example, of the energy matrix elements $\langle \Psi \mid \hat{H} \mid \Psi \rangle$ is extremely cumbersome (note that the Slater rules cannot be applied here). Thus the use of this method is restricted to very small systems containing only two (or at least a few) electrons [617, 730, 1078, 1079].

(2) *Multiconfiguration SCF methods* (MCSCF) [1384, 1394, 1395]. The wave function is written as a sum of a *limited* number of configurations:

$$\Psi_{\mathrm{MCSCF}} = \sum_{K=1}^{N} C_K \mid \psi_{K_1} \psi_{K_2} \cdots \psi_{K_n} \mid$$

where ψ_{K_i} is the i'th one-electron orbital in the K'th configuration, n is the number of electrons and N is the number of configurations (determinants) to be considered. Both the linear combination parameters C_K and the form of the one-electron functions ψ_{Ki} are optimized variationally. (The latter are usually expanded in some finite set of basis orbitals, similar to the HF method, to which the MCSCF obviously reduces if $N = 1$.) This simultaneous optimization in the practice requires a special iterative procedure. Due to the increased variational freedom, the energy of the MCSCF wave functions is deeper than the HF energy in the same basis; therefore, this wave function is partly correlated. However, the MCSCF method does not provide a systematic account of correlation energy in general (the number of determinants is usually small), and its main value is to offer a better starting point for further calculations in cases where the one-determinantal SCF wave function is inappropriate. An example is the (quasi-) degeneracy of the highest occupied and the lowest virtual SCF orbital which clearly leads to a breakdown of the HF approximation, *cf.* Section 1.2.4.

A special class of multiconfiguration wave function methods is represented by the extended Hartree–Fock (EHF) schemes, known also as projected HF methods [827, 882]. The general HF equations (1.46) or (1.47) do not warrant necessarily that the corresponding one-determinantal wave function is an eigenfunction of all operators commuting with the Hamiltonian. We have already discussed (Section 1.2.4) the spin-projected extended HF method [882] where it is enforced by means of spin-projection operators that the DODS wave function be an eigenfunction of $\hat{S}^2$. Other types of projection operators can be applied to ensure the proper spatial symmetry of the one-determinantal wave function if it were violated [827, 837].

(3) *Valence bond type methods.* The Heitler–London wave function was already discussed in Section 1.2.7. We have seen that it accounts for correlation effects, and, in addition, it can be considered overcorrelated. The proper consideration of the ionic terms in VB methods can provide an appropriately correlated wave function.

In the generalized valence bond (GVB) method [454] one deals with optimized molecular orbitals instead of pure (hybrid) AOs. In the perfect pairing* approximation

* The "perfect pairing" approximation means that each orbital plays a role only in one bond and each bond is considered as a singlet subsystem. That is superpositions of Kekulé- or Dewar structures (see Section 1.2.7) cannot be treated by the GVB wave function. A method which overcomes this difficulty was published recently [1391].

one obtains nicely correlated wave functions—certainly at a very high cost. Note that the GVB procedure can also be considered as a special MCSCF method.

The valence bond type methods are very promising in obtaining accurate wave functions, but they are still under development. Their application is usually not a routine task, so their use is still far from common in applied quantum chemistry.

(4) *Configuration interaction.* The application of the CI method described in Section 1.2.3 for calculating correlation effects is possible by choosing the HF MOs as one-electron functions. As far as the HF model is selected as an initial approximation, the CI expansion (Eq. 1.27) can be rewritten as

$$\Psi = \phi_{\mathrm{HF}} + \sum_{i,j^*} C^S_{ij^*}\phi^{j^*}_i + \sum_{i,j,k^*,l^*} C^D_{ijk^*l^*}\phi^{k^*l^*}_{ij} + \ldots \tag{1.123}$$

where ϕ_{HF} is the single determinantal HF wave function, $\phi^{j^*}_i$ denotes a singly excited configuration obtained by replacing the spinorbital φ_i by φ_{j^*} in ϕ_{HF} (the asterisk indicates virtual orbitals), and $\phi^{k^*l^*}_{ij}$ stands for a doubly excited determinant, etc; in the general case one has to consider higher excitations as well. The numbers $C^S_{ij^*}$ and $C^D_{ijk^*l^*}$ etc. are the CI coefficients. Note that Ψ in Eq. (1.123) is not normalized to unity but the so-called *intermediate* or *correlation normalization* is used:

$$\langle \Psi \mid \phi_{\mathrm{HF}} \rangle = 1 \tag{1.124}$$

where the single determinant ϕ_{HF} is normalized to unity.

Since the HF MOs φ_i form an orthonormal set, the many-electron determinants ϕ_{HF}, $\phi^{j^*}_i$, $\phi^{k^*l^*}_{ij}$, etc. (or their spin-adapted linear combinations) all are mutually orthogonal and the matrix elements of the Hamiltonian can be obtained by the Slater rules. Then, the CI matrix consisting of the matrix elements of $\hat{\mathrm{H}}$ over the above determinants can be, in principle, diagonalized. The lowest eigenvalue corresponds to the ground state energy of the system. Using (1.123), this can be expressed (without any approximation) as follows [998]:

$$E = E_{\mathrm{HF}} + \sum_{i<j} \sum_{k^*<l^*} C^D_{ijk^*l^*}[(ij \mid k^*l^*) - (ik^* \mid jl^*)] \tag{1.125}$$

where $E_{\mathrm{HF}} = \langle \phi_{\mathrm{HF}} \mid \hat{\mathrm{H}} \mid \phi_{\mathrm{HF}} \rangle$ is the SCF energy and we exploited the Brillouin theorem (1.43) and the fact that the matrix elements of the Hamiltonian between ϕ_{HF} and all the triply and higher excited determinants are zero, *cf.* Slater rules [1286]. Introducing the notation

$$\varepsilon_{ij} = \sum_{k^*<l^*} C^D_{ijk^*l^*}[(ij \mid k^*l^*) - (ik^* \mid jl^*)] \tag{1.126}$$

we have

$$E = E_{\mathrm{HF}} + \sum_{i<j} \varepsilon_{ij} \tag{1.127}$$

then one has to manipulate with the large number of two-electron integrals. Except for small problems, all the necessary integrals cannot be stored simultaneously in the operative memory of present-day computers*, but must be placed on tapes or disks, the access of which is much slower. Therefore the effectiveness of the programs concerning the integral manipulation is of crucial importance. Current standard *ab initio* programs are well optimized in this respect, many ideas and tricks being incorporated, which result in saving at least an order of magnitude in the computational times as compared to early *ab initio* programs. We note, however, that more than half of this time saving is due to the effective evaluation of integrals.

The number of the SCF iterations can be reduced by finding the proper initial guess and by adopting some extrapolation techniques [1190]. However, the possible time saving here is less than in evaluating and manipulating the two-electron integrals. Much attention must be paid to avoid oscillations in the SCF iterations. For this purpose different damping procedures or the so-called level shift technique [491] can be applied. In principle, oscillations can always be avoided by means of these methods, but this may lead to an extremely slow convergence.

Standard ab initio SCF programs. Ab initio SCF calculations can be performed for ground states of small and medium-size molecules in a routine fashion. Effectively organized computer programs are available which are able to work within standardized basis sets (STO-*n*G, *k*-*nm*G, *k*-*nm*G* and *k*-*nm*G**). The most frequently used programs are the "GAUSSIAN 70" [530], HONDO [349], "GAUSSIAN 76" [103] and "GAUSSIAN 80" [104] system. Pulay's TEXAS [1135a] and the MONSTERGAUSS [1088] systems are also worth mentioning. In contrast to earlier *ab initio* programs (POLYATOM [267], IBMOL [1380]), which require significant experience from their users, these modern systems can also be used as "black boxes" having an intelligent input. One should only specify the types and coordinates of atoms and identify the selected basis set by a keynumber or keyword and the program is ready to run. The output usually consists of energetic quantities (total and orbital energies), MO coefficients, the density matrix and Mulliken population analysis. Optionally, other properties can also be calculated such as localized molecular orbitals, dipole moments, etc. Geometry optimization or potential surface scan options are also available. Computations in non-standard basis sets are possible, too, but in this case the specification of the input requires more work and needs some experience. The most popular and easy-to-handle program is the GAUSSIAN series. For computing molecular geometries, the use of TEXAS is recommended. GAUSSIAN 82 is the most modern and certainly the most effective and most universal program system, although it can be implemented only on large mini and mainframe computers due to its extreme size.

By using the above programs one is able to perform calculations for both closed and open shell systems, by the RHF and UHF methods, respectively. Appropriate versions

* Quantum chemists are looking forward to the new generation of computers with much larger operative memory.

of the programs are usually available for different systems of computers (IBM, CDC, VAX etc.).

Methods accounting for electron correlation

In studying chemical problems, the HF model often provides a satisfactory account of many important effects. However, as we have already noted in Section 1.2.4, the correlation energy E^{corr} is comparable with, or even larger than, chemical energy differences (see also Fig. A1). Therefore (at least approximate), conservation of the correlation energy during a chemical process is an essential condition for the applicability of the HF method for quantitative purposes. The problem is that one can never be sure beforehand that E^{corr} will conserved, though some conditions were proposed for this conservation (see *e.g.* [182], pp. 74–78). At the same time there are many reactions which are known to violate the conservation of E^{corr}. They are essentially connected with the abnormal dissociation behaviour of the HF wave function (see Section 1.2.4). That is, if a chemical bond is broken or formed in the course of the reaction, the correlation energy of the product(s) and reactant(s) can differ significantly, since the RHF energy contribution corresponding to the broken bond can become meaningless. Accordingly, the role of correlation energy is important in studying rotations about double bonds, ionization and excitation processes, dissociation, potential curves, intermolecular reactions with bond fission, etc., which cover a wide range of processes of chemical interest. In addition, there are some molecules for which the breakdown of the HF approximation is observed even at normal bond distances (see also later). For instance, the F_2 molecule would be predicted to be unstable by HF calculations: its HF energy at the equilibrium F—F distance is higher than the sum of the HF energies of the two constituent F atoms. The HF prediction for the equilibrium F—F bond length is not too bad, however.

There exist some important physical phenomena which can be considered as typical correlation effects. We mention here the *dispersion* interactions which contribute significantly, for example, to intermolecular binding energies. The essence of this effect is that, as two electronic systems approach each other, the motion of the electrons localized in different systems are also correlated. As with any true correlation effect, dispersion involves a decrease of the total energy.

The above examples indicate that it is often desirable to go beyond the HF level in the quantum chemical calculations. This is still a field of methodological research and no widely used standardized methods are yet available. Another serious problem is that all existing procedures are much more expensive than SCF computations. In the following we discuss briefly the most important *ab initio* methods for calculating the correlation energy.

(1) *The method of relative electronic coordinates:* one can build up molecular wave functions which are not expanded in terms of one-electron orbitals but contain also explicitly the distance between the electrons (the differences of their actual coordinates). Such wave functions are fairly correlated but the evaluation of the occurring integrals,

approach covers the dominant portion of the correlation energy, moreover, it gives an upper bound to the exact energy since the CI method is variational. Therefore, keeping its shortcomings in mind, the CI–SD method can be successfully applied in systematic investigations of correlation effects.

Another way of reducing the size of the CI problem is to exclude of some MOs when generating the excited configurations. One can assume, for instance, that the correlation energy assigned to inner shell MOs is conserved in many chemical reactions. In such a case one can construct excited determinants preserving the doubly filled character of inner shell orbitals (valence CI). In other words, only the valence MOs are used as configuration generating orbitals. This approach neglects the correlation between core electrons and between valence and core electrons; only the correlation between valence electrons is accounted for, which is possibly most sensitive to the chemical rearrangements (see [952] and references therein). The "fully optimized reaction space" method of Ruedenberg [1205, 1206] falls into this category; it has been applied successfully in treating various chemical reactions [203, 386, 647]. Since in this method the valence MOs are also reoptimized, it can also be considered as an MCSCF procedure.

(5) *Perturbational approaches.* Correlation energies can also be calculated by means of the perturbation theory (PT). One defines a zeroth order Hamiltonian $\hat{H}^0$ for which exact eigenvectors are known, and it is relatively close to the exact Hamiltonian $\hat{H}$ of the molecule thus the difference

$$\hat{W} = \hat{H} - \hat{H}^0 \tag{1.130}$$

can be handled as a relatively small perturbation.

As for the correlation problem, two widely used choices for $\hat{H}^0$ may be mentioned. In the Epstein–Nesbet partitioning [375, 997] $\hat{H}^0$ is represented by the diagonal elements H_{kk} of the CI matrix, while the off-diagonal elements H_{kl} $(k \neq l)$ give rise to the perturbation. Another partition of $\hat{H}$ is that of Møller and Plesset [921] where $\hat{H}^0$ is chosen as the sum of Hartree–Fock operators of the individual electrons. The Epstein–Nesbet partition often provides a better convergence of the perturbation series, but the energy correction formulae are slightly simpler if the Møller–Plesset partition is used.

To calculate the correlation energy, the Rayleigh–Schrödinger perturbation approach is preferable to the Brillouin–Wigner one, since the former is size-consistent while the latter is not. The Rayleigh–Schrödinger (RS) PT can be formulated by means of the diagrammatic many-body approach (MB–RSPT) [63, 147, 668, 1378]. This means, that the operators $\hat{H}^0$ and $\hat{H}$ are expressed in their second quantized forms [39, 653] and the perturbation formulae are represented by special diagrams serving as an efficient book-keeping technique for the rather complicated expressions [456] (see also [181]). The correlation energy at the various orders can be calculated by explicit formulae. The first order energy correction to the correlation energy in the MB–RSPT is zero if the Møller–Plesset partition is used, while at the second order one has:

$$E^{\text{corr}} \approx \sum_{ijk^*l^*} \frac{2(ik^*|jl^*)-(il^*|jk^*)}{\varepsilon_i+\varepsilon_j-\varepsilon_{k^*}-\varepsilon_{l^*}}(ik^*|jl^*) \tag{1.131}$$

where ε_i is the HF orbital energy.

By calculating the second order energy correction *via* Eq. (1.131) one obtains a rough estimate of the total correlation energy. The formulae at the third order are more complicated but still tractable. The third order MB–RSPT usually yields a satisfactory account of the correlation energy. There exist also fourth order calculations for small molecules.

It is to be emphasized that the total energy of a molecule as obtained by a perturbation procedure is not an upper bound to the exact energy. Moreover, the condition of the success of the MB–RSPT approach is that the HF wave function itself be more- or less reliable otherwise the perturbation becomes large and the series of energy corrections does not converge properly. If the HF approximation represents a good initial guess, the MB–RSPT approach serves as a relatively economic and widely-applicable tool in calculating the correlation energy.

(6) *Electron pair methods.* Some of the most successful approaches in the theory of electron correlation are based on the physical model which assigns a correlation energy contribution to electron pairs, and calculates these contributions separately. As was noted above, the correlation energy can be written exactly as a sum of pair contributions, *cf.* Eq. (1.127), and the aim of various electron pair methods is to guess these pair contributions. The simplest model is to consider the electron pairs assuming that their correlation is completely independent of each other—this is the independent electron pair approximation (IEPA) [747]. In the IEPA model one performs a small but accurate CI for each pair of occupied spinorbitals, using the whole set of virtual MOs in each CI subproblem. The resulting pair correlation energies are simply summed up. In other words, the IEPA treats each pair of electrons in the HF field (averaged electrostatic interaction by the other electrons treated at the HF level only). The IEPA is size consistent but it often significantly overestimates the correlation energy. The low cost of the calculations, however, permits us to apply the IEPA in many studies of correlation effects.

A very successful refinement of the electron pair model is represented by the coupled electron pair approximation (CEPA) proposed by Meyer [898]. In solving the CI problem for a given electron pair, the CEPA takes into account that the motion of other electron pairs is also correlated. As a consequence, the CEPA equations are to be solved iteratively. Similar to the IEPA, the CEPA also offers a size consistent method. The CEPA energies do not represent an upper bound, but they are usually so accurate that it doesn't matter. The results of the CEPA calculations are in excellent agreement with experimental results, provided that the basis set is sufficiently large and the HF wave function is not extremely bad. Due to the breakdown of the HF approximation, dissociation curves cannot be studied by CEPA, but it leads to very good potential curves in a rather wide interval around the equilibrium nuclear configurations.

that is, the correlation energy can be expressed as the sum of pair correlation energies ε_{ij}. Eq. (1.125) shows that, in order to calculate the correlation energy, one needs only the coefficients of the doubly excited configurations. These coefficients, however, are affected indirectly by all configurations. Practically, one must truncate somewhere the expansion (1.123) (which would be infinite if the set of MOs were complete), since only a finite matrix can be diagonalized in actual calculations. Moreover, not even the finite "full CI" problem corresponding to a given finite basis set is tractable usually. (For some impressive examples performing full CI computations, see Refs [66, 515, 1228].)

The rate of convergence of this expansion is very low (this is one of the bottlenecks in the theory of correlation), and the number of independent configurations (the dimension of the CI matrix) increases very rapidly. Therefore the straightforward application of the CI method (usually referred to as "brute force CI") soon becomes prohibitive as one considers larger systems and/or higher excitations.

Another problem is that in the elements of the CI matrix there appear two-electron integrals expressed over MOs φ_i which are complicated combinations of the integrals over the basis AOs:

$$(ij \mid kl) = \sum_{\mu\nu\lambda\sigma} c_{i\mu} c_{j\nu} c_{k\lambda} c_{l\sigma} (\chi_\mu \chi_\nu \mid \chi_\lambda \chi_\sigma) . \tag{1.128}$$

Here the $c_{i\mu}$'s are the LCAO-MO coefficients and χ_μ's are the atomic basis orbitals. The two-electron integrals over AOs can be evaluated directly (they are usually available, as they are necessary for the SCF calculation); the $(ij \mid kl)$ integrals over the MOs are to be computed by an integral transformation procedure which, even if is optimally organized, needs a computation time proportional to the 5th power of the number of basis functions [1326]. Therefore, especially for larger systems, CI calculations are much more expensive than SCF calculations where the computer time increases at most as N^4.

As a consequence of the above computational difficulties, the effective organization of the CI procedure is of crucial importance. Among several technical ideas, we mention the "direct CI" method of Roos and Siegbahn [1188] who could obtain the CI energies and coefficients avoiding the explicit construction of the CI matrix. A very promising tool is the unitary group approach proposed originally by Paldus [1058], and reformulated later by Shavitt [1264, 1265]. Shavitt's formulation, the graphical unitary group approach (GUGA), permits us to solve the CI problem in an extremely effective manner by analysing mathematically the structure of the CI matrix. As a consequence, GUGA calculations are faster by about an order of magnitude than the best conventional CI computations.

An important tool in accelerating the convergence of the expansion in Eq. (1.123) is the use of natural orbitals (see Section 1.2.3). The HF orbitals themselves can be considered as "approximately natural" in the sense that they diagonalize the HF first order density matrix, which is often very close to the exact one. If one constructs a correlated but still approximate wave function, for example, by a truncation of the

series (1.123), a new first order density matrix can be obtained, which is no more diagonalized by the HF MOs. The diagonalization of this correlated density matrix leads to new orbitals which are closer to the natural ones ensuring in this manner a better convergence of the CI expansion. The drawback of this procedure is the need of the repetition of the expensive integral transformation step.

In actual applications of the CI method one must somehow reduce the number of configurations considered. This introduces new approximations into the theory and the reliability of these new approximations is not always clear. Therefore, the correlation problem cannot be considered to be solved by the present state-of-art to the same extent as is the HF problem of molecules. The simplest way of reducing the size of the CI is the aforementioned truncation of the expansion (1.123). That is, all occupied and virtual MOs are used, but only some specified type of configurations are considered. A common method is the single + double (SD) CI where one constructs all the singly and doubly excited configurations, but neglects higher excitations. (Note that single excitations do not interact with the HF ground state by virtue of the Brillouin theorem. As a consequence, singly excited configurations appear only through the interaction with the doubly, and possible higher, excitations. Doubly excited configurations are, therefore, the most important terms of the CI expansion, following the leading HF determinant.)

The main problem with the CI–SD procedure is that it violates the *size-consistency* requirement: it is obvious that the energy of a system consisting of two noninteracting subsystems must be the sum of the energy of the separated subsystems. This requirement is very important in comparing molecules of different size. It is easy to show, however, that a CI–SD procedure performed for the "supersystem" is not size-consistent. Let us consider, for example, a He atom for which the energy is obtained by an SCF + CI procedure the latter being a CI–SD (no higher excitations exist for a two-electron system, of course). If two noninteracting He atoms are computed simultaneously, the full CI wave function is an appropriately antisymmetrized product of the wave functions of the two individual atoms. So it contains quadruply excited configurations as well, namely the product of the two local double excitations on both He atoms. Such quadruply excited configurations are dropped if a straightforward CI–SD procedure is performed for the He–He supersystem which leads to an energy higher than the sum of the energies of the two He atoms. A useful approximate formula which permits us to estimate the energy loss ΔE due to size-inconsistency in the CI–SD procedure was proposed by Langhoff and Davidson [761]:

$$\Delta E = (1 - C_{\mathrm{HF}}^2) E_{\mathrm{SD}}^{\mathrm{corr}} \tag{1.129}$$

where $E_{\mathrm{SD}}^{\mathrm{corr}}$ is the correlation energy obtained by the CI–SD approach and C_{HF} is the coefficient of the HF configuration in the CI expansion of the *normalized* wave function.

Another shortcoming of the CI–SD method is that it does not account for the dissociation of molecules with multiple bonds properly, since it contains the inherent error of the MO model. At equilibrium interatomic distances, however, the CI–SD

[340, 341, 356]. The SAMO Fockian is constructed by transferring its elements from calculations on smaller pattern molecules.

There are nonempirical Hartree–Fock–Roothaan schemes, which are not *ab initio* in a strict quantum chemical sense, but in which different approximations are made for the $(\mu\nu|\lambda\sigma)$ two electron integrals.

The ZDO approximation (see below) which is widely used in semiempirical models is too drastic to be applied in a nonempirical theory, though many of the three- and four centre integrals, as well as the $(\mu\nu|\mu\nu)$ two-centre exchange-type integrals can be very small. This feature leads to the introduction of the method of "partial retention of the diatomic differential overlap", PRDDO [504, 505].

Several approximate formulae have also been proposed to estimate polycentric integrals. For the approximation of the charge distribution $(\mu\nu)=\chi_\mu(\mathbf{r})\chi_\nu(\mathbf{r})$ due to the product of two different orbitals (usually called differential overlap, see below), Mulliken proposed the following expression [946]:

$$(\mu\nu)=\frac{1}{2}S_{\mu\nu}[(\mu\mu)+(\nu\nu)]$$

where $S_{\mu\nu}$ is the overlap integral of the orbitals μ and ν.

Using 1.152, the two-electron integrals in the Mulliken approximation become:

$$(\mu\nu|\lambda\sigma)=\frac{1}{4}S_{\mu\nu}S_{\lambda\sigma}[(\mu\mu|\lambda\lambda)+(\mu\mu|\sigma\sigma)+(\nu\nu|\lambda\lambda)+(\nu\nu|\sigma\sigma)].$$

This approximation often reflects correctly the qualitative features of a multicentre integral, but the introduced error can be rather large especially for very small and very large internuclear distances. Other possibilities for evaluating approximately multicentre integrals were proposed *e.g.* by Sklar [1283], Čižek [217] and Ruedenberg [1201]. These integral approximation schemes can, in principle, be incorporated into nonempirical methods, though no widely accepted quantum chemical method has yet been proposed making use of one of these approximations. A promising tool in developing a successful approximate but nonempirical procedure, applying a Ruedenberg-like approximation, is offered by Mayer's "chemical Hamiltonian" method [886].

1.3.2 SEMIEMPIRICAL METHODS

Indications and philosophy of semiempirical schemes. Computer time and storage requirements of *ab initio* procedures make computations on large molecules prohibitive. *Ab initio* SCF calculations can be routinely performed only up to 100–150 basis orbitals. For comparison, the benzene molecule in the 4-31G and 4-31G* basis sets possesses 66 and 96 basis orbitals, respectively. Computations on slightly larger systems are still possible but very expensive. In addition, the answer to many

chemically interesting questions requires more than one computation on the same molecule (geometry optimization, potential surface scan, etc.). The speed of the computer is certainly an important factor, but since the computational time increases with the fourth power of the number of basis orbitals, if the speed increases by as much as an order of magnitude, this allows only the treatment of a roughly two times larger molecule.

Thus, many molecules of chemical and biological interest are not available for *ab initio* computations. This makes it necessary that new approximations be incorporated which allow us to reduce the computer time by *several* orders of magnitude. Such approximations concern the neglect of overlaps between some AOs, the neglect of certain types of one- and two-electron integrals, approximate evaluation of integrals, and the restriction that only certain groups of electrons (valence or π-type) be treated explicitly. These approximations could easily destroy the reliability of the procedures, since they are, from the numerical point of view, rather crude or sometimes even quite unrealistic. Within the given approximation scheme, however, some quantities appear which can be estimated by making use of experimental data. For example, one-centre integrals in the diagonal elements of the core Hamiltonian can be related to the atomic ionization potential *(see below)*, which can be taken from experiment instead of being computed analytically. In this manner the computational work decreases further, and, what is much more important, the incorporation of empirical data may compensate for some of the errors due to the crude approximations. Such procedures are called *semiempirical.* A semiempirical calculation presupposes the specification of the empirical parameters as well. The parameters can be taken not only from experiments but also from some model calculations on other (*e.g.*, smaller) molecules. As we will see later, there exist extremely simple semiempirical methods which, despite the inherent rough approximations, work unexpectedly well, providing sometimes finer results than *ab initio* procedures using small basis sets. Therefore, theoreticians often try to derive the semiempirical schemes by searching for the justifications or theoretical basis of these (otherwise heuristic) models. In spite of considerable effort in this field [301, 390, 409, 1065, 1066] the theoretical backgrounds of most semiempirical methods, explaining their success and failures, are not yet completely understood.

The philosophy of the parametrization of semiempirical schemes is slightly controversial. Roughly speaking, there are two main ways for finding the "best" parameters. One possibility is to consider the semiempirical method as providing some "interpolation formula" among experimental results based on an ensemble of selected sample molecules: the parameters can be determined, for example, by a least-square fit procedure in order to reproduce properties of that class of molecules as exactly as possible. Then, it is expected that a computation on a new molecule using the same parameter set will yield results of an accuracy similar to the standard deviation of the least-square fit. The advantage of this method of selecting the parameters is that it often leads to very accurate predictions. The disadvantage is that the results are expected to be satisfactory only if the electronic structure of the molecule under study is at least

Considering its very high power, the time requirement of a CEPA run is quite economic, since for small molecules, for example, it is comparable with that of the HF procedure including the integral evaluation [182]. For a recent application, see for example [1303].

We note that the use of approximate (pseudo-) natural orbitals combined with the electron pair model leads to the pair-natural orbital (PNO) scheme [6, 661, 744].

(7) *Other approaches.* Some other methods for taking correlation effects into account should be mentioned. The cluster expansion of the wave function [1281, 1282] serves as a theoretical framework of various alternative approaches, including the methods discussed above. Sinanoğlu's many electron theory [1281], the coupled cluster method [218, 1059], and the coupled-pair many electron theory [747] are based explicitly on the cluster expansion. Nesbet's formulation of the Bethe–Goldstone method represents a variational approach [999]. The methods using two-electron functions, called also *geminals* [611, 665, 666] are related to the IEPA and to the VB and GVB models [1063]. The antisymmetrized product of strongly orthogonal geminals (APSG) approximation [6] is worth mentioning. Geminals can also be combined with many-body perturbation theory [1332]. The electron propagator methods [652, 795, 1018, 1033, 1069, 1100, 1279] are of extreme importance in obtaining accurate excitation energies, ionization potentials and electron affinities, because they offer the possibility of calculating these energy differencies directly (*i.e.*, not as a small difference between the large energies of two states). There is no room here to discuss these methods, but the quoted references permit the interested reader to find the necessary informations (see also [64, 67, 1123, 1330a]).

There is a continuous effort in present-day quantum chemistry to develop more and more efficient algorithms and methods which make it possible to go beyond the HF scheme in cases of larger and larger (and perhaps chemically more and more interesting) molecules. The success of electron pair methods suggests that good physical models are needed even in this field. However, the treatment of really large organic molecules and inorganic complexes by means of *ab initio* methods, whether they account for correlation or not, is prohibitive at present. This is possible only by the so-called nonempirical methods applying rather crude approximations (see below), or by semiempirical procedures which will be discussed in the next section.

Nonempirical methods. Before closing this section we have at least to mention some quantum chemical procedures which are neither *ab initio* in a strict sense nor semiempirical in the conventional manner. Their common features are (1) the introduction of certain approximations which are not admitted in the pure *ab initio* framework, and (2) the approximate formulae used do not contain empirical parameters. The use of pseudopotentials discussed in Section 1.2.6 may belong to this category, provided that the pseudopotential is derived by some analytical consideration and not parametrized empirically.

Another attempt in the HF method concerns the approximation of the nonlocal exchange operator. In the X_α method [239, 424, 425, 1288] proposed originally by Slater, one approximates the exchange interaction by the following *local* potential:

$$U^X(\mathbf{r}) = -3\alpha\left[\frac{3}{8\pi}\rho(\mathbf{r})\right]^{1/3} \tag{1.132}$$

where $\rho(\mathbf{r})$ is the electron density, and α is a parameter* in the 2/3-1 range. In spite of the presence of this parameter, the X_α method is not considered as semiempirical since analytical considerations were originally invoked to derive the value for α. These considerations are based on the theory of free-electron gas. Different derivations lead to slightly different values for the parameter α. In the name of the method, the "α" refers to this parameter while "X" refers to "exchange". If no further approximation is made, the X_α is called also the Hartree–Fock–Slater method. The advantage of the X_α method lies in its simplicity which is achieved by using the local exchange potential (1.132). The X_α method obeys the Hellmann–Feynmann and the virial theorems.

The Hartree–Fock–Slater approximation was proposed originally to make the approximate solution of the atomic *numerical* HF problem easier. Compared with the simple Hartree method, the main difficulty in the atomic HF procedure is the handling of the nonlocal exchange operator. This problem is by-passed if we use the approximate formula (1.132).

Johnson introduced a further approximation into the X_α model [645]. In this version the interatomic potential is called properly the "muffin-tin" potential referring to its characteristic shape. The molecule is divided into closely packed spheres around all atoms; the potential inside the spheres is $1/r$ (r is the distance from the centre of the sphere in question), while it is constant outside the spheres. The whole molecule is embedded in a larger sphere outside of which the potential is again $1/r$. This represents a very great simplification, thus great saving of computational time; however, the method is somewhat ambiguous.

As to the accuracy of X_α calculations, it is very good for individual atoms but slightly uncertain for molecules. The X_α excitation energies are usually better than those calculated by HF orbitals. Obviously, the X_α method to some extent fills a gap between *ab initio* and semiempirical calculations. In our opinion, however, the intuitive steps leading to the X_α scheme are based on a very physical model and not on a chemical one in the sense that the concept of chemical bonding is not incorporated. Anyway, the usefulness of the X_α method is unquestionable for many systems as in, for example, transition metal complexes.

Nonempirical schemes sometimes try to utilize the fact that much information about the electronic structure of a larger molecule is available from calculations on smaller component subunits. Such an example is the simulated *ab initio* MO (SAMO) method

* Not to be confused with the Coulomb parameter in the Hückel method.

thogonal AOs $\{\chi_\mu\}$ as much as it is possible in the least-square sense, *i.e.* $\sum_\mu \|\chi_\mu - \varphi_\mu\|^2$ is minimal*.

It was shown that the values of different integrals neglected by the ZDO approximation are really small if one turns to a Löwdin-orthogonalized atomic basis set, while the values of the pure Coulomb integrals are not much affected.

It is important to notice, that in approximating the off-diagonal matrix elements of the core Hamiltonian the ZDO condition cannot be completely utilized. The core matrix element is

$$H^c_{\mu\nu} = \left\langle \chi_\mu \left| -\frac{1}{2}\Delta - \sum_A Z_A/r_A \right| \chi_\nu \right\rangle \tag{1.135}$$

so it contains the kinetic energy operator for the matrix element of which the ZDO approximation cannot be used. In fact, in the integral $\langle\chi_\mu|\Delta|\chi_\nu\rangle$ differential overlap $f_{\mu\nu} = \chi_\mu(\mathbf{r})\chi_\nu(\mathbf{r})$ does not really appear because Δ is a differential operator. Thus off-diagonal $H^c_{\mu\nu}$ matrix elements should be evaluated or parametrized even in ZDO methods. This is, however, a formal reasoning and it is much more important that one must keep at least some of the matrix elements $H^c_{\mu\nu}$ $(\mu \neq \nu)$ in order to have a reliable model. As we will see later, in the ZDO schemes just these types of matrix elements are responsible for the appearance of the chemical bonding.

All-valence-electron schemes. Semiempirical methods usually do not include inner shell orbitals. (Pseudopotentials are often parametrized semiempirically, but then the valence shell is mostly treated at the *ab initio* level.) As was already discussed in Section 1.2.6, the so-called all-valence-electron schemes emerge if one compresses the core electrons into the nuclei, and works with an effective core charge of atom A:

$$Z^c_A = Z_A - n^c_A \tag{1.136}$$

where Z_A is the atomic number and n^c_A is the number of the inner shell electrons. Accordingly, one deals explicitly only with the valence orbitals, *e.g.* with $1s$ AO for hydrogens and with the $2s$, $2p_x$, $2p_y$, and $2p_z$ AOs for the first row atoms.

One of the most successful semiempirical all valence electron methods is referred to as "complete neglect of differential overlap", CNDO [1121]. This makes a consequent use of the ZDO approximation, complemented by the assumption that the surviving two-electron integrals depend only on the kinds of atoms in question, and are independent of the azimuthal quantum number of the AOs. For the main group elements in which all the valence electrons have the same principal quantum numbers

* Another important procedure is the successive orthogonalization of the orbitals called Schmidt-orthogonalization. Here a reference orbital is picked up which remains unchanged. The second orbital is modified by mixing a component of the reference orbital to it by demanding orthogonality. Then a third orbital is selected and orthogonalized to the first two, etc. Obviously, the result of the Schmidt procedure depends on the order of selecting the orbitals. Such an unsymmetric procedure is useful, for example in orthogonalizing the STOs to mimic the orthogonal AOs—here the 1s AO can be chosen as a reference since it has no nodal surface.

one simply has:

$$(\mu\mu|\nu\nu)=\gamma_{AB} \tag{1.137}$$

where $\mu \in A$ and $\nu \in B$. The use of Eq. (1.137) is necessary for preserving the rotation and hybridization invariance of the ZDO model, which requires that the results of the calculations should be invariant if one performs a unitary transformation mixing basis orbitals centred on the same atom. The γ_{AB} integrals are evaluated for *s*-type Slater orbitals either analytically or by using some approximate formulae (*see below*). The elements of the Fockian then become:

$$F_{\mu\nu}=H_{\mu\nu}+\delta_{\mu\nu}\sum_{C}\gamma_{AC}\sum_{\lambda\in C}P_{\lambda\lambda}-\frac{1}{2}P_{\mu\nu}\gamma_{AB} \tag{1.138}$$

where the label C runs over all atoms of the molecule.

The most widely used version of CNDO-type methods is the CNDO/2 [1121]. Here the diagonal elements of the core Hamiltonian are written as

$$H_{\mu\mu}=\left\langle \mu\left| -\frac{1}{2}\Delta-r_A^{-1}\right|\mu\right\rangle-\sum_{B\neq A}\left\langle \mu\left| r_B^{-1}\right|\mu\right\rangle \tag{1.139}$$

for $\mu \in A$. The first term is monoatomic, and the second term is diatomic, describing kinetic energy and the interaction of the electron on the orbital χ_μ with the core of that and other atoms, respectively. The one-centre term is calculated semiempirically by relating it to the average of the experimental atomic ionization potential I_μ and the electron affinity A_μ *via*

$$\left\langle \mu\left| -\frac{1}{2}\Delta-r_A^{-1}\right|\mu\right\rangle=-\frac{1}{2}(I_\mu+A_\mu)+\left(\frac{1}{2}-Z_A\right)\gamma_{AA}.$$

The two-centre term is approximated heuristically [1121] as

$$\langle\mu|r_B^{-1}|\mu\rangle=Z_B\gamma_{AB}. \tag{1.140}$$

The off-diagonal two-centre matrix element $H_{\mu\nu}$ ($A\neq B$, $\mu \in A$, $\nu \in B$) is called the resonance integral; it is characteristic of the strength of the binding between orbitals χ_μ and χ_ν. The resonance integrals (often called also beta-integrals) in the CNDO scheme are approximated as

$$H_{\mu\nu}=\frac{1}{2}(\beta_A^0+\beta_B^0)S_{\mu\nu} \tag{1.141}$$

where the β_A^0's are the bonding parameters determined semiempirically to give the optimal fit to the results of *ab initio* calculations on diatomics. The overlap integrals $S_{\mu\nu}$ are evaluated over STOs analytically. (For the aforementioned reason, the ZDO approximation must not be applied here. We shall note once again that the overlap integrals $S_{\mu\nu}$ ($\mu\neq\nu$) are absent in the formalism due to the ZDO assumption; they are, however, used to determine the values of the core parameters $H_{\mu\nu}$.) The one-centre off-

slightly similar to that of the set of molecules for which the parameters are obtained (*e.g.*, no bonds of a quite new type occur). Moreover, only those properties can be studied which were considered in the fitting procedure: parameter sets providing, for example, good molecular geometry may predict false spectroscopic properties and *vice versa*. Furthermore, it is also obvious that this parametrization scheme does not use any physical model, it allows us to gain only limited insight into atomic contributions, and many may have therefore present some difficulties in chemical interpretation.

Another possibility for finding appropriate semiempirical parameters is to relate them to certain chemically meaningful properties. We have mentioned above the experimental ionization potentials which, together with experimental electron affinities, can be used for estimating one centre core matrix elements. Two-centre off-diagonal core integrals are characteristic of two-centre binding. One-centre two-electron integrals can also be related to atomic energy levels, etc. This method of parametrization offers perhaps a less accurate fit to experimental data, but the resulting method may have a wider range of applicability. The main advantage of this parametrization scheme lies in its conceptual simplicity.

Ab initio methods, using sufficiently large basis sets and a sophisticated wave function, are in principle able to reproduce experimental results for any properties and they can be used instead of a measurement if experimental predictions are not available. The same is not true for semiempirical methods which may sometimes contradict experiments as a consequence of the crude approximations applied, or the inappropriate parameter set. The main aim of semiempirical procedures is not to substitute but to supplement the experimental results by providing a possibility of interpreting the experiments, *cf.* assignation of excitation spectra. There can be, of course, some special fields of application where the reliability of the semiempirical method in question has already been proven; thus one can use the approximate method even in the absence of the experimental control. Such calculations, however, are to be handled always with some care. Fortunately, the very large number of diverse semiempirical calculations documented in the literature permits one to draw conclusions easily on the reliability and shortcomings of different semiempirical methods.

Further on in this section we will discuss the typical features of most widely used semiempirical techniques. Theoretical backgrounds of the methods will not be treated here in detail. As some useful references, we mention the monograph by Pople and Beveridge [1121], the volume edited by Segal [1253], and Salem's [1219] and Streitwieser's [1313] books on π-electron theory.

The zero differential overlap scheme. Before reviewing the actual methods, it is worthwhile to discuss a special feature of many semiempirical procedures. The scalar product of the atomic orbitals χ_μ and χ_ν is defined as their overlap integral:

$$S_{\mu\nu} = \langle \chi_\mu | \chi_\nu \rangle = \int \chi_\mu(\mathbf{r}) \chi_\nu(\mathbf{r}) \, \mathrm{d}V = \int f_{\mu\nu}(\mathbf{r}) \, \mathrm{d}V$$

where, if $\mu \neq \nu$, the function $f_{\mu\nu}(\mathbf{r})$ equal to the product of basis functions $\chi_\mu(\mathbf{r})\chi_\nu(\mathbf{r})$ is

usually called the *differential overlap* of the orbitals χ_μ and χ_ν. If χ_μ and χ_ν are centred on far-lying atoms or they are of quite different orientations in space, their differential overlap $f_{\mu\nu}(\mathbf{r})$ is nearly zero for all $\mathbf{r}$. This feature is often utilized in semiempirical methods by neglecting all or most of the integrals where $f_{\mu\nu}$ $(\mu \neq \nu)$ is present [1064, 1119]. If all such integrals are neglected, we arrive at the so-called *zero differential overlap* (ZDO) approximation. The ZDO assumption implies that the overlap integral matrix, $\mathbf{S}$ becomes the unity matrix, as we obtain:

$$\mathbf{S}_{\mu\nu} = \int f_{\mu\nu}(\mathbf{r})\, \mathrm{d}V = \delta_{\mu\nu}. \tag{1.133}$$

Note that the opposite statement is not true: the orthogonality of two orbitals does not necessarily mean that their differential overlap is zero everywhere.

Semiempirical methods applying the ZDO condition are usually referred to as "ZDO schemes".

The ZDO approximation represents a drastic simplification. Not only the orthogonality of the basis orbitals follows immediately from it, but also most multicentre two-electron integrals vanish:

$$\begin{aligned}(\mu\nu|\lambda\sigma) &= \int \chi_\mu(\mathbf{r}_1)\chi_\nu(\mathbf{r}_1) r_{12}^{-1} \chi_\lambda(\mathbf{r}_2)\chi_\sigma(\mathbf{r}_2)\, \mathrm{d}V_1\, \mathrm{d}V_2 \\ &= \int f_{\mu\nu}(\mathbf{r}_1) r_{12}^{-1} f_{\lambda\sigma}(\mathbf{r}_2)\, \mathrm{d}V_1\, \mathrm{d}V_2 \\ &= \delta_{\mu\nu}\delta_{\lambda\sigma}(\mu\mu|\lambda\lambda).\end{aligned} \tag{1.134}$$

That is, only the one-centre and some two-centre two-electron integrals survive. The two-centre integrals $(\mu\mu|\lambda\lambda)$ which are conserved in the ZDO theory describe the Coulomb repulsion between electrons on AOs χ_μ and χ_ν. As a consequence of Eq. (1.134), the construction of the Fockian, the computation of the energy, etc. become very simple and very fast in ZDO methods. As to they reliability of the ZDO approximation, it is far from being accurate: the differential overlap of orbitals centred on the same or on neighbouring atoms can be rather large. Therefore, one cannot expect that ZDO methods provide good numerical approximations to exact theories. However, justifications of the ZDO approximation have been widely discussed in the literature [390, 391, 1066]. One important reasoning is based on the use of Löwdin-orthogonalized orbitals.

It is well known from elementary mathematics that a set of nonorthogonal functions $\{\chi_\mu\}$ with an overlap matrix $S_{\mu\nu}$ can be transformed into an orthogonal set $\{\varphi_\mu\}$ by an appropriate linear transformation $\varphi_\mu = \sum_\nu t_{\nu\mu}\chi_\nu$. The choice for the transformation matrix $\mathbf{t}$ is not unique: orbitals obtained by different orthogonalization procedures from the same nonorthogonal set are related to each other by a unitary transformation. If one chooses $t_{\nu\mu} = (\mathbf{S}^{-1/2})_{\nu\mu}$ one speaks about the *symmetric* or *Löwdin-orthogonalization* [819]. The φ_μ's then are called *Löwdin-orbitals* and have the important property that though $\langle\varphi_\lambda|\varphi_\sigma\rangle = \delta_{\lambda\sigma}$, they resemble the original nonor-

TABLE 1.5

The reliability of all-valence electron methods

Method	Geometry	Conformation	Charge distribution	Spin density	Electronic excitation
CNDO/2	Good	Good	Good	Bad	Poor
CNDO/S	Bad	Poor	Poor	Bad	Good
INDO	Good	Good	Good	Good	Poor
MINDO/3	Good	Good	Good		Poor
MNDO	Good	Good	Good		Poor
EHT	Bad	Good	Bad	Bad	Bad

diagonal core matrix elements, $H_{\mu\nu}$ ($\mu \neq \nu$, A = B) are taken equal to zero since no direct chemical binding between different orbitals on the same atom exists.

Due to the orthogonality of the AOs which follows from the ZDO assumption, the HFR equations are written simply as

$$\sum_{\nu} F_{\mu\nu} c_{k\nu} = \varepsilon_k c_{k\mu}. \tag{1.142}$$

The set of semiempirical parameters $\frac{1}{2}(I_\mu + A_\mu)$ and β_A^0, together with the above equations, define completely the CNDO/2 model. This heuristic method is very simple (it requires computations proportional only to the third power of the number of basis orbitals), but accounts for many important tendencies and often leads to qualitative or semiquantitative agreement with experimental results for ground state electronic properties (see Table 1.5).

The most important reparametrization of the CNDO scheme is the CNDO/S method [294, 295, 359] where 'S' refers to the term 'spectroscopic'. In this version the semiempirical parameters are changed to provide better energies of electronic excitations. For the same reason Eq. (1.141) is modified as

$$H_{\mu\nu} = \frac{1}{2} k(\beta_A^0 + \beta_A^0) S_{\mu\nu} \tag{1.143}$$

where $k = 1$ if orbitals χ_μ and χ_ν are of type σ, while $k = 0.585$ if they are of type π. The Coulomb repulsion integrals are not evaluated analytically as in the CNDO/2 scheme, but they are parametrized empirically. The one-centre integrals γ_{AA} are chosen as [294]:

$$\gamma_{AA} = I_A - A_A \tag{1.144}$$

where I_A is the experimental ionization potential, A_A is the electron affinity of atom A. The two-centre integrals γ_{AB} are obtained by the approximate Mataga–Nishimoto [1021] formula:

$$\gamma_{AB} = [r_{AB} + 2/(\gamma_{AA} + \gamma_{BB})]^{-1} \tag{1.145}$$

where r_{AB} is the distance of atoms A and B. (Note that in an earlier version of the CNDO/S method another expression was used.)

The SCF step in the CNDO/S calculation is often followed by a limited CI calculation for the excited states formed of the singly excited configurations. That is, the ground state wave function remains a single determinant while the excited state wave function is represented by a linear combination of singly excited determinants. If all possible single excitations are involved, one speaks about an "all single" CI. (The name "Tamm–Dancoff approximation", TDA, is also often used.) The purpose of this CI is not to account for correlation effects (though the excited state contains some correlation), but merely to offer a more reliable description of the excited state configurations. As a matter of fact, a spin-adapted excited wave function resulting from a single excited configuration is not invariant to a unitary transformation of the occupied (or virtual) MOs (*cf.* Sections 1.2.4 and 1.4), thus it should be considered as ambiguous. Excited states obtained by an all-single CI obey such invariancy, similar to the ground state. For larger molecules, the size of this CI is quite large, thus in actual computations only some of the singly excited determinants are considered usually. The selection of the most important configurations requires some care and experience.

The CNDO/S + CI method has been successfully used for calculating low lying electronic transitions of some molecules, but the generality of this scheme is much less than that of the CNDO/2 for ground state properties.

As widely documented in the literature, and as will be discussed in several examples throughout this book, the cost/performance ratio is very advantageous for the CNDO scheme. There are, however, some special fields of applications where it cannot be used due to the approximations inherent in this model. An example is the case when the role of inner shell electrons is important; one cannot then apply a valence-electron model. Furthermore, several properties of open shell systems cannot be studied by CNDO methods due to the ZDO approximation. As a matter of fact, the neglect of the one-centre $(\mu\nu|\mu\nu)$ $(\mu, \nu \in A)$ exchange-type integrals for $\mu \neq \nu$ results in the failure of the CNDO method in predicting correctly the energy splitting between states of the same configuration but different multiplicities. Similarly, spin densities as calculated by the UHF–CNDO method are usually wrong. (We have described above the CNDO method for the closed shell RHF case. Its extension to the UHF level [1121] is also quite straightforward and it is a part of most CNDO programs.) These shortcomings can be eliminated by retaining the $f_{\mu\nu}$ monoatomic differential overlap $(\mu \neq \nu, \mu, \nu \in A)$ in one-centre two-electron integrals $(\mu\nu|\mu\nu)$. These integrals can be determined empirically by means of the spectroscopic Slater–Condon parameters [1287] which are tabulated for each atom to give best fits to atomic energy levels. The resulting semiempirical scheme is called the intermediate neglect of differential overlap (INDO) method [1121]. For closed shell systems, the results of INDO calculations are similar to that of CNDO/2 (the standard INDO calculation uses the same values for the $\frac{1}{2}(I_\mu$

$+A_\mu$) and β_A^0 parameters as CNDO/2 does). For open shell systems, for example to study ESR spectra, one should use preferably the INDO method.

Various reparametrizations and modifications of the INDO scheme have been published in the literature. One of the most important ones is the family of MINDO [318] ("modified INDO") methods (MINDO/2, MINDO/3). This scheme uses a large number of semiempirical parameters which are determined by least-square fit procedures to reproduce heats of formations and molecular geometries. As a result, these quantities can be calculated by MINDO/3 with quite good accuracy. At the present time, probably this scheme is the most popular one among the all-valence electron semiempirical methods. Conceptually, a further improvement of the INDO approximation is possible by retaining the monoatomic differential overlap even in the two-centre integrals, that is, to neglect only the integrals with a differential overlap of AOs centered on different atoms. This approach is called the "neglect of diatomic differential overlap", NDDO [1121]. The approximations inherent in this scheme are much less drastic than the ZDO, and, certainly, they could be more easily established theoretically. Despite this, the NDDO method was not so widely used as CNDO or INDO due to its relative complexity and since no standardized set of semiempirical parameters had been proposed [105, 700, 1325] until the introduction of the "modified neglect of diatomic differential overlap" (MNDO) method [323]. This latter scheme is a reparametrization of the NDDO method according to the philosophy of the MINDO methods described previously. The MNDO method is proven to be superior to MINDO/3 in most applications.

Among the all-valence-electron semiempirical methods, a very promising approach, the HAM/3 method [37, 37a, 147a] has been proposed a few years ago. The underlying theory is based on Slater's atomic shielding concept. Although it is not easy to understand the source of the success of this scheme, the HAM/3 method has been used to predict diverse molecular properties (for example, ionization potentials, excitation energies) with a surprisingly good accuracy.

Quite another type of all-valence electron method is represented by Hoffmann's "extended Hückel theory" (EHT) [575]. The name of this method reflects that EHT is, in some sense, an extension of the simple Hückel π-electron method (which will be discussed later) to the valence shell. The most important feature of the EHT is that it does not take the electron–electron interaction explicitly into account: all two-electron integrals are set equal to zero. The two-centre core-electron attraction and the core–core repulsion is neglected as well. As a consequence, one should not deal with the SCF problem but one has simply to construct the effective one-electron Hamiltonian and solve its secular equation. Formally, the EHT corresponds to a model where the electrons are completely independent, but the core Hamiltonian is parametrized in such a way that it accounts implicitly also for the interelectronic interaction. Another characteristic feature of the extended Hückel (EH) scheme is that it considers the overlap of basis orbitals explicitly, in contrast to the ZDO type schemes discussed above. That is, the HFR equations are written as

$$\sum_{\nu} H_{\mu\nu} c_{k\nu} = \varepsilon_k \sum_{\nu} S_{\mu\nu} c_{k\nu} \tag{1.146}$$

where $H_{\mu\nu}$ is the effective one-electron Hamiltonian which is now independent of the coefficients $c_{k\nu}$. The diagonal elements $H_{\mu\mu}$ are empirical parameters, related to experimental ionization potentials. The off-diagonal elements $H_{\mu\nu}$ are calculated by means of the Wolfsberg–Helmholtz formula [1433]:

$$H_{\mu\nu} = \frac{1}{2} K (H_{\mu\mu} + H_{\nu\nu}) S_{\mu\nu} \tag{1.147}$$

where K is another empirical parameter which should be chosen in the $1 < K < 2$ range. In the original EH calculations [575] the value $K = 1.75$ was used. Note that a similar expression for estimating the off-diagonal core integrals is applied in the CNDO method as well (see. Eq. 1.141).

As may be seen, the EHT offers the simplest all-valence electron method: the only thing to do in an EH calculation is to evaluate the overlap integrals $S_{\mu\nu}$ over STOs, to build up the Hamiltonian by Eq. (1.147), and solve the generalized eigenvalue problem within the nonorthogonal basis set (Eq. 1.146). The eigenvalues ε_k are interpreted as the orbital energies. The total energy of the molecule, in the absence of any explicit electrostatic effects in the theory, is simply the sum of the energies of the MOs weighted by the occupation numbers g_k:

$$E = \sum_{k} g_k \varepsilon_k \tag{1.148}$$

which, for a closed shell system, obviously reduces to

$$E = 2 \sum_{k}^{\text{occ}} \varepsilon_k \,. \tag{1.149}$$

It is not very easy to understand what effects in EHT are really accounted for. Clearly, electrostatic interactions are predominant in the electronic structure of molecules from a physical point of view, but they are still not considered explicitly. However, one cannot say that EHT neglects the electron repulsion—this would be unrealistic. What is really neglected in the EH scheme, is the *difference* of electron–electron and core–core repulsion and electron–core attraction; these quantities are of opposite signs and obviously cancel each other to a large extent. (This cancellation is complete for neutral atoms at larger distances.) Moreover, the overlap effects of basis orbitals are also very important in describing the electronic structure, and they are, in contrast to the ZDO-type methods, properly accounted for in the EHT. The surprising success of the EH scheme (mainly in qualitative models) is certainly related to the proper treatment of the overlap. There are, however, some properties in charged or very polar systems where the net electrostatic effects are predominant; thus the EH method cannot be used without further refinements. In the iterative extended Hückel

theory (IEHT) some additional charge transfer effects are taken into account by allowing the parameters $H_{\mu\mu}$ to depend on the density matrix.

The EHT turned out to be useful in calculating conformational properties (relative stabilities of conformers and barriers to rotations) of neutral and non-polar molecules, overall forms of valence shell molecular orbitals, and in studying the dependence of orbital energies on different chemical effects. The method is inappropriate for determining reasonable bond lengths and angles, isomerization energies and for describing ionization and excitation processes. An extremely important field of application for the EH scheme is the qualitative MO model, which will be discussed in Section 1.3.3.

Some benefits and limitations of the most important semiempirical all-valence electron methods are listed in Table 1.5. It should be emphasized that, in contrast to the qualification of the *ab initio* schemes in Table 1.4, the term "good" refers to a semiquantitative agreement with experimental results.

Another important all-valence electron semiempirical method is the PCILO, which will be reviewed in Section 1.4, discussing localized molecular orbitals.

π-electron methods. We have seen in Section 1.2.6 that in conjugated systems the π-electrons can be treated separately of the σ core to a certain degree of approximation. Earliest attempts in quantum chemistry were made mainly at the π electron level.

The AO basis set in a π-electron theory consists of the $2p_z$ atomic orbitals (one on each atom), provided that the conjugated molecule, which has a planar geometry, lies in the xy plane. For example, in naphthalene one has ten $2p_z$ AOs, while the all-valence electron treatment of this molecule requires the consideration of 48 valence AOs. Such a large save of computational work means that π-electron methods are, even nowadays, rather attractive if one is studying the electronic structure of large π-electron systems which are not amenable to study by more sophisticated quantum chemical methods.

In principle, π-electron theories could be formulated in an almost *ab initio* manner [474] which means that the SCF(+CI) wave functions for the π-electrons could be obtained exactly within the given $\{\chi_{2p_z}\}$ atomic basis set, assuming that the effective potential due to the σ core is specified. Unfortunately, the $\sigma-\pi$ separation, which is the theoretical basis for π-electron schemes, is usually the source of quite a rather large error which requires a semiempirical compensation in order to obtain results in agreement with experiment. Therefore, π-electron methods are usually formulated in a semiempirical framework.

An SCF π-electron theory is represented by the Pariser–Parr–Pople (PPP) method [1062, 1066, 1119]. The PPP makes use of the ZDO condition: the $2p_z$ AOs on different centres are considered to be orthogonal and all integrals containing their differential overlap is neglected. Since in the π-electron framework one has only a single AO on each centre, there are no such different levels of approximation as are CNDO, INDO, and NDDO in the all-valence electron theories. As only diatomic differential overlaps

are neglected in PPP the ZDO is not a too drastic approximation. Moreover, the justification of the ZDO by the implicit use of Löwdin-orbitals (see above) can also be invoked in connection with the PPP method [1066].

The parametrization scheme of the PPP method is similar to that of CNDO. An important difference is that the beta integrals (*i.e.* off-diagonal elements of the core Hamiltonian) are chosen empirically for first-neighbour atoms, while for others they are neglected. In parametrizing the diagonal core matrix elements the valence–state atomic ionization potentials and electron affinities are used. Only one centre γ_{AA} and two-centre γ_{AB} two-electron integrals survive the ZDO approximation. The former are chosen empirically by Eq. (1.144). The empirical determination of γ_{AA} permits us to incorporate some effects of correlation and $\sigma-\pi$ interaction implicitly. The two-centre γ_{AB} integrals are estimated in different versions of the PPP method as

$$\gamma_{\mu\nu}=R^{-1} \qquad (\mu \in \mathrm{A}, \nu \in \mathrm{B}) \tag{1.150}$$

where R is the distance between A and B; or

$$\gamma_{\mu\nu}=[R+(\gamma_{\mu\mu}+\gamma_{\nu\nu})/2]^{-1} \tag{1.151}$$

(Ohno-formula [1034]); or by the Mataga–Nishimoto approximation given in Eq. (1.145). The simple Coulombic formula, Eq. (1.148), is equal to the $\gamma_{\mu\nu}=(\mu\mu|\nu\nu)$ integral in the $R\to\infty$ asymptotics; it is easy to see that both the Mataga–Nishimoto and the Ohno formulae possess the same asymptotics. For $R\gtrsim 5\text{Å}=500$ pm Eq. (1.150) represents a very good approximation to the $(\mu\mu|\nu\nu)$ integral, and for $R\gtrsim 10\text{Å}=1$ nm it is almost exact. For small R, the $1/R$ expression slightly overestimates the value of the $\gamma_{\mu\nu}$ integrals evaluated over STOs, thus the corrections represented by Eqs (1.145) and (1.151) are justified. Moreover, in contrast to the Coulombic formula Eq. (1.150), the Mataga–Nishimoto and the Ohno formulae behave more correctly for $R\to 0$ tending to $\gamma_{\mu\mu}$ at the homonuclear case (*i.e.*, if $\gamma_{\mu\mu}=\gamma_{\nu\nu}$). (We note, however, that this customary reasoning is in disagreement with the assumption that the AO basis is tacitly Löwdin orthogonalized (I. Mayer, personal communication).) Main features of actual PPP calculations are not sensitive to the choice among the above possibilities for the two-centre $\gamma_{\mu\nu}$ integrals. Let us note that in the PPP method all integrals are determined by semiempirical parameters, none of them is evaluated over atomic orbitals. Consequently, in order to define the PPP model one need not specify the actual form of the atomic orbitals: the above parameters and integrals, together with an initial guess of the π-electron density matrix, are sufficient to construct the PPP and then the SCF procedure can be performed in the usual way.

Within the framework of the PPP method one can go beyond the SCF approximation by considering correlation effects. Obviously, only the correlation in the motion of π-electrons can be taken into account, while the correlation among σ-electrons and the σ–π correlation is neglected. A successful procedure to obtain a significant part of the π-electron correlation energy in the ground state is represented by Löwdin's "alternant MO" (AMO) method [821, 1071] which is essentially a

simplified version of the DODS EHF procedure mentioned in Section 1.2.4. Valence bond type methods are also very powerful for estimating the π-electron correlation energy [363, 798].

Being a π-electron model, the PPP method can only be used in calculating those physical properties for which the π-electrons are mainly responsible. The most important application of the PPP method is the calculation of electronic excitation spectra of conjugated systems. The energies and intensities of $\pi - \pi^*$ transitions can be obtained with a fair accuracy by an appropriate set of semiempirical parameters.

The π-electron density and some reactivity indices for conjugated systems can also be calculated successfully by the PPP method. It may be noted that the PPP model is inapplicable without further refinements to molecules having a nonplanar structure.

The Hückel method. The earliest quantum chemical method, which permitted one to perform calculations on large conjugated molecules routinely is the simple Hückel π-electron theory [1313]. The Hückel molecular orbital (HMO) method is certainly the simplest MO model: only one orbital per atom is considered and no electrostatic interaction is treated explicitly. Formally, the HMO model can be "deduced" from the PPP one by setting $\gamma_{\mu\nu} = 0$. (Actually, the HMO model is much older than the PPP one, and the latter can be considered as its refinement or generalization.) Essentially, HMO is an extremely successful heuristic model of conjugated systems. The Hückel Hamiltonian is parametrized simply in the following way:

$$H_{\mu\mu} = \alpha_\mu$$

$$H_{\mu\nu} \begin{cases} = \beta_{\mu\nu} & \text{if } \mu \text{ and } \nu \text{ are first neighbours,} \\ = 0 & \text{otherwise } (\mu \neq \nu). \end{cases} \tag{1.152}$$

The α's are called Coulomb integrals, the β's resonance integrals. The values for parameters α_μ depend on the kind of atom A($\mu \in$ A), while the parameters $\beta_{\mu\nu}$ are determined by the nature of the chemical bond between atoms having the orbitals μ and ν. A stronger bond implies a more negative value for β. By a simple shift of the origin on the energy scale the parameter α of carbon atoms is usually taken equal to zero. The β parameter of the C–C bond can be used as the energy unit. (Note that this "β-unit" is negative.)

The Hückel method implies the diagonalization of Hamiltonian (1.152), assuming that $S_{\mu\nu} = \delta_{\mu\nu}$ (*i.e.*, the set of $2p_z$ AOs is considered orthogonal). The eigenvalues of the Hamiltonian are interpreted as π-orbital energies. For the ground state of a molecule possessing $2n$ electrons, the n lowest energy orbitals are all considered as occupied by two electrons. Note that the orbitals and orbital energies are completely determined by the set of parameters α and β, and do not depend on the actual number of the π-electrons in the system*. This is a consequence of the neglect of explicit electron–electron interaction. Therefore, the orbital energies are the same for the neutral and ionized molecule in the HMO scheme.

* This is, however, far from being true in reality and is to be considered as a typical limitation of the Hückel model.

The Hückel total energy is the sum of the energies of all electrons; that is for closed shell systems Eq. (1.149) can be applied. For open shell molecules one should use the more general expression (1.148) which gives also the energy formula for the Hückel excited states.

The parameters α and β defining the Hamiltonian are usually determined merely by the nature of the corresponding atoms, and the nuclear coordinates do no enter the formalism. In other words, the Hückel Hamiltonian defined in Eq. (1.152) is closely connected to the *molecular topology*, the latter being essentially the set of classical bonding relations between the constituent atoms as indicated in usual structural formulae. The latter can be considered just as a graphic representation of the Hückel–Hamiltonian provided that all β's are equal. Therefore, a graph-theoretical analysis gives an insight into the essential aspects of the Hückel problem [476, 494].

The extreme simplicity of the Hückel method permitted one to obtain quantitative information on the electronic structure of planar conjugated systems even before the appearance of fast electronic computers. The Hückel MOs and orbital energies, as well as some physical quantities obtained from them (*e.g.*, π-electron polarizabilities), were tabulated and printed in books [260, 541] for a number of representative conjugated molecules.

At the present time, in the era of modern computers, much more sophisticated quantum chemical calculations can be performed, even for quite large molecules. Nevertheless, the simple HMO model is still timely, mainly in two respects. First, it represents almost the only possibility of obtaining semiquantitative informations on the structure of very large conjugated systems containing for example, several dozen or a few hundred atoms [688, 689, 750]. Second, and more importantly, the simplicity of the Hückel scheme allows us to develop "paper and pencil methods" which permitting to gain a qualitative understanding of the systems studied. Furthermore, we can derive many results analytically, as well as to formulate different rules concerning, for example, the relative stabilities of π-electron systems. These rules can be obtained just from the form of the Hückel Hamiltonian, or in other words, from the molecular topology. One may say that the most important value of the Hückel method lies in offering us the possibility of understanding how far the molecular topology alone determines the electronic structure of π-electron systems.

Let us see how some important quantities are defined at the Hückel level. The bond order between atoms possessing orbitals μ and ν is given by the corresponding elements of the Hückel density matrix $P_{\mu\nu}$ (*cf.* Section 1.2.5, Eq. (1.81)). The π-electron population on the atom A is given by the diagonal element $P_{\mu\mu}$ ($\mu \in$ A). The matrix **P** was originally introduced just in the HMO framework, and was called the "charge–bond order matrix". The *free valence index* of atom A, which characterizes the ability of the molecule to react with free radicals, is defined as

$$f_A = \sqrt{3} - \sum_{\substack{\nu \\ (\nu \neq \mu)}}^{\text{(nearest neighbours)}} P_{\mu\nu} \qquad (\mu \in A). \tag{1.153}$$

TABLE 1.6

Grouping of most frequent semiempirical methods. The equations in brackets indicate whether the basis set is supposed to be orthonormal [$S_{\mu\nu}=\delta_{\mu\nu}$] or not [$S_{\mu\nu}\neq\delta_{\mu\nu}$]

	all-valence electron models	π-electron models
SCF methods accounting for electrostatic interactions	CNDO INDO MINDO [$S_{\mu\nu}=\delta_{\mu\nu}$] NDDO MNDO	PPP [$S_{\mu\nu}=\delta_{\mu\nu}$]
Non-SCF methods neglecting electrostatic interactions	EHT [$S_{\mu\nu}\neq\delta_{\mu\nu}$]	Hückel [$S_{\mu\nu}=\delta_{\mu\nu}$]

Another important concept in the Hückel model is that of the delocalization energy. It is defined as follows. The conjugated molecule can be approximated as a system of independent two centre π-bonds, like the Kekulé structures of benzene. The delocalization energy is the difference between the total Hückel energy and the sum of the energies of the constituent two-centre π-bonds.

The delocalization energy measures the stability of the conjugated molecule as compared to the constituent two-centre bonds.

A very important feature of the HMO method is that several conclusions can be drawn without specifying the actual values of the parameters α and β. For obtaining quantitative results, however, numerical relations between these parameters should be established. Such considerations are often uncertain since there is some ambiguity in selecting the values for the α's and β's. More precisely, different sets of parameters must be used for obtaining reasonable estimations for physical quantities of different types. More or less balanced sets of Hückel parameters for carbon and several heteroatoms, which offer a compromise between accuracy and generality, are available in the literature [1145, 1313]. The results of Hückel calculations are worse if there are heteroatoms in the molecule studied.

The HMO model can be reliable only if (1) the role of σ electrons is negligible, and (2) net electrostatic effects are unimportant. Note that condition (1), as in any π-electron model, involves the neglect of the role of hydrogen atoms as well; σ-type substituents can be taken into account at best by their effect on the parameters of the adjacent π-centre.

A very simple semiempirical method using the philosophy of the Hückel scheme for σ electrons was proposed by Del Re [298] (see Section 1.4). An extension of the HMO scheme for describing the effect of the σ core by an empirical potential was proposed by Longuet–Higgins and Salem [812] (for a recent application, see [688, 689]).

In this section we have reviewed the most common semiempirical methods listed also in Table 1.6. In actual calculations, the choice among these methods should be directed by the nature of the problem under consideration. Before performing a semiempirical computation, one should ascertain whether the effect in question is accounted for in that semiempirical scheme, since such schemes are much less universal than *ab initio* methods.

1.3.3 QUALITATIVE METHODS IN QUANTUM CHEMISTRY

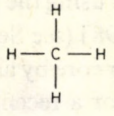
In the preceding sections the general principles of the current computational methods in quantum chemistry were outlined. Although rigorous calculations can be successfully used for the theoretical evaluation of the physical properties of individual molecules, we need also some qualitative concepts which may help to understand trends in molecular characteristics. This aim can be best accomplished by appropriate qualitative models in which theoretical and experimental data fit together. These models are invaluable tools both for theoreticians and experimentalists as means of guided speculations about molecular structure and properties, and they may serve as starting points for new experiments and more detailed quantum chemical investigations.

The qualitative quantum chemical models stress the most important aspects of the electronic structure under study and try to handle the problem without doing extensive calculations. In the following we present some of these "paper and pencil" procedures and outline a few concepts which may help in elucidating molecular structure.

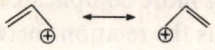
Valence bond methods. The chemist's ideas about molecular structure are based on the concept of the chemical bond. Qualitative valence bond theory [1415], which has grown from the work of Pauling [1070] explains molecular electronic structure in terms of localized electron-pair bonds and lone pairs. Basic ideas behind the VB method were outlined in Section 1.2.7. Classical chemical formulae can be considered as graphical representations of the various electron pairing schemes (or valence bond structures). Vertices, edges and pairs of dots represent atoms, pairs of shared electrons with opposite spins and lone pairs, respectively. The "standard" valence bond structures (so called Lewis structures) are characterized by the following properties:

(a) they have the maximum number of bonds permitted by the rules of valence for the given AO basis set (*e.g.* the octet rule for the first row elements);
(b) the bonds are located between adjacent atoms only.

A great number of molecules can be described by considering only one standard valence bond structure, like methane:



while for other molecules (*e.g.* allyl cation, benzene) several equivalent standard valence bond structures can be given. The qualitative valence bond method describes these latter molecules as "resonance hybrids" of several structures, for example, for the allyl cation:



The term "resonance" has often been the source of some misunderstanding. It has to be stressed that the different valence bond structures have no physical reality in themselves. The only meaningful object is the appropriate linear combination of the valence bond structures, that is, the approximate wave function of the molecule.

As a matter of fact, not only the standard valence bond structures can be constructed for a given molecule. Various ionic structures and pairing schemes connecting distant atomic orbitals may contribute to the wave function, however only with a minor weight compared to that of the standard structures (Fig. 1.16).

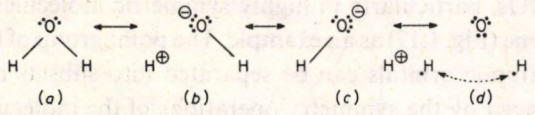


Fig. 1.16 Valence bond structures for water. *(a)* Standard valence bond (Lewis-) structure; *(b)* and *(c)* ionic structures describing the polarity of the bonds; *(d)* "long-bond" structure

Qualitative valence bond theory has been extensively used in organic chemistry for the representation of the electronic structure of conjugated molecules. A drawback of this procedure is the lack of a corresponding quantitative method, which may justify and put on a sounder basis the qualitative predictions. In spite of this fact, the attractive feature of having the bond concept inherently built in the theory, stimulated a renewal of interest for this kind of approach [374, 510].

Molecular orbital models. The current computational methods of quantum chemistry are based, almost exclusively, on the molecular orbital (MO) theory. Therefore it is quite natural that most of the qualitative models are closely related to this approach.

The first problem one has to solve by using simple models is the qualitative prediction of the shape and the energy sequence of the molecular orbitals, prior to doing numerical calculations. The general principles governing molecular orbital formation can be exploited for this purpose. In qualitative MO considerations the LCAO approximation is used, that is, the MOs are linear combinations of the χ_μ atomic orbitals:

$$\varphi_i = \sum_\mu c_{\mu i} \chi_\mu \,. \tag{1.154}$$

Usually only valence electrons, or only the π-electrons are treated explicitly.

First we discuss briefly some uses of the orbital symmetry in qualitative arguments. Secondly a few important properties of the π MOs of conjugated systems are reviewed. Various applications of perturbation theory are presented, which can be used to draw qualitative conclusions concerning more complicated systems. Finally, the method of correlation diagrams, which reveals the relations between MOs of different molecular structures, is discussed.

Symmetry. Molecular orbitals describing electronic states of a given symmetry, must behave appropriately with respect to the symmetry operations of the molecule. For instance they must be either symmetric or antisymmetric with respect to an inversion centre; more generally, the occupied MOs must be bases for the irreducible representations of the molecular point group. This property of the MOs follows directly from the fact that the Hamiltonian (and the Fockian) commutes with the molecular symmetry operations. The symmetry restrictions limit severely the number and kinds of atomic orbitals (AOs) that can combine in a given MO. This helps in constructing the MOs, particularly in highly symmetric molecules.

Let us take ethylene (Fig. 1.17) as an example. The point group of the molecule is D_{2h}. The valence shell atomic orbitals can be separated into subsets of equivalent AOs, which are interchanged by the symmetry operations of the molecule. Supposing that the z coordinate axis is perpendicular to the molecular plane (Fig. 1.17), the following atomic orbital subsets span reducible representations in the D_{2h} point group:

$\{(2s)_1, (2s)_2\}$; $\{(2p_x)_1, (2p_x)_2\}$; $\{(2p_y)_1, (2p_y)_2\}$;

$\{(2p_z)_1, (2p_z)_2\}$; $\{(1s)_3, (1s)_4, (1s)_5, (1s)_6\}$.

Instead of going into the details of group theoretical methods, which are available to decompose these reducible representations into their irreducible components (see *e.g.* [249]), we show another procedure leading to the desired set of symmetry orbitals in a pictorial way. The generator orbital approach proposed by Ruedenberg and his coworkers [574] offers a very simple procedure to construct the symmetry orbitals. The method consists of placing some auxiliary hydrogen-like atomic orbitals at the centre of the molecular framework which are used as templates to reveal the nodal properties of the corresponding LCAO symmetry orbitals. These template orbitals, called the *generator orbitals* are, of course, deleted at the end of the procedure. An application on the example of the ethylene molecule using a minimal AO basis set is illustrated on Fig. 1.18.

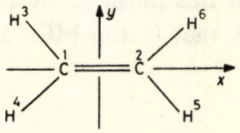


Fig. 1.17 The ethylene molecule with the coordinate axes and the numbering of atoms

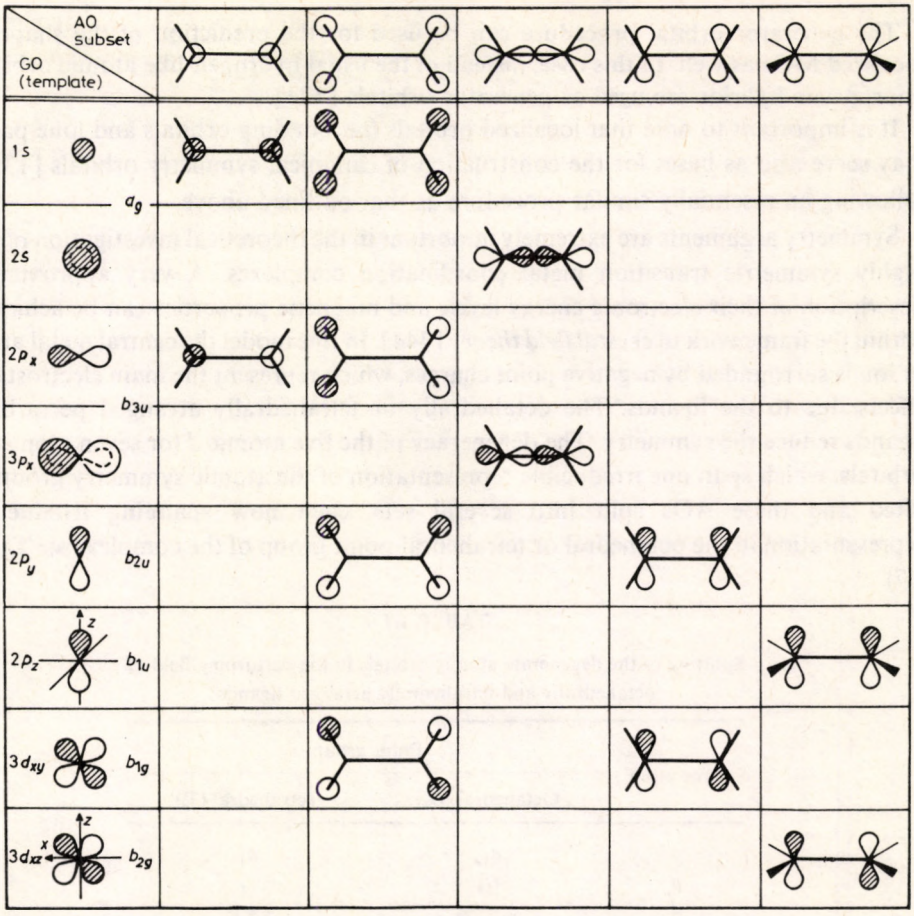


Fig. 1.18 Construction of symmetry orbitals using the generator orbital technique. Note that 2*s* and 3*p* generator orbitals have an inner nodal surface. The symmetry notations refer to the D_{2h} point group. Only symmetry orbitals in the same row can be combined to form canonical molecular orbitals

For example, the molecular orbitals belonging to the b_{2u} irreducible representation have the general form:

$$\varphi_{b_{2u}} = c_1[(2p_y)_1 + (2p_y)]_2 + c_2[(1s)_3 + (1s)_4 - (1s)_5 - (1s)_6]\,. \tag{1.155}$$

It has to be borne in mind that symmetry considerations alone are insufficient to predict the values of the coefficients c_1 and c_2 in the above equation; they can be obtained (along with the corresponding orbital energies) by solving the appropriate secular equation, *cf.* Section 1.2.5. As to the b_{1u} and b_{2g} molecular orbitals of ethylene, which are composed of $2p_z$ carbon orbitals exclusively, symmetry arguments give directly the exact MOs (bonding and antibonding π-orbitals) in the actual minimal AO basis set.

The generator orbital procedure can be used for the prediction of the shape of localized MOs as well. In this case, instead of the usual hydrogen-like atomic orbitals appropriate hybrids are used as generator orbitals [574].

It is important to note that localized orbitals (*i.e.* bonding orbitals and lone pairs) may serve also as bases for the construction of canonical symmetry orbitals [1352] following an essentially similar procedure as that outlined above.

Symmetry arguments are extremely important in the theoretical investigation of the highly symmetric transition metal coordination complexes. A very approximate description of their electronic energy levels and magnetic properties can be achieved within the framework of *crystal field theory* [344]. In this model the central metal atom or ion is surrounded by negative point charges, which represent the main electrostatic effects due to the ligands. The octahedrally or tetrahedrally arranged perturbing ligands reduce the symmetry. The degeneracy of the five atomic *d* (or seven atomic *f*) orbitals, which span one irreducible representation of the atomic symmetry group, is lifted and these AOs split into several sets, each now spanning irreducible representation in the octahedral or tetrahedral point group of the complex (see Table 1.7).

TABLE 1.7

Splitting of the degenerate atomic orbitals in the perturbing field of octahedrally and tetrahedrally arranged ligands

Free atom	Point group	
	Octahedral (O_h)	Tetrahedral (T_d)
s	a_{1g}	a_1
p	t_{1u}	t_2
d	e_g+t_{2g}	$e+t_2$
f	$a_{1u}+t_{1u}+t_{2u}$	$a_2+t_2+t_1$

The *d*-orbitals are of outstanding importance in the description of transition metal complexes. The d_{xy}, d_{xz} and d_{yz} orbitals belong to the three-dimensional t_{2g} and t_2 irreducible representations in the octahedral (O_h) and tetrahedral (T_d) point groups, respectively; while the $d_{x^2-y^2}$ and d_{z^2} orbitals span the two-dimensional e_g and e representations in the same point groups. Elementary considerations can be used for predicting the order of the split AO levels. In octahedral complexes the electrons on t_{2g} orbitals, and in tetrahedral complexes the electrons on e orbitals are located far in space from negative point charges representing the ligands. These orbitals will be of lower energy, while electrons on other *d*-orbitals exhibit destabilizing effect because of their proximity getting too close to the ligand negative charges (Fig. 1.19).

The *ligand field theory* of transition metal complexes treats the relevant metal and ligand orbitals explicitly, so this scheme allows investigation of the metal-ligand

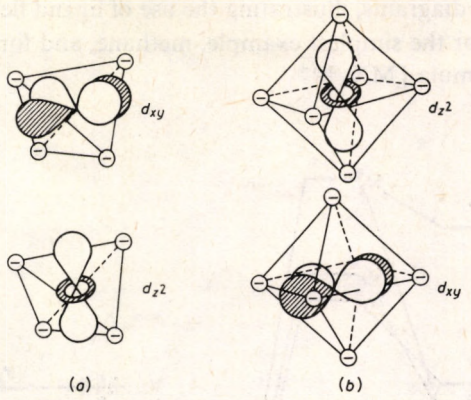


Fig. 1.19 Interaction of ligand charges with *d* orbitals

bonding. The working rules, which use extensively the symmetry properties of the orbitals, have been summarized according to Dunn [344] as follows:

(1) Decide upon the symmetry of the complex, that is, it is necessary to know the structure of the complex in advance.

(2) Construct linear combinations of available ligand orbitals such that they transform according to the irreducible representations of the point group of the complex.

(3) Ascertain to which irreducible representations of the point group the orbitals of the metal belong in the presence of the perturbing field created by the ligands, *cf.* Table 1.7.

(4) Form linear combinations of the symmetry adapted ligand orbitals with the metal orbitals of the same symmetry in order to obtain the final MOs. (The actual extent of mixing between ligand and metal orbitals can be determined only by solving the corresponding MO equations using an appropriate model Hamiltonian.)

(5) Decide upon the energy order of the MOs (either by appeal to experiment or by using the results of appropriate calculations).

(6) Fill the MOs with the appropriate number of electrons.

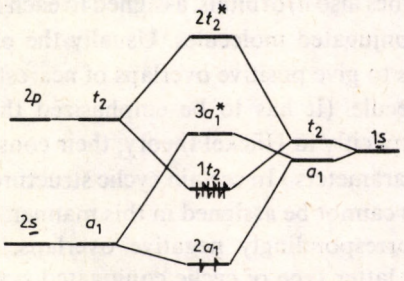


Fig. 1.20 Energy levels of methane derived on the basis of ligand field theory

Molecular orbital diagrams, illustrating the use of ligand field theory, are shown in Figs 1.20 and 1.21 for the simplest example, methane, and for a tetrahedral complex with the general formula $[MX_4]^{m+}$.

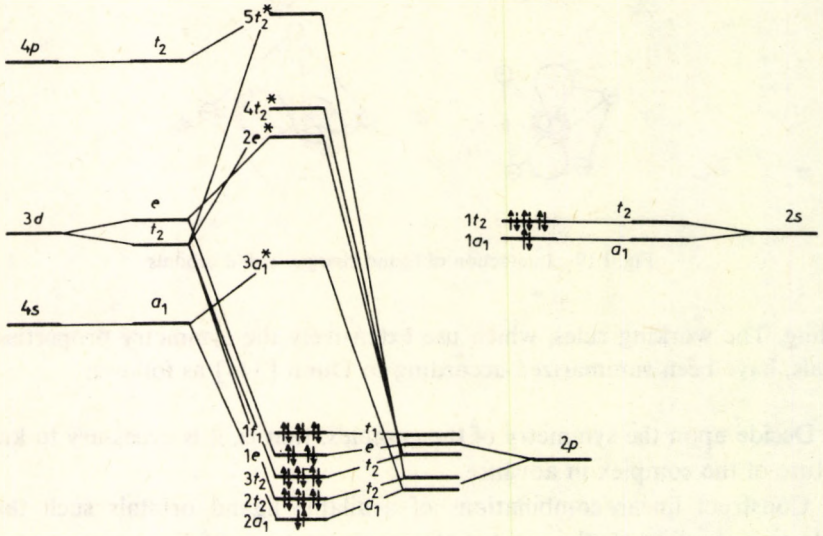


Fig. 1.21 Electron configuration derived on the basis of ligand field theory for a tetrahedral complex of general formula MX_4 possessing 32 electrons

MOs of conjugated systems. The chemical and physical properties of conjugated molecules, which are of great importance in organic chemistry, are determined by their π-electron structure. Symmetry arguments cannot be used effectively for qualitative study of the great majority of π-electron systems. Fortunately, an ingeniously simple molecular orbital model of π-systems, the Hückel theory, provides a reasonable description for qualitative and semi-quantitative purposes. A detailed discussion of the Hückel-theory has been given in Section 1.3.2. Here some rules, which are important in qualitative considerations, are briefly recapitulated.

Pure atomic *p* (sometimes also *d*) orbitals, assigned to each π-centre serve as a basis in the MO treatment of conjugated molecules. Usually the phases of the AOs can be selected in such a way as to give positive overlaps of nearest neighbour basis orbitals throughout in the molecule. (It has to be emphasized that although the overlap integrals do not enter explicitly in Hückel theory, their consideration is necessary for the estimation of the β parameters.) In certain cyclic structures, however, the phases of the atomic basis orbitals cannot be assigned in this manner: one or an odd number of sign inversions, and correspondingly negative overlaps, occur between adjacent orbitals (Fig. 1.22). This latter type of cyclic conjugated systems is called a Möbius-

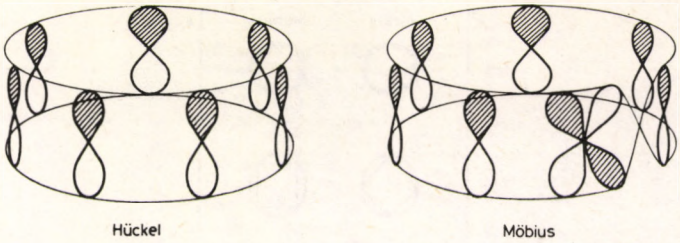


Fig. 1.22 Schematic representation of Hückel and Möbius-type π systems. The phase change in the Möbius system is due to a d_π orbital

system [539] in contrast to the more common, Hückel-system. The analytic expressions of the MO energies for these type of conjugated systems are:

$$\varepsilon_k = \alpha - 2\beta \cos\left(\frac{2\pi k}{N}\right) \quad \text{Hückel} \tag{1.156}$$

$$\varepsilon_k = \alpha - 2\beta \cos\left(\frac{2\pi k + 1}{N}\right) \quad \text{Möbius} \tag{1.157}$$

where α is the Coulomb integral, β is the resonance integral and N is the number of atoms constituting the ring, integer k runs over the values $0, \pm 1, \pm 2, \ldots \pm N - 1$.

A useful mnemonic device can be used for deriving these energy levels. Let us take a polygon with N sides inscribed inside a circle of radius 2β. The energy levels of a Hückel system are represented by the vertices of a polygon placed in a circle by one of its vertices at the bottom. On the other hand, if the polygon is placed by one side at the bottom, the Möbius energy levels are reproduced (Fig. 1.23). In Hückel-systems, the number of electrons, N, needed to fill all bonding orbitals equals to $4n+2$ with $n = 0, 1, 2$. This is closely related to the well-known Hückel $4n+2$ rule, the criterion for aromaticity. The aromaticity is defined as the extra stability of the given compound with respect to the corresponding open chain conjugated system. (*cf.* Section 2.6.) (In chemical literature this comparison is frequently taken as obvious and is not stated explicitly.) As to the Möbius-structures, an extra stability is expected in systems containing $4n$ electrons. This latter rule plays important role in estimating the stability of the transition-states in certain reactions (Section 4.5.).

Finally, we note that the orbital energies of a linear conjugated polyene ($C_N H_{N+2}$) is given by the formula:

$$\varepsilon_k = \alpha - 2\beta \cos\left(\frac{\pi k}{N+1}\right) \tag{1.158}$$

where the k integer runs over the values $1, 2, 3, \ldots N$.

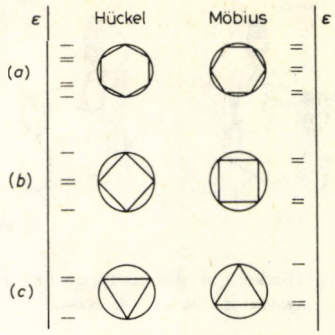


Fig. 1.23 Mnemonic for the Hückel and Möbius molecular orbital energy levels

Another even simpler MO method is the free electron molecular orbital (FEMO) model of linear polyenes [1105], where the orbitals describe electrons moving in a simple linear one-dimensional potential well. The length of this well is determined for even and odd membered chains by the relations $L=N\cdot l$ and $L=(N+1)\cdot l$, respectively, where the bond length is l, and N is the number of atoms constituting the chain. The solution of this model can be obtained in a closed form. The one-electron FEMO orbitals have the energies:

$$\varepsilon_k = \frac{k^2h^2}{8mL^2} \tag{1.159}$$

where L is the dimension of the "well", and k is a quantum number.

In a comparison of Eq. (1.159) to the Hückel result, Eq. (1.158), we notice that the energy spacing of the FEMO orbitals increases with increasing quantum number k, and there are no pairing properties of these orbitals as is the case with Hückel MOs (see below).

A closely related free electron model, the "perimeter model" has been proposed for the description of catacondensed hydrocarbons (whose carbon atoms lie on a single periphery). Here the electrons are restricted in a one dimensional circular well of constant potential. These orbitals have the energy

$$\varepsilon_k = \frac{k^2h^2}{2mL^2} \qquad (k=0, \pm 1, \pm 2, \ldots \pm N) \tag{1.160}$$

Both FEMO and perimeter models have been successfully used for the prediction of electronic absorption spectra of certain conjugated polyenes (*cf.* Section 3.6.3.). Here we emphasise the property that these simple methods lead to MOs which reflect correctly the nodal characteristics of the π-MOs. Consequently one can expect that they can

serve as appropriate generator orbitals for π-systems. In effect, quite close mathematical resemblance can be found between the form of Hückel and free electron MOs as illustrated in Table 1.8. Two simple applications of free electron MOs as generator orbitals are shown on Fig. 1.24.

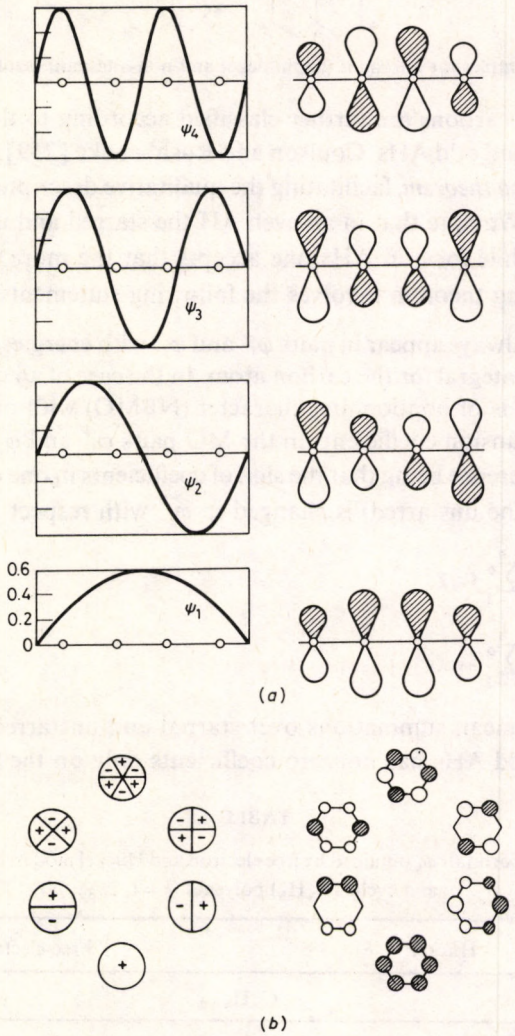


Fig. 1.24 Free-electron (FE) molecular orbitals as generator orbitals: *(a)* linear polyene (1,3-butadiene); *(b)* monocyclic polyene (benzene)

An important class of conjugated molecules is that of the *alternant hydrocarbons* (AHs), in which the conjugated atoms can be divided into two groups ("starred" and "unstarred") in such a way that each atom of a given group is bonded directly only to atoms of the other group. It can be easily shown that conjugated systems are alternant

if, and only if, they contain no odd-membered rings. For example, naphthalene is alternant, whereas the division of atoms in the above way to starred and unstarred ones is impossible in the nonalternant azulene (Fig. 1.25).

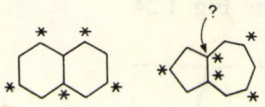


Fig. 1.25 Examples for alternant (naphtalene) and non-alternant (azulene) hydrocarbons

Alternant hydrocarbons are further classified according to the number of their π-centres into even and odd AHs. Coulson and Rushbrooke [259] derived an important theorem, the *pairing theorem*, facilitating the qualitative description of these systems at the Hückel level. We note that in an even AH the starred and unstarred atoms form equivalent sets, while for odd AHs one accepts that the more numerous set will be starred. The pairing theorem involves the following statements.

(1) The π-MOs always appear in pairs φ_i^+ and φ_i^- with energies $\alpha-\varepsilon_i$ and $\alpha+\varepsilon_i$ where α is the Coulomb integral for the carbon atom. In the case of an odd AH a further MO φ^0 appears which is of nonbonding character (NBMO) with orbital energy α.

(2) The AO expansion coefficients in the MO pairs φ_i^+ and φ_i^- are numerically the same, the only difference being that the sign of coefficients in one complete set (either in the starred or in the unstarred) is changed in φ_i^- with respect to φ_i^+:

$$\varphi_i^+ = \sum_{\mu=1}^{n}{}^{*} c_{\mu i}\chi_\mu + \sum_{\nu=1}^{n}{}^{o} c_{\nu i}\chi_\nu \tag{1.161}$$

$$\varphi_i^- = \sum_{\mu=1}^{n}{}^{*} c_{\mu i}\chi_\mu - \sum_{\nu=1}^{n}{}^{o} c_{\nu i}\chi_\nu \tag{1.162}$$

where Σ^* and Σ^o mean summations over starred and unstarred atoms, respectively. The NBMO of odd AHs has nonzero coefficients only on the starred atoms.

TABLE 1.8

Comparison of orbitals ϕ_k obtained by free electron and Hückel models for linear (C_NH_{N+2}) and cyclic (C_NH_N) polyenes ($k=1, 2, \ldots N$)

Hückel	Free-electron
C_NH_{N+2}	
$\phi_k=\sqrt{\frac{2}{N+1}}\sum_{r=1}^{N}\sin\left(\frac{k\pi r}{N+1}\right)\chi_r$	$\phi_k=\sqrt{\frac{2}{L}}\sin\left(\frac{k\pi x}{L}\right)$
C_NH_N	
$\phi_k=\frac{1}{\sqrt{N}}\sum_{r=1}^{N}\exp\left(i\frac{2\pi kr}{N}\right)\chi_r$	$\phi_k=\frac{1}{\sqrt{L}}\exp\left(i\frac{2\pi kx}{L}\right)$

(3) For neutral AHs the π-electron density is unity and the bond order between atoms of the same set (starred or unstarred) is zero.

(4) In odd AH anions or cations the π-electron densities (q_{μ^*}) and bond orders ($p_{\mu^*\lambda^*}$) follow the rules:

$$q_{\mu^0} = 1 \tag{1.163}$$

$$q_{\mu^*}^{\pm} = 1 \pm c_{0\mu^*}^2 \tag{1.164}$$

$$p_{\mu^*\lambda^*}^{\pm} = \mp c_{0\mu^*} c_{0\lambda^*} . \tag{1.165}$$

Here the upper signs refer to anions the lower ones refer to cations.

Although the pairing theorem provides a wealth of information about MOs and about the overall charge distribution in the π-system, the actual values of the MO coefficients remain to be determined. In the case of the especially important NBMO in odd alternant hydrocarbons, this can be done simply by a "paper and pencil" procedure [310]. Let us consider an unstarred atom ν in an odd AH, which is attached to, at most, three neighbouring atoms μ^*, $\lambda^*\sigma^*$. Since the latter necessarily belongs to the starred set, and according to the pairing theorem the NBMO will contain coefficients only on the starred atoms, Longuet–Higgins' rule [807] states that if the NBMO coefficients are $c_{0\mu^*}$, $c_{0\lambda^*}$, $c_{0\sigma^*}$ and the resonance integrals are $\beta_{\nu\mu^*}$, $\beta_{\nu\lambda^*}$, $\beta_{\nu\sigma^*}$ the following equation holds:

$$c_{0\mu^*}\beta_{\nu\mu^*} + c_{0\lambda^*}\beta_{\nu\lambda^*} + c_{0\sigma^*}\beta_{\nu\sigma^*} = 0 \tag{1.166}$$

or, if the β's are all the same:

$$c_{0\mu^*} + c_{0\lambda^*} + c_{0\sigma^*} = 0 \tag{1.167}$$

i.e. the sum of the NBMO coefficients at starred atoms adjacent to a given unstarred atom vanishes. The corresponding graphical procedure is illustrated on the example of the α-naphthylmethyl molecule (Fig. 1.26). Similar procedure can be used in the framework of the free-electron model (FEMO) [1334].

Perturbation of the MOs. When dealing with complicated unsymmetric structures, the experience gained in the studies of relatively simple, symmetrical molecules can be

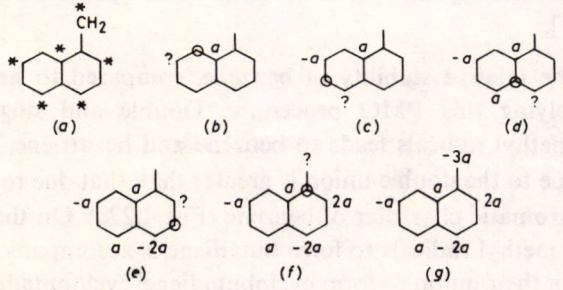


Fig. 1.26 Calculation of NBMO coefficients in α-naphthylmethyl

successfully used *via* perturbation theory (PT). This offers a convenient way of relating MOs of complex molecular structures to the MOs of its simple fragments. In other cases it is possible to treat unsymmetric molecules by relating them to previously investigated, simple, symmetrical systems.

A very popular, widespread version of the perturbative treatments is the perturbation molecular orbital (PMO)-theory of conjugated systems elaborated by Dewar [307]. The stability and reactivity of conjugated molecules can be explained in a simple, pictorial way using the PMO-theory, thus giving a theoretical interpretation of many problems arising in organic chemistry [310]. The main ideas of the method are the following:

(1) Actual HMO calculations or the relations (1.161)–(1.165) are utilized to get charge densities, bond orders, orbital energies and the most important MO coefficients for the conjugated hydrocarbon under study.

(2) It is supposed that practically all the conjugated systems can be related to an appropriate isoelectronic hydrocarbon, as far as a zeroth order approximation is required.

(3) The variation of the total π-electron energy (δE_π) is calculated by PT for the following perturbations:

(a) Substitution of a carbon by a heteroatom (monocentric perturbation), where first order PT yields:

$$\delta E_\pi = q_\mu \delta\alpha_\mu + \sum_\lambda p_{\mu\lambda}\delta\beta_{\mu\lambda} \tag{1.168}$$

where the atom μ is substituted and the corresponding changes in the Coulomb and resonance integrals are $\delta\alpha_\mu$ and $\delta\beta_{\mu\lambda}$, respectively.

(b) Union of two conjugated systems by making one or more crosslinks between them. The general expression of the second order perturbation energy for this case will be given later. The union of odd AHs is of special importance in PMO theory. Here the energy of union is given by first order PT, since the NBMOs are of the same energy α in all odd AHs:

$$\delta E_\pi = 2a_{0\mu}b_{0\nu}\beta_{\mu\nu}\,. \tag{1.169}$$

(The NBMO coefficients $a_{0\mu}$ and $b_{0\nu}$ can be found by the "paper and pencil" Longuet–Higgins' rule [807].)

For example, the relative stability of benzene, compared to hexatriene may be explained by applying this PMO procedure. Double and single union of the pentadienyl and methyl radicals leads to benzene and hexatriene, respectively. The energy lowering due to the double union is greater than that due to the single union: this explains the aromatic character of benzene (Fig. 1.27*a*). On the other hand, the union of allyl and methyl radicals to form butadiene is accompanied by a greater π-energy change than their union to form cyclobutadiene; cyclobutadiene is considered to be antiaromatic (Fig. 1.27 *b*).

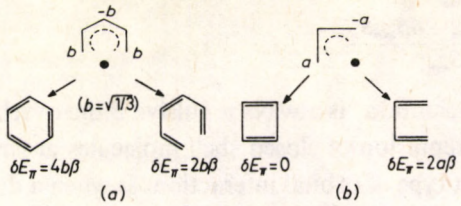


Fig. 1.27 PMO derivation of the aromatic character of benzene *(a)* and the antiaromatic character of cyclobutadiene *(b)*. The a and b are coefficients of NBMOs, β is the resonance integral

The simple formulae applied in PMO theory are special cases of a more general perturbational method, which is valid for the all-valence-electron case too. When σ orbitals should also be included, the molecules are usually treated at the Extended Hückel level, considering explicitly the overlap of the basis orbitals [621]. An effective way of rationalizing substituent effects, conformational preferences and even reaction paths, is to consider the interaction of the orbitals on two or more relevant molecular fragments. The interaction of φ_m^0 on fragment A and φ_n^0 on fragment B ($\varepsilon_m^0 < \varepsilon_n^0$) leads to the new orbitals φ_m and φ_n with energies

$$\varepsilon_m, \varepsilon_n = \frac{\varepsilon_m^0 + \varepsilon_n^0 - 2S_{mn}\beta_{mn} \mp T}{2(1-S_{mn}^2)} \tag{1.170}$$

where the minus sign applies to ε_m, the plus sign applies to ε_n, S_{mn} and β_{mn} are the overlap and resonance integrals and

$$T^2 = ([\varepsilon_m^0 + \varepsilon_n^0] - 2S_{mn}\beta_{mn})^2 + 4(1-S_{mn}^2)(\beta_{mn}^2 - \varepsilon_m^0\varepsilon_n^0)\,. \tag{1.171}$$

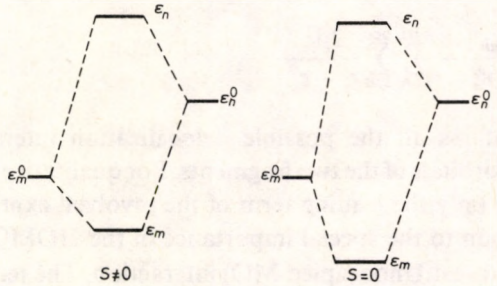


Fig. 1.28 Schematic illustration of the interaction of two orbitals φ_m and φ_n. If there is a nonvanishing overlap between them the splitting of levels is non-symmetrical; if $S_{mn}=0$ the splitting is symmetrical

The bonding combination φ_m is always stabilized to a lesser extent with respect to the mean energy of the initial orbitals than the antibonding combination is destabilized. This rule does not hold if the overlap is zero: in non-overlapping basis, the destabilization of the antibonding combination is the same as the stabilization of the bonding one (Fig. 1.28).

If both φ_m^0 and φ_n^0 are doubly occupied, the net energy change due to the interaction is given by:

$$\Delta E_{mn}(4) = \frac{2(\varepsilon_m^0 + \varepsilon_n^0)S_{mn}^2 - 4\beta_{mn}S_{mn}}{1 - S_{mn}^2}. \tag{1.172}$$

This "four-electron interaction" is always repulsive if the overlap is nonzero and this can be related to the repulsion of closed shell molecules at small distances.

The other important type of orbital interactions is when a doubly occupied orbital φ_m^0 interacts with an empty orbital φ_n^0 on another fragment. This "two-electron interaction" is always attractive, since it involves the lower energy (bonding) combination of the initial orbitals filled by two electrons. For the overlapping case the net energy change is given by second order perturbation theory as:

$$\Delta E_{mn}(2) = \frac{2(\beta_{mn} - S_{mn}\varepsilon_m^0)^2}{\varepsilon_m^0 - \varepsilon_n^0} \tag{1.173}$$

which for the case of nonoverlapping orbitals simply reduces to:

$$\Delta E_{mn}(2) = \frac{2\beta_{mn}^2}{\varepsilon_m^0 - \varepsilon_n^0}. \tag{1.174}$$

The above formulae are very useful in the analysis of results of detailed *ab initio* calculations in terms of orbital interactions. This quantitative PMO approach has proved to be an appropriate way of rationalizing, for example, conformational barriers calculated by accurate methods [87, 88, 1413].

Let us take now the total interaction energy of two molecular fragments A and B. Second order perturbation theory applied for a nonoverlapping model yields approximately

$$\Delta E_{\text{deloc}} \approx \sum_{m\in A}^{\text{occ}} \sum_{n\in B}^{\text{virt}} \frac{2\beta_{mn}^2}{\varepsilon_m^0 - \varepsilon_n^0} + \sum_{k\in A}^{\text{virt}} \sum_{l\in B}^{\text{occ}} \frac{2\beta_{lk}^2}{\varepsilon_l^0 - \varepsilon_k^0}. \tag{1.175}$$

This expression contains all the possible delocalization interactions between the occupied and virtual orbitals of the two fragments. For qualitative purposes it would be sufficient to estimate only the leading term of the involved expression. It was Fukui who draw the attention to the special importance of the HOMO (Highest Occupied MO) and LUMO (Lowest Unoccupied MO) interaction. The term, corresponding to the interaction of the HOMO and LUMO, has usually the smallest denominator; consequently it dominates the interaction energy expression Eq. (1.175). In most cases the interaction of these "*frontier orbitals*" provides enough information about the preferred stereochemical path of concerted chemical reactions (Section 4.5) or conformational changes.

The frontier orbital rule has been formulated [394, 418, 419] by saying that the majority of chemical reactions and conformational changes take place at the position and in the direction of maximum overlap between the HOMO and LUMO of the reactants or of the appropriately selected molecular fragments A and B. Examples for the application of the frontier orbital method will be given in Sections 4.4.2 and 4.5.

A simple graphical procedure can be used when applying the above overlap criterion. The molecular orbital diagrams of the HOMO and LUMO are sketched in the stereochemical drawing of the nuclear frame, and the favoured reaction path, i.e. that one which is accompanied by the most significant HOMO–LUMO overlap, can be selected by inspection.

Note that the existence of nonzero overlap is equivalent to a symmetry rule, namely, the HOMO of the first fragment and the LUMO of the second one must be of the same symmetry in order to provide a favourable reaction path. However, in some instances the overlap criterion may help to distinguish between different paths each of which are "symmetry-allowed" the greater overlap is generally associated with the stronger interaction, *cf.* Wolfsberg–Helmholtz formula, Section 1.3.2.

The distortion of the nuclear framework itself can also be considered as a source of the perturbation affecting the electronic structure. Results of second order perturbation theory show [44, 1075] that the existence of low-lying excited states of the same symmetry as that of the ground state is a necessary condition of having a low energy barrier along the reaction coordinate under study. This specific situation, when the mixing of two electronic states makes favourable a given nuclear deformation, is called the "*second-order Jahn–Teller effect*". Its application ranges from the prediction of molecular geometries to establishing symmetry rules for various chemical processes [1076].

In the framework of the simple MO theory the existence of low-lying excited electronic states of the same symmetry as that of the ground state corresponds to the requirement that the symmetries of the HOMO and LUMO are the same. This is exactly the criterion cited for the frontier orbital method.

Finally, it is worth mentioning that the conservation of orbital symmetry in the course of a reaction path, the famous rule of Woodward and Hoffman (Section 4.5), may be considered as a simple symmetry consequence of the specific perturbation theory applied in the derivation of the second-order Jahn–Teller effect [1075].

Correlation diagrams. The method of correlation diagrams has great importance among the qualitative methods of quantum chemistry. The classical applications of this procedure can be traced back to the spectroscopy of diatomic molecules [555], where experimentally known atomic energy terms and symmetry arguments were combined in the framework of MO theory to the picture of the unknown energy levels of the diatomic molecules. "Two-sided" correlation diagrams have been used for this purpose, that is, the levels of the separated atoms were correlated to the levels of the united atom (the hypothetical state where the interatomic distance tends to zero).

The general rules for the construction of correlation diagrams are the following:

(1) The symmetry of each molecular orbital remains unchanged.

(2) Molecular orbitals of the same symmetry cannot cross (noncrossing rule, see *e.g.* [1161]).

(3) No orbitals are gained or lost ("matching rule").

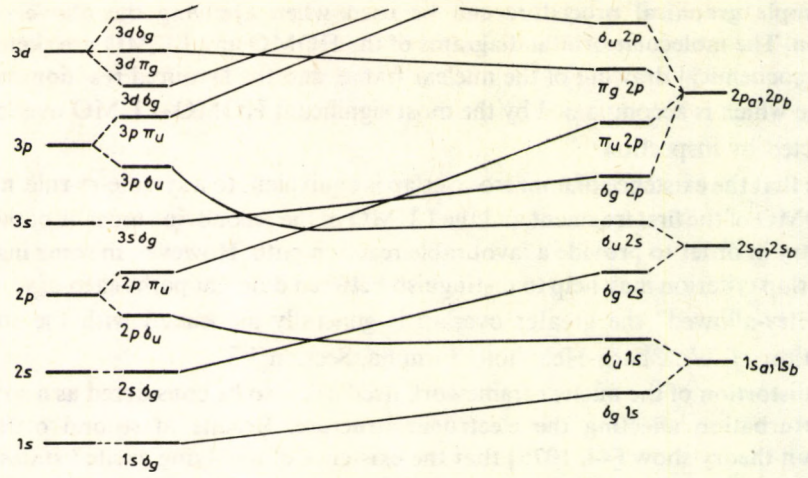


Fig. 1.29 Correlation diagram for homonuclear diatomics

The classical correlation diagram of a homonuclear diatomics is represented in Fig. 1.29.

It was Walsh [1399] who proposed using correlation diagrams for the prediction of the molecular shape. He studied "one-sided" correlation diagrams, that is, the variation of the orbital energies plotted against the angular deformation of the molecule. Walsh concluded that the molecular geometry in a given type of system was mainly determined by the number of the valence electrons ("Walsh's rules"). This method was extended later by Gimarc [449] and a thorough analysis of the procedure, based on *ab initio* calculations performed by Buenker and Peyerimhoff [158] contributed to the deeper understanding of the theoretical foundations and the limits of this approach. Note that these rules are connected with the approximate relations between the total energies and the sum of orbital energies (*cf.* Extended Hückel method, Section 1.3.2 and Ref. [158]). An application of Walsh diagrams is illustrated in Section 3.1.

The rules, applied in the method of Walsh-diagrams, or in qualitative MO theory (QMOT) are essentially those which have already been mentioned on previous pages in connection with the simple MO results or perturbation theory. They can be summarized as follows [816]:

(1) An increase of overlap population between two AOs tends to lower the MO energy, a decrease tends to increase it.

(2) The effect of a given change in the overlap population is more pronounced for the orbital energy of the higher lying MOs. This is in accordance with the result, discussed above, that the destabilizing effect of an antibonding combination of two AOs is greater than the stabilizing effect of a bonding combination between them, if other factors are the same.

(3) The change in the total energy approximately equals that of the sum of one-electron energies for the nonpolar, neutral systems, if the nuclei are separated by the distance of a normal bond length or more. This rule corresponds to a basic assumption in the Extended Hückel Theory, so its limitations are the same as were discussed in Section 1.3.2.

The method of correlation diagrams has also been proposed for the investigation of the stereochemistry of concerted reactions [810, 1436, 1437]. Various types of correlation diagrams have been successfully used for the prediction of the selection rules, which will be presented in detail in Section 4.5.

Finally we should like to stress that the importance of the qualitative methods remains unchanged even in the presence of increased computational facilities. It is important that the logic of qualitative methods should be incorporated into the analysis if we want the results of computational quantum chemistry to become an integral part of chemical thinking.

1.4 THE FRAMEWORK OF LOCALIZED MOLECULAR ORBITALS

The molecular orbitals discussed so far were obtained as solutions of the canonical HF equations

$$\hat{F}\psi_k = \varepsilon_k \psi_k. \tag{1.176}$$

The orbitals ψ_k are called canonical MOs. As was discussed briefly in Section 1.2.4, the above equation represents only a special case of the general Hartree–Fock equations which can be written as

$$\hat{F}\varphi_k = \sum_l^{\text{occ}} \varepsilon_{kl}\varphi_l \tag{1.177}$$

where the summation runs over the occupied orbitals. The mathematical significance of Eq. (1.177) is as follows. Let the Fock operator $\hat{F}$ act on a given occupied molecular orbital φ_k; then the transformed orbital $\hat{F}\varphi_k$ can be completely expanded *within the subspace of the occupied orbitals* with expansion coefficients ε_{kl} as $\sum_l^{\text{occ}} \varepsilon_{kl}\varphi_l$. In other words, the occupied subspace is an invariant subspace of operator $\hat{F}$. (Of course, the same is expressed by the local Brillouin theorem, Eq. (1.44), discussed in Section 1.2.4.) This consideration suggests that any set of MOs spanning the same occupied subspace can be considered as a solution of the general HF equations. Therefore the occupied MOs can be transformed among one another (*i.e.*, without leaving their subspace) by any nonsingular linear transformation, and they still can be considered as true solutions of the HF problem.

The origin of this transformational freedom in the HF scheme is in the fact that the HF wave function is a Slater-determinant of the occupied (spin-) orbitals, and this

determinantal wave function remains unchanged—up to a constant which influences only the normalization of the wave function—if one performs a (nonsingular) linear transformation among the columns (or rows) corresponding to the individual MOs. Thus, a linear transformation of the MOs may affect only the norm of the many-electron determinantal wave function [397, 780]*.

Moreover, if (and only if) the transformation is unitary, it does not influence even the normalization of the one-determinantal wave function. This is connected with the unitary nature of the MO transformation: if the initial orbitals form an orthonormal set, the transformed MOs remain also orthonormal. Since the canonical MOs are always orthonormal being obtained as eigenvectors** of the hermitian operator $\hat{F}$, one gets an orthonormal set of transformed MOs φ_k, too. A unitary transformation $\mathbf{U}$ connecting the orbitals φ_k of Eq. (1.177) with the canonical MOs ψ_k of Eq. (1.176), can be written as

$$\psi_k = \sum_l U_{kl} \varphi_l .$$

Substituting into Eq. (1.176) and utilizing the unitary character of matrix $\mathbf{U}$ ($\mathbf{U}^{-1} = \mathbf{U}^+$), by some algebra we obtain:

$$\hat{F} \varphi_k = \sum_{lm} U^+_{km} \varepsilon_m U_{ml} \varphi_l .$$

By comparing with Eq. (1.177) we find

$$\varepsilon_{kl} = \sum_m U^+_{km} \varepsilon_m U_{ml} .$$

A similar connection between the orbital energies ε_k of the canonical MOs and the general matrix elements ε_{kl} exists even in the case when the $\varphi \rightarrow \psi$ transformation is not unitary. Of course, in this case the adjoint of the unitary matrix ($\mathbf{U}^+$) is to be substituted by the inverse of the corresponding linear transformation.

The fact that the subspace of occupied MOs defines alone the solution of the HF problem means that, one can freely consider transformations within the virtual subspace as well, as far as only the ground state properties are studied.

It should be realized that this possibility of transforming the MOs without altering the wave function and thus any expectation value, is in some sense connected to the Pauli principle as applied to the independent particle theory. The Pauli principle requires that the total many-electron wave function be antisymmetric with respect to

* One can prove this result on the basis of the well known theorem according to which the determinant det ($\mathbf{A}\,\mathbf{B}$) of the matrix product $\mathbf{A}\,\mathbf{B}$ is equal to the product of the two determinants, det $\mathbf{A}$ and det $\mathbf{B}$.

** In case of orbital degeneracy, *i.e.* for $\varepsilon_k = \varepsilon_l$ though $\psi_k \neq \psi_l$ for certain k and l, the MOs ψ_k and ψ_l are not necessarily orthogonal but there exists always an appropriate linear transformation of the degenerate MOs making them orthogonalized. Practical computational schemes of finding the eigenvectors always ensure their orthogonality as well.

the interchange of the electronic coordinates. This requirement is obeyed by the *determinantal form* of the HF wave function which allows us to transform the MOs within the occupied subspace. A Hartree-product wave function would not possess a similar transformational freedom.

The above transformational degree of freedom means that the one-electron functions φ_k or ψ_k themselves have no true physical significance. The set of MOs is by no means unique: in a certain sense there is an ambiguity in the choice of the one-electron functions. It is only the many-electron wave function which is physically meaningful: neither the electron density, nor any other physical quantities change by the transformation of occupied MOs. We shall see below that the shape of individual MOs strongly depends on the kind of (unitary) transformations they result from. Only an analysis of the physical or chemical problem studied can be invoked as a guide to select among the different kinds of MOs. The significance of canonical orbitals was already mentioned in Section 1.2.4 in connection with the Koopmans theorem and with the description of excited electronic states in the HF framework. The present section is devoted to a discussion of the chemical significance of another type of orbitals, the so-called localized molecular orbitals (LMOs).

The essence of the concept of LMOs can be well illustrated on the following simple analytically solvable model. Let us consider the four-electron four-orbital Hückel problem of the 1,3-butadiene molecule. If all β's are taken equal, the Hückel Hamiltonian is diagonalized by the following canonical MOs [260]:

$$\psi_i = \sqrt{\frac{2}{5}} \sum_{\mu=1}^{4} \sin \frac{i\mu\pi}{5} \chi_\mu \tag{1.178}$$

where $i = 1, 2, 3, 4$ labelling the MOs in order of ascending energy, and χ_μ is the $2p_z$ AO on the μ'th carbon atom of butadiene. The two MOs occupied by four electrons in the ground state are ψ_1 and ψ_2; they are depicted schematically in Fig. 1.30. Notice that both MOs extend over the whole molecule and they transform according to different species (irreducible representations) of the C_{2h} point group of s-*trans* 1,3-butadiene (ψ_1: a_u; ψ_2: b_g). Let us now consider the following 2 by 2 unitary transformation of the occupied MOs:

$$\varphi_1 = \sqrt{2}^{-1}(\psi_1 + \psi_2) \tag{1.179a}$$

$$\varphi_2 = \sqrt{2}^{-1}(\psi_1 - \psi_2). \tag{1.179b}$$

These transformed orbitals, as was discussed above for the general case, describe exactly the same ground state of butadiene; thus their use is completely equivalent to that of the canonical MOs ψ_1 and ψ_2. The transformed MOs are depicted schematically in Fig. 1.31. They are obviously of quite a different shape compared with the canonical MOs: they do not correspond to a symmetry species of butadiene, and do not show the nearly uniform weights of the different AOs as the canonical MOs do. One can observe that the MO φ_1 is localized almost completely on atoms 1 and 2, while it

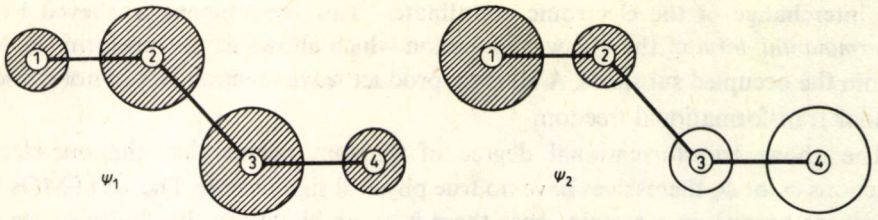


Fig. 1.30 Occupied canonical MOs in *trans*-butadiene. The figures in the small circles indicate the numbering of AOs. The larger circles depict the weight of the MO on the corresponding centre, with a radius proportional to the value of the LCAO–MO coefficient. The shaded and empty circles refer to different signs of the coefficients

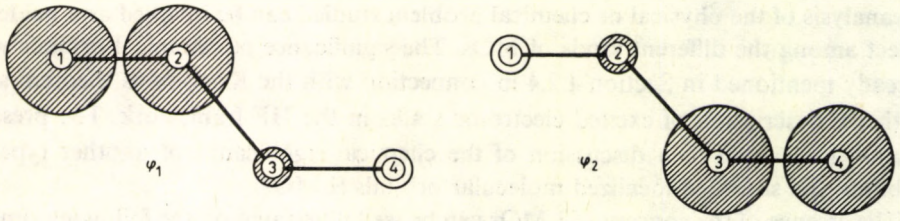


Fig. 1.31 Localized MOs in *trans*-butadiene (for designations, see Fig. 1.30)

has only a small "tail" on atoms 3 and 4. The opposite is true for φ_2 which is localized to a large extent on the bond between atoms 3 and 4, and has a tail on atoms 1 and 2. This feature justifies the nomenclature in which φ_1 and φ_2 are called localized molecular orbitals (LMOs). It is very interesting that the picture which emerges after localizing the MOs closely resembles the classical chemical model of 1,3-butadiene, namely the system of two double bonds isolated by a single one. As is seen in Fig. 1.31, the localized part of the LMOs φ_1 and φ_2 is an *in-phase combination* of the two corresponding $2p_z$ AOs; thus it can be considered as a bonding orbital describing a localized π-bond between the two atoms. On the other hand, the tails of MOs φ_1 and φ_2 in Fig. 1.31 are *out-of-phase combinations* of the two constituent AOs: we can say that the localized orbital corresponding to one fragment contains a small tail on the antibonding orbital of another fragment.

Generally, it turns out that the shape of LMOs reflects nicely the chemical valence structure of most molecules: the LMOs are usually concentrated in the regions of classical inner shells, lone pairs or individual chemical bonds, while in other parts of the molecule they possess small tails only. We may say that LMOs connect the concept of the chemical bond and the concept of one-electron orbitals. For another example, the schematic view of the canonical and localized MOs of the water molecule is shown in Fig. 1.32. The LMOs clearly represent the inner shell 1s AO on the oxygen, the two OH σ-type bonding MOs and the two lone pair orbitals of the classical chemical picture.

While the canonical MOs themselves reflect the symmetry of the molecule (they transform according to the irreducible representation of the point group), the LMOs

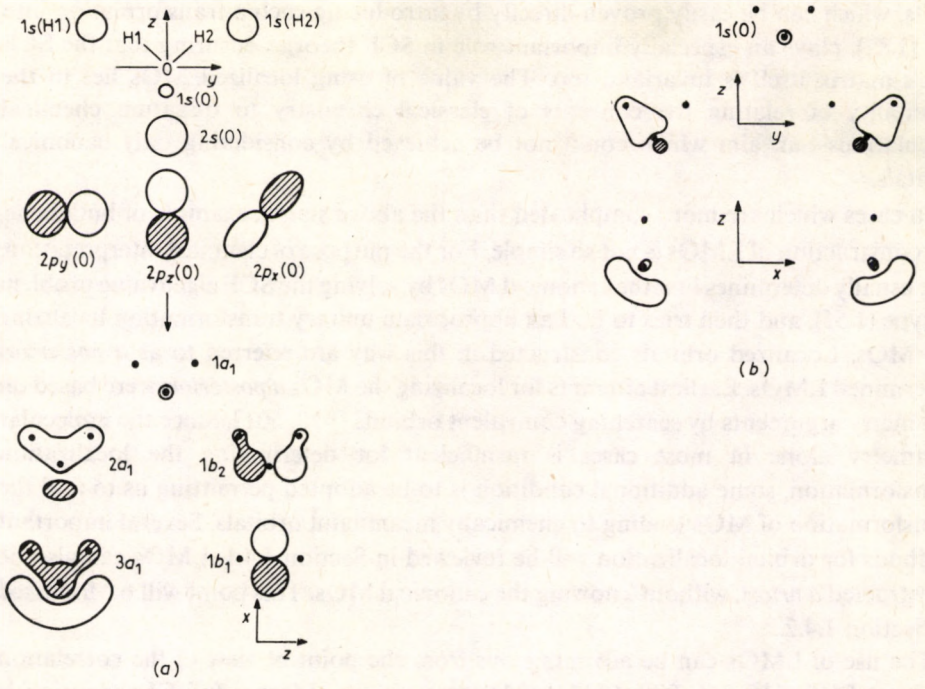


Fig. 1.32 Canonical *(a)* and localized *(b)* MOs of the water molecule in a schematic representation. Nuclei are indicated by dots

may possess another type of symmetry property. A similar LMO may correspond to each of the equivalent chemical bonds in a molecule, if any. These LMOs transform into each other under the symmetry operations, and thus correspond to reducible representations of the molecular point group. Such LMOs are called *equivalent orbitals* (*cf.* the two C=C bonds in butadiene and φ_1, φ_2 in Fig. 1.31; or the two equivalent O—H bonds of water and the two equivalent bonding orbitals in Fig. 1.32.) In such a way, by using localized MOs the equivalent groups can be described by means of equivalent orbitals which is not the case if using canonical MOs. This feature represents an important advantage of the localized orbital framework. Note that the determination of equivalent orbitals is usually not unique, and sometimes not even possible [667].

It cannot be overemphasized that the canonical and localized (or any other type of) MOs represent a completely equivalent description, from the physical point of view, of the ground state electronic structure at the Hartree–Fock level. All physical properties, any expectation values and the whole density matrix **P** is invariant under a localization transformation*. The invariance of matrix **P** to any unitary transformation of the

* Note that the Slater rules for evaluating matrix elements over determinantal wave functions and the simple definition of matrix **P** given in Eq. (1.66) remain valid only if the localization transformation is unitary; otherwise one should use more general expressions due to the nonorthogonality of the resulting MOs.

MOs, which can be easily proven directly by introducing such a transformation into Eq. (1.81), plays an especially important role in SCF theories ensuring that the SCF Fock matrix itself is invariant, too. The value of using localized MOs lies in the possibility of relating the concepts of classical chemistry to quantum chemical calculations—an aim which could not be achieved by considering only canonical orbitals.

In cases which are more complicated than the above simple example of butadiene, the construction of LMOs is not so simple. For the purpose of chemical interpretation, one usually determines first the canonical MOs by solving the SCF eigenvalue problem of type (1.55), and then tries to find an appropriate unitary transformation localizing the MOs. Localized orbitals constructed in this way are referred to as *a posteriori* determined LMOs. Earliest attempts for localizing the MOs *a posteriori* were based on symmetry arguments by searching equivalent orbitals [499, 501]. Since the molecular symmetry alone in most cases is insufficient for determining the localization transformation, some additional condition is to be adopted permitting us to find the transformation of MOs leading to chemically meaningful orbitals. Several important methods for orbital localization will be reviewed in Section 1.4.1. LMOs can also be constructed *a priori*, without knowing the canonical MOs. This point will be discussed in Section 1.4.2.

The use of LMOs can be advantageous from the point of view of the correlation problem [668, 746, 866, 998, 1282, 1424]. As a matter of fact, a full CI expansion is invariant to a unitary transformation of one-electron orbitals, as was already noted in Section 1.2.3. However, if the wave function is approximated by a truncated CI expansion, this invariance is lost, thus the canonical and localized description of configurations may result in different fractions of correlation energy which can be accounted for. The use of LMOs may be advantageous in two respects: (a) It provides a CI expansion where the intraorbital correlation is large, while the interorbital contributions are relatively small and diminish quickly with the distance between LMOs; thus a better convergence of CI is expected. (b) The approximate transferability of LMOs (which will be discussed later) results in an approximate transferability of correlation contributions, too, making chemical interpretations easier.

Methods for constructing LMOs, optimal for multideterminantal wave functions, were reported by Certain and Hirschfelder [192] and Adams [2]. A successful semiempirical scheme based on a perturbative CI in terms of LMOs, the PCILO method [866], will be reviewed in Section 1.4.2. With this exception, the discussion of using LMOs is restricted in this book to the Hartree–Fock level. We call the reader's attention to an important collection of review papers on the localization problem with more detailed information on some aspects of the problem and a more complete bibliography [193].

1.4.1 A POSTERIORI LOCALIZATION CRITERIA

In larger molecules possessing many AOs and many electrons, the definition of the LMOs is slightly arbitrary: many sets of MOs spanning the same occupied subspace can be found which are all "localized" from a certain point of view. Several localization criteria have been proposed which can be divided into two main categories:

(1) The *internal localization criteria* make no reference to concepts such as chemical bonds, atoms or molecular fragments; they determine the localization transformation by demanding some specific inherent properties for the LMOs. Among the procedures discussed below, the *energetic* [351, 352], *density* [1009, 1010] and the *spatial* [138, 400] criteria fall into this category.

(2) The use of *external localization criteria* pressupposes the specification of AOs, hybrids, atoms or molecular fragments on which the LMOs are to be localized on. Various external criteria have been proposed. They differ in the definition of the fragments and in the definition of what the term "localized on a given fragment" means.

The Edmiston–Ruedenberg energetic localization [351, 352]. Given a set of canonical MOs ψ_k, $k=1, 2, \ldots n$. For the sake of simplicity only the case of doubly filled orbitals is considered. The Coulomb part of the electron–electron repulsion energy of the molecule is expressed as, *cf.* Eq. (1.60):

$$E_J = 2 \sum_{i,k}^{occ} (\psi_i \psi_i | \psi_k \psi_k). \tag{1.180}$$

E_J is the expectation value of the Coulomb operator $\hat{J}$, and it is invariant under a unitary transformation of the occupied MOs. Let us consider the following decomposition of E_J:

$$E_J = 2 \sum_{i}^{occ} (\psi_i \psi_i | \psi_i \psi_i) + 2 \sum_{i \neq k}^{occ} (\psi_i \psi_i | \psi_k \psi_k).$$

Here the first sum measures the sum of Coulomb repulsions of the two electrons placed on MO ψ_i ("intraorbital repulsion"), while the second sum represents the Coulomb repulsions of electrons on different MOs ("interorbital repulsion"). Clearly, these two sums separately are not invariant to unitary transformations: the partition of E_J into intra- and interorbital parts depends on the nature of the orbitals. One can search for those type of MOs which minimize as far as possible the interorbital repulsion; it is expected that the resulting MOs will be concentrated in relatively small and far-lying regions "avoiding" each other to a great extent. The invariance of E_J means that if the interorbital repulsion is minimized, the intraorbital repulsion is maximal at the same time. Thus, one can seek a unitary matrix **U** for the localization transformation so that the intraorbital repulsion of the transformed orbitals $\varphi_k = \sum_i U_{ki} \psi_i$ be maximal:

$$\sum_k (\varphi_k \varphi_k | \varphi_k \varphi_k) = \max. \tag{1.181}$$

This is the energetic localization criterion of Edmiston and Ruedenberg.

As for the actual search for orbitals φ_k, one does not consider the general condition of Eq. (1.181) at once, since it would be too complicated to find the unknown matrix **U**. Instead, one performs an iterative procedure, according to the scheme called "two-by-two" rotations, in each step of which one mixes only two MOs, say ψ_i and ψ_j, by the transformation

$$\psi_i' = \cos\alpha\, \psi_i + \sin\alpha\, \psi_j$$

$$\psi_j' = -\sin\alpha\, \psi_i + \cos\alpha\, \psi_j. \tag{1.182}$$

Here α is the parameter of the 2×2 rotation defined by the requirement of maximizing the intraorbital repulsions for the MOs ψ_i' and ψ_j' in question:

$$\frac{\partial}{\partial \alpha} [(\psi_i' \psi_i' | \psi_i' \psi_i') + (\psi_j' \psi_j' | \psi_j' \psi_j')] = 0 \tag{1.183}$$

This equation can be solved for α, and the pair of new orbitals ψ_i' and ψ_j' can then be constructed. One should apply the two-by-two rotations to each pair of MOs and repeat the whole procedure until it converges and one obtains the final set of LMOs.

It turns out that the Edmiston–Ruedenberg LMOs are in most cases in very close agreement with the chemical picture and represent clearly the inner shells, lone pairs and bonds of the molecules. Since one should deal with the whole list of the two-electron integrals in each step, the Edmiston–Ruedenberg procedure is rather time-consuming for larger molecules.

Von Niessen's density criterion [1009, 1010]. A similar approach was proposed by von Niessen using the charge density instead of the Coulomb repulsion for deriving a localization criterion. The charge density due to the MO φ_i is given simply by

$$\rho_i(\mathbf{r}) = |\varphi_i(\mathbf{r})|^2 . \tag{1.184}$$

The overlap of the charge densities ρ_i and ρ_j is defined as

$$D_{ij} = \int \rho_i(\mathbf{r}) \rho_j(\mathbf{r})\, \mathrm{d}^3\mathbf{r} . \tag{1.185}$$

Again, the sum of all density overlaps, $\sum_{ij}^{\text{occ}} D_{ij}$ for all pairs of MOs is invariant to any unitary transformation of MOs but its intra- and interorbital components $\sum_{i}^{\text{occ}} D_{ii}$ and $\sum_{i \neq j}^{\text{occ}} D_{ij}$, respectively, are not invariant separately. Accordingly, the density localized orbitals are defined by demanding that the sum of interorbital density overlaps be minimal:

$$\sum_{i<j} D_{ij} = \min . \tag{1.186}$$

This condition, of course, involves the maximization of the sum of intraorbital density overlaps D_{ii}.

It was found that the density localized MOs are similar to those obtained by the Edmiston–Ruedenberg energetic criterion. The density localization procedure is cheaper than the energetic one, but it uses the D_{ij} density overlap integrals which are not calculated by standard SCF MO programs.

The Foster–Boys spatial criterion [138, 400]. Let us define the centre of MO φ_i as $\langle\varphi_i|\hat{\mathbf{r}}|\varphi_i\rangle$ where $\hat{\mathbf{r}}_i$ is the coordinate operator with respect to an arbitrary fixed origin. A unitary transformation can be defined by demanding that the following sum be of maximal value:

$$S=\sum_{i<j}|\langle\varphi_i|\hat{\mathbf{r}}|\varphi_i\rangle-\langle\varphi_j|\hat{\mathbf{r}}|\varphi_j\rangle|=\max. \tag{1.187}$$

This requirement results that the "distance" between the centroids of different MOs will be as large as possible. This is the Foster–Boys or spatial localization*. In actual calculations, the Foster–Boys criterion is also achieved by 2×2 rotations as was explained above.

The spatially localized MOs are usually also similar (but not identical) to the energetically localized ones. The main advantage of the Foster–Boys procedure is that it is very economic as compared to the Edmiston–Ruedenberg method, since the former works only with one-electron matrix elements.

External localization criteria. The most important one was proposed by Magnasco and Perico [858]. In this approach one works with so-called local Mulliken populations. We recall that the Mulliken population is defined as $P_{\mu\nu}S_{\mu\nu}$ (*cf.* Section 1.2.5) where $\mathbf{P}$ is the usual density matrix as defined in Eq. (1.81), and $S_{\mu\nu}$ is the overlap of AOs μ and ν. Now, the basis set is partitioned into fragments (atoms, bonds, etc.) according to the chemical picture. The fact that an AO μ belongs to the fragment K can be denoted by the symbol $\mu\in K$. The Mulliken local electron population on fragment K is given by

$$P_K=\sum_{\mu,\nu\in K}C_{K\mu}C_{K\nu}S_{\mu\nu}. \tag{1.188}$$

The Magnasco–Perico or population localization consists in maximizing the sum of fragment populations P_K. Similar to the previous methods, the actual search for population localized orbitals can be performed by 2×2 rotations iteratively. The cost of this procedure, however, is very low since one works only with the easily accessible $\mathbf{C}$ and $\mathbf{S}$ matrices. A comparison of the population and energetically localized MOs can be found, for example, in Ref. [1362]. The generality of this Magnasco–Perico localization is not so wide as that of the internal schemes, since (a) the specification of the fragments can be ambiguous in some cases, and (b) it is presupposed that the

* Originally not the sum but the product of the squares of interorbital distances was maximized.

Mulliken populations are relevant for the given molecule and in the given basis set. In most cases, however, the population localized MOs turn out to be similar to those obtained by other criteria. The Magnasco–Perico criterion has also been extended to the virtual MO space [140].

The density matrix **P** can be used to determine LMOs in other contexts, too. Caldwell *et al.* [176] utilized the fact that eigenvalues of monoatomic, diatomic, etc. blocks of **P** can be interpreted as occupancies of one-centre nonbonding, two-centre, etc. orbitals which are close to the LMOs if the occupancy approaches the value of 2 for occupied orbitals, and the value of 0 for virtual orbitals. Such *bond order orbitals* were constructed previously by Jug [657] (see below). The elements of the canonical MO LMO transformation matrix are defined by the overlaps of the bond order orbitals and the canonical MOs. Projection properties of the density matrix can also be exploited to construct *a posteriori* LMOs [1324].

Analyzing the large body of numerical data documented in the literature concerning the shape and structure of *a posteriori* localized MOs, the following picture has emerged. The molecules can be classified according to their localizability. Systems which can be described by their classical Lewis-structures (*i.e.*, in terms of inner-shell, lone pair AOs and a unique set of two-centre chemical bonds) turn out to be well-localizable. This means that there exists a localization transformation which provides LMOs corresponding to the orbitals conserving atomic character even in the molecule and to the chemical bonds in the Lewis structure having only small tails over the molecule. A quantitative index of the localizability is given, for example, by the weight l_l of the localized part of the LMO (see below; *cf.* also Section 2.1). Since the LMOs are normalized to unity, $l_l + l_t = 1$ where l_t is the weight of the tails. The localizability l_l is usually expressed in percents; for well localizable systems $l_l \gtrsim 95\%$.

In terms of VB language, the well-localizable systems are those which have a single dominant VB structure. Saturated organic compounds, molecules containing independent (unconjugated) double or triple bonds, etc. fall in this category. (It is somewhat surprising that linear conjugated polyenes are also relatively well localizable systems which is connected with the alternation of their C—C bond lengths.)

Molecules with more than one dominant VB structures were found weakly localizable: here the LMOs may have large tails and they do not necessarily correspond to the chemical picture which is inherently delocalized (or involves a simultaneous consideration of more than one resonance structure) in these cases (*cf.* also Section 2.6).

As to their localized parts, the LMOs in well-localizable systems were found to be approximately transferable from molecule to molecule, reflecting the existence of similar bonds in different molecules [669, 981, 1086]. The small tails of LMOs, however, are strongly affected by the molecular environment and are definitely non-transferable.

In large molecules, the tails of LMOs are not only small but also quickly diminish with the distance from the given bond if the system is well-localizable. An unambigous *a priori* measure of localizability for extended systems, based on the long-range

behaviour of the SCF density matrix **P**, was proposed recently [1320]. As a matter of fact, simple Hückel-type considerations [927, 1374] suggest that in linear extended systems density matrix elements $P_{\mu\nu}$ fall off either exponentially with the distance r between AOs μ and ν or, or as $1/r$. The former is the case for well-localizable systems while the latter corresponds to a weakly localizable set. *Ab initio* numerical calculations [1320] also confirm this result, and it turns out that the localizability of a system is the greater the faster is the fall-off of the corresponding density matrix elements.

As far as the localizability is large, and the tails of LMOs are small, a reasonable approximation to the exact LMOs is to consider only their localized parts, that is, to neglect their tails. Such LMOs are completely localized on the given fragment of the molecule, and will be referred to as *strictly localized molecular orbitals* (SLMOs). If a minimal basis is used, the SLMOs possess of two hybrid AOs in case of two-centre bonds, while a single hybrid in case of a lone pair. In general, the SLMOs do not span exactly the SCF occupied subspace, thus they cannot be considered as true solutions to the HF problem. However, they may give good initial approximations to the latter and, at the same time, they can easily be constructed *a priori* from the chemical formulae as will be discussed in the next section. Methods for *a posteriori* determination of optimum SLMOs, based on the analysis of the SCF density matrix, were proposed by McWeeny and Del Re [853, 854]. Polák [1106–1109] and Jug [657]. This latter approach was discovered also by Caldwell *et al.* [176], and by Weinhold and coworkers [401, 1163, 1181].

1.4.2 A PRIORI LOCALIZED MOs

As was mentioned above, the computation of canonical MOs is not a necessary step to find LMOs: there exist special procedures which are able to produce LMOs directly. One can proceed in two different ways:

(a) One does not solve the canonical HF equations but works with the general nondiagonal ones carrying all ε_{kl} matrix elements over the whole SCF procedure. In this case one should modify the Fockian by introducing a special *localization potential* in order to ensure localization of the final MOs, which were otherwise not defined uniquely by the general HF equations. This potential is constructed so that the occupied subspace remains its invariant subspace; thus the general HF equations remain valid. The form of the localization potential determines the nature of the LMOs, or so to speak, defines a localization criterion. Such (rather laborious) procedures leading to nonorthogonal LMOs were developed, for example, by Peters [1085], Adams [2, 3] and Gilbert [445–447].

(b) Another way of finding LMOs directly (*i.e.*, without solving the canonical HF equations) consists of constructing an appropriate initial guess from approximate LMOs (*e.g.*, strictly localized MOs), and to adopt a procedure which permits us to improve them systematically but preserves their localized nature.

Further on in this section we will focus our attention on procedures of type *(b)*. First of all, we have to discuss the strictly localized MOs (SLMOs) in some detail. In the subsequent discussion, we will treat well-localizable systems where the chemical bonds possess only two atomic centres. The generalization to aromatic systems, for example, where the "strictly localized" units are two-centre only for the σ-core but may extend over a few $2p_z$ AOs for the π-system, is straightforward*.

Strictly localized MOs. Given a set of directed atomic hybrid orbitals (HYOs) $h_{i\mu}$ where the label i indicates a two-centre bond which the HYOs belong to, and μ labels the two HYOs h_{i1} and h_{i2}. Then, the two-centre SLMO takes the form:

$$\varphi_i = \mathcal{N}_i[h_{i1} + \lambda_i h_{i2}] \tag{1.189}$$

where $\mathcal{N}_i$ is chosen to normalize φ_i to unity, and the coefficient λ_i determines the *polarity* of bond i. If $\lambda_i = 1$, the bond is neutral. Once the HYOs are determined, λ_i represents the only free parameter of the SLMO φ_i. These bond polarities can be obtained by solving the following set of 2×2 HFR problems:

$$\begin{bmatrix} F^i_{11} & F^i_{12} \\ F^i_{21} & F^i_{22} \end{bmatrix} \begin{bmatrix} 1 \\ \lambda_i \end{bmatrix} = E_i \begin{bmatrix} 1 & S^i_{12} \\ S^i_{21} & 1 \end{bmatrix} \begin{bmatrix} 1 \\ \lambda_i \end{bmatrix} \qquad i = 1, 2, \ldots m \tag{1.190}$$

where m is the total number of bonds, $F^i_{\mu\nu}$'s are the elements of the Fockian at the i-th bond in the hybrid basis, and $S^i_{12} = \langle h_{i1} | h_{i2} \rangle$ is the overlap of the two HYOs spanning the bond i. Equation (1.190) can be solved easily for the bond polarities λ_i and the bond energies E_i. (Note that, due to SCF effects, the $F^i_{\mu\nu}$ Fock matrix elements depend on all λ_j's so Eqs (1.190) are coupled. Since the two HYOs h_{i1} and h_{i2} are directed towards each other (Fig. 1.23), their overlap S^i_{12} is rather large (S^i_{12} is usually 0.5–0.7 depending on the bond distance and on the form of the HYOs.) Therefore, in actual calculations it must not be neglected, though it does not appear in semiempirical ZDO schemes where the basis set is assumed to be orthogonalized. However, in order to gain insight into the basic characteristics of SLMOs, the following simple model example is illuminating. Let us assume that (1) $S^i_{12} = 0$, *i.e.* we have an orthonormalized HYO basis, and (2) the $F^i_{\mu\nu}$ matrix elements do not depend on the polarity λ_i. These conditions correspond to a Hückel-type approximation which is never acceptable from the numerical point of view but often contains the most important qualitative features allowing us to study the essence of the chemical bonding**. Applying these simplifications, Eq. (1.190) reduces to

$$\begin{bmatrix} \alpha_1 & \beta \\ \beta & \alpha_2 \end{bmatrix} \begin{bmatrix} 1 \\ 2 \end{bmatrix} = E \begin{bmatrix} 1 \\ 2 \end{bmatrix} \tag{1.191}$$

* One can consider in aromatic systems (or in other ones with more than one resonance structure, like the carboxyl group) transferable building blocks consisting not of two-centre MOs but of the whole "delocalized" π-system [301, 992].

** Note that these approximations are not so crude since (a) Eqs (1.190) can be subjected to an explicit Löwdin-orthogonalization providing $S^i_{12} = 0$, and (b) the matrix elements of the Fockian, $F^i_{\mu\nu}$ do not depend strongly on λ_i's within the usual range of the latter.

where we dropped the label i for the sake of simplicity, and applied the usual Hückel notation for the matrix elements of the Hamiltonian. Further, let us consider a homonuclear bond for which $\alpha_1 = \alpha_2 = \alpha$. Then, the two solutions of Eq. (1.191) are, after normalizing the SLMO:

$$\lambda = 1, \quad \text{thus} \quad \varphi_i = \frac{1}{\sqrt{2}}(h_{i1} + h_{i2}) \quad \begin{matrix} \text{with the energy} \\ E_i = \alpha + \beta \end{matrix} \tag{1.192}$$

$$\lambda = -1, \quad \text{thus} \quad \varphi_{i^*} = \frac{1}{\sqrt{2}}(h_{i1} - h_{i2}) \quad \begin{matrix} \text{with the energy} \\ E_{i^*} = \alpha - \beta \end{matrix} . \tag{1.193}$$

Equation (1.192) describes the in-phase combination of the two HYOs h_{i1} and h_{i2}, while Eq. (1.193) corresponds to the out-of-phase combination (Fig. 1.33). It is easy to

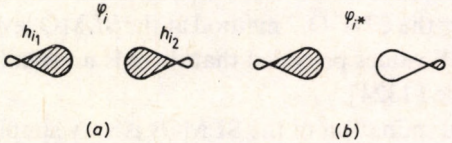


Fig. 1.33 Hybrid orbitals in a two-centre bond. *(a)* Bonding, *(b)* antibonding combination

demonstrate that electrons on the in-phase level increase, while on the out-of-phase level decrease the bond order. Accordingly, we say that φ_i is a bonding, φ_{i^*} is an antibonding orbital. (Here and further on the asterisk refers to antibonding levels.) The energy of a bonding MO is deeper than that of an antibonding one; thus the β "bonding parameter" should always be negative.

If $\alpha_1 \neq \alpha_2$ then $|\lambda| \neq 1$; thus one obtains an intrabond charge transfer: the electron populations on the HYOs h_{i1} and h_{i2} become different. Such a polarized bond carries a dipole moment contribution.

Whenever the electrostatic interaction among different bonds is taken into account, the Fock matrix elements are to be modified appropriately [866, 1125, 1324]. However, the electrostatic effects can be taken into account introducing an effective core potential for each bond which contains the electrostatic potential due to both nuclei and electrons in the other bonds. In fact, if the electrostatic (Coulomb + exchange) interactions are included, the elements of the Fockian for the i-th bond become:

$$F^i_{\mu\nu} = H^i_{\mu\nu} + \sum_{j(\neq i)} \sum_{\lambda,\sigma \in j} P^j_{\lambda\sigma} \left[(\mu\nu \mid \lambda\sigma) - \frac{1}{2}(\mu\lambda \mid \nu\sigma) \right]$$

$$+ \sum_{\lambda,\sigma \in i} P^i_{\lambda\sigma} \left[(\mu\nu \mid \lambda\sigma) - \frac{1}{2}(\mu\lambda \mid \nu\sigma) \right]. \tag{1.194}$$

Here $\mathbf{H}^i$ and $\mathbf{P}^i$ are the 2×2 blocks of the core and density matrices, respectively, corresponding to the bond i. ($\mathbf{H}^i$ includes the kinetic energy and the attraction to all the

nuclei in the molecule.) The second term [the sum over $j \neq i$ in Eq. (1.194)] describes the coupling between bonds i and j, and, together with $H^i_{\mu\nu}$ serves as an effective core for the bond i:

$$H^{i,\mathrm{eff}}_{\mu\nu} = H^i_{\mu\nu} + \sum_{j \neq i} \sum_{\lambda,\sigma \in j} P^j_{\lambda\sigma} \left[(\mu\nu \mid \lambda\sigma) - \frac{1}{2} (\mu\lambda \mid \nu\sigma) \right].$$

The j'th block of the density matrix, $\mathbf{P}^j$, is determined by the corresponding bond polarity λ_j of the j'th bond. As a result, the $\mathrm{F}^i_{\mu\nu}$ matrix elements of the given bond i will depend on the polarities of other bonds as well, which requires an iterative procedure for determining the polarities. This procedure, however, is very fast since one deals only with simple 2×2 problems in each step. The λ_i's determined in this way are said to be *optimized* bond polarities. The SLMOs with optimized polarities often give a satisfactory account of the net electrostatics of the molecule. The atomic charges for example, as obtained by the CNDO/2 method at the SLMO level, are quite close to the standard CNDO/2 SCF values provided that there is no significant interbond charge transfer in the molecule [1324].

It seems that the determination of the SLMOs is very simple: one has to deal with several 2 by 2 problems (one for each bond). Lone pairs are left as one-centre HYOs so they are not included. Moreover, it was observed that the polarities of SLMOs are roughly determined by the nature of the two atoms in question. Such polarities are approximately transferable from molecule to molecule and can be determined either by using some standardized sets extracted from a series of calculations on sample molecules [981], or can be estimated by the electronegativities χ_1 and χ_2 of the atoms possessing the HYOs according to the formulae [467, 1122]:

$$\lambda = \sqrt{\frac{1+\xi}{1-\xi}} \tag{1.195}$$

where

$$\xi = 1 - \mathrm{e}^{-\frac{1}{4}(\chi_1 - \chi_2)}. \tag{1.196}$$

With these transferable bond polarities, it is possible to give a rough estimation of the electrostatics of the molecule (atomic charges, dipole moments, electrostatic potentials [973, 981]). Rotation barriers can also be calculated provided that the overlap between different SLMOs is properly accounted for [209, 247, 597, 598, 658, 1299], as in the case of the *ab initio* or Extended Hückel levels (see also in Section 3.2).

Using transferable bond polarities, no actual interbond interactions can be taken into account. The optimization of the polarities permits us to obtain non-transferable SLMOs capable of describing *inductive effects*.

In constructing the SLMOs, one is faced with the problem of determining appropriate hybrid orbitals. The quality of the SLMO level of description strongly depends on how suitable are the HYOs themselves. Several procedures have been

proposed for obtaining atomic hybrids. These can be divided into three category: (a) standard, fully transferable (*e.g.*, Pauling-type HYOs (*cf.* Section 1.2.5) [101, 1070]); (b) *a posteriori* HYOs which are obtained by extracting information from the full SCF results [401, 657, 853, 854, 1107, 1108, 1163, 1181]; and (c) *a priori* determined non-transferable hybrids based on for example the analysis of the overlap matrix [115, 299, 435, 908]. Among hybrids of type (c), the maximum overlap criterion by Del Re [299] is of greatest importance. The hybridization on first-row atoms is much better understood than that on the higher elements, and this is the reason why the SLMO schemes are usually adopted for molecules built up only by first-row atoms and hydrogens. At the SLMO level, the case of atoms bearing two or three lone pairs (LPs) is rather interesting. As was discussed in Section 1.2.5, one can choose the direction of these LPs in quite different ways (see Fig. 1.13) obtaining the tetrahedral and spectroscopic LPs. It is noteworthy that using SLMOs the tetrahedral and spectroscopic choice for the LPs represents a completely equivalent description, since these LPs can be obtained from each other by a 2×2 (or 3×3) unitary transformation within a completely occupied subspace by the two (or three) LPs in question. Such a transformation does not affect the many-electron determinantal wave function built up by the SLMOs, thus one can use both kinds of LPs as long as the strictly localized character of the MOs is maintained. The effectivity of procedures going beyond the SLMO approximation, however, does depend on the representation of lone pairs [112, 115, 435, 1315].

The Del Re method [298]. A very simple procedure, using conceptually SLMOs, was proposed by Del Re, as early as 1958. Here the 2×2 Hamiltonian of Eq. (1.191) is parameterized in the spirit of the Hückel method, therefore the explicit construction of the HYOs is not necessary. The α and β parameters depend not only on the type of corresponding atoms, but also on the parameters of the neighbouring ones. As a consequence, the Del Re method accounts for inductive effects. For the determination of the actual values of the parameters one has to solve an inhomogeneous system of equations of order N_{at}, N_{at} being the number of atoms in the molecule. Once the actual values of the parameters have been obtained, bond energies, polarities and net atomic charges can easily be calculated by explicit formulae resulting from the solutions of the 2×2 problem. The method offers a rough description of electron distribution in saturated molecules with a negligible computational cost. For unsaturated compounds, it is usual to perform a Hückel or PPP calculation for the π-system while the charge distribution in the σ core is taken into account by Del Re's method; for an application see *e.g.* [433].

Utilization of SLMOs for initial guess. The conceptual and computational simplicity of SLMOs makes them very suitable for using as starting points for further calculations. The density matrix **P** as obtained by the SLMOs may, for example, represent a good initial guess for standard SCF procedures [783, 784, 1269] (*cf.* also Section 1.3.1). Another idea was utilized by Daudey [278] who determined the SCF LMOs directly, avoiding the construction of canonical MOs, the following iterative

procedure:

$$\varphi_i^{(n+1)} = \varphi_i^{(n)} - \sum_{k^*}^{(\text{virt})} \frac{F_{ik^*}^{(n)}}{F_{k^*k^*}^{(n)} - F_{ii}^{(n)}} \varphi_{k^*}^{(n)} \tag{1.197}$$

where the superscript n labels the steps of iteration, $\mathbf{F}^{(n)}$ is the Fockian built up by the LMOs of the corresponding step:

$$F_{ik^*}^{(n)} = \langle \varphi_i^{(n)} \mid \hat{\mathrm{F}} \mid \varphi_{k^*}^{(n)} \rangle . \tag{1.198}$$

Using SLMOs $\varphi_i^{(0)}$ as initial guesses, he obtained the SCF LMOs spanning the exact occupied subspace in a few iteration steps. (Note that $F_{ik^*} \to 0$ as the iteration procedure converges, in accord with the local Brillouin theorem, Eq. (1.44).)

Improvements of the SLMO description. The inherent drawback of SLMOs is that they do not account for interbond charge transfer effects. This shortcoming can be eliminated by adding delocalization corrections (tails) to the SLMOs. The tails can be obtained, for exampe, by the so-called SCF perturbation theory [1140, 1225]. A first-order approach is represented by the "linearized SCF approximation" [1321]. It is based on the fact that the tails of LMOs though significant in many respects, are small quantities. Accordingly, in this procedure, any terms of the relevant SCF equations, containing products or squares of the tails, are neglected, and the resulting linearized SCF equations are solved analytically leading to explicit tail formulae. (In writing down the SCF equations, namely, the local Brillouin theorem, the orthogonality of the SLMOs was assumed.) A natural result of the linearization is that the SLMOs representing the chemical bonds of the molecule at the zeroth order interact in a pairwise manner; thus the tails can be calculated independently. The linearized SCF method has been successfully applied at the CNDO/2 level in conformation analysis [1323].

In order to improve this linearized approximation, one can apply some version of higher order perturbation theory which is special in the sense that it provides an expansion for the *tails* and not for *eigenvectors* as usual perturbation theory does. By this approach introduced recently [1322], recursive formulae have been derived at any order of PT for the case when the SLMOs form an orthonormal set and the effective one-electron Hamiltonian (Fockian) is assumed to be known. Very recently, this scheme was generalized to the non-orthogonal case as well [890]. Apart from computational advantages, there are some qualitative and conceptional results which can be learned from this approach of generating the tails. First, it turned out [883] that there always exists a set of non-orthogonal LMOs φ_i spanning the exact occupied subspace and having a special structure so that they can be written in terms of SLMOs φ_i^0 as

$$\varphi_i = \varphi_i^0 + \sum_{k^*}^{\text{virt}} \eta_{ik^*} \varphi_{k^*}^0 \tag{1.199}$$

where η_{ik^*}'s are the tail coefficients. (Note that φ_i is not normalized to unity.) It seems from Eq. (1.199) that in the expansion of the exact LMOs over SLMOs the tails are generated only on antibonding orbitals, that is, no mixing of bonding-bonding type need to be considered. (As a matter of fact, the occupied and virtual SLMOs together span the same space as the original basis AOs, thus any set of orbitals ψ_i (whether localized or not) can be trivially expanded as

$$\psi_i = \varphi_i^0 + \sum_{l(\neq i)}^{\text{occ}} \vartheta_{il}\varphi_l^0 + \sum_{k^*}^{\text{virt}} \kappa_{ik^*}\varphi_{k^*}^0 . \tag{1.200}$$

The freedom of linear transformations among occupied orbitals means that the coefficients ϑ_{il} and κ_{ik^*} are not uniquely determined by the SCF conditions. Now, it was proven [883] that the choice $\vartheta_{il}=0$, leading to the special form of Eq. (1.199), *introduces no approximations*, and exact nonorthogonal LMOs having the form of Eq. (1.199) can always be found. Thus, one concludes that the mixing between the strictly localized bonding MOs represents no physical delocalization effects. Note that if the LMOs φ_i are subjected to an orthogonalization procedure, the special form of Eq. (1.199) cannot be maintained since *orthogonality tails* appear which mix also the bonding SLMOs. We stress further that the form of Eq. (1.199) is rather special; the SCF LMOs as obtained by, for example, an *a posteriori* localization procedure or by Daudey's method (see above) do not have this property. For instance, Eq. (1.197) mixes also the bonding zeroth order strictly localized orbitals from the second iteration step on. In fact, the condition $\vartheta_{il}=0$ turned out to be a useful external localization criterion [30, 883, 890, 1322].

A second important value of this perturbational approach is that it allows us to gain some insight into the propagation of delocalization interactions, by analysing the results obtained at different orders of PT. As noted above, the aim of this PT is to find expressions for the tails. At the first order of PT, only direct (through space, see below) bond-antibond interactions appear. The corresponding tail formula determines the tails to a reasonably good accuracy in the vicinity of the central part of the LMO in question, but the first-order tails diminish too quickly with distance as compared to the tails of exact LMOs. Usually, the first order tails on geminal (first neighbour) bonds are good. The situation is improved at the second order of PT which produces tails of correct sign and magnitude on second neighbours, etc. (see Fig. 1.24). The second order tails result from indirect (through bond, *vide infra*) delocalization interactions [890, 1322].

The origin of the terminology of "through space" and "through bond" interactions is connected to that of Hoffmann and coworkers [540, 576, 578, 579] which was used for studying changes in orbital energies. An interaction is said to be *through space* if there exists a direct interaction matrix element between the orbitals in question. One speaks about a *through bond* interaction if there is no direct matrix element, but there is a third intervening bond which interacts with both orbitals directly. The interaction then propagates through this third bond. We have used these terms in connection with

delocalization interaction, and the PT developed in Refs [890, 1322] permits us to give a well defined meaning to this terminology. We note that slightly different definitions for through-space and through-bond delocalization effects, based on an *a posteriori* analysis instead of a direct perturbational treatment, were given by Brunck and Weinhold [148] and Imamura and coworkers [623–627, 1036–1039].

Through-space and through-bond interactions appear at the first and second order of PT, respectively. These concepts can easily be generalized to the higher orders too; it turns out that at the n-th order the delocalization propagates through $n-1$ bonds [890, 1322].

In order to recover the correct asymptotics of the density matrix [927, 1320], which is a typical "infinite order" effect in the LMO-PT approach, one has to consider such through-many-bond interactions.

An important feature of through-space delocalization interaction is that it has a short radius of action (about, 4–5 Å only). The through-one-bond interaction has about twice as large radius of action. Long range delocalization (*i.e.*, charge transfer) can appear only as a through-many-bond effect. The distinction between through-space and through-bond delocalization interactions permits us to understand, for example, why intermolecular charge transfer effects are usually much smaller than intramolecular ones. The delocalization between two molecules can propagate only through-space, thus this charge transfer is generally weak at usual intermolecular distances. On the contrary, in the intramolecular case, the delocalization can spread along a sequence of bonds allowing significant long range charge transfer to occur.

This perturbation approach was applied to the study of conformational problems (Section 3.3) and electronically excited states and optical rotatory strengths [30] (see Section 3.3 and 3.7). In the latter, the use of LMOs is very advantageous since it permits us to analyse the electronic spectra in terms of chemical chromophores.

The PCILO method. Though we focus our attention mainly on the HF problem, no treatment of localized orbitals can be complete without discussing the PCILO method (perturbative CI using localized orbitals). This very important all-valence-electron method was originally introduced by Malrieu and coworkers [325, 866, 868] at the CNDO level. The PCILO is a CI calculation (see Section 1.2.7) where SLMOs are chosen as configuration-generating one-electron functions. The zeroth order wave function consists of the single determinant of occupied SLMOs whose polarities can be optimized, if desired. The SLMOs are built up by HYOs determined by Del Re's criterion [299]. Standard perturbation theory is then applied in solving the CI problem. In this sense, the PCILO is a many-body approach [752] where the Epstein–Nesbet partition was originally applied. A modification of the procedure for using the Møller–Plesset partition has also been proposed [113, 114]. Since the SLMOs, having no tails, differ significantly from the HF orbitals, the aim of the perturbation theory in the PCILO method is twofold. First, it has to improve the orbitals towards the Hartree–Fock ones by giving polarization and delocalization corrections to the SLMOs. Secondly, intra- and interbond correlation energy contributions are also

calculated. Thus, in principle, the PCILO wave function, being correlated, can be of much better quality than the HF wave function corresponding to the same model Hamiltonian. (In fact, this is not always the case since some genuine SCF effects such as delocalization are taken into account in PCILO by calculating only contributions by the low orders of PT.) In contrast to other approaches mentioned previously, the PCILO energy is also obtained from a perturbation series instead of being calculated as an expectation value. The drawback of this is that the energy is not an upper bound, but this approach results in considerable computational advantages. The PT procedure is usually performed up to the third order in energy; recently fourth order PCILO calculations were also reported [269]. The convergence of the perturbational series is not *a priori* guaranteed; for example, sometimes the fourth order contributions are comparable with the third order ones. Nevertheless, the third order energy serves already as an acceptable approximation provided that the zero order description (SLMO level) is not improper. This feature permits to use the PCILO method in extensive systematic numerical studies on many molecules. The reliability of the zero order SLMO level depends on (1) the choice of hybrid orbitals and on (2) whether the molecule in question can be represented by two centre bonds and atomic lone pairs, at least to a reasonable initial approximation. Point (1) represents a problem only when there are atoms bearing more than one lone pair [115, 435], or for atoms in an unusual bonding situation. Question (2) is connected with the representation of strongly delocalized (*e.g.* aromatic) systems. In such cases the delocalization corrections can be so large that they lead to the breakdown of the perturbation theory, or, one is faced with the problem that different Kekulé structures used for constructing the zero order wave function do not yield the same results up to the highest order of PT considered. It is important to realize that for the infinite order of PT, any zero order wave function can be equally well used provided that the perturbational series converges. Thus, in principle, any strictly localized structure could be used in an infinite order PCILO method. Hence the problem is due to the application of a *finite* order perturbation calculation: the third order energy, for example, may depend strongly on the choice of the zero order wave function. Different Kekulé structures thus lead to the same results only if they are equivalent by symmetry. The natural solution of this problem is the handling of delocalized (π-) electrons as undivided systems involving more than two centres already at the zero order. Such a scheme was utilized recently in connection with the PCILO method [114].

The use of CNDO/2 parametrization is also an unnecessary restriction; the method has already been extended to the INDO and NDDO levels [113, 114, 334]. Some effort has also been made to generalize the PCILO method to the *ab initio* level [279, 1050], but no really efficient procedure has yet been proposed. The main problem here is the nonorthogonality of the SLMOs if we abandon the ZDO approximation. This difficulty is usually bypassed in a formal manner introducing an explicit orthogonalization of the basis set of the zero order LMOs. This is, however, very unfavourable from the computational point of view since one should perform a four-

index transformation of all the two-electron integrals to the orthogonal basis. Moreover, the introduction of orthogonalized LMOs destroys the transferability of the zero order description which makes difficulties in chemical interpretations.

As to the reliability of the standard PCILO method, it is similar to that of the CNDO/2. An important advantage of PCILO is that some correlation effects are also considered. The PCILO has been successfully applied in extensive calculations on many molecules. The computer time requirement of the procedure increases with the third power of the number of orbitals, but the factor of proportionality at the third order term is quite small, so PCILO is very fast as compared to standard CNDO/2. (In semiempirical SCF theories the most time-consuming step is usually the repeated diagonalization of the Fock matrix. There is no such diagonalization in PCILO.)

Although the computational benefits of PCILO are apparent, in the opinion of the original authors "the main advantages of the method are certainly conceptual... PCILO provides a bridge to chemical »intuition«, and makes clear the local character of the energy, building it as a sum of one- two- three-body terms, as do empirical systematics" [866].

Group function formalisms. In conclusion, we shall comment briefly on an approach which is, in its general intention, closely related to the theory of localized orbitals: the group function method. The point here is to study the distortion and interaction of chemical fragments (groups) in a molecule. In this sense, the group function method can be considered as a generalization of the LMO approach. In the latter, the fragments are usually chosen to contain at most two centres and two electrons, and they are identified with localized bonds, inner shells and lone pairs. No such restriction is applied in the more general group function formalism. Analogous to the SLMO approach, in the group function theory each electron is assigned initially to a particular fragment of the molecule. The principal aim of the theory is to derive the relevant equations for the fragment wave functions by taking into account those interactions among the groups which preserve the groups separated, that is, which do not involve an electron transfer from one group to another. Such interactions describe Coulomb repulsion, mutual polarization and dispersion; the former two effects result from the averaged electrostatic interaction between the fragments and can be treated already at the HF level. At the same time dispersion is caused by the correlation of electrons assigned to different groups and cannot be accounted for within the HF scheme at all.

In principle, the group function theory can be formulated at the HF level or for correlated wave functions. Once the wave functions of the separated groups have been obtained, one can calculate the exact wave function of the molecule in terms of the fragment wave functions by switching on the charge transfer interaction between the different groups. Note that one should ensure the proper antisymmetry of the wave function both within and between the individual groups.

Important pioneering works in group function theory were done by Lykos and Parr [839, 1067] and McWeeny [710, 852, 853]; see also [616, 992]. In order to obtain

tractable formulae, these theories usually assume the *strong orthogonality* between the fragment wave functions which is expressed as

$$\int \phi_A(\mathbf{x}_1, \mathbf{x}_2, \ldots)\, \phi_B(\mathbf{x}_1, \mathbf{x}_2 \ldots)\, d\mathbf{x}_1 = 0, \qquad A \neq B\,. \tag{1.201}$$

That is, if ϕ_A and ϕ_B belong to different groups, one obtains zero by integrating over the variables of (at least) one of the electrons. The strong orthogonality restriction can be fulfilled by expanding the fragment wave functions over distinct and orthogonal basis functions. (This is easy to ensure in the ZDO-type methods.) This partitioning of the basis set is, however, not a necessary requirement in the group function formalism. Electron pair methods such as APSG (see Section 1.3.1), which can also be considered as group function formalisms since each group contains two electrons, do not apply such a restriction. The partitioning of basis orbitals represents an approximation which simplifies the treatment.

Group function methods can also be classified whether they account for correlation or not. Among recent approaches working at the HF level we mention Klessinger's "fragments in molecule" method [708, 709] and the "fragment SCF" procedure by Náray-Szabó and Surján [978, 986] which both were developed at the semiempirical CNDO/2 level. Klessinger solves the SCF equations on the basis of the strongly orthogonal fragment orbitals. In the latter approach [986] a "central part" is cut out forming a closed shell subset of the basis orbitals, which contains the chemically most important part of the molecule directly affected by the molecular rearrangement in the chemical process in question. For the central part the SCF equations are solved exactly, for other fragments the wave function is constructed by using SLMOs only, that is the strict localization is maintained and no tails are taken into account. In this manner an accurate description is ensured for the central part, while interactions with far-lying fragments are taken into account only approximately without considering delocalization effects. This represents a great simplification in computations and permits us to study conformational properties in very large systems quantitatively.

The generalization of the above approaches for the case of non-orthogonal basis sets (necessary for the extension to the *ab initio* level) is by no means straightforward. Some possibilities were proposed by Adams [4, 5] and Mehler [893, 894]. A very simple fragment method working at the *ab initio* level is that of Christoffersen [210] which was also combined with pseudopotential calculations for the inner shells [426].

We note finally that there is some connection between group function methods and different approaches such as Kirtman's recent density matrix treatment [696, 697], the "atoms in molecules" [34, 321], "diatomics in molecules" [361, 1371] and the "molecules in molecules" [811] methods.

Closing remarks. The framework of localized orbitals, and the group function methods as well, permit us to extract chemically relevant information from standard quantum chemical calculations, to discuss complicated effects in simple terms, and to construct more-or-less accurate wave functions using transferable building blocks. Deviations from transferability can be taken into account in an approximate manner.

Actual procedures can be efficient only if they utilize some chemical and/or physical model concerning the localization and delocalization. Such schemes are widely accepted in order to pick up the most significant effects and drop the unimportant ones, when calculating electron correlation, cf. APSG, IEPA, CEPA, etc; see Section 1.3.1, and many quantum chemists are looking forward to see how these approximate but reliable approaches gain importance in simplifying HF calculations as well. This requires a lot of future developments but the authors of the present book feel that such methods represent the only possibility of solving the "N^4 catastrophe" inherent in "brute force" *ab initio* HF computations for large systems.

1.5 REPRESENTATION OF ENVIRONMENTAL EFFECTS IN QUANTUM CHEMICAL CALCULATIONS

Although most chemical and physical phenomena are studied experimentally in condensed phases, the theoretical framework outlined in preceding sections is valid, in principle, only for isolated molecules, that is the corresponding macroscopic system is assumed to be an ideal gas. In order to be able to describe properly the molecules in the liquid phase or in solutions, as impurities in crystals or as molecular subsystems (*e.g.* active sites of enzymes) in large biomolecules, we need special quantum chemical methods taking into account the effect of the chemical environment. The purpose of the present section is to discuss briefly current theoretical models and computational methods for the representation of environmental effects in quantum chemical calculations.

The current theories of surrounding medium (solvent) effects have been worked out to describe rather differents situations, like "solvated electrons", solvated molecules and ions, electron and proton transfer reactions in solutions, hydrogen bonds in liquids, crystals and biomolecules. Probably as a consequence of the great variety of subjects, the theoretical treatments of them have been developed more or less independently. Tapia [1341, 1342] recently attempted to discuss all these situations in the framework of a unifying theory.

Theoretical studies of environmental effects may have various purposes, for example, the determination of solvent structure, the evaluation of the thermodynamic parameters of solutions, or quantum chemical investigation of the medium effects on solute molecular properties, spectral characteristics or reactivities. Although throughout this book we are concerned mainly with problems falling into the last category, we shall attempt to give an overall idea about the most important theoretical procedures and about their interrelationships.

The basic microscopic model system in the theories of environmental effects consists of one solute molecule and usually a large number of N solvent molecules* in a volume V at absolute temperature T. This model is appropriate for the description of cases

* The terms "solvent" and "solute" may have generalized meaning as environment and subsystem.

where the solute–solute interactions are negligible, that is, for dilute solutions. It is assumed that the translational and rotational motions of the molecules are decoupled from their electronic and vibrational degrees of freedom, which are, in turn, separated by the usual Born–Oppenheimer approximation. The solvent molecules are assumed to be in their ground electronic and vibrational states. The low-frequency translational and rotational motions, which are usually limited by the presence of surrounding molecules *(librations)*, can be treated by neglecting quantum effects.

The Hamiltonian of the overall system is partitioned as

$$H = H_S + H_\Sigma + H_{\Sigma S} \tag{1.202}$$

where H_Σ stands for the solute Hamiltonian, H_S represents the Hamiltonian of the N interacting solvent molecules, $H_{\Sigma S}$ is an operator of the solute-solvent interaction. Within the Born–Oppenheimer approximation the ground state solutions of the Schrödinger equation corresponding to the Hamiltonian (1.202) yield information about the system at zero absolute temperature at a given nuclear configuration. Temperature dependence can be introduced afterwards by statistical mechanical treatment of a large number of nuclear geometries.

The methods, which lay emphasis on the microscopic molecular representation of the solvent environment (in contrast to the continuum models, to be discussed later on) are usually treated under the term of "*discrete molecular complex approximations*". An adiabatic potential energy surface is associated with the system consisting of one solute and the N solvent molecules. The minima of the surface correspond to more or less stable structures, each of which can be characterized by the positional and orientational parameters of individual molecules. In the discrete models a given, single structure, preferably the most stable one, is considered to represent the environment. A theoretical basis of the discrete molecular complex approximation is provided by the quasi-structure hypothesis formulated originally by Yomosa [1446]. This hypothesis is based on the fact that the lifetime of "quasi-structures", which correspond to the system at the minima of the *adiabatic potential energy* surface*, is far longer than the periods of the stationary motions not only of electrons but also of nuclei: the solute and solvent molecules undergo librations around their equilibrium positions. It has been shown [1341, 1342] that the optimization of the electronic wave function of the system or, under certain assumptions, that of the subsystem, yields also the minimum of the *free energy*, having a central importance in the statistical mechanical description of the bound state corresponding to the quasi-structure.

In crystals without disorder, in inclusion complexes, and in biological macromolecules with restricted conformational flexibility, there is only one quasi-structure which is known experimentally in many cases. In these situations the use of discrete

* The system cannot be characterized unequivocally by rigid structures, defined by unique geometrical arrangements of the nuclei, due to the large-amplitude librational motions. The term "quasi-structure" is used to emphasize this fact and give a "quasi" description by considering the geometry of local minima of the global potential energy surface.

models is a well founded approximation even from the statistical thermodynamic standpoint. On the other hand, a large number of quasi-structures are thermally accessible in liquid phase solutions, so a statistical average of them is necessary if correct temperature dependence is to be accounted for by the theoretical treatment. Discrete models based on a single quasi-structure are widely used for liquid state problems too, mainly for the investigation of the solvent structure in the so-called cybotactic region.

In solutions, the spatial distribution and the electronic structure of the solvent are somewhat perturbed by the solute-solvent interactions. There is, in general, a volume, called the *cybotaxis* or *cybotactic region*, around the solute molecule where relatively important rearrangements of the solvent structure are brought about; in constrast, the solvent outside this volume, the "*bulk*", is not significantly perturbed. If the cybotactic region contains tightly bound solvent molecules, it can be expected that the consideration of a relatively small number of solvent molecules provides an appropriate model for the description of the main portion of solvent effects.

The *supermolecule method* is the most important quantum chemical approach, which is used within the framework of the discrete molecular complex models. The supermolecule procedure consists of the solution of the Schrödinger equation in the "clamped nuclei" (Born–Oppenheimer) approximation for the whole molecular complex containing one solute and a certain number of solvent molecules. Usually this is done at SCF level [224]; correlation effects are neglected, mainly due to computational limitations. In general, within this approach, the total interaction energy is defined as the difference between the total energy of the supermolecule and the sum of energies of the isolated constituent (one solute and N solvent) molecules:

$$\Delta E = E^{(\mathrm{sup})} - \sum_{\mathrm{I}}^{N+1} E_{\mathrm{I}}^{0}. \tag{1.203}$$

According to the traditional approach in the theory of intermolecular forces the interaction energy is considered as a sum of individual contributions. While these contributions appear as distinct terms in the perturbational development of intermolecular interactions [154, 222], there is no such natural decomposition of the interaction energy in the supermolecule method. However, in order to get insight into the nature of interactions, we can apply certain model assumptions, which permit partitioning of the interaction energy.

One of the most widely used decomposition schemes has been proposed by Kitaura and Morokuma [706]. Let us consider four trial wave functions $\psi^{(i)}_{\mathrm{AB}\ldots\mathrm{N}\Sigma}$ with the corresponding energy expectation values $\mathrm{E}^{(i)}$:

$$\begin{aligned}
\psi^{(1)}_{\mathrm{AB}\ldots\mathrm{N}\Sigma} &= \psi^{0}_{\mathrm{A}}\psi^{0}_{\mathrm{B}}\cdots\psi^{0}_{\mathrm{N}}\psi^{0}_{\Sigma} \\
\psi^{(2)}_{\mathrm{AB}\ldots\mathrm{N}\Sigma} &= \hat{\mathrm{A}}[\psi^{0}_{\mathrm{A}}\psi^{0}_{\mathrm{B}}\cdots\psi^{0}_{\mathrm{N}}\psi^{0}_{\Sigma}] \\
\psi^{(3)}_{\mathrm{AB}\ldots\mathrm{N}\Sigma} &= \psi_{\mathrm{A}}\psi_{\mathrm{B}}\cdots\psi_{\mathrm{N}}\psi_{\Sigma} \\
\psi^{(4)}_{\mathrm{AB}\ldots\mathrm{N}\Sigma} &= \psi^{\mathrm{SCF}}_{\mathrm{AB}\ldots\mathrm{N}\Sigma}
\end{aligned} \tag{1.204}$$

where ψ_I^0 is the wave function of the isolated subsystem (solute or solvent molecule) I with energy E_I^0. $\psi_{AB...N\Sigma}^{(1)}$ is a simple Hartree product of the wave functions ψ_I^0 for the isolated subsystems. As a next step, $\psi_{AB...N\Sigma}^{(2)}$ accounts for the exchange interactions by antisymmetrizing $\psi_{AB...N\Sigma}^{(1)}$. In $\psi_{AB...N\Sigma}^{(3)}$ the electron densities of all subsystems are "relaxed" in the electrostatic field of the N other subsystems, *i.e.* the wave functions ψ_I^0 of the isolated subsystems are replaced by the variationally reoptimized functions ψ_I. Up to this stage no electron delocalization between subsystems has been permitted. Finally $\psi_{AB...N\Sigma}^{(4)}$ represents the best single determinant wave function of the whole supermolecule. The interaction energy $\Delta E^{(i)}$ accounted for by the wave function $\psi_{AB...N\Sigma}^{(i)}$ is defined as:

$$\Delta E^{(i)} = E^{(i)} - \sum_{I}^{N+1} E_I^0. \tag{1.205}$$

Then the electrostatic (Coulomb), exchange repulsion and polarization components of the interaction energy are defined as:

$$\Delta E^{cou} = \Delta E^{(1)}$$

$$\Delta E^{ex} = \Delta E^{(2)} - \Delta E^{(1)} = E^{(2)} - E^{(1)}$$

$$\Delta E^{pol} = \Delta E^{(3)} - \Delta E^{(1)} = E^{(3)} - E^{(1)}. \tag{1.206}$$

There is a fourth contribution

$$\Delta E^{RES} = \Delta E^{(4)} - \Delta E^{(3)} - \Delta E^{(2)} + \Delta E^{(1)} \tag{1.207}$$

which is the difference between the sum of the first three contributions and of the total supermolecule energy of interaction. This residual term contains among others the effect of delocalization (charge transfer). Although the charge transfer interaction energy component is frequently used in qualitative discussions, its correct definition is rather problematic [1245].

In addition to the above contributions, which are generally properly accounted for in supermolecule calculations, the dispersion forces have also an important role, mainly in the interaction of nonpolar molecules. The dispersion interactions are of correlational origin, *cf.* 2.11, so they are missing from the SCF supermolecule treatments; CI techniques are needed to include them [460].

There is a systematic error inherent in supermolecule calculations which is manifested by the appearence of spurious, nonphysical contributions in the residual component of the interaction energy. This is the so-called *basis set superposition error* (BSSE), which is essentially a mathematical artefact due to the incompleteness of the basis sets used in the actual calculations. What happens is a virtual "improvement" of the description of the constituent molecules in the presence of additional basis functions (with respect to the isolated molecule case) centred on the neighbouring molecules. The artificial lowering of the supermolecule energy is less pronounced if the

basis set used for individual molecules is sufficiently large, while supermolecule calculations with small or minimal basis sets should be handled with great care. However, the increase of the size of basis set is quite impractical because of the high computational costs. There is the possibility of estimating the upper bound to the BSSE by the method of Boys and Bernardi [139], which involves calculations on the isolated molecules including all basis functions of the whole supermolecule. Recently Mayer [886] proposed a formula which affords the direct calculation of only the physically meaningful part of the supermolecule energy, free from any BSSE.

According to the (1.202) partition of the Hamiltonian of the model system, it is possible to determine the energy of the solute and of the solvent (the latter may be itself a supermolecule) and to get the solute-solvent interaction energy in various nuclear configurations. Although the supermolecule method describes, in principle, the intermolecular forces governing the solvent organization in the cybotactic region and the interactions, which are in effect in crystals or in biomolecules almost completely, the rapidly increasing computational cost with increasing supermolecule size makes extensive calculations prohibitive.

Completed by statistical thermodynamical considerations, the study [1246] of "gas-phase solvation" phenomena (*cf.* the hydrogen bond, Section 2.9 and van der Waals complexes, Section 2.11) is quite an important field of application of the supermolecule procedure. These investigations, greatly helped the understanding of the specific interactions which determine the short-range structure in some solvents. The supermolecule method is well-suited also for the investigation of "solvated electrons", where the predominant effects are played by the short-range electron–molecule interactions [1002]. Sophisticated procedures have been elaborated by the Pullmans and their coworkers for the determination of the solvent structure in the cybotaxis [1143].

The statistical thermodynamical simulation methods, which are able to provide a correct temperature dependence, are out of the scope of the present book. However, these procedures merit a brief discussion. The Monte Carlo method involving configurational averages and the molecular dynamics method, involving time averages, both require repeated computation of the potential energy corresponding to the different configurations of the $N+1$ molecules modelling the solvent, at least $\sim 10^6$ times. In order to accomplish this enormous computational task some simplifying assumptions are needed in the energy calculations [225].

The potential energy surface is described by the following cluster expansion

$$E = \sum_{I}^{N+1} E_I + \sum_{I<J}^{N+1} V_{IJ} + \sum_{I<J<K}^{N+1} V_{IJK} + \ldots \tag{1.208}$$

where the first term is simply the sum of the isolated molecule energies and the other terms correspond to binary, ternary and higher order interactions. The cluster expansion converges quite rapidly: in most cases it can be truncated after the second term, i.e. the pair-wise additivity of interactions can be assumed (*cf.* Section 2.11). This

assumption is strictly valid as far as the electrostatic interactions are concerned; the polarization and dispersion forces are markedly nonadditive and may have three-body or higher contributions of significant value [1247]. The supermolecule calculations are very important in elucidating the role of such cooperative effects in intermolecular interactions.

The two-body interactions are supposed to have some analytical representation, for example, they are brought in the form of a sum of atom–atom pair potentials:

$$\Delta E_{AB} = \sum_{i \in A < j \in B} V_{ij}^{AB} = \sum_{i<j} \left(-\frac{A_{ij}^{AB}}{r_{ij}^{6}} + \frac{B_{ij}^{AB}}{r_{ij}^{12}} + \frac{C_{ij}^{AB} q_i q_j}{r_{ij}} \right). \tag{1.209}$$

Besides empirical and semiempirical approaches, the parameters of the pair potentials can be determined by fitting them to the results of *ab initio* supermolecule calculations on model dimers. A great number (10^3) of nuclear configurations have to be included in the fitting procedure in order to get reliable analytical potentials at every intermolecular separation. The number of parameters to be fitted is usually reduced using transferability properties: parameters for atoms in different molecules but in similar electronic environment, are taken to be identical. Quite recently some attempts have also been made to include analytical three-body functions in the statistical thermodynamical calculations [230].

The significance of statistical thermodynamical methods with respect to quantum chemistry is twofold. First, the results obtained by quantum chemical procedures on the intermolecular forces may enter the statistical treatment as input data. Secondly, it is hoped that the output of statistical thermodynamical theories concerning solvent structure can be built into some sophisticated quantum chemical treatment of solvent effects [1260].

Turning back to the procedures yielding explicitly the wave function of the solute molecule, and thus giving information about the modifications of the electronic structure and molecular properties under the influence of the environment, we shall mention some methods which can be considered as providing approximate solutions of the supermolecule problem.

Group function methods, which have already been mentioned in Section 1.4 are based on the assumption that the system can be decomposed to distinct electron groups. This separability criterion is particularly well fulfilled for supermolecules composed of moderately interacting individual molecules. As has already been discussed, the dimensionality of the SCF problem can be reduced when using the group function procedure, but the number of two-electron integrals in the *ab initio* formalisms remains prohibitive for the treatment of larger molecular complexes; in this respect, the situation is the same as with supermolecule calculations. However, recent methodological progress has led to some promising results both at semiempirical [986] and the *ab initio* levels [894].

The group function formalism provides a good theoretical framework for the discussion of the various approximate procedures used in quantum chemical

calculations using discrete models. The mutually consistent field (MCF) procedure of Otto and Ladik [403, 1049] is, for example, a simplified group function approach. Here, at the first step the exchange interactions are neglected and some simplifications are introduced for the calculation of the intermolecular Coulomb integrals. Afterwards the exchange, delocalization and dispersion effects, neglected so far are evaluated in a perturbative manner over the wave function containing polarization effects.

The methods described so far treat the whole supersystem on the same footing. However, in most practical cases the main interest centres on the wave function of the solute molecule. Considerable savings in computational effort can be achieved if the quantum chemical description is limited only to the solute molecule and the remaining part of the system, that is, the environment, is represented by suitable model potentials. There are many computational procedures falling into this category. In these methods one has to solve the following effective equation for the electronic wave function of the solute molecule:

$$\left[\hat{H}_\Sigma + \sum_{S=1}^{N} (\hat{V}_{\Sigma S}^{COU} + \hat{V}_{\Sigma S}^{EX})\right] \psi_\Sigma = E_\Sigma^{EFF} \psi_\Sigma \tag{1.210}$$

where the $\hat{V}_{\Sigma S}^{COU}$ and $\hat{V}_{\Sigma S}^{EX}$ effective potentials stand for the Coulomb and exchange interactions with the environment. Explicit use of the wave function for the environment can be avoided by considering these potentials as functions of the charge density of the solvent molecules. In principle, this is possible for both Coulomb and exchange interactions; however, in most of the actual applications only Coulomb potentials are retained. Further simplifications are possible by introducing some appropriate model charge distributions for the environment.

Following these principles a hierarchy of approximations can be derived from Eq. (1.209). For example, one can consider the classical electrostatic (Coulomb) interaction between the charge distribution of the solute and its environment, and neglect polarization effects. Let us denote the electrostatic potential (*cf.* Section 4.4.1) of the environment by $V_S(\mathbf{r})$. Then a very simple approximate formula can be used for the interaction energy $E_{\Sigma S}$:

$$E_{\Sigma S} \approx \sum_{i \in \Sigma} q_{\Sigma i} V_S(\mathbf{r}_i) \tag{1.211}$$

where a set of point charges $\{q_{\Sigma i}\}$ (*e.g.* net atomic charges) stands for the approximate representation of the solvent charge distribution [27, 1251]. More refined procedures, involving higher atomic multipoles have also been used for this purpose [1251].

Polarization effects on the electronic structure of the solute can also be included in the calculations, if the electrostatic potential emerging from the rigid (unpolarized) charge density distribution of the environment is put into the effective Hamiltonian (and Fockian) of the solute. In practice this can be done, for example, by taking point charge sets, which are selected in order to mimic the solvent (water) molecules in the first solvation shell [1025], the enzyme field in the catalytic site [339, 525] or the exact

electrostatic (Madelung) potential or crystal lattice [12, 60]. Net atomic charges obtained by Mulliken population analysis cannot be used directly in most cases; but Mulliken charges, scaled in such a way that they reproduce the total dipole moment of the solvent molecules, have proved to be adequate in many cases [1025]. The electrostatic effect of the water molecules in the cybotactic region has also been represented by appropriately selected point dipoles, the potential of which had been included directly in the Fock operator of the solute [91, 1441].

The reverse effect, the polarization of the solvent (environment) charge distribution by the field of the solute (and, in turn, the influence of this polarization on the solute creating it) proved to be quite important in the correct description of environmental effects, especially in processes accompanied by charge separation [1341, 1342]. In group function methods this mutual polarization is accounted for by optimizing both charge distributions in the field of each other. Since we would like to avoid here the explicit use of the solvent wave function, we can assume an analytic dependence of the changes in the solvent charge distribution on the charge distribution of the solute molecule. The potential created by the solvent polarized by the solute, and acting back on the solute, is the polarization potential $\hat{V}^{POL}$. This can be written in the following general form [794, 1001]:

$$\hat{V}_{\psi}^{POL}(\mathbf{r}) = \int g(\mathbf{r}, \mathbf{r}') \rho_{\psi}(\mathbf{r}') \, d\mathbf{r}' \tag{1.212}$$

where $\rho_{\psi}(\mathbf{r})$ is the charge density depending on the wave function ψ, and $g(\mathbf{r}, \mathbf{r}')$ is a "response function", with explicit forms to be given later. V^{POL} depends explicitly on the charge distribution of the solute molecule, *i.e.* on the wave function, which we are searching for by solving the following equation:

$$[\hat{H}_{\Sigma} + \hat{V}_{\Sigma S} + \hat{V}_{\psi_{\Sigma}}^{POL}] \psi_{\Sigma} = E_{\Sigma}^{EFF} \psi_{\Sigma} . \tag{1.213}$$

Here

$$\hat{V}_{\psi_{\Sigma}}^{POL} = - \sum_{i=1}^{n_{el}} \hat{V}_{\psi_{\Sigma}}^{POL}(\mathbf{r}_i) + \sum_{A=1}^{N_{nucl}} Z_A \hat{V}_{\psi_{\Sigma}}^{POL}(\mathbf{r}_A) \tag{1.214}$$

is the operator of the polarization potential acting on the different particles (electrons and nuclei) of the solute molecule. Owing to this wave function dependence of the Hamiltonian, the Schrödinger equation (1.213) is *nonlinear*.

Nonlinear Schrödinger equations are often invoked in the quantum chemical theories of environmental effects. A special feature of this class of equations is that they cannot be derived by applying the variational principle to the expectation value of the Hamiltonian $\hat{H}$ of the solute molecule containing nonlinear terms:

$$\hat{H} = \hat{H}_0 + \hat{V}_{\psi}^{POL} . \tag{1.215}$$

Here $\hat{H}_0$ is the linear and $\hat{V}_{\psi}^{POL}$ is the nonlinear part of $\hat{H}$. Based on the analysis of the nonlinear Schrödinger equations, the following appropriate variational functional had been proposed by Sanhueza *et al.* [1223]:

$$J=\langle\psi|\hat{H}_0+\hat{V}_\psi^{POL}|\psi\rangle-\frac{1}{2}\langle\psi|\hat{V}_\psi^{POL}|\psi\rangle=\left\langle\psi\left|\hat{H}_0+\frac{1}{2}\hat{V}_\psi^{POL}\right|\psi\right\rangle. \tag{1.216}$$

It is quite interesting to look at the physical meaning of the functional (1.216). Recalling the (1.202) partition of the total Hamiltonian for the model system, it is obvious that $\hat{H}=\hat{H}_0+\hat{V}_\psi^{POL}=\hat{H}_\Sigma+\hat{V}_{\Sigma S}+\hat{V}_\psi^{POL}$ provides an estimate for the terms $\hat{H}_\Sigma+\hat{H}_{\Sigma S}$ of (1.202), and the expectation value

$$\langle\psi_\Sigma|\hat{H}_\Sigma+\hat{V}_{\Sigma S}+\hat{V}_{\psi_\Sigma}^{POL}|\psi_\Sigma\rangle$$

can be considered as an approximation to the corresponding energies, $E_\Sigma+E_{\Sigma S}$. However the model system contains also the solvent. In the framework of the hypothesis that $\hat{V}_\psi^{POL}$ can be written in the form of Eq. (1.212) *i.e.* the polarization charge density of the solvent is a linear function of the solute charges, the change in the solvent energy ΔE_S can be shown [108] to be equal to

$$\Delta E_S=-\frac{1}{2}E_{\Sigma S}. \tag{1.217}$$

Thus the energy functional (1.216) gives the expectation value of the total energy of the whole solvent-solute model system (by taking the zero point of the energy scale at the energy of the unpolarized solvent system).

Solution of the nonlinear Schrödinger equation (1.213) within the independent particle model leads to a system of effective Hartree–Fock equations with the modified Fock operator:

$$\hat{F}(\mathbf{r})=\hat{F}_\Sigma(\mathbf{r})-\hat{V}_{\Sigma S}(\mathbf{r})-\hat{V}_{\psi_\Sigma}^{POL}(\mathbf{r}) \tag{1.218}$$

where $\hat{F}_\Sigma$ is the Fockian corresponding to $\hat{H}_\Sigma$, the molecular Hamiltonian and $\hat{V}_{\psi_\Sigma}^{POL}$ is given by Eq. (1.212).

In certain situations the perturbational method of solution of Eq. (1.213) may be preferred to the variational one. Standard Rayleigh–Schrödinger PT cannot be used for this purpose because of the nonlinearity of the perturbation $\hat{V}_\psi^{POL}$. Recently a special perturbation theory had been worked out for this purpose [1318].

Let us see now an actual example for the form of the $\hat{V}_\psi^{POL}$ effective potential. The polarization density $\mathbf{P}(\mathbf{r})$ associated with the induced dipole moment per unit volume of the solvent is given by the relation [25, 1344]:

$$\mathbf{P}(\mathbf{r})=\bar{\chi}(\mathbf{r})\mathbf{F}(\mathbf{r})=\int\bar{\chi}(\mathbf{r})\mathbf{T}(\mathbf{r},\mathbf{r}')\rho_\psi(\mathbf{r}')\,d\mathbf{r}' \tag{1.219}$$

where $\mathbf{T}(\mathbf{r},\mathbf{r}')$ is defined as*:

$$\mathbf{T}(\mathbf{r},\mathbf{r}')=\frac{(\mathbf{r}-\mathbf{r}')}{|\mathbf{r}-\mathbf{r}'|^3}$$

* $\mathbf{T}(\mathbf{r},\mathbf{r}')$ gives either the field $\mathbf{F}(\mathbf{r})$, created at $\mathbf{r}$ by a unit charge placed at $\mathbf{r}'$, or the potential at $\mathbf{r}'$ by a unit dipole parallel with $\mathbf{r}-\mathbf{r}'$, placed at $\mathbf{r}$.

and $\bar{\bar{\chi}}(\mathbf{r})$ is a susceptibility tensor, which can be approximated in a discrete model of the solvent as a sum of effective point polarizabilities [1349]:

$$\bar{\bar{\chi}}(\mathbf{r}) \approx \sum_k \bar{\bar{\alpha}}_k \delta(\mathbf{r} - \mathbf{r}_k) . \tag{1.220}$$

In Eq. (1.220) the summation runs over the points representing the environment. The polarization potential can be written now as

$$\hat{V}_\psi^{\mathrm{POL}}(\mathbf{r}) = \int \mathbf{T}(\mathbf{r}, \mathbf{r}'') \bar{\bar{\chi}}(\mathbf{r}'') \mathbf{T}(\mathbf{r}'', \mathbf{r}') \rho_\psi(\mathbf{r}') \, d\mathbf{r}' \, d\mathbf{r}'' \tag{1.221}$$

i.e. the $g(\mathbf{r}, \mathbf{r}')$ response function becomes:

$$g(\mathbf{r}, \mathbf{r}') = \int \mathbf{T}(\mathbf{r}, \mathbf{r}'') \bar{\bar{\chi}}(\mathbf{r}'') \mathbf{T}(\mathbf{r}'', \mathbf{r}') \, d\mathbf{r}'' . \tag{1.222}$$

In practical applications of (1.222) Taylor series expansion of $g(\mathbf{r}, \mathbf{r}')$ in $\mathbf{r}$ and $\mathbf{r}'$ makes numerical calculations feasible practically [25, 1344, 1349].

The effective potentials calculated from discrete models of the environment suffer from the shortcoming of not being able to describe appropriately the temperature dependent orientational polarization of the solvent molecules. It has to be stressed that discrete models include orientational effects, simply through the geometrical arrangement of the solvent molecules, but in the case of liquid solutions such a rigid model is not realistic due to the large number of equally probable arrangements of the solvent molecules around the solute. Recently some attempts have been made to set up temperature dependent effective electrostatic potentials on the basis of structural information gained in statistical thermodynamical (Monte Carlo) studies [1260].

A thorough analysis of both quantum chemical and statistical thermodynamical aspects of liquid solvent effects had been carried out by Tapia in the context of the self-consistent reaction field (SCRF) theory [1343]. In this theory, a simple model of polar solvent–polar solute interactions is introduced; namely the solvent is represented by a set of polarizable point dipoles and their statistically averaged field enters into the effective Hamiltonian of the solute molecule:

$$\{\hat{H}_\Sigma - \mu_\Sigma(\langle \mathbf{F}_\Sigma \rangle + \langle \bar{\bar{g}} \mathbf{M}_\Sigma \rangle)\} \Upsilon = \langle E_\Sigma^{\mathrm{EFF}} \rangle \Upsilon \tag{1.223}$$

In Eq. (1.223) $\langle \mathbf{F}_\Sigma \rangle$ denotes the average field of the permanent dipole moments of the oriented solvent molecules in the cybotactic region around the solute, and $\langle \bar{\bar{g}} \mathbf{M}_\Sigma \rangle$ is the average field due to the dipole moments induced in the solvent molecules by the field of the solute. The sum of these two fields is a sort of reaction field. It has to be emphasized that the appearance of statistical mechanical averages over solvent configurations demands that the Schrödinger equation (1.223), the resulting wave function Υ and effective energy $\langle E_\Sigma^{\mathrm{EFF}} \rangle$ of the solute molecule have also statistical significance. This implies that the wave function Υ cannot be associated with any particular solvent configuration, not even with the optimum one. Since both orientational and inductive (polarization) parts of the reaction field acting on the solute can be represented as the function of the solute dipole moment, one obtains the following nonlinear Schrödinger

equation [1343]:

$$\{\hat{H}_\Sigma - \mu_\Sigma(\bar{g}_0 + \bar{g}_I)\langle\Upsilon \mid \mu_\Sigma \mid \Upsilon\rangle\}\Upsilon = \langle E_\Sigma^{EFF}\rangle\Upsilon \tag{1.224}$$

where $\bar{g}_0$ is the orientational, and $\bar{g}_I$ is the inductive part of the response tensor $\bar{g}$. Tensor $\bar{g}$ is usually parametrized based on empirical data, however in the realm of discrete models some attempts have been made to evaluate its inductive component from available structural information [25, 1344].

The SCRF theory can be considered as an attempt to fill the gap between the statistical thermodynamical treatment of solutions and the classical reaction field concept of Onsager [1043]. In the classical reaction field model, the solute molecule is considered as being embedded in a cavity inside a continuous dielectric medium. The *continuum models* of quantum chemical solvent effect theories use the same assumptions for setting up an effective potential acting on the solute molecule. This reaction potential inside the cavity created by the polarized dielectrics is a function of the cavity shape and size, of the static relative permittivity of the pure solvent and of the solute charge distribution. The reaction potential formally plays the same role as the polarization potential in discrete models, however, its physical meaning is more complex: it contains both electronic and orientational polarization components. The physical interpretation of the functional (1.216) is somewhat different in the continuum models with respect to the discrete model case. Due to the temperature dependence of the solvent-solute interaction (through the relative permitivity of the dielectrics) J corresponds now to the *free energy* of the solvent-solute system [108].

The electrostatic equations which describe the situation corresponding to the continuum model have solutions in closed form only for some special cases. For example, Born's model for ionic solvation gives the reaction potential V_{Born} [128]:

$$V_{Born} = \frac{Q}{a}\frac{1-\varepsilon}{\varepsilon} \tag{1.225}$$

where a is the radius of the cavity assumed to be of spherical form, Q is the charge of the ion and ε is the relative permittivity of the solvent. Onsager's theory for dipolar solutes yields the following formula for the reaction field [1043]:

$$\mathbf{F}_{ONS} = \frac{2}{a^3}\frac{\varepsilon-1}{2\varepsilon+1}\mathbf{M} \tag{1.226}$$

where $\mathbf{M}$ is the dipole moment of the solute.

Formulae (1.225) and (1.226) can be considered as special cases of a more general treatment given originally by Kirkwood [694] for an arbitrary charge distribution in a spherical cavity. Quantum chemical generalization of the Kirkwood formula [1180] and its extension to the case of ellipsoidal cavity have also been used in both semiempirical and *ab initio* calculations [1178].

A serious problem in the application of continuum models is how to select the size and the form of the cavity. Spherical or ellipsoidal cavities quite often do not fit well to

the molecular shape. More realistic cavity shapes can be obtained by considering interlocking van der Waals spheres around each atoms. In this case rather complicated numerical methods have to be used for the solution of the corresponding electrostatic equation for the reaction potential [612]. Recently an efficient approximate procedure had been proposed by Miertuš *et al.* [912] for this purpose. The method consists of the calculation of apparent charges on the surface of the cavity, and the magnitude of these charges is taken to be proportional to the derivative of the molecular electrostatic potential at the cavity surface. (The approximation consists of using discrete apparent point charges on the cavity surface, instead of a continuous surface charge density predicted by the strict electrostatic treatment.) The apparent charges can be included directly into the molecular Hamiltonian. The procedure has been implemented at both *ab initio* and semiempirical levels [912].

The above continuum and discrete models treating explicitly solvent polarization effects involve reaction potentials, which depend on the quantum mechanical expectation value of the solute charge distribution. In contrast to these "*average reaction field*" approaches, some authors have proposed to put the instantaneous value of the reaction field (instead of its average value) into the Hamiltonian directly. This *direct reaction field* approach leads to a linear Schrödinger equation. The direct reaction field method was considered both in discrete [1349] and continuum [618] models, and it has been claimed to involve an approximation to the dispersion interactions besides polarization (induction) effects between the solvent and the solute [1350]. The rationale behind this model is the assumption that polarizable surroundings respond instantaneously to the fluctuations of the electric field caused by electronic motions in the solute. A quite serious problem in these types of procedure is that there is no reason to restrict the instantaneous positions of the electrons inside the boundaries of the cavity or solvent cage [1341]. The probability of finding the electrons outside the cavity is practically (but not formally) zero. These electron configurations do not contribute to an appreciable extent to any expectation values, but may lead to some divergencies in the direct reaction field method, as was found by Hylton *et al.* [618] using the Kirkwood model. To avoid the divergencies one has to restrict the allowed positions of the electrons inside the cavity.

Finally we have to mention an interesting class of solvent effect theories, the *effective charge* (solvaton [711], virtual charge [246]) methods. An attractive feature of these models is that the corresponding formulae are extremely simple and one can implement them in current semiempirical quantum chemical computer programs by inserting a few lines. Effective charge methods are popular, but attention should be paid to some misconceptions and theoretically unfounded computational methods, which have appeared in the literature. None of the existing effective charge models can be considered as being based on a firm theoretical ground.

The effective charge models of solvation grew out from the generalization of the classical Born formulae for the ionic solvation energy in the case of polyatomic ions [585]. The generalized Born formulae corresponds to a simple physical picture, when

the atoms of the solute molecule (or ion) bearing fractional charges are immersed into a dielectric of relative permittivity ε. Then the classical Born formula (Eq. (1.225)) applies to each atom separately, while their Coulomb interactions are attenuated by a factor of ε^{-1}. A quantum chemical adaptation was due to Jano [637], who obtained in the framework of the ZDO approximation for the solvation free energy (*i.e.* including the solvent polarization energy ΔE_S, which is equal to $-\frac{1}{2}E_{\Sigma S}$):

$$E_{solv} = E_{\Sigma S} + \Delta E_S = \frac{1}{2}\frac{1-\varepsilon}{\varepsilon}\sum_{AB} q_A q_B \gamma_{AB} . \tag{1.227}$$

Here q_A and q_B are net atomic charges and the double summation runs over the atoms of the solute; γ_{AB} is the usual gamma integral. The heuristic "*solvaton*" model of Klopman [711] had also been proposed for calculating a first order solvation energy correction to the quantum chemical energy of the solute. Klopman's model gives practically the same free energy functional as that following from the Jano formula. There have been several implementations of the solvaton model into the SCF equations of the solute. Following the general considerations outlined above one gets the following diagonal Fock matrix elements from the solvaton model [1341]:

$$F_{\mu\mu} = F^0_{\mu\mu} - \sum_{B,\nu}\frac{1-\varepsilon}{\varepsilon}(Z_B - P_{\nu\nu})\gamma_{AB} (\mu \in A) \tag{1.228}$$

while off-diagonal matrix elements contain no correction due to solvation. The Fock-matrix elements derived by Germer [437] and Miertuš and Kysel [911] contain an incorrect factor of 1/2. Moreover, the correction term had the wrong sign in the equations of Germer and due to an additional parametrization problem his method leads to unphysical results [911]. Recently Klopman and Andreozzi [715] proposed an extended solvaton model, but this procedure does not fulfil some basic requirements of self-consistency [245]. A quite general formulation of effective charge methods can be achieved by observing [24] that the extremely simple form

$$g(\mathbf{r}, \mathbf{r}') = f(\varepsilon)\frac{1}{|\mathbf{r}-\mathbf{r}'|} \tag{1.229}$$

of the response function leads to Eqs (1.227) and (1.228) with

$$f(\varepsilon) = \frac{1-\varepsilon}{\varepsilon} .$$

The method of Miertuš *et al.* [912] can also be considered as a sophisticated solvaton model, where the solvaton charges are calculated nonempirically [911].

2. THE CHEMICAL BOND

The concept of the chemical bond is more than one hundred years old and it was deduced from a huge amount of experimental observation. According to this concept, molecules are constructed of transferable building blocks: the chemical bonds. Molecular properties are obtained as simple or vectorial sums of bond increments *(additivity)*. These increments are not measurable so all definitions of the chemical bond necessarily bear some ambiguity. However, the role of the bond concept in systematization and rationalization of experimental facts is unquestionable.

An intrinsic feature of all bond theories is their qualitative nature. The astonishingly high accuracy by which the energy content of saturated compounds can be calculated from bond contributions has not found a satisfactory explanation till now [14]. If we abandon the full quantitative treatment, a very useful scheme of transferable bond properties can be constructed which may be refined through consideration of secondary (inductive, delocalization, etc.) effects. For a brief survey of the topic see [782].

In this part we discuss chemical bonds in terms of localized molecular orbitals. This treatment is becoming more and more popular and we feel that further developments of the theory may lead to a deeper understanding of bonding than ever before. In each chapter we give a pictorial representation of the bond, that is, the contour map of the localized molecular orbital, if available. Afterwards localizability, transferability and secondary effects are handled. At last, experimental bond properties are summarized.

2.1 DEFINITIONS AND ORIGIN OF BONDING

Since bonds are forming *molecules*, we have first to define what we mean by this term. Let us consider a set of nuclei and electrons. The wave function of this system, Ψ, depending only on electronic coordinates, describes its possible electronic states within the Born–Oppenheimer approximation. If the whole ensemble can be partitioned into subsystems $M_1, M_2, \ldots, M_n$ to which separate wave functions $\Psi_{M1}, \Psi_{M2}, \ldots, \Psi_{Mn}$ can be ascribed and the differential overlap between these latter is approximately zero everywhere the subsystems may be called isolated molecules. Due to the neglect of differential overlap, charge transfer between isolated molecules is negligible and their interaction energy is relatively small. For example, a system of twenty electrons, four hydrogen and two oxygen nuclei is decomposed into two water molecules if

internuclear distances within each set are smaller than 180 pm and distances between nuclei of different molecules are larger than 1 nm. On the other hand, a diamond lattice of, say, a thousand carbon atoms each having four neighbours in a distance of 154 pm, cannot be partitioned as above therefore it makes no sense to speak about individual molecules within this system. There are cases, where differential overlap between Ψ_{M1} and Ψ_{M2} and, accordingly, interaction energy between M1 and M2, are non-negligible though small. An example is the water dimer with an O . . . O distance of 280 pm. These systems exhibit intermolecular interactions and if they are more or less stable they may be called *van der Waals molecules* [572].

Let us now discuss how the relative stability of the molecules can be understood. In general, destabilization of a molecule is a consequence of internal geometry changes; therefore, stability is best treated on the basis of the *energy hypersurface*, which is a function of all nuclear coordinates. Physically observable states of a molecule correspond to minima on this surface. These can be determined by calculating an approximate solution of the Schrödinger equation for a given set of nuclear coordinates. The explanation for stability or instability is inherent in this equation. However, it is often useful to have a simple and didactic model for bonding which allows us to construct working hypotheses to be tested numerically or experimentally.

Such a model, with close reference to exact numerical results but using relatively simple physical concepts, was constructed by Ruedenberg [1202–1203]. Let us define the bond or interaction energy for a diatomics by the relation

$$E_{int} = E_{AB} - E_A - E_B \tag{2.1}$$

where E_{AB}, E_A and E_B stand for the energies of the molecule and of the noninteracting atoms A and B. Bonding occurs if $E_{int} < 0$ *i.e.* if the system gains in energy upon molecule formation. E_{int} can be partitioned into promotion (*p*), interference (*i*), quasiclassical (*qc*) sharing penetration (*sp*) and mixed terms. Accordingly, hypothetical steps in the formation of a diatomic molecule are defined. These steps have no physical meaning the distinction merely allows a better understanding of the phenomenon.

Both X-ray diffraction measurements and accurate calculations indicate that in the vicinity of the nuclei, electron density increases in molecules as compared to free atoms [86]. Figure 2.1 shows the qualitative trend of calculated values along the axis of the H_2 molecule [1202]. Considering this change, the first hypothetical step of molecule formation may be *promotion:* increase of electronic density around nuclei as two atoms get sufficiently close to each other. In this step no chemical bond is formed but atoms get into a promoted or *valence state.* Upon promotion, potential energy of the electrons decreases while their kinetic energy increases. This leads to a net increase in the total energy. The change in electronic density around nuclei is responsible for alteration of some atomic properties, depending on molecule formation like the ESR hyperfine coupling constant.

As atoms in valence states get bonded, electronic density increases in the space between them (*interference*, see Fig. 2.2 [86]). Therefore the density decreases slightly

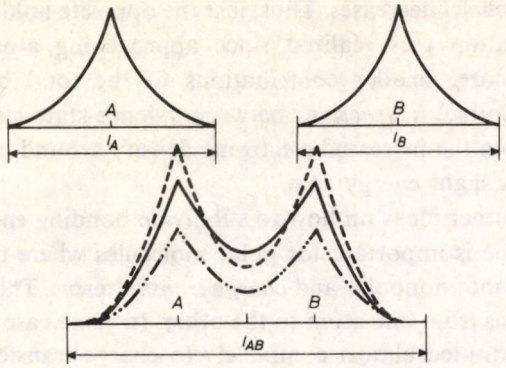


Fig. 2.1 Electron density change upon molecule formation. Full line: molecule or free atoms, dashed line: sum of valence-state atomic densities, dash-dotted line: quasiclassical sum of free atomic densities

around nuclei though it remains higher than in free atoms. These density changes lead to an increase in potential energy, since electrons get far from attracting nuclei and close to each other. On the other hand, kinetic energy considerably decreases due to the larger room available for electronic motion *(delocalization)* [1203]. Notice that this term is different from the delocalization concept used in other fields of quantum chemistry, *e.g.* delocalization of SLMOs where tails are formed, see Section 1.4.

Let us define closed-shell molecules as "classical" if they are composed of only H, C, N, O and F atoms. For most of these interference is the largest contribution to bond stabilization. Therefore we can state that the most important single factor of bond formation is electronic delocalization allowing a decrease in the potential energy as compared to free atoms.

The above model holds only if electrons, forming a bond, have opposite spins. Due to the Pauli principle electrons with parallel spins keep away from each other; therefore

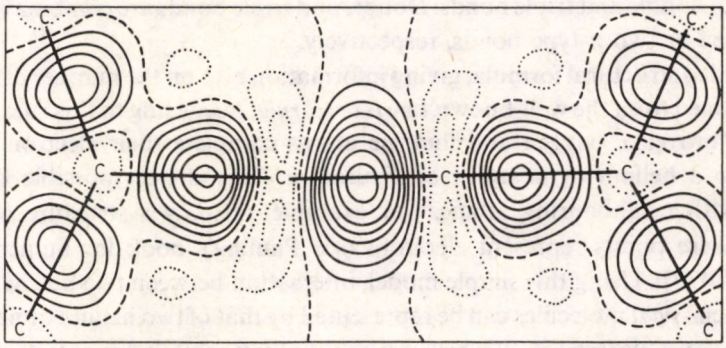


Fig. 2.2 Electronic difference density map for tetraphenyl-butatriene as measured by X-ray diffraction. Full and dotted lines denote excess and lack of charge, respectively. Note the charge accumulation along bonds and the different shape of the central region indicating the perpendicular orientation of the central and terminal π-bonds. (With permission from Ref. [86])

the density between nuclei decreases. Thus, just the opposite holds to the former case: an *antibonding* situation gets realized since approaching atoms see a repulsive potential. Furthermore, smaller contributions to the total bonding energy are *quasiclassical* (Coulombic) *interactions* between valence-state electrons and *sharing penetration* arises from the increased electronic density around neighbouring atoms. Both terms lead to a slight energy gain.

There are several other ideas on how to subdivide bonding energy into physically meaningful parts. One is important for polar molecules where the total interaction energy is partitioned into nonpolar and *charge transfer* terms. This latter corresponds to transfer of electrons from one atom to the other. In some case (metal halogenides) bonding may be attributed almost completely to charge transfer. Another concept treats electronic correlation separately and discusses its role in bonding. In general, it is not important for closed-shell molecules (except *e.g.* F_2) but it is essential for most open-shell systems (*e.g.* triaziridenyl dication $N_3H_3^{2+}$ [126]).

On the basis of the Ruedenberg model it is clear that atoms have to get close to each other in order to form a classical covalent bond [745]. Interference occurs only if wave functions of approaching atoms sufficiently overlap. The corresponding integrals vanish exponentially with increasing interatomic distance therefore only neighbouring atoms can be treated as bonded. This is why a *structural formula* can be ascribed to classical molecules allowing a topological treatment of, for example, aromaticity [476], reaction paths [902] and even biological activity [690].

It is easy to construct the structural formula for classical molecules since the number of edges (two-centre bonds) belonging to a certain type of vertex (H, C, N, O, or F atom) is constant. This valence number is one for hydrogen and fluorine, two for oxygen, three for nitrogen and four for carbon. A molecule is called *saturated* if the valence number equals the coordination number. Saturated molecules may be characterized solely in terms of one-centre lone pairs (Section 2.4) and two-centre σ-bonds (Section 2.2). It may occur that two vertices are connected by more than one edges indicating the formation of double and triple bonds. Double and triple bonds are combinations of a σ-type and one or two π-type bonds, respectively.

An extended structural formula, giving information also on the number of lone pairs, can be obtained from the well-known *Lewis octet rule*. According to this rule, hydrogen or carbon, nitrogen, oxygen and fluorine atoms complete their electron shell in a molecule to a helium or neonlike configuration. This is only possible by sharing electrons with neighbouring atoms. For example, the Lewis structure of water is $H:\ddot{O}:H$ where points represent electrons (see Pauling's book for numerous other examples [1070]). Using this simple model, interaction between two atoms belonging to different classical molecules can be represented by that of two helium or neon atoms. This is unfavourable (see Fig. 2.3) because antibonding orbitals are occupied therefore the charge density between the two atoms gets smaller. Interference is lacking and repulsion, instead of attraction, occurs if the two electrons get within covalent distances. The opposite is true for two open-shell molecules (*e.g.* hydroxyls $\cdot\ddot{O}:H$)

modelled by hydrogen atoms where the antibonding orbital is vacant. Though attraction is possible at larger interatomic separations it is at least one order of magnitude smaller than in the covalent case. This is why supermolecules are loosely bound. The octet rule and our conclusions can be extended to molecules with second and higher row atoms but only with sufficient care.

The short-range nature of covalent bonding has further far-reaching consequences. It is the basis of the approximate additivity of several molecular properties. Mathematically

$$w \approx \sum_{A} w_A^1 + \sum_{A,B}^{(\text{neighbours})} w_{AB}^2 + \dots \tag{2.2}$$

i.e. a property, w, of a saturated molecule can be written as a sum of one and two-centre

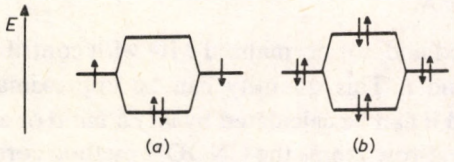


Fig. 2.3 Change of electron configurations upon molecule formation. *(a)*: H_2, *(b)*: He_2

increments, w_A^1 and w_{AB}^2, respectively. To a good approximation, two-centre increments correspond to bonds. This means that contributions arising from atoms which are not nearest neighbours may be neglected. In general, the bond increments are approximately transferable between molecules. For some classes of compounds, like boron hydrides, aromatic molecules, transition metal complexes, etc., two-centre increments alone are not transferable. They have to be combined to give three-centre or higher increments to ensure transferability. In these cases we speak about three-centre or many-centre bonds.

Now the question is how additivity and transferability can be expressed in quantum chemical terms. Several theories are known [193, 275, 1070] of which resonance is frequently used in everyday practice. This is, however, difficult to put into quantitative terms. We feel that the concept of localized molecular orbitals offers a solid basis for bond theory, better than resonance, and it makes it possible to treat intra- and interbond effects in a quantitative, yet simple and didactic, way [368, 464, 586, 670, 671, 698, 1012]. We ascribe just one strictly localized and doubly occupied molecular orbital (SLMO, φ_i°) to each bond of a molecule [119].

This can be done, in principle, within an arbitrary (large) LCAO basis set or even by applying off-centered bond functions, *cf.* Section 1.3.1. However, most of the qualitative features of bond formation can also be studied conceptually within a minimal basis set. Therefore, for the sake of simplicity and clearness, in what follows we restrict the discussion to the case of minimal basis. Then, each SLMO is a single atomic (hybrid)

orbital for an inner shell or a lone pair, combination of two hybrids for a two-centre σ-bond, or combination of two or more p_z-type orbitals for isolated or delocalized π-bonds [972]. More mathematical details are given in Section 1.5.

Except for diatomic molecules, SLMOs are not identical to localized molecular orbitals (LMO, φ_i) which are obtained from canonical solutions of the Hartree–Fock–Roothaan equations by a localization procedure. Though the latter have largest coefficients on atoms belonging to the given bond, nonnegligible tails are located at neighbouring or even far lying centres. In the following, we call a bond LMO that which has largest coefficient(s) at atom(s) A (for a lone pair), AB (for a σ-bond), AB...C (for many-centre bonds). Neglecting tails and after renormalization we obtain the corresponding SLMO. A useful quantity for the characterization of bond LMOs is *localizability* which may be defined for the i-th localized molecular orbital as [119]:

$$l_i = \int \varphi_i \varphi_i^\circ \, dV \equiv \langle \varphi_i | \varphi_i^\circ \rangle. \tag{2.3}$$

φ_i means the truncated and not normalized MO with contributions only from atoms belonging to the bond i. This quantity can be approximated by various simple expressions [985] and it can be calculated by an *ab initio* or a semiempirical method. For molecules with first-row atoms the CNDO/2 method correctly reproduces trends given by an *ab initio* method with minimal basis set [699, 985].

Once we relate bonds to SLMOs it is possible to partition molecular properties to obtain intrabond and interbond contributions. Such a partition for the SCF expression of the molecular electronic energy is given by Bonaccorsi *et al.* [119]. They defined an intrinsic bond energy, E_i^0, which is transferable between molecules. Note that E_i^0 is much larger than "experimental" bond energies since it is related to the molecular total energy and not to the dissociation energy. For example, in the case of twelve three-membered rings, E_i^0 of the CH bond varies between $-18{,}375$ and $-19{,}005$ kJ/mol: the deviation is only 3.3 per cent. Partitioning of other one-electron observables, like electric field gradient, electrostatic potential or electric dipole moment, is also possible and transferability is nicely fulfilled. On the other hand, deviations from transferability, like *substitution effects* may be treated as interbond contributions to the total molecular property [119, 440, 1420]. Certainly, numerical accuracy is far from that provided by computational quantum chemistry but it is enough to shed light on the origin of the bond concept widely accepted and exploited in chemistry.

Ruedenberg's simple model holds for strong covalent bonds. However, intermolecular forces, responsible for other types of bonding (hydrogen bond, sandwich molecules, etc.) are one or two orders of magnitude weaker than those acting between closest neighbour atoms in a classical molecule, *cf.* Table A1 in the Appendix. For such types of structures another physical picture is needed. Several propositions are known [1245] which are based on perturbation theory [14, 154] or on a suitable partitioning of the total SCF energy [706].

As we have mentioned previously, classical molecules with covalent bonds may associate to form van der Waals molecules. The stability of noncovalent bonding is

characterized by the interaction energy which is defined in Eq. (2.1). E_{int} can be partitioned into physically meaningful contributions

$$E_{int} = E_{Coul} + E_{pol} + E_{ex} + E_{ct} + E_{mix} + E_{disp} \tag{2.4}$$

where lower indices correspond to Coulombic, polarization, exchange, charge-transfer, mixed and dispersion terms, respectively. Each will be disccussed shortly.

E_{Coul} is the classical Coulombic interaction between the non-overlapping charge distributions of the isolated molecules. It is very important for most combinations of charged or dipolar molecules and for these it varies roughly parallel to the total interaction energy. This is why purely electrostatic models work so well for such systems. If A and B are dipolar molecules and R_{AB}, the distance between their charge centroids, is large E_{Coul} decreases as R_{AB}^{-3}, *i.e.* relatively slowly.

Polarization is due to the distortion of free molecular charge densities upon complex formation. It leads in general to an energy decrease which is vanishing as R_{AB}^{-4} if A (or B) is a charged and B (or A) is a dipolar molecule [935]. If both A and B are dipolar molecules the interaction energy decreases with R_{AB}^{-6}.

Exchange of electrons, ascribed to different closed-shell molecules, leads to a repulsive term in the interaction energy. Since it varies approximately parallel to the overlap integrals between molecular wavefunctions, it vanishes exponentially with R_{AB} so it is negligible at larger distances.

Delocalization effects, charge transfer from one molecule to the other, may also play an important role in bonding. Within the molecular orbital picture this corresponds to an interaction between occupied orbitals of molecule A and vacant orbitals of molecule B and *vice versa*. E_{ct} is in most cases negative and it vanishes with R_{AB} as rapidly as E_{ex}.

Mixed terms with no descriptive meaning are included into E_{mix}. It is relatively small for most associations though it may become large for some transition-state complexes. Dispersion plays an important role in classical van der Waals interactions. Its source is electronic correlation and it vanishes as R_{AB}^{-6}.

2.2 SIGMA BONDS

The simplest and best characterized bond type is the two-centre σ-bond [256]. It is formed for example between nearest neighbours in *saturated molecules* like alkanes, ammonia, or tetrahydrofuran. σ-Bond LMOs possess a quasiaxial symmetry which is perfect in diatomic molecules. The orbital amplitudes have maxima along the lines connecting bonding atoms (see Fig. 2.4 [366, 367]) and negative lobes outside the bonding region. These lobes correspond to p orbital components of atomic hybrids, consequently they are absent in the vicinity of the hydrogen atoms.

σ-Bond LMOs are in most cases well localizable. For a variety of first-row atom molecules l_σ of Eq. (2.3) exceeds 0.98 [119]. However, there are cases where they are strongly delocalized. This occurs mostly in *hyperconjugation* where delocalization is

due to the interaction between a π-bond LMO and a quasi π-type combination of XH(X = C, N or O) bond LMOs *e.g.* in a methyl group [1150]. Hyperconjugation may be the source of important physical and chemical effects like shifts in ultraviolet absorption bands or reactivity changes [310]. This phenomenon explains why the dipole moment of toluene differs from zero (0.11 aC. pm [871] in spite of the negligible inductive effect of the methyl substituent of the apolar benzene. An extreme example is the dimethylsulphimide (Me_2SNH) molecule [984]. According to CNDO/2 calculations l_{NH} of Eq. (2.4) ranges from 0.952 to 0.959 while $l_{CS} = 0.999$ and $l_{NS} = 0.997$. CH bonds of dimethylsulphimide are also hyperconjugated but to a smaller extent (l_{CH} = 0.981). Even more striking is *N*-sulphinosulphimide (H_2SNSO_2H) where strong delocalization of a bond, containing no hydrogen atom, is observed: $l_{S(VI)N} = 0.923$. In all the above cases delocalization occurs almost exclusively to vacant *d*-orbitals of the neighbouring sulphur atom [984].

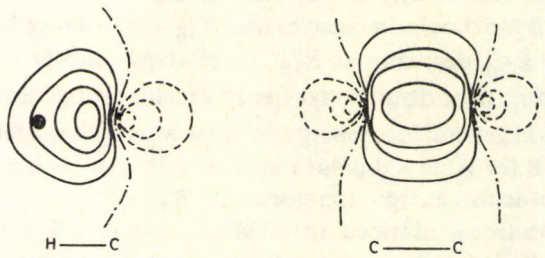


Fig. 2.4 Schematic representation of CH and CC-type bond LMOs for ethane. Full and dashed lines denote positive and negative values, respectively

Transferability of σ-bond LMOs may be judged from *s-characters* (λ^s) and *bond polarities* (σ) as given for some simple molecules in Table 2.1. Using a minimal basis set, these quantities may be defined from an AB bond LMO (A and B are first-row atoms) as

$$\lambda_A^s = c_{2sA}^2 / n_A \tag{2.5}$$

$$\sigma_A = n_A / (n_A + n_B) \tag{2.6}$$

with

$$n_A = c_{2sA}^2 + c_{2p_xA}^2 + c_{2p_yA}^2 + c_{2p_zA}^2 \tag{2.7}$$

c_{2sA}, c_{2p_xA}, etc. are AO coefficients in the bond LMO.

According to Table 2.1 *s*-characters are poorly transferable, though some trends may be seen. λ_C^s depends primarily on the coordination number of the carbon atom. This indicates that it is reasonable to use sp^3, sp^2 and *sp* hybrids to describe a σ-bond fraction with a tetra-, tri- and bicoordinated carbon atom, respectively. The corresponding *s*-characters are 0.25, 0.33 and 0.5. Thus, *hybridization* may have a meaning in minimal basis MO theories, too. However, it is not an observable

TABLE 2.1

s-Characters and polarities of CH bonds in some saturated molecules as obtained from CNDO/2 SCF calculations [970]

Coord. number of C atom	Molecule	λ_C^s	σ_H
4	Methane	0.272	0.505
	Ethane	0.269	0.509
	Methanol[a]	0.293 – 0.297	0.517 – 0.524
	Methylamine[a]	0.275 – 0.281	0.520 – 0.524
3	Ethylene	0.323	0.502
	Benzene	0.303	0.510
	Formaldehyde	0.396	0.518
2	Acetylene	0.458	0.475

[a] Limiting values for different CH bonds

phenomenon, though certainly has some physical significance and it provides only a simple rule to construct appropriate basis sets of AOs. It is especially important for transition metal compounds where computational difficulties are formidable and reasonable simplifications play a vital role [577].

Bond polarities are, in general, well transferable; the deviations from the mean do not exceed 10 per cent for a number of classical molecules [981]. This means that polarities are determined only by the atom forming the bond. Secondary effects, like hybridization, polarization by the environment and delocalization, play only a minor role though they may be decisive in some cases (*e.g.* reactivity). Bond polarity depends on the relative power of an atom to attract electrons to itself. This quantity is called *electronegativity* [1070] and it has several definitions [565, 945]. All these give about the same relative scale which corresponds to experimental observations on a variety of different molecules. A straightforward definition can be given if we ascribe SLMOs to bonds. Using a minimal basis of Slater orbitals the electronegativity can be defined as the exponent of the valence AOs which are given by the Slater rules. Notice that in most minimal basis set methods *s* and *p* exponents are equal to each other. The larger the exponent, the stronger the AO and the corresponding charge distribution is concentrated around the core. Thus the orbital exponent is a direct measure of electron attracting power. In fact, Pauling electronegativities, χ_A^P [1070], and valence atomic orbital exponents, ζ_A, show a close relation for atoms between H and Kr:

$$\chi_A^P = 1.357\zeta_A + 0.210\,, \qquad r^2 = 0.893\,. \tag{2.8}$$

If only first-row atoms are considered an excellent correlation with $r^2 = 0.992$ is obtained [970].

There are some chemically important cases where systematic deviations from the transferability of bond polarities are observed (see Table 2.1). A well known example is the decrease of CH reactivity in saturated carboxylic acids (*e.g.* butyric acid) as the number of bonds between the carbon atom and the carboxyl group gets larger. This phenomenon is due to polarization of the CH bond by its environment and arises from the superposition of two effects [871, 1168, 1358]. The first is the *inductive effect*. The C^{α} atom, having been deprived of some of its charge by the electron withdrawing power of the carboxyl group, is drawing the $C^{\alpha}C^{\beta}$ electrons closer to itself. As a consequence, this bond is polarized and the C^{β} atom becomes slightly positive. The inductive effect is greatest for adjacent bonds but it may also be important farther away [573]. However, in general it vanishes for third and higher neighbours. The other dominating contribution is the electrostatic *field effect* which operates over larger distances through space (or through solvent). This can be illustrated on substituted acrylonitriles [119]. The electrostatic field of the molecular environment polarizes the three CN banana bonds directly. This may be seen from the good correlation ($r = 0.993$) between the corresponding components of the bond dipole moment and the electric field originating from the rest of the molecule. The variable substituent is separated from the polarized bond by at least one σ-bond.

Let us characterize now the σ-bond on the basis of experimental data. Our goal is to analyze transferability and additivity of some so-called bond properties, like length, force constant, energy, reactivity, etc.

Bond lengths between atoms of given type are constant to a good approximation in a wide variety of compounds [1327]. Best transferable is the CC distance: it ranges in various saturated hydrocarbons between 153.7 and 154.5 pm. Similarly, the CH distance in these compounds is 107–110 pm depending on the number of nonhydrogen substituents on the carbon atom. Transferability is thus better fulfilled if the local environment of the bond is also considered. Bond distances depend also on the coordination number, they are 109.3, 108.5 and 105.9 pm for the CH bonds in ethane, ethylene and acetylene, respectively [1327].

Rotation around σ-bonds is easy, rotational barriers range between 4 and 40 kJ/mol [1383]. The actual value of the barrier depends strongly on the local environment of the bond, steric hindrance or hydrogen bond formation may cause considerable changes. Therefore transferability is not fulfilled.

Stretching force constants may be ascribed to σ-bonds and they are fairly transferable. This is the basis of the relative constancy of bond (or group) frequencies in infrared spectra. Molecular environment and solvent may influence these frequencies to some extent but they are characteristic of the bond in most cases.

Electronic excitation of saturated molecules having exclusively σ-bonds and occasionally lone pairs is possible only by high-energy (ultraviolet) light. Maxima of the UV spectra appear mostly under 180 nm [760]. The high energy excitation leads often to bond breaking.

Dipole moment increments are well transferable. Exploiting the additivity rule, dipole moment of saturated molecules can be calculated as vectorial sums of bond increments with a relatively small error [918]. This allows us to gain information on the conformation of the molecule by comparing calculated and experimental values.

The σ-bond is chemically stable; considerable energy is needed to break it. Average bond energies, as derived from observable data, are between 100 and 565 kJ/mol [1070]. For bonds containing carbon atoms the range is 250–420 kJ/mol. Additivity, especially for nonstrained saturated hydrocarbons, is excellent; the deviation between calculated and experimental values is only a few kJ/mol. Saturated molecules, especially hydrocarbons, are inactive in chemical reactions.

2.3 PI BONDS

As mentioned in Section 2.1 isolated double bonds are composed of a σ- and a π-part. The π-type bond LMOs are essentially different from σ ones as may be seen from Fig. 2.5. Molecular fragments with π bonds have local planar symmetry; the orbital has a nodal plane which contains the line connecting the two bonded atoms. Consequently, the electronic density corresponding to a π LMO vanishes in this nodal plane. This has some physical consequences, too (*e.g.* Mössbauer isomeric shift, see Section 3.4.3). π-type SLMOs can be constructed in most cases from atomic p_z orbitals. They do not possess an axial symmetry since the axes of p_z orbitals are not collinear. The lack of axial symmetry for a π-bond may also be seen from experimental difference densities. The difference density map for the CC double bond in tetracyanoethylene, in a plane bisecting the interatomic distance, is distorted if compared to the almost perfectly symmetric map of the CC single bond [76].

π-Bonds with one or two second-row atoms may involve *d*-orbitals of the appropriate symmetry. An example is Me_2SO where the SO π-bond LMO is composed primarily of $d_{xz}-p_z$ and $d_{yz}-p_z$ AO combinations [984]. If *d*-orbitals are mixed ($d\pi - p\pi$ bonding [754]) the bond may have special features compared with "pure" p_z-p_z type ones. The analogy between bonds obtained by replacing a first-row atom with its second-row counterpart may be absent. Such an analogy exists between CO and CS

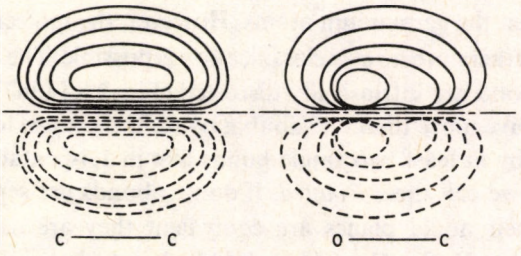


Fig. 2.5 Schematic representation of CC and CO π-type bond LMOs. Full and dashed lines denote positive and negative values, respectively

double bonds which are similar in many respects. On the other hand, the SO bond in Me_2SO has no analogy with any OO link. In dimethylsulphoxide, the oxygen lone pair delocalizes strongly to the vacant sulphur *d*-orbitals and a π-bond is formed. Lone pairs are much better localized in peroxides, thus, the oxygen atoms are singly bonded in these compounds.

Heteropolar π-bonds are much more distorted than σ-bonds involving the same atoms since they are more easily polarizable. If two perpendicular π-bonds and one σ-bond are located between two atoms a *triple bond* is formed. π-Bonds may have just one common centre involving perpendicular *p*-type AOs which combine with the neighbouring *p*-orbital of the appropriate symmetry (*cumulated double bonds e.g.* in butatriene $H_2C{=}C{=}C{=}CH_2$). The perpendicular arrangement of cumulated double bonds is seen from Fig. 2.2 [86]. The experimental difference density in hexatriene is different for the central CC double bond from the neighbouring ones. The central bond is a combination of *p*-type AOs which lie in the molecular plane, while the two others involve perpendicular orbitals.

An interesting π-only bond is present in cyclic S_2N_2 (see Fig. 2.6) where no σ-bond between the interacting sulphur atoms is formed. The existence of this bond is supported by CNDO/2 calculations of the corresponding LMO [97, 974] and also by experimental evidence. SNS and NSN bond angles are nearly the same in this molecule while in other SN rings the former tend to be larger [1185]. Thus both sulphur atoms get closer than expected supporting the idea that a weak diagonal bond is formed.

If canonical orbitals of molecules with double bonds are obtained by an *ab initio* or INDO method and these are localized σ- and π-type bond LMOs mix and bent banana (τ) LMOs are obtained [366]. Clearly, if σ and π orbitals are localized separately this is not the case. A banana orbital for the N_2 molecule is depicted in Fig. 2.7 [371]. The three banana LMOs corresponding to the triple bond are placed symmetrically around the molecular axis.

The σ–π or banana representation of LMOs for double bonds in planar molecular fragments is completely equivalent from the physical point of view. The difference is essentially didactic. For some purposes (*e.g.* demonstration of the high barrier to rotation around a bond) the banana representation is better. However, in general we prefer the σ–π classification. There are cases where the local environment of a double bond is not planar like in Ge_2H_4 This molecule should be analogous to ethylene with a double bond between the germanium atoms. However, the molecule has a *trans* bent nonplanar structure therefore no σ–π classification is possible. The LMOs corresponding to the double bond are intrinsically distorted (Fig. 2.8 [1367]).

Molecules may have more than one double bond. If these are located far away, *i.e.* they are separated by at least two single bonds like in 1,4-pentadiene, $H_2C{=}CH{-}CH_2{-}CH{=}CH_2$, we call them *isolated*. If double bonds are separated by just one single bond and their nodal planes are equivalent they are called *conjugated*. In *cumulenes* like allene, $H_2C{=}C{=}CH_2$, double bonds have one common atom. Localizability of π-LMOs assigned to isolated double bonds is very close to unity. This

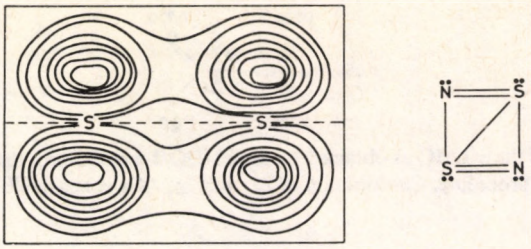


Fig. 2.6 Isodensity contour map for the SS π-type bond LMO in S_2N_2. (From Ref. [974])

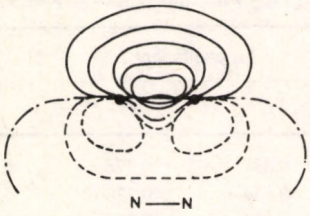


Fig. 2.7 Schematic representation of the banana bond LMO in N_2. Full and dashed lines denote positive and negative values, respectively



Fig. 2.8 Isodensity contour map of the GeGe bond LMO in *trans*-bent digermene. (With permission from Ref. [1367])

is due to symmetry reasons since π-type MOs belong to different species and they do not mix with σ MOs, only with each other. If they are far from each other their mixing will be indeed small. If a planar molecule has just one π LMO, it is perfectly localizable ($l = 1$). An exception from strong localizability is *hyperconjugation* where CH bonds of a methyl group interact with a conjugated π-bond. The CO π-bond LMO of acetaldehyde is delocalized to the neighbouring carbon and hydrogen atoms (Fig. 2.9 [970]). Conjugated π-LMOs in acylic molecules delocalize to a given extent (see Table 2.2).

Transferability of π LMOs is fair if these are well localizable. If delocalization gets important transferability is also worse (see glyoxal in Table 2.2). Bond characteristics, as extracted from experiment, are also transferable to a given extent, though not so well as for σ-bonds.

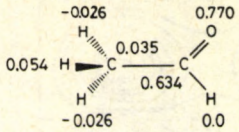


Fig. 2.9 Coefficients of the π-LMO as obtained by the CNDO/2 method with the Edmiston-Ruedenberg procedure. Contribution of $2p_x$ and $2p_y$ AOs is negligible

TABLE 2.2

Coefficients of π-type CO bond LMOs in some simple molecules as obtained by the CNDO/2 method [970] with the Edmiston–Ruedenberg procedure

Molecule	$2p_z$ coefficient		σ_C	Localizability
	C	O		
Formaldehyde	0.631	0.776	0.398	1.0
Acetaldehyde	0.634	0.770	0.404	0.995
1-F-acetaldehyde	0.651	0.755	0.422	0.994
Acrolein	0.624	0.767	0.399	0.978
Glyoxal	0.652	0.738	0.442	0.975

Since the electron excess between bonding atoms, consequently the interference effect also is increased in double and even more in triple bonds these are stronger than a single σ-bond. As a consequence bond lengths get shorter

$$R_{\text{triple}} < R_{\text{double}} < R_{\text{single}} . \tag{2.9}$$

The validity of the above rule may be judged from experimental bond lengths (C≡C : 120.5, C=C : 133.7, C—C : 154.1; C=N : 115.8, C=N : 132.0, C—N : 147.2, in pm [1327]. Transferability of bond lengths is good for isolated double and triple bonds but it becomes worse in the conjugated case. The CC double bond length is 135 pm in butadiene, 136 pm in acrolein and 133.7 pm in ethylene [1327].

Barriers to rotation around isolated double bonds are very high, more than 200 kJ/mol, (*cf.* Section 3.2) since the π-bond has to be cleaved during rearrangement. If conjugation is strong the barrier may diminish [664].

Stretching force constants and bond energies of single, double and triple bonds increase in this order: f_{CC} in ethane, ethylene and acetylene is 445, 939.5 and 1595 N/m, *cf.* Section 3.3 and the corresponding bond energies are 347, 552 and 960 kJ/mol, respectively. This has the same origin as the decrease of bond lengths: the bond gets stronger.

Excitation and ionization of double bonds is easier than for the corresponding single bonds. This is due to the existence of a nodal plane in π-bond LMOs. It is known that observable excitation and ionization energies may be related to orbital energies, *cf.*

Section 3.6 and these latter increase with increasing number of nodal planes (see *e.g.* [1313]).

Dipole moment increments are reasonably transferable for isolated double and triple bonds. Transferability gets worse in conjugated molecules.

Double and triple bonds are more reactive than corresponding single ones. This seems to be in contradiction to the increased strength but, however, the electron cloud ascribed to π-bond LMOs is not so strongly concentrated around the bond as in the case of single bonds. Therefore polarization by a reactive group is easier. Another factor increasing the reactivity is the decrease of the coordination number, making double bonds sterically more easily accessible than single ones.

2.4 LONE PAIRS

In most classical molecules with N, P, O, S or halogen atoms a special "bond" called lone pair is formed where the corresponding LMO is located almost exclusively on a single atom. It is always the heteroatom which bears one or more lone pairs, carbon atoms may have these only in nonclassical structures (*e.g.* singlet methylene, H_2C:). Lone pairs are best discussed in terms of the corresponding LMO though canonical lone pair orbitals are also defined especially for the treatment of electronic excitation and ionization phenomena (see Section 3.6). Canonical lone pairs are not necessarily identical with localized ones—they may differ even if located on the same atom (*e.g.* $3a_1$ and $1b_1$ orbitals in H_2O (see Section 1.5)). Peaks in the photoelectron spectra which correspond to ionization from a canonical lone pair have no vibrational structure therefore their classification as a pure atomic orbital is justified.

One of the two identical lone-pair LMOs on the oxygen atom in water is depicted in Fig. 2.10 [970]. Comparing this with Fig. 2.4 it is seen that the lone-pair LMO occupies a larger solid angle than a bonded pair. This statement is quantified on the basis of *ab initio* calculations [266, 671]. It means that lone pairs tend to separate farther from each other than bonding σ or π orbitals; this has consequences in the Gillespie valence-shell electron repulsion theory of molecular geometry (see Section 3.1).

Table 2.3 shows some characteristic figures for the lone-pair LMOs in simple molecules [970]. Localizability is smaller than for σ and isolated π LMOs [1324]. Consequently, resonance effects due to substituents containing lone pairs may be important [871]. Transferability of *s*-characters is usually fair, though it is bad for glyoxal where the oxygen atom bears two nonequivalent lone pairs. A similar situation holds for the hypothetical vinylalcohol molecule. λ_s remains constant in different conformations of the same molecule. Transferability of oxygen lone pairs can be judged also by comparing the angle ϑ, between them. We define ϑ as the angle between vectors with components c_{p_x}, c_{p_y} and c_{p_z}. These latter are coefficients of lone-pair LMOs obtained by the INDO method. For the molecules in Table 2.3, except for vinylalcohol, transferability is fair. The stronger separation of lone pairs than of σ-bonds is reflected

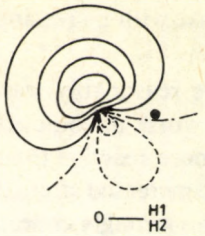


Fig. 2.10 Schematic representation of the lone-pair LMO in H_2O. Full and dashed lines denote positive and negative values, respectively

by values of ϑ which are larger than the angles between σ-bonds in saturated molecules ($<110°$). The slight increase of ϑ with respect to the ideal 120° in carbonyl compounds where the coordination number of oxygen is 1 indicates also a stronger separation. The numbers of Table 2.3 reflect nicely the rule of Pauling which states that the angle between lone pairs is proportional to their average *s*-character [1070]. We obtained the following linear regression equation [970]:

$$\vartheta = 119.5\,\lambda_s + 80.7; \qquad r = 0.987\,. \tag{2.10}$$

Delocalization of lone-pair LMOs to π-orbitals may be considerable if the former have appropriate steric orientation (*e.g.* planar phenol). If an atom bears two lone pairs it is often advantageous to define nonequivalent σ- and π-type lone-pair LMOs. This can be done with a simple linear transformation of the equivalent pairs. Distinction of

TABLE 2.3

Characterization of oxygen lone pair MOs in some simple molecules (CNDO/2 calculations) [970]

Coord. number	Molecule		Coefficient				
			$2s_O$	$2p_O$[a]	λ_O^s	ϑ Degree	l%
2	H_2O		0.574	0.815	0.330	120	100.0
	H_2O_2	*cis*	0.585	0.808	0.342	122	99.6
		trans	0.589	0.806	0.342	122	99.9
	CH_3OH	staggered	0.559	0.821	0.312	119	98.6
		eclipsed	0.557	0.817	0.310	119	97.7
	$H_2C{=}CHOH$		0.430	0.889	0.184	102	97.9
1	H_2CHO		0.600	0.785	0.360	123	97.8
	$H_2C{=}CHCHO$	*a*	0.620	0.793	0.385	124	99.9
		b	0.583	0.800	0.340		98.0
	$(CHO)_2$	*a*	0.680	0.723	0.467	123	98.6
		b	0.506	0.851	0.258		98.4

[a] $(c_{p_x}^2 + c_{p_y}^2 + c_{p_z}^2)^{1/2}$

π-type lone pairs may be important in the appropriate definition of π-systems which are needed in several semiempirical methods (see Sections 1.2.6 and 1.3.2) and in qualitative argumentations.

Lone pairs on atoms of the second and higher rows may consist of *d*-orbitals. Accordingly, several types of hybrid orbitals may be constructed which allows a straightforward description of various structural features [1070]. This becomes especially important for transition metal compounds. As for first-row atoms, localizability of lone-pair LMOs with *d*-orbital participation is smaller than that of a corresponding bond LMO [490].

It is difficult to relate experimentally observable quantities directly to lone-pair properties. It makes no sense to speak about bond length, bond energy, stretching frequency, etc. Lone-pair effects are easiest discernible if we study the shape of molecules. Lone pairs have to be considered as real ligands attached to a given atom. If the number and nature of ligands is correctly settled the valence-shell electron pair repulsion (VSEPR) model [448] works well for an astonishingly large number of classical and nonclassical molecules. This model will be treated in more details in Section 3.1.

Lone pairs contribute also the total dipole moment of a molecule. For example, it could not be understood without lone-pair contribution why the NF_3 molecule has a small dipole moment. The NF bond is strongly polar and the corresponding dipole increment would result in a large moment if the lone pair contribution did not cancel this effect.

Chemical reactivity is often influenced by the presence of lone pairs at a given reaction centre. Lone pairs are easily polarizable; thus, for example, protonation is facilitated. This has important consequences in various reaction mechanisms [871]. Lone pairs play an essential role in formation of hydrogen bonds (see Section 2.9).

2.5 THREE-CENTRE BONDS

Closed-shell molecules containing only H, C, N, O and F atoms may be described in practically all cases in terms of relatively well localizable σ-bonds or lone pairs and localized or delocalized π-bonds. There exist, however, important nonclassical molecules where two-centre σ-bonds are so strongly delocalized that only the term "three-centre" is appropriate. Typical representatives are the *electron-deficient* molecules. These contain atoms which have fewer occupied valence AOs than their coordination number implies [1070]. For example, due to the bridged structure of diborane the coordination number of boron is four though it has only three valence AOs occupied. Accordingly, the localization of MOs to two centres is ambiguous and we have to discuss molecular properties in terms of three-centre LMOs.

Let us now study diborane, B_2H_6, more detail. This molecule is not similar to ethane; rather it has a bridged structure as shown in Fig. 2.11. Localization of canonical MOs,

as obtained by the *ab initio* method with a minimal STO-3G basis set, yields four equivalent two-centre BH bond LMOs and two three-centre LMOs localized on both boron and one of the two bridge hydrogen atoms [24], respectively. A similar result is obtained using the INDO semiempirical method [970]. According to this calculation AO coefficients of the BHB LMO are 0.258 (2*s*) and 0.487 (2*p*) for both boron atoms and 0.655 for the bridge hydrogen; *s*-characters at boron are 0.235 (BHB bonds) and 0.335 (BH bonds). These numbers explain the difference between HBH angles (for definition see Fig. 2.11). Using Eq. (2.10) we obtain 109° and 121° for α and β; the experimental values are 96° and 121°, respectively. This difference may also be predicted by the VSEPR model. In this the spatial extension of three-centre bonds is considered to be smaller than that of two-centre σ-bonds. This is why α is smaller than β.

Up to now a large variety of boron hydrides has been synthesized [1080] and several of them consist of three-centre BHB or HBH bonds (e.g. $B_3H_8^-$, B_4H_{10}, B_5H_9). An example of the latter is BH_5 for which high-quality *ab initio* calculations were performed [583]. In this molecule the pyramidal BH1H3H5 moiety is loosely bound to the H2H4 one and a structure with C_s symmetry is formed (Fig. 2.12). The binding energy with respect to the dissociation to BH_3 and H_2 is small, 8 kJ/mol, but the formation of a H2BH4 three-centre covalent bond is unquestionable. The contour plot of the corresponding LMO is given in Fig. 2.13. Explicit calculations indicate that binding of H_2 to BH_3 in BH_5 is essentially due to electron correlation; therefore the HBH bond is atypical even if compared to the BHB bond in diborane.

Another important class of molecules with three-centre bonds are carbocations (*e.g.* CH_3^+). These can also be treated as electron deficient since the carbon atom bearing the formal positive charge has less occupied valence AOs than its maximum coordination number is. Carbocations are formed as intermediate products in certain chemical reaction mechanisms (alkylation, nitration, etc.) [95]. They are, in general, short-lived species and easily transform into some more stable compound (*e.g.* alkane). A subclass of carbocations are carbonium ions possessing pentacoordinated carbon atoms (*e.g.* CH_5^+). These are formed upon protonation or alkylation of saturated hydrocarbons.

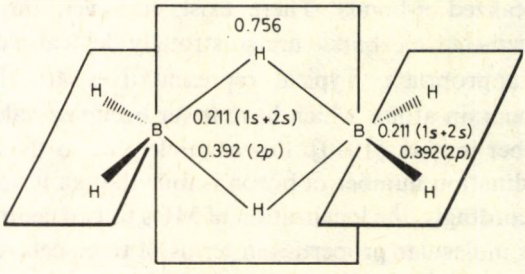


Fig. 2.11 Renormalized AO coefficients in the BHB LMO in diborane as obtained by the *ab initio* SCF method with an STO-3G basis set

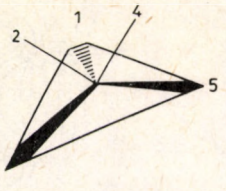


Fig. 2.12 Geometrical arrangement of hydrogen atoms in BH_5

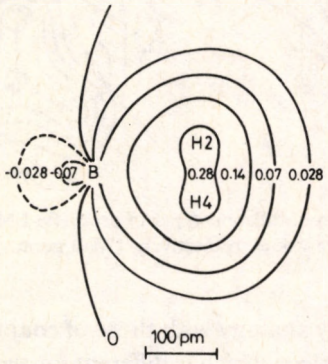


Fig. 2.13 Schematic representation of the BHH LMO in BH_5. (With permission from Ref. 583)

The simplest carbonium ion, CH_5^+, has been the subject of several theoretical investigations [1081, 1171]. It is similar to BH_5 (Fig. 2.12) though its dissociation energy to CH_3^+ and H_2 is very much larger (180 kJ/mol [583]), and the portion due to electron correlation is relatively small. This is attributable to electrostatic and polarization effects of CH_3^+ on the H_2 moiety. Similarly, as in BH_5, a three-centre H2CH4 bond is formed [1081].

Three-centre bonds can consist of exclusively nonhydrogen atoms, too. Such a bond exists in PH_3F_2 which has a D_{3h} trigonal bipyramidal structure [681]. The linear FPF moiety is strongly polar in this molecule both F atoms bearing a net charge of -650 millielectrons while *d*-orbital participation is unimportant in bonding. Other interesting examples for X—Y—X bonds are metal alkyls, *e.g.* $Al_2(CH_3)_4$, where Al—C—Al bonds exist.

2.6 AROMATICITY

In certain planar molecules which have a ring structure conjugated double bonds are especially strongly delocalized. Bonding in these *aromatic systems* (*e.g.* benzene, pyridine, naphthalene) is essentially different from the cases described in previous chapters. These molecules possess characteristic physical and chemical properties

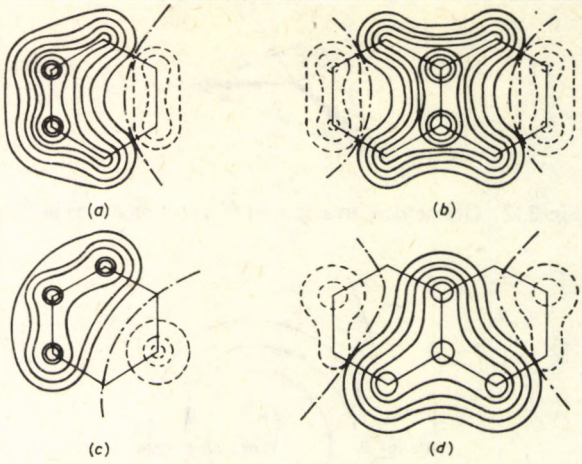


Fig. 2.14 Schematic representation of different types of aromatic LMOs. Full and dashed lines denote positive and negative values, respectively. (With permission from Ref. 369)

which cannot be discussed by analogy with those of conjugated dienes. An example is the CC bond length in hexatriene which is different for the single (146 pm) and double bonds (135 pm). This is not the case for the cyclic analogue, benzene, where all CC bond lengths are equal, 139 pm.

The most striking property of aromatic molecules, distinguishing them from linear or branched conjugated systems, is the strong delocalization of their π-orbitals. Planarity and cyclic structure favour delocalization as will be shown later. Two-centre localizability of π-orbitals on different aromatic molecules varies between 70 and 80 per cent as obtained from *ab initio* minimal basis set or CNDO/2 semiempirical calculations [326, 982]. On the other hand, σ-bond and lone pair LMOs which do not delocalize to the aromatic system are localizable to about the same degree as their counterparts in saturated molecules. In aromatic systems π-type LMOs, having at least one nodal plane (the molecular one), extend to three or even four atoms of the molecule. England and Ruedenberg classified these for various mono- and polycyclic systems, the latter containing only six-membered rings. Their results, obtained on the basis of simple Hückel MO calculations, are visualized in Fig. 2.14 [369]. In six-membered heteroaromatic systems type *(c)* dominates while for three-, four- and five-membered cycles (besides cases *(a)* and *(c)*) other, special types are obtained [982].

Due to the considerable delocalization, aromatic bond LMOs are not transferable from one molecule to another. Even in such relatively simple systems as substituted benzene derivatives, considerable differences are observed in the positions of LMO centroids if substituents are changing [1011]. Lack of bond transferability is also reflected in the chemical behaviour of aromatic compounds. For example, aniline (Ph—NH_2) behaves essentially different in electrophilic substitution reactions than nitrobenzene, Ph—NO_2. The only case where transferability is maintained is

substitution by a $—CH_2X$ group bridge. The "insulating" effect of the methylene prevents delocalization to the X moiety thus ensuring transferability.

The first step towards a unified treatment of aromaticity is to define which molecules are considered as aromatic. In classical chemistry, experimental properties, and primarily reactivity, determine aromatic character. For example, benzene may be substituted relatively easily while in the case of the corresponding open-chain hexatriene addition to a double bond is more common. Theoretical treatment of reactivity is often problematic even in modern quantum chemistry therefore aromaticity is, in general, expressed in terms of the extra stability as compared to the corresponding open-chain structure. A possible, widespread experimental method to measure this is as follows [1313]. We know that heats of atomization of saturated molecules may be calculated with a fair accuracy from bond increments (Section 2.2). This is also true for molecules with isolated double bonds. Increments for C—H, C—C and C=C bonds are 417, 332 and 591 kJ/mol, respectively. Using these values the heat of atomization which corresponds to the Kekulé structure of benzene is 5271 kJ/mol while the experimental value is 5539 kJ/mol. The difference, 268 kJ/mol is the *empirical resonance energy* of benzene which is a measure of extra stability. Aromatic molecules have large, positive empirical resonance energies. However, the opposite is not true, a molecule with large resonance energy is not necessarily aromatic.

Quantum chemistry helps to select molecules possessing special aromatic stability. According to the *Hückel* $4n+2$ rule all monocyclic, conjugated hydrocarbons having a number of $4n+2$ ($n=0, 1, 2, \ldots$) "π-electrons" are aromatic. This rule is discussed in more detail in Section 1.3.3. Stable, configurations are those where 2, 6, 10, ... electrons are ascribed to π-type MOs. These are often called 2, 6, 10, ... "π-electron" systems. According to the $4n+2$ rule, not only "six-electron" systems may resemble benzene in being aromatic (*e.g.* triphenylcyclopropenyl cation, $C_3Ph_3^+$, cycloocta-tetraenyl dianion, $C_8H_8^{2-}$).

Using Eq. (1.156) we can simply calculate the resonance energy. Note that the corresponding theoretical quantity, often called *delocalization energy*, is always negative since it is a measure of the energy *gain* upon formation of a conjugated system from ethylene units. However, both definitions differ only in sign. Treating benzene as an example, we have 2 and 4 electrons on the lowest and subsequent levels. Since the Kekulé structure of benzene contains three ethylene units each with a π-orbital energy of $2\alpha+2\beta$ in the Hückel approach, the delocalization energy is as follows

$$E_d = 2(\alpha+2\beta)+4(\alpha+\beta)-3(2\alpha+2\beta)=2\beta\,. \tag{2.11}$$

Similarly, Hückel delocalization energies of the tropylium cation ($C_7H_7^+$), cyclo-pentadienyl anion ($C_5H_5^-$), tropylium anion ($C_7H_7^-$) and cyclobutadiene (C_4H_4) are 2.988β, 0.472β, 0.098β and zero, respectively.

If the number of "π-electrons" in a molecule is $4n$, according to the Hückel rule no aromatic stabilization occurs. In this case the molecule is called *antiaromatic* since its π-electron system is less stable than the corresponding open-chain species (*i.e.*

cyclobutadiene, cyclooctatetraene). Antiaromatic molecules are very reactive in most cases. For large values of n ($n=4, 5, \ldots$) the difference between aromatic and antiaromatic molecules gradually vanishes. Concerning aromatic stabilization, cyclic conjugated polyenes (annulenes) with 20 or more carbon atoms are practically equivalent to their acyclic counterparts. This can be proven with mathematical rigour on the basis of the Hückel formalism [370].

The $4n+2$ rule works, in its original formulation, only for monocyclic systems which contain exclusively carbon atoms. For heteroaromatic molecules with atoms other than carbon (N, O, S, etc.) Eq. (1.156) is no more true. Similar problems arise for polycyclic systems. For these, various *aromaticity indices* were introduced [85, 479]. We treat two families which, we feel, are most popular at present.

A natural way to decide whether a molecule is aromatic or not is to compare its experimental resonance energy (or the corresponding theoretical delocalization energy) to a suitable reference [1313]. In a first approximation, cyclic, conjugated molecules with a large resonance energy are considered as aromatic. The larger the resonance energy, the more aromatic the molecule should be. This definition has some drawbacks. First of all, it is rather difficult to define the resonance energy unequivocally since measured heats of atomization may be influenced by factors other than aromaticity (*e.g.* ring strain). Owing to its high strain energy, cyclopropenyl cation is highly unstable, thus its resonance energy would be negative, indicating antiaromaticity [1313]. However, Hückel's rule, localization [982] and other [476] studies indicate strong aromaticity for this molecule. Furthermore, if the resonance energy is estimated by calculating the delocalization energy, some molecules which are nonaromatic or antiaromatic, would be considered to be aromatic. Using the Hückel method, delocalization energy of cyclooctatetraene is found to be 1.657β. This strongly antiaromatic molecule would be predicted to be almost as aromatic as benzene.

A further and serious problem with the above definition is that delocalization energy, as calculated by the simple Hückel approach, is roughly proportional to the number of occupied π-orbitals [370]. Therefore, aromaticity is best estimated by comparing the delocalization energy to that of the corresponding open-chain molecule and not of isolated double bonds [307]. The idea was developed further by Hess and Schaad [559, 560]. Thus the above mentioned delocalization energy divided by the number of "π-electrons" (REPE, resonance energy per electron) serves as a good aromaticity index. They calculated REPE for a large number of different molecules which helps in discussing reactivity and other properties of cyclic conjugated molecules. Trinajstić and coworkers derived REPE using solely molecular topology (topological REPE, TREPE) [493]. We give TREPE for a number of molecules in Table 2.4.

Table 2.4 allows us to explain some experimental trends. On the basis of TREPE the following stability order among carbon ring species is predicted in accord with experimental observations

$$C_3H_3^+ > C_3H_3^- ; \quad C_5H_5^- > C_5H_5^+ ; \quad C_8H_8^+ \approx C_8H_8^- .$$

TABLE 2.4

Topological resonance energies per electron (TREPE) for some conjugated cyclic molecules (in β units) [493]

Molecule	TREPE	Molecule	TREPE
$C_3H_3^+$	0.268	Benzofuran	0.027
$C_5H_5^-$	0.094	Azulene	0.015
Benzene	0.046	Furan	0.007
Pyrrole	0.040	[18] Annulene	0.005
Naphtalene	0.039	$C_8H_8^-$	−0.023
Phenantrene	0.039	$C_8H_8^+$	−0.029
Anthracene	0.034	$C_5H_5^+$	−0.153
Thiophene	0.033	C_4H_4	−0.307
$C_7H_7^+$	0.032	$C_3H_3^-$	−0.366

Aromaticity of benzenoid hydrocarbons decreases in the order benzene > naphthalene > anthracene. A similar decrease is found for pyrrole, thiophene and furan. If this latter, which is practically nonaromatic, is fused with a benzene ring to give benzofuran, its aromaticity considerably increases. Azulene is less aromatic than its isomer, naphthalene. The $4n+2$ rule is correctly reflected; rings with $4n$ electrons ($C_5H_5^+$, C_4H_4, $C_3H_3^-$) are antiaromatic with a negative TREPE. The topological approach allows treatment of radicals, too, which is a considerable practical advantage.

Another useful concept, discussing aromaticity at last semiquantitatively, is localizability of π-type LMOs [97, 329, 498, 982]. It is a generally accepted concept that the extra stability of aromatic molecules comes from the considerable delocalization of double bonds in cyclic systems (see Fig. 2.14 and [1313]). This qualitative argumentation can be founded more precisely [370, 371]. We mentioned in Section 2.1 that delocalization of bond LMOs lowers the energy of electrons which are ascribed to them. Since the total energy of aromatic molecules is a simple sum of MO energies in the Hückel approach (see Section 1.3.2) the delocalized π-orbitals yield lower total energies for aromatic systems than for the corresponding acyclic ones. The gain is just equal to the difference in the delocalization energies.

Characterization of aromaticity in terms of MO localizability is not necessarily linked to the simple Hückel approximation. This is especially useful in treating strange (*e.g.* inorganic) aromatic molecules [498, 974]. SN rings are so special that applicability of the Hückel method is questionable, though there exist some examples in the literature [450, 451]. However, analyzing localizabilities of MOs, obtained by the CNDO/2 method, it could be established that S_2N_2, $S_3N_2^+$ and $S_4N_3^+$ are of moderate aromaticity, about the same as pyrrole and imidazole [974].

An interesting case which was treated by Haddon in detail, is the MO theory of homoaromaticity [498]. A homoaromatic compound contains one or more sp^3

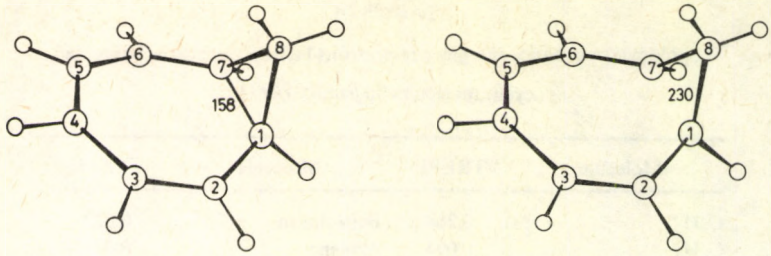


Fig. 2.15 Geometric structures of the homotropenylium cation *(a)* and cyclooctatrienylium cation *(b)*. Distances are in pm. (With permission from Ref. 498)

hybridized carbon atoms in an otherwise conjugated cycle. In order to ensure stability, sp^3 atoms are forced out of the plane of the aromatic sextet [1430]. Haddon discussed, among others, the structure of the homotropenylium cation (Fig. 2.15 *a*). This is a case where somewhat arbitrary assumptions have to be made in the simple Hückel theory to give a qualitative description of the phenomenon [620]. The reason is that this method is based exclusively on molecular topology and the effect of the geometry cannot be studied. Homotropenylium cation has an isomer, cyclooctatrienylium cation (Fig. 2.15*b*). This has the same topology as the former, the only difference is in the geometry. On the basis of *ab initio* STO-2G calculations this isomer was found to be formed in the flipping process as a stable intermediate. Analyzing the π-type LMOs of these species they proved to be essentially different (Fig. 2.16), while the 1–7 LMO in homotropenylium cation is strongly localized no counterpart is found in cyclooctatrienylium cation. This is certainly due to the considerable change in the 1–7 distance from 158 pm to 230 pm (*cf.* Fig. 2.15).

Schleyer and coworkers described "double aromaticity" in the 3,5-dehydrophenyl cation, $C_6H_3^+$ [197]. This cation is planar (see Fig. 2.17) and it has an aromatic sextet like benzene. Furthermore, there is an additional stabilizing interaction of three σ-orbitals in the molecular plane. A special three-centre bond is formed in which delocalization is similar to that in the cyclopropenyl cation. However, the plane of the bond LMO is perpendicular to the axes of the atomic *p*-orbitals which form the conventional π-bonds. Another special case is "acyclic aromaticity" in the Y-shaped

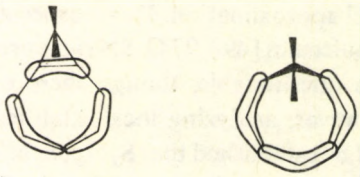


Fig. 2.16 π-type LMOs in homotropenylium cation *(a)* and cyclooctatrienylium cation *(b)*. (With permission from Ref. [498])

trimethylenemethane dianion, $C(CH_2)_3^{2-}$, where cyclic delocalization among three fragment π-type MOs is observed [628]. Though it is merely a matter of nomenclature, we would classify the above special cases rather as many-centre bonds.

After defining aromatic character, let us discuss its effects on molecular properties. Aromatic bond lengths lie between those of isolated single and double bonds [1327]. In benzene, a prototype of an aromatic molecule, all bond lengths are equal. This is exploited in a definition of aromaticity on the basis of bond length alternation in polycondensed hydrocarbons [660]. The less the molecule is aromatic the more CC bond lengths differ.

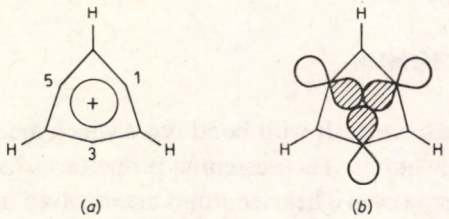


Fig. 2.17 Double aromaticity in 3,5-dehydrophenyl cation. *(a)* π-system, *(b)* delocalized σ-system

Excitation of aromatic molecules is easier than that of the corresponding saturated systems. Electronic transition energies are smaller, *i.e.* the wave length of the absorbed light is longer. This is why several aromatic compounds are coloured. A special group of conjugated hydrocarbons is called *alternating*. In these molecules carbon atoms can be classified into two groups, say A and B, in such a way that all bonded pairs involve atoms belonging to different groups: C_AC_B. For example, benzene, naphthalene and phenantrene are alternating while azulene is nonalternating (see [257] for details). It can be proven within the framework of the Hückel and PPP theories that in the ground state of alternating aromatic hydrocarbons π net charges are exactly zero on all atoms. This theorem does not hold rigorously in more sophisticated semiempirical and *ab initio* methods but numerical examples support its approximate validity.

Aromatic molecules have characteristic nuclear magnetic resonance spectra. Some signals are considerably shifted compared to the nonaromatic reference. This effect has been explained by the *ring current* concept (see Section 3.5.1). However, recent studies indicate that the π-electron cloud has no extra mobility; therefore its contribution to electric current density is less than that of σ-electrons even in benzene [771, 772]. Another important property of aromatic molecules is their enhanced stability, which is a consequence of delocalization (see above). Using the simple Hückel model Haddon was able to derive a formula which explicitly relates delocalization (resonance) energy to ring current in $(4n+2)$ annulenes [497].

Chemical reactions of aromatic molecules are unique from several points of view. Substitution is easier, while for isolated double bonds addition occurs more often. This difference may be explained most simply by the enhanced aromatic stability. During

addition at least one double bond is broken, so cyclic delocalization is interrupted and this is connected with an energy loss. Substitution leaves double bonds unchanged; therefore it is energetically more favourable. For molecules with isolated double bonds, no distinction between these types of reactions can be made merely on the basis of LMO localizability. We suppose that the attacking group does not influence localization properties of the reactant.

Aromatic molecules form preferentially charge transfer complexes which can be stable under laboratory conditions or which are formed as intermediate products of chemical reactions (Section 2.10).

2.7 METAL–METAL BONDS

In previous chapters we have dealt with bond types which are common in molecules with first- or second-row atoms. Their essential properties (shape, localizability, etc.) remain practically the same even if heavier atoms are involved in bonding. The σ-bond in XeF_2, though strongly polarized, is similar as in most simple organic molecules [55]. Recently, important and essentially new forms of bonding between transition metal atoms were described (see *e.g.* [251, 1182, 1259] for reviews). These cannot be compared to any of the bond types discussed above. Due to the rich variability of the electronic configuration of *d* elements quadruple and even sextuple bonds can be formed between them. From lithium to uranium a variety of metal-metal links is known and bonding between *d* elements is particularly strong; therefore it is especially important. In the last decade a great number of metal clusters, all involving metal-metal bonds, were synthesized from binuclear (*e.g.* $Re_2Cl_8^{2-}$) to nine-atom aggregates, like $[Pt_9(CO)_9(\mu_2-CO)_9]^{2-}$. Study of these compounds opens a new direction in chemistry.

Before characterizing metal–metal bonds it may be useful to briefly discuss quantum chemical methods, quantitative as well as qualitative, which are applicable to compounds of *d* elements. Since this field of quantum chemistry, though rapidly developing, is not yet elaborated as deeply as conventional methods we did not treat them in detail in Part 1. Now we summarize some methods and models in order of decreasing sophistication.

First of all it is important to know that for heavy elements, like transition metals, relativistic effects may be especially important [1147]. These are mainly of secondary character: inner shells contract strongly and this has an effect on the valence shell, too. Fortunately, it is possible to construct appropriate effective core potentials which include relativistic effects [663]. Using these, experimental spectra and potential curves can be reproduced with a sufficient accuracy. Therefore an adequate qualitative description of the metal–metal bond is possible, even if relativistic effects are neglected or considered only as corrections to the effective core potential. This is supported by the work of Benard *et al.* [81] who found a sufficient agreement between experimental and theoretical valence electron densities for dichromium tetraacetate dihydrate.

A factor which is much more important in describing metal–metal bonds is electron correlation. This is considered by most workers through a limited configuration interaction calculation. In a variety of cases a strong mixing of configurations can be observed [81, 168, 519]. This has important effects on some physical properties. For dimolybdenium (Mo_2) a limited CI calculation used 64 configurations involving paired excitations from the bonding orbitals to their corresponding antibonding orbitals. An equilibrium bond length (R_e) of 209 pm and a stretching frequency (ω_e) of 414 cm^{-1} was obtained, the value of the first anharmonicity constant, $\omega_e x_e$, was found to be negative. Including all single and double excitations out of the above 64 configurations, a total of 3212 spin-adapted configurations were obtained. Combining these in the final wave function $R_e = 197$ (193) pm, $\omega_e = 475$ (477) cm^{-1} and $\omega_e x_e = 2.3$ (1.5) cm^{-1} was obtained (experimental values are given in parentheses). Since relativistic effects were neglected in this calculation we may say that they are not important in the calculation of the above properties though their role is not negligible in excitation processes. Hay used a relativistic effective core potential for $Re_2Cl_8^{2-}$ [520] to describe electronic excitations of the weak δ bond which has two nodal planes containing the Re atoms.

Due to the diffuse character of the *d*-orbitals which are directly involved in bonding, basis set effects may be important for metal–metal bonds. This leads to computational problems. *Ab initio* calculations for compounds with *d* elements are very expensive. However, if only a qualitative description of bonding (*e.g.* electron density analysis [81]) is needed even a minimal basis can be used. It is primarily due to the basis set problem that the scattered wave X_α method has such wide applications in describing metal–metal bonds [1259]. Reviews on technical details are found in Refs 239 and 646. We feel that at present it is this method which is best suited to the study of metal–metal bonds. Though some physical parameters obtained from the calculations, may be erroneous, analysis of bonding in terms of electronic densities is possible.

A qualitative study of electronic configurations in transition metal complexes, including metal–metal bonds, is possible with the Extended Hückel method (see Part 1). This allows the analysis of trends in orbital populations, variation of overlap with bond lengths and bond angles. Though this method is very useful for systematizing the enormous amount of experimental data, it is only exceptionally applicable to obtain quantitative values of physical parameters (geometry, excitation energies, etc.).

Finally, we should mention a very useful concept which is an extension of the Lewis octet rule (Section 2.1). Apart from some exceptions (*e.g.* Sc) transition metal atoms tend to form a 18-electron configuration around them. This comes from the fact that the metal has 9 valence orbitals (one 4*s*, three 4*p* and five 3*d*). Group theory shows that for most coordination geometries the $n(\leq 9)$ ligand orbitals find a match in number and symmetry properties among the hybrids that can be formed from the nine metal orbitals. Bonding, nonbonding and antibonding combinations will be formed and the 18-electron rule can be formulated as the statement that only bonding and nonbonding combinations may be occupied by electrons.

Before we start discussing metal–metal bonds we mention that several binuclear complexes are known (these contain two metal atoms) in which no bond between *d* elements is present. A nice and thorough discussion of this problem for M_2L_{10} complexes is given by Hoffmann and coworkers [1262]*.

These compounds can be divided into three classes. The first class, derived from the Cotton compounds [251], (*e.g.* $Re_2Cl_8^{2-}.2H_2O$) are those containing a quadruple bond. In the second class, the Vahrenkamp compounds [1379], $[M_2(CO)_8(PMe_2)_2$, M = Mn, Cr, V, see Fig. 2.18], in agreement with the 18-electron rule there exists no bond

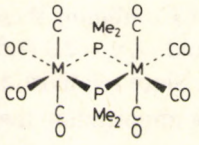


Fig. 2.18 Schematic structure of Vahrenkamp compounds (M = Mn, Cr, V)

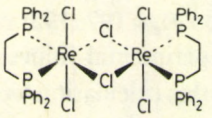


Fig. 2.19 Schematic structure of a Walton compound, $Re_2Cl_6(PPh_2CH_2)_4$

for Mn, a single bond for Cr and a double bond for V. A third class is also known, the paramagnetic, high-spin Walton compounds [640] where the metal atoms are very far from each other (see Fig. 2.19 for an example, the Re–Re distance is 381 pm). Though the Mn–Mn distance in $Mn_2(CO)_8(PMe_2)_2$ is not so large, there is direct evidence that in this molecule there is no bond between the metal atoms. We shall discuss these compounds in a bit more detail in Section 2.8. Here we mention only that it is the coupling between the bridging ligands which stabilizes the molecule in such a form. It makes no sense to speak about metal–metal bonding at all in these compounds.

Let us now treat various types of metal–metal bonds [253]. First, it has to be noticed that bond lengths are relatively large: they range between 180 and 250 pm [251]. Therefore metal orbitals overlap only slightly. In dichromium complexes, supposing a Cr–Cr distance of 220 pm, the overlaps between σ, π and δ-type hybrids amount to 0.25, 0.1 and 0.01, respectively. For comparison, the π overlap in benzene is 0.25 while the overlap of *sp* hybrid AOs forming σ-bonds is usually much higher (0.7–0.8). Because overlap is so small, it is found, in general, that effects facilitating increased overlap will favour metal–metal bonding [1368]. This is why metal cluster complexes usually contain *d* elements in low oxidation (electron rich) states: the electron–electron repulsion leads to the radial extension of the orbitals which, in turn, maximizes interatomic overlap.

σ and π bonds are similar to those described in Section 2.2 and 2.3 though *d*-orbital participation is important since 3*d* electrons are lower in energy than 4*p* ones. A wide variety of examples is known, *e.g.* binuclear clusters with single bonds are $Mn_2(CO)_8$ and $Rh_2(CH_3CO_2)_4[SO(CH_3)_2]_2$, larger clusters with single bonds are $Mo_6Cl_8^{4+}$ and

* Hereinafter M and L stand for metal and ligand, respectively.

$CO_6(CO)_{15}^-$ [252]. A binuclear cluster with a Ta=Ta double bond is $Ta_2[S(CH_3)_2]_3Cl_6$ while in the $Re_3Cl_{12}^{3-}$ anion Re=Re double bonds exist and metal atoms form a regular triangle [252]. In some cases heteronuclear single bonds are also formed between transition metals, like in $FeMn_2(CO)_{14}$ or in $Ru_3CoH_3(CO)_{12}$ [1182].

There are two classes of metal–metal triple bonds [167]: both are composed of one σ- and two π-type bonds (see Section 2.3). In the first category atoms with $3d^3$ configuration form the bond (d^3—d^3 triple bond). In these molecules σ and π levels are filled while higher lying δ levels are empty; the configuration is $\sigma^2\pi^4$. In d^5—d^5 triple bonds all bonding and antibonding δ levels are doubly occupied, leading to a $\sigma^2\pi^4\delta^2\delta^{*2}$ configuration with a net bonding number of three. The d^3—d^3 triple bonds exist *e.g.* in $Mo_2(OCH_2CMe_3)_6$ and in $W_2(NMe_2)_6$, while $Re_2Cl_4(PEt_3)_4$ and homologous compounds possess d^5—d^5 type triple bonds. In some compounds with metal–metal triple bonds the electron density along the M–M line has a quasiaxial symmetry, therefore ligands, attached to the metals, can rotate freely. In other cases this is not true since *d*-orbital mixing is strong; therefore the axial symmetry is destroyed. Owing to computational and interpretation problems, some controversies over internal rotation in a number of compounds can be found in the literature [9, 167].

The most interesting bond type which is formed between transition metal atoms is the *quadruple bond*. It was first described in $Re_2Cl_8^{2-}$ by Cotton [250]. Using the 18-electron rule, this molecule has a $\sigma^2\pi^4\delta^2$ valence configuration *i.e.* the formal bonding

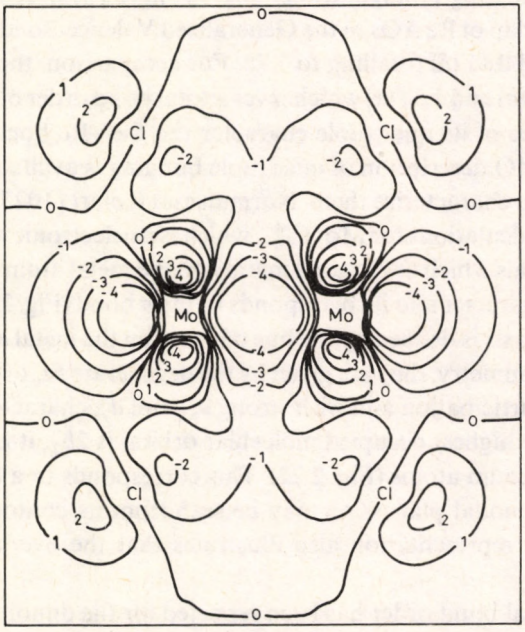


Fig. 2.20 Contour map of the $4a_{1g}$ orbital for $Mo_2Cl_8^{4-}$. The contour values are: 0, ±1, ±2, ±3, ±4=0, ±0.02, ±0.05, ±0.09, ±0.13, respectively. (With permission from Ref. [1027])

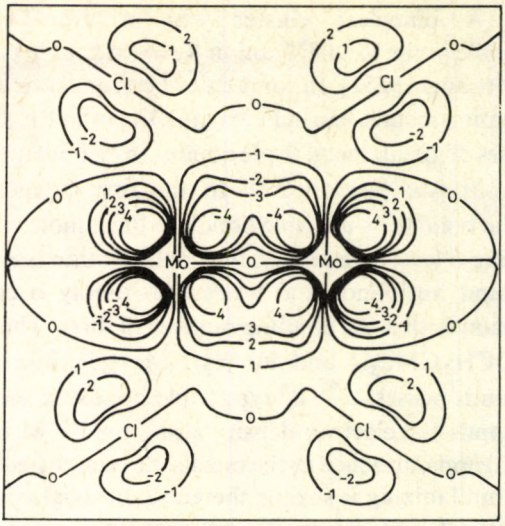


Fig. 2.21 Contour map of one of the two degenerate $5e_u$ orbitals for $Mo_2Cl_8^{4-}$. The contour values are 0, ± 1, ± 2, ± 3, $\pm 4 = 0$, ± 0.04, ± 0.07, ± 0.092, ± 0.135, respectively. (With permission from Ref. [1027])

number is four. However, *ab initio* MO calculations with configuration interaction indicate that antibonding configurations mix strongly [519, 520] therefore the net "bond orders" (overlap of Re AOs in the Generalized Valence Bond representation) are 0.65 (σ), 1.02 (π) and 0.11 (δ) totalling to 1.78. For comparison, the overlaps in the N_2 triple bond are 0.89 (σ) and 1.38 (π) which gives a total bond order of 2.3. These numbers indicate that in spite of its quadruple character the Re—Re bond is weak.

At present no LMO description of quadruple bonding is available, therefore we use canonical orbitals to characterize them. Norman and Kolari [1027] performed SCF—X_α scattered wave calculations for $Mo_2Cl_8^{4-}$ which is isoelectronic with $Re_2Cl_8^{2-}$. They identified four orbitals which are located mainly on the metal atoms. The $4a_{1g}$ orbital is of 83 per cent Mo character and it corresponds to the σ bond (Fig. 2.20) with a major d_z^2 contribution (the z-axis is defined by the line connecting the metal atoms). The π bonds are equivalent by symmetry; they are given by the degenerate $5e_u$ orbital (Fig. 2.21) with 76 per cent metal participation and with strong d_{xz} and d_{yz} character which is assigned to them. Finally the highest occupied molecular orbital is $2b_{2g}$ it is localized in 89 per cent to the molybdenum atoms (Fig. 2.22). This corresponds to a δ-bond between d_{xy} orbitals; it has two nodal planes. As may be seen from its contour map, it is rather diffuse, the graphic representation also illustrates that the overlap between AOs is small.

The highest formal bond order has been reported for the dimolybdenium molecule. The valence configuration is $9\sigma_g^2 5\pi_u^4 2\delta_g^4 10\sigma_g^2$ which corresponds to a sextuple bond. The experimental bond length is shorter than that of any known Mo—Mo bond.

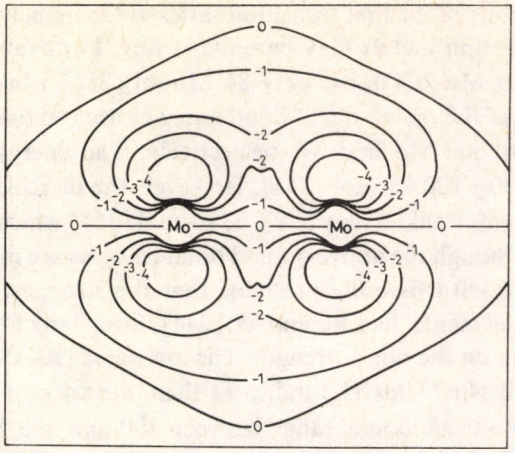


Fig. 2.22 Contour map of the $2b_{2g}$ orbital for $Mo_2Cl_8^{4-}$. The contour values are 0, ±1, ±2, ±3, ±4=0, ±0.01, ±0.0.4, ±0.75, ±0.14, respectively. (With permission from Ref. [1027])

Sophisticated configuration interaction calculations [168] predicted the following electronic structure

$$(9\sigma_g)^{1.88}(5\pi_u)^{3.78}(2\delta_g)^{3.42}(10\sigma_g)^{1.92}(9\sigma_u^*)^{0.08}(2\delta_u^*)^{0.58}(5\pi_g^*)^{0.22}(10\sigma_u^*)^{0.12}.$$

The sextuply bonded leading configuration gives 61 per cent of the total wave function which gave spectroscopic parameters in excellent agreement with experiment (see above). The $10\sigma_g$ orbital is mostly of 5*s* in character and it has an important role in making the Mo_2 bond length shorter than in any quadruple bonds. The formation of this second bond is restricted to the pure metal clusters since the addition of ligands will force the molecular orbital to higher energy resulting in a weaker bonding situation.

The non-heme iron-sulphur proteins (high potential iron protein and ferredoxin) are important electron carriers in many biological systems. Their active sites and synthetic analogues, $[Fe_4S_4(SR_4)]^{2-}$, (R = alkyl, aryl) have been studied by theoretical methods, too [439]. This cluster has a distorted cubic structure where weak Fe—Fe bonds may exist.

Let us summarize now some experimental properties characterizing metal–metal bonds. Bond lengths get shorter, the larger the formal bond order. Thus, the Mo—Mo distance in the metal is 272 pm [142] and it becomes 270 pm for the single, 217–224 pm for the triple, 207–215 pm for the quadruple and 193 pm for the sextuple bond [168, 251, 1259]. It is generally accepted that a bond between two metal atoms exists if their distances are of the same order as in the metal. Another criterion for bridged structures may be the MLM angle (L is the bridging ligand), see *e.g.* [1262]. However, at present the bond length is the most important tool to decide on the existence and multiplicity of a metal–metal bond.

Bonds between metals of the first transition series are extremely weak while bonds between heavier transition metals may be quite strong. For example, the Mn—Mn single bond energy in $Mn_2(CO)_{10}$ is only 84 kJ/mol [252] while in triply bonded $M_2(NR_2)_6$ type dimers the metal–metal bond energies are estimated to be 592 ± 196 and 775 ± 218 kJ/mol for Mo and W, respectively. The energy of the Mo—Mo quadruple bond is 640 ± 120 kJ/mol [244]. However, the dissociation energy of the sextuply bonded Mo_2 molecule is only 398 ± 63 kJ/mol [355] which is small compared to the above values. Though the above quoted bond energies are inferior to that of the N_2 molecule (940 kJ/mol) it is quite probable that the strongest bonds known are formed by heavier *d*-elements, like Re and W [244]. Stretching force constants yield also some information on the bond strength. The low value (50–150 Nm^{-1}) for single bonds [1259] (*cf.* 570 Nm^{-1} for H_2) indicates their weakness. Force constants for Mo—Mo and Re—Re triple bonds range between 300 and 450 Nm^{-1}, indicate the existence of a relatively weak bond, *cf.* 1900 Nm^{-1} for CO and 445 Nm^{-1} for the single CC bond. Since definition of bond dissociation energies is often uncertain [244] no strict parallelism between these and the corresponding stretching force constants can be found as in the case of lighter elements (see Section 3.3).

Metal–metal interactions may also be studied through magnetic susceptibility measurements. Due to the rich variability of the electronic structure of *d*-elements, open-shell, high or low spin configurations are often observed in di- or polynuclear complexes. For example, all four Cu atoms interact magnetically in the tetranuclear $[Cu_2OH(O_2CCF_3)_3$ (quinazoline)$_2]_2$ molecule and it seems that the metal–metal distance is not a major factor in determining the strength of the interaction [331].

Due to the easy polarization of the electronic cloud around metal–metal bonds and to the rich variety of possible stable configurations, interesting and unusual chemical reactions involving such bonds have been described [251, 252]. Since δ-bonds are easily excitable, photochemical reactions are also interesting. Metal–metal bonds play an important role in heterogeneous catalysis and in biology.

2.8 TRANSITION METAL COMPLEXES

Bi- and polycentric bond types, described in previous sections, have a common property: they are relatively strong. Formation of such bonds can be attributed mainly to electron delocalization between atoms (see Section 1.1). From now on, we shall discuss bonds which are essentially different from classical ones. Therefore not all concepts which proved to be useful for the treatment, of for example, σ- or π-bonds, can be used. Thus, it is very difficult to define classical structural formulas, and the meaning of valence is also unclear.

A very important class of nonclassical bonds is found in compounds of transition metals. In these metals atomic electron configurations include partly filled *d*-orbitals, too. Note that ions of nontransition metals with partly filled *d*-shells (Cu^{2+} : $3d^9$ or

Au^{3+} : $5d^8$) also form similar bond types. While for classical molecules containing only first- or second-row atoms, *d*-orbitals (*i.e.* their inclusion in the LCAO basis set) play a secondary role, description of transition-metal complexes is impossible without them. Since *d*-orbitals are easily polarizable, they readily participate in forming a wide variety of stronger and weaker bonds. These may be ordinary σ- or π-type bonds or lone pairs [749] like in OsO_4 [399] but in most cases new types of associations are formed. These are often called coordination complexes and the discipline discussing their properties and reactions is coordination chemistry which considerably overlaps with organometallic chemistry [1425]. The prototype of a transition-metal complex molecule consists of a central metal atom surrounded by a number of ligands which may be in themselves stable molecules, like CO, H_2O or cyclopentadiene (Cp). However, recently a great number of compounds were synthesized which contain more than one metal atoms.

We shall characterize bonds in transition–metal complexes through canonical MOs. (See Refs [169] and [1346] for some recent examples.) This is practical since LMOs are only rarely given in the literature and because of the relatively weak interaction

TABLE 2.5

Composition of the valence MOs of the MnO_4^- molecule (*ab initio* calculations with minimal basis set) [243]

MO	Energy		Composition (%)				
	MJ/mol	eV	4*s* (Mn)	4*p* (Mn)	3*d* (Mn)	2*s* (O)	2*p* (O)
$5t_2$	−1.153	−11.91	–	2.7	50.8	6.4	40.1
$1e$	−1.102	−11.38	–	–	44.0	–	56.0
$6f_2$	−0.704	−7.28	–	3.2	1.6	1.8	92.7
$6a_1$	−0.642	−6.63	0.7	–	–	3.7	95.2
$1t_1$	−0.556	−5.75	–	–	–	–	100.0

TABLE 2.6

AO populations in the MnO_4^- molecule (*ab initio* calculations with minimum basis set) [243]

MO	Mn_4^--ion configuration	MnO_4-orbital population	MO	O-atom configuration	MnO_4^--orbital population
1*s*	2	2.0000	1*s*	2	1.9982
2*s*	2	2.0000	2*s*	2	1.9096
3*s*	2	1.9999	2*p*	4	4.5734
4*s*	2	0.1471			
2*p*	6	5.9983			
3*p*	6	5.9666			
4*p*	0	0.5152			
3*d*	6	5.4479			

between atoms canonical MOs may be constructed from those of fragments. Bonds are characterized by the interaction of these fragments. We shall outline theoretical concepts which are used to classify bonding types for the extremely rich variety of transition-metal complexes. These concepts will be exemplified by some prototype molecules which are, by no means, the most important representatives of their class, rather they serve as good models for the calculations. To compare classical and nonclassical bonds in transition-metal compounds we discuss two examples, thoroughly investigated by *ab initio* calculations.

Let us first consider the tetrahedral permanganate ion (MnO_4^-) where only classical bonds exist even though Mn is a transition metal [243]. The constitution of canonical valence MOs is given in Table 2.5. It is seen that MOs of lower energy ($5t_2$ and $1e$) correspond to $(d–p)\pi$ bonds between Mn and O. The $6t_2$, $6a_1$ and $1t_1$ orbitals are of lone-pair character they are localized almost exclusively on the oxygen atoms. Population of AOs is given in Table 2.6. Core orbitals of manganese (1*s*, 2*s*, 2*p*, 3*s* and 3*p*) and oxygen 1*s* and 2*s* AOs are practically completely filled, they correspond to the configuration of the free atom. Occupancy of 4*s*- and 3*d*-orbitals on manganese decreases upon bonding while electrons appear on the 4*p* AO which is empty in the free atom. Bonding is due to the overlap between Mn 3*d*- and O 2*p*-orbitals. This is also seen from the high value of the corresponding overlap population (0.477). Overlap between other orbitals is much smaller. The net charge on Mn is $+0.93$ while it is -0.48 on each oxygen atom. This is due to the considerable charge transfer from the 4*s* AO of Mn to the oxygens. The strong polarization of bonds indicates that classical electrostatic effects are also important in bonding.

Chemical bonds in the permanganate ion do not differ essentially from classical ones. It is only the *d*-orbital participation which is much more important than in an organic molecule. Specific properties of a coordination bond will be exemplified on $Mn(CO)_5H$ for which *ab initio* calculations were performed [488]. This molecule is depicted in Fig. 2.23. The ligands form a distorted octahedron around the central manganese atom. The space group is C_{4v}. Composition of MOs and AO populations are given in Tables 2.7 and 2.8. It is seen that a simple covalent MnH σ-bond is formed ($17a_1$ AO) where *d*-orbital participation is important. Other MOs are strongly localized either on the metal atom or on the carbonyl ligands. A weak ($d\pi–p\pi$) bond is formed ($11e$ and $2b_2$

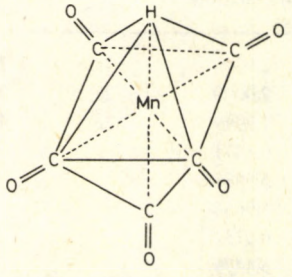


Fig. 2.23 Schematic structure of $Mn(CO)_5H$

TABLE 2.7

Composition of the valence MOs of the $Mn(CO)_5H$ molecule (*ab initio* calculations with minimal basis set) [488]. Orbital energies increase downwards. Core orbital participation is omitted

Orbital	Composition (%)							
	4*s* (Mn)	4*p* (Mn)	3*d* (Mn)	2*s* (C)	2*p* (C)	2*s* (O)	2*p* (O)	1*s* (H)
$14a_1$	2	–	–	4	29	13	52	–
$7e$	–	–	2	2	36	1	59	–
$1b_2$	–	–	4	–	36	–	60	–
$15a_1$	–	−3	1	4	34	1	62	1
$8e$	–	−1	1	2	32	1	65	–
$5b_1$	–	–	–	–	28	–	72	–
$9e$	–	–	–	–	27	–	73	–
$1a_2$	–	–	–	–	26	–	74	–
$16a_1$	–	2	11	28	29	2	28	–
$6b_1$	–	–	16	32	31	2	19	–
$10e$	–	6	–	29	30	1	33	–
$2b_2$	–	–	79	–	4	–	16	–
$11e$	–	–	82	–	4	–	13	–
$17a_1$	8	18	17	1	3	–	6	47

TABLE 2.8

AO populations in the $Mn(CO)_5H$ molecules (*ab initio* calculations with minimum basis set) [488]. MO symmetry and spatial arrangement are given in parentheses

Orbital	Population	Orbital	Population	
			$Mn(CO)_5H$	CO
4*s* (Mn)	0.019	2*s* (C, ax)	1.529	1.631
4*p* (Mn, a_1)	0.282	2*p* (C, σ, ax)	0.969	0.942
4*p* (Mn, *e*)	−0.084	2*p* (C, π, ax)	1.323	1.058
3*d* (Mn, a_1)	0.618	2*s* (C, eq)	1.528	
3*d* (Mn, b_1)	0.395	2*p* (C, σ, eq)	0.978	
3*d* (Mn, b_2)	1.674	2*p* (C, π, eq)	1.290	
3*d* (Mn, *e*)	3.415	2*s* (C, ax)	1.829	1.839
3*d* (Mn, total)	6.029	2*p* (O, σ, ax)	1.547	1.592
1*s* (H)	0.982	2*p* (O, π, ax)	2.971	2.942
		2*s* (O, eq)	1.830	
		2*p* (O, σ, eq)	1.549	
		2*p* (O, π, eq)	2.970	

MOs) while the $6b_1$ and $16a_1$ MOs correspond to an MnC σ-bond. AO populations (Table 2.8) indicate that the configuration of Mn in this molecule is $3d^6$. The nonzero p-population (Mn $4p$, a_1) corresponds almost exclusively to the $17a_1$ MnH bond.

The $Mn(CO)_5H$ molecule offers a good example of *π-back-bonding*. Owing to the weak σ-bonding between Mn and C a charge transfer from the ligands to the metal occurs. $2s$- and $2p$-populations of the C and O atoms slightly decrease compared to the free carbon monoxide. This decrease is overcompensated by a charge transfer from N to the carbonyls which is due to the π-bond. Population of the $2p\pi$ AOs on the carbon atoms considerably increases with respect to the unperturbed CO molecule. The gross charge transfer from the metal to the ligands is almost as large as a unit charge therefore back bonding is of decisive importance. $2p\pi$ population of axial and equatorial carbon atoms is different, the former being larger. Accordingly, the $3d$(Mn)–$2p$(C, π, ax) overlap is 0.156, larger than for the equatorial case (0.118). This may account for the physical and chemical differences in axial and equatorial bonds between metal and ligands.

Another example of back donation is Zeise's anion, $PtCl_3Et^-$, for which very accurate SCF-X_α scattered wave calculations were performed [1199]. Figure 2.24 illustrates the donation of electron density from the ethylene π-bonding MO to the platinum d_{z^2} orbital, while back donation is seen on Fig. 2.25. A characteristic feature of

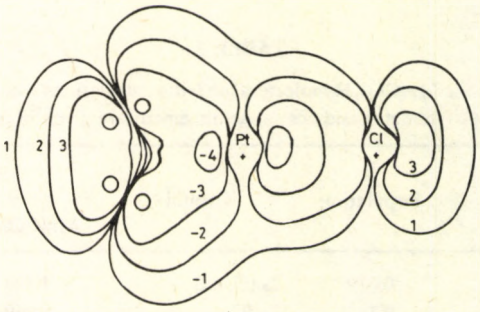


Fig. 2.24 Donation of electrons from the ethylene π-orbital to the metal in Zeise's anion, $PtCl_3Et^-$. Contour map of the $5a_1$ orbital. The contour values increase in absolute magnitude with increasing absolute values of the contour labels. (With permission from Ref. [1199])

these orbital plots is that the ethylene molecule is retained as a subunit within the complex. This is due to the weakness of bonding: delocalization between metal and ligands is small. It is this small delocalization which allows to use simple perturbation approaches in discussing transition-metal complexes (see Section 1.3.3). Some typical applications will be presented later in this section.

As we have mentioned in Section 2.1, an interpretative energy partitioning for weak bonds is possible using perturbation theory. Now we discuss Morokuma's decomposition scheme [935]. Since the mixed term, E_{mix}, of Eq. (2.4) is large for transition-

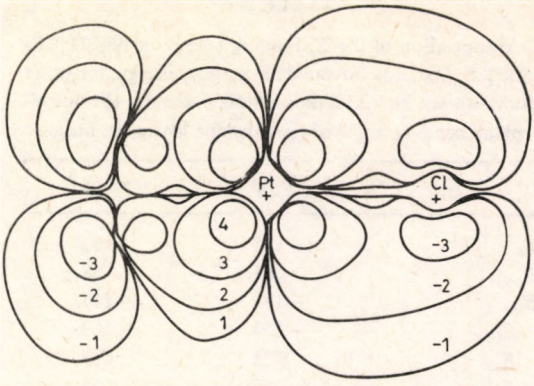


Fig. 2.25 Back-donation of electrons from the metal to the ethylene π-orbital in Zeise's anion, $PtCl_3Et^-$. Contour map of the $2b_2$ orbital. The contour values increase in absolute magnitude with increasing absolute values of the contour labels. (With permission from Ref. [1199])

metal complexes a modified energy decomposition scheme was suggested

$$E_{int} = E_{Coul} + E_{ex} + E_{fctpol} + E_{bctpol} + E_r \tag{2.12}$$

where E_{Coul} and E_{ex} has the same meaning as in Eq. (2.4). E_{fctpol} and E_{bctpol} are mixed charge-transfer and polarization terms, *f* (forward) stands for the "donative interaction" while *b* for the "back-donative interaction". This decomposition allows to estimate the relative importance of the two bonding components quantitatively. This is possible only qualitatively in other models [916, 1199]. Furthermore, it became clear also that the word "donation" does not necessarily correspond to charge transfer. Rather, it means an overall reorganization of electrons including both charge transfer and polarization. The electron cloud of transition metals is easily polarizable, this in turn, facilitates charge transfer. This interplay would be the origin of the large E_{mix} in Eq. (2.4).

Numerical values for $Ni(PH_3)_2Et$ are given in Table 2.9 (Et stands for ethylene). The calculated binding energy agrees well with the experimental value, 138 kJ/mol. It is seen that the back-donative interaction from the metal to the ligand (E_{bctpol}) is about 3 times as large as the donation from the ligand to the metal. Furthermore, the pyramidalized ethylene binds more strongly than the planar one. The pyramidalization mixes *p* and *s*-orbitals and pushes the electron density toward the nickel atom which results in a large electrostatic stabilization and exchange repulsion. The increase of the back-donation component is caused by the lowering of the energy of the antibonding orbital of Et upon bending. It is noticeable that the energy change upon deformation is surprisingly correctly predicted using the Coulombic term alone.

To introduce some order into the rich variety of metal–metal and metal–ligand bonding types a unifying concept is needed. It seems that this is found in the *isolobal analogy* proposed by Hoffmann [577] and others [916, 1312, 1392]. The principal idea of this concept is that most properties of transition-metal complexes are determined

TABLE 2.9

Decomposition of the E_b binding energy in $Ni(PH_3)_2Et$ [935]. E_{def} stands for the deformation energy, for other notations see Eq. (2.12) (in kJ/mol). ϑ denotes the out-of-plane bending angle of the ethylene hydrogen atoms

Term	$\vartheta = 26°$	$\vartheta = 0°$
E_b	−126	−80
E_{def}	63	38
E_{int}	−188	−117
E_{Coul}	−553	−502
E_{ex}	703	657
E_{fctpol}	−67	−54
E_{bctpol}	−226	−184
E_r	−46	−84

primarily by the highest occupied and lowest unoccupied molecular orbitals (frontier orbitals, see Section 1.3.3). By inspection, close resemblance between frontier orbitals of apparently different fragments like $Mn(CO)_5$, MnH_5^{5-}, d^7-ML_5 in general and CH_3 can be discovered (*cf.* Fig. 2.26). H^- serves here as a model ligand for CO. In the isolobal analogy, $Mn(CO)_5$ and CH_3 behave similarly. In fact, both molecules readily dimerize and each has a radical-type chemistry. Organic and inorganic fragments can be combined to give $Mn(CO)_5CH_3$ which is a stable compound. The isolobal analogy

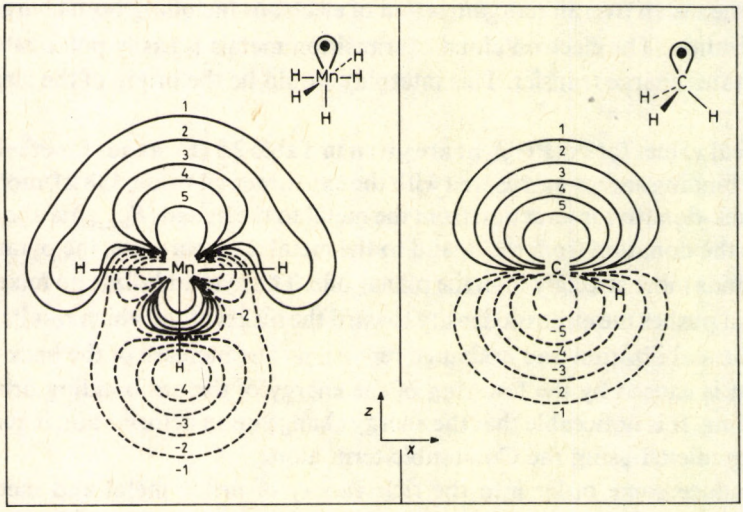


Fig. 2.26 Contour map of the isolobal a_1 orbitals of MnH_5^{5-} (left) and CH_3 (right). The contour values are ± 1, ± 2, ± 3, ± 4, $\pm 5 = \pm 0.01$, ± 0.025, ± 0.055, ± 0.1, ± 0.2, respectively. (With permission from Ref. [577])

offers a link between well understood classical organic chemistry and modern, yet somewhat obscure, transition-metal chemistry.

It should to be noticed that the two fragments, CH_3 and d^7-ML_5 are certainly not isostructural, nor are they isoelectronic. Two fragments are called *isolobal* if the number, symmetry properties, approximate energy and shape of their frontier orbitals and the number of electrons in them are similar (not necessarily identical). This definition can be extended as follows.

— If $Mn(CO)_5$ is isolobal with CH_3, so are $Tc(CO)_5$ and $Re(CO)_5$ as well as $Fe(CO)_5^+$ (*cf.* Table 2.10).

— If $Mn(CO)_5$ is isolobal with CH_3 then $Cr(CO)_5$, $Mo(CO)_5$ or $W(CO)_5$ are isolobal with CH_3^+ and $Fe(CO)_5$ with CH_3^-.

— If $Mn(CO)_5$ is isolobal with CH_3 so are any d^7-ML_5 species. Cyclopentadienyl anion (Cp^-) may be replaced by the isolobal equivalent of three carbonyls.

— The d^8-ML_4 and d^9-ML_3 species are isolobal with CH_2 and CH, respectively. Further isolobal analogies are given in Table 2.10.

TABLE 2.10

Isolobal analogies. L denotes a neutral two-electron ligand, *d*-electron configurations are indicated in superscripts

Organic fragment	Transition-metal coordination number				
	9	8	7	6	5
CH_3	d^1-ML_8	d^3-ML_7	d^5-ML_6	d^7-ML_5	d^9-ML_4
CH_2	d^2-ML_7	d^4-ML_6	d^6-ML_5	d^8-ML_4	d^{10}-ML_3
CH	d^3-ML_6	d^5-ML_5	d^7-ML_4	d^9-ML_3	— —

The beautiful isolobal analogy can be used effectively to find a relation between a number of very differently looking structures. For example, the d^8-ML_4 fragment, $Fe(CO)_4$ is isolobal with CH_2 and so $Fe_2(CO)_8$ is isolobal with ethylene, $(CO)_4FeCH_2$ and $(CO)_4MnPR_2$, respectively. The last analogy is obtained if we shift an electron formally from the metal to the carbon changing Fe to Mn and C to P and we notice that the hydrogen can be replaced by substituents. Realizing that $Fe(CO)_4$ is analogous to $FeCOCp^-$ and this to RhCOCp it is immediately seen that $Rh_2(CO)_2Cp_2$ is analogous to $Fe_2(CO)_8$. Some really fantastic further examples are found in Hoffmann's Nobel lecture [577].

Further interesting types of transition-metal complexes are the *sandwich compounds* (*e.g.* ferrocene, $FeCp_2$) [496, 917]. In these molecules two aromatic rings (cyclobutadienyl dianion, Cp, benzene, *etc.*) are bound to the central metal atom as ligands. Bonding is due to the overlap of metal valence orbitals with π-type MOs of the

aromatic ligands. If it is understood that carbocyclic ligands are analogous to a group of "ordinary" ligands, like Cp^- to $(CO)_3$ sandwich compounds can be discussed on the same basis as other transition-metal complexes. The analogy with bent sandwich compounds, like $TiCp_2(CO)_2$ and half sandwich compounds, like $MnCp(CO)_3$ or $Fe(\eta\text{-}C_4H_4)(CO)_3$, is obvious [577, 916]. An interesting sandwich compound is $U(\eta\text{-}C_8H_8)_2$ where besides metal *d*-orbitals *f*-orbitals also play a considerable role in binding [1200].

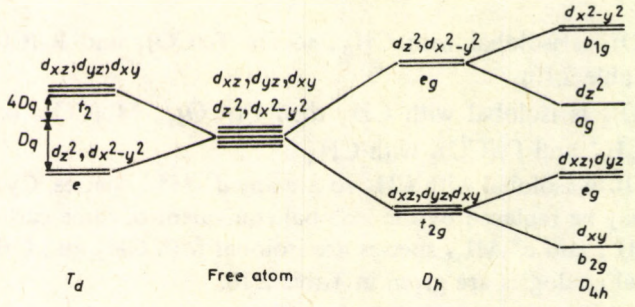


Fig. 2.27 Splitting of free atom energy levels in a field of negative charges. Left: T_d symmetry, right: O_h and D_{4h} symmetry

Owing to the weak bonding in transition-metal complexes the perturbational *ligand-field theory* (*cf.* Section 1.3.3) is well applicable. This postulates that the overlap between the central metal atom and ligands is small [436, 650, 1292]. This theory is a very useful tool in explaining and classifying experimental facts which seem completely unrelated at a first glance. An even simpler approach is *crystal-field theory* considering exclusively symmetry and electrostatic properties of transition-metal complexes [344]. We shall discuss it in a little more detail.

If the metal atom is placed into an electrostatic field of point charges, the degeneracy of *d*-orbitals is lowered. Splitting of energy levels depends on sign and symmetry of perturbing charges. Figure 2.27 shows this splitting for some symmetry point groups. If the symmetry of the external field is spherical, the degeneracy is conserved only the energy is shifted to higher or lower values if the charge is negative or positive, respectively. For a tetrahedral arrangement of ligands, the t_2 level raises by four, the e level lowers by six units, respectively, as compared to the unperturbed atom. Total splitting is just 10 units, this is conventionally called $10D_q$. An octahedral arrangement leads to the opposite splitting while for lower symmetries the degeneracy gradually disappears. The above rules can be derived on the basis of group theory, they can be rationalized using simple electrostatics. Energy levels will be filled by electrons consecutively. The resulting configuration may be used for characterizing and rationalizing electronic spectra and magnetic properties of transition-metal complexes.

Physical and chemical properties of transition-metal complexes are determined by their specific electronic structure. Since the link between metal atom and ligands is

weak the coordination number may vary. In most cases its value lies between 1 and 8. Therefore complex molecules may have a variety of different shapes.

Owing to the relatively small splitting of *d*-electron energy levels, transition-metal complexes are easily excitable. Since they absorb long-wave light they are mostly coloured. Ionization is easy, therefore in contrast to classical organic molecules, several ionized forms of the same complex may be stable. In several states, electron spins are unpaired; therefore paramagnetic states of higher multiplicity are common. A specific phenomenon may be observed: depending on the quality of ligands, the magnetic properties of molecules with the same symmetry and number of ligands may considerably change. The energy gain coming from a *weak ligand field* does not cover the energy loss due to spin pairing. According to Hund's rule the molecule will tend to reach a state of maximal multiplicity *(high spin)*. It will be strongly paramagnetic, *e.g.* FeF_6^{3-} with a configuration of $t_{2g}^3 e_g^2$ with all electrons having the same spin. If the ligand field is strong the pairing energy is relatively small, therefore multiplicity will be minimal. Such *low-spin* complexes are diamagnetic or weakly paramagnetic like $Fe(CN)_6^{3-}$ which has the same symmetry and number of *d*-electrons as FeF_6^{3-} though its configuration is t_{2g}^5. Magnetic properties can be judged by comparing $10Dq$ and the electron-pairing energy. The qualitative trend of $10Dq$ for various ligands is given by the *spectrochemical series* [1045]:

$$I^- < Br^- < SCN^- < Cl^- < OH^- < F^- < C_2O_4^{2-} < H_2O < N_3^- < NH_3$$

$$< NO_2 \ll CN^- \approx CO\,.$$

Ligands at the left side of the series, like I^- or Br^-, produce weak fields and, consequently, they form high-spin complexes. On the other hand, cyano complexes are, in general, of low spin. The spectrochemical chemical series is of course not absolutely valid it has to be changed for some cases. So the relative strengths of OH^- and F^- are reversed for N^{2+} complexes [1045]. It is important to know that for weak-field ligands the crystal-field theory works well while for strong fields a more sophisticated method (*e.g.* ligand-field theory) must be used.

Ligands bind loosely to the metal. It is this feature which makes transition-metal complexes especially important in catalysis. The binding energy depends primarily on the electronic configuration. Octahedral complexes with one, two or three electrons are relatively stable since in these all electrons are on lower energy levels than in the free metal. Further electrons can be put on antibonding e_g orbitals; therefore the stability decreases, and it becomes approximately zero for the five-electron case. Adding further electrons the same trend can be observed, the electronic configuration changes similarly to the above. This simple model gives an explanation for the experimental finding that from Sc to Ti and V the lattice energy of the pure metal increases (t_{2g}^1, t_{2g}^2 and t_{2g}^3 configurations) while it decreases for Cr and Mn ($t_{2g}^3 e_g^1$ and $t_{2g}^3 e_g^2$ configurations). The trend is the same for Fe, Co and Ni as for Sc, Ti and V.

2.9 THE HYDROGEN BOND

Electron-rich atoms or groups (called X), like atoms with lone pairs (N, O, F, P, S, Cl, etc.) and multiple bonds (>C=C<, —C≡C—, aromatic rings, etc.) readily associate with polar H—Y bonds where the hydrogen is electron-deficient, i.e. Y is the more electronegative. The X . . . HY link is called a *hydrogen bond* and it has great importance in chemistry and biology. For reviews see [572, 643, 724, 1245, 1246]. The atom or group X is called the *proton acceptor* while atom Y is the *proton donor.*

Several experimental and theoretical studies indicate that within hydrogen-bonded supermolecules constituent molecules preserve their properties to a high extent. This may be interpreted in terms of the small delocalization of monomer LMOs in the dimer (see Table 2.11 [970] and compare with Table 2.3). Therefore, electron delocalization may not be specified as an important factor for hydrogen bonding.

The origin of hydrogen bonding is best understood by splitting up the interaction energy into terms which have physical meaning, as in Eq. (2.4) [1376]. Some numerical values are given in Table 2.12. It is seen that in the equilibrium nuclear configuration, the total interaction energy is well approximated by the Coulombic term alone. This is true for nonequilibrium geometries too [1376]. The exchange term is a relatively large positive value but it is approximately cancelled by polarization, charge transfer and mixed terms. Dispersion, due to electron correlation, is of minor importance, it is only -6.3 kJ/mol for the $(H_2O)_2$ dimer while the total SCF binding energy is -32.6 kJ/mol [1245]. Therefore hydrogen bonds are strongly electrostatic in nature with a small contribution of charge transfer.

The Coulombic attraction arises from the mutual polarization of the interacting molecules. This is also observed experimentally in accord with theoretical calculations [552, 553]. As may be seen in Fig. 2.28 the electronic density in $(Li^+)_2(H_2O)_2OH^-$ gets considerably larger at the water oxygen atom while it decreases at the bridge hydrogen and hydroxyl oxygen atoms if compared to the free molecules. This phenomenon is correctly accounted for by CNDO/2 calculations of charge shifts [970]. For the $HO^- \ldots HOH$ dimer $\Delta q_{O(HOH)}$, Δq_H and $\Delta q_{O(HO-)}$ are -146, 108 and 72 millielectrons, respectively; though in this special case the loss of charge on the hydroxyl oxygen is partly due to the polarizing effect of the Li^+ ions polarization of the H—Y bond is observed for other hydrogen bonded complexes too.

From Table 2.11 a relation between charge transfer, Δq, and delocalization of the lone-pair LMO, Δl_X can be derived

$$\Delta q = 20.7 \Delta l_X + 8; \quad r^2 = 0.986 . \tag{2.13}$$

Gordon and coworkers did CNDO/2 calculations on several hydrogen-bonded complexes and they found a linear relationship between charge transfer and interaction energy [465]. This is confirmed in the case of the $(FH \ldots NH_3) . 6H_2O$ system for different positions of the bridge proton [27].

TABLE 2.11

Delocalization effects in some simple hydrogen-bonded dimers (CNDO/2 calculations with the Edmiston–Ruedenberg localization procedure). For lone-pair localizabilities, l_X the delocalization to the donor hydrogen atom is given in parentheses [970]

Bond X...H—Y	Acceptor	Donor	$l_X(\Delta l_X)$ %	H—Y bond	Delocalization to the acceptor	Charge transfer[a] millielectrons			
				$1s_H$		Δq_X	Δq_H	Δq_Y	Δq
N...H—N	NH_3	NH_3	99.9 (0.0)	0.673	0.2	−44	19	−47	1
N...H—O	NH_3	H_2O	98.9 (0.7)	0.641	0.4	−45	23	−24	20
N...H—F	NH_3	HF	98.7 (1.2)	0.602	0.2	−12	18	−54	36
O...H—O	H_2O	H_2O	99.2 (0.5)	0.642	0.1	−8	23	−32	15
	OH^-	H_2O	94.2 (4.5)	0.571	0.1	72	108	−146	122
	H_2O	CH_3OH	97.6 (1.7)	0.622	0.4	19	51	−59	45
O...H—S	H_2O	H_2S	100.0 (0.0)	0.689	0.1	−105	45	−83	0
S...H—S	H_2S	H_2S	100.0 (0.0)	0.691	0.1	−78	38	−78	0
F...H—F	HF	HF	98.9 (0.7)	0.604	0.3	−5	25	−46	21
	F^-	HF	81.7 (17.4)	0.417	0.9	348	77	426	348
	HF	HFH^+	90.2 (9.4)	0.368	0.6	31	5	176	231

[a] $\Delta q_X = q_X$ (associate)—q_X (isolated molecule), $\Delta q = \Sigma_i \Delta q_i$

TABLE 2.12

Energy partitioning in some hydrogen bonded complexes (in kJ/mol) at equilibrium geometries. See Eq. (2.4) for notations [1376]

Acceptor	Donor	E_{Coul}	E_{pol}	E_{ex}	E_{ct}	E_{mix}	E^{a}_{SCF}
HF	HF	−34.3	−1.7	18.8	−13.4	−1.3	−31.9
H_2O	HF	−79.1	−6.7	44.0	−13.0	−1.7	−56.5
	H_2O	−44.0	−2.5	26.0	−10.0	−2.1	−32.6
	H_3N	−19.3	−1.3	10.5	−6.3	−0.8	−17.2
	H_4C	−2.1	−0.4	2.1	−3.8	0.0	−4.2
H_3N	HF	−107.2	−8.4	67.0	−17.2	−2.9	−68.7
	H_2O	−58.6	−4.6	37.7	−10.0	−1.7	−37.2
	H_3N	−23.9	−2.5	15.1	−5.4	−0.8	−17.5
	H_4C	−2.5	−1.3	2.1	−2.9	0.0	−4.6

[a] $E_{SCF} = E_{int} - E_{disp}$

Transferability of hydrogen-bond properties (energy, length, etc.) is rarely found. Energies of ordinary hydrogen bonds range form 4 to 70 kJ/mol (*cf.* Table 2.12) and even the O...H—O bond energy varies between 14 and 32 kJ/mol [287, 288]. Even for the $H_2OO...HOH$ and $H_2O...HOOH$ complexes a considerable difference in the interaction energies is observed: it is 14.3 kJ/mol for the former and 31.9 kJ/mol for the latter [288]. The only property for which transferability is fulfilled, is the X...H—Y bond angle. This is approximately 180° for most complexes, though it is only 162° for the $(H_2O_2)_2$ dimer [288].

Though transferability of bond properties may not serve as a unifying concept in discussing the hydrogen bond in several molecular aggregates, simple and pictorial

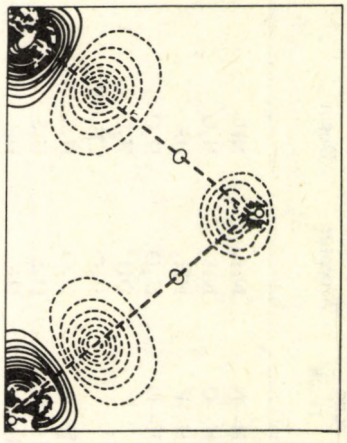


Fig. 2.28 Electronic difference density map along the hydrogen bonds in $(Li^+)_2(H_2O)_2OH^-$. Full and dashed lines denote excess and lack of charge, respectively. (With permission from Ref. [553])

models are at hand [10, 723, 727]. Allen has developed a simple model on the basis of *ab initio* calculations on pure and mixed dimers of NH_3, H_2O, HF, H_2S and HCl [10]. Based on the fact that hydrogen-bond energies are small and electronic structure of the subsystem is only slightly affected by complex formation the following approximate formula for the interaction energy was suggested

$$E_{int} = K\mu_{H-Y}\Delta I_X R_{XY}^{-1} . \tag{2.14}$$

Here K is an energy scale factor, μ_{H-Y} is the H—Y bond dipole moment, ΔI_X is the difference between the first ionization potentials of proton acceptor atom X and the noble gas atom in the same row (Ne for N, O and F; Ar for P, S and Cl). R_{XY} is the distance between atoms X and Y. Equation (2.15) gives quite a fair approximation of experimental and theoretical dimerization energies, the error for M_2 systems ($M = H_2O$, H_3N, HCl and H_2S) being smaller than 3 kJ/mol. Using the above quantities Allen was able to systematize other physical properties characterizing the hydrogen bond. These will be discussed later in this section.

Allen's formula reflects the essentially electrostatic nature of the hydrogen bond and the influence of the charge transfer represented by ΔI_X. Electrostatics was also exploited in another formula, given by Kollman [723]

$$E_{int} = C \cdot V_X \cdot V_Y \tag{2.15}$$

where V_X and V_Y are electrostatic potentials in certain points in the vicinity of atoms X and Y, C is a proportionality constant. Both Eqs (2.14) and (2.15) allow us to estimate hydrogen-bond energy from properties of the individual molecules.

Hydrogen-bonded molecules get closer to each other than would be expected on the basis of van der Waals radii. The reduction of the interatomic distance is one of the most important factors indicating the existence of a bond. The hydrogen-bond length, $R_{H\ldots X}$, is inversely proportional to μ_{H-Y}, *cf.* Eq. (2.14), and nearly independent of X for a series of related proton donors (*e.g.* H_3N, H_2O and HF) [10]. From this it follows that the interatomic distance, $R_{X\ldots Y}$, gets smaller the larger the bond energy, E_{int}. This rule

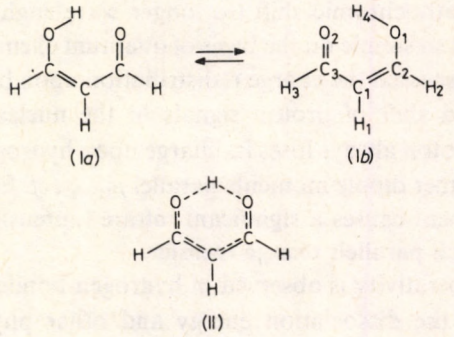


Fig. 2.29 Asymmetric (I) and symmetric (II) forms of malondialdehyde

has several quantitative forms, too [643]. Owing to the X...Y interaction, H—Y bonds get somewhat longer though this effect is small [1055].

Not only different molecules but different groups of the same molecule can form a hydrogen bond. An example is the enol form of malondialdehyde (Fig. 2.29) [673, 675]. There was some controversy in the literature as to whether this compound exists in an asymmetric or symmetric form [629]. *Ab initio* SCF calculations with careful geometry optimization [675] showed that the molecule is asymmetric and the proton moves in a double-well potential field. Inclusion of electron correlation gave the same result only the barrier height of the potential changed slightly [673]. For malondialdehyde the enol form is stabilized by aromatization which is indicated by the relatively high value of the aromaticity index defined in Refs 974 and 982, this is 10.5% and 2.5% for the symmetric and asymmetric forms, respectively [970] (CNDO/2 calculations). This value indicates that the hydrogen-bonded, cyclic enol form of malondialdenyde is about as aromatic as pyrrole. The stabilization of hydrogen-bonded cyclic systems is, however, not the consequence of aromatization alone; it is also observed for σ-bonded rings [1144]. As a consequence, conformational properties of a molecule are strongly influenced by intramolecular hydrogen bonds.

Group frequency of H—Y stretching vibrations is also affected by hydrogen bonding as a consequence of the slight delocalization of the electrons of the H—Y bond to the acceptor atom (*cf.* Table 2.11). Delocalization leads to bond weakening and lowering of the stretching force constant. This is why a red shift of H—Y bonds in the infrared spectrum is observed if a hydrogen bond is formed. Relative to the proton–donor monomer, the H—Y stretching frequency is inversely proportional to μ_{H-Y} for a given atom X and to ΔI_X for a given H—Y bond [10]. Further empirical relationships are summarized in Ref. 643.

Electronic excitation processes are also dependent on hydrogen-bond formation. It is a well-known experimental fact that in protic solvents (*e.g.* dimethylformamide, water) the energy of $n \rightarrow \pi^*$ electronic transitions increases, leading to a hypsochromic shift (to shorter wavelengths) of the absorption band [1302]. This phenomenon was explained by *ab initio* calculations [289, 291]. The $n \rightarrow \pi^*$ excitation breaks the hydrogen bond; the energy shift is practically equal to the bond-breaking energy. Explanation of the bathochromic shift (to longer wavelenghts) of $\pi \rightarrow \pi^*$ transition bands is, however, not so simple on the basis of quantum chemical calculations [934].

We have already discussed the charge redistribution upon hydrogen bonding. This results in a downfield shift of proton signals in the nuclear magnetic resonance spectrum, since the proton always loses its charge upon hydrogen-bond formation. In Allen's model [10], dimer dipole moments parallel μ_{H-Y}, *cf.* Eq. (2.15). The change in the bond dipole moment causes a significant infrared intensity enhancement for all hydrogen bonds, which parallels charge transfer.

An interesting cooperativity is observed in hydrogen-bonded chains. This leads to the nonadditivity of the dissociation energy and other physical properties. In a O—H...O—H...O chain of hydrogen bonds in water trimer, the contraction of the

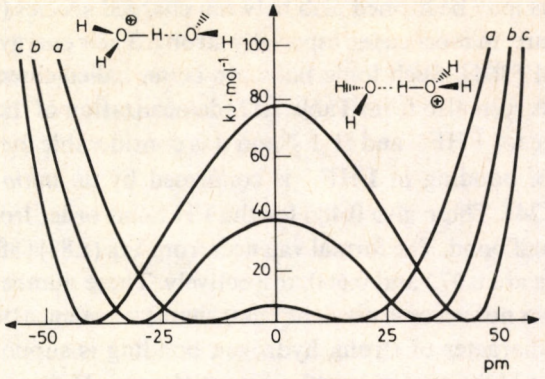


Fig. 2.30 Relative energy change as the function of the bridge proton position in $H_5O_2^+$. *(a)* $R_{O...O}=250$ pm, *(b)* $R_{O...O}=270$ pm, *(c)* $R_{O...O}=290$ pm

O...O distance is 100 pm while the trimer stabilization energy increases by 11.3 kJ/mol relative to two isolated water dimers [297]. This effect is attributed to the polarization of electron density which accompanies dimer formation [1246]. The cooperativity is especially important in α-helical structures of polypeptide chains where, for example, electrostatic potentials at the ends of the helix are considerably larger than it is expected on the basis of additive models [338].

A characteristic phenomenon in hydrogen-bonded systems is proton migration. Figure 2.30 depicts the relative energy of the $H_5O_2^+$ molecule as a function of the bridge proton position [638]. The proton is stabilized in the potential wells in the neighbourhood of both oxygen atoms. The potential wells are separated by relatively low barriers, the height of which depend on the O · · · O distance. If this distance is small (*e.g.* $R_{O...O}=250$ pm) the barrier height is smaller than the zero-point energy, the proton movement is almost unhindered. Proton transfer is strongly influenced by the tunnel effect (see Ref. [514] for an overview). Due to this, the proton may be transferred even if its energy is lower than the barrier height. The probability of proton transmission depends on the height and width of the barrier.

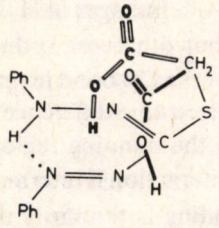


Fig. 2.31 Schematic structure of 3-carboxymethylthio-1,5-diphenylformazan. Empty and solid lines represent symmetric and asymmetric arrangements, respectively

Hydrogen bonds may be formed also between charged species (like in $H_5O_2^+$ or in FHF^-) and these are, in most cases, especially strong. Their energy may vary between 50 and 100 kJ/mol [364]. Such ionic links are better called three-centre bonds (see Section 2.5). This is seen also from Table 2.11: delocalization of the lone pair and HY LMOs is very large for FHF^- and $H_3F_2^+$ and it is considerable for $H_3O_2^-$. The three-centre character of bonding in FHF^- is confirmed by *ab initio* minimal basis set calculations, too [24]. These give 0.486 for the FH bond order from Eq. (1.82) which corresponds to a half bond. The formal valences from Eq. (1.83) [884] of the hydrogen and fluorine atoms are 0.972 and 0.660, respectively. These numbers indicate that the hydrogen atom does not become divalent but it shares its valence between both bonds. The three-centre character of strong hydrogen bonding is supported by the single-minimum character of the proton transfer potential curve. However, the simple model of hydrogen bonding by Allen may be extended to strong hydrogen bonds if some modifications are introduced [10].

If the proton acceptor group, X, is a π-bonded structure, like ethylene or an aromatic ring, the hydrogen bond is weaker than in other cases [290]. However, it may be stable enough to form even intramolecular bonds, like in 3-carboxymethylthio-1,5-diphenylformazan (see Fig. 2.31). The intramolecular bond formation is inferred on the basis of experimental evidence [613]; the model may be refined using theoretical calculations [974].

2.10 ELECTRON DONOR–ACCEPTOR COMPLEXES

There are some molecular associations where interaction can be formally attributed to charge transfer between a donor and an acceptor molecule. Donation occurs from an occupied (n = lone pair, σ- or π-type) to a vacant (v) or antibonding (σ^* or π^*) orbitals. Complexes of the $n \rightarrow v$ type are the strongest (*e.g.* $H_3N—BH_3$) while those of the $\pi \rightarrow \pi^*$ or $\sigma \rightarrow \pi^*$ type are the weakest (*e.g.* ethylene–formaldehyde or benzene–fluorine). These associations are called electron donor–acceptor or charge–transfer complexes.

Table 2.13 gives the interaction energy decomposition of Eq. (2.4) for some prototype donor–acceptor complexes [935]. It is seen that borane adducts, like all $n \rightarrow v$ or $\sigma \rightarrow v$ complexes, are very strongly bound and various energy terms have about the same weight. Therefore the N—B or C—B linkages in $H_3N—BH_3$ and $OC—BH_3$ resemble very much to a strongly polar but otherwise ordinary σ-bond. This is inferred by, amongst other things, the value of the CB bond length which is 157 pm corresponding to a simple covalent bond. The electronic difference density map of Fig. 2.32 shows a considerable gain in electrons in the bonding region [1375].

In other complexes where the interaction is intermediate or weak the most important term is E_{Coul} indicating that bonding is primarily due to the Coulombic interaction between the donor and the acceptor. A common feature of these complexes is that the charge–transfer contribution is less important though it is essential in determining the

TABLE 2.13

Decomposition of the interaction energy for some electron donor–acceptor complexes (in kJ/mol) at the optimized intermolecular separation [935]. For the definition of various terms see Eq. (2.4)

Donor	Acceptor	E_{Coul}	E_{pol}	E_{ex}	E_{ct}	E_{mix}	E^{a}_{SCF}
H_3N	BH_3	−389	−72	364	−113	23	−187
OC	BH_3	−255	−259	414	−286	266	−120
H_2O	$OC(CN)_2$	−40.6	−4.2	18.4	−7.5[b]		−33.9
C_6H_6	$OC(CN)_2$	−11.7	−7.1	7.5	−6.7	0.4	−17.6
C_6H_6	ClF	−6.7	−0.4	2.5	−3.3	0.0	−7.9
H_3N	Cl_2	−16.7	−3.3	16.3	−9.6	1.3	−12.0
H_2O	TCNE[c]	−14.6	−0.8	2.9	−0.4	0.2	−12.7

[a] $E_{SCF} = E_{int} - E_{disp}$
[b] $E_{ct} + E_{mix}$
[c] TCNE = tetracyanoethylene $(CN)_2C{=}C(CN)_2$

geometry of the molecular association [831]. To obtain correct potential curves exchange repulsion and sometimes dispersion terms have to be considered, too [766, 767]. The dispersion term is 5.0 and 10.9 kJ/mol for the $H_2O\ldots OC(CN)_2$ and $C_6H_6\ldots OC(CN)_2$ complexes, *i.e.* in the latter case its absolute value is also considerable.

Since the electrostatic term is of primary importance in electron donor–acceptor complexes, it is natural that simple electrostatic models work well for these associations (see Ref. [572] for a review). These give a qualitative account on several experimental facts which arise as a consequence of complex formation. The semiempirical CNDO/2 and PCILO methods [806] proved to be useful in discussing several properties of electron donor–acceptor complexes though, in general, they give too small internuclear distances and too large interaction energies. If using an *ab initio* method the minimal basis set is certainly not enough [831]. For example, with a minimal or double-zeta basis set the intermolecular distance in the formaldehyde-ethylene complex is 400 or 375 pm while the interaction energy is −0.38 or −2.85

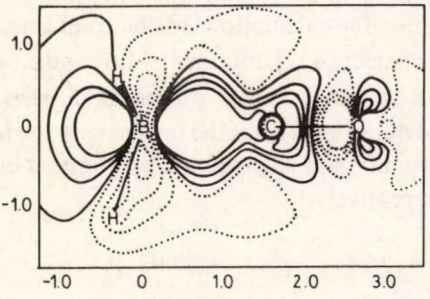


Fig. 2.32 Electronic difference density map along the B–C bond in $OCBH_3$. Full and dotted lines denote excess and lack of charge, respectively. (With permission from Ref. [1375])

kJ/mol, respectively [767]. Despite basis set problems, Hobza and Zahradník conclude that nonempirical SCF methods combined with a suitable estimation of dispersion effects can yield sufficiently accurate prediction of both the structure and the stabilization energy for electron donor–acceptor complexes [572].

Like hydrogen bonding, donor–acceptor complex formation also influences the properties of isolated molecules. A variety of molecular shapes is formed and several of these can be predicted on the basis of electrostatic potential maps of the isolated molecules [725]. Negative and positive regions of the potential should match in the complex and this is a good criterion to gain information on its shape. The power of the electrostatic method is illustrated on the OCO...HCl complex. For this, the HOMO–LUMO interaction scheme predicted a $HCl...CO_2$ structure while experiment confirmed the electrostatic prediction [725]. The HOH valence angle increases from 102.9° to 104.4° upon formation of the $H_2O...Cl_2$ complex [407]. Such geometry distortions were observed for other cases, too.

Donor–acceptor complexes have characteristic electronic spectra with a typical long-wave band in the visible region. This is attributed to a charge transfer from the electron donor to the acceptor molecule. The transition energy, ΔE, can be determined roughly from Mulliken's expression

$$\Delta E = I_D - E_A - C \tag{2.16}$$

where I_D and E_A are the ionization potential of the donor and the electron affinity of the acceptor, respectively. C is the Coulombic energy between the ionized species D^+ and A^-. If it is large ΔE is small. Consequently it is primarily the Coulombic interaction which is responsible for the appearance of the long-wave band in the spectrum.

Complex formation has a strong influence on the dipole moments of the interacting molecules. Even if these apolar dipole moments are induced in the complex which are perpendicular to the molecular planes of the associating units and which are proportional to the electrostatic and charge–transfer contributions to the total interaction energy [799]. Since it is the dipole–dipole term which determines the Coulombic energy and hence almost the total interaction energy of donor-acceptor complexes, the failure of minimal basis set *ab initio* methods to predict the correct sign of dipole moments for numerous weakly polar molecules is the origin of the aforementioned poor results for calculations of the total interaction energy by these methods. Lucchese and Schaefer [832] obtained −1.67 and 5.34 aC × pm for the dipole moment of FCl using a minimal and a double-zeta basis set, respectively. The experimental value is 2.94 aC × pm. This is the reason why the interaction energy of the $H_3N...ClF$ complex is so different if calculated by minimal or double-zeta basis sets: 0.71 and 32.2 kJ/mol, respectively.

2.11 VAN DER WAALS MOLECULES

The weakest associations of atoms or molecules, held together mainly by dispersion forces, are often referred to in the literature as *van der Waals molecules*. Some examples are noble gas associations, the N_2 dimer, the CO_2 dimer, etc. Though their binding energy is extremely small (0.2–0.5 kJ/mol) if compared to that of a classical chemical bond, several experimental and theoretical arguments suggest that van der Waals molecules are, in certain conditions, stable entities and they have to be discussed as such. Since the majority of potential curves between closed-shell molecules or noble-gas atoms have shallow minima at relatively large intermolecular separations ($\sim$200–300 pm) the corresponding geometry defines a van der Waals molecule.

The concept of van der Waals molecules arose from experimental and theoretical study of bulk properties of real gases and condensed phases. It became clear very early on that there exists a direct connection between bulk properties (gas imperfections, transport properties, scattering cross sections, etc.) and intermolecular forces (potentials) which may be adjusted by fitting simple analytic expressions to experimental properties. A recent, excellent review of experimental and theoretical determination of intermolecular forces is given by Maitland *et al.* [861]. (see also [719]). Hence, theories of intermolecular forces and van der Waals molecules are very closely related.

In contrast to intramolecular atom–atom potential curves in classical molecules intermolecular van der Waals potentials can often be derived simply from classical electrodynamics using only a few quantities which come from experiment. This approach gets worse as the intermolecular distance diminishes. Because of this, intermolecular potentials are discussed separately for large, intermediate and short distances [460].

Three types of long-range interactions are known: electrostatic, induction and dispersion ones, E^C, E^I and E^D, these correspond to E_{Coul}, E_{pol} and E_{disp} in Eq. (2.4). The electrostatic component was extensively studied by Buckingham [153] starting from the classical theory of electric charge distributions. The interaction energy between two neutral pointlike molecules, A and B, is given as

$$E^C = \frac{\mu_A \mu_B}{r_{AB}^3} F_\mu(\theta) + \frac{3}{4} \frac{Q_A Q_B}{r_{AB}^5} F_Q(\theta) \tag{2.17}$$

where μ and Q denote dipole and quadruple moments (see Section 3.4.2), r_{AB} is the intermolecular distance, F_μ and F_Q are orientation-dependent factors and θ is the angle between the dipole moment vectors. For the collinear (and parallel) arrangements cases $F_\mu = \mp 2$ (∓ 1), the upper and lower signs refer to the equivalent and opposite dipole moment directions, respectively. F_Q equals 8 and 3 for the above cases [572].

Induction energy is due to the polarization of the charge distribution of one molecule by the electrostatic field of another. This induces a dipole moment which interacts with

the inducing dipole to produce an attractive force. The corresponding mathematical expression is deduced from classical electrostatics. For the combination of a linear dipolar and an uncharged spherically symmetric molecule A and B it is as follows

$$E^I = -\frac{1}{2}\frac{\mu_A^2 \alpha_B}{r_{AB}^6}(3\cos^2\theta + 1). \tag{2.18}$$

Here μ_A and α_B are the dipole moment and polarizability of molecules A and B (see Section 3.4.2), θ is the angle between the vectors $\boldsymbol{\mu}_A$ and $\mathbf{r}_{AB}$.

Dispersion interaction between two molecules is entirely due to electron correlation. According to a classical model molecular electrons are in continuous motion; therefore the electron density oscillates continuously in time and space. Thus, at any moment, any molecule possesses an instantaneous electric dipole fluctuating with the electronic density. This instantaneous dipole in one molecule induces an instantaneous dipole in the second one and *vice versa*, producing the always attractive dispersion interaction. Between two neutral molecules with no permanent multipole moments dispersion is the only interaction. A simple oscillator model [336] yielded the following general formula for the interaction energy

$$E^D = -\frac{C_6}{r_{AB}^6} - \frac{C_8}{r_{AB}^8} - \frac{C_{10}}{r_{AB}^{10}} - \ldots. \tag{2.19}$$

The functional form of Eq. (2.19) was confirmed by rigorous quantum mechanical calculations, too (see Ref. 861 p. 63 for a derivation). The coefficients C_6, C_8, C_{10}, are all positive which means an attractive interaction. It has been shown that the coefficients of Eq. (2.19) depend on dipole and higher multipole polarizabilities for time-varying electromagnetic fields.

Calculation of potential curves of intermolecular interactions is most difficult for intermediate distances. Special perturbation theories were proposed [591, 955, 1331] but, the LCAO–MO method is also applicable if electron correlation is satisfactorily considered [800]. For short intermolecular distances the multipole expansion of the electrostatic energy does not converge, so other models have to be selected. Evidently, the best is a good quality *ab initio* calculation, but simple electron-gas models such as the Thomas–Fermi–Dirac [458] and Kim–Gordon [466] approximations work surprisingly well. These latter often represent the best that can be done at present for heavier inert gases.

To judge the power of quantum chemical methods we present the attractive part of the He...He interaction potential curve as taken from Ref. [861] (Fig. 2.33). The agreement between sophisticated *ab initio* and experimental results is excellent and even the electron-gas model yields a qualitatively good potential curve. Similar excellent agreement is achieved for the repulsive part of the potential [861]. Such success cannot be achieved for heavier noble gases or for di- and polyatomic molecules. However, experiments for these systems are not always reliable therefore an interplay between theory and experiment is necessary to understand all details quantitatively [1246].

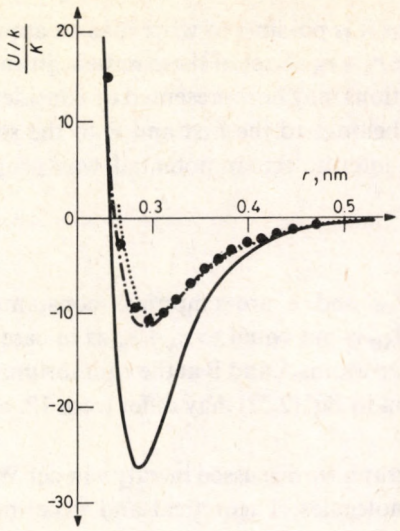


Fig. 2.33 The attractive pair potential for helium. Full line: electron-gas model, dashed-dotted line: exchange perturbation theory, dotted line: configuration interaction calculation. Dots indicate experimental results obtained by the low-energy molecular beam technique. (With permission from Ref. [861])

The expressions for the interaction energy in Eqs (2.17–19) are valid for fixed relative orientations. In gases, however, this orientation may change corresponding to the Boltzmann distribution law and, consequently, the average interaction energy expression is altered, too. For E^C the averaging process always leads to an attractive net term which is inversely proportional to the temperature and has an r_{AB} dependence equal to the square of that for the fixed orientation form. For E^I and E^D the r_{AB} dependence does not change. Hence, the orientationally averaged potential energy function for the interaction of two identical, neutral, linear, dipolar molecules (A and A) is simply [861]

$$\langle E\rangle = -\frac{1}{r_{AA}^6}\left(\frac{2\mu_A^4}{3x^2kT} + \frac{2\mu_A^2\alpha_A}{x^2} + C_6\right) \tag{2.20}$$

where $x = 4\pi\epsilon_0$, k is the Boltzmann constant, T is the absolute temperature.

Owing to the extreme importance of intermolecular forces in understanding, interpreting and modelling bulk properties of macroscopic systems simple analytical expressions were proposed to represent pair potentials (for an exhaustive account see Ref. [861]). We mention here only the two simplest. The hard-sphere potential has the form

$$E_{HS} = \begin{cases} \infty & r_{AB} < d_{AB} \\ 0 & r_{AB} \geqq d_{AB}. \end{cases} \tag{2.21}$$

d_{AB} is an empirical constant which is, in principle, different for each AB pair. However,

if both A and B are atoms it is possible to write it as an approximate sum of so-called *van der Waals radii*, $d_{AB} \approx r_A + r_B$. A set of these radii is given in Table 2.14 after Bondi [125]. Molecular interactions may be represented by considering Eq. (2.21) for each AB pair of atoms, where A belongs to the first and B to the second molecule.

The other important intermolecular potential was proposed by Lennard–Jones [779]

$$E_{LJ} = \varepsilon(R_{AB}^{-12} - 2R_{AB}^{-6}) \tag{2.22}$$

where $R_{AB} = r_{AB}/d_{AB}$, d_{AB} and ε are empirical constants fitted to experimental quantities. Frequently, d_{AB} is put equal to $r_A + r_B$ as in case of Eq. (2.21). ε is just the interaction energy between atoms A and B at the equilibrium separation. The exponent of the first, attractive term in Eq. (2.22) may differ from 12, in this case the parameters also change.

In the preceding paragraph we discussed mostly van der Waals molecules composed of atoms or diatomic molecules. Theoretical and experimental treatment of more complicated systems is difficult, the results are at most of semiquantitative value [572]. Quantum chemical calculations may serve to predict molecular shapes or trends in

TABLE 2.14

Van der Waals radii of atoms after Bondi [125] (in pm)

				H	He
				120	140
B	C	N	O	F	Ne
165[a]	170	155	152	147	154
Al	Si	P	S	Cl	Ar
–	210	180	180	175	188
Ga	Ge	As	Se	Br	Kr
–	198[a]	185	190	185	202
In	Sn	Sb	Te	I	Xe
–	216[a]	212[a]	206	198	216

[a] Calculated from the Pauling relationship r_A = covalent bond radius + 76

interaction energies which may be used for example in the treatment of solvent effects [590, 1159] or of biologically important molecular associations [1207].

As a rule the assumption that molecular interactions can be well approximated by simple sums of pair potentials is satisfied. However, in some cases, and especially in condensed phases, higher terms (particularly the three-body term) have to be considered. This latter is always of repulsive character and it is important if the nature of gas imperfections, relative stability of given crystal structures or dependence of pressure in liquids on temperature is to be understood [861].

3. MOLECULAR STRUCTURE

In principle, quantum chemistry is able to predict physical properties of molecules to any desired accuracy. In some cases the magnitudes of experimental and computational errors are comparable and quantum chemistry may serve as a "precision instrument" to determine a given physical quantity (bond length, force constant, etc.). However, computational difficulties often arise, especially for polyatomic molecules and the uncertainty of the calculated values gets larger. In such cases theory is useful primarily as a unifying concept giving a sound interpretation to experimental trends. Computations may serve sometimes also as an interpolation technique by which missing experimental information can be completed.

In the following chapters the efficiency of quantum chemical approximations will be discussed for some important quantities measured experimentally. In addition, we emphasize qualitative models, too. Some references to experimental techniques are given at the beginning of each section.

3.1 GEOMETRY

Experimental methods [787]: X-ray diffraction [343], electron diffraction [672], microwave spectroscopy [469].

The notion of molecular geometry presupposes that nuclei are pointlike and "clamped", *i.e.* their spatial positions can be unequivocally determined: quantum mechanical uncertainty and molecular vibrations are neglected. This rigid model is very useful in interpreting a great number of molecular properties.

Within the Born–Oppenheimer approximation, *cf.* Section 1.2.2 the total energy of a molecule as a function of all nuclear coordinates (in other words: as a function of the *nuclear configuration*) is:

$$E(\mathbf{R}_1, \mathbf{R}_2, \ldots, \mathbf{R}_m) = E_{\mathrm{el}}(\mathbf{R}_1, \mathbf{R}_2, \ldots, \mathbf{R}_m) + \sum_{m<n} \frac{Z_m Z_n}{|\mathbf{R}_m - \mathbf{R}_n|} \tag{3.1}$$

where $\mathbf{R}_m$ and Z_m denote the spatial coordinates and the charge of the m-th nucleus, E_{el} is the electronic part of the total energy which can be calculated by applying the appropriate quantum chemical approximation method. The second term in Eq. (3.1) is the Coulombic interaction between nuclei, it can be derived exactly for a given nuclear configuration. The multivariate function E is called *potential hypersurface* or simply

potential surface. Equilibrium geometries correspond to local minima on this surface. Each minimum defines an *isomeric structure* and all such structures are observable in case of systems for which the Born–Oppenheimer approximation applies.

The simplest potential surface is the one-dimensional potential curve of diatomic molecules (Fig. 1.3). It can be obtained point by point from spectroscopic data and the location of its minimum is simple [555]. For polyatomic systems the problem is much more difficult: equilibrium geometries are obtained from experimental data only indirectly and molecular vibrations have to be considered if accurate results are desired.

Owing to the approximate transferability of bond properties a straightforward way to define molecular geometries is using "internal" or *chemical coordinates i.e.* bond lengths, bond angles and dihedral (torsional) angles. It has to be noticed that dihedral angles corresponding to rotation around single bonds are, in general, nontransferable: they may considerably alter in different molecular arrangements. Several computer programs are known which use chemical coordinates as input to derive Cartesian ones which are more practical for computational purposes [563, 813, 1148]. While conversion from Cartesian to chemical (internal) coordinates is unequivocal the reverse is not true since for a molecule with M atoms there are $3M$ and $3M$—6 of such Cartesian and internal coordinates, respectively. Therefore, if one has to calculate Cartesian coordinates from chemical ones the spatial position and orientation of the molecule as a whole have to be specified. They are, however, irrelevant in the study of isolated molecules.

Quantum chemical determination of the equilibrium geometry may be done by a search point-by-point on the potential surface. It is easy to see that this is completely impracticable for more than one or two degrees of freedom; therefore one of the *force* (or gradient) *methods* has to be used [395, 846, 957, 1134, 1141]. For reviews on *ab initio* and semiempirical applications see [393, 1135, 1232]. In order to find local minima on potential surfaces first derivatives of the energy must be computed, which correspond to forces acting on the nuclei. In non-equilibrium points of the potential surface forces point towards local minima where they become zero. Mathematically, the force acting on the m'th nucleus, located at $\mathbf{R}_m$, in direction x in the i'th optimization step is

$$F^i_{xm} = -\left(\frac{\partial E}{\partial x_m}\right)_{x_m = x^i_m}. \tag{3.2}$$

Analogous expressions can be written for the y and z components, too. In the vicinity of the equilibrium position the displacement is calculated as follows

$$x^{i+1}_m = x^i_m + \mathbf{H}^i_m F^i_m. \tag{3.3}$$

$\mathbf{H}^i_m$ is called the Hessian which is constructed of the second derivatives of the energy (force constants), *e.g.* $H^i_{xym} = \partial^2 E/\partial x_m \partial y_m = \partial F^i_{xm}/\partial y_m$. An initial guess for the Hessian can be obtained from simple considerations (*e.g.* diagonal form). Iteration may be

TABLE 3.1

Bond lengths as obtained by different quantum chemical methods (in pm). STO–3G and 6–31G* denote the basis set in the *ab initio* calculation

Bond	Molecule	CNDO/2 [1121]	FSGO [211, 415]	STO–3G [1120]	6–31G* [285]	HF+CI [285]	Exp. [285]
C—H	CH_4	111.6	111.5	108.3	108.4	109.1	109.2
	C_2H_6	112.0	112.0	108.6	–	–	109.6 [1120]
	C_2H_4	111.0	110.1	108.2	107.6	108.4	108.5
	C_2H_2	110.0	107.9	106.5	105.7	106.5	106.1
	CH_3F	112.0	–	109.7	108.2	109.0	110.0
	H_2CO	112.0	–	110.1	109.2	110.1	111.6
N—H	NH_3	107	101.1	103.3	100.2	101.6	101.2
O—H	OH_2	103	88.1	99.0	94.7	96.6	95.8
	CH_3OH	112.0	–	–	94.6	96.3	96.3
C—C	C_2H_6	146.0	150.1	153.8	–	–	153.1 [1120]
	C_2H_4	131.0	135.1	130.6	131.7	132.8	133.9
	C_2H_2	120.0	121.4	–	118.5	120.2	120.3
F—F	F_2	111.9	148.9	131.5	134.5	139.9	141.2
C—F	CH_3F	134.8	–	138.4	136.5	138.2	138.3
Li—F	LiF	216.1	144.1	–	155.5	156.2	156.4
Mean deviation from experiment		9.7	3.8	2.0	1.7	0.5	–

continued till equilibrium is reached, *i.e.* the displacements, $x_m^{i+1} - x_m^i$ or the absolute value of forces get lower than a prescribed threshold.

The most advantageous feature of the force method is that all coordinates can be updated simultaneously in the direction of the equilibrium. Forces in Eq. (3.2) can be evaluated for most quantum chemical methods (*ab initio* with Gaussians, FSGO, CNDO/2, MINDO) analytically. This allows a considerable simplification of the numerical procedure. The force constants may play an important role. If they are considered to be equal for all forces, most probably the convergence will be very slow even oscillations may occur. The origin of this problem is that various types of chemical degrees of freedom (bond lengths, bond angles, dihedral angles) possess force constants differing by about two orders of magnitude. One way out is to transform Cartesian coordinates into chemical ones and to use the appropriate force constants which in this case are approximately transferable [969]. For the optimization of stretching, bending and torsional coordinates the force constant may have the value of 500, 50 and 5 Nm^{-1}, respectively (see Section 3.3). Modern geometry optimization methods construct the new Hessian in each iteration step.

Let us see now the reliability of quantum chemical methods when calculating the molecular geometry. Some representative figures are given in Tables 3.1 and 3.2. If electronic correlation is taken properly into account the reliability of calculations competes with measurements: deviations are within standard experimental errors

TABLE 3.2

Bond angles as obtained by different quantum chemical methods (in degrees). STO–3G and 6–31G* denote the basis set in the *ab initio* calculation

Angle	Molecule	CNDO/2 [1121]	FSGO [211, 415]	STO–3G [1003]	6–31G* [285]	HF+CI [285]	Exp. [285]
H—C—H	C_2H_4	124.3	118.7	115.4	116.4	116.3	117.8
	CH_3F	109.8	–	108.3	109.8	109.8	110.6
	H_2CO	115.0	–	114.5	115.7	115.8	116.5
H—N—H	NH_3	106.4	87.6	104.2	107.2	106.3	106.7
H—O—H	CH_2	104.7	88.4	100.0	105.5	104.3	104.5
H—O—O	H_2O_2	108.8	–	101.1	–	–	94.8 [1120]
F—O—O	F_2O_2	108.4	–	104.2	–	–	109.5 [1120]
Mean deviation from experiment		3.5	12.0	3.6	0.9	0.7	–

[285]. Very good results are achieved by large basis set *ab initio* SCF calculations for closed shell classical molecules [285]. As is seen from Table 3.1, bond lengths are systematically underestimated but trends are almost quantitatively reproduced. It is highly probable that this is also true for classical molecules with second or higher row atoms [179]. However, for nonclassical molecules (radicals, excited species, etc.) electronic correlation may essentially influence molecular geometry [280].

Experimental values, given in Tables 3.1 and 3.2, come from measurements on small molecules in the vapour phase. For larger systems experimental techniques are not so refined, therefore, requirements for theoretical methods are also smaller. The STO-3G minimal basis *ab initio* method is therefore usually satisfactory for larger molecules

TABLE 3.3

Covalent radii of some atoms (nm) in different bond types after Pauling [1070]

Bond	H	B	C	N	O	F
Single	0.030	0.081	0.077	0.074	0.074	0.072
Double			0.067	0.062	0.062	
Triple			0.060	0.055		
			Si	P	S	Cl
Single			0.117	0.110	0.104	0.099
Double			0.107	0.100	0.094	0.089
Triple			0.100	0.093	0.087	
			Ge	As	Se	Br
Single			0.122	0.121	0.117	0.114
Double			0.112	0.111	0.107	0.104
			Sn	Sb	Te	I
Single			0.140	0.141	0.137	0.133
Double			0.130	0.131	0.127	0.123

though it severely underestimates the F–F distance in F_2 but this is a very specific molecule. Similarly, FSGO and CNDO/2 methods may be well used for a variety of compounds to analyze trends in bond lengths or bond angles [1364]. The original CNDO/2 method fails, however, for molecules with second-row atoms [875]. Attempts to overcome this problem seem to be promising [1233].

Several semiquantitative or qualitative models are known in the literature to describe trends in molecular geometry. Maybe the most important of these models is the use of covalent radii (see Table 3.3) to reproduce bond lengths [1070]. Atoms are considered as rigid spheres with radii which are independent of their bonding partners. The model works best for well localizable σ- and π-bonds and its success traces back to the strongly repulsive character of the interatomic potential curves at short distances (Fig. 1.3). Transferability of covalent radii corresponds to transferability of atomic cores which are, in fact, not easily perturbed. Schomaker and Stevenson have observed that deviations from transferability are approximately proportional to the electronegativity differences [1242]. The interatomic distance R_{AB} can therefore be approximated by the following formula

$$R_{AB} = R_A + R_B - c\,|\,\chi_A - \chi_B\,| \tag{3.4}$$

where R_A, R_B and χ_A, χ_B are covalent radii and electronegativities of atoms A and B, respectively. The constant c was originally assigned the value of 9 pm but if one allows it to have different values for bonds involving at least one first row atom (8 pm), or for bonds between Si, P or S and a more electronegative atom (6 pm), etc. the mean deviation of Eq. (3.4) from experiment gets as low as 1–2 pm [1070].

Another formula by which bond lengths in aromatic hydrocarbons can be estimated was proposed by Coulson [256] (in pm)

$$R_{AB} = 151 - 17 p_{AB} \tag{3.5}$$

where p_{AB} is the π-bond order as calculated by the simple Hückel method [(*cf.* Eq. (1.143)]. Equation (3.5) can be well used to reproduce experimental trends in the CC bond lengths even in ionized and excited species. It may be adapted for heteronuclear bonds, too, though if bond polarity is too large the reliability becomes smaller. Bond orders may be calculated not only by the Hückel method but also by the PPP one. Overlap populations obtained by EHT procedures can also be applied. Needless to say, in such cases the proportionality constant in Eq. (3.5) assumes another value.

Bond lengths depend also on the *s*-character of bonded hybrids. A classical example is the decrease of the CH distance in the series of ethane, ethylene and acetylene. In these compounds the *s*-character of the hybrids on the carbon atom gets larger (*cf.* Table 2.1). The phenomenon may be interpreted as a consequence of increase in overlap with the increasing *s*-character [948] of the carbon hybrid directed to the H atom, *cf.* Section 2.1.

Transferability of bond angles is fair in most cases though deformation is easier than that of bond lengths. This is due to the smaller value of bending force constants as

compared with the stretching ones (see Section 3.3). Therefore bond angles depend more on molecular environment than bond lengths. Highly strained structures like cyclopropane or cyclobutadiene are experimentally detectable, even if sometimes with difficulty. In these molecules the CCC angles are 60° and 90° differing considerably from the standard sp^3 and sp^2 values, 109.5° and 120°, respectively. Ring strain may play an important role in the chemistry of some specific molecules (*e.g.* small ring propellanes [1421]). The origin of strain may be connected with the maximum overlap principle (Section 1.3.3): optimum atomic hybrids are not oriented along bonds therefore overlap is reduced.

As with bond lengths, several qualitative models are known which may be used for more or less correct predictions on molecular shapes. We discuss two of them, the Walsh rules [1399] and Gillespie's valence-shell electron pair repulsion (VSEPR) model [448]. There is strong evidence which indicates that these two models are linked with each other in a certain sense [503].

The Walsh rules are based on the observation that the total energy of a molecule may be approximated by a simple sum of orbital energies. This assumption is exploited in the simple and extended Hückel theories, *cf.* Section 1.3.2. As in other qualitative MO models (*cf.* Section 1.3.3). changes of orbital energies as functions of the molecular geometry can be followed relatively easily using group theory. Supposing that trends are the same for similar molecules, general rules are derived which hold for a wide variety of compounds.

Let us discuss now the example of molecules with the general formula AH_2 (A denotes an atom with $Z>2$). The correlation diagram, *i.e.* the variation of the orbital energies as a function of the bond angle, is shown on Fig. 3.1. If the HAH angle is 180° the molecule is axially symmetric ($D_{\infty h}$ point group). The lowest one-electron states are $1\sigma_g$ (essentially the core level of atom A), $2\sigma_g$ followed by $1\sigma_u$ and $1\pi_u$. For the case where the bond angle is 90°, the point group is C_{2v}, and the lowest one-electron states

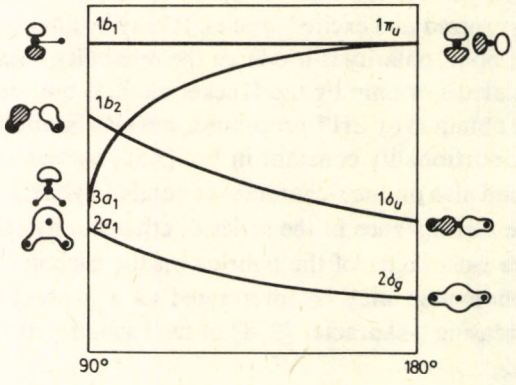


Fig. 3.1 Walsh diagram of water-type molecules.
Schematic plot of MOs is depicted on both sides of the graph

are the totally symmetric $2a_1$ and $3a_1$. The core level of atom A is practically independent of the molecular shape and we shall not discuss this further. Pairing the MOs by symmetry, the correlations $2a_1$-$2\sigma_g$, $1b_2$-$1\sigma_u$ and $1b_1$-$1\pi_u$ are obvious. These can be proved also by strict group theoretical methods, giving the non-trivial $3a_1$-$1\pi_u$ correlation in addition. In the real situation the bond angle varies until the minimum energy is obtained. Consequently, we can predict the molecular shape merely by considering the occupation of the different MOs. For example, the electron configuration of BeH_2 in the ground state is $2\sigma_g^2 1\sigma_u^2$. Both orbital energies are the

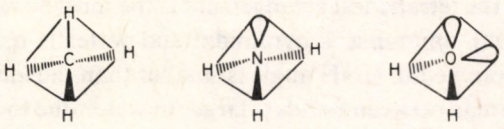


Fig. 3.2 Formations, corresponding to the VSEPR theory, for methane, ammonia and water

lowest for a bond angle of 180° and the molecule is linear. On the other hand, the configuration of the NH_2 radical is $2a_1^2 1b_2^2 3a_1^2 1b_1$ and it is bent, since the energy of the $3a_1$ MO strongly decreases if the bond angle gets close to 90°. This energy lowering is larger than the increase due to the distortion of the $2a_1$ and $1b_2$ MOs. In the first excited state an electron gets from the $3a_1$ to the $1b_1$ MO. Since the energy of the latter is independent of the bond angle the bending effect reduces and the molecule opens. Our qualitative considerations reflect experimental reality: the bond angles in the ground and excited states are 103.3° and 144°, respectively. Other examples are discussed by Burdett [166].

Buenker and Peyerimhoff did *ab initio* calculations for several dozens of molecules to establish the validity of the quantum chemical model used in the Walsh rules [158]. They found that for example, for the F_2O molecule the total energy and the sum of orbital energies change parallel as a function of the FOF bond angle. This is not completely true for the O_3 molecule and the model completely fails for FOH and CO_2. Similarly, total energy and the sum of orbital energies do not change parallel as a function of the bond length. However, these authors have shown that the Walsh rules are always applicable if we are interested in geometry changes upon ionization or electronic excitation. This is why correct comparisons can be made between molecules of the same type but containing a different number of valence electrons.

Another, popular and successful model is the VSEPR theory [448]. It is based on the localized MO picture of the chemical bond (see Sections 2.1–2.5). Each electron pair forming a bond or a lone pair is treated as a closed entity; these repel each other as a result of the "Pauli repulsion forces" so they tend to localize in space as far apart as possible (Fig. 3.2). Lone pairs are "larger" than bonded pairs in the sense that lone pairs extend to a larger solid angle in space than bonded pairs [266, 671]. Accordingly, repulsion between different types of electron pairs decreases in the following order

(l: lone pair, b: bonded pair)

$$ll > lb > bb\,. \tag{3.6}$$

The validity of Eq. (3.6) may be proved by *ab initio* calculations [671]. Several electron pairs may be attached to the atomic core of a central atom, the more the larger radius and charge belongs to the latter. The maximum number of electron pairs (which is also the maximum coordination number or the number of available valence AOs) therefore increases for higher rows and for higher atomic numbers within the same row of the periodic table. Owing to the repulsion between electron pairs for the case of four ligands or lone pairs the tetrahedral arrangement is the most advantageous. Therefore methane is tetrahedral, ammonia is pyramidal and water is bent. As the lone pair extends to a larger volume the HNH angle is smaller than the ideal tetrahedral value. The decrease of the angle between bonds is larger in water due to the stronger effect of two lone pairs. Experimental values of bond angles are: CH_4 : 109.5°, NH_3 : 106.7°, H_2O : 104.5°, in full accord with the above considerations.

The VSEPR theory is applicable for a large number of molecules. It is especially useful for the qualitative prediction of geometries of molecules for which experimental data are not available (*e.g.* noble gas compounds [619]). Some authors denied the existence of "Pauli forces" [100] though it seems that this is only a matter of terminology [503]. If the Pauli principle is considered merely as the inclusion of the exchange term in the total energy expression for the single-determinant wave function, its effect is almost negligible. However, the most important consequence of the Pauli exclusion principle, that is, maximum spatial separation of electrons of the same spin, is implicitly accounted for even by a simple Hartree product wave function if MOs are orthogonal. Violation of the orthogonality condition may lead to serious errors in predicting molecular geometries. This is why mutual repulsion of electron pairs, the basis of the VSEPR theory, can be related to "Pauli forces". It is important to notice that the present rationale holds only for a Hartree product wave function. In the Hartree–Fock approximation the orthogonality condition is only of minor importance. The problem will be discussed in more detail in Section 3.3 in connection with barriers to rotations around single bonds.

Bond lengths and bond angles, detectable in the vapour phase, change only little in condensed phases. CNDO/2 calculations on hydrated methanol [1055] indicate that the change of the CO bond length is less than 1 pm. It is the OH bond length which changes a bit more as a consequence of H-bond formation, though its elongation is not more than 2 pm. Bond angle changes are 0.6° and 0.4°, for the COH $\measuredangle$ and HCO $\measuredangle$, respectively. Experimental measurements also indicate that gas-phase and solid-phase geometries are close to each other [233].

3.2 CONFORMATION

Experimental methods: X-ray diffraction [343], electron diffraction [672], microwave spectroscopy [469], dipole moments [1048], acoustic relaxation [1048], summary [1048].

Under molecular conformations we mean different nuclear configurations which may be transformed into each other by changing one or more dihedral angle(s). Examples of such different configurations, often called *conformers*, are the staggered and eclipsed forms of ethane or the chair and boat forms of cyclohexane. In a somewhat wider sense, however, conformational changes may include inversion and Berry pseudorotation, too (see Fig. 3.3). Conformational analysis studies geometries and

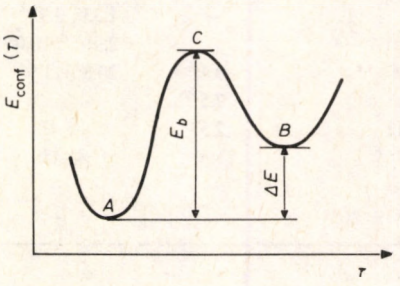


Fig. 3.3 Schematic energy profile for a conformational change. *A* and *B* denote equilibrium conformations *C* is the transition-state complex. $E_b = E_C - E_A$ is the rotational barrier

relative energies of different conformers as well as energy barriers to conformational changes. Experimental techniques yield, as a rule, indirect information on these quantities, while direct calculations may be performed by using various theoretical methods.

All conformers correspond to local minima on the molecular potential surface, these are separated by saddle points (hypothetical "transition states" see Section 4.3 for more detail). The energy difference between the minimum and the saddle point is called the *rotational barrier*. A conformational change involves the motion of the system (principally by alteration of one or more dihedral angles) on the minimum energy path from one conformer to the other. For internal rotations in acyclic molecules the dihedral angles serve as the best choice for the reaction coordinate while in cyclic molecules various puckering coordinates may be defined [265].

In principle, localization of equilibrium conformations can be done by the force methods used for geometry optimization. However, torsional force constants are very small; therefore the total energy depends on dihedral angles slightly. Consequently, joint optimization of bond lengths, bond angles and dihedral angles by a force method yields accurate values for the former two and does not necessarily give the optimum torsional angle. It seems that at present the best method of locating equilibrium dihedral angles is to construct conformational energy maps point by point.

TABLE 3.4

Comparison of experimental and calculated rotational energy barriers (kJ/mol). If not specified, the data are from Ref. [1383]

Molecule	Ab initio	PCILO [970]	CNDO/2	EHT	Experimental
$H_3C—CH_3$	10...15, 12.8[a,b]	8.3	2.9...10	17	12.2
$H_3C—SiH_3$	6.54	–	3.58[c]; 10.3[d]	–	7.12
	–	–	1.50[a]; 8.00[a,d]		
$H_3Si—SiH_3$			1.42[c]; 24.4[d]	–	4.58
			0.46[a,c]; 59.8[a,d]		
$H_3O—NH_2$	8.3...10	6.2	6.54	–	8.24
$H_3C—OH$	4.2...6.7	3.3	3.25; 5.37[a,e]	1.7	4.41
$H_3C—SH$	5.04	–	1.33[c]; 3.91[d]	–	5.29
			2.96[a,c]; 10.0[a,d]		
$HO—OH$[f]	34.6[a,b]; 4.6[a,b]	0.4; 7.5	20.8[a]; 11.9[a]	–	29.1; 4.6
$H_3C—CHO$	3.3...6.2	2.5	3.41	–	4.83
$H_2N—CHO$	79...87[a,b]	11.3	41.1[a]	105	71...87
$O_2N—NO_2$	21[a]	–	–	8.7	12
$H_2C=CH_2$	441...579; 265[g]	–	–	335	271

[a] Optimized geometry
[b] Polarization functions
[c] Using *sp* basis
[d] Using *spd* basis
[e] [1054]
[f] The first figure stands for the *cis*-, the second for the *trans*-barrier
[g] Using configuration interaction and with partial geometry optimization

Let us discuss now the reliability of various quantum chemical approximations to reproduce rotational barriers and relative energies of different conformers [1383]. First, it has to be noted that electron-correlation does not play a significant role in determining barriers to rotation around single bonds [1456], even if these latter are delocalized to some extent, as in acetaldehyde or in 1-propene [90]. The rotational barrier in ethane, using a large basis set, is calculated to be 13.3 kJ/mol; it changes only to 13.7 kJ/mol if correlation effects are also considered [1456] (the experimental value is 12.2 kJ/mol). Relativistic effects may also be neglected [1383].

For simple systems, like ethane, minimal basis set *ab initio* calculations yield satisfactory results, *cf.* Table 3.4. This is not true for H_2O_2, where the rotational barrier is strongly basis set dependent [1381] and polarization functions have to be considered, too.

To reproduce barriers to rotations accurately, minimum energy paths have to be calculated. When altering the actual rotational freedom all other coordinates have to be optimized which leads to a considerable increase in the computational work. In *ab initio* calculations experimental geometries are used, as a rule, since full optimization is

costly. This rigid rotor approximation is allowed in most cases since the HF geometries are rather close to the experimental ones, *cf.* Section 3.1. Optimization of the transition states leads to a small decrease in the barrier heights. Geometry optimization may lead to essentially different results from the rigid rotor approach if semiempirical methods are applied to calculate the barrier. Thus, semiempirical methods do not reproduce experimental bond lengths and bond angles quantitatively. It has to be noted that optimization does not necessarily improve the value of the barrier. It is seen from Table 3.4 that CNDO/2 barriers may change by 200% upon optimization. This is especially important for rotations where hydrogen bonds are formed or broken or if nonbonded interactions become significant.

Precise results are achieved by *ab initio* calculations even with minimal basis sets; with larger basis sets including polarization functions (6-31G**) and optimizing the geometry quantitative agreement with experiment is achieved for ethane, hydrogen peroxide and formamide (*cf.* Table 3.4). Various calculations using smaller (*e.g.* 4-31G) basis sets yield barrier heights close to the experimental values. If double bonds are examined where π-bond components break during rotation electron correlation has to be considered. The effect of π-bond breaking is for ethylene as large as about 200 kJ/mol. *Ab initio* calculations are able to reproduce even finer details of the rotational curve. For ethane it is approximated by the following truncated Fourier series (τ is the dihedral angle around the threefold axis):

$$E(\tau) = \frac{1}{2} V_3(1 - \cos 3\tau) + \frac{1}{2} V_6(1 - \cos 6\tau) . \tag{3.7}$$

V_3 is the rotational barrier, V_6 characterizes the shape. *Ab initio* calculations yield 0.03–0.05 kJ/mol for V_6 [1383]. Recently successful attempts have been made to fit analytical expressions to more complicated conformational energy surfaces (*e.g.* those in *n*-butane, formic acid) [1087]. The fitted expressions reproduce quantitatively geometries and relative energies, obtained by the *ab initio* force method. They are especially useful for cases (*e.g.* methyloxirane) where classical stereochemistry cannot be applied to locate critical regions (minima, cols, maxima) on the potential surface. Location of these regions is much easier if an analytic fit for the potential surface is available.

The PCILO method is often used for conformational analysis. It often underestimates barriers to rotation around single bonds. In general, geometries and relative energies of various conformers are reproduced correctly [737]. The method is very rapid, so it is advantageous for larger systems like biomolecules. Pullman and coworkers widely applied it with success to the study of dipeptides [1144].

The CNDO/2 method underestimates barrier heights. It reproduces correctly experimental geometries and relative energies of the conformers for rotations around well localized σ-bonds (*e.g.* Me—N_2Me, Et—SCN). If slight delocalization occurs (*e.g.* Me—COCN, Ph—Me, Ph—OH) results are in general but not always realistic. However, if the delocalization is strong (*e.g.* HOOC—COOH, Ph—COOH, Ph—

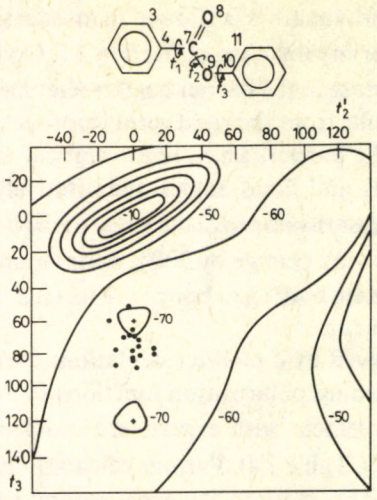


Fig. 3.4 Isoenergy contour map (in kJ/mol) for internal rotations in phenylbenzoate as obtained by the NDDO method. $t'_2 = 180° - t_2$. Crosses denote local minima, circles indicate experimental equilibrium conformations for related molecules

NO_2) the CNDO/2 results are in error [1274]. For molecules containing second-row atoms, *d*-orbitals have to be considered though even in this case erroneous results may be obtained, *cf.* disilane in Table 4.3.

In some of the above delocalized cases the NDDO (neglect of diatomic differential overlap) method yields good results [105, 1325]. An example is phenylbenzoate [106], for which the low-energy region of the theoretical potential surface (*cf.* Fig. 3.4) corresponds to molecular conformations which were found experimentally for some selected model molecules included in the Cambridge Crystallographic Data File [954].

Recently a breakthrough by molecular mechanics (or empirical force field) methods is observed in the literature [11, 995, 1400]. Strictly speaking these are beyond the scope of this book since they represent purely interpolation techniques based on experimental data, quantum mechanics is only indirectly exploited. The methods deserve, however, a short discussion. Regions of potential surfaces around their local minima can be approximated as a sum of simple analytical expressions

$$E = E_b + E_i + E_{nb} \tag{3.8}$$

where the subscripts refer to bonded, intermediate and nonbonded contributions. Bonded interactions are expressed as a sum of stretching, bending and cross terms

$$E_b = \frac{1}{2}\sum k_r(r - r_0)^2 + \frac{1}{2}\sum k_\vartheta(\vartheta - \vartheta_0)^2 + \text{cross terms}\,. \tag{3.9}$$

r, r_0, ϑ and ϑ_0 denote actual and equilibrium bond lengths and angles, respectively; k_r and k_ϑ stand for quadratic force constants. Summation runs over all stretching and

bending degrees of freedom. Cross terms, if considered, include stretch–stretch, bend–bend or stretch–bend contributions.

Intermediate interactions are described by torsional potentials, which can be expressed as a periodic function of the dihedral angle

$$E_i = \frac{1}{2} \sum V_\tau^n (1 - \cos n\tau) . \tag{3.10}$$

V_τ^n is the n-fold rotational barrier (*e.g.* $n = 3$ for ethane) and summation runs over all torsional degrees of freedom.

The nonbonded term can be described as an atom–atom interaction potential (*cf.* Section 2.11); neglecting three-body interactions

$$E_{nb} = \varepsilon^{-1} \sum q_i q_j r_{ij}^{-1} + \sum V_{Hb}(r_{ij}) + \sum V_{vdW}(r_{ij}) . \tag{3.11}$$

The first term corresponds to electrostatic interactions between atoms i and j bearing net charges q_i and q_j. These are taken either from quantum chemical calculations on model molecules [227, 924] or from fitting to experimental properties of hydrocarbon, amide or amino-acid crystals [1400]. The choice of the ε dielectric constant is somewhat arbitrary; it may range between 1 and 4 from author to author. The form of the hydrogen-bonding potential, V_{Hb} is also problematic [1101]. The van der Waals potential, V_{vdW}, is the same as in Eq. (2.23); however, the constants are different.

The main advantage of molecular mechanics calculations lies in their simplicity, which allows complete geometry optimization even for large molecules [1400]. If the parameter set is carefully fitted an accuracy of 2 kJ/mol can be achieved. However, much experimental data are needed for such a fitting; therefore, if these are not available, the accuracy of the method lowers drastically. Maybe this is the reason that, except hydrocarbons and some simple families of saturated systems (alcohols, amines, etc.) [11], no single version of parametrizations became popular and results coming from different laboratories are difficult to compare.

If an atom A, bearing a lone pair, is bonded to three other ones the corresponding AXYZ molecule will be pyramidal (X, Y and Z may denote equivalent or different atoms or groups). For such molecules (*e.g.* ammonia or methylamine) two equivalent arrangements are possible which can be transformed into each other via a planar intermediate structure (Fig. 3.5). Similar rearrangement is possible for bent molecules

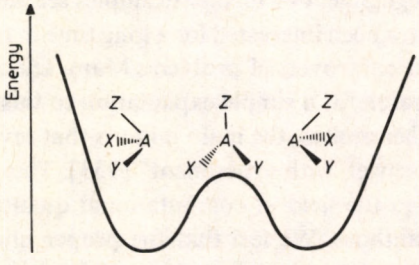


Fig. 3.5 Schematic plot of the inversion energy curve for a molecule of the type AXYZ

TABLE 3.5

Comparison of experimental inversion barriers (kJ/mol) with calculated values obtained by different methods [1383]

Molecule	Method			
	Ab initio	CNDO/2	MINDO	Experimental
NH_3	1.7...42.1; 24.6[a]	13.3...85.8	15.4	23.9
NF_3	–	252...320	–	233...246
NH_2CH_3	32	17...95	24	20
NH_2CN	7.5	0.8	–	8.3
NH_2COH	0.4	0.04	6.2	4.6

[a] Using polarization functions

of the type BXY (B bears two lone pairs like O in H_2O). In this case the intermediate structure is linear. The above transformations are called *inversion* and they are also studied by conformational analysis.

The efficiency of various computational methods is compared in Table 3.5 [1383]. The effect of electron correlation is negligible. The Hartree–Fock method is able to quantitatively reproduce inversion barriers, the energy differences between planar or linear intermediate and initial structures, if polarization functions are also included in the basis set. In ammonia, the polarization functions almost alone account for the appearance of inversion barriers [1155]. Accuracy of semiempirical methods (CNDO/2, MINDO) is in some cases sufficient though in others they fail.

Solvent effects are sometimes especially important for conformational changes. Tvaroška and Kozár calculated the effect of solvent upon the conformational behaviour of the glycosidic segment in methoxytetrahydropyran [1373]. The obtained results, in excellent agreement with experimental data, made it possible to determine relative population of various conformers in various solvents. Hoffmann and coworkers calculated the effect of carbon tetrachloride solvent on the amide group rotation in 1-methyl-1, 4-dihydronicotamide, a model for the pyridinoid component of the reduced form of NAD^+-coenzymes [582]. As it is seen from Fig. 3.6 the solvent effect is small but not negligible. For further examples see Refs 23, 121, 655 and 1054.

Quantum chemists have been interested for a long time in the origin of barrier forces which represents a most controversial problem. Many scientists feel that "too much effort has gone into a search for a simple explanation to this phenomenon..." [575] and "this is perhaps rather useless: the main point is that several computations of the difference in energy agree well with experiment" [953]. This view is characteristic for some authors working in the field of computational quantum chemistry but is not shared by the present authors. We feel that the proper understanding of a general phenomenon or, at least, a particular effect is interesting in its own right on one hand,

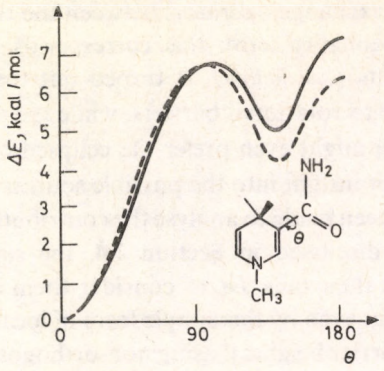


Fig. 3.6 NDDO potential energy curves for 1-methyl-1,4-dihydro-nicotamide. Full line: gas phase, dashed line: solution in carbon tetrachloride (With permission from Ref. [582])

and may be *practically useful* on the other hand. The practical value is partly connected with the fact that sophisticated computational schemes can be applied only for relatively small molecules. The treatment of larger systems requires a knowledge of the physical sources of the effects to be studied: in the absence of such knowledge one is not able to find the proper approximate method. As we will see, the case of rotational barriers represents a typical example for this need.

The facts that the values of barriers to internal rotations around single bonds are generally of the same order of magnitude (see Table A1 in the Appendix), and that the staggered conformations are generally stable, suggests that the barriers in different molecules may be attributed to similar sources.

One has to find a repulsive interaction between vicinal bonds, since the distance between vicinal hydrogens is slightly larger in this conformation. Among the possible origins, the electrostatic repulsion was proven to be negligible in the case of neutral and unpolar systems, such as ethane [209, 1299]. Van der Waals effects can also be neglected because they are connected to the electron correlation and, as we have pointed out above, electron correlation has little influence on rotational barriers.

Morokuma and Umeyama presented an analysis of some simple molecules [936, 1375] using the energy decomposition scheme of Morokuma which has been already discussed in Section 1.5. This decomposition was originally developed for the study of interaction between two molecular fragments or molecules at the HF level. To analyse the rotational barrier, Morokuma and Umeyama considered, for example, the ethane molecule as an ensemble of two methyl radicals. Among different contributions (electrostatic, polarization, exchange, charge transfer and mixed terms), the exchange interaction alone was found to be significant. This finding is in agreement with many other conclusions (see *e.g.* [209]).

The exchange interaction consists of two different terms. One is the so-called direct exchange effect which is connected to the value of the exchange integrals (*i.e.*

expectation values of the exchange operator) between the two fragments. The second term is called the orthogonality term; this corresponds to the overlap repulsion between the two fragments *(see below)*. It turned out that essentially the latter is responsible for giving rise to rotational barriers, while the direct exchange effects are very small and they alone might even prefer the eclipsed conformation [936].

In order to gain a deeper insight into the possible sources of the rotational barriers, many attempts have also been made to analyse the contributions to barriers in terms of localized MOs. As was discussed in Section 1.4, the simplest approximation to localized MOs is to drop their tails, *i.e.* to consider them as being strictly localized (SLMOs). It was found that even by this simple form of localized orbitals, one obtains good estimations of the barrier heights if using non-orthogonal SLMOs in the *ab initio* framework [247, 597, 598, 685, 958, 1316, 1317]. (We recall that, due to the non-orthogonality of the atomic orbitals centred at different atoms, the *ab initio* SLMOs *do* overlap.) The ability of pure non-orthogonal SLMOs to account for barriers means that no electron delocalization effects are necessary to understand the origin of barrier forces. This conclusion agrees well with the finding that, in Morokuma's decomposition, the charge transfer contributions play no role in governing the conformation.

Clearly, if the SLMOs were completely noninteracting no barrier could appear, since in this case the total electronic energy would be the sum of the energies of the individual SLMOs which are unaffected by the steric arrangement. Thus, the origin of the barrier forces is certainly hidden in *those interactions between SLMOs which do not directly produce electron delocalization.* Such interactions are either electrostatic (Coulomb repulsion, polarization) or they are connected to the overlap repulsion resulting from the non-orthogonality of the SLMOs. As we have mentioned above, the former are insufficient to explain the phenomenon, thus one concludes that, also in this framework, the *overlap repulsion of SLMOs is responsible for giving rise to barrier forces.* More physically, it is the repulsion of closed shell electron clouds at short distances (*cf.* the repulsion of two He atoms) which usually provides a higher energy for the eclipsed configuration (where the vicinal bonds are slightly closer to each other) than for the staggered one.

To elucidate the essence of overlap repulsion, let us consider a simple model of the interaction of two slightly overlapping doubly filled orbitals at the extended Hückel level. The two orbitals may represent, for example, the two 1*s* AOs of two He atoms, or two SLMOs describing vicinal C—H bonds in ethane. As was discussed in Section 1.3.2, in the extended Hückel theory one takes into account the overlap of basis functions, but does not consider the electron repulsion (nor the electrostatic interaction of the nuclei with the electrons or each other) explicitly. Thus, for the Hamiltonian and overlap matrices in this four-electron two-orbital model we have:

$$\mathbf{H}=\begin{pmatrix}\alpha & \beta\\ \beta & \alpha\end{pmatrix}; \qquad \mathbf{S}=\begin{pmatrix}1 & s\\ s & 1\end{pmatrix}; \qquad \mathbf{s}=\begin{pmatrix}0 & s\\ s & 0\end{pmatrix} \tag{3.12}$$

where α and β are the intra- and inter-orbital matrix elements, respectively, while s is

the overlap between the two orbitals in question. Since both orbitals are doubly filled, the energy of the system is given by the following formula, *cf.* Eqs (1.51)–(1.52):

$$E=2\sum_{i,k=1}^{2}(\mathbf{S}^{-1})_{ik}\mathbf{H}_{ik}=2\sum_{i=1}^{2}H_{ii}-2s\sum_{i\neq k}H_{ik}+o(s^2) \tag{3.13}$$

where i and k label the two orbitals, and we have expanded the inverse overlap matrix in a Taylor series as

$$\mathbf{S}^{-1}=(\mathbf{I}+\mathbf{s})^{-1}=\mathbf{I}-\mathbf{s}+o(\mathbf{s}^2)\,. \tag{3.14}$$

The terms of the second and higher orders in $\mathbf{s}$ are dropped. Substituting the matrix elements of the Hamiltonian, Eq. (3.12), one obtains for the energy

$$E=4\alpha-4s\beta\,. \tag{3.15}$$

Since the overlap integral s and the corresponding Hamiltonian (resonance) matrix element β are usually of opposite signs, we have $s\beta=-|s\beta|$ and Eq. (3.15) becomes

$$E=4\alpha+4|s\beta|\,. \tag{3.16}$$

The first term of the energy, 4α, is the sum of the energies of the two noninteracting orbitals, while the second term describes the overlap interaction. The latter is positive, so it raises the energy, thus the overlap interaction is always repulsive. In agreement with the above fact two closed shell electron configurations always repel each other (this is valid not only at the Extended Hückel level). If one considers also SCF and correlation effects, there can appear some attraction terms as well (*cf.* van der Waals attraction), but they are rather weak and for short distances the overlap repulsion always dominates. Accordingly, this effect can be considered as the main source of interbond repulsion which gives rise to barrier forces.

In the light of the above example it is clear that it is *not the value of the exchange integral* which affects the barrier heights. If one speaks about "exchange effects" in this connection one always means the overlap repulsion which is also connected to the exchange, since it expresses the repulsion of closed shells as required by the Pauli principle. The appearance of the overlap integral in the energy expression in Eq. (3.13) is a consequence of the determinantal form of the wave function.

A more detailed analysis of overlap repulsion and the relevant SCF effects permits us to derive simple bond–bond pair potentials which are approximate but nonempirical by their nature and describe qualitatively the interbond interactions influencing the molecular conformation [1316, 1317].

It was mentioned already that semiempirical ZDO schemes, such as CNDO, PCILO, usually predict accurate values for barriers to rotations. In the framework of these methods, however, the "origin" of barriers should be attributed to quite different sources since the corresponding atomic basis sets are assumed to be orthogonalized; thus no explicit overlap effects take place if using SLMOs. In fact, the SLMOs are orthogonal to each other in these schemes and it was found that they are unable to

account for barriers to rotations [148, 464, 1322, 1323]. In order to obtain good barriers, interbond delocalization effects should be taken into account. These delocalization interactions can be classified, as was discussed in Section 1.4.2: one can distinguish between *through space* and *through bond* delocalization effects [1322]. The former results from the direct interaction between different bonds, and it is very sensitive to the relative bond orientations. Through bond delocalization effects are rather independent of the relative orientation of the bonds; thus their contribution to the barrier is negligible [1322]. Hence one arrives at the conclusion that, in semiempirical theories working in orthogonal atomic basis sets, the origin of barrier forces lies in *direct through space delocalization interactions* between vicinal bonds [148, 1322]. This is also true at the *ab initio* level if the basis set is explicitly orthogonalized [247].

This conclusion was recently utilized in developing efficient computational schemes [986, 1321, 1323] permitting us to study conformational properties of very large (bio-) molecules.

3.3 MOLECULAR VIBRATIONS

Experimental methods: infrared spectroscopy [219, 234], Raman spectroscopy [219, 234].

Molecular motions can be appropriately modelled by treating the nuclei as a classical system of mass points. This is true within the Born–Oppenheimer approximation since it means that the light electrons follow the (heavy and therefore slow) nuclei instantaneously. A molecule consisting of M atoms has $3M$ nuclear degrees of freedom. The translational motion of a molecule as a whole can be described by defining the centre of mass and considering its motion separately. Furthermore, rotation is described by means of three axes of rotation, thus, six of the $3M$ independent coordinates, necessary to locate the M mass points in space, describe translation and rotation of the molecule and only $3M-6$ coordinates, called internal or chemical coordinates, are necessary to define relative nuclear positions*. Translational motion is of no quantum chemical interest. On the other hand, rotations are quantized: this is why rotational spectra are observed within the microwave region. We do not discuss molecular rotations here, only refer to one of the numerous monographs on this subject [469].

In the following we suppose that electronic, rotational and vibrational motions are separable within the molecule. This is valid only approximately since molecular vibrations and rotations can influence electronic transitions (*e.g. vibronic interactions* [358]). An example of the interaction of vibrational and rotational motions is the *Coriolis coupling*, which allows that some bands corresponding to forbidden transitions may appear in the infrared spectra [937].

* These considerations are valid for nonlinear molecules consisting of three or more atoms. For linear molecules the number of internal coordinates is $3M-5$.

Nuclear vibrations can be discussed on the basis of the Schrödinger equation, similar to the electronic motion. Applying the Born–Oppenheimer approximation the basic equation is as follows

$$\hat{H}_n(\mathbf{R})\psi_n(\mathbf{R}) = E_v\psi_n(\mathbf{R}) \tag{3.17}$$

where $\mathbf{R} = \{x_1, x_2, \ldots, x_{3M-6}\}$ is the vector of the internal nuclear coordinates. The nuclear Hamiltonian writes

$$\hat{H}_n(\mathbf{R}) = \hat{T}(\mathbf{R}) + \hat{V}(\mathbf{R}). \tag{3.18}$$

The first term represents the kinetic energy while the second stands for the potential energy, which is just the potential surface given by Eq. (3.1). The latter has to be determined first to solve Eq. (3.17). This is a complicated task. Furthermore, if no simple analytical expression for $\hat{V}(\mathbf{R})$ is known, formidable mathematical problems arise in treating Eq. (3.17). Therefore, the potential surface is usually expressed in the form of a Taylor series

$$V = V_0 + \sum_a f_a \Delta x_a + \frac{1}{2}\sum_{a,b} f_{ab}\Delta x_a \Delta x_b + \frac{1}{6}\sum_{a,b,c} f_{abc}\Delta x_a \Delta x_b \Delta x_c + \ldots \tag{3.19}$$

where Δx_a, Δx_b, Δx_c, etc. are relative coordinates giving displacements from the equilibrium geometry corresponding to the minimum of V. For the sake of simplicity, V_0 can be put equal to zero by shifting the origin of the energy scale. Furthermore, the forces f_a (first derivatives of V with respect to Δx_a) vanish at the equilibrium geometry; therefore only second and higher order terms survive in Eq. (3.14).

The potential curve of diatomic molecules is often approximated by a *Morse function* [937]:

$$V = D_e[1 - \exp(-\beta\Delta R)]^2 \tag{3.20}$$

where D_e is the dissociation energy ΔR is the distortion from equilibrium and β is an empirical constant.* By expanding Eq. (3.20) into series we have for small ΔR values $V \approx D_e\beta^2\Delta R^2$ [234]. This latter expression corresponds to the second order term in Eq. (3.19).

If the potential is given by Eq. (3.19) the vibrational energy of a diatomic molecule can be written as [177]

$$E_v = hcv_e\left(v + \frac{1}{2}\right) - hcx_e v_e\left(v + \frac{1}{2}\right)^2 + \ldots \tag{3.21}$$

where $v = 0, 1, 2, \ldots$ is the vibrational quantum number; h is Planck's constant; c is the

* Usually D_e is substracted from V to ensure $V = 0$ at infinitely large distortions.

velocity of the light; $\nu_e = \frac{1}{c}(f_{RR}/\mu)^{1/2}/2\pi$ the wave number, *i.e.* the vibrational frequency, $1/\lambda_e$ where λ_e is the wavelength. f_{RR} is the force constant and the reduced nuclear mass is $\mu = M_a M_b (M_a + M_b)^{-1}$. The product, $x_e \nu_e$, is called the anharmonicity constant.

The special feature of Eq. (3.21) is that the energy does not become zero even if $v = 0$, which means that molecules vibrate even at absolute zero temperature. This is in agreement with the Heisenberg uncertainty relation. In fact, if the energy of the vibrating nucleus were zero, both its momentum (zero) and position (the equilibrium value) would have definite values simultaneously, which is impossible. The energy corresponding to $v = 0$, according to Eq. (3.21), is $E_0 = \frac{1}{2} hc\nu_e$; it is called *zero-point energy*. E_0 is important for example in determining dissociation energies of chemical reactions (*cf.* Sections 4.1 and 4.2). The characteristic band structure of the infrared spectra is due to the quantized nature of the vibrational energy as given in Eq. (3.21). The characteristic frequency shift in Raman scattering (*cf.* Section 3.7) also has the same origin.

If molecular vibrations are discussed quantum mechanically it is found that in the ground vibrational state the vibrating nuclei are located with greatest probability around the equilibrium position. Classical mechanics yields the opposite result: since the velocity of the vibrating mass point is maximal when passing the equilibrium geometry it is mostly located at turning points where the velocity becomes zero [234].

If one treats small-amplitude vibrations around the equilibrium it is enough to consider only the second-order terms in Eq. (3.19). This is the *harmonic approximation* for which Eq. (3.21) reduces exactly to the first leading terms on the right-hand side: $\frac{1}{2} \sum f_{ab} \Delta x_a \Delta x_b$. This means that the potential function is approximately replaced by a quadratic form. Deviation from the harmonic approximation is called *anharmonicity*. One of the consequences of anharmonicity is that the maximum probability position of the nuclei does not exactly coincide with the minimum on the potential surface. "Experimental" bond lengths are therefore found to be larger by some pm if anharmonicity corrections are also considered in the vibrational analysis. To give some impression of the differences we give in Table 3.6 the vibrational frequencies of the chloroform ($CHCl_3$) molecule as they were calculated in the harmonic and anharmonic approximations [234]. For comparison, experimental frequencies are also given. It is seen that for higher overtones, the anharmonicity corrections become more and more important.

A central point in treating molecular vibrations is the choice of the relative coordinates in Eq. (3.19). Since in the harmonic approximation we have only quadratic terms the mathematical expression greatly simplifies if the so-called *normal coordinates* (Q_i) are introduced. With these mixed terms vanish and the potential is a simple sum of

TABLE 3.6

Frequencies of the CH stretching vibrational transitions (cm^{-1}) from the ground to higher ($v = 1 \ldots 6$) vibrational levels in the $CHCl_3$ molecule [234]

Transition $v=0 \rightarrow n$	Harmonic	Anharmonic	Exp.	Relative intensity
1	3 019	3 019	3 019	170
2	6 038	5 912	5 912	15
3	9 057	8 679	8 677	0.55
4	12 076	11 320	11 318	0.08
5	15 095	13 835	13 850	0.001
6	18 114	16 224	16 270	0.0001

squares

$$V = \frac{1}{2} \sum_i k_i Q_i^2 . \tag{3.22}$$

The total vibrational energy can be thus written as a sum of independent terms. These correspond to the energies of so-called *normal modes of vibration*. In a hypothetical case, when just one normal mode is excited, all atoms of the molecule vibrate with the same frequency and in the same phase. Using normal coordinates, the quantum mechanical treatment is considerably simplified but, unfortunately, normal coordinates cannot be transferred from one molecule to the other or even to an isotope substituted version of the same molecule. Normal coordinates are applied primarily for investigating individual molecules (*e.g.* derivatives of dipole moments) but not for comparisons between different species.

For nonsymmetrical molecules it is better to choose coordinates which are directly linked to the chemical structure. These are, for example, the chemical coordinates mentioned in Section 3.1. Deviations of chemical coordinates from their equilibrium values are sometimes also called internal coordinates. For characteristic groups of atoms, like $—XY_3$ (*e.g.* methyl) or $\gtrless XY_2$ (*e.g.* methylene), appropriate combination of internal coordinates yields new ones which correspond to the local symmetry. Molecular vibrations are then described by internal or local symmetry coordinates. Since the latter, in general, differ from the normal coordinates, independent decomposition of the vibration energy as in Eq. (3.17) is impossible: vibrations get coupled. Vibrations depending exclusively on changes in bond lengths, bond angles and dihedral angles are called *stretching*, *bending* and *torsional* ones, respectively. Stretching vibrations usually have frequencies characteristic for the bond in question. Several types of bending vibrations are known: *in-plane deformation* ones, changing ABC bond angles, *out-of-plane deformation* ones which characterize the situation when an atom D changes its position relative to the ABC plane. Distortion is characterized by the bending of the CD bond from the ABC plane (*e.g.* rocking vibrations of CH

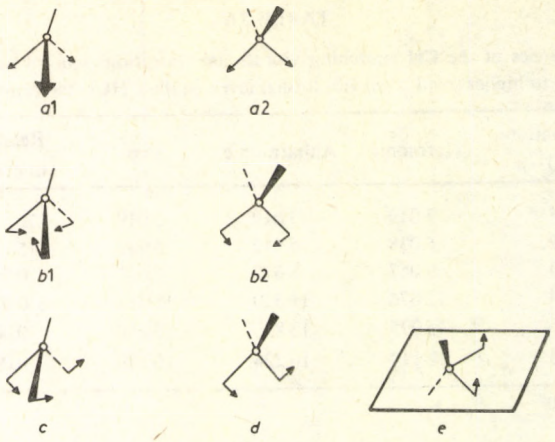


Fig. 3.7 Schematic representation of some simple vibration types. (a1): symmetric CH (methyl), (a2): symmetric CH (methylene), *(b):* scissoring, *(c):* rocking, *(d):* twisting, *(e)* wagging

groups in benzene). Torsional vibrations are observed if dihedral angles, mentioned in Section 3.1, are changing. Group vibrations involve a concerted movement of a group of atoms and can be constructed from various stretching and bending modes. Figure 3.7 depicts some of the more important vibration modes of groups of the types $—XY_3$ and $>XY_2$, respectively.

Let us see how force constants can be calculated by quantum chemistry. The most popular way is to obtain the second derivative of the potential surface by the force method [393, 1135], where the first and second derivatives are calculated analytically and numerically, respectively. To have a reliable value of the force constant it is sufficient to calculate the forces in two or three points near the equilibrium since their dependence on normal coordinates is nearly linear here.

Using sophisticated computer programs which include also electron correlation, vibrational force constants can be calculated with an accuracy close to that of their determination from the experimental data (see *e.g.* [874]). Some values for a couple of characteristic diatomics are given in Table 3.7. The Hartree–Fock calculations also yield good values though stretching and bending force constants are systematically overestimated. This can be corrected by appropriate scaling [1137]; thus the deviation between corrected *ab initio* and experimental values falls off to some few per cent [109]. Hartree–Fock calculations yield an especially good tool to predict coupling force constants though there are exceptional cases where the effect of correlation is also important [495]. The point is that the experimental determination of these quantities is uncertain; even the sign cannot be obtained from the analysis of the spectra in some cases. Calculated coupling force constants of ethylene were used by Pulay and Meyer [1138] to assign the experimental vibrational bands which was not possible without invoking the results of calculations. Another example is the work of Čársky *et al.* [181] who studied the Hückel $4n$ heterocycles, azirene, oxirene and thiirene. An experimental

TABLE 3.7

Stretching vibration frequencies (in cm^{-1}) for some diatomic molecules as calculated by various *ab initio* methods [900]

Molecule	Near HF	PNO-CI[a]	CEPA[a]	Exp.
LiH	1428.2	1408.6	1401.5	1405.7
CH	3044.1	2883.5	2841.7	2858.5
NH	3546.5	3342.6	3269.3	3282.1
OH	4045.5	3833.3	3743.6	3739.9
HF	4476.2	4251.5	4169.3	4138.7
NaH	1184.2	1172.1	1172.3	1172.2
HCl	3141.1	3034.0	2977.2	2991.2

[a] See Section 1.3.1

vibration spectrum is available only for thiirene but by making use of analogies for these closely related molecules, force constants for azirene and oxirene are predicted with a fair accuracy. The theoretical spectra for various isotope substituted derivatives of thiirene generally agree well with the experimental ones, but they strongly suggest that the C—S stretching frequency might be misassigned.

Reliability of some quantum chemical methods to estimate force constants can be judged from Table 3.8 [736, 1140]. It is somewhat astonishing how good the results obtained by the MINDO/2 method are. Similarly, the MINDO/3 method is able to predict vibrational force constants with a fair accuracy if an appropriate scaling procedure is applied [312]. The CNDO/2 method strongly overestimates stretching force constants, but scaling is possible [736, 1083], the method yields primarily qualitative information [592].

If force constants are defined in terms of internal coordinates, they are transferable among similar molecules to a large extent. This is a consequence of bond transferability, *cf.* 2.1. The most important consequence of the transferability of force constants is the transferability of group frequencies, which can be understood as follows. Let us treat a molecule AX consisting of two groups A and X. This is illustrated in Table 3.9 [110]. A mean value for the symmetric stretching force constant of the methyl group is *e.g.* $490.7 \pm 5.0\ Nm^{-1}$ and it changes only slightly for ethane, propane, propene, methanol and dimethylether. Coupling force constants are also well transferable.

If transferability breaks down this may usually be attributed to one of the following factors:

— inductive effect;
— conjugation, hyperconjugation;
— steric effects (ring strain, steric hindrance, rotational isomerism, etc.);
— tautomerism;
— external effects (phase, temperature, solvent).

For similar molecules, however, the above factors have similar effects and do not destroy transferability; thus it can be observed for a large variety of related compounds.

If the mass of the group X is considerably less than that of A its vibrations can be treated separately from the others. This is easy to see on the basis of classical mechanics: the moiety A has a large inertia, so its vibrations do not couple appreciably with those of X. An example is chloroform ($CHCl_3$) where $A = CCl_3$ and $X = H$. A similar situation is realized if the stretching force constant of the A—X bond is small in relation to that of the vibrating group of moiety X. This is the case for acetone (H_3CCOCH_3), where $A = H_3C—.—CH_3$, $X = \succ C{=}O$. If force constants are transferable, group frequencies also remain constant. This is exploited in practical IR spectroscopy to detect functional groups like —OH or —CN, based on their characteristic bands.

There is experimental evidence that force constants vary parallel to the bond strength and more generally, with the strength of the interaction between the atoms, the relative positions of which change in the given vibration. The interactions are strongest for covalent bonds, so stretching force constants are the largest (200–1000 Nm^{-1}).

TABLE 3.8

Experimental and theoretical force constants (Nm^{-1}) calculated by different methods [736, 1140]

Type	Molecule	HF	MINDO/2	CNDO/2	Experimental
Stretching					
Symmetric CH	CH_4	566.2	–	–	505.0
	C_2H_6	567.8	591	1380	490.0
	C_2H_4	594.3	482	1370	562.0
	C_2H_2	697.7	633	1500	639.1
CC	C_2H_6	507.3	510	1230	445.0
	C_2H_4	993.9	962	2300	939.5
	C_2H_2	1802	1829	3460	1595.3
Bending					
Scissoring	C_2H_6	75.6	52.2	81.1	60.6
	C_2H_4	55.6	32.2	57.9	47.0
Rocking	C_2H_6	85.0	52.9	80.9	68.2
Twisting	C_2H_4	62.8	41.0	59.9	57.2
Wagging	C_2H_4	32.2	22.0	40.4	24.3
CCH deformation	C_2H_2	36.7	26.7	66.9	25.8
Coupling					
CC/Symmetric CH	C_2H_6	+14.0	+44.0	+55.7	–
	C_2H_4	+13.6	+46.1	+65.1	+25.7
	C_2H_2	−13.4	+36.3	+41.5	−9.8
CC/Scissoring	C_2H_6	+39.0	+35.7	+45.9	+34.6
	C_2H_4	+24.2	+26.6	+39.5	+22.2
Scissoring/ Scissoring	C_2H_6	+3.3	+3.9	+4.3	+3.3
	C_2H_4	+2.4	+2.0	+2.7	+1.8

Nonbonded interactions are considerably weaker. They are relatively large for the X–Y interactions in groups of the type XAY, as in this case the XY distance is relatively small. This type of interaction determines the bending force constants which are by about one order of magnitude smaller than stretching ones. Torsional vibrations affect the mutual positions of atoms which lie relatively far from each other. The energy effects are small, so torsional force constants are by a further order of magnitude smaller than bending ones.

TABLE 3.9

Transferability of force constants in saturated molecules. The data are taken from *ab initio* calculations [110]

Type	C_6H_6	C_3H_8	C_3H_6	CH_3OH	$(CH_3)_2O$
Symmetric CH stretching	492.9	490.7	486.5	495.7	485.8
CC(O) stretching	431.2	429.8	466.0	526.7	519.3
Scissoring HCH	56.4	55.5	57.5	64.8	65.0
Rocking	65.3	64.2	66.3	87.9	85.6
CC(O) stretching/ symm. CH stretching	11.4	11.4	11.5	26.8	29.1
CC(O) stretching/rocking	32.2	31.2	32.3	52.0	54.1

We have mentioned in Section 2.1 that the bond strength varies parallel to the quantum chemical bond order index. The same is valid for stretching force constants: the larger the bond order the larger the force constant. This rule is often used in a quantitative form, as in the paper of Perrin and coworkers. They derived the following relation between CNDO/2 off-diagonal density matrix elements and CH stretching force constants, k_{CH}

$$k_{CH} = 791 P_{1sH,\,2sC} + 94 P_{1sH,\,2p_xC} \text{ Nm}^{-1}. \tag{3.23}$$

The 2_{p_x} orbital is directed to the carbon atom. Equation (3.23) reproduces experimental force constants for more than twenty molecules with an error of ± 0.3 Nm^{-1} (0.1 per cent) [1083].

It was shown in Section 3.1 that bond lengths and bond orders vary antiparallel. Comparing this with the statement in the previous paragraph it is logical that force constants and bond lengths vary antiparallel. Several empirical rules, demonstrating the validity of this statement, are known [460]. Maybe the best known is Badger's rule [50]

$$k_{AB}(R_{AB} - d_{ij})^3 = \text{const.} \tag{3.24}$$

Here k_{AB} is the AB force constant, R_{AB} is the equilibrium bond length, while d_{ij} is a constant with different values for different rows of the periodic table, *e.g.* $d_{22} = 68$ pm (N_2, O_2, CO, etc.), $d_{23} = 90$ pm (CS, PN, SiO, etc.).

3.4 ELECTRIC PROPERTIES

The chemical behaviour of molecules depends on the charged particles they are composed of: the electrons and the nuclei. The distribution of these particles gives the overall charge density of the molecules, which is one of their most important characteristics. The charge distribution determines the behaviour of molecules in electrostatic fields and it has an important role in the description of the reactivity. We treat some aspects of the molecular charge distribution in Section 3.4.1. The charge density and the electric field at the nuclei are important in the interpretation of Mössbauer and nuclear quadrupole resonance spectroscopic data: this problem is discussed in Section 3.4.2. The behaviour of molecules in electrostatic fields is discussed in Section 3.4.3.

3.4.1 CHARGE DISTRIBUTION

Experimental methods: X-ray diffraction [343], microwave spectroscopy [469].

The atoms and molecules are composed of charged particles; nuclei and electrons. The average distribution of these particles is defined by the probability densities associated with the nuclear and electronic wave functions, respectively. The overall charge distribution of a molecule containing N electrons and M nuclei is the expectation value of the following operator:

$$\hat{\rho}(\mathbf{r}) = -\sum_{i=1}^{N} \delta(\mathbf{r}-\mathbf{r}_i) + \sum_{A=1}^{M} Z_A \delta(\mathbf{r}-\mathbf{R}_A) \tag{3.25}$$

where $\mathbf{r}_i$ and $\mathbf{R}_A$ are electronic and nuclear coordinates respectively, Z_A is the nuclear charge and $\delta(\mathbf{x})$ is Dirac's delta function. The total charge distribution $\rho(\mathbf{r})$ can be decomposed into an electronic $\rho_{el}(\mathbf{r})$ and a nuclear $\rho_{nucl}(\mathbf{r})$ contribution:

$$\rho(\mathbf{r}) = \rho_{el}(\mathbf{r}) + \rho_{nucl}(\mathbf{r}). \tag{3.26}$$

In the framework of the Born–Oppenheimer approximation it is reasonable to consider the nuclei as simple point charges Z_A fixed at their equilibrium positions. On the other hand, the electron density associated with the probability distribution derived from the electronic wave function corresponding to the equilibrium nuclear configuration, is a continuous function, which falls off to zero only at infinity.

There are several alternative ways for the pictorial representation of the electron densities. The simplest method is to draw contour maps representing isodensity curves in a specified plane of the molecule (Fig. 3.8). More instructive are the plots of cross-sectional electron density diagrams. An example is presented on Fig. 3.9 for the case of the water electron density in the molecular plane. It is apparent that $\rho_{el}(\mathbf{r})$ has its highest value in the nuclear regions and falls off rapidly with increasing distances from the nuclei.

Still another possibility for the pictorial representation of electron densities is to use density shape plots, originally proposed for the illustration of molecular orbital shapes by Jørgensen and Salem [654]. One of the major advantages and attractive features of the electron density shape plots is that they are able to give a pictorial idea about the shape of the molecule itself. However, since the electron density decreases exponentially in all directions, the electron density value defining the encompassing envelope remains a matter of an arbitrary choice. Figure 3.10 represents a series of shape plots for water. It can be seen that if one chooses either too low (Fig. 3.10*a*) or too high (Fig. 3.10*e*) electron density value for the limiting surface, the resulting formation is practically spherical and conveys no information about the molecular shape. According to some authors, the electron density values characteristic of the regions of

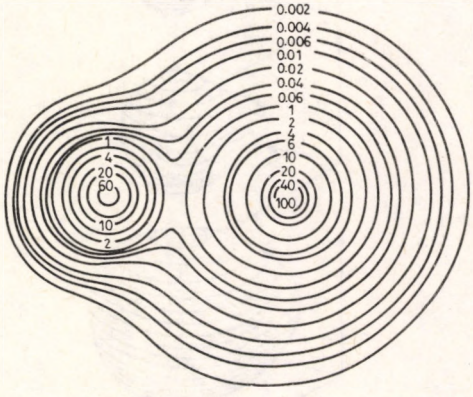


Fig. 3.8 Contour plot of the electron density in the LiF molecule. The electron density values corresponding to the contours are given in atomic units. (With permission from Ref. [1294])

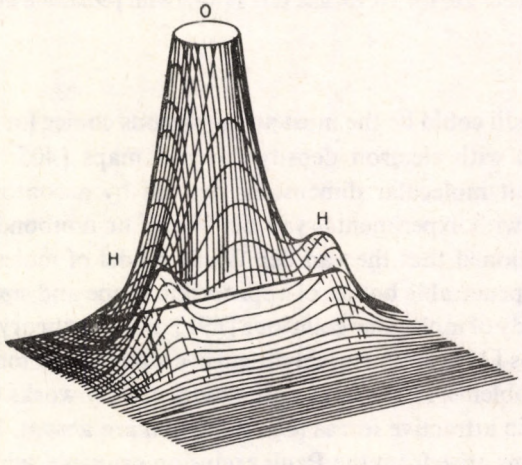


Fig. 3.9 Cross-sectional diagram for the total electron density of water in the molecular plane. (With permission from Ref. [1294])

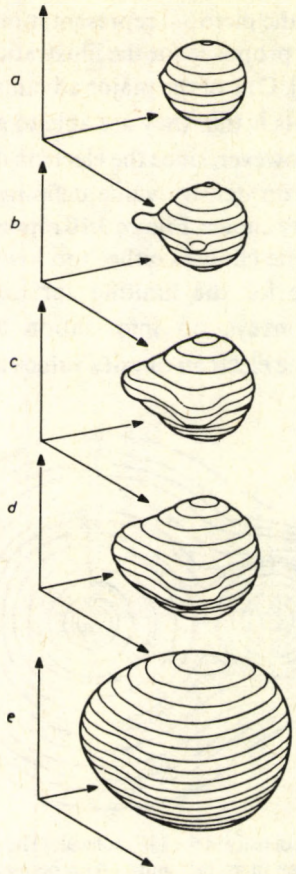


Fig. 3.10 Three-dimensional shape plots of the electron density of water. The contour surfaces correspond to electron densities of 2.0, 1.7, 1.0, 0.6 and 0.07 $e/(Å)^3$. (With permission from Ref. [1294])

the van der Waals radii could be the most advantageous choice for the representation of molecular shapes with electron density contour maps [405, 1405]. Bader and coworkers found that molecular dimensions defined by a contour of density 13.5 $e/(nm)^3$ agreed well with experimental van der Waals or nonbonded radii [46].

It should be mentioned that the van der Waals model of molecules, that is, their representation as impenetrable bodies of appropriate shape and size, has proved to be very useful in the study of molecular collisions [691] or in the theory of liquid structure and phase transitions [194, 195]. Harshly repulsive short-range forces play a decisive role in the above problems, so the hard-core model usually works well in these cases, provided that specific attractive forces (*e.g.* H-bonds) are absent. Remembering that short-range repulsions arise from the Pauli exclusion principle, which does not allow electrons on different molecules to be in the same place at the same time, it can be

understood that any attempt to push molecules together too closely will distort their electron distributions in such a way as to avoid such an overlap. At the van der Waals distances, the overlap of electron densities reaches that critical value, at which these forces become very strong and rapidly varying. However, any effort to find a quantitative quantum chemical criterium for molecular sizes seems useless. The actual "experimental" values of molecular radii depend strongly on the model, which has been set up for the phenomenon under study. For example, the molecular radius of methane varies between 0.33 and 0.42 nm [1314] depending on the specific experimental conditions.

Recently the electron density shape plots became popular in connection with molecular graphics facilities in computer aided rational drug design studies. The receptor–drug interactions are often supposed to be governed mainly by steric factors. In such cases the "chicken-wire electron density plots", as they are familiarly called [1170], are useful tools for the comparison of the shapes of potential drug molecules (Fig. 3.11).

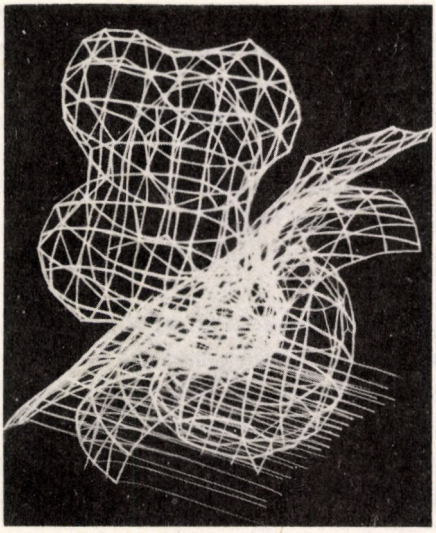


Fig. 3.11 The so-called "chicken-wire" representation of the electron density of a drug molecule. (With permission from Ref. [1170])

The detailed knowledge of the electron density in molecules is of central importance in elucidating many structural problems [58]. Platt wrote [1104]: "a theory of chemistry and the chemical bond is primarily a theory of electron density". This idea has been supported by the considerable success of the Hellmann–Feynman theorem [387, 545] in the study of molecular structure. According to this theorem the net force acting on a nucleus is the sum of electrostatic forces due to the electron distribution and to the other nuclei, *cf.* Eq. (1.20) in Section 1.2.2.

Another important theorem by Hohenberg and Kohn [584] states that under certain assumptions the energy of a nondegenerate ground state is a unique functional of the electron density. The theorem merely establishes the existence of such a functional, but does not give the way how to determine its explicit form. Much work has been devoted to find or approximate the appropriate functional. Density functional methods related to this approach may become powerful tools of future quantum chemistry.

Finally we note that the evaluation of expectation values of one-particle electrostatic operators (momenta, potentials, fields, etc.) involving only multiplication, but no differentiation or integration, reduces to a simple integral over the charge density function of the molecule:

$$\left\langle \Psi \left| \sum_{i=1}^{N+M} \hat{O}(\mathbf{r}_i) \right| \Psi \right\rangle = \int \hat{O}(\mathbf{r})\rho(\mathbf{r})\,\mathrm{d}\mathbf{r}. \tag{3.27}$$

The analysis of molecular electron charge distributions may help a lot in the understanding of the nature of chemical bonding [74]. When looking at the total electron density maps, it is very difficult to detect the characteristic features and subtle differences associated with bond formation. For this reason, in order to study bonding effects, the use of deformation density was proposed. The deformation density is the difference $\Delta\rho(\mathbf{r})$ between the molecular charge density $\rho(\mathbf{r})$ and the "reference density" $\rho_{\mathrm{ref}}(\mathbf{r})$ corresponding to the superimposition of the free atom densities arranged according to the molecular geometry [1196]:

$$\Delta\rho(\mathbf{r}) = \rho(\mathbf{r}) - \rho_{\mathrm{ref}}(\mathbf{r}). \tag{3.28}$$

The reference density $\rho_{\mathrm{ref}}(\mathbf{r})$ is chosen somewhat arbitrarily. According to the most widely accepted definition, $\rho_{\mathrm{ref}}(\mathbf{r})$ should be computed for the "*promolecule*", *i.e.* for the superimposed spherically averaged ground state charge densities of the constituting free atoms [569]. The free atom densities are usually determined with the same basis set as employed in the molecular calculation. When the bonding is presumed to be highly ionic, the sum of superimposed free ion densities may be the relevant reference state [45].

The basis set superposition error can be taken into account by calculating the free atom densities with the basis set of the whole molecule. Such corrections may be quite important in some cases, as it is illustrated on the example of LiH (Fig. 3.12).

Exhaustive examples for the use of various difference density maps have already been given in Part 2 dealing with chemical bonding; more details on this subject can be found there.

The experimental determination of electron densities and deformation densities in the crystal phase using X-ray diffraction techniques (sometimes combined with neutron diffraction experiments) [232, 389] is possible in the bonding regions with an accuracy of about 30 $e/(\mathrm{nm})^3$ and 50 $e/(\mathrm{nm})^3$, respectively [74]. The experimental error is much higher in the immediate vicinity of the nuclei [74]. Experimental densities

always contain the effect of thermal smearing due to lattice vibrations, which has to be considered as a correction when comparison with theoretical results is made. Only high quality quantum chemical calculations are able to compete with this experimental accuracy: sophisticated *ab initio* methods are necessary for calculating the electron density functions [1294].

The influence of the quality of the basis set may be enormous and it is now widely accepted that large, flexible basis sets, preferably of double zeta + polarization quality

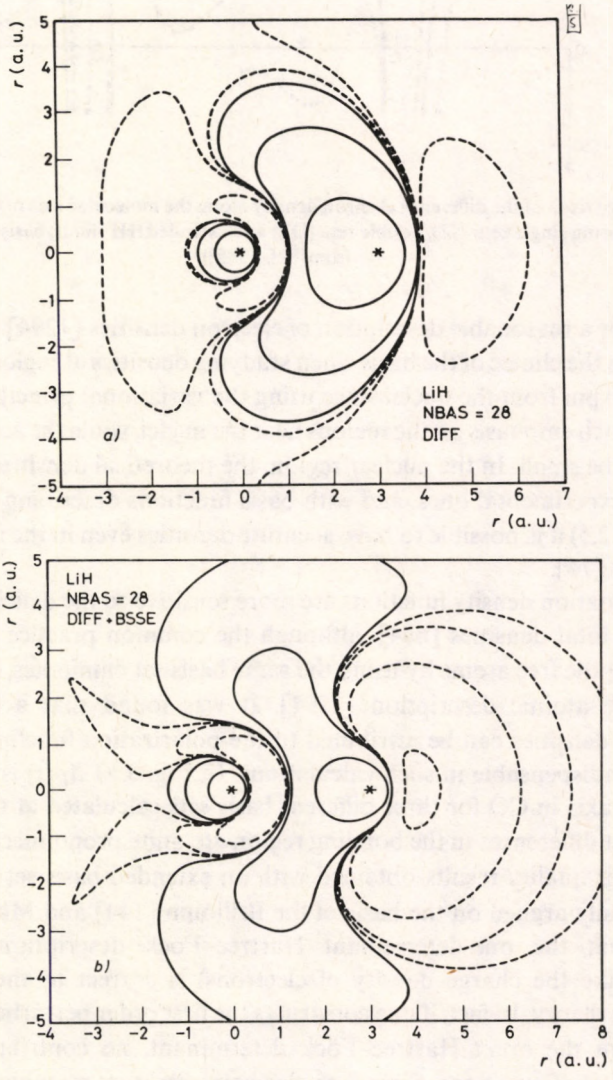


Fig. 3.12 Plot of the difference electron density of the LiH molecule *(a)* without and *(b)* with basis set superposition correction. Solid contour lines mean positive $\Delta\rho(\mathbf{r})$, (*i.e.* electron density excess w.r.t. the reference state), dashed lines mean negative $\Delta\rho(\mathbf{r})$ values. (With permission from Ref. [206])

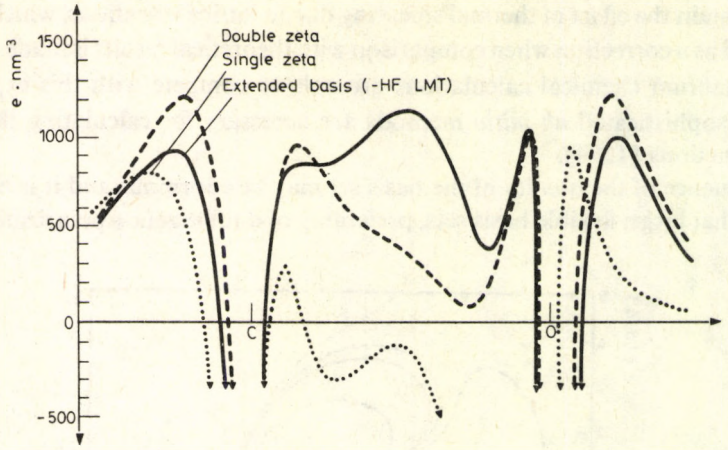


Fig. 3.13 Comparison of the difference electron density along the molecular axis of CO calculated by SCF wave functions using single zeta (SZ), double zeta (DZ) and extended (HF-limit) basis sets. (With permission from Ref. [385])

are needed for a reasonable description of electron densities [1294]. Special care must be devoted to the choice of the basis when studying densities at regions which are apart more than 30 pm from the nuclei since using the variational principle, one essentially places too much emphasis on the regions near the nuclei, while the accuracy in far-lying regions may be small. In the nuclear region, the theoretical densities are undoubtedly superior to experimental ones, and with basis functions describing properly the cusp (*cf.* Section 1.2.5) it is possible to have accurate densities even in the immediate vicinity of the nuclei [74].

The deformation density functions are more sensitive to the deficiencies of the basis set than the total densities [684], although the common practice of calculating the molecule and the free atoms by using the same basis set eliminates, at least partly, the errors in the atomic description [1294]. It was found that a large part of the deformation densities can be attributed to the polarization functions [171], so their presence is indispensable in such calculations. In Fig. 3.13 $\Delta\rho(\mathbf{r})$ is plotted along the internuclear axis in CO for three different basis sets calculated at the SCF level. It is apparent that differences in the bonding region are quite pronounced compared to the near HF-limit quality results obtained with an extended basis set [385].

It is generally argued on the basis of the Brillouin [144] and Møller–Plesset [942] theorems that the one-determinant Hartree–Fock description of one-electron properties (like the charge density of electrons) is correct to the second order of perturbation theory. In fact, if one constructs the first order perturbed correlated wave function from the *exact* Hartree–Fock determinant, no contributions come from monoexcited configurations. Since one-electron operators may have nonzero matrix elements only between determinants that differ by no more than one orbital, *cf.* Slater rules, Section 1.2.3., it is concluded that the expectation value of these operators (*e.g.* the

electron density) is correct to the second order. However, in practice it is impossible to get *exact* Hartree–Fock wave functions, and it has been shown [461] that any difference from the Hartree–Fock quality leads to one electron properties that are correct only to first order with respect to the extension of the bases set.

In actual calculations it turns out that the role of single excitations, coupled with the Hartree–Fock determinant through the double excitations, make the most important contribution to the correlation correction of the electron density [1294]. The effect of electron correlation can be represented by the difference plot of the correlated and uncorrelated electron charge densities. Studies using mainly the "all single and double excitations" configuration interaction method lead to the conclusion that correlation causes electrons to be drained from the bonding region and to accumulate behind the nuclei [1294]. This trend is quite well illustrated in the example of the water molecule, shown in Fig. 3.14.

Multipole moments. When overall characteristics of $\rho(\mathbf{r})$ are to be given quantitatively, the tabulation of the charge density function is rather impractical. Instead, various multipole moments of the charge distribution function can be evaluated for having a compact representation of the most important features of $\rho(\mathbf{r})$.

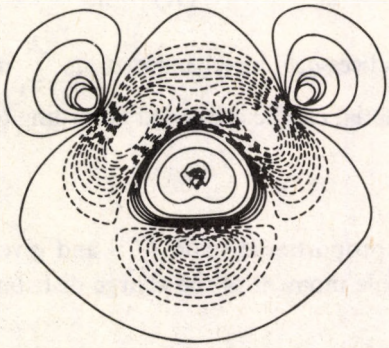


Fig. 3.14 Contour map of the correlational difference electron density $\Delta\rho_c = \rho_{corr} - \rho_{SCF}$ for water in the molecular plane. Positive and negative contours are drawn with solid and dashed lines, respectively. The contour values (e/bohr^3) are 0, ± 0.001, ± 0.0015, ± 0.002, ± 0.003, ± 0.004, ± 0.0045, ± 0.005, ± 0.0055, ± 0.006, ± 0.0065, 0.008, 0.02, 0.04, 0.08, 0.2 and 0.4. (With permission from Ref. [1294])

The multipole moments can be introduced by considering the potential $V(\mathbf{R})$ created by the molecular charge distribution $\rho(\mathbf{r})$ at the point $\mathbf{R}$:

$$V(\mathbf{R}) = \int \rho(\mathbf{r}) \, |\mathbf{R} - \mathbf{r}|^{-1} \, d\mathbf{r} \, . \tag{3.29}$$

We note that in the following the origin of the coordinate system is assumed to be selected somewhere within the volume occupied by the molecule and we are interested in the potential in those parts of the space (points $\mathbf{R}$), where $\rho(\mathbf{r})$ can be completely neglected owing to its exponential decay with the distance from the molecule in question (Fig. 3.15). Let us expand $|\mathbf{R} - \mathbf{r}|^{-1}$ in a Taylor series about the origin

according to the Cartesian components $r_\alpha(\alpha = x, y, z)$ of $\mathbf{r}$ [152, 153]:

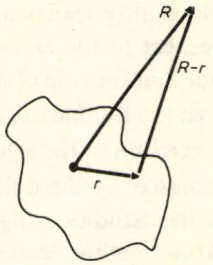


Fig. 3.15 Explanation of the meaning of the vectors **R**, **r**, and **R** − **r** in Eq. (3.29). The area within the curved line represents the charge distribution, the potential $V(\mathbf{R})$ is to be calculated at the point **R**

$$|\mathbf{R}-\mathbf{r}|^{-1} = \frac{1}{R} + \left(\frac{\partial}{\partial r_\alpha}\frac{1}{|\mathbf{R}-\mathbf{r}|}\right)_0 r_\alpha + \frac{1}{2!}\left(\frac{\partial^2}{\partial r_\alpha \partial r_\beta}\frac{1}{|\mathbf{R}-\mathbf{r}|}\right)_0 r_\alpha r_\beta + \ldots =$$

$$= \frac{1}{R} - r_\alpha \nabla_\alpha\left(\frac{1}{R}\right) + \frac{1}{2!} r_\alpha r_\beta \nabla_\alpha \nabla_\beta\left(\frac{1}{R}\right) - \frac{1}{3!} r_\alpha r_\beta r_\gamma \nabla_\alpha \nabla_\beta \nabla_\gamma\left(\frac{1}{R}\right) + \ldots \quad (3.30)$$

Hereafter the repeated indices $a_\alpha b_\alpha$ mean summation: $\sum_{\alpha=1}^{3} a_\alpha b_\alpha$ (Einstein convention). Using Eq. (3.30) the potential can be expanded according to the inverse powers of R:

$$V(\mathbf{R}) = \sum_{l=0}^{\infty} V_l(\mathbf{R}) \quad (3.31)$$

where the term $V_l(\mathbf{R})$ is proportional to $R^{-(l+1)}$ and gives the contribution to the potential due to the 2^l-pole moment of the charge distribution:

$$V_l(\mathbf{R}) = \frac{(-1)^l}{l!} T^{(l)}_{\alpha\beta\ldots\nu}(\mathbf{R}) \int \rho(\mathbf{r}) r_\alpha r_\beta \ldots r_\nu \, \mathrm{d}\mathbf{r} \,. \quad (3.32)$$

In the above equation the l-th order interaction tensors (l is just the number of suffixes) are defined as [153, 154]:

$$T = R^{-1}$$

$$T_\alpha = \nabla_\alpha R^{-1} = R_\alpha R^{-3}$$

$$T_{\alpha\beta} = \nabla_\alpha \nabla_\beta R^{-1} = (3R_\alpha R_\beta - R^2\delta_{\alpha\beta})R^{-5}$$

$$T^{(l)}_{\alpha\beta\ldots\nu} = \nabla_\alpha \nabla_\beta \ldots \nabla_\nu R^{-1} \quad (3.33)$$

and the integral

$$\int \rho(\mathbf{r}) r_\alpha r_\beta \ldots r_\nu \, \mathrm{d}\mathbf{r} \quad (3.34)$$

can be considered as a possible definition of the 2^l-pole moment of the charge

distribution [238]. For example, the overall *charge* of the system, or the *monopole moment*, is:

$$q=\int \rho(\mathbf{r})\,\mathrm{d}\mathbf{r} \tag{3.35a}$$

while the *dipole moment* components are:

$$\mu_\alpha=\int \rho(\mathbf{r})r_\alpha\,\mathrm{d}\mathbf{r}\,. \tag{3.35b}$$

Several alternative definitions can be found in the literature for the higher order ($l\geq 2$) moments. Let us consider the $l=2$ case. The diagonal elements of the second ($l=2$) moment tensor according to Eq. (3.34):

$$\langle r_\alpha^2\rangle=\int \rho(\mathbf{r})r_\alpha^2\,\mathrm{d}\mathbf{r} \tag{3.36}$$

measure the distance over which the charge distribution extends in the $r_\alpha(=x, y, z)$ directions of the space. The quantities $\langle r_\alpha^2\rangle$, the *second moments*, are frequently used to measure the size of the electronic charge distribution in various excited states in order to characterize the Rydberg nature of the state in question (*cf.* Section 3.6.2).

From another point of view it seems more convenient to define the $l=2$ moment in such a way that it measures the departure of the charge distribution from spherical symmetry. By virtue of the fact that $\left(\frac{1}{R}\right)$ satisfies Laplace's equation

$$T_{\alpha\alpha}(\mathbf{R})=0\,, \tag{3.37}$$

the $V_2(\mathbf{R})$ term can be rearranged as:

$$V_2(\mathbf{R})=\frac{1}{2}\,T_{\alpha\beta}(\mathbf{R})\int \rho(\mathbf{r})r_\alpha r_\beta\,\mathrm{d}\mathbf{r}=$$

$$=\frac{1}{3}\,T_{\alpha\beta}(\mathbf{R})\frac{1}{2}\int \rho(\mathbf{r})\,(3r_\alpha r_\beta-r^2\delta_{\alpha\beta})\,\mathrm{d}\mathbf{r}=\frac{1}{3}\,T_{\alpha\beta}(\mathbf{R})\Theta_{\alpha\beta}\,. \tag{3.38}$$

The quadrupole moment tensor $\Theta_{\alpha\beta}$, appearing in Eq. (3.38) is defined as

$$\Theta_{\alpha\beta}=\frac{1}{2}\int \rho(\mathbf{r})\,(3r_\alpha r_\beta-r^2\delta_{\alpha\beta})\,\mathrm{d}\mathbf{r} \tag{3.39}$$

and describes quadrupolar distortions of the charge distribution from spherical symmetry. Similar manipulations can be carried out on higher order terms and the following general definition of the l-th order contribution to the potential and of the corresponding multipole moment is obtained [154]:

$$V_l(\mathbf{R})=\frac{(-1)^l}{(2l-1)!!}\,T^{(l)}_{\alpha\beta\ldots\nu}(\mathbf{R})\xi^{(l)}_{\alpha\beta\ldots\nu} \tag{3.40}$$

$$\xi^{(l)}_{\alpha\beta\ldots\nu}=\int \rho(\mathbf{r})\frac{(-1)^l}{l!}\,r^{2l+1}\nabla_\alpha\nabla_\beta\ldots\nabla_\nu\left(\frac{1}{r}\right)\mathrm{d}\mathbf{r}\,. \tag{3.41}$$

The $\overset{\leftrightarrow}{\xi}^{(l)}_{\alpha\beta\ldots\nu}$ 2^l-pole moments are l-th order tensors, which are symmetric with respect to the interchange of any pair of suffixes (*e.g.* $\Theta_{\alpha\beta}=\Theta_{\beta\alpha}$) and they are reduced to zero on contraction (*i.e.* $\xi^{(l)}_{\alpha\alpha\ldots\nu}=0$, *e.g.* $\Theta_{\alpha\alpha}=\Theta_{xx}+\Theta_{yy}+\Theta_{zz}=0$). These properties imply that although a 2^l-pole moment has $(l+1)(l+2)/2$ distinct components, only $2l+1$ components are linearly independent in the most general case. Some of the independent components may be zero by symmetry [153, 154].

The above Cartesian tensor formalism is adequate for the study of low order multipole contributions to the potential, but a systematic investigation of higher order terms becomes tedious owing to the large number of distinct Cartesian multipole moment components. A much more compact formulation of the potential outside the molecular volume can be obtained if $|\mathbf{R}-\mathbf{r}|^{-1}$ is expanded into Neumann series

$$|\mathbf{R}-\mathbf{r}|^{-1}=\sum_{l=0}^{\infty}\sum_{m=-l}^{l}\frac{4\pi}{2l+1}\frac{r^l}{R^{l+1}}Y^*_{lm}(\Theta,\Phi)\,Y_{lm}(\vartheta,\varphi) \tag{3.42}$$

where $\mathbf{R}=(R,\Theta,\Phi)$ and $\mathbf{r}=(r,\vartheta,\varphi)$ are the spherical coordinates and Y_{lm} are the normalized spherical harmonics with Condon and Shortley phases* [238], *i.e.*

$$Y_{lm}(\vartheta,\varphi)=(-1)^m Y_{l-m}(\vartheta,\varphi)\qquad(m>0) \tag{3.43}$$

The l-th order contribution to the potential can be written as follows:

$$V_l(\mathbf{R})=\frac{1}{R^{l+1}}\sum_{m=-1}^{l}\left(\frac{4\pi}{2l+1}\right)^{1/2}Y^*_{lm}(\Theta,\Phi)Q^l_m \tag{3.44}$$

where the components of the l-th order multipole moment, Q^l_m are given in the spherical tensor representation as:

$$Q^l_m=\int\rho(\mathbf{r})r^l\left(\frac{4\pi}{2l+1}\right)^{1/2}Y_{lm}(\vartheta,\varphi)\,\mathrm{d}\mathbf{r}\,. \tag{3.45}$$

The Q^l_m tensors are irreducible representations of the 2^l-pole moments, *i.e.* all of their $2l+1$ components are linearly independent. Since the spherical tensor multipoles transform much simpler than the Cartesian ones, the use of the former representation is preferable in the theory of intermolecular forces, where the orientation dependent interactions can be conveniently written in terms of the multipole moments (and multipole polarizabilities) expressed in body fixed frame [480].

There is a one-to-one correspondance between the 2^l-pole moments in both representations. For example, the first order moment components in the spherical tensor representation Q^1_m, are related to the Cartesian dipole moment components μ_α by the following relations [480]:

$$Q^1_0=\mu_z \tag{3.46a}$$

* The phase of spherical harmonics is not standardized in the literature. The question of phase choice may cause some confusion in the relative phases of the multipole moment components, that is why the phase convention actually used always has to be specified.

$$Q^1_{\pm 1} = \mp \frac{1}{\sqrt{2}}(\mu_x \pm i\mu_y) \tag{3.46b}$$

where $i = \sqrt{-1}$.

Similarly, the second order moments Q^2_m can be expressed with the Cartesian quadrupole moment components as:

$$Q^2_0 = \Theta_{zz} \tag{3.47a}$$

$$Q^2_{\pm 1} = \mp \frac{2}{\sqrt{6}}(\Theta_{zx} \mp \Theta_{yz}) \tag{3.47b}$$

$$Q^2_{\pm 2} = \frac{1}{\sqrt{6}}(\Theta_{xx} - \Theta_{yy} \pm 2i\Theta_{xy}) . \tag{3.47c}$$

Higher multipole moments, like octupole- and hexadecapole moments ($\Omega_{\alpha\beta\gamma}$ and $\Phi_{\alpha\beta\gamma\delta}$ in the Cartesian representation), are not accessible to direct experimental studies. However, they may be quite important in the description of intermolecular electrostatic interactions.

The first nonvanishing multipole moment of a system is always independent of the choice of the origin, while all the higher order multipole moments are origin-dependent. For example the dipole moment of a system with a charge q is altered if one shifts the origin by $\mathbf{r}'$ as:

$$\mu'_\alpha = \mu_a - qr'_\alpha . \tag{3.48}$$

It follows from this relation that every ion has a centre of charge, that is, the point relative to which its dipole moment vanishes [154].

The number of nonvanishing independent multipole moment components is determined by the symmetry of the molecule. For example, heteronuclear diatomics ($C_{\infty v}$), directed along one of the coordinate axes, have only one nonzero dipole moment component. A homonuclear diatomic ($D_{\infty h}$) has one idependent quadrupole moment component, while the dipole moment obviously vanishes. (For any system with a centre of inversion the dipole moment is zero). In the methane molecule, which belongs to the T_d point group, the dipole and quadrupole moments are both zero, while the octupole and hexadecapole moments each have one-one independent components.

The computation of multipole moments proceeds by the evaluation of expectation values of operators in Eqs (3.41) or (3.45) over the molecular charge distribution. Analytical expressions for multipoles up to hexadecapole according to definition (3.41) can be found in the literature in terms of the density matrix elements and moment integrals over the atomic basis functions [850]. If Cartesian Gaussian basic functions are used, the moment integrals can be evaluated analytically in a simple way [879] by expressing explicitly the operators as homogeneous polynomials of the coordinates x, y, z. General expressions of this type for both multipole moment definitions have been given in Ref. [214].

Dipole moments are routinely evaluated in most quantum chemical calculations. In general, the Hartree–Fock approximation yields reasonable dipole moments. Concerning the role of the basis set, the same conclusion applies as to the charge density. It means that for an adequate description one needs at least double zeta + polarization quality basis sets [482]. In a series of diatomics the maximal error due to basis set deficiencies is about 0.7 to 1.4 10^{-30} Cm [482].

Difficulties in predicting the dipole moment of the CO molecule [481], for which SCF calculations yielded even the wrong sign, shed light to the role of electron correlation. Green [482] pointed out some interesting trends found in the error due to the neglect of correlation in diatomics. For molecules with single bonds the error is only 0.3 to 0.7×10^{-30} Cm. The general trend, that SCF dipole moments are larger than experimental ones (in an algebraic sense, with the convention that a positive value means A^+B^-, where B is the more electronegative) was supposed in [1294] to reflect the well-known property of the Hartree–Fock model of overemphasising in the wave function the ionic contribution compared to the covalent one.

It should be noted that the breakdown of Hartree–Fock theory in describing the dipole moment of the CO molecule is certainly not characteristic. In general the correlation causes only subtle changes in the electron charge density, as discussed above. This small redistribution proves to be sufficient in the case of carbon monoxide to alter the direction of the dipole moment of a very small absolute value [1294].

In Table 3.10 theoretical dipole moments calculated with *ab initio* SCF, SCF–CI and semiempirical CNDO/2 methods are compared with the best experimental data.

TABLE 3.10

Calculated and experimental dipole moments in 10^{-30} Cm units ($=0.29979$ D $=0.11795\ ea_0$)

Molecule	Hartree-Fock	Hartree-Fock and correlation	CNDO/2 [970]	Exp.
HF	6.41[a] [19, 844]	6.00 [19]	6.16	5.99 [774]
HCl	3.93 [860]	3.35 [860]	2.0	3.65 [774]
HCN	10.71 [873]	9.91 [789]	8.34	9.94 [994]
H_2O	6.65 [214]	6.25 [214]	7.16	6.19 [214]
NH_3	5.72 [214]	5.37 [214]	6.94	4.94 [842]
SO_2	6.74 [42]	–	13.18	5.44 [42]
CH_2O	9.99 [605]	8.76 [968]	7.55	7.77 [994]
CO[b]	−0.934 [481]	0.404 [850]	−2.13	0.374 [482]
CH_3NH_2	5.27 [873]	–	6.44	4.37 [994]
CH_3OH	6.14 [873]	–	6.36	5.67 [994]
CH_3F	6.61 [873]	–	5.59	6.17 [994]
Pyridine	7.55 [873]	–	7.08	7.37 [918]
Pyrimidine	8.14 [873]	–	5.48	8.07 [918]

[a] HF-limit

[b] Positive sign means that the dipole moment vector points towards the oxygen atom

TABLE 3.11

Calculated and experimental higher multipole moments: quadrupole moment $\Theta_{\alpha\beta}$ in 10^{-40} Cm^2 ($=0.29979\ 10^{-26}$ esu) octupole moment $\Omega_{\alpha\beta\gamma}$ in 10^{-50} Cm^3 ($=0.29979\ 10^{-34}$ esu) hexadecapole moment $\Phi_{\alpha\beta\gamma\delta}$ in 10^{-60} Cm^4 ($=0.29979\ 10^{-42}$ esu)

Molecule	Multipole moment component	Hartree–Fock	Hartree–Fock correlation	Exp.
CH_4	Ω_{xyz}	6.20 [18]	6.03 [18]	–
	Φ_{zzzz}	−10.70 [18]	−10.39 [18]	–
C_2H_6	Θ_{zz}	−4.30	–	−2.7 [155]
	Φ_{zzzz}	−24.9 [20]	–	–
C_2H_4	Θ_{xx}	6.27	–	6.9
	Θ_{yy}	−13.0 [20]	–	−13.5 [594]
	Θ_{zz}	6.72	–	6.6
C_2H_2	Θ_{zz}	23.8 [20]	–	28.0 [516]
	Φ_{zzzz}	72.7	–	–
NH_3	Θ_{zz}	−7.47 [214]	−7.03 [214]	−7.74 [994]
H_2O	Θ_{zz}	−0.598 [636]	–	−0.434 [1386]
	Θ_{yy}	7.697	–	8.339
HF	Θ_{zz}	7.69	7.58	7.37 [774]
	Ω_{zzz}	5.95 [860]	5.67 [860]	–
	Φ_{zzzz}	6.25	6.02	–
HCl	Θ_{zz}	11.87	11.49	11.78 [774]
	Ω_{zzz}	8.62 [860]	8.16 [860]	–
	Φ_{zzzz}	16.30	15.69	–

Ab initio investigations on quadrupole and higher multipole moments of molecules are less numerous (*e.g.* [18, 20, 944]). Accurate experimental values for quadrupole moment components are available only in a few cases [155, 396], and higher moments generally cannot be measured experimentally. Since the higher moments are usually origin-dependent, as they are not the first non-vanishing ones, the relative magnitude of the exactly known nuclear component, and of the approximately known electronic component may be varied by changing the origin. One expects that maximum reliability of the calculated moments can be attained by minimizing the electronic contribution. It was demonstrated that in this respect the centre of nuclear charges is the appropriate choice for the origin, although conventionally the centre of mass of the nuclei is usually chosen [214]. Some examples for calculated quadrupole, octupole and hexadecapole moments are given in Table 3.11.

In larger molecules, semiempirical methods can be applied for the calculation of multipole moments. The conventional Extended Hückel method overestimates the dipole moment [1166], but iterative Extended Hückel theory gives more or less reasonable charge distributions and multipole moments [1149]. The PPP-method has been used for estimating the π-component of molecular dipole [1142] or quadrupole

moments [378]; the effect of σ-skeleton has been considered in an approximate way, *e.g.* by using the Del Re procedure [1142], *cf.* Section 1.4.

When determining expectation values of one-electron operators, like the charge density or multipole moments, using semiempirical wave functions of ZDO-type, the question arises whether or not one should retain the ZDO assumption also in evaluating the moment integrals over atomic basis functions. For example, the consequent application of the ZDO assumption in dipole moment calculations with the CNDO wave function would lead to the expression:

$$\mu_{\mathrm{ZDO}} = -\sum_{\mathrm{A}} \sum_{\mu \in \mathrm{A}} P_{\mu\mu} \mathbf{R}_{\mathrm{A}} + \sum_{\mathrm{A}} Z_{\mathrm{A}} \mathbf{R}_{\mathrm{A}} = \sum_{\mathrm{A}} Q_{\mathrm{A}} \mathbf{R}_{\mathrm{A}} \tag{3.49}$$

where indices μ and A run over the atomic orbitals and atoms, respectively; $P_{\mu\mu}$ is the element of the charge-bond order (density) matrix; Z_{A} is the charge of the effective core of nucleus A, and Q_{A} is the net atomic charge. Thus the total dipole moment originates only from net atomic charges Q_{A}. However, it appears that another term, emerging from the monoatomic off-diagonal matrix elements of the dipole moment operator should also be considered if reasonable dipole moment values are required [1126]. This latter term, arising from the non-symmetrical nature of the atomic charge distributions in the molecule, is called the hybridization dipole moment component and reads:

$$\boldsymbol{\mu}^{\mathrm{hibr}} = \sum_{\mathrm{A}} \boldsymbol{\mu}_{\mathrm{A}}^{\mathrm{hibr}} = -\sum_{\mathrm{A}} \sum_{\lambda\sigma} P_{\lambda\sigma} \langle \lambda \,|\, \mathbf{r} - \mathbf{R}_{\mathrm{A}} \,|\, \sigma \rangle \,. \tag{3.50}$$

Similar approximations, retaining only monocentric matrix elements proved to be inappropriate for the calculation of the quadrupole moment with CNDO/2 [1165], since the contribution from the bicentric overlap densities is rather important for the quadrupole moment [1149]. Therefore a "reinterpretation" of the ZDO wave functions [1222] in terms of symmetrically (Löwdin-) orthogonalized atomic orbital basis is necessary and the expectation values should be calculated with this "deorthogonalized" density matrix. All mono- and bicentric matrix elements of the moment operator must be included. This method was found to be successful also for the calculation of the molecular electrostatic potential maps from CNDO/2 wave function [443].

Partitioning of the charge density. Much work has been done to define reasonable partitioning of the total charge (or electron) density of molecules [75]. The partitioning schemes constitute the basis for setting up model charge densities, which may be appropriate for interpretational purposes (in the understanding of the chemical bond [74]) or which can be used for the approximate evaluation of some one-electron properties (like multipole moments or electrostatic potentials and fields) [659], and for the calculation of intermolecular electrostatic interaction energies in multicentre–multipole expansions [222].

One possibility for the partitioning of charge densities involves the appropriate definition of boundary surfaces which enclose atomic or bonding regions in the molecule. Such a spatial partitioning scheme has been proposed, for example, by

Politzer and Harris [1115], who defined atomic regions such that in the limiting case of noninteracting atoms, the electronic charge associated with each one is the same as for the free atom. In linear molecules this can be realized by placing two planes perpendicular to the molecular axis such that the integrated promolecule density (see above) be equal to the negative of the nuclear charge Z_A. Politzer's idea has been generalized by Hirschfeld for molecules of more general shape [568].

An alternative spatial partitioning technique, which lies on a firm quantum mechanical basis, has been introduced by Bader [47, 48]. Making use of some general

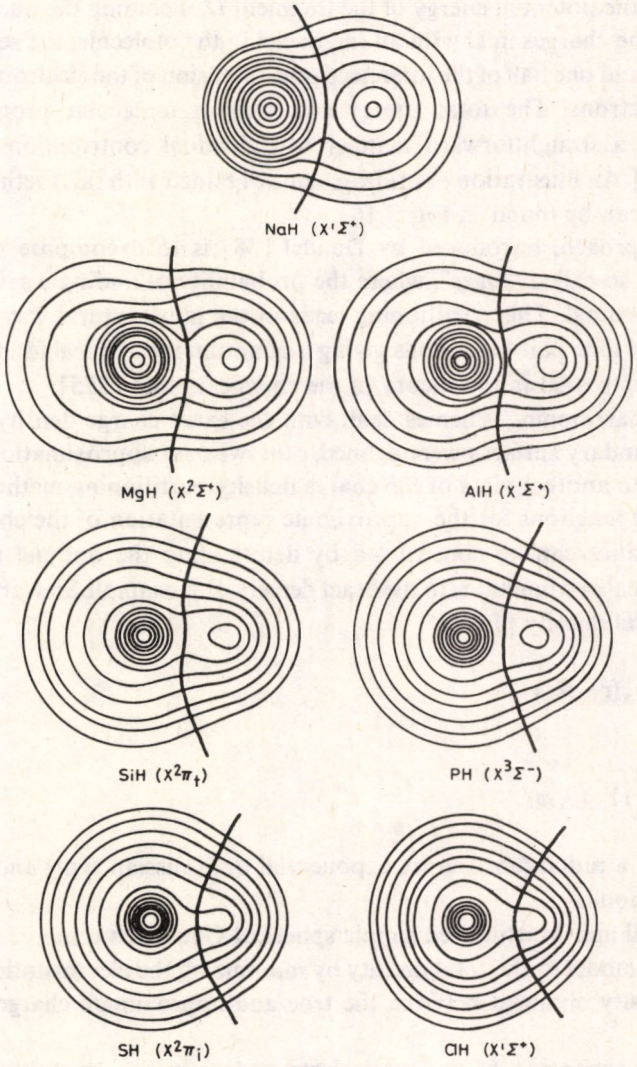


Fig. 3.16 Contour maps of the electron density in some hydrides with the virial partitioning surfaces indicated by dashed lines. (With permission from Ref. [49])

topological properties of the molecular charge distributions, he found that $\rho(\mathbf{r})$ can be divided into nonoverlapping atomic regions enclosed by boundary surfaces (the so-called "zero-flux surfaces") that satisfy the following equation:

$$\nabla\rho(\mathbf{r})\mathbf{n}(\mathbf{r})=0 \tag{3.51}$$

where $\mathbf{n}$ is the unit vector normal to the surface at $\mathbf{r}$. It can be shown that the kinetic energy, $T(\Omega)$ of such a fragment satisfies the following virial relationship [49], *i.e.*:

$$2T(\Omega)=-V(\Omega) \tag{3.52}$$

where $V(\Omega)$ is the potential energy of the fragment Ω, including the nuclear virial, the attraction of the charges in Ω with all the nuclei in the molecule, the self-repulsion of electrons in Ω and one half of the interelectronic repulsion of the electrons in Ω with the remaining electrons. The total energy and various molecular properties can be partitioned in a straightforward manner to individual contributions from atomic fragments [47]. An illustration of the fragments obtained with this method for second-row hydrides can be found in Fig. 3.16.

Another approach, introduced by Daudel [38] is to decompose the space into subspaces, the so-called "loges", where the probability of finding a given number of electrons is maximal. This partitioning leads in the most natural way to core loges, bond loges and lone pair loges, thus giving a quantum mechanical foundation for the classical concepts used in the theory of the chemical bond [275].

The above partitioning schemes dealt with the exact charge density function and only some boundary surfaces were defined; otherwise no approximations were made. We turn now to another class of the charge density partitioning methods, which use some localized functions for the approximate representation of the charge density.

Model densities can be constructed by determining the optimal fit of a set of appropriate localized functions to the exact density. For example Stewart proposed the following model density [1311]:

$$\rho_{\text{model}}(\mathbf{r})=\sum_{\text{A}}\rho_{\text{A}}(\mathbf{r}-\mathbf{R}_{\text{A}}) \tag{3.53a}$$

with

$$\rho_{\text{A}}(\mathbf{r})=\sum_{lm}R^{l}_{\text{A}}(r)\,Y_{lm}(\vartheta,\varphi) \tag{3.53b}$$

where $R^{l}_{\text{A}}(r)$ is a radial function (of exponential or Gaussian type) and $Y_{lm}(\vartheta,\varphi)$ is a spherical harmonics.

Instead, Hall and Martin used simple spherical Gaussians centered on the atoms, and fitted this model to the total density by minimizing the electrostatic energy of the difference density obtained between the true and approximate charge distributions [502].

The LCAO expansion of the total electron density can be written in terms of elementary distributions $\rho_{\lambda\sigma}(\mathbf{r})=\chi_{\sigma}(\mathbf{r})\chi_{\lambda}(\mathbf{r})$ as:

$$\rho_{el}(\mathbf{r}) = \sum_{\lambda} \sum_{\sigma} P_{\lambda\sigma} \rho_{\sigma\lambda}(\mathbf{r}) . \tag{3.54}$$

In the above expression two types of elementary distributions can be distinguished. The monocentric distributions with $\lambda, \sigma \in A$ are quite well-localized on the atomic centres A, while the diatomic overlap distributions ($\sigma \in A$, $\lambda \in B$ with $A \neq B$) are more-or-less diffuse. If one wishes to represent the density as a sum of pure atomic contributions the following approximation, originally proposed by Ruedenberg [1201], can be used for the division of two-centre overlap distribution to monocentric ones [178]:

$$\rho_{\sigma\lambda}(\mathbf{r}) = \chi_{\sigma}(\mathbf{r})\chi_{\lambda}(\mathbf{r}) \approx \frac{1}{2} \sum_{\mu \in B} \sum_{\beta \in B} s^{-1}_{\mu\beta} S_{\beta\sigma} \chi_{\mu}(\mathbf{r}) \chi_{\lambda}(\mathbf{r})$$

$$+ \frac{1}{2} \sum_{\nu \in A} \sum_{\alpha \in A} s^{-1}_{\nu\alpha} S_{\alpha\gamma} \chi_{\sigma}(\mathbf{r}) \chi_{\nu}(\mathbf{r}). \tag{3.55}$$

Here $S_{\mu\nu}$ is the $\mu\nu$ element of the overlap matrix, $s^{-1}_{\mu\beta}$ ($s^{-1}_{\nu\alpha}$) is the inverse overlap matrix of the AOs centered on B(A). Combining Eqs (3.54) and (3.55) and introducing the notation:

$$T_{\sigma\nu} = \frac{1}{2} \left\{ \sum_{\alpha \in A} \left(s^{-1}_{\sigma\alpha} \left[\sum_{B} \sum_{\lambda \in B} S_{\alpha\lambda} P_{\lambda\nu} \right] + \left[\sum_{B} \sum_{\lambda \in B} P_{\sigma\lambda} S_{\lambda\alpha} \right] s^{-1}_{\alpha\nu} \right) \right\} \tag{3.56}$$

the total electron density is approximately decomposed into a sum of monocentric elementary distributions:

$$\rho_{el}(\mathbf{r}) \approx \sum_{A} \sum_{\sigma,\nu \in A} T_{\sigma\nu} \rho^{(A)}_{\sigma\nu}(\mathbf{r}) . \tag{3.57}$$

We have outlined above some possibilities for the partitioning of the molecular charge distributions into components which can be assigned to individual atoms or bonds. One can consider the various multipole moments of these fragments as characteristic parameters of the total charge distribution. For example, the total charge (sum of the electronic and nuclear charges) of atomic fragments defined by one of the partitioning methods, yields the net atomic charge. It has to be emphasized in this respect that net atomic charges are not observables. There are methods yielding "experimental" atomic charges. They can be derived, for example, from XPS chemical shifts (*cf.* Section 3.6.2), or infrared intensities (*cf.* Section 3.7.2). However, these methods always include some theoretical model on which the analysis of experimental results is based. As a consequence the values of atomic charges thus obtained depend considerably on the model applied. One should keep in mind that "experimental" atomic charges have no deeper physical meaning, so their agreement or disagreement with theoretical values cannot be considered as an objective criterion of the quality of the quantum chemical method, of the wave function or of the partitioning scheme applied [492].

The most widely used definition of atomic charge, first given by Mulliken [950] (*cf.* Section 1.2.5) can also be obtained on the basis of the partitioning defined by Eq. (3.57). The gross atomic population q_A on atom A can be obtained by integrating the corresponding monocentric distributions:

$$q_A = \int \sum_{\sigma,\nu \in A} T_{\sigma\nu} \rho_{\sigma\nu}^{(A)}(\mathbf{r})\, d\mathbf{r} . \tag{3.58}$$

Using the fact that the integral of $\rho_{\sigma\nu}^{(A)}(\mathbf{r})$ gives $s_{\sigma\nu}$ Eq. (3.58) reduces to

$$q_A = \sum_{\sigma \in A} T_{\sigma\sigma} = \sum_{\sigma \in A} \sum_{B} \sum_{\lambda \in B} P_{\sigma\lambda} S_{\lambda\sigma} . \tag{3.59}$$

The net atomic charge Q_A is given by the following relation:

$$Q_A = Z_A - q_A . \tag{3.60}$$

In the LCAO formalism the above Mulliken charge has a privileged role. It has been shown for example that this definition has an associated operator [884, 886]. Since the validity of the approximation (3.55) depends strongly on the quality of the basis set (this relation would be exact only in a complete basis) the net charges derived from wave functions calculated with different basis sets may differ considerably. For example, two near Hartree–Fock quality wave functions, yielding practically the same energy and spatial electron density distribution, gave 0.23 and 0.48 as net charge of the hydrogen atom in hydrogen fluoride [1117]. This means that comparison of net atomic charges is allowed only when they are evaluated with the same basis set.

There have been many applications of Mulliken charges obtained with minimal basis STO-3G calculations for correlating chemical effects with the variation of the charge distribution. For example, the nature of substituent effects have been investigated in aliphatic [1359], unsaturated [1420], and aromatic [533] systems. The relationship of NMR chemical shifts [537], or ionization energies [1152] to Mulliken charges, substituent effects on energy and charge in various equilibria [536], effect of substituents on charged and neutral forms in proton transfer equilibria [1336], the possibility of obtaining scales of substituent-effect constants from theoretical calculations [905], all suggest that atomic Mulliken charges are chemically meaningful for comparison in a series of compounds [873]. The net atomic charges calculated from Mulliken population analysis and by direct integration of the charge density of an atomic fragment display similar variation in different molecules as is demonstrated in Fig. 3.17. Accordingly the net charges derived from simple semiempirical methods correlate well with various chemical effects.

Atomic charge definitions based on spatial partitioning schemes have the advantage of not being restricted only to LCAO wave functions, although their evaluation is rather cumbersome. For example, the atomic charges derived from Politzer's method correlate well with XPS chemical shifts and electronegativity differences [1112]. However, the linear relationship found between atomic charges obtained with the

spatial partitioning method [1420] and the Mulliken charges [873] add some confidence to the use of the latter in connection with LCAO wave functions for interpretational purposes.

In spite of the undoubted success of Mulliken charges for interpretational purposes, they proved to be less appropriate for the estimation of intermolecular electrostatic interaction energies and molecular electrostatic potentials or fields. The Mulliken charges are derived by dividing the charge of overlap populations equally between the atoms in question (Eq. (3.55)). Since the actual disymmetry of these two-centre

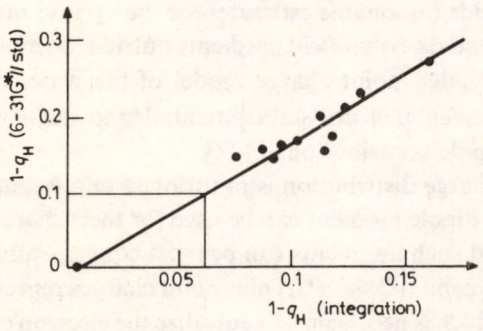


Fig. 3.17 Plot of the Mulliken atomic charges of the hydrogen in some CH_3X derivates *versus* the atomic charges obtained by direct integration of the charge density in the atomic region using 6–31G basis [873]

distributions is neglected in this way, the multipole moments (*e.g.* the dipole moment) calculated exclusively from Mulliken charges are wrong. This problem initiated several modifications in the LCAO definition of atomic charges, which conserve the multipole moments, or at least the total dipole moment of the molecule [656, 1351]. Only partial conservation of the dipole moment is attained with the method of Löwdin [818], who partitioned the bicentric distributions such that the dipole component along the internuclear axis be reproduced by the charges thus derived. For the purpose of intermolecular energy calculations, Claverie [222] suggested the use of effective atomic charges which reproduce the contribution of the hybridization dipoles to the total dipole moment in the CNDO framework. Numerical fitting of atomic charges in order to reproduce exact molecular multipole moments [70] or exact electrostatic potentials [262] has also been attempted. (See also the discussion in Section 1.2.5.)

However it seems that the use of point charges, the number of which is restricted to the number of atoms in the molecule, is not sufficient to yield a flexible description of both multipole moments and electrostatic potentials, and the construction of extended point charge models is required for this reason.

The mathematical properties of spherical Gaussians, used as basis functions in some *ab initio* methods, can be exploited for the construction of such extended point charge models. It is known that the product of two spherical Gaussians λ and σ with exponents

α_λ and α_σ centered at $\mathbf{r}_\lambda$ and $\mathbf{r}_\sigma$ is also a spherical Gaussian with exponent $\alpha_{\lambda\sigma}=\alpha_\lambda+\alpha_\sigma$ and centered at $\mathbf{r}_{\lambda\sigma}=(\mathbf{r}_\lambda\alpha_\lambda+\mathbf{r}_\sigma\alpha_\sigma)\alpha_{\lambda\sigma}^{-1}$. Thus all the elementary distributions appearing in the (3.54) expansion of the electronic charge density, reduce to spherical Gaussian distributions. According to the proposal of Hall these can be approximated by point charges placed at the centres of Gaussians [1338]:

$$\rho_{el}(\mathbf{r}) \approx \sum_{\lambda\sigma} P_{\lambda\sigma} S_{\lambda\sigma} \delta(\mathbf{r}-\mathbf{r}_{\lambda\sigma}) . \tag{3.61}$$

The point charge model of Eq. (3.61) conserves the total charge and dipole moment of the molecule and yields reasonable estimates for the various multipole moments, and the electrostatic potentials, fields, field gradients outside the molecular volume [1338]. Another type of extended point charge model of the water molecule, reproducing almost exactly the molecular electrostatic potential map, included 17 points selected to mimic atomic multipole contributions [122].

If the molecular charge distribution is partitioned into fragments each having zero resulting charge, the dipole moment can be used for their characterization. Following Gordon and England such fragments can be most conveniently defined as the charge density of a localized orbital $2\varphi(\mathbf{r})\varphi^*(\mathbf{r})$ plus point charges representing that fraction of the nuclear charge which is necessary to neutralize the electron charge. For example, in the case of a σ-bond, the charge of the two electrons are neutralized by two unit positive charges each placed at the nuclei, while for a lone pair a positive charge of value $+2$ is to be put at the atomic centre [463].

While the most interesting feature of atomic charges is their variation from one molecule to another, an appealing property of dipole moments associated with individual bonds (the bond dipole moments) is their relative independence of the molecular environment. This is the basis of the experimental interpretation of the measured molecular dipoles in terms of bond dipole moments [1293]. The "experimental" definition of bond dipoles is almost as controversial as that of the atomic charges. For example, in the case of the CH bond, arguments had been put forward for polarities of both type C^-H^+ and C^+H^- with absolute values ranging from 1.2 to 3.3 10^{-30} Cm [62, 1293]. (The generally accepted experimental value is $\mu(C^-H^+)=1.3\ 10^{-30}$ Cm.) CNDO/2 calculations predict $\mu(C^+H^-)=6.6\ 10^{-30}$ Cm [463]; an *ab initio* investigation yielded $\mu(C^+H^-)=5.7\ 10^{-30}$ Cm [564]. The calculated CH, NH, OH bond dipoles satisfy the expectations based on the electronegativity differences: $\mu(C^+H^-)=5.7\ 10^{-30}$ Cm $>\mu(N^+H^-)=3.7\ 10^{-30}$ Cm $>\mu(O^+H^-)=1.8\ 10^{-30}$ Cm [564], while the values used traditionally are $\mu(C^-H^+)=1.3\ 10^{-30}$ Cm, $\mu(N^-H^+)=5.0\ 10^{-30}$ Cm, $\mu(O^-H^+)=4.3\ 10^{-30}$ Cm [1293].

Bond polarities can be estimated on the basis of electronegativity differences, too. It was mentioned in Section 2.2 that electronegativity is a measure of the electron withdrawing power of an atom. In a molecule AB the electron population of A is the larger the greater is its electronegativity compared with atom B. Pauling [1070] proposed an empirical relation between the bond polarity and electronegativity

difference

$$\sigma_{AB} = 1 - \exp\left[-\frac{1}{4}(\chi_A - \chi_B)^2\right] \tag{3.62}$$

where χ_A and χ_B are the electronegativities, σ_{AB} is the bond polarity. According to Gordy [467] the relationship is linear

$$\sigma_{AB} = C(\chi_A - \chi_B)\,. \tag{3.63}$$

Summing the polarities for all bonds involving atom A we obtain the net charge

$$Q_A = \sum_B \sigma_{AB}\,. \tag{3.64}$$

If σ_{AB} is taken from Eq. (3.62) the more electronegative atom will be of negative polarity while the less electronegative one will be of positive polarity. A good correlation was found between the Pauling charges and, for example, the XPS chemical shifts [1273]. In the case of molecules containing delocalized bonds the approximation gets worse.

The bond polarity definition of Gordy can be rationalized on a quantum chemical basis. According to CNDO/2 calculations [970] on AH_n hybrides (A = Li, Be, B, C, N, O, F) the localizability on the H atom varies parallel to the orbital exponent differences of the atomic basis functions

$$l_H = 0.121\,(\zeta_H - \zeta_A) + 0.553 \qquad (r^2 = 0.986)\,. \tag{3.65}$$

The definition of l_H is given in Eq. (2.3). ζ_H is the exponent of the 1*s* orbital of hydrogen, ζ_A is the exponent of the 2*s* and 2*p* orbitals of A. The bond polarity can be related to the l_H localizability, which in turn determines the net charge on the hydrogen atom

$$\sigma_{AH} \approx Q_H \approx 1 - 2l_H\,. \tag{3.66}$$

The relation in Eq. (3.66) connects the localizability with the bond polarity. Since the orbital exponent and the electronegativity are related quantities (*cf.* Section 2.2), Eqs (3.63) and (3.65) express the same rule. An equivalent of the Gordy equation was derived by Hinze [565] in the framework of a very simple quantum mechanical model.

3.4.2 ELECTRON DENSITY AND ELECTRIC FIELD AT THE NUCLEI

Experimental method: Mössbauer spectroscopy [483].

In the description of the electron-nuclear interaction the nucleus is usually considered as a point charge. However, in reality the nuclei have small but finite volume: the effective ("charge") radius, R depends on the mass number A approximately as:

$$R = 1.20\,A^{1/3}\,10^{-13}\,\text{cm}\,. \tag{3.67}$$

The ground and excited (isomeric) states of the nuclei have different radii, so the electrostatic interaction with the electronic charge distribution is different in these states. Mössbauer spectroscopy [483] is able to detect extremely small shifts in the nuclear energy levels arising from the changes of the electronic charge density at the nucleus. The isomer shift δ of the Mössbauer transition, due to the above monopole charge interaction is given by [1396]

$$\delta = \frac{2\pi}{5} e^2 Z(\langle R\rangle_{IS}^2 - \langle R\rangle_{GR}^2)\,[\rho_A(0) - \rho_E(0)]\,. \tag{3.68}$$

where Z is the nuclear charge, the expression in the parentheses represents the difference between the mean square radii of the nucleus in the isomeric and ground states, $\langle R\rangle_{IS}^2$ and $\langle R\rangle_{GR}^2$, respectively. The square bracket stands for the difference of electron densities at the absorber (A) and emitter (E) nuclei, which are in different chemical environments, thus $\rho_A(0)$ and $\rho_E(0)$ are also different. The expression (3.68) can be written simply as a product of a nuclear (β) and of an electronic ($\Delta\rho(0)$) term:

$$\delta = \beta \Delta\rho(0). \tag{3.69}$$

The accurate theoretical determination of the nuclear factor β is almost impossible, since for the description of different nuclear states there is no reliable model, which would be able to predict the magnitude or even the sign of the change in the nuclear radius upon excitation. Using experimental data of isomer shifts and calculated electron density differences for d^5 and d^6 free ion configurations of iron, the relative change $\Delta R/R$ of the nuclear radius for the ^{57}Fe isotope, the most frequently used Mössbauer nucleus, was found to be about $(-0.5 \div -1.8) \times 10^{-3}$, with the effective radius of the ground state being larger than that of the excited state [1396]. It may be noted that the sign of the isomer shift has its origin in the fact that the lower the energy level of the nucleus the more compact is its charge distribution.

The theoretical evaluation of the electron density at the nucleus is a difficult, but manageable problem. In the nonrelativistic approximation, only the s electrons contribute to the density because atomic orbitals of higher principal quantum number have a node at the nucleus. This is not true any more in a relativistic approach where, for example, electrons on the relativistic p orbitals ($p_{1/2}$) may yield appreciable densities at the nucleus [1129]. According to the proposal of Shirley [1270] relativistic effects can be accounted for by applying a multiplicative correction factor, which is independent of the electron configuration and is a function of the nuclear charge only:

$$\rho_{el}^{rel}(0) = S(Z)\rho_{el}^{nonrel}(0). \tag{3.70}$$

The value of $S(Z)$ for ^{57}Fe isotope is about 1.3 [1270].

An accurate determination of $\rho_{el}^{nonrel}(0)$ would require the consideration of correlation effects as well. However, much simplification can be achieved due to the fact that for the theoretical interpretation of isomer shifts only the changes in the electron density are of interest. In a simplified model, proposed first by Walker, Wertheim and

Jaccarino [1396] the iron atom and the rest of the iron compound are treated separately. Accurate Hartree–Fock wave functions were used for the evaluation of the $\rho_{el}^{nonrel}(0)$ in various $3d$ electron configurations of the free iron atom, and less sophisticated molecular orbital methods were utilized to determine the appropriate effective oxidation state and electron configuration of Fe in the molecule. Then isomer shifts could be evaluated using the densities obtained for the free atom.

Accurate numerical Hartree–Fock calculations of Watson [1404] confirmed the expectation that the greatest (90%) contribution to the electron density at the nucleus comes from the $1s$ electrons; $2s$, $3s$ and $4s$ orbitals yield densities which are lower by an order of magnitude, while p and d electrons do not contribute at all. However, the electrons on these orbitals have an important influence on the s electron densities through electron–electron interaction. Some characteristic data for iron can be found in Table 3.12. It is apparent that the electron density $\rho_{el}(0)$ decreases with increasing d orbital occupation and that the occupation of the outer $4s$, and $4p$ orbitals have similar consequences [111]. Bloomquist *et al.* published interpolation formulas which can be used for the approximate evaluation of $\Delta\rho_{el}(0)$ for noninteger occupation numbers too [111]. This is very convenient when using simple semiempirical calculations for interpreting the data on isomer shifts. For example, Trautwein and Harris succeeded in reproducing experimental trends for iron complexes by combining the interpolation formula with the results of an iterative Extended Hückel method combined with spin-projected semiempirical CI calculations required for the proper description of spin-states [1366].

TABLE 3.12

The change of the electron density at the nucleus of ^{57}Fe atom in different electronic states [111] $\Delta\rho_{el}(0) = |\Psi_{el}(0)|^2 - 8.03 \times 10^7$ nm^{-3}

Change	Configuration	State	$\Delta\rho_{el}(0) \cdot 10^{-4}$
+4	$3d^4$	^5D	6.51
	$3d^3 4s$	^5F	17.07
	$3d^3 4p$	^5F	8.96
+3	$3d^5$	^4G	4.21
	$3d^4 4s$	^6D	12.65
+2	$3d^6$	^5D	2.53
	$3d^5 4s$	^5D	9.07
+1	$3d^7$	^4P	1.817
	$3d^7$	^2G	1.815
	$3d^6 4s$	^2D	6.01
	$3d^5 4s 4p$	^6H	8.14
0	$3d^8$	^3P	1.67
	$3d^8$	^1G	1.71
	$3d^7 4s$	^3D	3.91
	$3d^6 4s^2$	^3D	7.52
	$3d^6 4p^2$	^7P	2.52

Qualitative models have also been proposed for estimating isomer shifts. Factors affecting Mössbauer spectra of transition metal complexes were summarized by Shulman and Sugano [1272] on the basis of the Walker–Wertheim–Jaccarino model. They found that the occupation of 4*s* orbitals exerts a direct effect, while 3*p* and 3*d* orbitals have indirect effect on the *s*-electron distribution and consequently on the isomer shifts. If the metal–ligand bonding is due to the overlap of *d* orbitals of the metal with doubly filled ligand orbitals, the occupation of *d* orbitals increases due to the "back-donation" (*cf.* Section 2.8). This results in an enhanced screening of the 4*s*-electrons and the isomer shift increases. On the other hand, bonding interaction of *d* orbitals with empty ligand orbitals decreases the *d*-orbital occupancy. Owing to the decreased screening, the electron density and the isomer shift decrease also. It was found that the isomer shift changes linearly with the electronegativity of the halogen atom in the series FeF_2, $FeCl_2$, $FeBr_2$, FeI_2 [40].

Direct quantum chemical calculations on compounds containing Mössbauer nuclei is the most straightforward way to investigate characteristics of Mössbauer spectra. For example, isomer shifts of diatomic transition metal compounds have been interpreted by direct variational calculations using the X_α exchange interaction approximation (Au_2, FeX, X = transition metal) [487] and a similar SCF—X_α-scattered wave method was applied in the case of Fe_2 and FeCr [963]. Such refined calculations are able to predict even the hyperfine interaction parameters of the Mössbauer spectra: namely the quadrupole splitting (see below) and the magnetic hyperfine parameters (*cf.* Section 3.5) [1029, 1300].

The charge distribution of certain nuclei, with spin $S > \frac{1}{2}$, is nonspherical, and can be characterized by nonzero quadrupole moment Q. These quadrupolar nuclei, like deuterium, oxygen-17 or nitrogen-14 interact with the electric field gradient $F_{\alpha\beta}$ at the nuclear site. The electric field gradient tensor characterizes the spatial variation of the electric field created by other nuclei and the electrons, and in this way carries information about the chemical environment of the given nucleus. In the origin of the coordinate system the electric field gradient $F_{\alpha\beta}$ due to the molecular charge distribution $\rho(\mathbf{r})$ is given by:

$$F_{\alpha\beta} = \int \rho(\mathbf{r})[3r_\alpha r_\beta - \delta_{\alpha\beta} r^2] r^{-5} \, \mathrm{d}\mathbf{r}. \tag{3.71}$$

The interaction of the quadrupolar nucleus with the electric field gradient can be most conveniently expressed in a principal axis frame (where the $F_{\alpha\beta}$ tensor is diagonal) by the following "quadrupolar" Hamiltonian:

$$\hat{H}_Q = (1-R)\frac{e^2 Q F_{zz}}{4S(2S-1)}[3\hat{S}_z^2 - \hat{S}^2 + \frac{\eta}{2}(\hat{S}_+^2 + \hat{S}_-^2)]. \tag{3.72}$$

In this equation F_{zz} is the largest component of the electric field tensor in the principal axis system, (we suppose that $|F_{zz}| > |F_{yy}| > |F_{xx}|$), $\hat{S}$ is the nuclear spin, $\hat{S}_z$, $\hat{S}_+$ and $\hat{S}_-$ are the usual spin operators, Q is the nuclear quadrupole moment and η, the asymmetry

parameter is defined by the equation:

$$\eta = (F_{yy} - F_{xx})/F_{zz}. \tag{3.73}$$

The factor $(1-R)$ in Eq. (3.72) is the Sternheimer shielding factor [1308], which accounts for the polarization of the inner shell electrons by the quadrupolar field of the nucleus. The magnitude of the Sternheimer shielding was calculated by finite perturbation methods for some simple molecules [373].

Usually two parameters, the asymmetry parameter η, Eq. (3.72), and the nuclear quadrupole coupling constant ν_Q:

$$\nu_Q = \frac{e^2 Q F_{zz}}{h} \tag{3.74}$$

are used for the characterization of the nuclear quadrupole interaction in a given molecule. The most direct way for measuring this effect is by nuclear quadrupole resonance spectroscopy (NQR) [274, 483], but splitting of nuclear levels due to quadrupolar interactions can be detected in nuclear magnetic resonance or Mössbauer spectra too. While Mössbauer and NQR experiments are carried out in the solid phase,

TABLE 3.13

Comparison of calculated and observed field gradients [202]

Results from SCF MO calculations	O ‖ HCH	O ‖ HCF	O ‖ HCOH	HC(=O)O⁻
p_π	1.292	1.351	1.434	1.621
p_σ	1.313	1.245	1.251	1.318
Q_O	0.31	0.28	0.38	0.62
σ overlap pop.	0.584	0.763	0.773	0.398
π overlap pop.	0.433	0.417	0.393	0.264
eq_{yy}[a] (V_{zz})	−2.612	−3.310	−2.061	−1.742
eq_{xx}	1.916	1.425	1.093	0.420
eq_{zz}	0.697	0.786	0.968	1.322
e^2Qq/h, MHz	16.2	13.8	12.8	10.5
q_O[b]	0.47	0.28	0.06	0.51
Exptl results	O ‖ 4-ClC_2H_5CH	O ‖ C_2H_5CF	O ‖ $C_2H_5COC_2H_5$	HC(=O)O⁻
e^2Qq/h, MHz	10.65	8.51	9.50	7.34
	0.44	0.35	0.44	0.45
Q_O	0.84	1.03	0.92	1.17

[a] The labels *xx*, *yy*, *zz* refer to the diagonalized field gradient tensor. The field gradient tensors are labeled in accordance with the convention.
[b] Net charge on oxygen based on the Townes + Dailey analysis

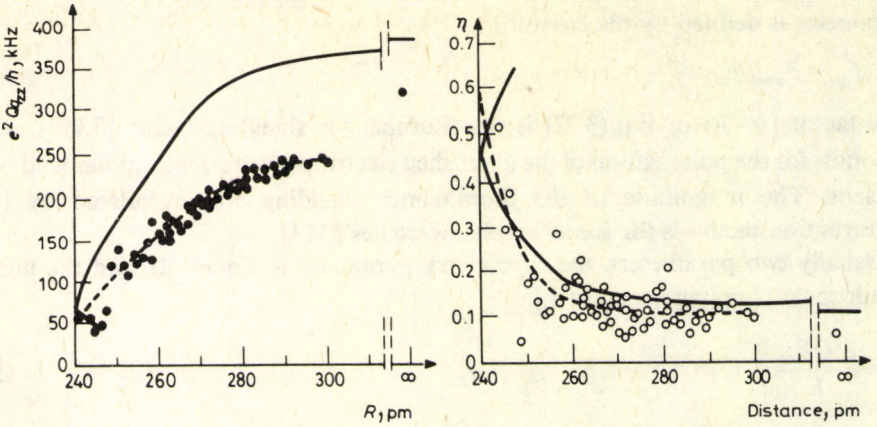


Fig. 3.18 Calculated and observed variation of *(a)* e^2Qq_{zz}/h and *(b)* η for deuterium in O—H...O hydrogen bonds as a function of the O...O distance [170]

in the liquid phase NMR measurements [1289], and in the gas phase microwave spectroscopy [469] can yield information about electric field gradients at the nuclei [833].

Since the electric field gradient operator has a $1/r^3$ dependence, one would expect that it is the inner shell electrons which mostly contribute to the field gradient at the nucleus. However this is not so, as the distribution of these electrons remains practically spherical even in bonded atoms, and the major effect is due to electrons and nuclei in the intermediate bonding region.

The simple model, put forth by Townes and Dailey in the early days of NQR spectroscopy, is based on the assumption that the electric field gradient tensor arises mainly from the imbalance in the populations of the valence level p and d orbitals centered on the atom in question [1360]. Let us consider the case of oxygen. According to the Townes-Dailey model the electric field gradient tensor can be written in terms of the p_σ and p_π populations and partial s characters of the bonding σ-hybrid orbitals. This simple model is appropriate to determine approximately the orientation of a principal axis frame on the atoms and makes possible the interpretation of the coupling constants and asymmetry parameters in simple chemical terms.

In Table 3.13 results of *ab initio* SCF calculations on carbonyl-containing model molecules [202] are compared with some experimental data. Although the trends are predicted correctly, the calculated quadrupole coupling constants are systematically larger than the experimental ones. This discrepancy can be explained partly by the fact that neither Sternheimer shielding, nor solid state effects were considered. The *ab initio* calculations gave only partial support for the validity of the Townes–Dailey model in the case of carbonyl compounds.

The fine structure of H-bonds can also be studied by analyzing nuclear quadrupole interactions of D, ^{14}N and ^{17}O nuclei. The quantum chemical model calculations are

indispensable for the interpretation of experimental data. For example, oxygen-17 and deuterium NQR parameters were calculated for formaldehyde–water complexes by an *ab initio* SCF method [170]. The comparison of the calculated and observed behaviour of the coupling constant, ν_Q and of the asymmetry parameter η as the function of the O...O distance is presented in Fig. 3.18. The agreement of theoretical and experimental results is very good. This enables us to assign O...O distances with high accuracy to solid state hydrogen bonds [170]. For further examples see Refs [1041] and [1162].

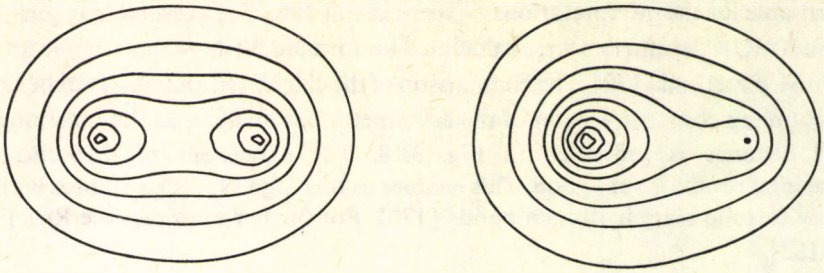
3.4.3 MOLECULES IN ELECTROSTATIC FIELD

When a molecule is placed in an external electrostatic field it is polarized, that is, its charge distribution is more or less changed. This polarization can be regarded as resulting from a redistribution of the electrons (electron polarization) and to some extent from the displacement of equilibrium positions of the atoms (atom polarization). Relatively weak fields cause only slight distortions in the electronic cloud; application of stronger fields may result in an appreciable change of molecular geometry and by the breaking of some bonds even chemical reactions may be induced.

Molecular fields may have quite high values locally. For example, the electrostatic field at 560 pm (10 a.u.) away from a positive ion of a unit charge amounts to 0.1 a.u. = 5.1423×10^{10} Vm^{-1} = 1.7153×10^{7} esu. Experimentally it is rather difficult to produce such strong fields. The characteristic electric field strengths in field ionization mass spectrometric experiments [77] are about 10^{9}—10^{11} Vm^{-1}, while the field strengths realized in electrooptic studies are in the range of 10^{6}—10^{7} Vm^{-1}. Strong fields of about 5×10^{9} Vm^{-1} arise at metal–electrolyte interfaces, and similar values were found in the active sites of proteins [644]. There is a lot of evidence that such high fields are responsible for a series of interesting chemical phenomena. A knowledge of the behaviour of molecules in the presence of fields is also important in the study of intermolecular interactions.

A pictorial illustration of what happens to the electron density of a molecule placed in a uniform external field is shown in the example of the H_2 molecule [43] (Fig. 3.19). The field was applied in the direction of the molecular axis. The effect of small fields has almost no apparent influence on the electron density (Fig. 3.19 *a*), while a field of about 5.1×10^{10} Vm^{-1} induces considerable changes (Fig. 3.19 *b*). The same field applied perpendicular to the molecular axis causes much weaker distortions [43].

The effect of electrostatic fields on the geometry of ethylene has been studied by the semiempirical INDO method [1061]. In the only stable orientation of the molecule, the C=C axis is parallel to the field direction. When applying fields higher than 6×10^{10} Vm^{-1}, the ethylene molecule decomposes to a hydride anion and a $C_2H_3^+$ cation. The equilibrium geometry of CH_4, C_2H_4, NH_3 and CO in the presence of an external field has been studied by *ab initio* SCF calculations. Changes in the bond lengths and bond angles up to 3.5 pm and 8.1 degrees, respectively, were found, and it was concluded that homopolar bonds should become longer in the external field. The same holds for



(a) (b)

Fig. 3.19 Electron density map of the H_2 molecule without *(a)* and with the presence of external uniform electric field *(b)*. The applied field is directed parallel to the internuclear axis and it is of 0.1 a.u. magnitude. The contour lines correspond to 0.05, 0.10...0.35 a.u. (With permission from Ref. [43]).

heteropolar bonds, if the applied field points in the direction of the more electronegative atom (this is the stable orientation for most molecules) [965].

The Hamiltonian of a molecule placed in an external uniform field **F** is:

$$\hat{H}(\mathbf{F}) = \hat{H}^0 - \hat{\boldsymbol{\mu}}\mathbf{F}, \tag{3.75}$$

where $\hat{\boldsymbol{\mu}}$ is the dipole moment operator and $\hat{H}^0$ is the molecular Hamiltonian in the absence of the field. The energy $E(\mathbf{F})$ of the molecule can be expressed as a power series in the field strength **F** [154]:

$$E(\mathbf{F}) = E^0 - \mu_\alpha F_\alpha - \frac{1}{2}\alpha_{\alpha\beta}F_\alpha F_\beta - \\ - \frac{1}{6}\beta_{\alpha\beta\gamma}F_\alpha F_\beta F_\gamma - \frac{1}{24}\gamma_{\alpha\beta\gamma\delta}F_\alpha F_\beta F_\gamma F_\delta - \ldots \tag{3.76}$$

where E^0 is the energy of the molecule in the absence of the field, the suffixes $\alpha, \beta, \gamma, \delta \ldots$ stand for the x, y, z Cartesian components and summation over the repeated indexes is assumed. $\alpha_{\alpha\beta}$ is the element of the static dipole polarizability tensor, $\beta_{\alpha\beta\gamma}$ is the first hyperpolarizability, and $\gamma_{\alpha\beta\gamma\delta}$ is the second hyperpolarizability tensor of the molecule. (Here the Cartesian tensor notation is used for the polarizabilities, the corresponding spherical tensor expressions can be found, for example in Ref. [480]).

The meaning of the different polarizabilities can be understood by considering the total dipole moment in the presence of the field **F**. One can define the following derivative:

$$\frac{\partial E(\mathbf{F})}{\partial F_\alpha} = \frac{\partial}{\partial F_\alpha}\langle\psi(\mathbf{F})\,|\,\mathbf{H}(\mathbf{F})\,|\,\psi(\mathbf{F})\rangle \tag{3.77}$$

which can be expressed using the Hellmann–Feynman theorem as:

$$\frac{\partial E(\mathbf{F})}{\partial F_\alpha} = \left\langle \psi(\mathbf{F}) \left| \frac{\partial \mathbf{H}(\mathbf{F})}{\partial F_\alpha} \right| \psi(\mathbf{F}) \right\rangle = -\langle\psi(\mathbf{F})\,|\,\mu_\alpha\,|\,\psi(\mathbf{F})\rangle = -\mu_\alpha(\mathbf{F}) \tag{3.78}$$

i.e. the total dipole moment reads as:

$$\mu_\alpha(\mathbf{F}) = \mu_\alpha + \alpha_{\alpha\beta}F_\beta + \frac{1}{2}\beta_{\alpha\beta\gamma}F_\beta F_\gamma + \frac{1}{6}\gamma_{\alpha\beta\gamma\delta}F_\beta F_\gamma F_\delta + \ldots . \tag{3.79}$$

It means that $\alpha_{\alpha\beta}$ describes the polarization of the molecule, which is linear in the external field, while $\beta_{\alpha\beta\gamma}$ corresponds to the initial departure from the linear polarization law [154].

We note that we have applied here a conceptually different definition of the dipole moment than that used in Section 3.4.1, when discussing the calculation of the permanent multipole moments. In fact, in Section 3.4.1 the dipole moment components have been defined as the expectation values of the corresponding operators:

$$\mu_\alpha = \langle \psi \mid \hat{\mu}_\alpha \mid \psi \rangle \tag{3.80}$$

while according to Eq. (3.79) they are defined by the first derivatives of the field-dependent total energy function $E(\mathbf{F})$:

$$\mu_\alpha = -\left(\frac{\partial E(\mathbf{F})}{\partial F_\alpha}\right)_{\mathbf{F}=0} . \tag{3.81}$$

However, by the virtue of the Hellmann–Feynmann theorem, these definitions are completely equivalent for the *exact* wave function and for any approximate (variational) wave function, for which this theorem holds. For example, these definitions give identical dipole moments for the SCF wave functions in the Hartree–Fock limit, but neither SCF, nor limited (or even "full") CI wave functions obtained with finite basis sets satisfy the requirements of the Hellmann–Feynman theorem. In the latter case, owing to theoretical considerations, the definition according to Eq. (3.81) is to be preferred.

The static dipole polarizability, α can be expressed from the relations (3.75–3.79) as:

$$\alpha_{\alpha\beta} = \left(\frac{\partial^2 E(\mathbf{F})}{\partial F_\alpha \partial F_\beta}\right)_{\mathbf{F}=0} = \left(\frac{\partial \mu_\alpha(\mathbf{F})}{\partial F_\beta}\right)_{\mathbf{F}=0} . \tag{3.82}$$

This definition of the polarizability is applied in the finite perturbation theory (FPT), in connection with numerical differentiation techniques [1124]. There is another expression for the polarizability, which is based on the conventional ("infinitesimal") Rayleigh–Schrödinger perturbation theory [154]:

$$\alpha_{\alpha\beta} = \sum_{k\neq 0}^{\infty} \frac{\langle \psi_0 \mid \mu_\alpha \mid \psi_k \rangle \langle \psi_k \mid \mu_\beta \mid \psi_0 \rangle + \langle \psi_0 \mid \mu_\beta \mid \psi_k \rangle \langle \psi_k \mid \mu_\alpha \mid \psi_0 \rangle}{E_k - E_0} . \tag{3.83}$$

The polarizability tensor α is symmetric ($\alpha_{\alpha\beta} = \alpha_{\beta\alpha}$), and it can be brought to a diagonal form by a unitary transformation (principal axis transformation). The mean polarizability $\bar{\alpha}$ describes the spherically averaged response of the molecular charge density to the external field (the isotropic part of the polarizability) and it is defined as the average of the diagonal polarizability components:

$$\bar{\alpha} = \frac{1}{3}(\alpha_{xx} + \alpha_{yy} + \alpha_{zz}) \tag{3.84}$$

while the anisotropy of the polarizability, η is defined as:

$$\eta^2 = \frac{1}{2}[(\alpha_{xx} - \alpha_{yy})^2 + (\alpha_{xx} - \alpha_{zz})^2 + (\alpha_{yy} - \alpha_{zz})^2]\,. \tag{3.85}$$

The distortions of the charge distribution due to uniform field are of a dipolar nature, that is an additional dipole moment is induced. If the applied field is non-uniform, additional distortions corresponding to higher multipole moments arise. Let us expand the Hamiltonian in a multipolar series (the repeated suffixes mean summation):

$$\hat{H}(F_\alpha, F_{\alpha\beta}, F_{\alpha\beta\gamma} \ldots) = \hat{H}^0 - \mu_\alpha F_\alpha - \frac{1}{3}\Theta_{\alpha\beta}F_{\alpha\beta} - \ldots \tag{3.86}$$

where F_α is the field, $F_{\alpha\beta}$, $F_{\alpha\beta\gamma}$, etc. are its derivatives:

$$F_{\alpha\beta} = \frac{\partial F_\alpha}{\partial r_\beta}; \qquad F_{\alpha\beta\gamma} = \frac{\partial^2 F_\alpha}{\partial r_\beta \partial r_\gamma}. \tag{3.87}$$

The total energy of the molecule can be written again as a power series of the field and its derivatives:

$$E(F_\alpha, F_{\alpha\beta}, F_{\alpha\beta\gamma} \ldots) = E^0 - \mu_\alpha F_\alpha - \frac{1}{3}\Theta_{\alpha\beta}F_{\alpha\beta} - \frac{1}{15}\Omega_{\alpha\beta\gamma}F_{\alpha\beta\gamma} -$$

$$- \frac{1}{2}\alpha_{\alpha\beta}F_\alpha F_\beta - \frac{1}{6}C_{\alpha\beta,\gamma\delta}F_{\alpha\beta}F_{\gamma\delta} -$$

$$- \frac{1}{30}R_{\alpha\beta\gamma,\delta\varepsilon\varphi}F_{\alpha\beta\gamma}F_{\delta\varepsilon\varphi} - \frac{1}{3}A_{\alpha,\beta\gamma}F_\alpha F_{\beta\gamma} \ldots \tag{3.88}$$

where C and R are the quadrupole and octupole polarizabilities giving rise to quadrupole and octupole moments induced by the field gradient and by the second derivative of the field, respectively; A is the dipole–quadrupole polarizability and it gives both the dipole moment induced by a field gradient and the quadrupole moment induced by a uniform field. The dipole polarizability and hyperpolarizabilities are independent of the choice of origin, but all higher multipole polarizabilities are origin dependent [154].

It is worth mentioning attempts to apply the continuum dielectric theory to describe the effect of an external field on molecular scale. If the source of the nonuniform field acting on the molecule is the ensemble of neighbouring molecules, difficulties arise due to the divergence of multipolar expansions at small distances. As shown by Oxtoby [1053], this problem can be circumvented by introducing a local susceptibility (or polarizability) density per unit volume describing the field-dependence of the induced charge distribution for arbitrary non-uniform fields.

The theoretical determination of atomic or molecular polarizabilities and hyperpolarizabilities is a very difficult task. Several alternative approaches have been proposed, but the considerable difficulties encountered practically in all the treatments made accurate calculations rather scarce. Before discussing some of the current methods used for the evaluation of polarizabilities, two general remarks, valid for all these procedures, should be made. At first, the use of large, extended basis sets, involving polarization functions, seems indispensable for the reasonable description of polarizabilities [1330, 1411, 1412]. The desired flexibility of the basis set can be ensured in other ways too, for example, by using basis functions with field-dependent exponents [1212] or by introducing "field-induced polarization functions" [943]. The extension of minimal basis sets employed routinely in semiempirical methods, has proved to be crucial in improving the theoretical polarizabilities and polarizability anisotropies calculated even by these methods [1007, 1347]. Secondly, the role of electron correlation seems to be important, as it was revealed by recent systematic studies [1214, 1451].

Among the several possibilities for calculating dipole polarizabilities, the utilization of the formula, one obtains from second order RS perturbation theory is usually rather problematic. This is because in general it is impossible to find a complete set of many-electron states $\{\psi_k\}$ and the selection of an appropriate (incomplete but sufficient) set is quite difficult. However, procedures based on Eq. (3.83), yielded reasonable polarizabilities even when using SCF wave functions (*i.e.* without correlation corrections), provided that sufficiently large basis sets were employed [324, 1254].

Computational methods based on the FPT (finite perturbation theory) of the polarizabilities seem to be more practical. They consist of performing a series of quantum chemical (usually Hartree–Fock) calculations for the system placed in different external fields (the interaction with the field is included explicitly in the molecular Hamiltonian). For example, by solving the Hartree–Fock equations for several values of the field, the dipole polarizability can be calculated from the first order coefficient of the dipole moment variation* [1124, 1248]. The finite perturbation procedure is a quite general one: it can be easily extended to higher multipole polarizabilities and hyperpolarizabilities [1248] and its application in connection with other than SCF wave functions is also straightforward (see *e.g.* Ref. [19]). However, the FPT method is very time consuming, since the calculation of each component of each property requires separate calculations. This difficulty can be partly overcome by using analytical derivatives of the energy expression with respect to the field components [996, 1151].

As an alternative to the direct variational solution of the Hartree–Fock equations in the presence of an external field, the application of the Hartree–Fock perturbation

* One may use either Eq. (3.80) or Eq. (3.81) for the definition of dipole moment. Owing to the approximate character of the wave functions with these two procedures somewhat different values are obtained for the polarizabilities.

theory can be considered. The system of equations given by perturbation theory for the Hartree–Fock orbitals in the external field is coupled through electron–electron interactions: this is the coupled Hartree–Fock (CHF) theory [272, 1310]. Here the coupling means that the external perturbation does not act independently on each one-electron orbital. The system of CHF-equations must be solved iteratively. This feature was considered undesirable and simpler uncoupled schemes have been proposed to reduce computational effort [15, 763, 769]. In these uncoupled Hartree–Fock (UCHF) theories the change of electron-electron interactions under the influence of external field is left out. Nevertheless, it is possible to obtain reasonable polarizabilities, if appropriate corrections are made [770]. An uncoupled perturbation scheme has been derived in the framework of the Hartree–Fock–Slater SCF procedure, and was successfully applied for electric dipole polarizabilities [1369].

The variational–perturbational procedure, originally developed for polarizability calculations in atoms by Kirkwood [693], and later extended for molecules by Pople and Schofield [1125], (the KPS-method), proved to be an economic and quite successful way of evaluating various multipole polarizabilities [183, 1179]. The most appealing feature of the method is that one needs to know only the unperturbed wave function of the system. The polarizabilities can then be expressed in terms of moments of the electron density calculated over the unperturbed wave function. Although in principle this procedure is justified only for exact wave functions, quite good results are obtained even at the SCF Hartree–Fock level due to a fortunate cancellation of errors [1213].

The correlation effects on polarizabilities have been studied by different procedures, *e.g.* PNO–CI, CEPA [1411, 1412] or by perturbational approaches like MBPT [65, 943].

Static dipole polarizability and the dipole moment of hydrogen-fluoride has been investigated by several authors performing SCF calculations as well as using methods accounting for electron correlation. Figure 3.20 summarizes relevant literature data after Mukherjee [943] by plotting theoretical dipole moment values and mean polarizabilities. Calculations involving electron correlation agree well with experimental data, but the methods at the SCF level of sophistication underestimate the polarizability and overestimate the dipole moment. Further characteristic theoretical values of dipole polarizabilities as compared with experiment can be found in Table 3.14.

Using semiempirical MO methods, polarizability calculations have been made with finite perturbation procedures (PPP [1248], CNDO/2 [1007], INDO [136], MINDO [897]) and with Rayleigh–Schrödinger second order PT (CNDO/S [872]). The good agreement of MINDO/3 results with experiment should be mentioned [314], although extended basis set is recommended if correct polarizability anisotropies are required [897].

The polarizabilities are quite sensitive to intermolecular interactions. The polarizability of dimer species formed in collisions of noble gas atoms, for example, is

different from the sum of polarizabilities of individual atoms. The deviation is the collisional pair-polarizability [430]. Either supermolecule approach can be used for the calculation of this quantity [758], or continuum dielectric theory adapted to molecular scale can be applied [1052].

The polarizabilities of ions in a vacuum are considerably different from the values determined in the crystalline state. It was predicted long ago [383] that electronic

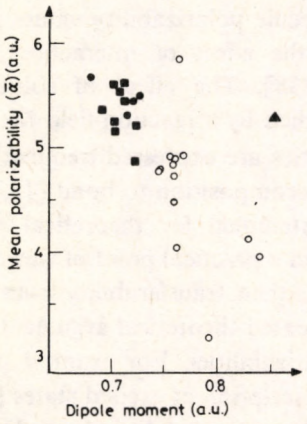


Fig. 3.20 Summary of calculated dipole moments and mean dipole polarizabilities of hydrogen fluoride. Open circles mean SCF level results, solid circles and squares mean beyond SCF calculations. The solid triangle corresponds to the result of a KPS-calculations [183]. The currently accepted experimental values are $\bar{\alpha}=5.5$ and $\mu=0.72$. (After Ref. [943]).

TABLE 3.14

Experimental and theoretical dipole polarizabilities (0.001 nm^3) calculated by different quantum chemical methods [897a]

Molecule	Component	Ab initio	MINDO/1	MINDO/2	MINDO/3 [314]	CNDO/2	Exp.
H_2	*xx*	0.0...0.80[a]	0.0	0.0	–	0.0	0.71
	zz	0.21...1.92[a]	1.02	0.47	0.76	0.46	1.03
N_2	*xx*	0.40...1.95[a]	0.60	0.60	–	0.39	1.53
	zz	1.10...5.75[a]	2.79	2.78	2.41	1.15	2.23
CO	*xx*	1.28...2.09[a]	0.95	0.90	–	0.71	1.80
	zz	1.67...4.80[a]	2.85	2.26	3.65	1.07	2.33
NH_3	*xx*	1.74	1.88	0.83	1.18	0.65	2.12
	zz	1.62	0.53	0.53	0.43	0.21	2.41
C_2H_4	*xx*	1.10...3.96[a]	3.72	2.00	–	1.09	–
	yy	0.50...3.38[a]	1.02	0.79	–	0.49	–
	zz	2.40...5.61[a]	5.45	4.29	–	2.46	–
	$\bar{\alpha}$	1.33...4.32[a]	3.40	2.36	–	1.35	4.22

[a] The results of calculations using different (variational, perturbational, etc.) methods fall within the indicated range.

polarizabilities of cations increase and those of anions decrease upon entering into a crystal from the free ion state. This was explained by the fact that the outer electron shell of a positive ion is loosening and that of a negative ion is tightening at the lattice site due to the Madelung potential (the electrostatic potential created by all the ions of the crystal) at the lattice site [1089]. The sensitivity of ion polarizabilities on crystal lattice effects have been demonstrated by calculations including Coulomb and exchange interactions using density functional methods [855]. In molecular crystal the deviation from the free-molecule polarizability values is expected to be smaller; its source is assumed to be the effect of interaction with induced moments on neighbouring molecules [838]. The effect of solvent environment on dipole polarizabilities has been studied by a reaction-field MO model [1177].

Experimental polarizabilities are expressed frequently as sums of bond polarizabilities [777, 778]. Similar decomposition to bond [13, 956] and atomic [897, 1169] contributions have been attempted for theoretical polarizabilities calculated by semiempirical methods. From a practical point of view an essential property of bond and atomic polarizabilities is their transferability from one molecule to another.

Several authors have presented theoretical arguments for explaining the observed transferability of bond polarizabilities. For example, Claverie [222] discussed the problem using an exciton description of excited states (*cf.* Section 3.6.3) entering the (3.83) expression of molecular polarizability. According to his analysis, there is a contribution to the bond polarizability which arises from the intrabond, localized excitations, and is essentially transferable from one molecule to another. However, the component of the bond polarizability, which can be associated with the interbond, charge transfer type excitations, depends strongly on the actual chemical environment of the given bond, thus giving rise to deviations from this transferability. Nevertheless, experimental bond polarizabilities obey the rule of additivity more closely than could be expected on a theoretical basis [777].

Pitzer considered the empirically found additivity of bond polarizabilities as fortuitous [1102]. He argued that owing to the effect of the induced moments in the surrounding bonds, the local electric field experienced by a given bond of a molecule should differ significantly from the external field [1102]. This idea of strong local fields proved to be quite fruitful in the refinement of the atomic polarizability model [33]. One can start from some transferable "basic" atomic polarizabilities and, by taking into account the mutual interactions of the induced atomic dipole moments a set of equations is obtained for the "effective" atomic polarizabilities which can be solved iteratively [1348]. This procedure has been found useful for the calculation of molecular polarizabilities as sums of atomic contributions.

We mention, that the local field effects discussed above must be non-negligible for bond polarizabilities too. However, owing to the relative invariance of the immediate surroundings of bonds, the variation of this effect from one molecule to another is small [222].

3.5 MAGNETIC PROPERTIES

Properties of molecules are influenced not only by electric but also by external magnetic fields. In the following we treat first the magnetic moments (Section 3.5.1), then possibilities for the theoretical calculation of the most important parameters in electron spin resonance (ESR) spectroscopy (Section 3.5.2) and nuclear magnetic resonance (NMR) spectroscopy (Sections 3.5.3, 3.5.4) will be discussed. The theory is presented in the non-relativistic form. Conceptually, relativistic theory is needed for a deeper understanding of the physics of magnetic properties and spin. However, a phenomenological inclusion of the spin into nonrelativistic quantum theory is also possible, and genuine relativistic effects can usually be considered as small corrections for atoms with atomic numbers $Z \lesssim 40$.

3.5.1 MAGNETIC MOMENTS AND SUSCEPTIBILITIES

Experimental methods: ESR [468, 1412a] microwave spectroscopy [469] magnetic permeability measurements [141a]

The energy change of molecules in magnetostatic fields can be decomposed into two parts, similar to that in the case of electrostatic fields. Accordingly, $E = E_m + E_s$, where E_m corresponds to the energy change due to the magnetic moment of the molecule, while E_s is caused by the diamagnetic susceptibility, which is analogous to the electrostatic polarizability [280a].

The expression for E_m is formally similar to the corresponding electrostatic one where the total interaction energy is determined by the electric moments of the molecule. The two different magnetic poles always occur together (no magnetic monopole has yet been found), therefore the term analogous to the electric charge q is absent. The contributions depending on the derivatives of the magnetic field are neglected; thus the energy change corresponding to the magnetic moment $\boldsymbol{\mu}^m$ in the non-relativistic approximation can be written as*

$$E_m = \sum_{\alpha=1}^{3} \mu_\alpha^m H_\alpha \equiv \mu_\alpha^m H_\alpha \tag{3.89}$$

where H_α is the α'th component of the magnetic field ($\alpha = x, y, z$). The magnetic moment can be calculated as the expectation value of the corresponding operators:

$$\mu_\alpha^m = \beta_B \langle \psi | \hat{L}_\alpha + g_e \hat{S}_\alpha | \psi \rangle \tag{3.90}$$

where $\beta_B = e\hbar/2m$ is the Bohr magneton (in SI units). The factor g_e is a universal constant characterizing the inherent magnetic moment of the free electron connected to its spin and having the value of 2.0023. (It may be useful to note that in the phenomenological nonrelativistic theory one has $g_e = 2$. The deviation from 2 is a

* In the second part of Eq. (3.89) the Einstein summation convention is adopted (*cf.* Section 3.4).

quantum electrodynamical correction.) The operator $\hat{L}_\alpha$ is the α'th component of the angular moment and $\hat{S}_\alpha$ is the operator of the α'th component of the resulting (total) electronic spin. The orbital momentum is defined as

$$\hat{\mathbf{L}} = \sum_{i=1}^{N} \hat{\mathbf{r}}_i \times \hat{\mathbf{p}}_i \tag{3.91}$$

where $\hat{\mathbf{r}}_i$ and $\hat{\mathbf{p}}_i$ are the position and linear momentum operators of the i'th electron, respectively. (We do not discuss here the small contributions due to nuclear spins.)

Accordingly, the magnetic moment of molecules consists of two parts. The first part corresponds essentially to the classical phenomenon of a moving charged particle which gives rise to a magnetic field. This classical analogy is not complete, however, because this magnetic field does not appear in the spatially non-degenerate states with all $\hat{L}_\alpha = 0$ ("orbital singlets"). Most organic molecules and free radicals belong to this category [280a]. Such states can be observed, for example, in atoms and diatomics, so the contribution of orbital momenta is important mainly in these cases. The states of polyatomic molecules described by spatially degenerate wave functions are unstable as a consequence of the Jahn–Teller effect (see Section 3.6.2). Because of the distortion, the contribution from the orbital moment disappears.

The spin can also give rise to magnetic moments in states with non-zero resulting spin (non-singlet states). This condition is obviously fulfilled by all molecules (free radicals) containing an odd number of electrons. There are also some molecules possessing an even number of electrons which have a non-singlet ground state. An example is the O_2 molecule whose ground state is a triplet.

The other contribution to the energy change of molecules in a magnetic field arises from the diamagnetic susceptibility. The applied magnetic field influences the motion of electrons, thus inducing a magnetic moment. The energy E_s, can be written as:

$$E_s \approx \frac{1}{2} \sum_{\alpha,\beta} \chi_{\alpha\beta} H_\alpha H_\beta \equiv \frac{1}{2} \chi_{\alpha\beta} H_\alpha H_\beta \,. \tag{3.92}$$

Here $\chi_{\alpha\beta}$ is the $\alpha\beta$ component of the diamagnetic susceptibility tensor. It consists of two parts:

$$\chi_{\alpha\beta} = \chi_{\alpha\beta}^{hf} + \chi_{\alpha\beta}^{L}$$

(see [280a]), where the first term $\chi_{\alpha\beta}^{hf}$ is the so-called high frequency contribution (incorrectly also called paramagnetic susceptibility by some authors); the second term $\chi_{\alpha\beta}^{L}$ is the so-called Langevin contribution (incorrectly: diamagnetic susceptibility). The term $\chi_{\alpha\beta}^{hf}$ can be presented in a form which resembles the expression Eq. (3.83) of the electrostatic polarizability:

$$\chi_{\alpha\beta}^{hf} = \beta_B^2 \sum_{k \neq 0} \frac{\langle \psi_0 | \hat{L}_\alpha | \psi_k \rangle \langle \psi_k | \hat{L}_\beta | \psi_0 \rangle + \langle \psi_0 | \hat{L}_\beta | \psi_k \rangle \langle \psi_k | \hat{L}_\alpha | \psi_0 \rangle}{E_k - E_0} \tag{3.93}$$

The Langevin term is determined by the following expression (in SI units):

$$\chi^L_{\alpha\beta} = \frac{e^2 a_0^2}{4m} \int \rho_{el}(\mathbf{r}) (r_\alpha r_\beta - r^2 \delta_{\alpha\beta}) \mathrm{d}\mathbf{r} \tag{3.94}$$

where a_0 is the Bohr-radius, $r^2 = r_x^2 + r_y^2 + r_z^2$, r_α being the α component of the position operator, and $\rho_{el}(\mathbf{r})$ is the ground state charge distribution. The values of the individual contributions to the diamagnetic susceptibility depend on the origin of the coordinate system, but the sum of all contributions is origin independent. The tensors $\chi_{\alpha\beta}$, ($\chi^L_{\alpha\beta}$ or $\chi^{hf}_{\alpha\beta}$) can be diagonalized by appropriate orthogonal transformations of the coordinate system. An inspection of Eq. (3.94) for the transformed (diagonalized) case shows that the diagonal elements of the Langevin term are necessarily negative. That is, the sign of the induced magnetic moment components is always opposite to that of the corresponding magnetic field component (diamagnetic behaviour). The high frequency term $\chi^{hf}_{\alpha\beta}$ usually has a smaller absolute value than the Langevin term. For this reason, most molecules with no permanent magnetic moment are diamagnetic. (See Ref. [1450] for BH as an exception.)

It is worthwhile noting that for well-localized σ-systems the susceptibility can be decomposed as a sum of bond contributions to a very good accuracy. This is indicated by the fact that the experimentally determined susceptibilities of saturated hydrocarbons can be calculated from the following empirical relation

$$\chi(C_nH_{2n+2}) = -1.136n - 0.576\ \mu\mathrm{J} \cdot \mathrm{T}^{-2}\,\mathrm{mol}^{-1} \tag{3.95}$$

with an accuracy of $\sim 1.5\%$. In this formula χ is the isotropic (averaged) value of the susceptibility:

$$\chi = \frac{1}{3}(\chi_{xx} + \chi_{yy} + \chi_{zz}) .$$

Eq. (3.95) agrees with the following scheme of additive bond contributions:

$$\chi(C_nH_{2n+2}) = (n-1)\chi_{CC} + (2n+2)\chi_{CH} ,$$

where χ_{CC} and χ_{CH} are the contributions due to CC and CH bonds, respectively. The value of the χ_{CC} and χ_{CH} bond contributions can be calculated theoretically by using localized MOs with good accuracy [570a]. We note also that the susceptibilities can be alternatively calculated in terms of atomic contributions as well [862].

It can be shown that the high frequency term $\chi^{hf}_{\alpha\beta}$ vanishes for free atoms if the nucleus is chosen as the origin of the coordinate system [96]. The calculation of the Langevin contributions is rather simple for atoms: one has only to evaluate the expectation value of r^2 and $r_\alpha r_\beta$ ($\alpha, \beta = x, y, z$) for the ground state wave function. This can be done with fair accuracy even in the one-particle approximation [280a].

For molecules, the computation of $\chi_{\alpha\beta}$ is more difficult since the high frequency contribution can be significant. Similar to the electrostatic polarizability, this term can be calculated by means of different approaches based on perturbation theory. Some results for small molecules are presented in Table 3.15.

The use of *ab initio* methods for determining the diamagnetic susceptibility of complicated molecules is rather difficult due to the significant increase of the necessary computational effort [500]. There are only a few calculations in the literature [570a, 600, 1409] using semiempirical all-valence electron schemes for this purpose. In turn, many attempts have been made to determine the diamagnetic susceptibility of homoaromatic molecules theoretically, mainly by means of the Hückel and PPP methods treated in Section 1.3.2. We discuss here the results in some detail (see also Ref. [280a]) for a review.

According to the experimental findings, the average diamagnetic susceptibility of aromatic compounds is surprisingly large (*e.g.* $-5.48\,\mathrm{JT^{-2}\,mol^{-1}}$ for benzene, $-22.0\,\mathrm{JT^{-2}\,mol^{-1}}$ for coronene). The anisotropy, $\Delta\chi$, of the susceptibility tensor is rather large as well. The anisotropy is defined by the following equation

$$\Delta\chi = \chi_{\perp} - \chi_{\parallel} \tag{3.96}$$

where $\chi_{\perp}$ denotes the component which is perpendicular to the molecular plane, while $\chi_{\parallel}$ stands for the parallel component. The value of $\Delta\chi$ for benzene is -5.97, for coronene $39.0\,\mathrm{J\,T^{-2}\,mol^{-1}}$. This phenomenon is related to the aromaticity of these molecules (*cf.* Section 2.6). The anisotropy of the diamagnetic susceptibility can be written to a good approximation as [280a]:

$$\Delta\chi = \Delta\chi^{\sigma} + \Delta\chi^{p} + \Delta\chi^{\pi} \tag{3.97}$$

where $\Delta\chi^{\sigma}$ and $\Delta\chi^{\pi}$ are the interatomic bond contributions due to the σ core and the delocalized π-system, respectively, while $\Delta\chi^{p}$ as an atomic p-orbital contribution. One usually assumes that $\Delta\chi^{p} < 0$, and it is often neglected in the simplest calculations. The

TABLE 3.15

Experimental and calculated values of averaged diamagnetic susceptibilities for some diatomics (J. $\mathrm{T^{-2}\cdot mol^{-1}}$) $\chi = \frac{1}{3}(\chi_{xx} + \chi_{yy} + \chi_{zz})$

Molecule	$\bar{\chi}_z^{\mathrm{L}}$		$\bar{\chi}_z^{\mathrm{hf}}$	
	Calculated [675a]	Exp. [280a]	Calculated	Exp.
H_2	−0.487	−0.473	0.0844[a]	0.0869[b]
N_2	−4.082	−4.36 . . . −0.3	2.349[a]	3.04[b]
FH	−0.9595	−0.92	0.0937[a]	0.0609[b]
CO	–	–	2.196[a]	2.82[b]
H_2CO	–	–	2.405[c]	4.108[d]

[a] [675a]
[b] [280a]
[c] [1356a]
[d] [742a]

value of $\Delta\chi^{\pi}$ can be estimated by computations based on PPP [280b] or Hückel-type [806a] methods.

A visual explanation of the phenomenon that aromatic compounds have much larger anisotropy of the diamagnetic susceptibility than others was given by Pauling [1069a]. He argues that this comes from the mobility of π electrons in aromatic rings, that is, a special *ring current* arises. A similar argument was given by London [806b]. It is supposed that $\Delta\chi \approx \Delta\chi^{\pi}$, and that one may neglect the high-frequency contribution working only with the Langevin term. This treatment is therefore similar to that of atoms for which the latter assumption holds exactly. For molecules, the model provides the explanation of the fact that the anisotropy of the diamagnetic susceptibility tensor of aromatic hydrocarbons increases with increasing number of rings, that is, with increasing molecular "area". The Langevin contribution, as defined in Eq. (3.94), contains the expectation value of r^2, the square of the position operator, which may really be interpreted as an area in some sense. On the other hand, recent sophisticated calculations on benzene have shown that there is no justification for speaking about a mobile π cloud flowing with equal intensity through every point of an aromatic ring [771, 772]. Symmetry considerations [771] suggest that σ electrons are also capable of sustaining delocalized currents which are even stronger than π currents. Therefore the phrase "ring current" possesses no more than a historical value (see also Ref. 459).

3.5.2 FREE RADICALS IN MAGNETIC FIELD

Experimental method: Electron spin resonance (ESR) spectroscopy* [468, 1412a]

As we have mentioned in the previous section, molecules having an odd number of electrons necessarily possess a permanent magnetic moment. It can be attributed to the unpaired electronic spins in most cases: if the spins are not compensated, the sum of the inherent magnetic moments of electrons also differs from zero. It may sometimes happen (*e.g.* in transition metal complexes) that a state with nonzero spin occurs, though the system contains an even number of electrons (so-called high-spin states, Section 2.8). According to quantum mechanics, the three components of the angular momentum (and thus that of the magnetic moment as well) do not have definite values simultaneously. One can determine only the absolute value of the moment and its projection corresponding to a given (arbitrary) single direction (the only exception is the case when all three components vanish). The arbitrary component (usually referred to as the z component) is quantized, which means that the orientation of the magnetic moment, relative to the z axis, is not arbitrary. The possible orientations of the resulting spin of value $S = 3/2$ for a system containing 3 unpaired electrons are illustrated by

* The term "electron paramagnetic resonance" (EPR) is also used.

Figure 3.21. The possible values of the z component of the spin momentum are $\pm 1/2$ and $\pm 3/2$. According to the general quantum mechanical properties of angular momenta, the absolute value is given by

$$\sqrt{S(S+1)} = \frac{1}{2}\sqrt{15} > \frac{3}{2} = S$$

thus the orientation of the spin momentum cannot coincide with the z axis. We shall recall that the orthogonal (x and y) components have no definite values. Pictorially one may visualize the situation by considering a precession of the spin momentum around the z axis; this classical analogy is often useful but is certainly not a strict one.

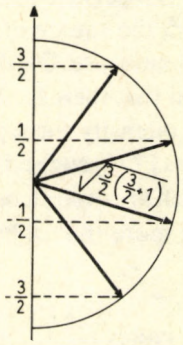


Fig. 3.21 Possible orientations of the magnetic moment vector of a molecule with spin 3/2

If the total magnetic moment of the system is due to the spin only, as is essentially the case for most organic free radicals, then there is a strict proportionality between the spin and the corresponding magnetic moment and the above considerations hold exactly for the behaviour of the magnetic moment, too. If there is also a non-zero "orbital" moment $\langle \hat{L} \rangle$, the situation becomes more complicated, not affecting, however, the fact that the magnetic moment has a quantized behaviour.

An important consequence of the existence of non-zero atomic and molecular magnetic moments is the *Zeeman-effect*. An external magnetic field removes the degeneracy of the states corresponding to different components of a level with non-zero multiplicity (*e.g.* the $S_z = 0, +1$, and -1 projections of a triplet), and the corresponding energy levels become split (see *e.g.* [280a]). According to Eq. (3.90), the magnetic moment consists of two terms: thus two types of Zeeman effects can be distinguished. The first type corresponds to the orbital moment; it has an analogue also in classical electrodynamics, if the electrons are supposed to move on some closed trajectory. Therefore, for historical reasons, this is called the *normal* Zeeman effect. The other type is the *anomalous* Zeeman effect which is connected with the spin and can be treated properly only in the framework of quantum mechanics.

If the orbital moment is zero, it is usually the case for molecules with low (or no) symmetry, the energy levels of spin multiplicity k are split to k distinct levels in a magnetic field. Accordingly, the Zeeman effect can be used for determining the multiplicity of energy levels experimentally.

The Zeeman effect is the basic phenomenon utilized in the electron spin resonance (ESR) spectroscopy. Let us discuss briefly the most important case of a molecule containing a single unpaired electron (doublet state). The vector of its magnetic moment has, accordingly, two possible orientations relative to the external field. The energy difference of the two states corresponding to the two possible orientations (*i.e.*, that of the two Zeeman levels), is proportional to the magnetic field H (see *e.g.* [1412a]):

$$\Delta E = g\beta_B H \tag{3.98}$$

where the value the factor g is $g_e = 2.0023$ for a free electron, *cf.* Eq. (3.90), but it can be slightly different for an electron in a molecule.

If, besides of the constant magnetic field H, there is also an electromagnetic radiation of a frequency ν, the latter can induce transitions between these Zeeman levels. Resonance occurs if

$$h\nu = \Delta E = g\beta_B H \tag{3.99}$$

This condition can be used for determining the actual value of the factor g.

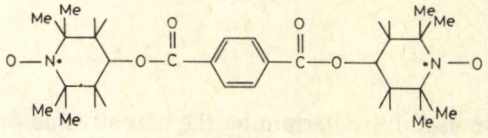
For technical reasons, in the practical ESR spectroscopy one usually varies slowly the intensity of the static magnetic field **H** and detects the absorption of radiation, the frequency ν of which is kept constant (actually, the derivative of the absorption curve is detected). As a consequence, the different parameters are often given in units of magnetic field and not in those of frequency.

In organic radicals, the difference between g and g_e can be attributed mainly to spin-orbit coupling. This phenomenon can be understood completely only in the framework of relativistic quantum theory. It can be explained as the magnetic moment due to the interaction of electronic spin with the magnetic field produced by the orbital motion of the given and other electrons. As a consequence, the energy levels are shifted slightly, leading to a change in ΔE, and hence in the value of g, compared with the case without such interactions. We shall note that, in order to give a satisfactory estimate of the spin-orbit coupling energy, one need not solve the relativistic Dirac equation; it is enough to take this energy change into account as a small correction to the nonrelativistic energy for example by means of a second order perturbation theory. This approach gives reliable results at least for atoms with $Z \lesssim 40$. In the case of organic radicals, one finds *e.g.* that $\Delta g = g - g_e$ depends on the orientation of the molecule relative to the external field. For such systems the value of Δg is in the $10^{-4} - 10^{-5}$ range [280a]. Large deviations of the g factor from the free electron value are observed for systems containing transition metal ions.

There are many (triplet) molecular states, where not just one but two electrons have unpaired spins. These are usually excited states, but the O_2 molecule and some

aromatic ions (triphenyl-benzyl dianion, pentaphenylcyclopentadienyl cation, etc. [1412a]) have triplet ground states. In these cases the spin-spin interaction is of great importance. This effect, similar to spin-orbit interaction, is of relativistic origin [280a]. For singlet levels the spin-spin interaction leads to only a very small shift of energy, but the triplet levels undergo a split due to its influence. The splitting can be detected in electronic spectra directly. This phenomenon is connected to the interaction of the magnetic moments of electrons, which removes the spin degeneracy of the molecule. The splitting can also be studied by ESR spectroscopy *(zero-field splitting)*: the energy difference of the Zeeman levels is not given exactly by Eq. (3.98) but does not vanish even if extrapolating to zero magnetic field.

The value of the zero-field splitting is determined by the exchange interaction (*cf.* Section 1.2) between molecular orbitals corresponding to electrons with unpaired spins. The larger is the exchange energy, the stronger is the spin–spin coupling [1412a]. If the exchange interaction is weak, a very interesting state, the so-called biradical or diradical can appear. An example is the following compound [1412a]:



The electrons with unpaired spins are marked by dots. They can be assigned primarily to the nitrogen atoms. In the limiting case, when the exchange interaction is much weaker than the hyperfine interaction between the unpaired electrons and any of the nuclear spins (see below), the ESR spectrum of the biradical is a simple superposition (sum) of the spectra of the two "independent" doublet radicals. One expects that the exchange interaction between the two unpaired electrons is negligible if the corresponding orbitals are localized in far-lying regions of space, thus having sufficiently small differential overlap (*cf.* Section 3.6.2). This is certainly the case for the above molecule since the two nitrogen atoms are separated by many σ bonds. It is to be emphasized that for smaller molecules the term "biradical" is often not justified, though it is widely used for example in photochemistry (in these cases it simply means triplet state). We note also that, although a biradical contains an even number of electrons, its electronic structure cannot be studied properly by the RHF method which works with doubly filled spatial orbitals. Here, similarly to the case of ordinary radicals, the UHF or some EHF type procedures must be applied (*cf.* Section 1.2.4).

The unpaired spins in free radicals can also interact with the spins of atomic nuclei, owing to the magnetic momenta associated with the electronic and nuclear spins. This effect causes the so-called *hyperfine structure* of the electronic spectra of atoms and molecules: the degeneracy of the Zeeman levels with respect to the different possible orientations of the nuclear spins is removed and the levels split to a very small extent into sublevels. The phenomenon is very important in ESR spectroscopy [1412a]; this is

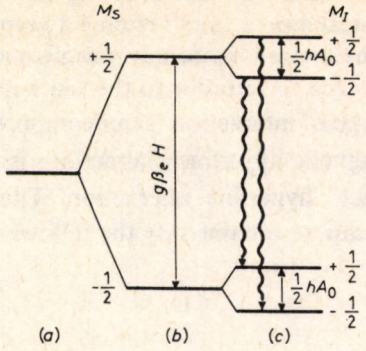


Fig. 3.22 Energy levels of the hydrogen atom in homogeneous magnetic field. *(a)* zero field; *(b)* Zeeman spliitting; *(c)* hyperfine splitting. M_S and M_I are the spin quantum numbers of the electron and the nucleus, respectively. Allowed transitions where nuclear spins remain unchanged are denoted by wavy lines

the very reason why ESR spectra show characteristic structures and can be analyzed to give important information on the molecular structure. As a result of the hyperfine interaction of spins of electrons and nuclei, the energy difference of the allowed transitions for the hydrogen atom, instead of Eq. (3.98), can be calculated as

$$\Delta E = g\beta_B H \pm \frac{1}{2} hA_0 \tag{3.100}$$

where h is Planck's constant, and A_0 is the hyperfine coupling constant often abbreviated as "hfc". The schematic view of energy levels and allowed transitions is presented in Fig. 3.22. Usually there is more than one nucleus in a molecule having non-zero spin and magnetic moment; thus the splitting can be much more complicated than that in Fig. 3.22. The number of levels is determined by the number and type of magnetic nuclei interacting with the unpaired electron; it also depends on how many of them are *equivalent*, that is represent the same isotope of the given atoms and are in the same chemical environment*. For example, in the methyl radical one has three equivalent hydrogen nuclei (protons) and, in the benzyl anion six equivalent. The extent of the splitting is determined by the hyperfine coupling constant(s).

The magnetic hyperfine interactions between the electrons and nuclei can be introduced strictly only in the framework of a relativistic theory. However, if we have obtained the appropriate expressions, there is no need for further explicit use of relativistic equations; we can substitute the appropriate parameters obtained from non-relativistic calculations. There are three types of such magnetic interactions. The first one is the coupling of nuclear spins with electronic orbital moments, the latter

* In some cases not only the chemical environment but also the spatial arrangement may be of importance (anisotropic hyperfine coupling).

resulting from the motion of electrons. This coupling can be neglected in most cases. The second type is the classical dipolar interaction between the magnetic moments of electrons and nuclei. This interaction is strongly anisotropic. It cannot be observed in solutions, because it is averaged to zero due to the fast and disordered motion of the molecules. However, this type of interaction is quite important in the solid state. The most significant type of magnetic hyperfine interactions is the third one, namely, the isotropic or "Fermi-contact" hyperfine interaction. The corresponding coupling constant at the nucleus A can be obtained by the following relation (*cf.* Ref. [96]).

$$A_A = \frac{8\pi}{3h} g_e \beta_B g_n \beta_n \rho_s(\mathbf{r}_A) \tag{3.101}$$

were g_e is the g-factor of electrons, β_B is the Bohr-magneton of electrons, β_n is the nuclear magneton,* and $\rho_s(\mathbf{r})$ is the spin density at the nucleus which is defined by the differences of the densities of electrons with spins α and β, *cf.* Eq. (1.25) in Section 1.2.5:

$$\rho_s(\mathbf{r}) = \rho^\alpha(\mathbf{r}) - \rho^\beta(\mathbf{r}) \tag{3.102}$$

where $\rho^\alpha(\mathbf{r})$ is the density of electrons with spin α at the space point $\mathbf{r}$, while $\rho^\beta(\mathbf{r})$ is that with spin β. In closed shell systems (singlet states) the spin density is zero at every point of space. As follows from Eq. (3.101), in order to determine the isotropic hyperfine coupling constant A_A, one should compute the spin density. As with total electron density at the nuclei, the spin density is determined merely by s-type orbitals, since AOs with higher azimuthal quantum number possess a nodal surface at the nuclei, leading to a zero spin density contribution there.

In treating open shell systems, different variants of the "open-shell RHF" methods cannot account for *e.g.* negative spin densities for example, thus the DODS-type wave functions are preferably applied. The UHF method (*cf.* Section 1.2.4) is commonly used to describe free radicals. However, as we have mentioned in Section 1.2.4, the UHF wave function is not an eigenfunction of the $\hat{S}^2$ operator. In calculating spin densities, this feature may lead to serious errors [1352a]. The extended HF (EHF)-type wave functions (*cf.* Section 1.2.4), which ensure the proper multiplicity of the wave function, give changes correctly but "overpolarized" spin densities (*i.e.* too large absolute values for both positive and negative spin densities). For obtaining quantitatively good results, however, large CI should be taken into account, which makes calculations on larger radicals prohibitive.

One of the methods most often used in calculating hyperfine coupling constants and spin densities, offering some compromise between accuracy and rigor, is the spin-projected UHF (PUHF) scheme [205, 1354, 1451a]. In this procedure one determines first the UHF solution, then selects that component of the wave function which is of the

* Similar to Eq. (3.98) for the case of electrons, the energy splitting in the magnetic field **H**, due to the nuclear magnetic moment is given as $\Delta E = g_n \beta_n H$.

desired multiplicity, by using appropriate spin projection operators [821]. It should be mentioned that the PUHF method does not necessarily improve the results of UHF computations concerning spin densities.

A detailed analysis of spin densities and the hfc of the methyl radical, performed at the *ab initio* level, can be found in a paper by Chipman [205]. Some other numerical examples are shown in Table 3.16. The data were taken from the paper by Zhidomirov and Chuvylkin [1451a]. It seems that the results, except a few cases, reflect very well the experimental findings. Moreover, the experimental determination of the sign of A_A is problematic; standard ESR measurements do not provide the sign [1412a]. In turn, quantum chemical calculations predict unique sign representing a nice example for the use of quantum chemistry as an "instrument".

For the calculation of the isotropic hfc a widely used semiempirical scheme is the INDO method [1121, 1121a, 1354] (see Section 1.3.2). As to the accuracy of the INDO results, it can compete with *ab initio* calculations using small basis sets (see Table 3.16). One inherent limitation is that, the INDO is an all-valence electron scheme, the effects of the core (inner shell) electrons cannot be taken into account explicitly. The trends for series of different compounds are well reflected. For the series of radicals BH_3^-, CH_3, NH_3^+ for example, the isotropic hfc calculated by the INDO method show the same trend as the experiment both for the hydrogen and heavy atoms. Similarly, the experimental findings are correctly reproduced for the three hydrogens with different positions in the vinyl radical. For further details, see for example, the book of Pople and

TABLE 3.16

ESR hyperfine coupling constants (10^{-4} T) for some simple molecules. Significant deviation from experiment is indicated by italic numbers [1451a]

Radical	Atom	Spinpolarized HF	INDO	Exp.
BH_3^-	H	−17.2	−16.9	−16.5
	B	13.6	34.6	25.0
CH_3	H	−18.0	−20.6	−23.0
	C	31.7	43.1	38.3
NH_3^+	H	−15.8	−21.2	−25.9
	N	14.8	19.2	19.5
HCN^-	H	140.3	148.9	137.5
	C	74.4	*156.1*	74.3
	N	4.9	3.1	6.5
CN	C	*339.2*	*149.4*	210.0
	N	−6.2	*4.1*	−4.5
$HCCH_2$	H	*−1.3*	10.7	13.4
	H	42.8	33.8	37.0
	H	62.4	74.0	65.9
	C	139.3	127.7	107.6
	C	−16.4	−14.9	−8.6

Beveridge [1121]. For performing INDO calculations, easy-to-handle computer programs are available [330a]. The use of this program is recommended in each case when the aim is to systematize the experimental results for a series of related molecules.

Organic radicals can be divided into two different groups from the point of view of ESR spectroscopy. In the first group, the electrons with unpaired spins can be assigned to σ-type orbitals. The radicals $HCCH_2$, C_6H_5 represent some examples for this case. In these compounds the spin density originates from the contributions of atomic s orbitals participating in the σ-bonds. Qualitative predictions can be made for the value of the coupling constant on the basis of the s-character of the σ-type orbitals [1188a], which can be estimated by analysing the Walsh-diagrams.

The second (and more important) group contains planar radicals in which the electron with the unpaired spin belongs to the delocalized π-system. One might expect

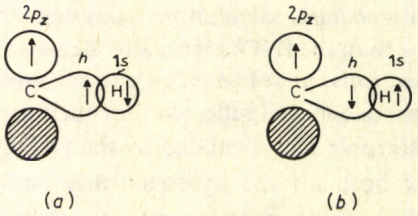


Fig. 3.23 Schematic view of spin polarization due to the magnetic field H. The hybrid orbital on the carbon directed along the C—H bond is denoted by h, while $1s$ stands for the orbital of the hydrogen

in this case that, the isotropic hfc for such molecules (like the benzyl radical) should be zero on each atom, since the π orbitals have a nodal surface in the molecular plane which leads to a zero spin density. This is by no means the case and however the ESR spectra of such compounds show rather characteristic structures. This phenomenon cannot be accounted for by maintaining the assumption of σ–π separability. Separate treatment of π electrons is not justified in calculating isotropic hyperfine coupling constants.

The breakdown of σ–π separability can be explained as follows. Let us assign the electron with the unpaired spin to a π orbital. Due to the interaction between the σ and the π system, a non-zero spin density contribution of the σ orbitals appears, leading to a hyperfine coupling with the protons. The phenomenon is illustrated schematically in Fig. 3.23. Let us consider a carbon atom of the aromatic system and the corresponding CH σ-bond. Let us further assign the unpaired electron to the $2p_z$ AO of the carbon. The CH bond may have two different configurations as it is illustrated by Fig. 3.23*a* and *b*. We recall that the pictorial formulation of the Pauli principle states that electrons with parallel spins avoid each other (Fermi hole). In other words, the situation depicted in Fig. 3.23 *a* is more realistic due to Hund's rule (*cf.* Section 1.2.1) than that in Fig. 3.23 *b*. This means that the energy of the configuration of Fig. 3.23 *a* will be lower than that of Fig. 3.23 *b*. The probability of the state (a) is therefore larger, thus increasing the

density of electrons at the H atom having a spin opposite to the field. Accordingly, one finds a negative spin density on the hydrogen *(spin-polarization)*. The above pictorial reasoning is far from being strict (especially because none of the cases in Fig. 3.23 represents a pure spin state), although it provides a satisfactory explanation to the essence of this phenomenon [843].

The spin polarization is expressed quantitatively by the McConnell relation [842a]

$$A_{H(i)} = Q\rho_s^{\pi}(\mathbf{r}_i)\,. \tag{3.103}$$

This relation says that the isotropic hyperfine coupling constant of the proton attached to the i'th atom of the aromatic system is proportional to the π electron spin density $\rho_s^{\pi}(\mathbf{r}_i)$ at the i'th atom. The sign of the proportionality factor, Q, is negative, indicating that the sign of the spin densities on the C and H atoms is opposite. The value of Q depends on the atomic number of the i'th atom and, in general, on the method by which ρ_s^{π} is calculated. (There are, however, some "reference points" where ρ_s^{π} does not depend on the particular method applied; *e.g.* for CH_3 $\rho_s^{\pi}=1$ or for C_6H_6 $\rho_s^{\pi}=1/6$ due to symmetry.) For more detailed discussions, see [1313, 1412a]. Comparing Eqs (3.103) and (3.100), it turns out that the McConnell equation expresses essentially a relation between the spin densities of the carbon and the neighbouring hydrogen atoms. In the framework of the INDO method the reliability of the McConnell relation can be checked since it is possible to calculate explicitly the π electron spin density on the carbon and the spin density due to the σ electrons on the hydrogen. One finds that the latter is proportional to the former with a very good accuracy. Based on the correlation between the experimental hfc and calculated hydrogen spin densities, this proportionality corresponds to the value $Q \approx -2.2 \times 10^{-3}$ T [1121]. This is in excellent agreement with the "experimental" value of Q deduced from other sources, such as from the hyperfine structure of ESR spectra of systems like $C_6H_6^-$. Since in this ion one has $\rho_s^{\pi}=1/6$ on each carbon, the experimental hfc of 0.375×10^{-3} T corresponds to a value $|Q| = 2.25 \times 10^{-3}$ T.

Using the McConnell relation, isotropic hyperfine coupling constants of organic radicals can also be studied by simple π electron (PPP, Hückel) methods [1313]. In the Hückel framework the following expression was proposed to calculate the spin density (McLachlan, [848a]):

$$\rho_s^{\pi}(\mathbf{r}_\mu) = c_\mu^2 - \lambda \sum_\nu \pi_{\mu\nu} c_\nu^2\,. \tag{3.104}$$

Here c_μ is the coefficient of the μ'th AO on the singly occupied MO which corresponds to the electron with unpaired spin. The value of the parameter λ has been estimated to be within 1 and 1.2; in practice it may be chosen within some limits so as to obtain the best possible fit with experimental data. The Eq. (3.104) was derived by means of perturbation theory; the factors $\pi_{\mu\nu}$ are the so-called atom–atom polarizabilities [1313] (not to be confused with the polarizability of the molecule discussed in Section 3.5.2):

$$\pi_{\mu\nu} = \frac{\partial q_\mu}{\partial \alpha_\nu} = \frac{\partial^2 E}{\partial \alpha_\mu \partial \alpha_\nu} = 4 \sum_{i}^{\text{occ}} \sum_{k^*}^{\text{virt}} \frac{c_{i\mu} c_{k^*\mu} c_{i\nu} c_{k^*\nu}}{\varepsilon_i - \varepsilon_{k^*}} \tag{3.105}$$

where q_μ is the π-electron density on atom μ, and α_μ is the Coulomb-parameter of atom μ. Owing to the simplicity of the Hückel method, the calculation of ρ_s^π through Eq. (3.104) represents no computational problem by this approach. Moreover, the values for c_μ and $\pi_{\mu\nu}$ have been tabulated for hundreds of molecules [260, 541]. If the effect of all neighbouring atoms is neglected, one has $\lambda = 0$ in Eq. (3.104) leading to an even simpler approach (see *e.g.* [1313]). In this case, however, the spin density is necessarily positive though it has been observed for several molecules (*e.g.* pyrene, [280a]) that experimental findings can be explained only by assuming a negative spin density. In such a case the use of the full McLachlan equation (3.104) is inevitable. Note that the importance of negative spin densities holds also in NMR spectroscopy.

A generalization of the McConnell relation was given by Colpa and Bolton:

$$A_{H(i)} = (Q + K\varepsilon_i)\rho_s^\pi(\mathbf{r}_i) \tag{3.106}$$

where K is an empirical constant, $\varepsilon_i = 1 - q_i$, q_i being the π-electron density on the i'th carbon atom. We note that, though Eq. (3.106) leads to slightly better results than Eq. (3.103), the deviations are usually less than $\pm 15\%$ [1412a].

ESR spectra are mostly recorded in solution, so investigation of solvent effects is important [382a, 741, 909]. Miertuš and Kysel compared spin densities as calculated without and with consideration of solvent effects for a number of radical anions [909]. They calculated spin densities by a restricted SCF π-electron method and applied the solvaton model (*cf.* Section 1.4) to treat solvent effects. It was found that for hydrogen, carbon and nitrogen hyperfine coupling constants the linear relationship in Eq. (3.100) is better fulfilled if solvent effects are also taken into account. This means that spin densities are influenced by the solvent. The origin of this influence for substituted methoxycarbonyl and acetylpyridinyl radicals is the polarization of the carbonyl group by the solvent [741].

3.5.3 ELECTRON-MEDIATED COUPLING BETWEEN NUCLEAR SPINS

Experimental technique: NMR spectroscopy [364a, 1297a]

The spins of nuclei can interact directly. This interaction is independent of the chemical environment of the nuclei in question. In addition to this direct interaction, coupling may also occur through the electrons of the molecule (a detailed discussion can be found *e.g.* in [1297a]). This effect results in splitting of lines in the NMR spectra. The extent of the splitting is determined by the *nuclear spin—nuclear spin coupling constant* [1056a]. The theoretical analysis of this coupling is formally similar to that of hyperfine coupling (*cf.* Section 3.5.2), thus these two effects are often treated on the same basis.

There are two parts to the coupling of nuclear spins through electrons. The first one is an anisotropic contribution, which cannot be studied experimentally in solution because the molecules undergo a fast random motion. This contribution may be significant in the solid state but is beyond the scope of the present discussion. We will focus here only on the second term, the isotropic contribution.

Similar to the case of the coupling between electron spin and nuclear spin, the theory of nuclear spin—nuclear spin coupling is based on relativistic quantum theory [280a]. The relativistic formulation can be used for deriving appropriate formulae to calculate the isotropic nuclear-nuclear spin coupling constant (from here on, the abbreviated term "coupling constant" will be used). For references, see [280a] and [1151a]. It was found that the coupling constant can be decomposed into three components:

$$J = J_1 + J_2 + J_3 . \tag{3.107}$$

All three terms in this equation have their own physical significance, as illustrated by Fig. 3.24. The third part of the coupling denoted by J_3 arises form the so-called *contact interaction* at the nuclei between the electronic and nuclear spins. This is analogous to the isotropic hyperfine coupling constant discussed in Section 3.5.2. The contact interaction affects the electronic distribution indirectly, in the internuclear space and at the neighbouring nucleus as well. The energy of the latter is therefore altered, leading to a coupling of the nuclear spins through the electronic cloud. Based on the derivation by Ramsey [1151a], and using the notations of Pople [1121], we give here the relevant expression for the contact term of the coupling between nuclei A and B:

$$J_3^{AB} = \hbar \gamma_A \gamma_B K_{AB} . \tag{3.108}$$

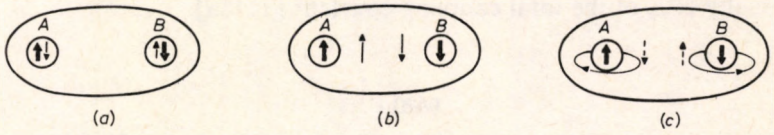


Fig. 3.24 Isotropic nuclear spin-nuclear spin coupling in a diatomics possessing two electrons. *(a)* contact nuclear spin-electron spin interaction; *(b)* classical nuclear spin-electron spin interaction; *(c)* interaction between the nuclear spin and the electronic orbital momentum. Fat arrow: nuclear spin; thin arrow: electronic spin; dashed arrow: orbital moment. The *A* and *B* stand for the nuclei

Here γ_A and γ_B are the gyromagnetic coefficients of nuclei A and B, respectively, defined as

$$\gamma_A = \frac{g_A}{\hbar} \beta_n \tag{3.109}$$

and similarly for γ_B, see Eq. (3.108). The factor K_{AB} in Eq. (3.108) is given by the following relation:

$$K_{AB} = -\left(\frac{8\pi}{3}\right)^3 \frac{8\beta_B^3}{3} \sum_{n \neq 0}^{\infty} \frac{D_{0n}^A - D_{n0}^B}{E_n - E_0} \tag{3.110a}$$

$$D^{A}_{mn} = \langle \psi_m \left| \sum_i \delta(\mathbf{r}_i - \mathbf{r}_A)\hat{s}_i \right| \psi_n \rangle \qquad (3.110b)$$

where the summation in Eq. (3.110a) is to be extended over all excited states ψ_n with the energy E_n. In Eq. (3.110b) $\hat{s}_i$ is the spin operator of electron i and the summation is over all electrons in the system. The appearence of the infinite sum in Eq. (3.110a) is inconvenient. To bypass this problem, several solutions have been proposed [280a, 364a, 1121].

The second part of the coupling, denoted by J_2, can be attributed to the "classical" interaction of the electronic and nuclear spins.

Besides the coupling of the electronic and nuclear spins, there exists a coupling between the nuclear spins and the electronic orbital moments which is denoted by J_1 in Eq. (3.107). The explicit expressions for J_1 and J_2 are rather complicated and there is no room to give them here. The relevant formulae can be found, for example in [364a].

Let us discuss now the importance of different contributions to the coupling constant in actual cases. Table 3.17 presents some data for terms J_1, J_2 and J_3 as calculated for selected molecules by *ab initio* methods. (The details of the calculations can be found in the references given for each molecule separately.) These data show that the contact interaction, J_3, is the most important in determining the coupling constant in most cases. The experimental situation is well reflected for the changes of J_3 for example for the ethane — ethylene — acetylene series and for the different couplings of methyl fluoride. The term J_2 originating from the classical spin coupling is usually small, but it is of essential importance for the ^{19}F — ^{19}F couplings shown in Table 3.17. The term J_1, corresponding to the spin-orbit interaction, is also small for well localizable systems. It can be significant in aromatic molecules, though even in this case it does not exceed usually 20% of the total coupling constant [1118a].

TABLE 3.17

Components of nuclear spin–nuclear spin coupling constants (Hz) for different molecules

Molecule	Coupling	J_1	J_2	J_3	Sum	Exp.
CH_3F [328b]	^{13}C—H	0.4	−0.4	172.8	172.8	148.8
	^{13}C—^{19}F	32.4	19.6	−149	−97.5	−161.9
	^{19}F—H	12.3	−4.2	58.5	66.6	46.3
	H—H	1.0	0.6	−31.6	−30.0	−9.6
CH_2F_2 [1181a]	^{19}F—^{19}F	—	117.8	60.6	178.4	—
	^{19}F—H	—	5.6	34.8	40.4	—
C_2H_6 [60a]	^{18}C—^{13}C	0.04	0.55	17.4	17.9	34.6
C_2H_4 [60a]	^{18}C—^{13}C	−4.83	3.67	69.2	70.9	67.6
FHCCHF *cis* [1181a]	^{19}F—^{19}F	—	51.0	−0.7	50.3	18.7[a]
C_2H_2 [60a]	^{13}C—^{13}C	1.89	0.35	190.7	192.9	171.5

[a] [1121].

Having obtained some insight into the importance of different contributions to the coupling constant, let us study the efficiency of different quantum chemical methods in calculating this quantity. Some numerical examples are shown in Table 3.18. Let us recall that the "*ab initio*" calculations reported in Table 3.18 were performed by different authors applying different levels of sophistication. For example, Barbier and coworkers [60a] evaluated the multicentre integrals by using approximate formulae, while Robb *et al.* [1181a] took into account electron correlation effects as well, by means of perturbation theory. These latter authors concluded that, though the role of electron correlation is important in calculating the value of the coupling constant, the tendencies and relative changes of J reflect the experimental findings even if neglecting the correlation [1181a]. However, the negative sign of the C—H—C coupling constant in difluorethane can be explained only by considering electron correlation. The data

TABLE 3.18

Nuclear spin–nuclear spin coupling constants (Hz) as calculated by *ab initio* and INDO methods

Molecule	Coupling	*Ab initio*	INDO[a]	Exp.[a]
CH_4	H—C—H	−25.0[b]	−6.1	−12.4
CH_3F	H—C—H	−30.0[c]	−1.9	−9.6
C_2H_6	H—C—H[d]	7.1[c]	9.3	8
C_2H_4	H—C—C—H	8.4[c]	9.3	11.7
	cis			
	H—C—C—H	13.2[c]	25.2	19.1
	trans			
Cyclopropane[f]	H—C—H	—	1.5	−7.0
Ethyleneimine[f]	H—C—H	—	8.9	2.0
Ethylene oxide	H—C—H	—	9.1	5.5
CH_4	^{18}C—H	—	122.9	125
C_2H_6	^{18}C—H	—	140.3	157.5
CH_3F	^{18}C—H	172.8[c]	—	148.8[c]
C_2H_6	^{18}C—^{18}C	17.9[e]	41.5	34.6
C_2H_4	^{18}C—^{18}C	70.4[e]	82.1	67.6
C_2H_2	^{18}C—^{18}C	192.[e]	163.8	171.5
CH_3F	^{18}C—^{19}F	−97.5[c]	−237.2	−161.9[c]
$C_2H_2F_2$	^{19}F—C—C—H	50.3[b]	10.3	18.7
	cis			
Cyclopropane[f]	^{18}C—H	—	157.7	161
Ethylene-imine[f]	^{18}C—H	—	161.4	168.1
Ethylene oxide[f]	^{18}C—H	—	167.8	175.8

[a] [1121]
[b] [1181a]
[c] [328b]
[d] Average of *gauche* and *trans* values
[e] [60a]
[f] [462a]

presented in Table 3.18 are not yet sufficient to draw general conclusions on the efficiency of different *ab initio* methods. The results of the semiempirical INDO method are of more uniform quality, but in these calculations only the J_3 term describing the contact interaction was evaluated [1121]. As is shown by the data presented in Table 3.17, neglect of J_1 and J_2 is not always justified. Anyway, the INDO results of Table 3.18 are in overall accord with the experimental findings. However, for the cyclopropane—ethylene imine—ethylene oxide series the INDO results are inadequate concerning the H—C—H geminal coupling constants [462a]: neither the signs, nor the absolute values are correct. In Ref. [462a] one can also find some results obtained by the Extended Hückel method (see Section 1.3.2). They are acceptable only for the constants of ^{13}C—H couplings while they fail to agree with the experiment in case of geminal H—H (H—C—H) coupling.

There are a number of qualitative rules establishing connections between coupling constants and the molecular structure. We shall now discuss some of them. As is reflected by Eqs (3.108)–(3.110), among various factors determining the value of the coupling constant the electron density at the nucleus in question is of essential importance. The electron density at the nuclei originates from the electron population of *s*-type atomic orbitals. Thus, if one studies the coupling constant in terms of localized orbitals, the *s*-characters of the corresponding hybrid AOs entering the bonding orbitals (*cf.* Section 1.5) contain essential information concerning the magnitude of J. The *s*-characters of the hybrid AOs characterize the hybridization state of the corresponding atom quantitatively. For instance, the value of the ^{13}C–^{13}C coupling constant increases along the series

$$C_2H_6 \ldots C_2H_4 \ldots C_2H_2$$

(*cf.* Table 3.17). In this series the *s*-characters of the standard hybrids on the carbons in sp^3, sp^2 and sp states, respectively, vary as 1/4, 1/3, 1/2; *i.e.*, they also increase. The situation is similar in the case of the ^{13}C—H coupling (for a detailed discussion, see [364a]).

There is a simple way to predict the signs of H—H coupling constats. According to a generally accepted rule, this coupling constant is positive (or negative) in saturated open chain hydrocarbons if the two protons are separated by an odd (or even) number of intervening bonds (see *e.g.* [1297a]). This rule is also valid for other open chain compounds with a limited number of exceptions [364a]. The theoretical background of this rule can be understood by considering Fig. 3.25. If the nuclei *A* and *B* are connected

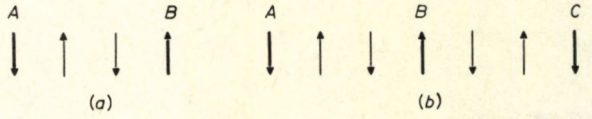


Fig. 3.25 Coupling of nuclear and electronic spins for the case of an *(a)* odd, *(b)* even number of bonds. Nuclei are denoted by *A*, *B* and *C*

by one bond (*i.e.* by a single electron pair), they possess opposite spins as a consequence of the coupling, since the neighbouring spins are preferably opposite (*cf.* Hund's rule). In turn, if there are two electron pairs (and one intervening nucleus *B*) between the two protons, as is the case for nuclei *A* and *C* in Fig. 3.25, the orientation of the spins of *A* and *C* will be parallel for the same reason. By definition [280a], the state with opposite nuclear spins has a positive coupling constant. Accordingly, the sign of *J* in the case illustrated by Fig. 3.25 *a* is positive, while for that on Fig. 3.25*b* it is negative. The above development can be generalized for the case of an arbitrary number of intervening bonds. This rule was extended by McConnell [842b] for aromatic alternant hydrocarbons containing an even number of carbon atoms. His formula is valid not only for proton–proton coupling, but for other types of couplings as well.

The value of the coupling constant J^{AB} between nuclei A and B is the smaller, the larger is the number of bonds separating the two nuclei [364a]. It was assumed that the mechanism of the coupling is mainly connected with a *through bond* effect. This means that the interaction is propagated through the intervening bonds. In other words, the through bond coupling would not appear between the two nuclei in question if the other bonds were not present. Theoretical analyses supporting experimental findings show that there exists a direct *through space* coupling as well [364a, 1181a], which is unaffected by the presence of other bonds and depends on the distance of the corresponding nuclei. Through space coupling can appear only if there exists a considerable overlap between the orbitals of the two atoms. This mechanism is very important in the case of ^{19}F–^{19}F couplings (*e.g.* in the $H_2FC—CFH_2$ molecule). We note that an analogous distinction between through space and through-bond effects can be done in many fields of quantum chemistry; it was introduced first by Hoffmann and coworkers [540, 578, 579] in connection with orbital interactions; we have discussed analogous effects also for electron delocalization interactions [890, 1322] (*cf.* Section 1.5).

The effect of polar solvents on NMR coupling constants is important in some cases (see Ref. [61] for a review). Rivail and coworkers investigated this problem by INDO calculations [1210] using a spherical cavity model and a multipole expansion of the charge distribution of the solute. The variation of coupling constants with that of the solvent dielectric constant is quite large especially for C—F coupling. For example the value of $\Delta J_{CF(2-20)} = J_{CF(2)} - J_{CF(20)}$ (the index in parentheses stands for the value of the dielectric constant) is +18.8 Hz for *cis*-1,2-difluoroethylene and it is as large as +49.0 Hz for trifluoroethylene. The effect is smaller, but not negligible, for H—H, C—H and F—H coupling constants. The calculations of Rivail and coworkers were able to reproduce signs and order of magnitude of ΔJ for most cases.

3.5.4 MAGNETIC FIELD AT THE NUCLEI

Experimental method: NMR spectroscopy [364a, 1297a]

Nuclei possessing non-zero spin interact with the external magnetic field. This field, however, is screened by the electronic clouds around nuclei [635]. This effect has a pronounced role in nuclear magnetic resonance (NMR) spectroscopy which provides useful pieces of information about the electronic structure of diverse molecules.

As a consequence of the screening, the external magnetic field H_0 will decrease to H_A at the nucleus denoted by A. This can be expressed mathematically as

$$H_A^\alpha = H_0^\alpha - \sum_{\beta=1}^{3} \sigma_{\alpha\beta} H_0^\beta \tag{3.111}$$

where the labels α and β stand for the x, y and z components of the magnetic fields, and $\sigma_{\alpha\beta}$ is the corresponding element of the *shielding tensor*. This tensor is symmetric, that is

$$\sigma_{\alpha\beta} = \sigma_{\beta\alpha}. \tag{3.112}$$

In an isotropic solution the screening, averaged due to the fast irregular motion of the solute molecules, is independent of the orientation, thus the formula of the screening reads

$$H_A = H_0 - \sigma H_0 \tag{3.113}$$

where we used the following notation:

$$\sigma = \frac{1}{3}(\sigma_{xx} + \sigma_{yy} + \sigma_{zz}). \tag{3.114}$$

The σ is called the shielding constant. The anisotropy of the shielding tensor is important only in the solid state.

In the practice of organic chemistry the shielding manifests itself by the so-called *chemical shift* δ_A measured relative to some reference sample:

$$\delta_A = \frac{H_A - H_R}{H_R} = \frac{H_0(1-\sigma_A) - H_0(1-\sigma_R)}{H_0(1-\sigma_R)} = \frac{\sigma_R - \sigma_A}{1-\sigma_R}. \tag{3.115}$$

Here H_A and H_R are the magnetic fields at the nucleus A and in the reference sample R, respectively; σ_A and σ_R are the corresponding shielding constants. Since the shielding is small, the above equation in a linearized approximation becomes:

$$\delta_A \approx \sigma_R - \sigma_A. \tag{3.116}$$

The chemical shift is usually expressed in parts per million (p.p.m.). The chemical shifts and the elements of the shielding tensor can be calculated in quantum chemistry. The shielding tensor is decomposed into diamagnetic and paramagnetic parts, denoted by σ^d and σ^p, respectively:

$$\sigma_{\alpha\beta,A} = \sigma^d_{\alpha\beta,A} + \sigma^p_{\alpha\beta,A}. \tag{3.117}$$

These two contributions can be calculated on the basis of expressions analogous to those of the diamagnetic susceptibility tensor (see Section 3.5.1 and Ref. [155a]):

$$\sigma^d_{\alpha\beta,A} = \frac{e^2}{2m}\left\langle \psi_0 \left| \sum_{i=1}^{N} \frac{\hat{r}^2_{iA}\delta_{\alpha\beta} - \hat{r}^{\alpha}_{iA}\hat{r}^{\beta}_{iA}}{\hat{r}^5_{iA}} \right| \psi_0 \right\rangle \tag{3.118}$$

$$\sigma^p_{\alpha\beta,A} = -\frac{e^2}{2m}\sum_{n\neq 0}^{\infty} \frac{A^{\alpha}_{0n}B^{\beta}_{n0} + B^{\alpha}_{0n}A^{\beta}_{n0}}{E_n - E_0} \tag{3.119}$$

where

$$A^{\alpha}_{mn} = \left\langle \psi_m \left| \sum_{i=1}^{N} \hat{L}^{\alpha}_i r^{-3}_{iA} \right| \psi_n \right\rangle \tag{3.120}$$

and

$$B^{\alpha}_{mn} = \langle \psi_m | \hat{L}_{\alpha} | \psi_n \rangle \tag{3.121}$$

(in SI units). In the above formulae r_{iA} is the norm of the position vector of the electron i relative to the nucleus A, $\hat{L}^{\alpha}_i$ is the α component of the angular momentum operator of electron i, while E_0 and E_n are the energies of the molecule in the ground and n'th excited states ψ_0 and ψ_n, respectively. By comparing these equations to Eqs (3.93) and (3.94), it seems that the diamagnetic term of Eq. (3.118) is analogous to the Langevin contribution to the susceptibility, *cf.* Eq. (3.94), while the expression of the paramagnetic shielding tensor σ^p_A as given in Eq. (3.119), resembles slightly the formula for the high-frequency susceptibility defined by Eq. (3.93).

As in the case of susceptibility discussed in Section 3.5.1, both the diamagnetic and paramagnetic contributions to the shielding constants are important. These two contributions are of opposite signs and in most cases the former has a larger absolute value, leading to a positive shielding constant. This is quite natural since as a result of the shielding by the electronic cloud, the magnetic field at the nuclei becomes weaker than the external field. However, the opposite is also possible: *e.g.*, in the case of the nucleus ^{17}O, the shielding constant was found to be negative in certain molecules [328a].

Note that Eq. (3.119) contains a sum over all excited states which causes some difficulties in calculating the paramagnetic shielding constant [416].

As for the possibility of computing the nuclear shielding by quantum chemical methods, recent calculations show [420] that about 20% of the paramagnetic contribution to the nuclear shielding can be attributed to correlation effects. The role of the basis set in *ab initio* calculation of σ is also important [785]; the results of split-valence 4-31G basis set calculations are still uncertain [328a]. Another point is that usual quantum chemical methods may provide results in the case of the presence of external magnetic fields, which violate the translation and the gauge-invariance

requirements of electrodynamics, leading to serious errors in calculating, for example, shielding constants. This problem can be solved by using special gauge invariant London-type atomic orbitals [271, 500, 806a] which have the following form:

$$\chi_\mu^{\mathrm{L}}(\mathbf{r}, \mathbf{H}) = \chi_\mu(\mathbf{r}) \exp\left\{-\frac{i}{2c}\mathbf{A}_\mathrm{A} \cdot \mathbf{r}\right\} \tag{3.122}$$

where $\chi_\mu(\mathbf{r})$ is the usual atomic orbital, $\mathbf{A}_\mathrm{A}$ is the vector potential corresponding to the external magnetic field at the centre of the AO $\mu(\mu \in \mathrm{A})$. That is, the London-type atomic orbitals depend on the external magnetic field through the exponential factor. This feature leads to the invariancy of magnetic properties to a translation of the origin of the gauge. The use of London orbitals results in a considerable improvement of chemical shifts calculated by *ab initio* quantum chemical methods.

Some numerical examples comparing theoretical and experimental chemical shifts are given in Table 3.19 [327a, 327b]. It seems that the experimental tendencies are very well reflected by the calculations, the average error is 0.39 p.p.m. for protons and 4.3

TABLE 3.19

Ab initio and experimental chemical shifts (p.p.m.)

Molecule	Hartree–Fock[a]	Exp.[a]
C_2H_6	−0.35	−0.75
C_2H_4	−5.61	−5.18
C_2H_2	−1.25	−1.35
CH_3F	−4.04	−4.00
H_2CO	−10.39	−9 . . . −10
HCN	−2.95	−2.83
NH_3	0.86	0.05
H_2O	0.06	−0.60
FH	−2.12	−2.50
C_2H_6	−7.4	−8.0
C_2H_4	−130.8	−125.6
C_2H_2	−75.2	−76
HCN	−123.5	−120 ± 10
CH_3F	−65.4	−77.5
CH_2F_2	−98.3	−111.3
CHF_3	−115.5	−118.7
CF_4	−126.2	−123.9
H_2CO	−199.6	−197
$CH_3CH_2CH_3$[b]	−16.8	−17.7
$CH_3CH_2CH_3$[c]	−15.4	−18.2

[a] [327, 327a]
[b] Relative to the proton of CH_4
[c] Relative to the carbon of CH_4

p.p.m. for ^{13}C nuclei. Similar results were obtained for ^{15}N and ^{19}F nuclei in the HCN and CH_3F molecules, respectively. The chemical shift for ^{17}O in formaldehyde, however, was calculated with a considerable error [327a]. The recent EHT calculation with London-type orbitals gave excellent results for carbon chemical shifts [337].

To gain some deeper insight into different chemical effects influencing the shielding constant, this latter quantity can be decomposed into several terms, each term having its own chemical significance. Among different possibilities, an important partition is the following [364a]:

$$\sigma_A = \sigma_{AA}^d + \sigma_{AA}^p + \sum_{B \neq A} \sigma_{AB} + \sigma_A^{deloc} . \tag{3.123}$$

As discussed in Ref. [1297a] in considerable detail, the terms of Eq. (3.123) have the following meaning. The first two terms contain the local diamagnetic and paramagnetic atomic contributions. The third term accounts for the effects of neighbouring atoms or groups (the subscript B runs over all atoms or chemical fragments of the molecule), while the fourth term describes the contributions due to delocalized (*e.g.*, aromatic) systems. These terms will be discussed below in some detail.

The most important contribution is σ_{AA}^d which corresponds to a "current" induced on atom A by the external magnetic field. Its magnitude is determined mainly by the net charge of atom A [631a]. The following linear relationship holds to a good degree of accuracy:

$$\sigma_{AA}^d = aq_A + b \tag{3.124}$$

where q_A is the net charge of atom A, and the parameters a and b are constant for a given family of molecules (*e.g.*, for substituted benzenes). It is often assumed that

$$\sigma_A \approx \sigma_{AA}^d .$$

Thus, the total screening constant is approximately a linear function of the net atomic charge. For example, semiempirical PPP + Del Re computations (*i.e.* a PPP calculation for the delocalized π electron system and a simple Del Re calculation for obtaining the electron distribution of the σ core, *cf.* Section 1.5) are able to provide net atomic charges which correlate well with proton chemical shifts, as is illustrated by Fig. 3.26 for the case of substituted *N*-pyrido-pyrroles [349a]. The correlation coefficient is $r = 0.936$. The four exceptional cases, indicated by double circles on the Figure, correspond to the chemical shifts of H3′ protons, which interact strongly with the oxygen atoms situated close to them. In this case, therefore, the assumption $\sigma \approx \sigma_{AA}$ does not hold since the term σ_{AB} describing neighbouring interactions should also be taken into account.

The computation of charge densities was already discussed in Section 3.4.1. Knowledge of the charge density permits us to systematize the values of chemical shifts in a series of related compounds. This systematization makes it easier to assign the experimental NMR signals to the relevant atoms. There are many such examples in the

literature; we cite here some papers using the simple Hückel [355a], and Extended Hückel [462b] methods, the combination of PPP and Del Re methods (see in Part 1) [349a], and the CNDO/2 scheme [648a]. For aromatic compounds, there exists some correlation between the observed chemical shifts and the π-electron densities as obtained by the PPP method, but it can be considerably improved by calculating also the σ-electron densities using, for example, the simple Del Re method [349a]. The dependence of chemical shifts on the charge distribution is indicated by the relation between substituent electronegativities and proton chemical shifts [631a]. This is quite obvious since, as it was discussed in Section 3.4.1, net atomic charges are strongly affected by the electronegativities of the corresponding atoms, which, in turn, influences the polarities of localized σ bonds.

The second term on the left-hand side of Eq. (3.123), the mono-atomic paramagnetic contribution, can be omitted from explicit consideration in many cases. In proton resonance spectroscopy it is usually considered as being constant for a series of similar compounds [427a], therefore it is unimportant in systematizing the experimental results. It can be very important, however, in the case of other nuclei [1297a].

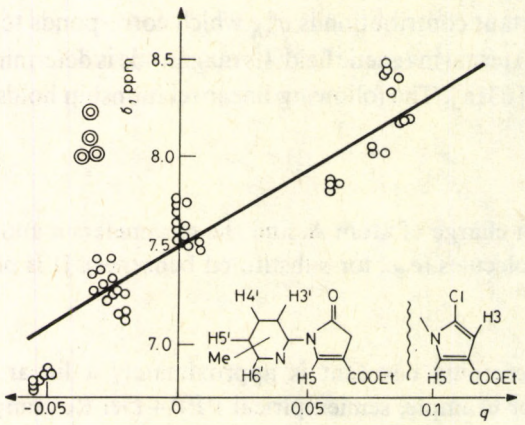


Fig. 3.26 Comparison of proton chemical shifts and net atomic charges for substituted *N*-pyrido-pyrrole derivatives. The charges are calculated by the PPP method augmented by the Del Re method for the σ core [349a]

The effect of neighbouring atoms, which is expressed by the sum of σ_{AB} contributions in Eq. (3.123), often modifies considerably the values of chemical shifts. It is of special importance if there is a group containing a π bond (>C=C<, —C≡C—, >C=O, —C≡N, etc.) in the neighbourhood of the atom in question. The magnitude of this term can be determined by the McConnell equation for NMR chemical shifts [842c] (not to be confused with the McConnell equation for hyperfine splittings). If the neighbouring group B represents a two-centre bond (or in a more general case is a linear group) the following formula was proposed for the contribution σ_{AB}:

$$\sigma_{AB} = \frac{\Delta\chi}{3R_{AB}^3}(1 - 3\cos^2\vartheta). \tag{3.125}$$

In this equation R_{AB} is the distance between atom A and the centre of the group B, ϑ is the angle between the axis of the group B and the vector $\mathbf{R}_{AB}$, while $\Delta\chi$ is the anisotropy of the diamagnetic susceptibility of the group B (see Section 3.5.1). On the basis of the McConnell equation (3.125) one can draw mainly qualitative conclusions. From the quantitative point of view it provides very approximate results for two reasons: (*i*) it was derived by utilizing severe simplifications, and (*ii*) the determination of $\Delta\chi$ is rather uncertain in most cases. Anyway, the McConnell equation is very useful for example, in studying diverse stereochemical problems [631a].

It is perhaps not too surprising that for unsaturated cyclic compounds the last term of Eq. (3.125) σ^{deloc}, is of crucial importance. It is often explained by the concept of the "ring current" which was already mentioned in Section 3.5.1. It was noted there also that this has no physical meaning. However, it can be shown that there is a part of the delocalization contribution σ^{deloc} to the shielding constant, which appears only in ring containing molecules [851a, 866a].

On the basis of the decomposition of the shielding constant given by Eq. (3.123), one can assign definite ranges (intervals) of chemical shifts to characteristic fragments of different molecules, *i.e.* to individual functional groups. These ranges are approximately transferable from molecule to molecule. For instance, the chemical shift of the protons in the —OCH_3 group, as compared to the tetramethyl silane reference, usually lies in the 3.2–4.3 p.p.m. range. On the basis of this transferability, it is possible to construct correlation tables which make the assignment of the signals in NMR spectra easier [1297a].

A recent theory [748] of NMR chemical shifts and magnetic susceptibilities [1238, 1239, 1240] based on localized quantities is proved to be very successful in *ab initio* computations of the above quantities.

NMR chemical shifts are also dependent on solvation. Solvent effects are mainly due to changes in atomic net charges and to hydrogen bond formation [22]. Quantum chemical calculation of chemical shift changes is not very simple: different methods may yield considerably different results [22].

3.6 EXCITED AND IONIZED ELECTRONIC STATES

In Sections 3.1–3.5 we have discussed some properties of molecules in the ground electronic state. Molecules, by absorbing energy, may get into various excited states having higher electronic energy. Properties, such as spin multiplicity, spatial symmetry, equilibrium geometry, charge distribution, polarizability, the potential energy hypersurface, etc. differ considerably in various electronic states.

A host of spectroscopic methods are used for getting information about higher electronic states. In the case of small molecules accurate energy measurements are

possible, but the short lifetime of most excited states (10^{-9}–10^{-15} s) makes experimental investigation of the excited state properties difficult. Usually they can be deduced only in some indirect manner from spectroscopic measurements. Theoretical elucidation of the characteristics of these unstable states may help to understand many photophysical and photochemical processes.

In the present section we restrict our discussion to the quantum chemical aspect of ionized and excited electronic states, with special attention to energetic features and to some molecular properties; phenomena governing the probability and dynamics of spectroscopic transitions will be treated in more detail later, in Section 3.7, dealing with the interaction of molecules with light.

Atomic spectroscopic measurements were the most stringent test for the quantitative predictions of early quantum theory [238]. However, the formidable computational difficulties had prevented for a long time a similar spectacular success of molecular quantum chemistry, but the results in qualitative interpretation of ionization potentials and electronic transitions using MO methods, proved the efficiency of the theory. The qualitative picture emerging from molecular orbital theory still serves as the theoretical framework for systematization and interpretation of various spectroscopic data related to ionized and excited states. Recent developments in computational facilities made possible nearly quantitative agreement with experiment, at least in the case of small molecules, and quantum chemistry has an increasing role in elucidating the nature of higher electronic states not easily amenable to experimental studies.

First, the single configurational model, which serves as the basis for qualitative discussion of the properties of various ionized and excited states is presented briefly in Section 3.6.1. Although there are many similarities between the various phenomena concerning ionized and excited states, these two topics are treated separately in Sections 3.6.2 and 3.6.3, respectively.

3.6.1 SINGLE CONFIGURATIONAL DESCRIPTION OF ELECTRONIC STATES AND SPECTROSCOPIC METHODS

According to molecular orbital theory, electronic states can be approximately described on the basis of the single configurational model by using the Aufbau Principle (*cf.* Section 1.2.4). This method provides a useful tool for the interpretation and classification of spectroscopic data.

An *electron configuration* means a set of molecular orbitals with the corresponding occupation numbers (0, 1, or 2), which can be considered as a short-hand notation for the single determinantal wave function. Usually, it is supposed that the same set of canonical orbitals, which emerges from the SCF treatment of the ground state, is appropriate for the description of different ionized and excited states, only the occupation scheme varies. We will see that this approximation has its limitations, but it works well for qualitative purposes in the majority of cases.

The orbitals are categorized by spectroscopists on the basis of their binding energy and spatial extent, as core, valence and Rydberg orbitals.

Core orbitals, although delocalized in a canonical MO description among the atoms of the same type, are tightly bound and compressed to the specific atomic centres and are only slightly influenced by other atomic centres of the molecules. They retain to a large extent their atomic nature, as it is stressed by the usual notation ($1s_C$, $1s_O$ etc.).

Electrons on *valence orbitals* have binding energies in the order of magnitude of chemical bonding energies. Usually valence orbitals are delocalized over the whole molecular frame. According to local symmetry properties σ and π bonding orbitals are distinguished. Their antibonding counterparts, the σ^* and π^* orbitals usually become populated only in some excited states. The non-bonding orbitals, which are denoted by the letter n are related to the lone pairs of a localized model.

Rydberg orbitals have an important role in the higher excited states of molecules. These are diffuse and only loosely bound orbitals resembling atomic orbitals with higher principal quantum numbers. Details of molecular architecture exert only a small perturbative influence upon them; consequently, they behave as quasi-hydrogenic orbitals. Although Rydberg orbitals are practically of atomic character, they are so diffuse that they do not belong to any of the individual atoms in the molecule. Rather they are related to the orbitals of the so-called "united atom", which would be formed by "compressing" all the nuclei of the molecule to one point. Correspondingly their notation is simply that of atomic orbitals: *ns*, *np*, *nd* etc, where n is the principal quantum number.

Molecular orbitals can also be denoted by the symbol of the irreducible representation according to which they are transformed in the molecular point group. In order to make distinction between the symmetry of electronic states and that of the individual orbitals, the former are denoted by upper-case letters, while the orbitals are marked with lower-case ones. For example the $^1A_1$ ground state of formaldehyde (H_2CO) is represented by the following electronic configuration:

$$^1A_1 : (1a_1)^2(2a_1)^2(3a_1)^2(4a_1)^2(1b_2)^2(5a_1)^2(1b_1)^2(2b_2)^2$$

where the orbitals follow each other in the order of increasing energy, and the occupation numbers are indicated by superscripts. The symmetry notation refers to the C_{2v} point group. According to the generally accepted conventions a and b stand for molecular orbitals, which are respectively symmetric and antisymmetric to the C_2 twofold rotation; while the subscripts 1 and 2 mean symmetric and antisymmetric behaviour, respectively, with reference to reflection to the plane perpendicular to the molecular plane. Left superscripts of the state symbol denote the spin multiplicity (singlet = 1, doublet = 2, triplet = 3) etc.).

The many-electron wave function of a molecule transforms according to one of the irreducible representations of the molecular point group. (Owing to the Jahn–Teller theorem, this irreducible representation is usually non-degenerated.) We may call this representation the symmetry of the electronic state. The symmetry of the electronic

state is closely related to orbital symmetries in one-determinantal wave functions. If there is no singly occupied molecular orbital in the given configuration, in most cases the state belongs to the totally symmetric representation of the molecular point group (A_1 in the case of formaldehyde, but the $4n$ antiaromatic conjugated hydrocarbons, for example, form an exception to this rule). In other cases usually the singly occupied levels determine the overall symmetry. If there is only one singly occupied molecular orbital, the symmetry of the state is the same as that of the singly occupied orbital; otherwise, the direct product formed from the irreducible representations provided by the singly occupied levels gives the overall symmetry. The above rule applies well for point groups without degenerate irreducible representations; further considerations should be applied if the direct product representation turns out to be reducible.

Besides the symmetry notation of the molecular orbitals, the chemical notations may also be very instructive. It has to be stressed that in the theory of electronic spectra we use canonical orbitals (at least in most cases). Although the chemical notation is similar to the symbols of localized orbitals by appearance, it also refers to canonical orbitals, albeit emphasising the most significant localized components of each orbital (*cf.* Section 1.4). The formaldehyde ground state with chemical notation is:

$$(1s_O)^2(1s_C)^2(\sigma_{CO})^2(\sigma_{CH})^2(\sigma_{CH})^2(\sigma n_{CO})^2(\pi_{CO})^2(n_{CO})^2 .$$

In the *single configurational model* negative and positive ionic states are formed from the neutral ground state configuration by adding or removing one electron from one of the occupied orbitals. The ground state of a positive ion formed from the formaldehyde molecule is of $^2B_2$ symmetry:

$$^2B_2 : (1a_1)^2(2a_1)^2(3a_1)^2(4a_1)^2(1b_2)^2(5a_1)^2(1b_1)^2(2b_2)^1 ; \qquad \pi \rightarrow \infty .$$

Similarly, excited states are generated by removing one electron from an occupied orbital and putting it on a virtual one. Some excited states of formaldehyde stand here as example. Only the four highest-energy occupied orbitals are indicated explicitly, because inner valence shell and core orbitals are unchanged. In these cases a simplified notation of the nature of excited states is also presented, referring to the electron "jump" from the occupied to the virtual orbital (*cf.* Fig. 3.27 where a pictorial illustration of the electron promotions is also presented).

$$^{1,3}A_2 : (5a_1)^2(1b_1)^2(2b_2)^1(1b_1^*)^1 ; \qquad n \rightarrow \pi^*$$

$$^{1,3}A_1 : (5a_1)^2(1b_1)^1(2b_2)^2(1b_1^*)^1 ; \qquad \pi \rightarrow \pi^*$$

$$^{1,3}B_1 : (5a_1)^1(1b_1)^2(2b_2)^2(1b_1^*)^1 ; \qquad \sigma_n \rightarrow \pi^*$$

$$^{1,3}B_2 : (5a_1)^2(1b_1)^2(2b_2)^1(6a_1^*)^1 ; \qquad n \rightarrow 3s .$$

The first three states are intravalence excited states (both occupied and virtual levels are of valence type) whereas the last one is a Rydberg state involving a $3s$ orbital.

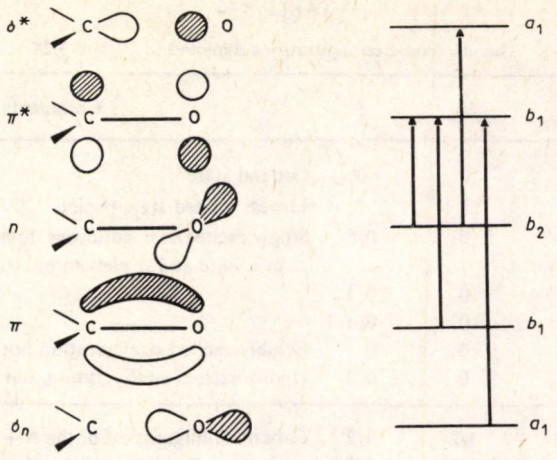


Fig. 3.27 Schematic representation of the valence molecular orbitals of formaldehyde and the most important intravalence electronic transitions. Both the chemical ($n, \pi, \sigma, \pi^*, \sigma^*$) and the symmetry ($a_1, b_1, a_2, b_2$) notation of the molecular orbitals are indicated

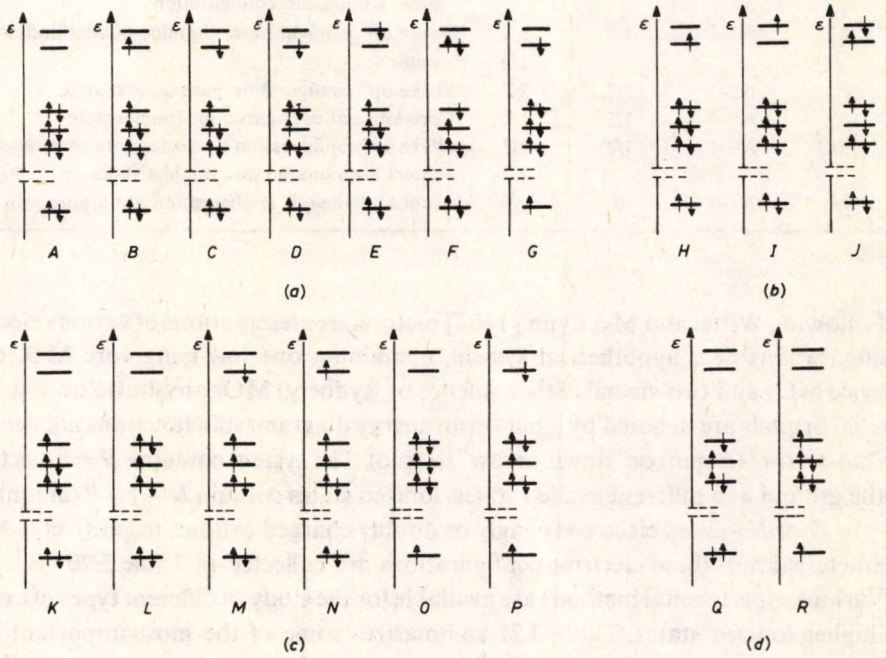


Fig. 3.28 Electron configuration diagrams for a system containing one core MO, three valence MOs and two virtual MOs. (A) $N=8$ electrons; (B) $N=9$ electrons; (C) $N=7$ electrons; (D) $N=6$ electrons. For explanation consult Table 3.20. (With permission from Ref. [1432])

TABLE 3.20

The electronic configurations depicted in Figure 3.28

Configuration	No. of electrons	M_s	S	Comments
A	N	0	0	Ground state
B	N	1	1	Lowest excited state triplet
C	N	0	0, 1	Singly excited configurations do not correspond to pure-spin state and triplet states
D	N	0	0, 1	
E	N	0	0, 1	
F	N	0	0, 1	Doubly excited configuration not a pure spin state
G	N	0	0, 1	Highly excited configuration, not a pure spin state
H	$N+1$	1/2	1/2	Ground configuration of the $N+1$ electron system
I	$N+1$	1/2	1/2	Excited configuration of the $N+1$ electron system
J	$N+1$	1/2	3/2 1/2	Excited configuration of the $N+1$ electron system, does not correspond to pure spin state, enters both quartet and doublet states
K	$N-1$	1/2	1/2	Ground configuration the $N-1$ electron system, doublet state, Koopmans' configuration
L	$N-1$	1/2	1/2	Excited configuration $N-1$ electron system, doublet state, Koopmans' configuration
M	$N-1$	1/2	3/2 1/2	"Shake up" configuration, contains quartet and doublet states
N	$N-1$	3/2	3/2	"Shake up" configuration pure quartet state
O	$N-1$	1/2	1/2	"Core-ionized" configuration, doublet state
P	$N-1$	1/2	3/2 1/2	"Shake up" configuration connected with core ionization, enters both quartet and doublet states
O	$N-2$	0	1, 0	Valence "shake-off" configuration not a pure spin state

Following Wittel and McGlynn [1432] pictorial representations of various electron configurations of a hypothetical system, containing one low-lying core MO, three valence MOs and two virtual (either valence or Rydberg) MOs are shown on Fig. 3.28. Spatial orbitals are denoted by a bar on an energy diagram; spin functions are denoted by "up-arrow" (α spin) or "down-arrow" (β spin). The system contains N=8 electrons in the ground and different excited states; ionized states contain $N+1$=9 (anion) and N—1=7 or N—2=6 electrons (singly or doubly charged cations, respectively). Main characteristics of these electron configurations are collected in Table 3.20.

Various experimental methods are available for the study of different types of excited or higher ionized states. Table 3.21 summarizes some of the most important ones following Wittel and McGlynn [1432]. In order to make clear the meaning of different excitation processes (shake-up, shake-off, Auger, emission etc.), a pictorial illustration is also presented on Fig. 3.29.

TABLE 3.21

Photoinduced electron transitions (*cf.* Fig. 3.29)

Confign excitation	Name of transition	Name of exptl process	Pictorial process of Fig. 3.29
$A \rightarrow B, C, D, E, F$	Electronic excitation	VIS/UV absorption spectroscopy	1
$A \rightarrow G$	Core excitation	X-ray absorption spectroscopy	2
$B \rightarrow A$	Phosphorescence	Emission spectroscopy	7
$C \rightarrow A$	Fluorescence		
$H \rightarrow A, B$	Ionization of the N+1 electron system		
$A \rightarrow K \ldots R$	Ionization	Photoelectron spectroscopy	3, 4
$A \rightarrow M, N, P$	"Shake-up"	Photoionization	5
$A \rightarrow Q, R$	"Shake-off"		6
$A \rightarrow (O \rightarrow Q)$	Auger transition	Auger spectroscopy	8
$A \rightarrow (O \rightarrow K)$	X-ray emission	X-ray emission spectroscopy	9

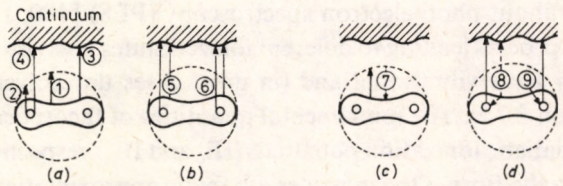


Fig. 3.29 Pictorial representation of different types of transitions. *(a)* "simple" events; *(b)* simultaneous events; *(c)* and *(d)* consecutive events. (With permission from Ref. [1432])

3.6.2 IONIZED STATES

Experimental methods: photoelectron spectroscopy [180, 1273], ultraviolet spectroscopy [632], mass spectroscopy [77].

In the course of an ionization process induced by some excitation source like UV radiation, X-rays, synchrotron radiation, electron- or atom beams the molecule M loses an electron and a positive ion is formed:

$$M \rightarrow (M^+)^* + e^- . \tag{3.126}$$

The resulting ionized species can be either in the ground or in an excited electronic state (the excited ionic state is denoted by a star). Spectroscopic methods which are concerned with the study of ionized states by measuring the binding energy (ionization

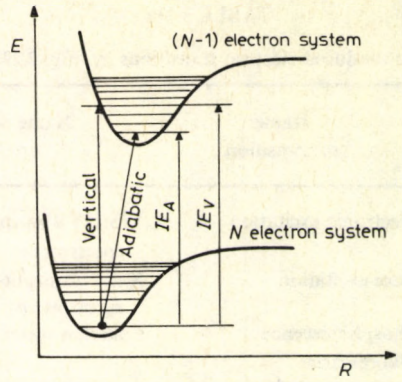


Fig. 3.30 Schematic illustration of a vertical and an adiabatic ionization event, with the corresponding vertical (IE_V) and adiabatic (IE_A) ionization energies

energy, IE) of the ejected electron, are called electron spectroscopies. Although the terms "electron spectroscopy" and "electronic spectroscopy" are identical in linguistic sense, they have acquired different meanings. Electronic spectroscopy is used for denoting processes which involve transitions among different electronic states of an N-electron system (N = constant) while electron spectroscopy refers to ionization processes ($N \neq$ constant). In particular, when photons are used as primary excitation sources, we speak about photoelectron spectroscopy (PES) [180, 1372].

Each ionization process leading to different ionized states give rise to a band in PES. The bands usually have vibrational and (in most cases unresolved) rotational fine structure (*cf.* Section 3.7.2). The fundamental quantities of theoretical interest are the vertical and the adiabatic ionization potentials (IE_v and IE_a, respectively). The *vertical ionization energy* in the Born–Oppenheimer adiabatic approximation is defined as the energy difference between the potential curves of the molecule and the ion at the nuclear configuration where the lower curve exhibits its minimum, while the *adiabatic ionization* potential measures the difference between the minima of the upper and lower potential surfaces (Fig. 3.30). The vertical ionization potential is that which is usually determined from the position of the maximum intensity on a PES band (*cf.* Franck–Condon principle, 3.7.1), although the appropriateness of this choice has been questioned [1295]. In addition to the simple ionization events, more complicated two-electron processes may take place (*e.g.* shake-up, shake-off processes), which give rise to satellite bands in the PES. In some cases the experimental photoelectron spectra cannot be interpreted in the framework of the Born–Oppenheimer approximation and non-adiabatic effects have to be considered. At the end of the section some examples of this type will also be presented.

The electron affinity (EA) is defined either as the IE of the corresponding negative ion, or using the following electron detachment process:

$$(M^-)^* \rightarrow M + e^- . \tag{3.127}$$

The experimental determination of electron affinities represents a rather difficult problem. Recently, due mainly to the development of laser photodetachment techniques, accurate atomic and diatomic EAs have become available, but only a few reliable measurements of EAs are known for polyatomic molecules.

The assignment of the PES requires the calculation of ionization potentials. The configuration description within the framework of MO theory has proven to be quite successful for this purpose, even in a quantitative respect. The appropriateness of the single configuration model is asserted by the Koopmans theorem [735, 1297] (*cf.* Section 1.2.4). Within the HF approximation the negative SCF orbital energies ε_k are equal to the vertical ionization energies:

$$IE_k = -\varepsilon_k \tag{3.128}$$

and similar relations hold for the virtual orbital energies and electron affinities. These equalities hold if the orbital relaxation is ignored, otherwise the Koopmans theorem requires corrections even within the Hartree–Fock model (*see below*).

According to the above model a one-to-one correspondence should be found between the bands of the photoelectron spectrum and the occupied molecular orbitals. Actually, the number of most prominent bands really equals the number of occupied orbitals; thus PES measurements provide direct experimental evidence for the orbital structure of atoms and molecules [68].

The Koopmans theorem applies only for simple one-electron ionization processes; it is not valid for the two-electron shake-up and shake-off events. There are other cases, where Koopmans theorem leads to qualitatively wrong predictions for the sequence of ionization potentials (see later), but apart from these cases, it serves as a useful guide in the approximate prediction of IEs in connection with MO calculations. However, if quantitative agreement between theory and experiment is required, Koopmans' theorem may be quite unsatisfactory due to the approximations inherent the model. Empirical relations, *e.g.*

$$IE_k = -0.92\varepsilon_k \tag{3.129}$$

may improve the matching of calculated and experimental ionization potentials within a particular class of compounds [149], but the usual error range, which amounts to 1–3 eV makes the assignment of ionized states differing by less than 1 eV dangerous [1432].

Deviations of the true IE from that predicted by the Koopmans theorem arise from three main sources due to the neglect of

(1) the change in relativistic energy corrections going from neutral to ionized states;

(2) the self-consistent readjustment ("relaxation") of the orbitals in the ionized state; as has already been noted (Koopmans' theorem) corresponds to a "frozen orbital" approximation;

(3) the difference of correlation energies in the molecule and in the ion.

Relativistic effects are important when electron velocities are comparable with the velocity of the light [1103]. This is the case in regions close to the nucleus (where both potential and kinetic energies are high in accord with the virial theorem) and the higher the atomic number, the higher the velocities expected. Consequently, relativistic corrections are greatest for inner shells (and *s* orbitals) of heavier atoms. The relativistic effects are manifested in the decrease of the *s* orbital radius and in the increase of the electron binding energy (Table 3.22). The effect on the *p* orbitals is in a similar direction, but smaller, because *p* orbitals have nodes at the nuclei. Relativistic interactions increase the shielding of the nuclear charge for *d* and *f* electrons, hence the net relativistic effect may be reversed for the latter, resulting in an increased orbital radius and decreased IE. In free atoms, relativistic effects remove the degeneracy of *p*, *d*. *f* orbitals. The above trends are illustrated by the example of argon (Table 3.22), where the diminishing amount of relativistic corrections for outer shells can also be seen.

The increasing importance of relativistic effects with increasing atomic number can be illustrated for example by the relativistic corrections to the 1s ionization potentials of CH_4, Ne and Ar, which are 0.1 eV [1078], 0.8 eV [1385], and 14 eV [53] respectively. It is usually argued that neutral ground states have larger relativistic energies than ionized states, which possess fewer electrons; consequently the non-relativistic ionization energies are smaller than the true ones [182]. However, this is not always the case. *Ab initio* calculations on positive ionic states of formaldehyde using a relativistic Hamiltonian led to the unexpected result that relativistic corrections to the $^2B_2(n)$ and $^2B_1(\pi)$ hole states were larger than for the ground state, and this increased the ionization potential [1098]. Simple theoretical approaches, like the use of the phenomenological spin-orbit coupling operator incorporated in the standard Extended Hückel Hamiltonian and the subsequent application of Koopmans' theorem, have proved to be successful for calculating relativistic ionization energies in larger molecules containing Br and I [870].

TABLE 3.22

Ionization energies of the argon atom calculated by relativistic and non-relativistic approaches (eV)

Orbital	Non-relativistic		Relativistic		Exp.
	Koopmans	ΔSCF	Koopmans	ΔSCF	
1*s*	3227.4	3195.2	3240	3209	3205.9
2*s*	335.3	324.8	336	327	326.3
$2p_{1/2}$	260.4	248.9	261	250	250.6
$2p_{3/2}$ } 2*p*			259	248	248.5
3*s*	34.8	33.2	34.9	33.3	29.3
$3p_{1/2}$	16.1	14.8	16.1	14.8	15.94
$3p_{3/2}$ } 3*p*			15.9	14.6	15.76
Reference	[53]	[53]	[1192]	[1192]	[1273]

In general the so-called Koopmans defect is defined as the difference of the true nonrelativistic ionization potential and that predicted by Koopmans' theorem. The Koopmans defect has two contributions arising from the neglect of effects 2 and 3 discussed above. Thus neglecting relativistic effects, the ionization potential becomes

$$IE_k^{nonrel} = -\varepsilon_k + \Delta R_k + \Delta C_k \tag{3.130}$$

where ΔR_k is the relaxation and ΔC_k is the correlation correction to the ionization potential for the removal of an electron from the k'th occupied MO.

Relaxation corrections come from the fact that although the MOs obtained by an SCF calculation for the neutral parent molecule minimize the single determinant energy of the ground state, they yield an energy for the cation which is higher than what would be obtained by an independent variational calculation. In other words, the single determinant wave function built up of the MOs determined for the neutral molecule is not the best single determinant for the ionic state. For this reason Koopmans' theorem always gives a higher IE than the value predicted by taking the difference between separate SCF calculations on the molecule and on the cation "hole state" (so-called ΔSCF prodecure).

Neglect of correlation corrections leads to errors, when the values of correlation energies are different for the ionic and for the ground states. Generally the neutral molecule has the greater correlation energy, which is qualitatively explained by the fact that a reduction of the gap between filled and empty MO levels usually increases the correlation energy. Production of a cation usually increases this gap and thus reduces the correlation energy with respect to the neutral parent molecule. Proper inclusion of electron correlation would lower the energy of the neutral molecule more than that of the cation, thus making the true IE larger than the value obtained by neglecting this effect. According to the above arguments the sign of relaxation and correlation corrections is opposite and, at least partial cancellation of errors can be expected when using the Koopmans theorem. A schematic representation of the various corrections to Koopmans' theorem for a positive ionic state is depicted on Fig. 3.31. Unfortunately,

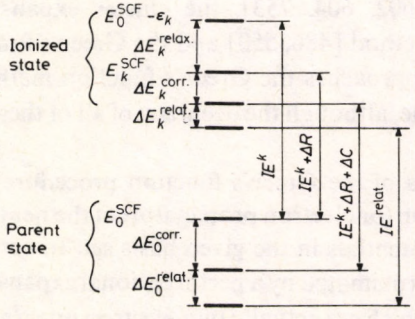


Fig. 3.31 Representation of the corrections to the Koopmans theorem. IE^k means the ionization energy in the Koopmans approximation, ΔR is the relaxation correction, ΔC is the correlation correction. $IE^{relat.}$ stands for the ionization energy if the relativistic approach. (After Ref. [182])

the correlation and relaxation corrections may have the same sign in certain cases, and due to the lack of cancellation of errors Koopmans' theorem may become a poor approximation. This situation is usually referred to as the nonvalidity (or breakdown) of Koopmans theorem.

It has to be noted that for electron affinities the situation is much less favourable than with ionization potentials. Production of an anion usually reduces the separation of the filled and empty MO levels, so the inclusion of correlation effects lowers the energy of the anionic state more than that of the neutral molecule. Since in this case the correlation and relaxation corrections practically always have the same sign, no cancellation of errors can be expected when using Koopmans' theorem for electron affinities.

Sophisticated procedures are required to take into account the relaxation or both the relaxation and correlation corrections to the ionization potentials. The improvement relative to Koopmans' theorem assessed by ΔSCF calculations (*i.e.* taking the difference of separately calculated SCF energies for the ion and the ground state molecule [53]) is usually identified with relaxation corrections exclusively, although there is some ambiguity about this definition (see later). Direct calculation of relaxation contributions to the Koopmans' defect, without forming the small difference of two large numbers, (the energies of ionized and ground states) is also possible by using the transition operator method (TOM) of Goscinski and coworkers [470] related to the transition state concept of Slater [1288].

In principle the correlation effects can be included in the computational procedure by carrying out separate CI calculations on both ground and ionic states ("ΔCI" method) [521].

However, more efficient direct procedures are preferred for this purpose. The main advantage of direct methods is that making use of only the ground state SCF wave function the ionization potential is evaluated directly without forming the small difference of large numbers. Relaxation and correlation effects are accounted for simultaneously. There are four main types of direct approaches for calculating ionization energies: the diagrammatic many-body Rayleigh–Schrödinger perturbation theory (MB–RSPT) [602, 604, 753], the cluster expansion method [1060], the equations of motion method [486, 550] and the Green's function method [186, 1006, 1015]. Among these approaches the Green's function method seems to be the most elegant and effective one, although the accuracy of all of these procedures are about at the same level [182].

The theoretical basis of the Green's function procedure is that the so-called one particle Green's function (or electron propagator) of the neutral parent molecule yields the exact ionization potentials in the given basis set. In actual calculations the exact Green's function is approximated by a perturbational expansion in terms of interaction matrix elements V_{ijkl}, which are actually two-electron integrals over molecular orbitals:

$$V_{ijkl} = \langle \phi_i(1)\phi_j(2) | r_{12}^{-1} | \phi_k(1)\phi_l(2) \rangle . \tag{3.131}$$

The second order expression for the ionization potential in this approach can be partitioned explicitly to the Koopmans term and to various corrections of different physical significance [1100]; thus making possible the analysis of the calculated results:

$$\mathrm{IE}_k \approx -\varepsilon_k + \Delta R_k^{(2)} + \Delta C_{\mathrm{REM},k}^{(2)} + \Delta C_{\mathrm{REL},k}^{(2)} \tag{3.132}$$

where the meaning of the various terms is explained in the following.

$\Delta R_k^{(2)}$ is the second order relaxation correction:

$$\Delta R_k^{(2)} = \sum_i^{\mathrm{occ}} \sum_a^{\mathrm{virt}} \frac{V_{kaki}^2 + (V_{kaki} - V_{kaik})^2}{\varepsilon_i - \varepsilon_a}. \tag{3.133}$$

The first part $\Delta C_{\mathrm{REM},k}^{(2)}$ of the second order correlation correction is due to the fact that a part of the pair correlation energies present in the ground state disappears at the removal of an electron from the orbital ϕ_k:

$$\Delta C_{\mathrm{REM},k}^{(2)} = \frac{1}{2} \sum_i^{\mathrm{occ}} \sum_a^{\mathrm{virt}} \sum_b \frac{V_{kiab}^2 + V_{kiba}^2 + (V_{kiab} - V_{kiba})^2}{\varepsilon_a + \varepsilon_b - \varepsilon_i - \varepsilon_k} \tag{3.134}$$

while the second part is the many-body relaxation term $\Delta C_{\mathrm{REL},k}^{(2)}$, which accounts for the change in pair correlation energies in the course of the orbital relaxation:

$$\Delta C_{\mathrm{REL},k}^{(2)} = \frac{1}{2} \sum_{i \neq k}^{\mathrm{occ}} \sum_{l \neq k}^{\mathrm{occ}} \sum_a^{\mathrm{virt}} \frac{V_{kail}^2 + V_{kali}^2 + (V_{kail} - V_{kali})^2}{\varepsilon_i + \varepsilon_l - \varepsilon_a - \varepsilon_k} - \sum_{i \neq k}^{\mathrm{occ}} \sum_a^{\mathrm{virt}} \frac{V_{kaik}^2}{\varepsilon_k - \varepsilon_a}. \tag{3.135}$$

These formulae afford a qualitatively reliable analysis of the Koopmans' defect, as will be shown later.

Core ionizations. SCF calculations turned out to be quite successful for the evaluation of core ionization potentials [53]. This success has been attributed to the fact that for core ionizations the relaxation correction to Koopmans' theorem dominates over the correlation terms. Accordingly, the transition operator method (TOM), which takes into account this orbital relaxation effect, is expected also to yield reliable core ionization potentials [207].

SCF calculations on core ionization potentials of homonuclear diatomics, like N_2 and O_2, raised an interesting question concerning the localized or delocalized nature of core hole states [54, 1297]. For example, in the O_2 molecule the localized $1s$ orbitals can be combined to give $1\sigma_g$ and $1\sigma_u$ symmetry adapted delocalized core orbitals. Localized core hole states emerge if an electron is ejected from either of the $1s$ localized orbitals, while delocalized core hole states can be formed by removing an electron from the $1\sigma_g$ or $1\sigma_u$ orbitals. Bagus and Schaefer performed unrestricted Hartree–Fock (UHF) calculations on the core ionized states of O_2, and found that the energy of the ion is lower for the localized core hole state (if the breaking of symmetry of the molecular orbitals is allowed) than for the symmetric Hartree–Fock solution (delocalized core hole state) [54]. The ionization potential obtained for the localized core hole state (543.1 eV) is in excellent agreement with experiment (542.0 eV), while calculations for the delocalized core hole state overestimated the experimental value by

more than 12 eV (554.4 eV). Bagus and Schaefer concluded that "the 1*s* core hole states of O_2^+ are localized—that is, the ejected electron has been specifically removed from one of the two atoms" [54]. The idea of such a physical localization has been supported by others too [1297].

However, such an interpretation of the above cited results is incorrect. The question of the physical localization of the core hole is essentially a time problem, which cannot be answered without considering the time-evolution of the wave function, as was pointed out by Denis *et al.* [306]. In particular, the special properties of the Hartree–Fock solution are irrelevant in this respect.

Cederbaum and Domcke analysed the problem using the (3.132) decomposition of the Green's function expression of the ionization potential [187]. They could demonstrate that in the delocalized representation the contributions of the $\Delta R^{(2)}_{1s(\mathrm{del})}$ and $\Delta C^{(2)}_{\mathrm{REM},\,1s(\mathrm{del})}$ relaxation and correlation terms are of the same sign and of about the same magnitude ($\Delta C^{(2)}_{\mathrm{REL},\,1s(\mathrm{del})}$ is negligibly small), while in the localized picture the entire second order correction to Koopmans' theorem comes from the relaxation effects $\Delta R^{(2)}_{1s(\mathrm{loc})}$. Similar conclusions were drawn by Denis *et al.* [306], who discussed the question in the framework of a configuration interaction analysis performed in the basis of determinantal wave functions built up from either localized or delocalized molecular orbitals. They showed that the second order correction to the Koopmans theorem is the same in both descriptions. In the localized picture the polarization of the valence orbitals is due to mainly single excitations (with respect to the zeroth order Koopmans description of the ion), which is an effect directly included in the Hartree–Fock theory. On the other hand, in the delocalized description the most important second order effects appear as double excitations, which formally correspond to correlation corrections. The equivalence of the symmetry adapted and broken symmetry solutions have been demonstrated in actual calculations at a limited CI level *e.g.* in Ref. 82.

The spatial-symmetry-broken description of hole states is a special example of the Hartree–Fock instabilities. For example, in the case of the N_2^+ ion, the $2a_g$ and $2b_{1u}$ ionization potentials were calculated as a function of the internuclear separation. (Although these are not core hole states, the qualitative behaviour of 1σ levels is expected to be similar.) At smaller internuclear distances the symmetry restricted (RHF) and the symmetry-broken (UHF) methods give the same results, but at distances greater than 1.8 Å "hole localization" occurs, *i.e.* the RHF solution becomes unstable with respect to the UHF one [814]. (*Cf.* the discussion on the "symmetry dilemma" in Sections 1.2.4 and 1.3.1 [822].)

In $Cr(CO)_6$ the reduction of the symmetry from O_h to C_{4v} resulted in an improvement of the calculated ionization potentials not only for 1*s* but for near valence levels also [52], showing that use of symmetry-broken solutions may be "advantageous" not only for core ionizations.

Let us note that according to the definition of the correlation energy given by Löwdin (the difference of the exact nonrelativistic energy and the energy of the

conventional RHF solution Section 1.2.4), the improvement brought about by the ΔSCF calculations with respect to the Koopmans theorem cannot always be related just to relaxation effects. When UHF methods are applied for the description of the hole states the ΔSCF results contain a certain amount of correlation corrections as well [413].

The core ionization potentials are investigated experimentally by X-ray photoelectron spectroscopy (XPS) [1273]. These studies showed that core ionization energies are characteristic of the atomic centre from which the ionization occurs. The influence of the neighbouring atoms is relatively small, and leads to shifts in the core ionization potentials with respect to the free atom positions. These "XPS chemical shifts" are in the order of magnitude of the chemical bond energies (1–4 eV) and reflect the effect of the chemical environment of the atom [1273]. Since the chemical shifts amount to only a few percent of the core ionization energies, their theoretical evaluation may proceed by perturbation theory. This type of treatment of the core-level orbital energies (*i.e.* we assume the validity of Koopmans' theorem for the core-level electron binding energies) leads to the ground state potential model (GPM) [431], where the chemical shifts are correlated with the electrostatic potential V_A calculated at the nucleus A:

$$V_A = \int \rho_{el}(\mathbf{r}) |\mathbf{R}_A - \mathbf{r}|^{-1} \, d\mathbf{r} + \sum_{B \neq A} Z_A |\mathbf{R}_A - \mathbf{R}_B|^{-1} . \tag{3.136}$$

Introducing an arbitrary partitioning of the molecular electron density into atomic components (*e.g.* according to Mulliken, or using the definition of Politzer; *cf.* Section 3.4.1), the following approximate equation is obtained for the XPS chemical shifts:

$$\Delta IE \approx -K_A P_{AA} + \sum_{B \neq A} Q_B R_{AB}^{-1}, \tag{3.137}$$

where K_A is the electrostatic potential of the charge distribution $\rho_{el}^{(A)}(\mathbf{r})$ assigned to atom A:

$$K_A = \int \rho_{el}^{(A)}(\mathbf{r}) |\mathbf{R}_A - \mathbf{r}|^{-1} \, d\mathbf{r}, \tag{3.138}$$

P_{AA} is the valence population of atom A and Q_B is the net atomic charge of atom B. Various empirical equations having the same structure as Eq. (3.137) have been successfully used to correlate experimental chemical shift data with atomic charges. The qualitative implication of relations of this type is rather simple: the energy required for removing an electron from the core orbital of an atom increases with its increasing positive or decreasing negative charge, and the core ionization energy is lowered when all atoms except A are negatively charged. Good correlations have been found between the chemical shift data and atomic charges derived by the method of Pauling from fractional ionic characters of bonds [1273], from net atomic charges obtained by Extended Hückel [548] or by CNDO [587] molecular orbital methods.

The GPM does not take into account the relaxation effects in the valence shell, which means that the valence electron density in the final ionic state is different from that in

the initial ground state. Such "final state effects" are approximated by the equivalent core model introduced by Hollander and Jolly [588]. The concept of equivalent cores means that when a core electron is removed from an atom in a molecule, the valence shell electrons relax as if the nuclear charge of the atom had increased by one unit. In other words atomic cores, which have the same charge may be considered to be chemically equivalent. A hypothetical reaction, the "core-replacement" reaction has been invoked in this connection. For example, the core hole state of N_2 (NN^{*+}) can be replaced by the ground state ion NO^+:

$$NN^{*+} + O^{6+} \rightarrow NO^+ + N^{*6+}. \tag{3.139}$$

We can write a similar reaction for other nitrogen compounds, for example:

$$^*NH_3^+ + O^{6+} \rightarrow OH_3^+ + N^{*6+}. \tag{3.140}$$

The thermochemical model of XPS shifts is based upon the assumption that the energy associated with the above reactions, the "core-replacement energy", is approximately constant for all the core replacement reactions of a given atom. In this case the energy of the following reaction

$$N_2 + OH_3^+ \rightarrow NO^+ + NH_3 \tag{3.141}$$

equals the shift in the core ionization energies from N_2 to NH_3. The equivalence of the core replacement reactions have been verified for certain families of compounds [1]. We note, that according to theoretical analyses, the thermochemical model, just like the ground state potential model, is able to predict shifts in the orbital energies (Koopmans' theorem) and not in ionization potentials [1271]. The relationship between core ionization potentials and thermochemical data, as predicted by the equivalent cores model, can be used for the determination of proton affinities or isomerization energies from measured core ionization potentials. This method may be valuable when experimental heats of formations cannot be obtained by traditional methods [73].

In order to include relaxation effects in a comparatively simple model, the GPM procedure has been generalized using the theory of transition operators [470]. The transition potential model [471] involves the evaluation of the charge density appearing in Eq. (3.136) with a Hamiltonian corresponding to a pseudoatom with nuclear charge $Z + 1/2$ for the ionization site. The transition potential model can be extended to Auger ionization processes, where doubly, triply etc. ionized species are formed, too. In these cases, pseudoatoms of nuclear charge $Z + 1$ or $Z + 1.5$ should be used [471].

The simultaneous electron excitation accompanying the primary ionization process gives rise to satellite peaks of lower intensity beside the main band, due to a Koopmans configuration. Such "shake-up" processes can be explained by the existence of "non-Koopmans" configurations, where one electron is ejected and another one is promoted to a virtual orbital. The shake-up processes usually appear in connection with core

ionizations. For example, a typical shake-up configuration is the $(1a_1)(2a_1)^2(1b_1)(3a_1)^2(1b_2)^2(2b_1)$ configuration of water (in a shorthand notation: $1b_1 \rightarrow 2b_1$, $1a_1$), which is associated with the 1*s* ionization.

In a configuration interaction (CI) approach the ionic wave function of the shake-up state $\Phi_{i\rightarrow j,k}$ (where the shorthand notation for the leading configuration $(i\rightarrow j, k)$ denotes an $i\rightarrow j$ excitation accompanying the k-level ionization), is expanded in terms of doublet configurations ($\Psi_{m\rightarrow n,k}$) obtained from the Koopmans configuration $(0\rightarrow 0, k)$ by allowing one-electron excitations $m\rightarrow n$:

$$\Phi_{i\rightarrow j,k} \approx \sum_{mn} c_{mn}^{ij} \Psi_{m\rightarrow n,k}. \tag{3.142}$$

In this approximation the relative intensities of the shake-up peaks of the photoelectron spectrum are given by the square of the expansion coefficients $|c_{00}^{ij}|^2$, which are interpreted as the "Koopmans characters" of the states. This model is referred to as the intensity borrowing mechanism of shake-up line intensities [182]. Besides the use of standard CI methods [489], Green's function techniques [1243], and quasidegenerate many-body RSPT [603] can be effectively used for the calculation of shake-up ionization spectra.

The strong mixing among different shake-up configurations connected to the same core ionization event may result in broad line systems in the spectrum, making difficult the reliable determination of the single core-ionization potential itself, which is of importance for obtaining experimental chemical shifts. In order to have an appropriate experimental quantity to which a unique core binding energy is related, Manne and Aberg [869] derived the following formula:

$$\sum_{ij} P_{i\rightarrow j,k} \mathrm{IE}(i\rightarrow j,k) = \mathrm{IE}^F(k) \tag{3.143}$$

where $P_{i\rightarrow j,k}$ is the normalized relative intensity of the ionization process $(i\rightarrow j, k)$ and IE $(i\rightarrow j, k)$ is the experimental ionization energy of the given process. The intensity weighted average ionization potential $\mathrm{IE}^F(k)$ can be referred to as the ionization energy of the frozen orbital ionic state and it can be used to derive the corresponding chemical shifts [413].

The theoretical treatment of Auger spectra (*cf.* Table 3.21) is also a rather difficult task. Green's function methods can be applied here also [791], and even Auger-satellites could be calculated in fair agreement with experiment, using a three-particle Green's function approach [790].

Valence ionization. The study of *valence ionization* processes is an important way of getting accurate information about the electronic structure of molecules. For valence ionizations, the balance between the relaxation and correlation effects is a much more complicated problem than for core ionizations. Here both contributions to the Koopmans defect are often in the same direction, and the sign of the correlation correction may vary from orbital to orbital even in the same molecule. There are

several examples for the non-validity of the Koopmans theorem, when the sequence of ionization potentials predicted by the Koopmans theorem is different from the experimental one. A well-known case is that of the N_2 molecule. Large basis set *ab initio* calculations predict an IE sequence on the basis of Koopmans' theorem as $1\pi_u$, $3\sigma_g$, $2\sigma_u$ [172]. The experimental order* of ionized states is quite different: $3\sigma_g$, $1\pi_u$, $2\sigma_u$ [353]. The unfavourable situation is not improved at all, if relaxation corrections are accounted for within the framework of a ΔSCF calculation: the ionization energy sequence remains unaltered [172]. In order to have agreement between the theory and experiment both relaxation and correlation corrections have to be considered, for example by a Green's function procedure [191]. The analysis of these results showed that while, for the $1\pi_u$ orbital, ΔR and ΔC tend to cancel each other, both corrections have the same sign and about the same magnitude for $3\sigma_g$ and $2\sigma_u$ orbitals. Among the numerous examples of the non-validity of the Koopmans theorem, one can mention the case of F_2 [184], formamide [1013], acrolein [1014], and nitrosomethane [377]. A comparison of the predictions of Koopmans' theorem with experimental data can be found on Fig. 3.32, which includes the above mentioned examples for the non-validity of the Koopmans' theorem along with cases, where it is valid. In these latter examples despite the often large deviations of the numerical value of experimental ionization energies and orbital energies, the sequence is correctly maintained.

It is desirable to have some idea when one would expect a violation of the Koopmans theorem. According to von Niessen and his coworkers the following rule of thumb may help: if in linear or planar molecules a low-lying $\pi(\sigma)$ virtual orbital of nondiffuse character and a $\pi(\sigma)$ occupied valence orbital exist, significant corrections to the valence ionization potentials and deviations from the sequence predicted by the Koopmans theorem may be expected [1017]. For example, in *trans*-oxacylfluoride $(COF)_2$, there is a low-lying virtual orbital of π^* type and there are outer valence occupied π orbitals too. Since the orbital energies of the n and highest π orbitals are very close (-16.98 eV and -16.21 eV) the corresponding ionization energy order is expected to be interchanged with respect to the Koopmans predictions [1017].

The role of the basis set is quite important in ionization potential calculations using *ab initio* methods. The various basis set effects have been summarized by Čársky and Urban [182]. Minimum basis sets are not recommended at all, apart from the level of sophistication at which the IEs are evaluated. With double zeta, double zeta plus polarization bases the Hartree–Fock quality Koopmans' theorem values are reproduced with an accuracy of 0.2–0.4 eV. If relaxation and correlation effects are accounted for in the calculation, DZ + P basis sets yield an agreement with experiment within 0.25 eV; without polarization function the errors may amount to 0.5 eV.

* A variety of criteria can be used in general for the experimental identification of IEs [1372]. Among these methods the analysis of the vibrational fine structure of the bands in the PES appears to be the most reliable.

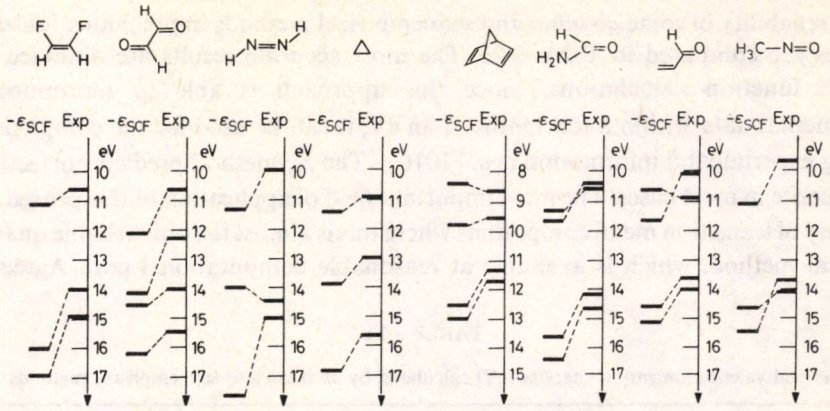


Fig. 3.32 Koopmans' defects for valence electrons in *(a)* 1,2-*cis*-difluoro-ethylene, *(b)* *trans*-glyoxal, *(c)* *trans*-diimide, *(d)* cyclopropane, *(e)* norbornene, *(f)* formamide, *(g)* acroleine and *(h)* nitrosomethane. In most cases the Koopmans theorem can be considered as valid in this energy range. Exceptions are the formamide, acroleine and nitrosomethane. (With permission from Ref. [876])

Obviously for larger molecules such large-scale calculations are impracticable and simpler approaches have to be found. Various approximate methods including local density functional procedures and different semiempirical molecular orbital theories have been applied for the calculation of ionization potentials. In local density functional schemes, like X_α [240, 242, 649, 1452] just the energy difference is formed between the neutral molecule and the ion. Since this theory may include, in principle, a certain amount of correlation effects through the scaled exchange–correlation potential, discussion of the deficiencies of these calculations cannot be carried out in the same terms as was done for Hartree–Fock theory [413].

In connection with semiempirical methods, like CNDO, INDO, the Koopmans theorem is usually applied for estimating ionization energies. In principle, one can go beyond the SCF level using the semiempirical Hamiltonian too. For example, an analysis of Green's function results obtained with an INDO model Hamiltonian for transition metal compounds, like ferrocene, cyclobutadiene-iron-tricarbonyl and iron-tetracarbonyl-dihydride, revealed some qualitative aspects for the quantum chemical origin of the nonvalidity of Koopmans' theorem for these compounds [141]. However, discussions about the validity of approximations inherent in Koopmans' theorem within the context of computational schemes, which are of lower quality than the Hartree–Fock theory can be rather dangerous [1432]. Numerous parametrized semiempirical computational schemes have been proposed for the evaluation of ionization potentials. Some examples are the SPINDO [36], HAM/3 [37], reparametrized Extended Hückel [641], which all yield fair agreement with experiment for given families of compounds. These methods should be viewed at best "as prescriptions for getting IEs rather than real MO calculations" [1432].

The reliability of some *ab initio* and semiempirical methods in predicting ionization energies are compared in Table 3.23. The most accurate results are obtained with Green's function calculations. Since this approach is able to reproduce the experimental data within a few tenths of an eV, it can be used for the completion of missing experimental information (*e.g.* [1016]). The X_α-method predicts correctly the IE sequence in most cases. The most important field of application of this procedure is the study of transition metal compounds where this is almost the only reliable quantum chemical method, which is available at reasonable computational cost. Agreement

TABLE 3.23

Vertical valence ionization energies (eV) calculated by *ab initio* and semiempirical methods

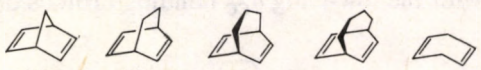
Molecule	Orbital	Green's function	Hartree-Fock, Koopmans	X_α	CNDO/2 Koopmans	Exp.
N_2	$3\sigma_g$	15.52	17.28	14.1	–	15.60
	$1\pi_u$	16.38	16.75	18.2	–	16.98
	$2\sigma_u$	18.98	21.17	18.3	–	18.78
Reference		[1015]	[172]	[242]	–	[1015]
NH_3	$3a_1$	–	11.6	14.6	17.4	10.9
	$1e$	–	17.1	16.2	19.3	15.8
	$2a_1$	–	31.3	26.9	38.1	27.5
Reference		–	[1178b]	[242]	[970]	[242]
H_2O	$1b_1$	12.69	13.24	15.0	17.9	12.78
	$3a_1$	14.91	14.28	15.5	19.7	14.83
	$1b_2$	18.96	17.24	15.7	22.0	18.72
	$2a_1$	34.82	34.57	30.1	40.8	32.2
Reference		[1015]	[241]	[220]	[1273]	[1015]
$(CH_2)_2O$	$2b_1$	10.59	12.31	–	–	10.6
	$4a_1$	11.64	12.34	–	–	11.7
	$1a_2$	13.88	14.97	–	–	13.7
	$2b_2$	14.07	14.82	–	–	14.2
	$3a_1$	16.42	17.93	–	–	16.6
	$1b_1$	17.48	19.23	–	–	17.4
Reference		[1016]	[1016]	–	–	[1016]
SF_6	$1t_{2g}$	–	22.2	18.8	24.2	19.9
	$2t_{1u}$	–	24.7	21.8	29.0	22.9
	$2a_{1g}$	–	29.6	29.7	30.8	27.0
	$1e_g$	–	45.3	35.6	43.1	39.3
	$1t_{1u}$	–	46.8	36.5	50.8	41.2
	$1a_{1g}$	–	50.4	39.3	57.0	44.0
Reference		–	[432]	[240]	[1273]	[1273]

between the CNDO/2 and experimental ionization energies is at most qualitative: the experimental values are overestimated by several eV's, but the sequence is generally good.

For example, in the case of simple alkanes and silanes a linear relationship has been found between the experimental and CNDO/2 ionization potentials; the regression coefficient is 0.94 [1335]. In this case the CNDO/2 method predicted the correct sequence of ionization energies for 52 of 58 cases. This may be encouraging for the usefulness of CNDO/2 calculations in assignment of the PES bands in related compounds. Furthermore these calculations pointed out that silicon *d* orbitals have no significant effect in bond formation of silanes. However, it should be mentioned that a thorough analysis of the semiempirical methods, in particular of CNDO/2 and MINDO/2, pointed out that the predicted orbital sequence are, more often than not, incompatible with the PES [540].

The orbital interaction concept, which had been introduced into quantum chemistry by Hoffmann [576] has become a good example of the fruitful application of qualitative MO theory (*cf.* Section 1.7) in photoelectron experiments. According to the orbital interaction model the molecule is dissected into two or more distinct fragments, whose molecular orbitals are allowed to interact. The shifts in the energies of the newly formed orbitals are estimated using perturbation theory. Since the orbital energies are directly related to the ionization potentials, photoelectron spectroscopic measurements may yield direct "evidence" for the existence of orbital interactions provided that Koopmans' theorem is valid. On the other hand, the observed data can be interpreted in terms of appropriate orbital interactions.

According to the terminology of Hoffmann [576] two types of interactions can be distinguished. *Through-space interacions* involve the interaction of two orbitals through their direct overlap, while in the case of *through-bond interactions* the splitting of orbital levels is realized *via* the participation of intervening other orbitals (bonds) (*cf.* Section 1.4). An illustrative example is the case of a series of ring compounds having two interacting ethylenic units:



The PES data for these compounds can be rationalized by assuming that the sequence of the two highest occupied π molecular orbitals in derivatives *1* and *2* is $b_2(\pi)$ above $a_1(\pi)$, while in compounds *3*, *4*, *5* the $a_1(\pi)$ orbital lies above the $b_2(\pi)$ one. This finding has been explained by assuming that in the former case, the through-space interactions dominate and lead to a splitting of the two π levels, in the sense that the antisymmetric combination of the π orbitals of the two ethylenic unit is of the higher energy (Fig. 3.33*a*). On the other hand, in compounds *3*, *4*, *5* through-bond effects dominate. The ethylenic units interact through those σ bonds of the CH_2 moieties which possess the appropriate symmetry (σ_π). The resulting splitting scheme, as is illustrated in (Fig.

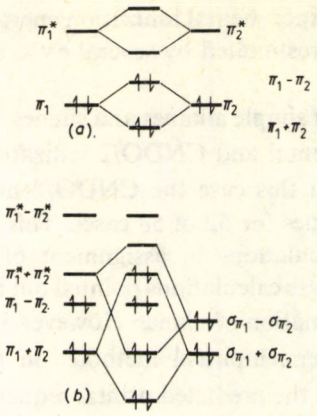


Fig. 3.33 Orbital interaction diagrams illustrating *(a)* through-space and *(b)* through-bond interactions in compounds **1**...**5** possessing two ethylenic units. For explanation see the text

3.33 *b*) places the symmetric a_1 combination of the ethylenic π orbitals at the highest energy among the occupied orbitals [578].

The concept of through-space and through-bond interactions has been reformulated after the original Extended Hückel theory, also in the terms of an SCF theory [540]. A detailed analysis of the above interactions with semiempirical SPINDO, MINDO/2 and CNDO/2 model Hamiltonians showed that the relative importance of the through-space and through-bond interactions may vary considerably depending on the computational method. In particular the CNDO/2 method was found to overestimate the amount of through-bond effects [540].

Another example may be the pyrazine molecule (Fig. 3.34). Here the direct, through-space interaction of the nitrogen lone pair orbitals n_1 and n_4 results in a symmetric (n_+) and antisymmetric (n_-) combination, placing the n_+ orbital at the lower energy. When considering through-bond interactions, simple symmetry arguments reveal that n_+ orbitals can interact with the low-lying σ_{CC} bonding orbitals of the carbon-skeleton,

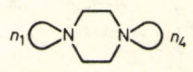


Fig. 3.34 The pyrazine molecule with two lone pairs n_1 and n_2 on the nitrogens

while the n_- orbital can mix to some extent with the antibonding σ^*_{CC} orbitals. The resulting orbital interaction scheme is analogous to that of Fig. 3.33 *b* and the order of the two highest occupied orbitals is reversed with respect to the through-space interaction case: the highest occupied orbital is practically of n_+ nature [1393]. Accordingly, provided that Koopmans' theorem is valid, the energy, which is required to remove an electron from the $a_g(n_+)$ orbital will be smaller than in the case of the

$b_{1u}(n)$ orbital. The application of VB (valence bond) arguments leads to similar conclusions concerning the sequence of the ionic states [1393].

Finally we mention the example of 7-oxanorbornane



where the through-space interactions between the oxygen lone pair and the σ-orbitals of the six-membered ring (the so-called "ribbon"-orbitals) is prohibited for symmetry reasons. Consequently the binding energy of the electron on the oxygen lone pair orbital is higher by about 0.2 eV with respect to the value, which is predicted on the basis of analogy with aliphatic ethers without a six-membered ring [580]. Various types of orbital interactions, which are manifested in the PES of organic molecules have been reviewed and explained by qualitative MO considerations by Martin and Mayer [876].

The qualitative interpretation of the sequence of electron binding energies can be done with the help of orbital correlation diagrams (*cf.* Section 1.3.3). Correlation of orbital energies of the same (or related) symmetry in a series of molecules affords prediction of the sequence of ionization potentials. Orbital correlation diagrams were constructed for several families of compounds [180].

Figure 3.35 illustrates the correlation diagram of electron binding energies for the CH orbitals in *n*-alkanes [56]. There are two distinct groups of orbitals, one corresponding to the $2a_1$ the other to the $1t_2$ orbital of methane. It is interesting to note that although these orbital energies correspond to canonical delocalized orbitals in alkanes there is a more-or-less clear distinction between the orbitals involving both carbon and hydrogen atoms and those which are overwhelmingly on carbon atoms. A similar distinction was found in simple silanes [1335].

There are several cases where canonical orbitals have such a "chemical" interpretation. For example, in water the $3a_1$ and $1b_2$ orbitals are localized on the oxygen: these are "lone-pair" orbitals, although they are not identical to the localized lone pair orbitals. Canonical "lone pair" orbitals are not equivalent, their energies differ

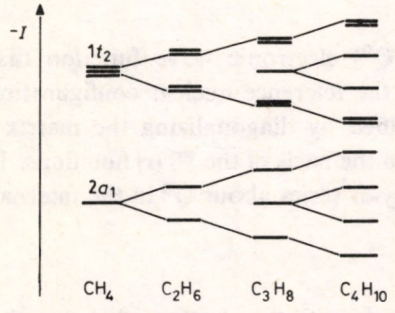


Fig. 3.35 Correlation diagram illustrating the relationship between the canonical CH orbitals in *n*-alkanes

considerably. It is important to stress again that Koopmans' theorem is valid only for canonical orbital energies.

Ionization energies are expected to shift when the molecule is incorporated in an intermolecular complex. The ionization potentials of various complexes like $(HF)_2$, $CH_3F.HF$, $H_2O.HF$, $CH_3OH.HF$, $(CH_3)_2O.HF$ have been calculated by an *ab initio* SCF method using 4-31G basis set [1077]. It has been found that the shifts of the IEs with respect to the corresponding monomer values are well approximated by the Koopmans theorem and relaxation corrections are only of minor importance. The ionization potential shifts were analysed by the interaction energy decomposition scheme of Morokuma [935], and for most cases the effects due to the electrostatic potential of each monomer transmitted through space to its partner had the dominating role. The reliability of these predictions has been confirmed by the good agreement with the experimental IE shifts available for the $(CH_3)_2O.HF$ complex [1077].

Thus far we did not speak about the question of the equilibrium nuclear configurations in various ionic states. In general, we can remark that it is a widespread phenomenon when the symmetry of the equilibrium geometry in the ionic (and also excited) electronic state is lower than the symmetry in the ground state [739]. This "*symmetry-lowering*" has quite important consequences regarding the vibrational fine structure (intensity distribution) of the photoelectron (and also electronic absorption) bands. A discussion of this subject can be found in Section 3.7.2.

The symmetry-lowering can be studied conveniently within the framework of the Born-Oppenheimer approximation. Simply, one has to determine the adiabatic potential surfaces in different electronic states with standard (SCF, CI, etc.) methods of quantum chemistry. This is a straightforward procedure which has been applied in a number of cases for the study of the equilibrium geometry in ionic states [1057]. Alternatively, one can apply another approach for the calculation of the "*dynamical electronic wave function*"* $\Psi_k(\mathbf{r};\mathbf{Q})$ by expanding it in a complete set of electronic wave functions $\Psi_l^0(\mathbf{r})$ determined at a reference nuclear configuration $\mathbf{Q}^0$ (usually the equilibrium nuclear configuration of the ground state molecule) [57, 808]:

$$\Psi_k(\mathbf{r};\mathbf{Q}) = \sum_l \Psi_l^0(\mathbf{r}) C_l^k(\mathbf{Q}) \tag{3.144}$$

where the $\Psi_k^0(\mathbf{r}) = \Psi_k(\mathbf{r};\mathbf{Q}^0)$ electronic wave function diagonalizes the electronic Hamiltonian $\hat{H}_{el}(\mathbf{Q}^0)$ at the reference nuclear configuration $\mathbf{Q}^0$. The $C_l^k(\mathbf{Q})$ mixing coefficients can be obtained by diagonalizing the matrix of the $\Delta\hat{H}_{el}(\mathbf{Q}) = \hat{H}_{el}(\mathbf{Q}) - \hat{H}_{el}(\mathbf{Q}^0)$ Hamiltonian in the basis of the $\Psi_l^0(\mathbf{r})$ functions. The $\Delta\hat{H}_{el}(\mathbf{Q})$ Hamiltonian can be expanded in a Taylor series about $\mathbf{Q}^0$ in the internal symmetry displacement coordinates Q_i:

* We use this name for the electronic wave function, which depends parametrically on the nuclear coordinates, $\mathbf{Q}$.

$$\Delta\hat{H}_{el}(\mathbf{Q}) \approx \sum_{i}^{N-6} \left(\frac{\partial \hat{H}_{el}(\mathbf{Q})}{\partial Q_i}\right)_{\mathbf{Q}^0} Q_i + \ldots . \tag{3.145}$$

Owing to the well defined symmetry properties of Q_i, $(\partial \hat{H}_{el}/\partial Q_i)_{\mathbf{Q}^0}$ and of the electronic wave functions Ψ_l^0, the (3.144) expansion is very useful in the qualitative analysis of the behaviour of the potential energy surface in the neighbourhood of $\mathbf{Q}^0$ [1301].

If the molecule belongs to a point group in its ground state equilibrium nuclear configuration which possesses degenerate irreducible representations, some of its ionized or excited electronic states may be spatially degenerate. Let us consider a doubly degenerate electronic state, and restrict the (3.144) expansion to only these states. Then the energy of the dynamical wave function, considering a distortion Q_i will be given by the roots of the following secular equation:

$$\begin{vmatrix} E_k^0 - E & Q_i V_{k1,k2} \\ Q_i V_{k1,k2} & E_k^0 - E \end{vmatrix} = 0 \tag{3.146}$$

where E_k^0 is the energy of the electronic state in $\mathbf{Q}^0$. Jahn and Teller have shown that for nonlinear molecules, which belong to degenerate point groups, one can always find a non-totally-symmetric distortion Q_i, so that the interaction integral

$$V_{k1,k2} = \left\langle \Psi_{k1}^0(\mathbf{r}) \left| \left(\frac{\partial \hat{H}_{el}(\mathbf{Q})}{\partial Q_i}\right)_{\mathbf{Q}^0} \right| \Psi_{k2}(\mathbf{r}) \right\rangle \tag{3.147}$$

be different from zero [633]. Accordingly, the *Jahn–Teller theorem* involves that a degenerate electronic state is not stable with respect to a nuclear deformation which is able to lift its degeneracy [633]. For example, in the benzene cation the e_{2g} "carbon stretching" distortion leads to a successful Jahn–Teller effect [1219]. Numerous examples of the Jahn–Teller effect can be found in the book of Englman [372].

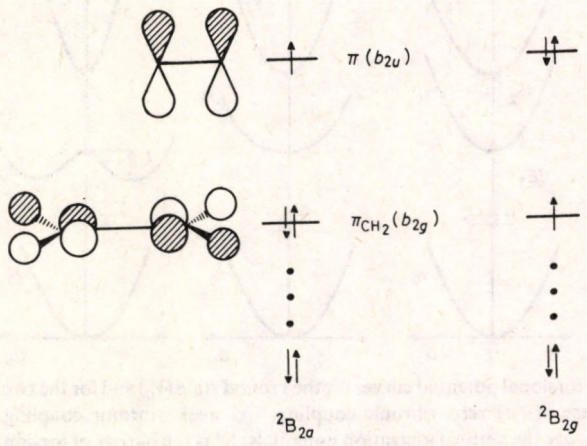


Fig. 3.36 Simple orbital picture of the $^2B_{2u}$ and $^2B_{2g}$ cationic states of ethylene

In general, if there are two or more relatively close lying electronic states, their "interaction" through nuclear motion (vibrations) leads to similar symmetry lowering effects. The method based on the expansions (3.144–3.145) is usually referred to as "*Herzberg–Teller vibronic coupling*" model, since this approach has been applied in the Herzberg–Teller theory of the intensities of electronically forbidden transitions (*cf.* Section 3.7.2). The qualitative implications of this model were discussed by Köppel *et al.* [739] using the cationic states of ethylene as an illustrative example.

The lowest cationic state of ethylene has a nonplanar structure. This symmetry lowering with respect to the planar molecular ground state can be described in the vibronic coupling model (Eq. 3.144) by considering the mixture of the wave functions for the $^2B_{2u}$ and $^2B_{2g}$ electronic states. Although these functions do not mix at the planar ground state equilibrium geometry, upon distortion, that is, upon torsion of the CH_2 groups, they mix considerably due to the nonvanishing overlap of the π (b_{2u}) and π_{CH_2} (b_{2g}) orbitals (see Fig. 3.36). The adiabatic potential curves can be obtained by taking the energy of these mixed states. The shape of the potential curves depends on the coupling constant:

$$\left\langle \Psi^0_{^2B_{2u}}(\mathbf{r}) \left| \left(\frac{\partial \hat{H}_{el}(\mathbf{Q})}{\partial Q_{tors}} \right)_{\mathbf{Q}^0} \right| \Psi^0_{^2B_{2g}}(\mathbf{r}) \right\rangle . \tag{3.148}$$

In Fig. 3.37 potential curves of the zero (Fig. 3.37 *a*), small (Fig. 3.37 *b*) and strong (Fig. 3.37*c*) coupling cases are depicted. For the strong coupling case one obtains a double minimum torsional potential curve for the $^2B_{2u}(\pi, \infty)$ state, with a barrier at 0° and with minima at $\pm 25°$ [79]. It is interesting to note that such vibronic coupling calculations were more successful in predicting the equilibrium geometry of the ethylene cation than the direct *ab initio* SCF calculations [79]. A possible reason for this is that in the variational treatment the energy of the lower cationic state, $^2B_{2u}$ is

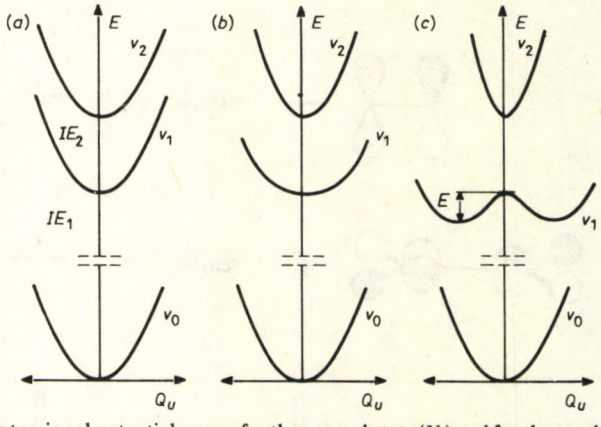


Fig. 3.37 Adiabatic torsional potential curves for the ground state (V_0) and for the two lowest cationic states of ethylene in the case of *(a)* zero vibronic coupling; *(b)* weak vibronic coupling; *(c)* strong vibronic coupling. IE_1 and IE_2 are the vertical ionization potentials, E^* is the barrier of torsion in the lowest cationic state ($^2B_{2u}$). After Ref. [739])

minimized, but simultaneously the energy of the higher state $^2B_{2g}$ becomes much too high. Since the geometry of the cation depends largely on the coupling of these states, conventional variational treatments underestimate the vibronic mixing and lead to a planar cation [739]. As can be judged from Table 3.24 the vibronic coupling calculations using Green's function method yield qualitatively correct, nonplanar geometry [188]. It is interesting to note that semiempirical methods, like CNDO, MINDO, MNDO give also nonplanar cation geometries [79].

TABLE 3.24

Torsional studies of the ethylene radical cation ($^2B_2$ state) with different quantum chemical approaches (from Ref. [79]

Method	Twist angle at energy min., deg	Energy at planar geometry (kJ/mol)	Energy at perpendicular geometry (kJ/mol)
CNDO	37	9.3	86.7
MINDO/3	44	14.2	64.0
Ab initio 4-31G	0	0.0[a] 6.7 30°	114
Ab initio 6-31G*	0	0.0[a] 8.8 30°	122
SCF-CI	23	–	–
MBPT	9	0.67	–
MNDO	20	0.21	72.4
MNDO/UHF	25	0.84	58.2
Experiment	25	2.80	–

[a] Planar minimum

Electron affinities. The difficulties arising in the theoretical determination of electron affinities using Koopmans' theorem have already been mentioned. Usually the calculations of molecular electron affinities (EAs) requires sophisticated and balanced treatment of electron correlation effects [1278]. Accordingly, ΔSCF calculations for negative ionic states quite often are unreliable.

The case of the ground state of the CO_2^- anion can be considered as one of the few exceptions to this rule. Here ΔSCF calculations yielded an electron affinity of -0.36 eV [1057] in excellent agreement with experimental findings: electron attachment and collisional ionization studies gave -0.4 to -0.6 eV [365]. Furthermore, the calculated equilibrium geometry of the CO_2^- anion is bent, with an OCO angle of 135°, again in fairly good agreement with experiment. These results have been rationalized by the fact that in the ground anionic state the electron is added to the diffuse $6a_1$ orbital, consequently the correlation energy difference between the neutral system and the negative ion turns out to be small [1057]. INDO calculations on the same system also predict correct equilibrium geometry (137° OCO angle), but the electron affinity is somewhat overestimated (-2.6 eV) [220].

TABLE 3.25

Electron affinities of formaldehyde calculated by different *ab initio* approaches [968]

State	Orbital	KT	ΔSCF	Corr.	Exp.
$^2A_1$	$a_1(3s)$	−0.775	−0.742	−0.734	−0.66
$^2B_1$	$b_1(\pi^*, 3p_z)$	−1.06	−1.05	−1.05	−0.86
$^2B_2$	$b_2(3p_y)$	−1.21	−1.20	−1.19	−1.06
$^2A_1$	$a_1(3p_zC)$	−1.27	−	−1.22	−1.24

Alternatively to the ΔSCF calculations direct methods, like equation of motion (EOM) [1278, 1279], Green's function techniques [189], or many-body perturbation theory [1442], can be applied for the theoretical determination of electron affinities. When the negative ion in its ground state is a closed shell system, the calculation of EAs may proceed also by the evaluation of the ionization potential for the negative ion. This procedure has been applied in several systems by using powerful approaches, like the EOM formalism for BeH^- systems [549] or the electron propagator (Green's function) technique for NH_2^- and PH_2^- anions [1047]. In the latter case the agreement with experimental results is quite good: the calculated 0.67 and 0.85 eV electron affinities compare well with the 0.78 and 1.27 eV experimental values [1047]. If the neutral molecule itself is a closed-shell system, it should be chosen as the reference state for the calculation. The role of the basis set is a crucial point in *ab initio* investigations of electron affinities, since the description of the negative ionic species requires the use of very large, extended basis sets [1057]. Electron affinities of formaldehyde calculated by Koopmans' theorem, ΔSCF method and with inclusion of electron correlation (using symmetry adapted cluster expansion theory [968]) are listed in Table 3.25. It seems that KT and ΔSCF calculations give practically similar, qualitatively acceptable results, but inclusion of correlation effects improves the agreement with experiment considerably.

The great difficulties encountered in both experimental and theoretical determination of accurate molecular electron affinities make it desirable to have relatively simple qualitative concepts which rationalize the existing data. A qualitative molecular orbital theory of electron affinities has been proposed by Lowe [815]. His considerations refer rather to the thermodynamic (adiabatic) EA's than to the vertical process. Figure 3.38 illustrates the relation, which holds for the adiabatic EA of a diatomic molecule A_2, the EA of the atom A, and the dissociation energies $D_0(A_2^-)$ and $D_0(A_2)$:

$$EA(A_2) = EA(A) + D_0(A_2^-) - D_0(A_2). \tag{3.149}$$

The advantage of this approach is that one can deduce the electron affinities using fairly simple considerations concerning the role of bonding and antibonding orbitals on the bond dissociation energies. According to Mulliken [947] the EA of I_2 can be estimated by assuming that $D(I_2^-)$ is the half as large as $D(I_2)$. This method works rather well for halogen diatomics and for other homonuclear diatomics [212].

Since errors in Koopmans' theorem cumulate for negative ions, the electron affinities cannot be equated usually with the virtual orbital energies of the neutral system. However, it is reasonable to assume that the change of MO energy upon molecular formation is similar to the difference in EA's when A is compared to A_2 [683]. This implies that the difference between the electron affinity calculated by Koopmans' theorem and the true one remains approximately constant as the internuclear distance varies. Based on this assumption a qualitative rule can be derived. The EA of diatomics is larger (smaller) than that of the constituting atom if the LUMO of the diatomic A_2 is bonding (antibonding). Lowe [815] established other simple rules concerning the electron affinities of heteronuclear diatomics. For example, if the LUMO of the AB molecule is bonding the EA (AB) is larger than the larger atomic EA. If the LUMO of the AB molecule is antibonding, the EA (AB) is approximately equal to the smaller atomic EA (we cannot predict whether it will be smaller or larger). The more polar is the AB molecule, the larger is the expected stabilization of the corresponding anion. The agreement between these qualitative predictions and the available experimental data is generally good [815].

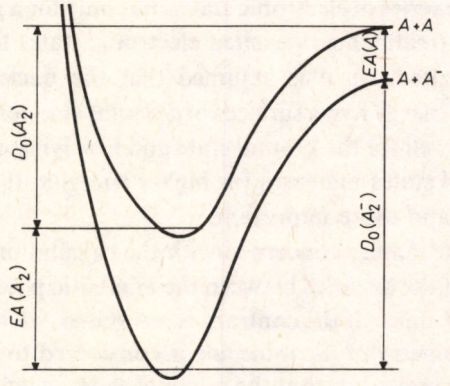


Fig. 3.38 The total energy *vs.* internuclear separation for a diatomic molecule A_2 and its anion A_2^-. EA means the electron affinity, D_0 is the dissociation energy [815]

For polyatomic systems like conjugated organic molecules the above simple ideas cannot be applied. Here one can attempt to find correlation between the electron affinities and the virtual orbital energies calculated by some simple MO method (*e.g.* HMO, EHT, PPP). In effect, good correlations were found between the LUMO energies evaluated by a modified version of the PPP method and the adiabatic electron affinities of conjugated organic molecules. In all cases where the existence of stable negative ions was established experimentally, positive EA's were predicted by the theory [1447].

3.6.3 MOLECULAR EXCITED STATES

Experimental methods: ultraviolet spectroscopy [632], electron beam spectroscopy [743].

The molecules may be excited by absorbing the energy of light or of other appropriate excitation sources, like electron beams [743, 1365]. In the course of excitations brought about by ultraviolet (UV) or visible (VIS) light an electronic transition takes place, which can be described as the promotion of an electron from a valence orbital to a higher energy antibonding or nonbonding virtual orbital or to a Rydberg orbital, while the core electrons remain practically unaffected. High energy X-ray radiation has to be applied to induce transitions of the core electrons (*cf.* Table A1).

Due to their short lifetimes, the experimental study of excited electronic states is rather difficult. The role of theoretical calculations is essentially twofold. First, the assignment of the spectra requires a reliable prediction of the energy sequence of the various excited electronic states. Second, often the theoretical calculations represent the only way to reveal the properties of the thermodynamically unstable excited state species. The main difficulty of these investigations lies in the fact that a well-balanced description for a whole series of electronic states, not only for a given state, is necessary.

In most theoretical treatments of excited electronic states the Born–Oppenheimer approximation is adopted, *i.e.* it is assumed that the nuclei move on completely independent potential energy hypersurfaces of different electronic states. Although this approximation works well for the ground state and low-lying electronic states in most cases, as the density of states increases for higher energies, the role of non-adiabatic effects becomes more and more important.

In this section we are mainly concerned with the calculation of excitation energies, which are a measure of the distance between the adiabatic potential energy surfaces of the excited and ground states. If the contrary is not stated, we will speak about vertical transitions, *i.e.* the geometry of the molecule is considered to be unchanged in going from the ground to the excited state at the minimal energy nuclear configuration of the ground state (*cf.* Franck–Condon principle, Section 3.7.2).

In general, sophisticated quantum chemical methods are required for the appropriate description of excitation energies and excited states. The overwhelming majority of theoretical procedures applied for this purpose are based on the Hartree–Fock description of the ground state and in a zero order approximation the electronic excitation is considered as a jump of a single electron from an occupied SCF space-orbital φ_k to a virtual one φ_{j^*} (*cf.* Section 1.2.4):

$$\varphi_k \rightarrow \varphi_{j^*}.$$

This "single transition approximation" (STA) corresponds to the single configurational qualitative picture outlined in Section 3.6.1. Since the more refined quantum chemical approaches can be considered as higher order approximations with respect to STA, first we recapitulate briefly the most important features of the single transition approximation.

It has already been shown that an electron promotion $\varphi_k \rightarrow \varphi_{j^*}$ from a singlet ground state may lead to excited states of either singlet (S) or triplet (T) spin multiplicity. The transition energies can be calculated from the energy difference of the ground state SCF determinant and of the spin-adapted determinantal wave functions of the excited states, constructed from ground state orbitals. The singlet ${}^1\Delta E_{k\rightarrow j^*}$ and triplet ${}^3\Delta E_{k\rightarrow j^*}$ transition energies are:

$$ {}^{1,3}\Delta E_{k\rightarrow j^*} = \varepsilon_{j^*} - \varepsilon_k - J_{kj^*} + K_{kj^*} \pm K_{kj^*} \tag{3.150} $$

where the + sign stands for the singlet, the − sign stands for the triplet case. ε_{j^*} and ε_k are canonical orbital energies, J_{kj^*} and K_{kj^*} are the Coulomb and exchange integrals in molecular orbital basis (*cf.* Section 1.2.4). We see that the excitation energy is not simply the difference of orbital energies: the J_{kj^*} Coulomb and the K_{kj^*} exchange integrals account for the change in the interelectronic repulsions upon excitation. Within the STA framework the singlet – triplet energy separation is due to the different strengths of interelectronic repulsions. It is always the triplet which is of lower energy than the corresponding singlet state. It has to be noted that in non-SCF Hückel-type MO methods the excitation energy reduces to an orbital energy difference, and the singlet–triplet separation cannot be accounted for.

One may put the question, whether the STA does provide for an adequate description of the electronic excitations or not. We have seen that a comparably simple configurational model for ionization potentials yielded quantitatively acceptable results due to the optimum property of the canonical orbitals in the description of ionized states (Koopmans theorem). The situation is less favourable for the excited states: the use of the ground state canonical SCF orbitals is not justified by an analogous theorem. Let us recall that canonical orbitals are eigenfunctions of the Fock operator, representing the average field of $N-1$ electrons when it acts on a filled spin-orbital. On the other hand, when it acts on a virtual orbital, it corresponds to the average potential of N electrons filling the occupied subspace. This implies that the physical situation arising in positive and negative ionic states is reflected properly by the ground-state Fock operator. This can be considered as the physical background to the Koopmans theorem. On the other hand for excited states the motion of the excited electron should be described by an orbital produced in the field of $N-1$ other electrons (rather than in the field of N electrons). The other electrons, which remain in the STA description on the occupied level, should feel the change of the average field accompanying the electron promotion. In other words, the canonical SCF orbitals of the ground state are not optimum orbitals for the excited state.

Introducing some modifications in the Fock operator, one can attempt the determination of optimum excited state orbitals. For example, improved virtual orbitals (IVOs) can be obtained by using a Fock operator which describes the average potential of $N-1$ electrons corresponding to the removal of one electron from the k-th occupied orbital [610, 615]. Similarly, improved ground state orbitals (IGOs) can be gained by including in the Fock operator the effect of an electron on the j^*-th virtual

orbital [933]. According to the terminology of Morokuma and Iwata [933] the IVOs are determined in the potential involving a "hole" in the occupied subspace (hole-potential method; HPM). On the other hand, the IGOs see effectively the potential of an electron placed on a virtual level; thus the corresponding method is called the "electron-potential method", EPM. It is interesting to note that the HPM is equivalent to a limited CI which involves all the single excitations starting from the orbital k, and the EPM wave function can also be interpreted as the combination of all the single excitations ending on the virtual orbital j^*. Self-consistent improved molecular orbitals can be obtained for a given excitation $k \rightarrow j^*$ by the iterative application of both the EPM and HPM Fock operators [630, 933]; this is the EHP (electron-hole-potential) method.

Of course, orbitals of the excited state can be optimized also by carrying out a separate SCF calculation. Unfortunately not all excited states are accessible for such a treatment, particularly those higher states, which cannot be distinguished on the basis of symmetry from each of the lower lying states. This problem is due to the fact that the variational principle ensures that the energy calculated with a trial function Ψ_i be the upper bound of the i-th eigenvalue of the Hamiltonian, only if Ψ_i is orthogonal to all the eigenfunctions belonging to lower energies. Since the exact eigenfunctions of lower energy are usually not known, exact orthogonality cannot be maintained, except in the case when the symmetry ensures orthogonality. It is due to this symmetry problem that the $^1(\pi, \pi^*)$ excited state of ethylene, which is of the same $^1A_1$ symmetry as the ground state, cannot be treated by the SCF method. Otherwise the procedure of calculating transition energies as the difference between SCF energies of the ground and excited states (the ΔSCF method) has proved to be appropriate for getting a correct ordering of states. ΔSCF calculations provide a considerable improvement with respect to the STA, since electron reorganization effects are included. The success of ΔSCF method in the assignment of electronic spectra depends on whether the variation of the correlation energy in different electronic states bypasses the gap between the states or not. Actually it was found for a series of compounds [1094] that although the correlation energies in states of different character are certainly not equal, a reliable ordering of states can be obtained even at the ΔSCF level.

In general, the required degree of balance in the quantitative treatment of a whole series of electronic states cannot be achieved unless one goes beyond the SCF level, and the introduction of certain amount of correlation effects in the various states becomes necessary [1094]. If correlation defects in the ground and excited states were of about the same magnitude, one could get correct transition energies without worrying about electron correlation. In fact, correlation defects do not cancel each other. It is usually assumed that the amount of correlation energy is greater for the closed shell ground state than for the open shell excited state; consequently ΔSCF calculations systematically underestimate the true excitation energy. However this is not always true; there are examples, such as ethane [160], where the contrary holds for

all the states depopulating the $1e_g$ MO and the ΔSCF excitation energies are higher than the experimental ones.

The usual methods of accounting for electron correlation (*cf.* Section 1.3.1) can be used for excited state problems as well. Both perturbational and variational (CI) techniques have been extensively applied for this purpose. However, there are some methods developed specifically for the treatment of excited states, which merit a few words of discussion.

The configuration interaction treatment affords a simultaneous consideration of both *relaxation* and *correlation* effects. (The definition of these effects is analogous to that discussed in connection with ionization potentials in Section 3.6.2.) It is known that the exact solution of the Schrödinger equation in the given basis set would be obtained by a full CI calculation, which would yield exact theoretical excitation energies within the limits of the Born–Oppenheimer approximation [1099]. However, this is practically impossible owing to the huge number of configurations arising for even small molecules in a reasonable basis set. The restrictions, to be introduced in the CI treatment are basically of two types. Either limitations are introduced in the number of molecular orbitals allowed for variable occupation, or one can eliminate the most weakly interacting configurations from the final CI problem in a systematic way [1094].

For example one can restrict the CI only to the π configurations, while the large core of doubly occupied σ-orbitals is kept fixed throughout the calculation. This full π–CI treatment of butadiene and benzene [522, 593] has permitted a reassignment of the experimental spectrum, but due to neglect of the polarization of σ-electrons large errors were found in some calculated excitation energies. The reorganization effects in the orbitals, which are excluded from the CI procedure can be accounted for by the method of Buenker and Peyerimhoff [157]. This procedure consists of the determination of the so-called "parent configuration molecular orbitals" (PCMOs), which are obtained from separate excited state SCF calculations. These orbitals are used in the limited CI calculation for the given excited state.

Even with severely restricted configuration spaces the CI treatment may turn out to be extremely lengthy. One must decide how to select the relevant configurations. It follows from the Slater rules that only those determinants which differ at most by two substitutions, interact directly with the parent configuration. This would assume that inclusion of only single and double excitations is sufficient. The approach where the ground state is treated as one determinant and the excited state is a linear combination of all singly excited configurations is the single excitation CI (SECI), or according to the terminology of Dunning and McKoy [345], the Tamm–Dancoff approximation (TDA).

Alternatively one can afford a multiconfigurational form for the ground state too by including doubly excited determinants: this is the single–double excitation CI (SDCI). Indirect interactions of considerable magnitude can take place between a singly or doubly excited and highly (triply or quadruply) excited species. The neglect of these

terms from the final CI matrix may lead to errors. However, it is a very difficult task to select the most important higher excited configurations. A controlled approach had been proposed by Buenker and Peyerimhoff, the multireference single and double excitation CI (MRD–CI) procedure [161, 164]. Here, several reference configurations are selected which interact all with the SCF or the leading term strongly. All single and double substitutions with respect to the reference configurations are tested to see whether they are in strong interaction with at least one of the reference configurations.

Other rational approaches have also been put forward. For example, only one reference configuration can be selected and all singly and doubly excited configurations plus a limited number of triple and quadruple excitations can be included [513]; or else, a large reference set can be selected and only single excitations related thereto can be included [1229]. In all these procedures, appropriate extrapolation formulas are recommended for estimating the effect of neglected configurations [161].

The CI calculations are quite easily manageable if the interacting determinants are orthogonal. The CI in nonorthogonal basis raises several technical problems; however, in connection with GVB type wave functions there have been several attempts in this direction too, *e.g.* [512].

The advantages of direct approaches for the calculation of transition processes (transition energies and probabilities) have already been mentioned in the context of ionization potential calculations. While for ionization potentials the relevant quantity was the one-body Green's function (electron propagator) of the system, for excitation processes the two-particle Green's function, the *polarization propagator*, is particularly useful [796, 1032]. As with the case of ionization processes, singularities (poles) of the polarization propagator occur at values of the energy parameter equal to the energy difference between stationary states; the polarization propagator contains information also about the amplitude of transition between stationary states [651, 796, 1032]. The Green function satisfies Heisenberg's equation of motion [651]. A hierarchy of approximations for solving this equation can be derived using various techniques, involving the theory of Green's functions [1241], equation of motion [345, 1197], superoperator formalism [651] (usually in the framework of second quantized representation). Derivations based on the wave function representation, which are more familiar to chemists, can also be found in the literature [410, 508]. In the wave function picture the problem can be formulated as the search for appropriate excitation operators which generate excited states from the ground state wave function of the system [410]. Different levels of approximation are defined according to the method of representation of the reference ground state and of the excitation operator. For example, the Hartree–Fock ground state can be taken as the reference state. The single transition approximation (STA) is defined by an excitation operator, which removes a single electron from one of the occupied HF orbitals, thus creating a "hole", and puts it into a virtual orbital to create a "particle" [345]. The linear combination of this type of elementary "particle-hole" operator leads to the Tamm–Dancoff approximation (TDA) [345].

These approaches bring nothing new to the usual indirect methods, discussed previously. Essentially new methods for treating excitation processes emerge from the simultaneous consideration of the particle-hole and hole-particle type excitation and de-excitation elementary operators: this is the time-dependent Hartree–Fock (TDHF) [849], or random phase approximation (RPA) [1353], if the reference state is again the Hartree–Fock ground state. The RPA (or the TDHF) equations lead to a linear eigenvalue problem which yields directly the transition energies and amplitudes without the explicit calculation of the ground and excited state wave functions. Nevertheless, wave functions consistent with the RPA can be constructed [1267]. Such type of ground state wave function consists of the Hartree–Fock ground state plus a linear combination of doubly excited configurations, while the corresponding excited state is a linear combination of singly excited configurations [651]. It means that in RPA the ground state correlation effects are implicitly accounted for in the transition energies and amplitudes. According to experience, these approaches yield quite satisfactory results for singlet excitations, but the calculated transition energies are much poorer for triplets [651]. This shortcoming can be remedied by taking more elaborate approximations for the reference ground state wave function. One possible choice is to take the HF ground state plus doubly excited determinants. In this way explicit ground state correlation effects are included. Applying again the TDHF or RPA excitation operator to this reference state, it seems a natural restriction to require that the reference state be identical to the ground state which is consistent to the RPA (TDHF) approximation [651]. Approaches of this type are the equations of motion (EOM) method of McKoy and his coworkers [1267, 1268], or self-consistent RPA (SCRPA) and the self-consistent polarization propagator approximation (SPPA) [1032].

The selection of the atomic orbital basis set is a crucial point of the *ab initio* excitation energy calculations. Single zeta quality basis sets can be used only for obtaining a very rough idea about the relative spacing of the intravalence excited states [1094]. For quantitative predictions, at least double zeta or preferably even more flexible basis sets are recommended [1094]. A special requirement is raised due to the presence of diffuse Rydberg states in the spectrum. These electronic states cannot be treated unless long-range, united-atom-type functions are introduced in the basis set. These functions also have an important role in the description of the semi-diffuse valence states which bridge the gap between the true valence and Rydberg electronic states.

Obviously, large-scale *ab initio* calculations are inappropriate for routinely treating molecules containing more than a few atoms, and there is a need for simpler approximate methods for calculating electronic spectra at lower cost. The X_α and related local density (Hartree–Fock–Slater HFS) methods [654] seem to be a possible alternative. The excitation energies are determined here either by the simple single-transition approximation (STA) or by using the transition-state concept of Slater [1288]. Although the reliability of these calculations is not comparable to those using

Hartree–Fock theory, for transition metal compounds it offers a unique possibility for the estimation of electronic transition energies.

The usual all-valence semiempirical methods like CNDO/2, INDO, MINDO, have been found inappropriate for the calculation of transition energies and excited state properties in most cases. For example, even the order of lowest electronic transition is incorrectly reproduced by CNDO/2 and INDO [442]. Specific parametrization schemes have been developed for spectroscopic purposes, among which the CNDO/S version of Del Bene and Jaffé [294, 295, 359] is by far the most popular (*cf.* Section 1.3.2). No uniquely accepted spectroscopic INDO parametrization exists; the results obtained by the few currently applied schemes are of comparable quality [423, 1176]. The PPP method is successful π-electron theory of the electronic spectra of conjugated molecules, primarily of conjugated hydrocarbons (*cf.* Section 1.3.2) [1066]. Examples concerning the reliability of the semiempirical methods in the calculation of electronic excitations will be presented later.

After getting acquainted with the most important computational procedures specifically developed for the quantum chemical study of excited states and electronic transitions, in the following we overview briefly the different types of electronic excitations in the light of theoretical results. First the Rydberg transitions are discussed, then various problems arising in the study of intravalence excitations are treated.

Rydberg transitions. There are bands in the vacuum ultraviolet region of the electronic spectra of molecules which obey the well-known Rydberg formula:

$$\Delta E_n = \mathrm{IE} - T_n . \tag{3.151}$$

Here ΔE_n is the excitation energy for the n'th member of the Rydberg series, IE is the ionization potential, and T_n, the term value, is

$$T_n = \frac{R}{(n-\delta)^2} \tag{3.152}$$

where R is the Rydberg constant, n is an integer and δ is the quantum defect, which characterizes the departure of the molecular Rydberg series from hydrogenlike behaviour. The *Rydberg excitations* [342, 1183] have been identified as transitions from a valence to a higher principal quantum number orbital, which is called by spectroscopists the Rydberg orbital.

For example, the acetylene molecule exhibits a number of Rydberg series (see Table 3.26). Its lowest ionization potential is attributable to the removal of an electron from a π_u orbital ($\mathrm{IE}_{\pi_u} = 11.40$ eV). In the progression towards this ionization limit the π_u electron may be excited to the $3s, 4s, 5s, \ldots$ orbitals. Similar Rydberg series converging on the same π_u ionization limit are formed involving excitations to the $3p, 4p, 5p, \ldots$ or the $3d\pi, 4d\pi, 5d\pi, \ldots$ orbitals.

It has already been mentioned that Rydberg orbitals are large, diffuse and only loosely bound to the molecular core. The size of Rydberg orbitals can be characterized

by the expectation value of the second moment operator (*cf.* Section 3.4.1). Data in Table 3.26 confirm that the expectation values $\langle x^2 \rangle$ and $\langle z^2 \rangle$ for acetylene lying on the z axis are of several orders of magnitude larger for Rydberg states than for intravalence excited states [304]. Thus, for practical purposes the Rydberg state can be defined as a state in which the orbital of the excited electron is large compared to the molecular core and which corresponds to a band in the electronic spectrum, which is a member of a Rydberg series [1221].

On the basis of experience, the simple model, describing Rydberg states as having a positively charged, pointlike core and a loosely bound hydrogenic orbital, seems quite reasonable. Deviations from this model are expressed by the magnitude of the quantum defect δ [951].

The quantum defect is positive for Rydberg AOs which have precursors, that is occupied orbitals of the same l value (*e.g.* 2*s* for a 3*s* Rydberg or 2*p* for a 3*p* Rydberg), due to the interaction of the Rydberg electron and the singly charged core. The degree of penetration decreases in the sequence $s > p > d$. Accordingly one may expect that deviations from hydrogen-like behaviour of the Rydberg states vary in the same order. In effect, this is witnessed by the values of the quantum defects for 2nd row atoms [1432]:

$$\delta(s) \approx 1; \qquad \delta(p) \approx 0.6; \qquad \delta(d) \approx 0.1$$

TABLE 3.26

Vertical valence- and Rydberg excitation energies of acetylene (C_2H_2) calculated by the frozen core approximation [304]; δ is the quantum defect, the second moments $\langle x^2 \rangle$ and $\langle z^2 \rangle$ characterize the spatial extent of the electronic state

Excited state	Excitation	MO	ΔE calc.	ΔE exp.	δ	$\langle x^2 \rangle$	$\langle z^2 \rangle$
$^1\Pi_u$	$(1\pi_u, n\sigma^*)$	3*s*	8.43	8.16	0.86	0.052	0.057
		4*s*	10.05	9.93	0.83	0.270	0.184
		5*s*	10.43	10.57	0.80	0.939	0.494
$^3\Pi_g$	$(1\pi_u, n\sigma^*)$	3*pσ*	8.83	–	0.70	0.032	0.118
		4*pσ*	10.18	–	0.66	0.169	0.524
		5*pσ*	10.71	–	0.55	0.650	2.004
$^3\Sigma_u^+$	$(1\pi_u, n\pi_g^*)$	Valence	5.02	5.2...5.3	–	0.008	0.010
		3*dπ*	9.97	–	−0.90	0.192	0.192
		4*dπ*	10.60	–	−0.13	0.743	0.743
		5*dπ*	10.90	–	−0.22	2.263	2.263
$^1\Sigma_u^-, {}^3\Sigma_u^-$	$(1\pi_u, n\pi_g^*)$	Valence	6.69	5.23	–	0.010	0.012
		3*dπ*	10.05	–	−0.18	0.213	0.213
		4*dπ*	10.63	–	−0.21	0.777	0.777
		5*dπ*	10.90	–	0.22	2.233	2.233
$^1\Pi_u$	$(1\pi_u, n\delta^*)$	3*dδ*	9.99	9.97	−0.11	0.180	0.057
		4*dδ*	10.60	10.59	−0.13	0.689	0.213
		5*dδ*	10.88	10.88	−0.12	1.597	0.491

(*cf.* also Table 3.26). The value of the quantum defect is affected also by the spin multiplicity of the state: this is the so-called "exchange contribution" to δ [951]. Finally, for nonpenetrating orbitals one should consider a further, polarization contribution [951].

The quantum defects of B_1 Rydberg states in water have been analyzed on the basis of *ab initio* CEPA clculations [1304] in terms of the simple quantum defect model. The interaction potential of the Rydberg electron with the core has been assumed to involve charge, dipolar, quadrupolar interactions and even the polarizability of the point-like core has been considered. A negative quantum defect for some of the *d* orbitals was found due to mainly quadrupolar interactions.

In the quantum chemical investigation of Rydberg states much care should be paid to the selection of the atomic orbital basis set. Naturally, minimal basis set calculations are appropriate at least for intravalence states, and higher principal quantum number atomic orbitals have to be included in the basis set for the description of Rydberg states. According to experience, in *ab initio* calculations using Gaussian basis sets quite satisfactory results can be achieved by using single primitive Gaussians centered either at the midpoint of the molecule (at the center of the united atom) or at one or more of the constituent nonhydrogenic nuclei [1094]. The careful optimization of the exponents of the diffuse functions is a critical factor in the evaluation of reliable energies for Rydberg states. It should be mentioned that the danger of having approximately linearly dependent basis sets is increased due to the use of a large number of diffuse Rydberg functions [1221].

Usual semiempirical methods involve only minimal valence basis sets. Attempts at the description of Rydberg states by these type of methods made it necessary to include in the basis AOs of higher principal quantum number [1218]. (2*s* and 2*p* orbitals for hydrogen and by 3*s* and 3*p* orbitals for atoms B to F.)

The difficulties in the correct theoretical representation of Rydberg (and also ionic) excited states have been reviewed by Malrieu [867]. According to the experience gained by *ab initio* calculations [1094] the spacing between members of a Rydberg series originating from the same valence orbital can be quite well reproduced by single configurational treatments, like ΔSCF. This is the basis of the success of the IVO-treatment of Rydberg states [776]. The IVO-approach is practically equivalent to the "frozen core approximation" [304] to the calculation of Rydberg transitions. This means that the Rydberg orbital is optimized in the field of the frozen core (a positive ion), which is left unaffected by the Rydberg-electron. This procedure was applied to the calculation of Rydberg states of acetylene [304]. The results, as witnessed by Table 3.26 are quite good, showing that correlation effects are relatively unimportant in this case.

In general, the excitation energies calculated by frozen-core method are shifted relative to the observed values by the amount of error due to the neglect of correlation and core-orbital relaxation effects. This discrepancy was empirically corrected by introducing the appropriate experimental ionization potential. Assuming that the

TABLE 3.27

The energies of the lowest vertical excited states of water (H_2O) in different approximations

Excitation	Excited state	SCF-CI [1431]	ΔSCF [1431]	Pert. CI [1156]	Eq. (3.153) [1156]	X_α [127]	INDO [221]	Exp.
$(b_1, 3sa_1)$	$^3B_1$	7.26	6.00	–	–	8.82	6.20	7.0...7.2
	$^1B_1$	7.61	6.37	8.59	7.40	8.93	7.43	7.49
$(1b_1, 3pb_2)$	$^3A_2$	9.34	8.10		–	–	7.49	8.9...9.2
	$^1A_2$	9.46	8.23	10.35	9.07	–	8.03	9.1
$(1b_1, 3pb_1)$	$^3A_1$	9.74	8.57	–	–	10.52	–	9.81
	$^1A_1$	10.16	8.64	11.45	10.17	10.65	–	10.17
$(1b_1, 3pa_1)$	$^3B_1$	9.99	–	–	–	10.50	–	9.98
	$^1B_1$	10.06	9.91	11.33	10.05	10.63	–	10.00
$(3a_1, 3sa_1)$	$^3A_1$	9.44	8.12	–	–	–	8.67	9.3
	$^1A_1$	9.82	8.44	10.56	8.70	–	10.85	9.73
$(3a_1, 3pb_1)$	$^3B_1$	11.87	10.63	–	–	–	–	–
	$^1B_1$	11.92	10.66	12.33	11.47	–	–	11.91

difference between the experimental ionization potential (IE_i) and the ionization potential estimated by Koopmans' theorem (E_i) can be taken as an approximate measure of the errors, the following formula can be used [1156]:

$$\Delta E_{i\to R} = \Delta E_{\text{calc}} - |\varepsilon_i - IE_i| \,. \tag{3.153}$$

The utility of this formula can be judged from the figures in Table 3.27: this empirical correction to the medium-quality theoretical values of water excitation energies leads to better agreement with experiment than that obtained by extensive CI calculations [1431]. The ΔSCF method underestimates the transition energies of water, but the calculated spacing of the Rydberg states is quite reasonable. The reliability of INDO calculations [220] without extended atomic orbital basis set is questionable for water, owing to the Rydberg nature of the lowest excited states.

In the calculations, which include correlation effects by some configuration interaction techniques, there is an important question in the interpretation of the CI wave functions as to what extent the Rydberg and valence states mix. Three main cases should be considered for the valence Rydberg mixing (see Fig. 3.39) [162, 1093].

(*i*) If the pure valence state lies well below the various Rydberg series, one expects essentially no mixing. As a rule of thumb we can say that when the absorption in a given band system lies about 2.0 eV below the expected location of the lowest pure Rydberg state of the same symmetry, mixing is unlikely. The location of the Rydberg states can be estimated from the experimentally known term values $T = E(A^+) - E(A^+ ns)$, which is for 3*s* 3.0–3.5 eV, for 3*p* 2.2–2.8 eV, and for 3*d* Rydberg transitions is about 1.0–1.8 eV. For example, in ethylene the $IE_{min} = 10.51$ eV, and the energy of the lowest-lying Rydberg transition of the same symmetry with the $^3(\pi, \pi^*)$ valence state, the $^3(\pi, 3d\pi)$ must not be lower than 8.5 eV. Consequently the $^3(\pi, \pi^*)$ state of energy 4.22 eV lies too low for any mixing with Rydberg states [1094]. A similar situation holds, for example, for most valence excitations of formaldehyde [1096].

(*ii*) In the second case the pertinent valence state coincides with low-lying pure Rydberg states. Under these conditions after CI mixing the lowest state can be found

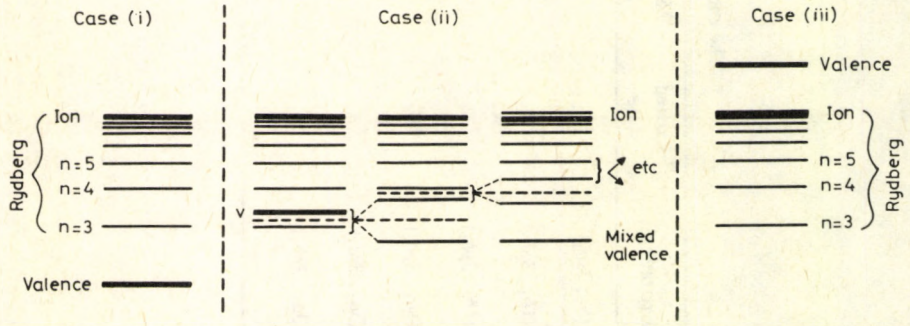


Fig. 3.39 Schematic diagram showing the interaction between the valence and Rydberg states in the three cases discussed in the text [162]

below the expected location of the lowest-lying pure Rydberg. In addition, it is likely that a good portion of valence character will be built into all Rydberg transitions, including the higher members of the series. An example of strong valence-Rydberg mixing is the $^1(\pi, \pi^*)$ state of ethylene [1094].

(*iii*) Finally we can consider the situation, when the valence state lies beyond the location of the ionization potential. In this case it is possible to have a large, usually infinite, number of Rydberg states below the valence species. Rydberg-valence mixing is unlikely unless the interaction matrix element is very large. Saturated molecules containing exclusively σ-bonds are good examples; the low-lying excited states of water and ethane, for example, are all Rydberg states.

Due to the closely related nature of the electronic structure of Rydberg and corresponding ionized states, their geometry is expected to be rather similar. A classical example is the ethylene molecule. The nonplanar structure of the radical cation has already been discussed (*cf.* Section 3.6.2). For similar reasons the Rydberg state of ethylene also aquires a nonplanar structure, as was noted by Mulliken [949]. He gave the name "isovalent hyperconjugation" to the delocalization of electrons from a pure π orbital to a pseudo-π (π_{CH_2}) orbital, which is allowed by the twisting of the molecular skeleton. The result of this delocalization in the excited state is the strengthening of the C=C bonding in the distorted structure (*cf.* vibronic coupling, Section 3.6.2 and also 3.7.1).

While intravalence transitions terminate at antibonding orbitals, the Rydberg orbitals involved in Rydberg transitions are essentially of nonbonding character between neighbouring atoms. On the other hand, just because of their size, the same orbitals may provide for a certain amount of bonding in the molecule. This feature has important consequences in the photochemical behaviour of Rydberg states. In particular, one might expect that the primary photochemical step for molecules in Rydberg states will be the extraction of smaller molecules or radicals, while for valence excited states involving antibonding orbitals the cleavage of bonds is thought to be favoured [1221].

Intravalence transitions. Now we turn our attention to the intravalence excitations which are responsible for most of the spectral features in visible and ultraviolet spectroscopy. An exhaustive discussion of all the subjects in this vast field exceeds the limits of this book, so we restrict ourselves to some selected examples.

In the following we overview the theoretical results concerning the excited states of formaldehyde in some detail, since the reliability and applicability of the various quantum chemical methods can be judged quite well in the light of this case. The formaldehyde molecule offers an important example where the interplay of theory and experiment led to the understanding of many physical effects. Furthermore, the formaldehyde molecule (H_2CO) can be considered as a prototype system for many diverse phenomena arising in molecular electronic spectroscopy. This is the simplest compound which contains the carbonyl chromophore (>C=O) the functional group

responsible for the spectral behaviour of many organic compounds. There are a great number of theoretical investigations concerning the formaldehyde molecule, which greatly helped the understanding of the spectrum of the carbonyl chromophore as well.

The most important intravalence excited states of formaldehyde have already been presented in connection with the single configurational model (see Fig. 3.27). Calculations using various *ab initio* and semiempirical methods confirmed the sequence of excited states predicted on the basis of simple qualitative considerations. Some representative theoretical results have been collected in Table 3.28 in comparison with the best experimental transition energies.

The lowest lying transitions of formaldehyde are of (n, π^*) type. All the theoretical calculations listed in Table 3.28 place the pair of the singlet and triplet (n, π^*) transitions at about 3.5 eV, in agreement with experiment. The triplet state is of the lower energy by a few tenths of electron volts.

The difference between the energies of the singlet and triplet states corresponding to the same spatial orbital promotion, is called the *singlet-triplet splitting*. In the single transition approximation (STA) this splitting δ_{ST} equals twice the exchange integral K_{kj^*} between the occupied and virtual molecular orbitals φ_k and φ_{j^*}:

$$\delta_{ST} = 2K_{kj^*} = 2\int \varphi_k^*(\mathbf{r}_1)\varphi_k^*(\mathbf{r}_2)|\mathbf{r}_1 - \mathbf{r}_2|^{-1}\varphi_{j^*}(\mathbf{r}_1)\varphi_{j^*}(\mathbf{r}_2)\,d\mathbf{r}_1\,d\mathbf{r}_2\,. \tag{3.154}$$

The exchange integral is always positive. This is in accordance with *Hund's rule*, which requires that the state of higher multiplicity (in this case the triplet), be of the lower energy. The exchange integral can be interpreted in a pictorial way as the electrostatic self-energy of the transition density ρ_{kj^*}.

$$\rho_{kj^*}(\mathbf{r}) = \varphi_k^*(\mathbf{r})\varphi_{j^*}(\mathbf{r})\,. \tag{3.155}$$

The magnitude of the singlet–triplet splitting can be estimated simply from the shape of the occupied and virtual orbitals. As a rule we can say that when both orbitals occupy the same region of the space, that is, the corresponding transition density function is high in certain regions, the exchange integral, and consequently the singlet–triplet splitting, is large. On the other hand, if the two orbitals occupy regions far away from each other, small exchange integral and accordingly, small singlet–triplet splitting is expected. The formaldehyde (n, π^*) transition can be considered as having a moderate value of singlet–triplet splitting. Very small splittings are characteristic of Rydberg transitions (*cf.* Tables 3.26, 3.27), where the exchange integral between the diffuse upper orbital and the valence orbital is very small. Large singlet–triplet splittings are found for the (π, π^*) transitions, where both the occupied and the virtual orbitals are in the same region. Examples will be the formaldehyde (π, π^*) transition ($\delta_{ST} = 4.5$ eV), or the benzene and naphthalene lowest (π, π^*) transitions (2.29 eV and 2.15 eV, respectively) [1432].

The geometry of the formaldehyde $^1(n, \pi^*)$ excited state has been investigated also by quantum chemical methods. Buenker and Peyerimhoff found with *ab initio* CI (PCMO) calculations a non-planar equilibrium geometry with an out-of-plane angle of

TABLE 3.28

Excitation energies of the formadehyde molecule calculated by different approaches

State	Orbital	Exp.	EOM	SAC-CI	GVB-CI	SDCI	PCMO-CI	EHP	SECI	CNDO/S
$^3A_2$	$^3(n, \pi^*)$	3.54	3.46	3.67	3.68	3.70	3.41	3.61	3.56	3.5
$^1A_2$	$^1(n, \pi^*)$	3.8–4.2	4.04	4.13	4.09	4.07	3.81	4.42	4.38	3.5
$^3A_1$	$^3(\pi, \pi^*)$	5.6–6.2	5.29	6.08	5.95	6.21	5.56	4.88	4.78	5.4
$^1A_1$	$^1(\pi, \pi^*)$	10.7	10.10	10.80	10.77	11.05	11.41	12.08	10.41	9.8
$^3B_1$	$^3(n_\sigma, \pi^*)$	8.5	–	8.49	–	–	8.14	–	–	8.6
$^1B_1$	$^1(n_\sigma, \pi^*)$	9.05	9.19	–	–	9.30	9.03	9.36	9.32	8.6
$^1B_2$	$^1(n, 3sa_1)$	7.13	7.28	6.99	7.16	7.10	7.38	–	–	–
$^1B_2$	$^1(n, 3p_za_1)$	8.14	8.12	7.91	8.08	–	8.39	–	–	–
$^1A_1$	$^1(n, 3p_yb_2)$	7.97	8.15	7.92	8.09	7.86	8.11	–	–	–
$^1A_2$	$^1(n, 3p_xb_1)$	–	8.35	8.13	8.32	–	9.07	–	–	–
Reference			[1443]	[968]	[511]	[762]	[1096]	[933]	[933]	[360]

32.7° [157]. The C=O bond length was found to be 0.29 Å longer than in the ground state. These results are in good agreement with the experimental data (33.6° and 0.12 Å), respectively [106]. A qualitative explanation of the nonplanarity of the $^1(n, \pi^*)$ excited state can be assessed by using Walsh rules (*cf.* Section 3.1). According to this model the occupation of π^* orbital in the excited state stabilizes the nonplanar nuclear configuration, and due to the antibonding character of this orbital the C=O bond length increases and the carbonyl stretching frequency drops in the $^1(n, \pi^*)$ excited state [158].

The first fully allowed electronic absorption band in the formaldehyde spectrum (the $^{1,3}(n, \pi^*)$ transitions are forbidden in a first approximation, *cf.* Section 3.7.2) is a Rydberg transition $(n, 3sa_1)$, whose location has been predicted correctly by various *ab initio* calculations to be about 7.1–7.7 eV. The next strong absorption system appearing about 8 eV had been attributed for a long time to the intravalence $^1(\pi, \pi^*)$ excitation. The precise assignment of these bands was made with the help of *ab initio* calculations. These showed unambiguously that the 7.97 and 8.14 eV absorption bands were due to $(n, 3p)$ type Rydberg transitions [1094].

Although the triplet $^3(\pi, \pi^*)$ state could be located quite well by different theoretical methods to be about 6 eV, the actual position of the singlet $^1(\pi, \pi^*)$ transition has been a matter of controversy for a long time [1094]. A considerable problem in the theoretical treatment of this state is that it possesses the same symmetry as the ground state. Therefore direct SCF calculations cannot be undertaken for the $^1(\pi, \pi^*)$ excited state, whilst CI calculations using the molecular orbital set obtained for the ground state represent a reasonable theoretical approach [762]. There are considerable problems also in the experimental identification of this transition. According to *ab initio* calculations the potential curve of the $^1(\pi, \pi^*)$ state is dissociative with respect to the CO stretching [157]. This is the reason why no sharp absorption band could be identified in the spectrum [941]. The experimental value of 10.7 eV appearing in Table 3.26 has been quoted by Harding and Goddard [511]; the theoretical estimates range from 9.9 to 11.4 eV.

The $^3(\pi, \pi^*)$ triplet state is a pure intravalence state. Although the corresponding $^1(\pi, \pi^*)$ singlet state is basically also of intravalence nature, it has a significant amount of diffuse character [968, 1094]. It is interesting to note that even without diffuse basis functions quite good transition energies can be obtained. On the other hand, the inclusion of a Rydberg basis leads to a significant change in the dipole moment and second moment of the excited state [968]. Considering that the first ionization potential of formaldehyde (10.9 eV) [941] lies closely to the expected location of the vertical $^1(\pi, \pi^*)$ transition energy, the diffuse, mixed valence-Rydberg nature of this state is not surprising. Since the singlet-triplet splitting is usually large for (π, π^*) transitions, distinction according to the diffuse character of these transitions of different multiplicity is quite common [1094].

The (n_σ, π^*) transition energy was predicted by CI (PCMO) and EOM *ab initio* calculations to be about 9 eV. Due to the dissociative nature of the potential curve of

this excited state, the theoretical calculations were indispensable in the identification of this transition too [941].

A particularly important class of organic molecules is that of *conjugated compounds.* These systems possess characteristic UV/VIS absorption spectrum due to (π, π^*) type transitions. The theoretical interpretation of these spectra is greatly simplified by applying the σ–π separability condition (*cf.* Section 1.2.6), which allows us to restrict the discussion to the π-electron system, and the σ electrons are considered only implicitly through an effective Hamiltonian. The two most important π-electron theories have been discussed in Section 1.3.2.

The basic structural unit of conjugated hydrocarbons is represented by the ethylene molecule. Various theoretical studies agree that the majority of low-lying excited states of ethylene are of Rydberg character (for a review see Ref. [1183]) (Table 3.29). However, most of the attention has been paid to the characterization of the (π, π^*) valence states. Similarly to the case of formaldehyde, the splitting of singlet and triplet (π, π^*) states is large. The triplet state lies at 4.2–4.4 eV, the singlet, which has some Rydberg character, is situated above the triplet by about 3–3.5 eV [1094]. Adiabatic torsional potential curves (including diagonal corrections to the Born–Oppenheimer, or clamped nuclei, potential curves) for the $^1(\pi, \pi^*)$ and $^1(\pi, 3s)$ excited states of ethylene were calculated with the MRD–CI method [1091]. At about 22° an avoided crossing of the potential curves could be found which explains the strong non-adiabatic effects in the vibrational structure of the (π, π^*) band system (*cf.* Section 3.7.2). The optimal conformations of the $^1(\pi, \pi^*)$ and $^1(\pi, 3s)$ states are at 90° and 24.8°, respectively*. The height of the torsional barrier in the $^1(\pi, \pi^*)$ state is 1.78 eV [1091]. It is interesting to note that the usual Born–Oppenheimer (clamped nuclei) approximation yields a torsional potential with a half as large barrier.

Theoretical studies on the charge distribution of ethylene and other alkenes in their twisted excited states revealed that these species should have a zwitterionic character, if

TABLE 3.29

Vertical transition energies of ethylene calculated by various *ab initio* methods

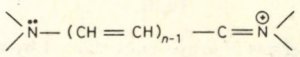
Excitation	MRD–CI	PCMO–CI	SAC–CI	RPA	Exp.
$^3(\pi, \pi^*)$	4.35	4.17	4.54	–	4.4—4.7
$^1(\pi, \pi^*)$	7.96	8.25	8.17	7.70	7.66
$^1(\pi, 3s)$	7.13	6.94	–	7.15	7.14
$^1(\pi, 3p_z)$	7.86	7.55	–	7.74	7.80
$^1(\pi, 3p_y)$	7.89	7.52	–	–	–
$^1(\pi, 3p_x)$	8.21	–	–	–	–
Reference	[1091]	[1094]	[964]	[133]	[428]

* Note the similarity of the geometries of the ground cationic state and of the $^1(\pi, 3s)$ Rydberg state.

their structure is, at least slightly, dissymmetric. For example, a 90°-twisted ethylene with one pyramidalized methylene group displays a 0.5*e* charge separation at 10° pyramidalization angle. Salem termed this phenomenon "sudden polarization" [124, 1220]. The zwitterionic excited states are supposed to play a key role in photochemistry and in particular, in the mechanism of vision [1220].

Linear polyenes can be built up from ethylenic units which are in a conjugated position. The simplest member of the polyene series is butadiene. *Ab initio* calculations with full-π-CI yielded quite good agreement with experiment for the intravalence triplet states. The theoretical excitation energies are 3.45 and 5.04 eV for the ^3B_u and ^3A_g states, while the corresponding experimental values are 3.20 and 4.91 eV, respectively [593]. Comparison of these full-π-CI results with all-valence MRD–CI calculations [165] confirms the accuracy of the π-electron approximation for these states. However, due to the neglect of the polarization of the σ-orbitals, π–CI calculations turned out to be less appropriate for the description of the diffuse singlet $^1(\pi, \pi^*)$ states. For example the ^1A_g excited state has been placed by 0.35 eV higher with all-valence CI than with π–CI calculations [165]. According to GVB–CI studies the carbon-carbon σ-orbitals contribute most to the σ-contribution of the correlation energy in the $^1(\pi, \pi^*)$ states [987].

The computational work needed in *ab initio* studies of the higher members of the polyene series increases rather fast, so the role of much simpler semiempirical models is crucial in the elucidation of the spectral characteristics of these systems. The Hückel theory offers such a possibility: the HOMO–LUMO orbital energy separation can be put into correspondence with the energy of the first (π, π^*) absorption band. If the single and double bonds of the polyene chain are considered to be all of the same length (*i.e.* the corresponding β-s are the same), Hückel theory predicts an $1/n$ decrease of the excitation energy with the increasing number n of conjugated double bonds [1219]. In effect, this linear dependence of the transition energy on the polyene size had actually been found experimentally for odd polyenes, like cyanine dyes of the type:



On the other hand, in the case of even polyenes, although the excitation energy decreases, it tends to a constant value (about 2.23 eV) in the limit of infinite chain length [1219]. This discrepancy between the simple Hückel model and experiment has been explained in a satisfactory manner by supposing an alternation of bond lengths in the polyene, that is, different β values had been considered for the double and for the single bonds in the Hückel Hamiltonian [751, 1219].

When the Hückel model is used for the study of spectroscopic properties, the usual parametrization, based on thermochemical data, turns out to be inappropriate [1313], and another set of (spectroscopic) parameters have to be introduced. For example, in the spectroscopic parametrization the β_{CC} is -3.04 eV (-70 kcal/mol) for linear polyenes and -3.60 eV (-83 kcal/mol) for alternant hydrocarbons; while the

corresponding values appropriate for the study of ground state properties are −0.78 and −1.56 eV (−18 and −36 kcal/mol) [1219].

In many cases, the single configurational model and the corresponding single transition approximation (STA) are acceptable starting points in the qualitative characterization of excited states. The alternant hydrocarbons (*cf.* Section 1.3.3) provide an example, when one should go beyond the single configurational model in order to have a qualitative description, since due to the pairing properties of molecular orbitals, degenerate singly excited configurations arise. Configurational interaction calculations are needed to lift this degeneracy and to yield the correct number of transitions in the electronic spectrum [319]. These limited CI calculations are sometimes called "first-order CI" [1219].

Benzene is a well-known example, where both the HOMO and the LUMO consist of a pair of doubly degenerate orbitals. In a simple Hückel model the four singly excited configurations are of the same energy, which would correspond to only a single absorption band in the electronic spectrum. Early attempts at interpretation of the benzene spectrum used limited "first-order CI" between these degenerate configurations [474]. Since in the Hückel model there is no explicit electron–electron interaction, the introduction of a CI can be accepted only as an "afterthought" [1219] in these calculations. By the way, the results of these studies were in agreement with experiment. Two forbidden transitions were found of $^1A_{1g} \rightarrow {}^1B_{2u}$ and $^1A_{1g} \rightarrow {}^1B_{1u}$ type, and one dipole-allowed $^1A_{1g} \rightarrow {}^1E_{1u}$ appeared at higher energy. Some theoretical excitation energies of the benzene molecule obtained with various *ab initio* and semiempirical approaches are compared with experimental data in Table 3.30.

The most successful semiempirical π-electron theory of conjugated molecules is the PPP method (*cf.* Section 1.3.2). This is an SCF procedure completed by a CI calculation including all singly excited determinants, so a reliable description of the low-lying (π, π^*) transitions is expected. Among the different parametrization schemes of the PPP model-Hamiltonian we mention an attempt at reproduction of the absorption

TABLE 3.30

Vertical excitation energies of benzene as calculated by different *ab initio* and semiempirical approaches

State	π-EOM	σ,π-EOM	SECI	π-CI	CNDO/S	PPP	Exp.
$^1B_{2u}$	5.7	5.5	6.30	5.00	4.7	4.9	4.9
$^1B_{1u}$	7.8	7.4	7.02	7.64	5.2	6.2	6.3
$^1E_{1u}$	9.5	8.3	8.42	8.34	6.9	7.0	7.0
$^1E_{2g}$	11.3	10.9	9.09	8.33	–	–	7.3
$^3B_{1u}$	2.7	3.8	3.67	3.83	–	–	3.9
$^3E_{1u}$	5.2	5.2	5.15	4.98	–	–	4.7
$^3B_{2u}$	7.0	6.7	6.01	7.00	–	–	5.6
$^3E_{2g}$	7.9	8.1	7.86	7.28	–	–	6.6
Reference	[1191]	[1191]	[522]	[522]	[294]	[970]	

TABLE 3.31

Experimental and CNDO/S theoretical excitation energies (eV). The electron repulsion integrals are parametrized according to either Pariser and Parr (PP) or Mataga and Nishimoto (MN)

Molecule	Excitation	Excited state	CNDO/S		Exp.	Ref.
			(PP)	(MN)		
Benzene	(π, π^*)	$^1B_{2u}$	4.7	–	4.7	[294]
	(π, π^*)	$^1B_{1u}$	5.2	–	6.1	
	(π, π^*)	$^1E_{1u}$	6.9	–	6.9	
Chlorbenzene						
	(π, π^*)	$^1B_1$	4.8	–	4.7	[742]
	(π, π^*)	$^1A_1$	6.0	–	6.0	
	(π, π^*)	$^1B_1$	6.7	–	6.7	
Pyridine	(n, π^*)	$^1B_1$	4.4	4.2	4.3	[293]
	(π, π^*)	$^1B_2$	5.0	4.9	4.8	[359]
	(π, π^*)	$^1A_2$	–	5.6	–	
	(π, π^*)	$^1A_1$	6.2	6.0	6.2	
	(π, π^*)	$^1A_1$	7.2	6.8	7.0	
Furan	(π, π^*)	$^1B_2$	5.2	–	5.9	[293]
	(π, π^*)	$^1A_1$	5.8	–	6.5	
	(π, π^*)	$^1A_1$	7.3	–	7.4	
Pyrimidine	(n, π^*)	$^1B_1$	–	4.2	3.9	[359]
	(n, π^*)	$^1A_2$	–	4.6	3.8	
	(π, π^*)	$^1B_2$	–	5.1	5.0	
	(n, π^*)	$^1A_2$	–	5.6	–	
	(π, π^*)	$^1A_1$	–	6.1	6.5	
	(n, π^*)	$^1B_1$	–	6.4	6.4	
	(n, π^*)	$^1A_2$	–	7.0	–	

spectrum of different mono- and disubstituted benzene derivatives [474]. It can be seen from Table 3.31 that quite good agreement with experiment has been achieved, making possible the assignment of some experimentally non identifiable electronic transitions.

The spectrum of conjugated molecules containing heteroatoms (*e.g.* nitrogen, oxygen, sulphur) becomes complicated due to the presence of (n, π^*)-type transitions beside the (π, π^*) excitations. The reliable prediction of these spectra and the need for at least a partial inclusion of σ–π polarization effects led to the development of all-valence electron methods of electronic transitions. Some illustrative examples for excitation energies obtained with the most successful procedure of this type, the CNDO/S, are collected in Table 3.32.

Localized description of excited states. Formaldehyde and various conjugated systems are all examples of so-called *chromophoric groups*, which have outstanding importance in the systematization and interpretation of the electronic spectra of more complicated molecules. It has been found on empirical grounds that the spectral characteristics of the molecules can be quite well described on the basis of the spectral behaviour of some of their functional groups, the chromophores.

TABLE 3.32

Comparison of experimental and theoretical excitation energies (eV) calculated by the PPP-method [701, 702, 703]

Compound	Calc.	Exp.	Compound	Calc.	Exp.
Benzene	4.91	4.88	Aniline	4.38	4.30
	6.20	6.08		5.31	5.30
	7.03	6.74		6.32	–
Chlorbenzene	4.72	4.68		6.65	–
	5.79	5.74	Benzaldehyde	4.53	4.46
	6.74	6.53		5.17	5.16
Phenol	4.61	4.57		6.24	–
	5.70	5.88		6.55	–
	6.67	–	Benzoic acid	4.64	4.52
	6.76	–		5.38	5.37
				6.16	–
				6.49	–
Nitrobenzene	4.56	4.32			
	5.07	4.95			
	5.90	–			
	6.08	5.96			
	6.45	–			

The main features of the observed spectrum can be built up from the nearly transferable absorption properties of the chromophores. The effect of the whole molecular framework is manifested in relatively small perturbations with respect to the idealized isolated chromophore state. Characteristic substituent shifts of the transition energies of the most common chromophores have been collected in the literature, and these effects could be explained on the basis of qualitative MO (or VB) considerations [632].

A straightforward way of introducing the chromophore concept into the quantum chemical treatment is based on the use of some localized description of the excited states [175]. This has two advantages. First, it offers a conceptually simple and natural way of analysis of the theoretical results in terms of the familiar chromophore picture, thus leading to deeper chemical understanding of the nature of various spectral characteristics of the molecules. Secondly, one can expect that with the help of localized orbitals correlation effects can be managed in a more economic manner. In particular, truncated CI expansions in localized orbital basis should have advantageous convergence properties with respect to the corresponding canonical expansions [175].

The localized treatment of excited states traces back to the early work of Simpson, who used such an approach for the interpretation of the spectrum of conjugated hydrocarbons [1280]. In Simpson's model the conjugated hydrocarbon is described as an assembly of strictly localized ethylenic units (no electron delocalization is allowed). The excited states are represented by linear combinations of local excitations

(excitons) within the ethylenic units. The excitonic states thus obtained become delocalized over the whole system. However, this "exciton delocalization" should be distinguished from the electron delocalization associated with the electron charge transfer between the localized units even in the ground state. Although the neglect of this latter effect is serious drawback in the application of the exciton model to polyene spectra [1219], this model is of outstanding importance in the study of weakly interacting systems, like molecular crystals [281].

The fact that symmetry adapted canonical molecular orbitals allow at least a qualitatively satisfactory single determinantal (STA) representation of the excited states explains the domination of canonical molecular orbital methods in spectroscopy [305]. In most cases a chemically meaningful zero order description of the excited states in a localized orbital framework requires us to go beyond the single determinantal approach. However, bearing in mind that even in the canonical MO representation the single determinantal wave function is only a crude approximation from the quantitative point of view, there is no reason to insist on the canonical MO framework if a CI is also performed. It has to be mentioned that if the localized and canonical orbitals span the same occupied and virtual subspaces, full CI expansions in both bases lead to identical results. The same holds for any full CI-subspace. For example the same results are obtained by all single CI calculations carried out in either canonical or localized MO bases, if these sets of orbitals are related to each other by a unitary transformation [305].

An *a posteriori* analysis in terms of localized orbitals of the STA or CI excited state wave functions evaluated in canonical MO basis is a possible use of localized orbitals in spectroscopy. For example Langlet and Malrieu [764] have undertaken an analysis of the canonical STA wave function. They found that this wave function can be represented in the localized picture as a "democratic mixture" of charge transfer excitations (involving an electron jump from a localized bond orbital to the virtual orbitals of other bonds), where the long-distance electron jumps are highly probable, while local excitations (within a given bond) have a vanishing weight [764]. Thus the single transition approximation in the canonical representation overestimates the delocalization of the excitation. Accordingly, the configuration interaction has usually a tendency towards a more localized excited state wave function [175, 764].

The inadequacy of the canonical single determinantal approach and the advantages of a localized description can be illustrated by the example of the glyoxal molecule (n, π^*) excitation. Glyoxal has two identical, strongly interaxting carbonyl chromophores. The delocalized canonical orbitals $n_\pm$ and $\pi^*_\pm$ involved in the lowest energy transition can be expanded in terms of the n_1 and n_2 and π_1 and π_2 orbitals localized on chromophores number 1 and 2. Neglecting the normalization we can write:

$$n_\pm = n_1 \pm n_2$$

$$\pi^*_\pm = \pi^*_1 \pm \pi^*_2. \tag{3.156}$$

The excited state wave function $\Psi(n_+, \pi^*_-)$ has the following form:

$$\Psi(n_+, \pi^*_-) = \Psi(n_1, \pi^*_1) - \Psi(n_2, \pi^*_2) - \Psi(n_1, \pi^*_2) + \Psi(n_2, \pi^*_1). \tag{3.157}$$

The first two terms are local exciton contributions, while the last two terms are charge transfer excitations between the chromophores. Although we would expect a significantly lower weight of the interchromophoric charge transfer excitations with respect to the intrachromophoric local excitations, these two types of configurations make equal contributions to the wave function [1022]. This feature of the symmetry constrained single determinantal description of the excited state explains the unexpected correlation effect on the corresponding transition energy. The ΔSCF excitation energy is higher by about 0.5 eV than the CI result [566, 1022]. Much better results are obtained in the single determinantal approach for the lowest energy transition if the symmetry constraint is released [1022].

This example illustrates the possible use of symmetry-broken localized description as a convenient zero order approximation in excited state problems. Other cases when localized approach to the transition energies and excited state geometries proved to be useful are *p*-benzoquinone [877] and pyrazine [707, 1393], where the generalized valence bond (GVB) method was applied.

The importance of the study of excited state potential energy surfaces has already been mentioned in connection with the formaldehyde and ethylene molecules. The progress in experimental techniques, mainly the availability of lasers, has led to an increasing interest in excited state reaction dynamics and photochemistry, and made possible the accurate measurement of spectroscopic constants. The interpretation of these experimental data relies heavily upon the theoretical predictions concerning the potential energy surfaces of excited state species [570].

These calculations should meet the basic requirements of potential energy surface investigations (*cf.* Section 3.2). Special attention should be paid to the account of correlation effects, since quite often dissociative processes are involved in the regions of the potential surface that are of interest. Furthermore, the calculations should give a reliable description of a series of different electronic states. There are several reviews on excited state potential surface calculations, see for example Ref. 570. The extensive *ab initio* calculations which are possible for diatomics yield results in good agreement with experiment. In order to have an illustrative example, the case of the N_2 molecule is presented in Fig. 3.40. The potential curves, which are in a spectacular agreement with the experimental ones, have been obtained with a special multiconfigurational SCF technique, the complete active space SCF (CASSCF) method [1187]. Direct methods, like the equation of motion procedure has also been used for the calculation of N_2, CO, and C_2H_4 potential surfaces [261].

The calculation of whole surfaces in the case of triatomics and larger systems is quite difficult, and the accuracy needed for dynamical studies can hardly be attained by the usual *ab initio* techniques. A specific approximate method, which is based on the use of accurate data on component diatomic systems, the diatomics in molecules (DIM)

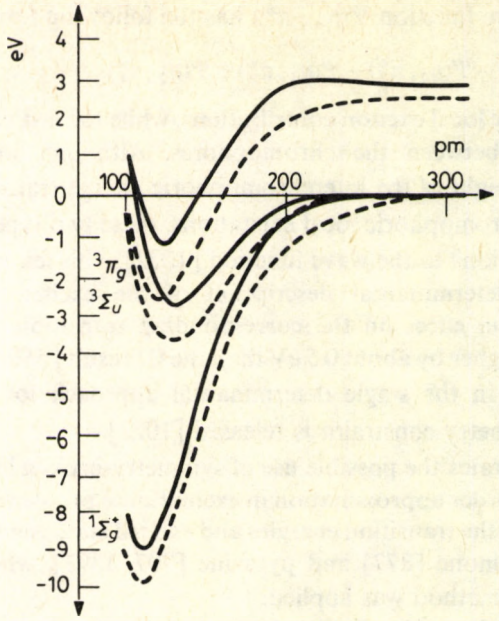


Fig. 3.40 Calculated (solid line) and experimental (dashed line) potential curves of the three lowest states of the N_2 molecule. (With permission from Ref. [1187])

method seems to be the most convenient procedure to study potential energy surfaces of several electronic states [1371].

The study of a relatively limited part of the potential energy surfaces is sufficient for the prediction of various spectroscopic constants. Examples concerning the vibrational structure of electronic absorption bands will be discussed in Section 3.7.2.

Several attempts have been made to develop semiempirical MO methods which are appropriate for the calculation of excited state equilibrium geometries. The CNDO/S method cannot be used for geometry optimization; it gives erroneous results. The combination of CNDO/2 geometry optimization with CNDO/S transition energy calculations proved to be a successful compromise in some cases [1224]. Other approaches are the MNDO–CI method [1249] and a special INDO-type parametrization scheme, the SINDO with CI [919].

The quantum mechanical extension of empirical force fields has been proposed for the study of excited state geometries of conjugated molecules. In the QCFF/PI method of Warshel *et al.* [1402] the quantum mechanical π-energy is calculated by a PPP-like method and the effect of the sigma framework is accounted for by empirical methods.

The effect of intermolecular complexation and of the solvent on the electronic spectra has also been studied by different methods. A thoroughly investigated case is the (n, π^*) transition of formaldehyde and of carbonyl compounds. The effect of hydrogen bonding solvents was simulated by considering the excitation energies in the

complexes HOH...OCHR [291] and ROH...OCH_2 [289]. In these complexes the transition energies are blue-shifted with a few tenth of eV with respect to the corresponding monomer (n, π^*) excitation energy. *Ab initio* calculations could reproduce well this tendency. The complex transition energies were found to be well approximated as the monomer (n, π^*) transition energy plus the hydrogen bond strength in the ground state complex. This relationship suggests that blue shifts reflect the energy required to break or weaken the hydrogen bond in the excited state [291].

The effect of the association of carbonyl compounds with Li^+ ion has also been studied. The excited state complexes were found to remain bound, but as was reflected by the large increase of the (n, π^*) transition energies (0.7–1.7 eV), they were destabilized with respect to the ground state [296]. The (n, π^*) excited state of the formaldehyde-water and acrolein-water complexes were found to be dissociative, while the (π, π^*) excited state of the formic acid dimer is an excimer state, *i.e.* it corresponds to a stable intermolecular complex [631].

The effect of the bulk solvent on the transition energies of formaldehyde has been calculated as well as of its complexes with water molecules within the framework of a continuum electrostatic model [116, 117, 216] (*cf.* Section 1.5), and quite reasonable solvent shifts were obtained. Other continuum models of the solvent effects were applied for the prediction of solvent shifts; namely the SCRF theory [1455], the solvaton [392, 910] and the virtual charge methods [130].

3.7 INTERACTION OF MOLECULES WITH ELECTROMAGNETIC RADIATION

One has to consider two main types of processes, when the interaction of molecules with electromagnetic radiation is studied. In the course of an *absorption* process the molecule gains energy from the radiation field by absorbing a photon and gets into an excited state. Depending on the frequency of the radiation rotational, vibrational, or electronic levels may be excited. In an *emission* process, on the other hand, the molecule which was initially in an excited state gets back to the ground state, or to another state of lower energy by emitting a photon. The full understanding of absorption and emission processes would require an involved quantum electrodynamical treatment [268, 1130]. However, in most cases a semiclassical theory, which treats the electromagnetic radiation field classically, and the molecule itself by means of the quantum theory, provides an adequate description [268, 1237, 1387].

In the following we shall be concerned with absorption processes. We have already surveyed in the preceding sections some quantum chemical methods, which were appropriate for the description of the ground and (vibrationally and/or electronically) excited states of the molecules. An interesting question is; what happens to the molecules while they are interacting with the radiation field.

Let us consider a ground state molecule, and put it into a radiation field. A formal description of the system, perturbed by the electromagnetic radiation, can be given in

terms of the stationary states of the molecule by the $\Phi(\mathbf{r}, t)$ "superposition function" [547]:

$$\Phi(\mathbf{r}, t) = c_0(t)\Psi_0(\mathbf{r}, t) + c_n(t)\Psi_n(\mathbf{r}, t) \tag{3.158}$$

where the stationary wave functions Ψ_0 and Ψ_n are defined by

$$\Psi_0(\mathbf{r}, t) = \Psi_0(\mathbf{r})e^{-iE_0t/\hbar} \tag{3.159a}$$

$$\Psi_n(\mathbf{r}, t) = \Psi_n(\mathbf{r})e^{-iE_nt/\hbar} \tag{3.159b}$$

and $\Psi_0(\mathbf{r})$ and $\Psi_n(\mathbf{r})$ satisfy the time-independent Schrödinger equation. The mixing coefficients $c_0(t)$ and $c_n(t)$ must satisfy the normalization condition:

$$|c_0(t)|^2 + |c_n(t)|^2 = 1. \tag{3.160}$$

It has to be emphasized that during the transition period the system is in a nonstationary state, *i.e.* the superposition function (3.158) is not an eigenfunction of the molecular Hamiltonian. Accordingly, the outcome of an energy measurement during this period cannot be predicted with certainty. The probabilities of observing E_0 or E_n in a single energy measurement at a given time t, are $|c_0(t)|^2$ and $|c_n(t)|^2$, respectively. Since such an experiment is incapable of revealing the time-dependent properties of nonstationary states, it is quite common to assume that the system gets from the initial to the final stationary state by a discontinuous "quantum jump" at some moment during the transition period, rather than exhibiting a continuous evolution [851]. However, recent experimental measurements using coherent radiation sources confirmed that there are no "quantum jumps" in the above sense. In effect, in the course of a transition process, the electric and magnetic properties of the system undergo smooth, continuous, periodic changes.

In order to have a somewhat more precise idea about the transition process, let us consider the probability function $P(\mathbf{r}, t)$ corresponding to the (3.158) wave function:

$$P(\mathbf{r}, t) = |\Phi(\mathbf{r}, t)|^2 = |c_0(t)|^2 |\Psi_0(\mathbf{r})|^2 + |c_n(t)|^2 |\Psi_n(\mathbf{r})|^2$$
$$+ 2c_0(t)c_n(t)\Psi_0(\mathbf{r})\Psi_n^*(\mathbf{r}) \cos\left[\frac{(E_n - E_0)t}{\hbar}\right]. \tag{3.161}$$

For specifying the actual time dependence of $P(\mathbf{r}, t)$ we must know the mixing coefficients, which can be calculated by time-dependent perturbation theory. The derivation can be found in standard textbooks [382, 678, 1237], only the final results are interesting in the present context. After making some approximations [1236] the following formula is obtained:

$$|c_n(t)|^2 \approx \frac{\pi}{4} \frac{|V_{0n}|^2}{\hbar^2} t\delta(\omega_{0n} - \omega). \tag{3.162}$$

Equation (3.162) implies that two conditions must be fulfilled for realizing a quantum transition. First, the V_{0n} matrix element, describing the interaction of the molecule and

the perturbing radiation field must be different from zero; second, the frequency of the incident radiation must be equal to the Bohr frequency of the given transition:

$$\omega_{0n} = \frac{E_n - E_0}{\hbar}. \tag{3.163}$$

Provided that the above conditions are met, the weight $|c_n(t)|^2$ of the final state in the probability function increases linearly with the time. Let us note that an interference term

$$2c_0(t)c_n(t)\Psi_0(\mathbf{r})\Psi_n^*(\mathbf{r})\cos[(E_n - E_0)t/\hbar]$$

arises also in $P(\mathbf{r}, t)$, which corresponds to oscillations of the $\Psi_0(\mathbf{r})\Psi_n(\mathbf{r})$ transition density with the ω_{0n} Bohr-frequency. The amplitude of these oscillations is also time dependent; it reaches its maximal value in the middle of the transition period [547].

The time evolution of the probability function is illustrated schematically for the *s–p* transition of a H atom on Fig. 3.41 [547]. As the transition progresses, the $P(\mathbf{r}, t)$ function, which is identical to the electronic charge density of the *s* state H atom at $t = 0$, resembles more and more closely the charge density of the final *p* state. During the transition period the centre of the electric charge density is displaced periodically in the positive and negative *z* directions (we suppose that the electron is excited to a p_z orbital) giving rise to an oscillating transition dipole moment. Using a classical analogy we can say that in the course of an $s \rightarrow p$ transition the H atom behaves like a dipole oscillator ("antenna") [547]. The conditions of the effective energy transfer from the radiation field to the molecule (or *vice versa* in an emission process) can be quite well understood from this classical picture. It is clear that a net transition dipole moment is required in order to have an interaction with the radiation field. This is the basis of the "dipole selection rule", which plays an important role in various branches of spectroscopy. Furthermore, the oscillator must be in resonance with the radiation field, that is, its frequency must be equal to the frequency of the radiation.

We have not yet specified the form of the interaction operator that promotes the transition between two (vibrational, electronic, etc.) quantum states of the molecule. In general, the interaction of the molecule and the radiation field is described in the dipole approximation, that is only the electric dipole term is retained in the multipolar expansion of the interaction operator $\hat{\mathbf{V}}$. Higher order terms, like electric quadrupole or magnetic dipole, have much smaller contributions to ordinary absorption intensities. The consideration of magnetic dipole interactions is important in the theory of chiroptical phenomena (see Section 7.3).

There are several formally equivalent representations of the interaction operators in the electric dipole spectroscopies [57, 507a]. In the *dipole length (position)* formalism the radiation-matter interaction is written as:

$$\hat{\mathbf{V}} = -\mathbf{F} \cdot \hat{\boldsymbol{\mu}} \tag{3.164}$$

where $\mathbf{F}$ is the electric field vector and $\hat{\boldsymbol{\mu}}$ is the electric dipole moment operator acting

on both electrons and nuclei (Eq. 3.35b). On the other hand, according to the *dipole velocity (momentum)* formulation the interaction operator reads as:

$$\hat{V} = \frac{e}{mc} \mathbf{A} \cdot \hat{\mathbf{p}} \tag{3.165}$$

where $\mathbf{A}$ is the vector potential of the electromagnetic field and $\hat{\mathbf{p}}$ is the linear momentum operator. The operators (3.164) and (3.165) correspond to different choices of the gauge used to express the field [473]. Although formally only the dipole length operator ensures the gauge-invariant description of the radiation–matter interaction, under certain limiting conditions the dipole velocity formalism leads to equivalent results [773].

The relation of dipole length and dipole velocity operators can be demonstrated also by means of quantum mechanical commutation rules, by the off-diagonal hypervirial relations [201]. These relations can be used for the derivation of different forms of the oscillator strength as well as the optical rotatory strength of electronic transitions (see Sections 7.2 and 7.3). It is important to emphasise that the equivalence of these different formulations of electric dipole transitions holds only for wave functions which are exact solutions of the Schrödinger equation.

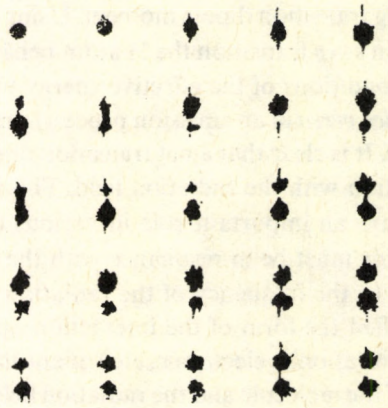


Fig. 3.41 Time-evolution of the electric charge density (probability density) of a hydrogen atom in the course of an $1s \rightarrow 2p$ allowed electronic transition. The series increases in time from left to right starting in the upper left corner. Note the presence of a persistent oscillating dipole moment during the transition. (With permission after Ref. [547]

In the following we briefly look at some quantum chemical methods for the calculation of the transition probabilities of vibrational and electronic excitations. We have just seen that this probability is proportional to the square of the matrix elements of the transition moment operator (either $\hat{\boldsymbol{\mu}}$ or $\hat{\mathbf{p}}$, depending on the actual formulation), thus our task is to calculate these matrix elements with the appropriate wave functions of the ground and excited states.

3.7.1 VIBRATIONAL TRANSITION PROBABILITIES

Experimental method: infrared spectroscopy [219].

When a molecule interacts with infrared radiation, its vibrational levels become excited (see Section 3.3 and Appendix 1). The probability of an infrared transition between the v and v' vibrational levels of the ground electronic state is proportional to the square of the corresponding transition moment matrix element. Let us consider a pure vibrational transition, that is let the change in the rotational state of the molecule be neglected. Then, we can write the transition dipole moment (in the dipole length formulation) using the Born–Oppenheimer approximation as:

$$\langle \Psi_0(\mathbf{r};\mathbf{Q})\xi_{0v}(\mathbf{Q})|\hat{\mu}|\Psi_0(\mathbf{r};\mathbf{Q})\xi_{0v'}(\mathbf{Q})\rangle = \langle \xi_{0v}(\mathbf{Q})|\hat{\mu}(\mathbf{Q})|\xi_{0v'}(\mathbf{Q})\rangle \tag{3.166}$$

The $\hat{\mu}(\mathbf{Q})$ quantity is the dipole moment function of the ground electronic state, and depends on the normal coordinates of the nuclei, $\mathbf{Q}$. The dipole moment function $\hat{\mu}(\mathbf{Q})$ can be expanded in Taylor series in terms of the normal coordinates, Q_i, about the equilibrium nuclear configuration $\mathbf{Q}^0$ as [177]:

$$\hat{\mu}(\mathbf{Q}) = \hat{\mu}(\mathbf{Q}^0) + \sum_{i}^{N-6} \left(\frac{\partial \hat{\mu}(\mathbf{Q})}{\partial Q_i}\right)_{\mathbf{Q}^0} Q_i + \ldots . \tag{3.167}$$

Putting this expansion into the (3.166) expression we obtain the following result for the transition dipole moment:

$$\hat{\mu}_{0v,0v'} = \sum_{i}^{N-6} \left(\frac{\partial \hat{\mu}(\mathbf{Q})}{\partial Q_i}\right)_{\mathbf{Q}^0} \langle \xi_{0v}(\mathbf{Q})|Q_i|\xi_{0v'}(\mathbf{Q})\rangle . \tag{3.168}$$

Within the framework of the harmonic approximation the integral $\langle \xi_{0v}(\mathbf{Q})|Q_i|\xi_{0v'}(\mathbf{Q})\rangle$ is zero, unless the vibrational quantum number of the i'th normal mode changes by ± 1 from the initial to the final vibrational state. The effect of anharmonicities can be judged from the data in the last column of Fig. 3.6. The most intense band in the spectrum of chloroform ($CHCl_3$) corresponds to the $0 \rightarrow 1$ transition for the CH stretching, while the intensities of the $0 \rightarrow 2$, $0 \rightarrow 3$, etc. transitions decrease rapidly. Thus the integrated intensity, A_i of the i'th fundamental band in the IR (infrared) spectrum can be expressed as:

$$A_i = \frac{1}{nl}\int \ln\left(\frac{I_0(\nu)}{I(\nu)}\right) d\nu = \frac{N_A \pi}{3c^2}\left|\left(\frac{\partial \hat{\mu}(\mathbf{Q})}{\partial Q_i}\right)_{\mathbf{Q}^0}\right|^2 . \tag{3.169}$$

where ν is the wave number (in cm^{-1}), n is the molar concentration, l is the path length, and $(\partial \hat{\mu}(\mathbf{Q})/\partial Q_i)_{\mathbf{Q}^0}$ is the derivative of the molecular dipole moment with respect to the i'th normal coordinate [1051, 1428]. It is interesting to note that the Born–Oppenheimer wave function used in Eq. (3.166) turns out to be inappropriate for the

calculation of IR intensities in the context of the dipole velocity formalism [892]. One is faced with the somewhat paradoxical situation that it is necessary to go beyond the Born–Oppenheimer approximation to get reasonable vibrational transition probabilities in the dipole velocity formalism, but this is not necessary in the dipole length formalism [1398]. The reason for this discrepancy lies in the fact that while the Born–Oppenheimer wave function contains information regarding the correlation of *electronic and nuclear positions*, it does not include the correlation of *electronic and nuclear moments*. This paradox has been resolved by the introduction of a "complete adiabatic" wave function, which preserves the separability of the electronic and nuclear motions, but contains a parametric dependence of the electronic wave function upon the instantaneous nuclear momenta as well as the usual dependence on nuclear positions [962].

The theoretical calculation of vibrational intensities is an important tool in the interpretation of IR spectra. Since the integrated intensities, A_i are proportional to the square of the dipole moment derivatives, only the absolute values of $\partial\hat{\mu}/\partial Q_i$ can be deduced from experimental data and the signs remain undetermined. Quantum chemical calculations are useful for resolving this sign ambiguity [1306]. Furthermore, the correct reproduction of the experimental dependence of the dipole moment on nuclear distortions is a stringent test for any molecular wave function.

A normal vibration of a molecule gives rise to an absorption band if the distortion of the nuclear framework along the corresponding normal coordinate Q_i leads to a change in the total dipole moment. This is the basis of the dipole selection rules for IR spectra [234]. For example, in the case of the symmetric stretching vibration of the CH_4 molecule all bond lengths increase simultaneously. The symmetry of the molecule is not destroyed, therefore the dipole moment does not change, and the corresponding band is missing from the IR spectrum. On the other hand, during the asymmetric stretching mode the high symmetry of the molecule is destroyed and a small dipole moment arises. It means that the asymmetric stretching mode is dipole-allowed and the corresponding band really appears in the IR spectrum. The selection rules can be formulated conveniently in the language of group theory. The normal modes belonging to those irreducible representations of the molecular point group which transform like the components of the dipole moment operator, are allowed. A detailed discussion of the IR selection rules can be found, for example in the book of Colthup [234].

The dipole moment derivatives can be determined by quantum chemical methods which are appropriate for the study of ground state molecular charge distributions. Usually numerical differentiation techniques are applied in these calculations. One possibility is to determine the molecular dipole moment at different geometries by taking small displacements along the internal local (**R**) or internal symmetry (**S**) coordinates and evaluate the $\partial\hat{\mu}/\partial R_i$ or $\partial\hat{\mu}/\partial S_i$ derivatives as finite differences. Usually step lengths of 0.02 Å and 2 degrees are sufficient for stretches and bendings, respectively [1291]. The $3 \times (3N-6)$ derivatives form the **P** polar tensor, which is defined on symmetry coordinate basis as [1084]:

$$\mathbf{P}_S = \begin{pmatrix} \partial\mu_x/\partial S_1 & \partial\mu_x/\partial S_2 & \dots & \partial\mu_x/\partial S_{3N-6} \\ \partial\mu_y/\partial S_1 & \partial\mu_y/\partial S_2 & \dots & \partial\mu_y/\partial S_{3N-6} \\ \partial\mu_z/\partial S_1 & \partial\mu_z/\partial S_2 & \dots & \partial\mu_z/\partial S_{3N-6} \end{pmatrix}. \tag{3.170}$$

In actual quantum chemical calculations one needs the space-fixed Cartesian coordinates for the distorted geometries. The transformation from the internal coordinates to the Cartesians [1136] should be carried out by taking into account the six Eckart conditions [350] for the translations and rotations of the molecule-fixed frame. Since these conditions depend on the atomic masses, for different isotropic species appropriate corrections should be applied [1136].

In order to calculate the theoretical intensities, A_i, the dipole moment derivatives must be transformed into a normal coordinate basis. This transformation depends on the molecular force field, which can be calculated theoretically or can be derived from experimental data. It is important to note that discrepancies between the measured and calculated intensities can sometimes be attributed, at least partly, to inaccuracies of the applied force fields [1306].

The above procedure, which can be called the "*finite nuclear displacement perturbation*" method [734] requires a large number of calculations for polyatomic molecules. An alternative "*finite field perturbation*" method, which had been proposed by Komornicki et al. [732, 734], offers a more economical way of evaluating dipole moment derivatives. The method consists of using the (3.81) definition of the dipole moment (as the first derivative of the energy with respect to the applied field **F**), and reversing the order of differentiations with respect to the field and the nuclear distortions:

$$\frac{\partial\mu_\alpha}{\partial Q_i} = -\frac{\partial}{\partial Q_i}\left(\frac{\partial E(\mathbf{F})}{\partial F_\alpha}\right)_{\mathbf{F}=0} = -\frac{\partial}{\partial F_\alpha}\left(\frac{\partial E(\mathbf{F})}{\partial Q_i}\right)_{\mathbf{Q}^0}. \tag{3.171}$$

A great computational advantage is that the basis set integrals have to be calculated only once at the reference geometry and just the energy gradients (forces) have to be evaluated at several values of the external field. The method can be easily extended for the calculation of polarizability derivatives which play an important role in the interpretation of Raman-intensities.

The calculated dipole moment derivatives are quite sensitive to the choice of the basis set (*cf. e.g.* [270, 805]). Minimal basis sets are not flexible enough to describe the changes of charge distribution with respect to nuclear distortions. The use of at least double zeta quality basis sets is strongly recommended. It is worth mentioning that the 4–21G split-valence basis yields dipole moment derivatives in good agreement with near HF-limit calculations [1136]. In certain cases the application of polarization functions is also important [1419]. According to Smit and van Dam, higher principal quantum number (p, d) polarization functions should to be used for ameliorating the description of bending mode derivatives, while stretching mode derivatives can be conveniently calculated by using bond functions [1290].

Although it is generally assumed that SCF calculations provide for appropriate dipole moment derivatives, there are some important exceptions [17]. The case of CO, where a correlated wave function is required even for the description of the dipole moment, is such an example [16]. The vibrational transition dipole matrix elements, calculated from the dipole moment function obtained by the MCSCF method, were in excellent agreement with experiment [1410]. In ozone the absolute magnitude of the IR intensities was found to vary considerably with the level of description, although the sign of the dipole moment derivative was given correctly by both SCF and CI calculations [270]. Valence CI investigations on HCN showed that when the CN bond is stretched the dipole moment decreases, while the SCF calculations predicted a wrong sign for the dipole derivative of this mode [805].

Semiempirical methods, like CNDO/2 are not able to give quantitative agreement with experiment. However, these methods are very useful in resolving sign ambiguities of the experimental dipole moment derivatives [1306]. Some *ab initio* and CNDO/2 results are compared in Table 3.33.

The analysis of the IR intensity data can be carried out with the help of *atomic polar tensors*, $\mathbf{P}^A$, which give the change in the total dipole moment $\Delta\hat{\mu}$ when the N atoms of the molecule undergo small Cartesian displacements $\Delta\mathbf{r}_A$:

$$\Delta\hat{\mu} = \sum_{A=1}^{N} \mathbf{P}^A \Delta\mathbf{r}_A. \tag{3.172}$$

The atomic polar tensor associated with the atom A:

$$\mathbf{P}^A = \begin{pmatrix} \partial\mu_x/\partial x_A & \dots \\ \partial\mu_y/\partial x_A & \dots \\ \partial\mu_z/\partial x_A & \dots \end{pmatrix} \tag{3.173}$$

first introduced by Morcillo *et al.* [98] and rediscovered by Person and Newton [1084], has several interesting properties. For example, one can define the square of the net atomic charge χ^2 as the one third of the squares of the components in Eq. (3.173).

$$\chi^2 = \frac{1}{3}\sum_{\alpha\beta}(P^A_{\alpha\beta})^2 = \frac{1}{3}\sum_{\alpha\beta}\left(\frac{\partial\mu_\alpha}{\partial(r_A)_\beta}\right)^2. \tag{3.174}$$

The effective atomic charges derived from experimental IR intensities using Eq. (3.174) fall within a relatively narrow range for a given atom (*e.g.* oxygen) in different molecules [692].

A quite different approach to a chemically comprehensive formulation of vibrational intensities is the bond moment theory of Gribov [485]. In this model the total dipole moment is resolved to bond moments directed along the bonds:

$$\hat{\boldsymbol{\mu}} = \sum_{k}^{\text{bonds}} \mu_k \mathbf{e}_k \tag{3.175}$$

TABLE 3.33

Dipole moment derivatives calculated by different quantum chemical methods

Molecule	Vibration	Units	CNDO/2	*Ab initio* SCF	Exp.
NH_3 [1139]	Sym. stretch	10^{-20} C	+0.3	−0.057	±1.33
	Sym. bending	10^{-30} C.m.	+3.8	−6.068	±5.07
CH_4 [899]	Asym. stretch	10^{-20} C	−2.1	−3.259	±2.779
C_2H_2 [634]	Asym. stretch	10^{-20} C	+0.981	+4.554	±3.903
	Sym. bend	10^{-30} C.m.	+2.819	+6.632	±4.580
H_2CO [634]	CH sym. stretch	10^{-20} C	−1.90	−2.50	−3.04±0.37
	CO stretch	10^{-20} C	+11.54	17.68	±11.3±1.0
	HCH bend	10^{-30} C.m.	+0.13	−0.27	−0.27±0.17
C_6H_6 [150]	Out-of-plane bend	10^{-30} C.m.	+2.67	–	±4.77±0.10
HCN [150]	CH stretch	10^{-20} C	+0.96	+4.49	±3.36
	CN stretch	10^{-20} C	+4.01	+1.83	±1.86
	Bend	10^{-30} C	−3.11	–	±3.54

where $\mathbf{e}_k$ is the unit vector of the k'th bond. The infrared intensities can be expressed with the help of the so-called *electro-optical parameters* μ_k and $\partial\mu_k/\partial r_k$. The simple bond moment hypothesis, in its most restrictive form implies, that [151, 485]:

a) the stretching of a bond by dr produces a change of the dipole moment in the direction of the bond by $(\partial\mu/\partial r)\,\mathrm{d}r$;

b) the bending of a bond by an angle dϑ produces a dipole moment change $\mu\,\mathrm{d}\vartheta$ perpendicular to the bond and in the plane of the movement;

c) when a bond is stretched or bent no changes occur in other bonds.

These assumptions were analysed by CNDO/2-LMO calculations on the NH_3 vibrations, and the contribution of the lone pair moment was found to be substantial for all vibrational modes [151].

Since the bond moment theory does not hold in its simple form even in a first approximation, if we want to insist on the bond moment hypothesis additional parameters of type $\partial\mu_k/\partial r_j$, describing the bond dipole moment changes induced by the variation of another bond geometry, must be introduced [485]. This correction arises from the fact that the molecular electronic charge distribution does not follow the atomic displacements in a rigid manner. For the same reasons the fixed partial atomic charges model [282] of the IR intensities proved to be unsatisfactory [1132]. We note in passing that the equivalence of the simple bond dipole and the fixed partial charge models have been demonstrated by the fact that they lead to the same atomic polar tensor expressions [1132].

The quantum chemical reorganization of the electronic charge density can be described in a qualitative manner by the rehybridization model [1422]. The application of this method to the dipole moment changes in the symmetric *(a)* and antisymmetric *(b)* bending modes of haloforms (CH_3X) is illustrated on Fig. 3.42. The

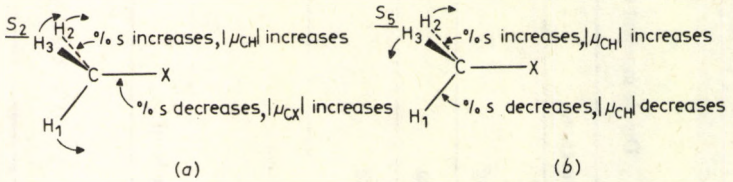


Fig. 3.42 The interpretation of the dipole moment derivatives in the symmetric *(a)* and antisymmetric (*b*) bending modes of a CH_3X molecule in the framework of the rehybridization model. (Ref. [1419])

changes in the CH and CX bond dipole moments are associated with the changes in the *s*-character of the corresponding hybrid orbitals [1419].

It is well-known that intermolecular complexation causes quite pronounced changes in the integrated intensities of vibrational bands. Such changes were investigated for the water dimer and the $H_2O\ldots Li^+$ complex by 4-31G *ab initio* calculations of Sadlej et al. [679]. A significant increase of the OH stretching band intensity was found in the

two cases by factors of 17.6 and 6.9, respectively, corresponding to the experimental factor of 12 observed in liquid water. The atomic polar tensor formalism may be relevant in the analysis of intensity changes in molecular complexes too [1453].

In Raman-experiments the intensities of the individual bands associated with vibrational transitions are proportional to the derivative with respect to the given vibrational mode of the dipole polarizability [219, 556]. Accordingly, the selection rules for the Raman and IR spectra are different [234]. The quantum chemical calculations of polarizability derivatives follow similar lines as those of dipole moment derivatives [402]. The approximate evaluation of Raman intensities can be attempted by using either bond polarizability [546, 929] or atom-dipole interaction [33, 929] models.

3.7.2 ELECTRONIC TRANSITION PROBABILITIES

Experimental method: ultraviolet spectroscopy [632].

In electronic absorption spectroscopy the transition probability is usually characterized by the *oscillator strength* f_{0n}, which is related to the integrated intensity of the absorption band by the following expression:

$$f_{0n} = \frac{2303mc}{2\pi^2 e^2 N_A} \int\limits_{\substack{0\to n \\ \text{band}}} \frac{\varepsilon(\omega)}{\omega} \mathrm{d}\omega = 4.32 \times 10^{-9} \int\limits_{\substack{0\to n \\ \text{band}}} \frac{\varepsilon(\omega)}{\omega} \mathrm{d}\omega \,. \tag{3.176}$$

Here $\varepsilon(\omega)$ is the molar extinction coefficient, ω is the (circular) frequency and the fundamental constants have their usual meaning.

The theoretical definition of the oscillator strength, $f_{0n}^{(\mathbf{r})}$ using the dipolar approximation and the dipole length (position) formalism is [508]:

$$f_{0n}^{(\mathbf{r})} = \frac{2m\omega_{0n}}{3\hbar} |\langle \Psi_0 | \hat{\mathbf{r}} | \Psi_n \rangle|^2 \,. \tag{3.177}$$

Alternative expressions can be obtained for the oscillator strength if we apply the off-diagonal hypervirial theorem [201], according to which for exact eigenfunctions of the molecular Hamiltonian the following relation holds between the matrix elements of the position ($\hat{\mathbf{r}}$) and gradient ($\hat{\nabla}$) operators:

$$\langle \Psi_0 | \hat{\nabla} | \Psi_n \rangle = \frac{m\omega_{0n}}{\hbar} \langle \Psi_0 | \hat{\mathbf{r}} | \Psi_n \rangle \,. \tag{3.178}$$

The dipole velocity (momentum) expression, $f_{0n}^{(\nabla)}$ emerges by putting the relation (3.178) into the (3.177) definition:

$$f_{0n}^{(\nabla)} = \frac{2\hbar}{3m\omega_{0n}} |\langle \Psi_0 | \hat{\nabla} | \Psi_n \rangle|^2 \tag{3.179}$$

while in a mixed formulation the transition frequency can be eliminated from the expression of the oscillator strength:

$$f_{0n}^{(\nabla)} = \frac{2}{3} \langle \Psi_0 | \hat{\nabla} | \Psi_n \rangle \langle \Psi_n | \hat{\mathbf{r}} | \Psi_0 \rangle . \tag{3.180}$$

The oscillator strengths obey different sum rules of which the most important is the *Thomas–Kuhn sum rule.* It states that the sum of the oscillator strengths of all the electronic transitions in a given system is equal to the total number of electrons [678].

Vibronic intensities. When studying electronic transitions we have to take into account that not only the electronic levels are excited by the incident light but rotational and vibrational degrees of freedom are also affected. Therefore it is more appropriate to speak about transitions between "*rovibronic*" and "*vibronic*" states. This implies that in principle we have to use the total wave function (involving both electronic and nuclear parts) for the description of the intensity distribution in electronic spectra. The complexity of this task can be reduced considerably by neglecting rotational degrees of freedom, and addressing only the problem of vibronic transitions. We note, that in this respect there is no substantial difference in the treatment of electronic absorption and photoelectron spectra, where the relative intensities of the vibrational sub-bands are governed by the same laws.*

Usually it is assumed that the *adiabatic approximation* is valid, *i.e.* the total wave function $\mathbf{\Psi}(\mathbf{r}, \mathbf{Q})$ can be written in a product form:

$$\mathbf{\Psi}(\mathbf{r}, \mathbf{Q}) = \Psi_{\text{el}}(\mathbf{r}, \mathbf{Q}) \chi_{\text{nucl}}(\mathbf{Q}) \tag{3.181}$$

where $\Psi_{\text{el}}(\mathbf{r}, \mathbf{Q})$ dynamical electronic wave function depends parametrically on the nuclear coordinates, and $\chi_{\text{nucl}}(\mathbf{Q})$ is the nuclear wave function. The physical picture behind this approximation is that the nuclei move independently on separate potential energy hypersurfaces, assigned to the different electronic states. Let us consider the transition moment for a $0v \rightarrow kw$ vibronic excitation:

$$\mathbf{A}_{0v,kw} = \langle \Psi_0(\mathbf{r}; \mathbf{Q}) \chi_{0v}(\mathbf{Q}) | \hat{\mathbf{A}} | \Psi_k(\mathbf{r}; \mathbf{Q}) \chi_{kw}(\mathbf{Q}) \rangle =$$

$$= \langle \chi_{0v}(\mathbf{Q}) | \mathbf{A}_{0k}(\mathbf{Q}) | \chi_{kw}(\mathbf{Q}) \rangle \tag{3.182}$$

where the operator $\hat{\mathbf{A}}$ may stand for either the position $\hat{\mathbf{r}}$ or the momentum $\hat{\mathbf{p}} = -i\hbar\hat{\nabla}$ operators, and after the second equality in (3.182) the integration for the electronic variables was carried out. The electronic transition moment $\mathbf{A}_{0k}(\mathbf{Q})$ as a function of the nuclear coordinates $\mathbf{Q}$, is often taken to be constant. This is the *Condon approximation* [235]. Provided that the transition is electronically allowed, *i.e.* the electronic transition moment $\mathbf{A}_{0k}(\mathbf{Q}^0)$, calculated at the equilibrium nuclear configuration $(\mathbf{Q}^0)$ of the initial state is nonvanishing, the oscillator strength of the $0v \rightarrow kw$ vibronic transition is:

* For the quantum chemical calculation of *absolute* intensities of photoelectron spectra (photoionization cross section) see *e.g.* Ref. [840].

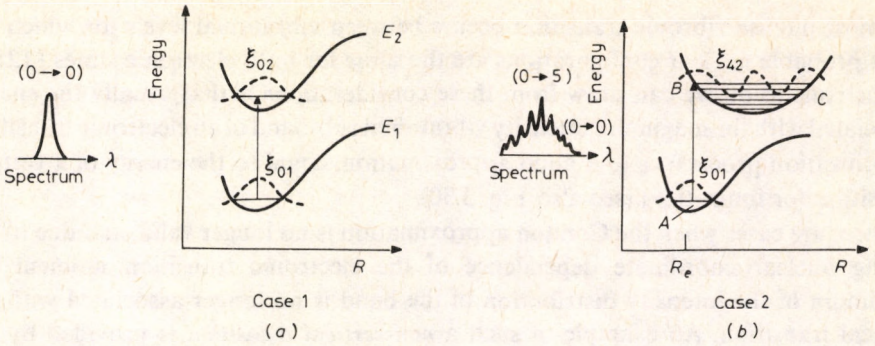


Fig. 3.43 The illustration of the Franck–Condon principle. *(a)* Case 1, when the ground and excited potential energy surfaces are similar. *(b)* Case 2, when the two potential surfaces are significantly different

$$\mathbf{A}_{0v,kw} \approx \mathbf{A}_{0k}(\mathbf{Q}^0) \langle \chi_{0v}(\mathbf{Q}) \mid \chi_{kw}(\mathbf{Q}) \rangle . \tag{3.183}$$

It means that the intensity of a vibrational sub-band of an electronically allowed transition is proportional to the absolute square of the overlap integral* between the vibrational wave functions of the initial and final states. This is the basis of the *Franck–Condon* principle [404], which conveys particular importance to vertical transitions in the theoretical interpretation of ionization and electronic spectra (*cf.* Sections 3.6.2 and 3.6.3). Let us consider the two cases illustrated on Fig. 3.43. [1219]. In the first case *(a)* the potential energy surfaces of the two electronic states are similar and their minima correspond practically to almost the same nuclear configuration. In the ground vibrational level of both electronic states the most probable nuclear configurations (measured by the maximum of $|\chi(\mathbf{Q})|^2$) are $\mathbf{Q}^0$, the ground state equilibrium geometry, and the transition between the ground vibrational levels is associated with the largest overlap of the vibrational wave functions (Fig. 3.43*a*). The spectrum consists of one highly peaked band corresponding to the $00 \rightarrow k0$ excitation, while other vibronic transitions are of much lower intensity. In the second case (Fig. 3.43 *b*) the potential energy surfaces of the two states are quite different and their minima correspond to different nuclear configurations. The overlap of the ground vibrational level wave functions (χ_{00} and χ_{k0}) is now small. For higher vibrational levels the largest amplitude of the wave function is at the turning point, *i.e.* at the positions of largest nuclear displacements from the equilibrium. Therefore it is expected that $\chi_{00}(\mathbf{Q})$ has the largest overlap with that vibrational wave function of the upper surface, which possesses its highest amplitude at the equilibrium nuclear configuration of the ground state (see Fig. 3.43 *b*). Thus, in general, we can formulate the Franck–Condon principle by saying that

* The $\langle \chi_{0v} \mid \chi_{kw} \rangle$ overlap integral (Franck–Condon factor) is not zero for $v \neq w$ since χ_{0v} and χ_{kw} are the vibrational wave functions of different electronic states.

the most intense vibronic transition occurs between vibrational levels for which the most probable nuclear configurations are the same for both electronic states [1219].

The conclusion we can draw from these considerations is that usually the energy associated with the maximum intensity vibrational sub-band of an electronic transition (or ionization process) is, to a good approximation, equal to the energy of a vertical transition (or ionization) (see also Fig. 3.30).

There are cases when the Condon approximation is no longer valid, and due to the strong nuclear coordinate dependence of the electronic transition moment the maximum of the intensity distribution of the band is no longer associated with the vertical transition. An example of such a *non-vertical transition* is provided by the $^1(\pi, \pi^*)$ excitation of ethylene. Various *ab initio* calculations of the vertical transition energy gave a consistently higher value (by about 0.4 eV) than the location of the maximum in the experimental absorption band. The electronic transition moment for this excitation depends strongly on the CH_2 torsional coordinate. When this feature was taken into account properly in the calculations, the most probable vibronic transition was found at 7.89 eV, in contrast to the vertical transition energy of 8.25 eV [1095]. However, it may be noted that the detailed intensity pattern found in these calculations failed to reproduce the rather diffuse experimental band shape. The source of this discrepancy is the breakdown of the Born–Oppenheimer (adiabatic) approximation for this transition, which necessitates consideration of non-adiabatic effects (see below).

A completely different but interesting approach for the study of band shapes has been proposed recently by Heller [543]. This theory avoids the explicit treatment of thousands of individual vibronic transitions, and describes the nuclear motions on the excited state potential energy hypersurface by the dynamical behaviour of a nonstationary nuclear wave function $\theta(\mathbf{Q}, t)$. Let us denote the ground state vibrational wave function by $\chi_{00}(\mathbf{Q})$, then the nuclear wave function of the upper state is an essentially localized wave packet at $t=0$;

$$\theta(\mathbf{Q}, t=0)=\boldsymbol{\mu}_{0k}(\mathbf{Q})\chi_{00}(\mathbf{Q}) \tag{3.184}$$

where $\boldsymbol{\mu}_{0k}(\mathbf{Q})$ is the electronic transition dipole moment. The wave packet $\theta(\mathbf{Q}, t)$ evolves according to the time-dependent Schrödinger equation as:

$$i\hbar\frac{\partial\theta(\mathbf{Q}, t)}{\partial t}=\hat{\mathrm{H}}_{\mathrm{vib}}\theta(\mathbf{Q}, t) \tag{3.185}$$

where $\hat{\mathrm{H}}_{\mathrm{vib}}$ is the vibrational Hamiltonian for the excited state potential surface. The absorption spectrum is given by the Fourier-transform of the overlap integral between the initial $\theta(0)=\theta$ and displaced $\theta(t)$ wave packets:

$$\varepsilon(\omega)=\mathrm{const}\cdot\omega\int_{-\infty}^{\infty}\mathrm{e}^{i(\omega+E_0)t}\langle\theta|\theta(t)\rangle\,\mathrm{d}t \tag{3.186}$$

where ω is the frequency of the incident radiation and E_0 is the energy of $\chi_{00}(\mathbf{Q})$ [544].

It follows from the uncertainty principle that the broadest features of the spectrum are associated with the shortest features in the time-dependent behaviour of the wave-packet. The steeper is the upper surface in the Franck–Condon region (*i.e.* in the region of the normal coordinate space, where the absolute value of the initial state vibrational wave function is appreciable), the faster is the decay of $\langle\phi|\phi(t)\rangle$ and the broader is the absorption envelope. Anything that happens at longer times adds only finer details to the structure of the spectrum, but cannot change the overall band shape [544].

An attractive feature of this method is that for sufficiently short times the wave-packet dynamics can be described to a good approximation classically or semi-classically [544]. Comparative calculations on the $^2A_2(\pi_u, \infty)$ state of N_2^+ revealed that classical wave packet dynamics is applicable only to the description of the primary structure of the spectrum, while a full quantum mechanical procedure yields very good agreement with experiment in all details [286].

Turning back to the conventional time-independent formulation of vibronic transition probabilities, let us see what happens if the electronic transition moment $\mathbf{A}_{0k}(\mathbf{Q}^0)$ vanishes for symmetry reasons, *i.e.* the transition is electronically forbidden. According to experience even in these cases the corresponding band appears in the absorption band. Of course, the intensities of such forbidden transitions ($\varepsilon_{max} = 100 \ldots 5000$) are considerably smaller than those of the electronically allowed ones ($\varepsilon_{max} > 5000$) and forbidden transitions usually exhibit characteristic vibrational fine structure [632].

Obviously one should go beyond the Condon approximation if description of the intensity in forbidden transitions is required. One possibility is to use directly Eq. (3.182), *i.e.* to evaluate the nuclear coordinate dependence of $\mathbf{A}_{0k}(\mathbf{Q})$ for a whole range of $\mathbf{Q}$-values, where the variation of the electronic transition moment is suspected to be strong [156]. For example, Kemper *et al.* used different quantum chemical methods (STA, TOM, ΔSCF) for the calculation of $\mathbf{A}_{(n,\pi^*)}(\mathbf{Q})$ in formaldehyde and found that it is, to a good approximation, a linear function of the normal coordinates [682]. They carried out numerically the integrations prescribed in Eq. (3.182) and calculated a total oscillator strength for the $^1(n, \pi^*)$ transition which was by an order of magnitude larger than the experimental one, in accordance with most earlier calculations. In the light of the theoretical results the authors proposed reexamination of the experimental oscillator strength [682].

Another example is the electrically forbidden $^1(n_+, \pi^*)$ transition of diimide, N_2H_2, where the calculated vertical electric energy difference is about 0.6–0.7 eV greater than the measured location of the intensity maximum. The *ab initio* CI potential curves were determined for six vibrational modes and the intensity distribution was calculated using Eq. (3.182). The discrepancy between experimental and theoretical vibronic levels could be thus reduced below 0.1–0.2 eV [1082].

Instead of carrying out lengthy calculations on the electronic transition moment for a number of nuclear configurations one can adopt the *Herzberg–Teller vibronic*

coupling theory for evaluating the intensity distribution of electronically forbidden transitions [557, 558, 1056].

In this method the dynamical wave function $\Psi(\mathbf{r};\mathbf{Q})$ in the (3.182) expression of the transition moment is expanded according to Eq. (3.144) which was discussed in Section 3.6.2. For most cases it is sufficient to take a three-state model, *i.e.* we consider only three electronic states, Ψ_0, Ψ_k and Ψ_l. If the electronic states are non-degenerate, for small displacements of the nuclei from the $\mathbf{Q}^0$ equilibrium geometry, the ground and excited state wave functions can be expanded into a perturbational series:

$$\Psi_0(\mathbf{r};\mathbf{Q}) = \Psi_0^0(\mathbf{r}) + C_k^0(\mathbf{Q})\Psi_k^0(\mathbf{r}) + C_l^0(\mathbf{Q})\Psi_l^0(\mathbf{r}) \tag{3.187}$$

$$\Psi_k(\mathbf{r};\mathbf{Q}) = \Psi_k^0(\mathbf{r}) + C_0^k(\mathbf{Q})\Psi_0^0(\mathbf{r}) + C_l^k(\mathbf{Q})\Psi_l^0(\mathbf{r}) \tag{3.188}$$

where the coefficients $C_l^k(\mathbf{Q})$ are given to the first order as:

$$C_l^k(\mathbf{Q}) \approx \sum_{i=1}^{N-6} \frac{\left\langle \Psi_l^0 \left| \left(\frac{\partial \hat{\mathrm{H}}_{\mathrm{el}}}{\partial Q_i}\right)_{\mathbf{Q}^0} \right| \Psi_k^0 \right\rangle}{E_l^0 - E_k^0} Q_i \,. \tag{3.189}$$

Accordingly the transition moment of a $0v \rightarrow kw$ vibronic transition can be written as:

$$\begin{aligned} A_{0v,kw} = {} & \langle \Psi_0^0 | \hat{\mathbf{A}} | \Psi_k^0 \rangle \langle \chi_{0v} | \chi_{kw} \rangle + \\ & + \langle \Psi_0^0 | \hat{\mathbf{A}} | \Psi_l^0 \rangle \sum_{i=1}^{N-6} \frac{\left\langle \Psi_l^0 \left| \left(\frac{\partial \hat{\mathrm{H}}_{\mathrm{el}}}{\partial Q_i}\right)_{\mathbf{Q}^0} \right| \Psi_k^0 \right\rangle}{E_l^0 - E_k^0} \langle \chi_{0v} | Q_i | \chi_{kw} \rangle + \\ & + \langle \Psi_l^0 | \hat{\mathbf{A}} | \Psi_k^0 \rangle \sum_{i=1}^{N-6} \frac{\left\langle \Psi_l^0 \left| \left(\frac{\partial \hat{\mathrm{H}}_{\mathrm{el}}}{\partial Q_i}\right)_{\mathbf{Q}^0} \right| \Psi_0^0 \right\rangle}{E_l^0 - E_0^0} \langle \chi_{0v} | Q_i | \chi_{kw} \rangle + \\ & + [\langle \Psi_0^0 | \hat{\mathbf{A}} | \Psi_0^0 \rangle - \langle \Psi_k^0 | \hat{\mathbf{A}} | \Psi_k^0 \rangle] \sum_{i=1}^{N-6} \frac{\left\langle \Psi_k^0 \left| \left(\frac{\partial \hat{\mathrm{H}}_{\mathrm{el}}}{\partial Q_i}\right)_{\mathbf{Q}^0} \right| \Psi_0^0 \right\rangle}{E_k^0 - E_0^0} \langle \chi_{0v} | Q_i | \chi_{kw} \rangle \,. \end{aligned} \tag{3.190}$$

One can recognize in the first term of Eq. (3.190) the Franck–Condon expression, Eq. (3.183), which vanishes identically for electronically forbidden transitions. In general, the third and fourth terms can be neglected, because the energy denominators $E_l^0 - E_0^0$ and $E_k^0 - E_0^0$ are considerably larger than $E_l^0 - E_k^0$. Provided that the $\mathbf{A}_{0l}(\mathbf{Q}^0)$ electronic transition moment is nonzero and the $\left\langle \Psi_l^0 \left| \left(\frac{\partial \hat{\mathrm{H}}_{\mathrm{el}}}{\partial Q_i}\right)_{\mathbf{Q}^0} \right| \Psi_k^0 \right\rangle$ matrix element is nonvanishing for the Q_i vibrational mode, we say that the $0 \rightarrow k$ transition "borrows" its intensity from the $0 \rightarrow l$ transition by coupling through the i'th vibrational mode. Detailed discussions about the symmetry selection rules associated with the vibrational borrowing model can be found in the paper of Sponer and Teller [1301].

A typical example of the electronically forbidden transitions is the carbonyl $^1(n, \pi^*)$ excitation [682, 1073]. In the formaldehyde molecule the out-of-plane wagging and partly the asymmetric CH stretching and bending modes are responsible for the intensification of this transition [682]. In diimide the majority of the vibrational bands of the $^1(n_+, \pi^*)$ transition were found to be induced vibronically *via* the asymmetric NH stretching mode [1082]. The first two electronically forbidden transitions of benzene borrow their intensities from the $^1A_{1g} \rightarrow {}^1E_{1u}$ allowed transition through coupling *via* the e_{2g} bending and stretching modes [384, 959].

Although the vibronic coupling term in Eq. (3.190) is only a higher-order quantity besides the zero order Franck–Condon contribution in electronically allowed transitions, there are cases where the relative importance of the two terms is reversed in favour of the Herzberg–Teller vibronic coupling. When the absorption band is due to a forbidden transition of a highly symmetric chromophore, which is embedded in an asymmetric molecule, the static perturbation of the molecular framework makes the transition formally allowed. However, this static perturbation may be considerably weaker than the vibronic interactions and the spectrum may be dominated by vibronic coupling terms [57].

The vibronic coupling effects are often even more pronounced in photoelectron spectroscopy than in electronic absorption processes [739, 333]. The Herzberg–Teller vibronic coupling theory, which remains within the framework of the Born–Oppenheimer (adiabatic) approximation, provides for a satisfactory description of the symmetry-lowering in ionic states (*cf.* Section 3.6.2) and of the intensity distribution of photoelectron spectra [185]. The symmetry-lowering effects in the core ionization spectrum of the CO_2 molecule have been studied by vibronic coupling method [332]. Another example of the successful application of this method is the study of the first

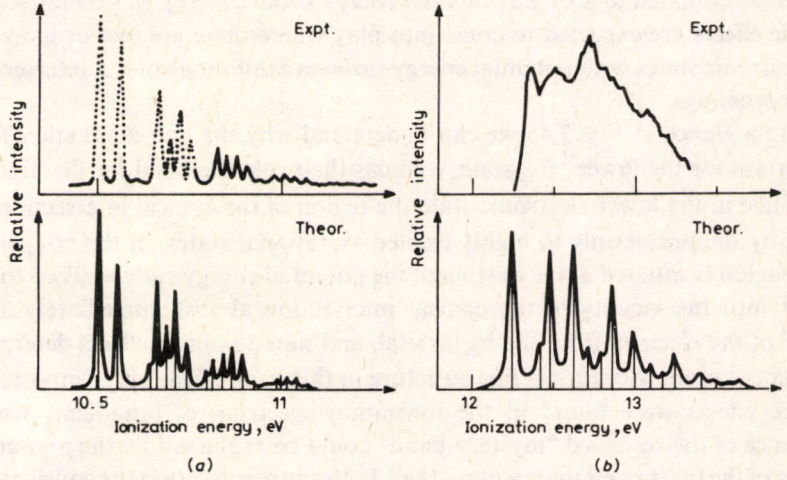


Fig. 3.44 Experimental and calculated (by the Herzberg–Teller vibronic coupling theory) photoelectron band for the (*a*) first cationic state; (*b*) second cationic state. (With permission from Ref. [739])

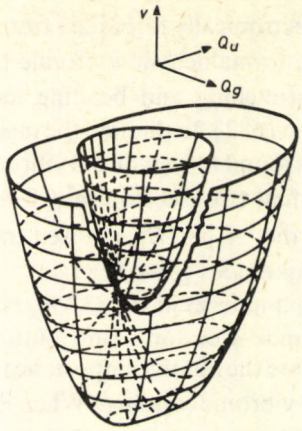


Fig. 3.45 Potential energy surfaces for the two lowest cationic states of ethylene. The two normal coordinates are the C=C torsion (Q_u) and the C=CC (Q_g) stretch. Note the conical intersection of the two surfaces. (With permission from Ref. [739])

band in the photoelectron spectrum of ethylene (Fig. 3.44 *a*) [740]. It is noteworthy that similar calculations on the second band, corresponding to the $^2B_{2u}$ cationic state of ethylene fail to reproduce the complicated vibrational fine structure (Fig. 3.44 *b*) [738].

The $^2B_{2u}$ state of ethylene is a typical example, where strong *non-adiabatic effects* govern the intensity distribution of the spectrum. As can be seen from Fig. 3.45, the potential energy surfaces of the upper $^2B_{2u}$ and of the lower $^2B_{2g}$ states touch each other in a certain region of the nuclear configuration space. This region is called the "*conical intersection*" [809]. In the vicinity of a conical intersection the nuclei jump extremely easily between the potential energy surfaces, therefore the nuclear motions cannot be described as confined to a single potential energy surface [739]. In general, such non-adiabatic effects are expected to come into play where there are two or more closely lying electronic states with potential energy surfaces exhibiting conical intersections or avoided crossings.

Taking a glance at Fig. 3.45 we can understand why the non-adiabatic effects are unimportant for the lower $^2B_{2g}$ state, whereas their role is crucial for the higher $^2B_{2u}$ state. While in the lower electronic state the region of the conical intersection can be reached by the nuclei only in highly excited vibrational states, in the $^2B_{2u}$ state this critical region is situated at the bottom of the potential energy surface. Thus the nuclei may get into the vicinity of the conical intersection almost immediately after the removal of the electron from the b_{2u} orbital, and non-adiabatic effects determine the development of the vibrational fine structure in this band [738, 740]. Important non-adiabatic effects were found in the ionization spectrum of butadiene, where the appearance of the so-called "mystery-band" could be explained by the non-adiabatic coupling of the two lowest ionic states [188]. In the nitrogen cation the consideration of about 20 closely lying ionic states was necessary for the interpretation of the structure

of the core ionization spectrum [190]. In the electronic spectrum of ethylene the non-adiabatic coupling between the $^1(\pi, \pi^*)$ and the $^1(\pi, 3s)$ states leads to a very diffuse, broad absorption band for the $^1(\pi, \pi^*)$ transition, while for the $^1(\pi, 3s)$ excitation the non-adiabatic effects are far less important, as was demonstrated by the accurate MRD-CI calculations of Petrongolo *et al.* [1091]. Non-adiabatic interactions come into play in various chemical reactions too, *e.g.* in the symmetric ring opening of dioxirane [215].

Electronic transition moments. Let us see now the problem of evaluating the electronic transition moment at a fixed nuclear configuration. Provided that the vibrational borrowing effects are negligible (*i.e.* the Franck–Condon principle is valid) this quantity plays a central role in the theoretical study of transition probabilities. It can be shown that in such cases the sum of the oscillator strengths for all the vibrational sub-bands of a given electronic transition equals to the pure electronic transition moment of the vertical excitation:

$$\sum_{vw} |\mathbf{A}_{0v,kw}|^2 = |\mathbf{A}_{0k}(\mathbf{Q}^0)|^2 \sum_{vw} |\langle \chi_{0v}(\mathbf{Q}) | \chi_{kw}(\mathbf{Q}) \rangle|^2 = |\mathbf{A}_{0k}(\mathbf{Q}^0)|^2 . \tag{3.191}$$

It means that the integrated intensity of the whole electronic absorption band can be directly compared with the electronic oscillator strength of the vertical transition. This results in a considerable simplification in the theoretical calculation of oscillator strengths, since it is sufficient to know only the electronic wave functions of the initial and final states at the equilibrium nuclear configuration of the initial state.

The first question one can put is whether the oscillator strength (or the transition moment) associated with the excitation is different from zero or not, *i.e.* the transition is allowed or forbidden. This can be answered by considering the symmetry properties of the electronic wave functions of the initial and final states. The rules thus derived are the *selection rules.* Selection rules based on the spatial symmetry of the electronic wave functions are the symmetry selection rules. In the language of group theory, they can be formulated by saying that the representation obtained as the direct product of the irreducible representations of the ground and excited state wave functions must contain the irreducible representation according to which one (or more) component(s) of the electric transition dipole moment transforms in the symmetry operations of the molecular point group. For example, in molecules possessing an inversion centre the states can be classified as even (gerade, g) or odd (ungerade, u). Since the electric dipole moment operator is antisymmetric with respect to the inversion, the $g \rightarrow u$ and $u \rightarrow g$ transitions are symmetry allowed, while the $g \rightarrow g$ and $u \rightarrow u$ transitions are symmetry forbidden. Further examples can be found in Ref. 557. The calculation of the intensity of electronically forbidden transitions was discussed above.

The spin selection rule says that transitions between states of different spin multiplicity (*e.g.* singlet–triplet transitions) are forbidden. This selection rule holds strictly as far as the space-spin factorization of the electronic wave function is not violated by spin-orbit coupling effects (*cf.* Section 3.5) [462]). In fact the singlet-triplet

transitions can be detected by absorption spectroscopy, although the corresponding bands have extremely small intensity ($\varepsilon \leq 1$) [632]. (A convenient method for observing singlet–triplet transitions is electron impact spectroscopy, where the spin selection rule is not valid [743].) The oscillator strength of spin-forbidden singlet–triplet transitions can be calculated by considering the mixing of the zero order triplet excited state ${}^3\Psi_k$ with a singlet excited state ${}^1\Psi_l$ through spin-orbit coupling. First order perturbation theory yields the following expression for the excited state wave function:

$$\Psi_k \approx {}^3\Psi_k + \frac{\langle {}^3\Psi_k | \hat{\mathrm{H}}_{so} | {}^1\Psi_l \rangle}{{}^1E_l - {}^3E_k} {}^1\Psi_l \tag{3.192}$$

where $\hat{\mathrm{H}}_{so}$ is the spin-orbit coupling operator. The transition moment is given by the following leading term:

$$\mathbf{A}_{0k} \approx \frac{\langle {}^3\Psi_k | \hat{\mathrm{H}}_{so} | {}^1\Psi_l \rangle}{{}^1E_l - {}^3E_k} \langle {}^1\Psi_0 | \hat{\mathbf{A}} | {}^1\Psi_l \rangle. \tag{3.193}$$

Provided that the spin-orbit coupling matrix element $\langle {}^3\Psi_k | \hat{\mathrm{H}}_{so} | {}^1\Psi_l \rangle$ is nonzero and the $0 \rightarrow l$ transition is allowed, the intensity of the singlet-triplet transition results from an intensity borrowing mechanism, analogous to the vibronic coupling case [462]. For example, in formaldehyde the most important path intensifying the spin-forbidden ${}^3(n, \pi^*)$ transition is due to coupling with the ${}^1(\pi, \pi^*)$ state. CNDO/S calculations using the (3.193) formula yielded an oscillator strength of 1.5×10^{-7} [360] for this transition, while relativistic *ab initio* calculations using the Tamm-Dancoff approximation (TDA) gave $f_{3(n,\pi^*)} = 5.3 \times 10^{-7}$ [32]. These results compare favourably with the experimental estimate of 1.2×10^{-6}.

Let us return now to the problem of calculating the oscillator strength of an allowed vertical transition. The main difficulty of such a calculation is that the transition moment matrix elements are extremely sensitive to the quality of the wave function. It is quite common that wave functions which provide for rather good excitation energies yield erroneous oscillator strengths. Therefore it would be desirable to have some reliability criteria for the calculated oscillator strengths. Rigorous upper and lower bounds to the electronic transition probabilities were established by Weinhold [1408]. Another practically useful criterion is based on the different formulations of the oscillator strength. As was mentioned, the forms (3.177) and (3.179) are related by the off-diagonal hypervirial relation, (3.178), which ensures the equivalence of these expressions for exact wave functions. One possibility for measuring the quality of the wave function (from the viewpoint of the transition probability calculations) is the angle β_{0k} between the transition moment vectors evaluated by the position and momentum formulations [508]:

$$\cos \beta_{0k} = \frac{\langle \Psi_0 | \hat{\mathbf{r}} | \Psi_k \rangle \langle \Psi_0 | \hat{\nabla} | \Psi_k \rangle}{|\langle \Psi_0 | \hat{\mathbf{r}} | \Psi_k \rangle| \cdot |\langle \Psi_0 | \hat{\nabla} | \Psi_k \rangle} = \frac{f_{0k}^{(rV)}}{(f_{0k}^{(r)} \cdot f_{0k}^{(V)})^{1/2}}. \tag{3.194}$$

In the ideal case, β_{0k} is zero ($\cos \beta_{0k}$ is one), but for some "pathological" wave functions

TABLE 3.34

Electronic oscillator strengths of the water molecule calculated by different *ab initio* approaches

State	Transition	ΔE (eV)	EOM	Pert. CI	FOTOS	MRD-CI	CEPA	Exp.
A_1	$(3a_1, 3s)$	9.54	0.06	0.097	0.091	0.069	—	0.05
A_1	$(1b_1, 3p_x)$	9.61	0.02	0.009	0.008	0.013	—	?
B_1	$(1b_1, 3s)$	7.22	0.05	0.046	0.059	0.044	0.029	0.044–0.06
B_1	$(1b_1, 3p_z)$	9.48	0.006	0.009	0.012	0.012	0.004	?
Reference			[1444]	[1156]	[1008]	[159]	[1304]	

TABLE 3.35

Electronic oscillator strengths for tetraoxy anions of Mn, Cr and V calculated by the X_α-method with separate optimization of the ground and excited states (ΔSCF) and with the single transition approximation (STA) [1157]

Transition	MnO_4^-			CrO_4^{2-}			VO_4^{3-}		
	ΔSCF	STA	Exp.	ΔSCF	STA	Exp.	ΔSCF	STA	Exp.
$(t_1, 2e)$	0.051	0.069	0.03	0.203	0.221	0.11	0.224	0.224	0.15
$(4t_2, 2e)$	0.054	0.067	0.02	0.185	0.210	0.10	0.116	0.120	0.12
$(t_1, 5t)$	0.070	0.070	0.04	0.035	0.034	—	0.120	0.115	—

β_{0k} may be even larger than 90 degrees. An example of such a case can be found in Ref. [1157].

The same quantum chemical methods can be used for the evaluation of transition probabilities as for the calculation of excitation energies (*cf.* Section 3.6.3). Let us look first at the methods which are based on the separate optimization of the ground and excited states. Usually the large-scale *ab initio* procedures which yield well-balanced correlated wave functions for both the ground and excited states (*e.g.* the MRD–CI method) provide for not only good excitation energies but reliable oscillator strengths too [163, 834]. However, the length of the CI expansion can be considerably reduced if one is able to select only those correlation effects which mostly influence the transition moment matrix elements. An effort in this direction is for example the "First Order Theory of Oscillator Strengths" (FOTOS) approach, which leads to good oscillator strengths at a considerably lower cost than calculations in the same basis set using the MRD–CI wave function [1008] (Table 3.34).

The effect of various CI expansions on the quality of the calculated oscillator strengths were analysed by Rauk and his coworkers [1156, 1157]. They found that one can obtain transition probabilities which are correct to the first order by using an excited state wave function including all singly excited configurations from the SCF ground state and a ground state wave function including doubly excited con-

figurations. The simple single excitation CI (SECI) approach, where the ground state is represented by a single SCF determinant, may be even worse than the single transition approximation (STA), which is a consistent zero order aproach [1156].

The ΔSCF procedure yields oscillator strengths of the correct order of magnitude [1094]. It may be mentioned that in this method there is some computational difficulty in treating the transition moment matrix elements between non-orthogonal determinants. Usually single configurational approaches are used for the description of electronic transitions in the density functional methods, like X_α [1157]. Table 3.35 shows some results obtained with this method.

Alternatively to the separate optimization of the ground and excited state wave function, one can calculate directly the transition energies and transition amplitudes without evaluating explicitly the wave functions of the initial and final states. Among these excitation (or direct) methods the RPA (random phase approximation) fulfils the hypervirial relation in complete basis [508]. It means that the difference of the oscillator strengths calculated by the position or momentum formalism is entirely due to the deficiencies of the basis set [508]. On the other hand, the Tamm–Dancoff approximation (TDA) does not satisfy the hypervirial relations, because this approach provides for a rather unbalanced description of the initial and final states [131]. This is illustrated in Table 3.36 where some oscillator strengths of the O_2 molecule calculated with the time dependent Hartree–Fock (TDHF) method (which is equivalent to the RPA), the multiconfigurational TDHF (MCTDHF) method and TDA are compared. Large discrepancies can be found between the position and momentum forms of the oscillator strength obtained by TDA, while the small deviations found in the TDHF and MCTDHF methods are due to the use of an incomplete basis [8].

For theoretical studies of larger molecules the semiempirical calculations of transition probabilities are of great importance. A common problem in the ZDO (or NDO) semiempirical methods, like CNDO, INDO, PPP, is that adoption of the ZDO (NDO) approximation in the evaluation of transition moment matrix elements over the atomic Slater-orbital basis may result in the neglect of such integrals which are of

TABLE 3.36

Electronic oscillator strengths for the lowest dipole-allowed transitions in O_2 using a double-zeta basis with diffuse functions. The experimental oscillator strength of the $X^3\Sigma_g^- \rightarrow B^3\Sigma_u^-$ transition is $f = 0.16$ [8]

Excitation	TDA		TDHF		MCTDHF	
	Length	Velocity	Length	Velocity	Length	Velocity
$X^3\Sigma_g^- \rightarrow B^3\Sigma_u^-$	0.207	0.003	0.181	0.190	0.178	0.186
$X^3\Sigma_g^- \rightarrow E^3\Sigma_u^-$	0.005	0.055	0.014	0.013	0.011	0.010
$X^3\Sigma_g^- \rightarrow 3\pi_u$	0.012	0.067	0.014	0.015	0.012	0.012
$X^3\Sigma_g^- \rightarrow 3\pi_u$	0.018	0.003	0.018	0.017	0.025	0.025
$X^3\Sigma_g^- \rightarrow 3\pi_u$	0.148	0.146	0.144	0.166	0.154	0.166

the same order of magnitude as others that are included. In order to overcome this problem, after a "deorthogonalization" procedure all the integrals are retained [624]. Another possibility is to use parametrized transition moment integrals which are consistent with the approximations introduced into the semiempirical model Hamiltonian, *e.g.* by requiring the fulfillment of the off-diagonal hypervirial relation [797]. Usually agreement of the experimental oscillator strengths with those determined by semiempirical calculations is only qualitative: the trends are more or less correctly reflected, but considerable errors may occur in the absolute magnitude of the transition probabilities.

The simple methods of qualitative MO theory can also be exploited for the estimation of transition moments. The procedure which will be shown in some details in the next section involves construction of the transition density as the product of the space orbitals participating in the transition. The net dipole moment of the transition density gives the transition dipole moment. Using simple graphical representation of the orbitals, one can construct the transition density on a piece of paper and get information about the forbidden or allowed nature of the excitation; even the expected direction of the transition dipole can be predicted easily [1296].

The influence of neighbouring molecules and of the solvent on absorption band shapes is a complicated problem which cannot be treated in detail by present-day quantum chemistry. A simple continuum model of the solvent effect (the SCRF method) was proved useful for the quantum chemical study of environmental effects on the shape of the absorption band of rhodopsin [1454].

3.7.3 CHIROPTICAL PHENOMENA

Experimental methods: optical rotatory dispersion and circular dichroism spectroscopy [213, 330]

Chiroptical phenomena are characteristic of *optically active* materials, which possess a different index of refraction (n) and absorption coefficient (ε) for left (l) and right (r) circularly polarized light:

$$\Delta n(\omega) = n_l(\omega) - n_r(\omega) \neq 0 \tag{3.195a}$$

$$\Delta\varepsilon(\omega) = \varepsilon_l(\omega) - \varepsilon_r(\omega) \neq 0. \tag{3.195b}$$

Both phenomena are frequency dependent. Under experimental conditions $\Delta n(\omega)$ is determined by measuring the angle of rotation $\alpha(\omega)$ of the polarization plane of plane polarized light, which is an equal mixture of left and right circularly polarized components. This is the *optical rotatory dispersion* (ORD). Due to the difference in the absorption coefficients $\Delta\varepsilon(\omega)$ of the circularly polarized components of the plane polarized incident radiation, the light leaving the sample becomes elliptically polarized. This is the *circular dichroism* (CD), which is measured by the ellipticity $\psi(\omega)$. The above simultaneous effects are illustrated schematically on Fig. 3.46.

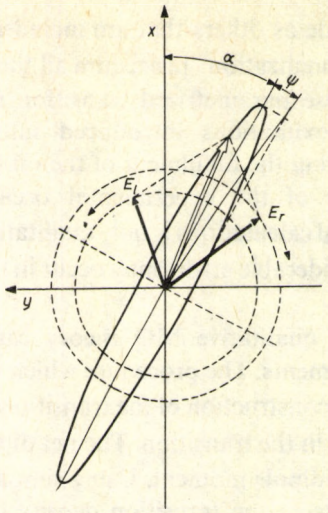


Fig. 3.46 Schematic illustration of the CD and ORD effects. An originally linearly polarized light beam with xz polarization plane leaving a dextrorotatory medium, as regarded from the direction of light propagation. E_r and E_l are the right and left circularly polarized components of the electric field, α is the angle of rotation (ORD), ψ is the angle of ellipticity (CD)

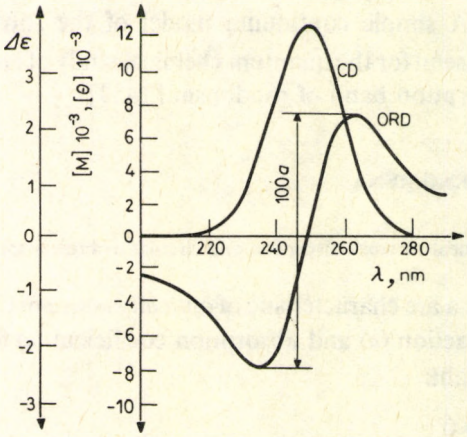


Fig. 3.47 Schematic representation of an idealized CD and ORD spectrum of an electronic transition (Cotton-effect)

In the vicinity of the absorption bands, ORD curves exhibit anomalous behaviour: they change sign, while in the same region $\Delta\varepsilon(\omega)$, the CD spectrum differs significantly from zero. This combined effect of CD and anomalous ORD within an absorption band is called the *Cotton-effect*. We speak about a positive Cotton effect if $\Delta\varepsilon(\omega)$ is positive and the corresponding ORD curve has negative values at higher energies; the negative Cotton effect is characterized by a negative CD maximum and an ORD curve which is positive at the higher energy side of the spectrum (Fig. 3.47). We note that CD

and ORD curves are in an unequivocal relation, expressed by the Krönig–Kramers transformations (see *e.g.* [330]).

The optical activity of homogeneous, isotropic phases requires the presence of *chiral* molecules which possess special symmetry characteristics; namely, they are not superimposable on their mirror images even after translation or rotation. Different quantum transitions of these molecules contribute to $\Delta n(\omega)$ and $\Delta\varepsilon(\omega)$ at a given frequency, and the contribution is proportional to the rotational strength R_{0k} associated with the transition. For molecules, which are small compared with the wavelength of the incident radiation*, the rotational strength is defined as the imaginary part of the scalar product of the electric $\boldsymbol{\mu}_e$ and magnetic $\boldsymbol{\mu}_m$ transition dipole moments [173, 200, 508, 1193, 1355]:

$$R_{0k} = \mathrm{Im}\{\langle\Psi_0|\hat{\boldsymbol{\mu}}_e|\Psi_k\rangle\langle\Psi_k|\hat{\boldsymbol{\mu}}_m|\Psi_0\}. \tag{3.196}$$

The operator of the magnetic dipole moment is

$$\hat{\boldsymbol{\mu}}_m = \beta_B \sum_{i=1}^{N} \hat{\mathbf{r}}_i \times \hat{\mathbf{p}}_i = \frac{e\hbar}{2mci} \sum_{i=1}^{N} \hat{\mathbf{r}}_i \times \hat{\boldsymbol{\nabla}}_i \tag{3.197}$$

where β_B is the Bohr-magneton ($e/2mc$), while the electric transition dipole moment is the same as that which appeared in the expression of the oscillator strength (Eq. 3.177). Using the off-diagonal hypervirial relation [201] for the electric transition dipole moment matrix elements, we get the following definitions for the dipole length ($R_{0k}^{(r)}$) and dipole velocity ($R_{0k}^{(v)}$) forms of the rotational strength [508, 938]:

$$R_{0k}^{(r)} = -\frac{e^2\hbar}{2mc}\langle\Psi_0|\hat{\mathbf{r}}|\Psi_k\rangle\langle\Psi_k|\hat{\mathbf{r}}\times\hat{\boldsymbol{\nabla}}|\Psi_0\rangle \tag{3.198}$$

$$R_{0k}^{(v)} = -\frac{e^2\hbar}{2m^2c\Delta E_{0k}}\langle\Psi_0|\hat{\boldsymbol{\nabla}}|\Psi_k\rangle\langle\Psi_k|\hat{\mathbf{r}}\times\hat{\boldsymbol{\nabla}}|\Psi_0\rangle \tag{3.199}$$

where $\Delta E_{0k} = E_k - E_0$ is the transition energy associated with the $0 \rightarrow k$ excitation.

The order of magnitude of the rotational strength for a transition which is both electrically and magnetically allowed is expected to be about 1 Debye × 1 Bohr-magneton ($1\ \mu_D \cdot 1\ \beta_B$)**. For the sake of convenience the rotational strength is often expressed in the units of hundredth of $1\ \mu_D \cdot 1\ \beta_B$: this dimensionless quantity is the reduced rotational strength [R] (*e.g.* [200]):

$$[R] = \frac{100}{\mu_D\beta_B} R = 1.08 \times 10^{40} R\ (\mathrm{cgs}). \tag{3.200}$$

* The (3.196) expression of the rotational strength is not valid for macromolecules, like polymers or proteins [1356].

** For the definition of different units *cf.* Appendix 2.

In principle, the rotational strengths can be determined experimentally from both ORD and CD curves. Since the Cotton-effect associated with a given transition has long-range tails in the ORD spectrum, at a given frequency $\Delta n(\omega)$ arises as a superposition of the contributions due to many transitions. On the other hand, the CD spectrum displays maxima only in the absorption regions, and the rotational strength can be readily measured as the integrated intensity of the corresponding CD band [1236]:

$$R_{0k} = \frac{3\hbar c \times 2303}{16\pi^2 N_A} \int_{\substack{0\to k \\ \text{band}}} \frac{\Delta\varepsilon(\omega)}{\omega} \, d\omega. \tag{3.201}$$

The rotational strength, being the scalar product of a polar (electric transition dipole moment $\boldsymbol{\mu}_e$) and of an axial (magnetic transition dipole moment, $\boldsymbol{\mu}_m$) vector, is a pseudoscalar quantity. It means that, owing to the different transformation properties of $\boldsymbol{\mu}_e$ and $\boldsymbol{\mu}_m$ under S_n improper rotations ($S_1 = i$, $S_2 = \sigma$, S_4), the rotational strength changes sign under the effect of these operations. Enantiomers of chiral molecules, which are mirror images of each other, have rotational strengths of opposite sign and of equal magnitude. On the other hand, in the case of achiral molecules, S_n is a symmetry operator of the molecule, which transforms the molecule into itself, therefore R_{0k} should also remain invariant with respect to sign inversion. It follows that the rotational strength of achiral molecules must be zero.

A more detailed analysis [200] shows that in molecules belonging to the C_1, C_2, and D_2 point groups all the transitions from the ground state are optically active. For systems of $C_n (n = 3 \text{ to } 8)$ and $D_n (n = 3 \text{ to } 6)$ symmetry, only transitions to nondegenerate excited states possess nonzero rotational strength. In the above cases we speak about *natural optical activity*. Degenerate transitions in C_n and D_n point groups and in some achiral point groups (*e.g.* C_{3v}, C_{4v}, C_{6v}, D_{2d}, S_4, $C_{\infty v}$) under the effect of an appropriate perturbation, which splits degeneracies, may acquire optical activity. Finally, those molecules which have either a center of inversion or both a reflection plane and a twofold axis (with the only exception of the C_s point group) are optically inactive. We note here that a magnetic field induces optical activity not only in degenerate transitions, but it also makes optically active all the transitions of optically inactive, achiral molecules. This is the basis of the magnetic ORD and CD (MORD and MCD) spectroscopies [200, 1307].

The above symmetry selection rules of optical activity apply to rigid and semirigid molecules. For nonrigid molecules, where vibrational amplitudes may be so large as to allow rapid interconversion among several sets of nuclear configurations at the time-scale of the experiment, analogous symmetry selection rules can be deduced on the basis of the Longuet–Higgins permutation group, which describes appropriately the symmetry of these systems [412].

The rotational strengths fulfil a number of sum rules. The most important one, established by Condon [236], states that in a molecule the sum of rotational strengths

for all the transitions equals zero:

$$\sum_{k}^{\infty} R_{0k} = 0 . \tag{3.202}$$

While the electric transition dipole moment is independent of the choice of origin for the coordinate system (remember that the total charge of the transition density is zero), this does not hold for the magnetic transition dipole moment of an electrically allowed transition. Let us consider a translation of the origin by $\mathbf{r}' = \mathbf{r} - \mathbf{R}$:

$$\langle \Psi_0 | \hat{\mathbf{r}}' \times \hat{\nabla} | \Psi_k \rangle = \langle \Psi_0 | \hat{\mathbf{r}} \times \hat{\nabla} | \Psi_k \rangle - \mathbf{R} \times \langle \Psi_0 | \hat{\nabla} | \Psi_k \rangle . \tag{3.203}$$

It can be seen by substituting Eq. (3.203) in Eq. (3.199) that the dipole velocity form of the rotational strength is always origin independent. By virtue of relation (3.178), the same should hold for *exact wave functions* in the dipole length formalism too. However, in the case of approximate wave functions, the extent of origin dependence of the dipole length rotational strength is an indication of the quality of the wave function [508].

The overwhelming majority of experimental and theoretical studies deal with investigations on the optical rotatory intensities of *electronic transitions*. Disregarding a few attempts at calculating vibrational fine structures of CD bands [599, 1445] most of the efforts have been devoted to correlating the integrated intensity of the electronic CD band with the theoretical rotational strength evaluated for vertical transitions [508].

Quantum chemical calculations of optical rotatory strengths involve almost the same problems as those encountered in the study of ordinary absorption intensities. The reliability of the various approaches is comparable to that discussed in Section 3.7.1. However, since not only the magnitude but also the relative orientation of the electric and magnetic transition dipole moments is crucial to the success of rotational strength calculations, this property is usually even more sensitive to the deficiencies of the approximate wave function than the oscillator strength. Unfortunately the size of even the smallest chiral molecules is prohibitive for carrying out highly sophisticated calculations and in most cases we are forced to adopt very approximate quantum chemical methods.

It is a common approach in the theoretical study of chiroptical properties to correlate the rotational strengths calculated for a smaller, chromophoric part of a complex molecule with the experimental Cotton effects. Following Moscowitz [939] the chromophores of chiral molecules can be divided into two main classes. The *inherently chiral* chromophores posses no S_n symmetry elements and their electronic transitions have nonvanishing rotational strengths even in the absence of interactions with the molecular skeleton they are embedded in. Inherently achiral chromophores may acquire optical activity due to the perturbing effect of their chiral molecular environment; this is the class of *chirally perturbed inherently achiral* chromophores. Snatzke [1296] proposed a more refined method for the rationalization of the optical activity of the chromophores. He divided the molecule into "chiral spheres" the

chromophore itself being the first sphere, any ring incorporating the chromophore is the second sphere, groups or rings connected to the second sphere form the third one, etc. (see Fig. 3.48). The chirality of each sphere is defined by its actual geometry, and the contribution of the chiral spheres to the final rotational strength is supposed to decrease with increasing distance from the chromophore.

This brief introduction to the basic terminology of the chromophore concept as applied to the theory of optical activity is indispensable for the discussion of actual quantum chemical calculations on rotational strengths. Let us first look at the reliability of the various methods for direct calculations of optical activity. Theoretical studies on the *trans*-cyclooctene molecule offer a good example, where both *ab initio* and semiempirical methods were applied to the same molecular system.

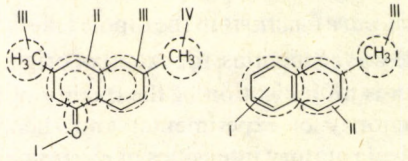


Fig. 3.48 Concept of chiral spheres illustrated on two simple examples

Trans-cyclooctene possesses an ethylenic chromophore, held in a dissymmetric position by the molecular framework (Fig. 3.49). The local geometry of the chromophore is twisted, therefore this chromophore can be considered as inherently chiral. The experimental CD spectrum is characterized essentially by two intense bands of opposite sign. The first one is due to a (π, π^*) excitation and the second one arises most probably from a (σ_{CH}, π^*) transition. Some theoretical results concerning the optical activity of these two transitions of *R-trans*-cyclooctene are collected in Table 3.37.

The simplest model able to describe appropriately the most important features of the CD spectrum of *trans*-cyclooctene is a twisted ethylene molecule, which represents the inherently chiral chromophore. For this small system, even large-scale *ab initio* calculations were feasible. It can be seen from Table 3.37 that for a 10° twisted ethylene model the perturbative CI calculations of Rauk and Barriel [1156, 1157], including doubly excited determinants in the ground state-, and singly excited configurations in the excited state-description, provide almost identical results to the RPA (random phase approximation) calculations of Bouman and Hansen [132]. The dipole length and dipole velocity rotational stregths are approximately equivalent in these well-



Fig. 3.49 The *R-trans*-cyclooctene molecule

TABLE 3.37

Calculations on the optical activity of the (π, π^*) and (σ_{CH}, π^*) transitions of the *R-trans*-cyclooctene molecule using various model compounds and different quantum chemical methods.

Model	Method	ΔE (eV)	$[R]^r$	$[R]^v$	ΔE (eV)	$[R]^r$	$[R]^v$	Ref.
R-trans-cyclooctene	exp.	6.3	−75.6	−75.6	7.9	+118.8	+118.8	[508]
R-trans-cyclooctene	1st order pert.CI	6.5	–	−104.2	–	–	–	[1157]
R-trans-cyclooctene	TDA	0.5	–	+160.5	–	–	–	[1157]
R-trans-cyclooctene	STA	4.4	–	−33.6	–	–	–	[1157]
R-trans-cyclooctene	HFS-STA	4.1	–	−64.5	–	–	–	[1157]
Trans-2-butene[b]	RPA single zeta	9.4	−84.5	−52.7	11.3	+129.5	+86.0	[132]
Twisted ethylene[a]	CI	7.5	−232.2	−165.2	9.7	+284.0	+194.4	[803]
Twisted ethylene[a]	RPA	7.2	−152.3	−128.5	9.1	+164.2	+145.8	[507a]
Twisted ethylene[a]	LORPA	7.1	−155.6	−126.4	9.1	+181.4	+190.8	
Twisted ethylene[b]	RPA double zeta	8.3	−94.5	−73.7	9.9	+138.1	+113.5	[132]
Twisted ethylene[b]	1st order pert.CI	8.2	−127.0	−112.2	9.4	+196.5	+185.1	[1156]
Twisted ethylene[b]	TDA double zeta	3.3	–	−215.9	–	–	–	[1157]
Twisted ethylene[b]	STA double zeta	–	–	−68.8	–	–	–	[1157]
Twisted ethylene[b]	X_α-STA	–	–	−130.4	–	–	–	[1157]
Twisted ethylene[b]	X_α-STA	11.9	−60.9	−25.3	10.6	+123.6	+82.6	[1158]
Twisted ethylene[b]	CNDO/2	–	−211.3	−109.2	–	+340.2	–	[1158]
	INDO	–	−84.0	−8.6	–	+167.4	–	
	CNDO/S-CI	–	−191.2	−102.4	–	+353.6	–	

[a] Geometry taken from X-ray diffraction data.

[b] The torsional angle around the C=C double bond is taken to be 10 degrees.

balanced computational schemes. Other less sophisticated *ab initio* and semiempirical calculations generally agree in the sign of the (π, π^*) rotational strength. It is worth mentioning that the single transition approximation (STA), which corresponds to a zero order approach to the description of transition moments, gives quite good results within the framework of both HF (Hartree–Fock) and HFS (Hartree–Fock–Slater) (density functional) theories. On the other hand, the rather unbalanced Tamm–Dancoff approximation (TDA) largely overestimates the rotational strength of twisted ethylene.

The all-valence semiempirical methods have important role in the study of rotational strengths. Table 3.37 also lists some data obtained with CNDO/2, INDO and CNDO/S methods for the twisted ethylene model molecule [1158]. Although these results are poor in comparison with the *ab initio* ones, for larger molecules these procedures provide the only method for the direct calculation of optical rotatory intensities (*cf.* Table 3.37).

Let us make a few general remarks here on the application of semiempirical NDO theories for rotational strengths studies. The first problem arises in the evaluation of the optical integrals involving operators $\hat{\mathbf{r}}$, $\hat{\nabla}$, $\hat{\mathbf{r}} \times \hat{\nabla}$ over the atomic orbital basis. Usually the STO basis is used directly for this purpose. The importance of the release of the NDO approximation in the course of the calculation of these integrals in connection with a deorthogonalization procedure have been demonstrated by several authors [624, 1174]. Optical integrals evaluated consistently to the parametrization of the semiempirical Hamiltonian have also been used for rotatory strength calculation by Linderberg and his coworkers [795]. A refined version of Linderberg's method, treating both electric and magnetic transition dipole moments by releasing the ZDO assumption, has been proposed by Surján and Kertész [1319].

The role of configuration interaction in semiempirical rotatory strength calculations has been also a matter of controversy. The effect of the truncation of the single excitation CI expansion on the rotational strength was analyzed by Volosov and Zubkov [1388]. They found in their CNDO/S calculations that the convergence of the CI expansion is wrong (see Fig. 3.50), and at least half of the total single excitation CI space has to be included in order to have reliable results. The analysis of Bouman and Lightner [134] led to similar conclusions. Therefore it was argued that as the limited TDA (single excitation CI, SECI) method is imbalanced and may lead to erroneous rotational strengths, simple STA calculations are superior to limited SECI method in certain cases [134, 554].

Returning to the chiroptical properties of *trans*-cyclooctene, the next step in a systematic study is to see what is the influence of the chiral second sphere on the optical activity of the twisted ethylene chromophore. According to RPA calculations with the single-zeta basis set on a *trans*-2-butene model, which is designed to include the effect of the dissymmetric C—C σ bonds in the vicinity of the olefin moiety, there is no significant change with respect to the twisted ethylene in the calculated rotational strengths [132].

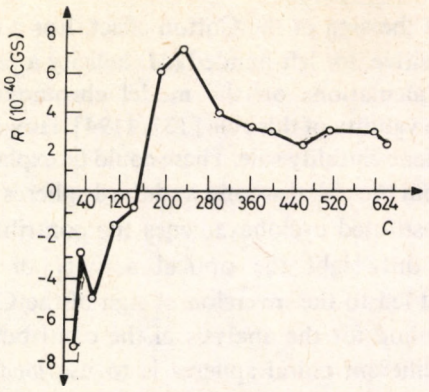


Fig. 3.50 The effect of the CI expansion length on the calculated rotational strength. The example is the (n, π^*) transition of dimethyl-cyclohexanone calculated by CNDO/S method with perturbative CI [1388]

Calculations of the rotational strengths of the whole molecule were also attempted by Rauk and his coworkers [1157]. Their results concerning the rotational strength of the (π, π^*) transition obtained by SCF + perturbative CI and HFS–STA methods are in good agreement with experiment. STA applied to the HF wave function underestimates the magnitude of the rotational strength and TDA gives completely erroneous results: even the sign of R is wrong.

The number of direct *ab initio* investigations on chiral molecules (without the application of model chromophores) is quite limited. For example, Rauk calculated the optical activity of small substituted three-membered rings (oxiranes, aziridines, diaziridines, and oxaziridines) [1154]. The lowest transitions were found to be of mixed valence–Rydberg character. The sign of the theoretical rotational strength of 2-methylaziridine (see also [472]) were in agreement with experiment, while the computations yielded incorrect sign for the rotational strength of 2-methyloxirane, probably due to the shortcomings of the CI procedure [1154].

The [4,4]-spirononatetraene molecule belongs to the D_{2d} point group in its normal state. Its degenerate excited states display Jahn–Teller instabilities with respect to a torsion, which takes them to chiral structures of D_2 symmetry. In the presence of a chiral solvent, one of the D_2 enantiomers can be stabilized, thus making possible in principle the determination of the CD spectrum. Minimal basis SCF–CI calculations on twisted [4,4]-spirononatetraene predicted a negative rotational strength of the lowest-frequency optically active electronic transition of the R enantiomer [263].

Returning again to an example where the rationalization of the observed Cotton effects is expected from calculations on model chromophoric systems, let us take the case of 1,3-cisoid dienes. Based on experimental data and semiempirical calculations an empirical rule has been established which states that the sense of the helicity* of the

* A diene is of positive (P) helicity if it is skewed in the sense of a right-handed helix, and of negative (M) helicity if skewed in the opposite sense.

diene moiety determines the sign of the Cotton effect. For a chromophore of right-handed (*P*) helicity a positive, for left-handed (*M*) helicity a negative Cotton effect is expected [199, 200]. Calculations on the model chromophore, the twisted 1,3-butadiene, confirmed the validity of this rule [131, 1194]. However, several exceptions have been found to the diene chirality rule. These could be explained by supposing that contributions coming from the chiral second and third spheres had an important role. In effect, for methyl-substituted cyclohexadienes the contribution of allylic methyl groups was found to outweight the optical activity of the inherently chiral chromophore [792], and led to the inversion of sign of the Cotton effect.

Probably the best method for the analysis of the contributions to the rotational strength coming from different chiral spheres is to use *localized MO basis* in the calculations. Bouman and coworkers carried out localized orbital RPA (LORPA) [133] studies for 1,3-cyclohexadienes [792]. It was found that the diene part of the ring system had a rotational strength with a sign opposite to that implied by the *P* helicity of the model and thus violated the diene helicity rule [792]. They demonstrate that owing to the nearly 90° angle between the electric and magnetic transition dipole moments, the diene rotational strength is extremely sensitive to the method of calculation and to the selection of the model. They analyzed the individual contributions of the various bonds and substituents to the rotational strength; the results are illustrated in Fig. 3.51.

The diene helicity rule can be considered as the special case of a more general one, established by Hug and Wagnière for the chromophores of C_2 symmetry [609]. This "C_2 rule" states that the lowest frequency symmetric (*A*) and antisymmetric (*B*) transitions in C_2 chromophores have negative and positive Cotton effects, respectively, for a righthanded (*P*) helicity [609]. Although in many cases this rule works well, there are exceptions, which call our attention to the fact that uncritical application of such chirality rules may be misleading.

A representative example of the *inherently achiral* chromophores is the carbonyl group. This moiety has an (n, π^*) transition, the Cotton effect of which had been studied

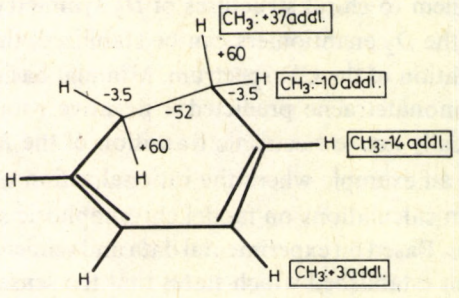


Fig. 3.51 Localized contributions to the optical activity of the 1,3-cyclohexadiene (*P*-helicity). The total rotational strength of the lowest transition can be obtained by summing up the appropriate contributions ([*R*] = +48) [792]

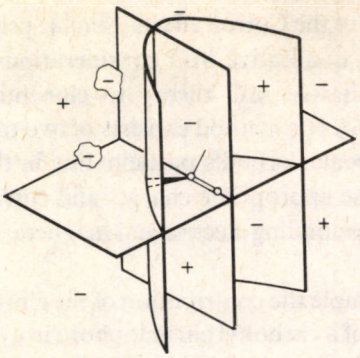


Fig. 3.52 Shape of the octant surfaces of a ketone chromophore determined by CNDO/S calculations [134]

very extensively from both experimental and theoretical aspects. The carbonyl (n, π^*) transition is electrically forbidden and magnetically allowed (see below), thus consideration of extrachromophoric contributions is needed for an understanding of its optical activity. An empirical relationship, the octant rule, had been established which claims that extrachromophoric atoms of the molecule make contributions to the rotational strength depending on their location with respect to the local symmetry planes of the carbonyl group and to a third surface intersecting the other two [923]. The nature of this third surface has been determined by CNDO/S STA calculations [134], as illustrated in Fig. 3.52. Localized orbital analysis of RPA results on chiral conformations of diethyl ketone demonstrated the most important source of the missing $\boldsymbol{\mu}_e$ electric transition dipole moment parallel to the $\boldsymbol{\mu}_m$ magnetic transition moment required for the rotational strength of the carbonyl group. It was found that $\boldsymbol{\mu}_e$ is provided primarily by a zigzag or W-shaped arrangement of the perturbing σ-bonds [135].

LORPA calculations and the analysis of atomic, bond and coupling contributions of the (n, π^*) rotational strength of thioketones supported the applicability of the ketone octant rule to this chromophore as well [793].

Further examples for the *a posteriori* localized orbital analysis of calculation for chiroptical properties can be found in Refs [7, 83, 623].

The usefulness of *a priori* localized orbitals in CNDO/2 calculations for the twisted glyoxal chromophore has been demonstrated in Ref [30].

The case of methyl-substituted pyrrolidones offers the possibility of comparison of some semiempirical methods. The calculated rotational strengths of *L*-5-methyl-pyrrolidone containing an inherently achiral amide chromophore generally agree in the sign of the Cotton effects (Table 3.38). In certain strained molecules the amide chromophore is nonplanar thus becomes inherently chiral. The optical activity of such nonplanar amides was investigated by the CNDO/S-CI method [865].

At the present state of the art, even good quality "quantitative" quantum chemical calculations on optical activity cannot be used for more than the prediction of the sign

and the order of magnitude of the Cotton effects. Similar predictions can sometimes be done even by using simple, qualitative MO considerations as well.

The application of qualitative MO theory to chiroptical phenomena has been attempted by Snatzke [1296]. His method consists of two main steps. First, one has to construct the relevant molecular orbitals participating in the transition. Secondly on the basis of these orbitals the appropriate charge- and current-densities are set up for the transition, and the corresponding electric and magnetic transition dipole moments are estimated from them.

Let us consider as an example the contribution of the chiral second sphere, the chiral ring, to the optical activity of a carbonyl chromophore in cyclic aliphatic ketones (Fig. 3.53). Following the general rules of orbital interactions, the mixing of orbitals can be undertaken in several consecutive steps. First of all, we mix the π orbital of the carbonyl moiety with the σ orbital of the neighbouring C—C σ-bond, and the higher energy combination is further combined with the highest occupied orbital, the carbonyl n orbital. Thus the lowest energy transition can be described as the promotion of an electron from an n orbital with an admixture of π character to a π^* antibonding orbital. Due to the presence of the π character in the highest occupied orbital, the corresponding transition density gives rise to a relatively small electric transition dipole moment parallel to the C—O axis. The most important contribution to the current density associated with the transition comes from the electronic motion from the p_y lobe of the n orbital to the p_x lobe of the π^* orbital. The current density is

TABLE 3.38

Reduced rotational strengths [R] and transition energies (eV) of the *L*-5-methyl-pyrrolidone molecule as calculated by different semiempirical SCF–MO–CI methods

Ring-conformation	Method	(n, π^*)		(π, π^*)		Ref.
		ΔE (eV)	[R]	ΔE (eV)	[R]	
Planar	INDO-CI[a]	6.56	−11.4	10.44	+2.90	[1175]
	CNDO/S-CI[b]	4.13	−4.10	7.09	+3.02	[1389]
	MINDO/3-CI[c]	4.43	−8.83	6.97	+3.45	[7]
Nonplanar	INDO-CI[a]	6.79	+0.44	10.47	−22.30	[1175]
	CNDO/S-CI[b]	4.13	−0.62	7.09	+16.63	[1389]
	MINDO/3-CI[c]	4.49	−2.88	6.99	+4.84	[7]
	CNDO-STA[d]	6.4	+28.1	—	—	[429]
	CNDO-CI[e]	4.8	−6.5	—	—	[429]
	Exp.	5.77	−7.34	6.70	+13.50	

[a] With a CI including 15 configurations
[b] With a CI including 50 configurations
[c] With a CI including 42 configurations
[d] Specific parametrization of the CNDO method
[e] With a CI including 120 configurations

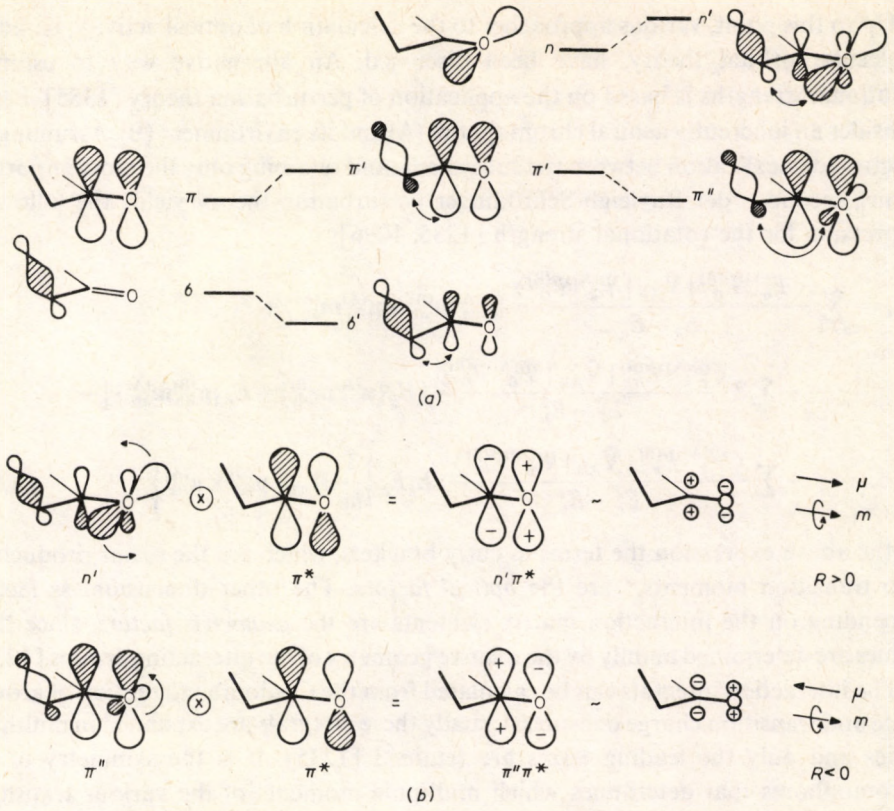


Fig. 3.53 Application of the qualitative MO theory to the prediction of the sign of rotational strength of a chiral cyclopentanone. *(a)* Mixing of the n and π orbitals of the carbonyl chromophore with the orbital of the ring. (The n and π orbitals of the carbonyl group mix through the extrachromophoric σ orbital). *(b)* Transition densities of the (n, π^*) and (π, π^*) excitations and the estimation of the sign of the rotational strengths

represented by the arrowed arc connecting the positive lobes of the occupied and the vacant orbitals. The corresponding magnetic moment direction comes from the application of a "lefthand rule" (if the 2nd and 5th fingers of the left hand follow the motion of the orbital lobes, then the thumb points to the direction of the magnetic moment; we note that the application of a "left-hand rule" and not "right-hand rule" was necessary since the electron is of negative charge). Furthermore, it has to be born in mind that only the relative direction of $\boldsymbol{\mu}_e$ and $\boldsymbol{\mu}_m$ is significant for the sign of the Cotton effect. It can easily be checked that another selection of phases for the orbital lobes at the beginning of the procedure, although altering the direction of the individual transition moments, leaves unaffected the estimated sign of the rotational strength [1296]. The sign of the Cotton effect thus derived for our example is in accord with the predictions of the octant rule.

Up to this point, various approaches to the calculation of optical activity, based on molecular orbital theory, have been discussed. An alternative way to estimate rotational strengths is based on the application of perturbation theory [1355]. Let us consider an inherently achiral chromophore (A) and its environment (B). Assuming no electron delocalization between the subsystems and retaining only the most important terms, second order Rayleigh-Schrödinger perturbation theory yields the following expression for the rotational strength [1235, 1296]:

$$R_{0k} = \sum_{a \neq k} \frac{\langle \Psi_a^{(A)} \Psi_0^{(B)} \mid \hat{V}_{AB} \mid \Psi_k^{(A)} \Psi_0^{(B)} \rangle}{E_k - E_a} \{ \boldsymbol{\mu}_{0k}^{(A)} \mathbf{m}_{a0}^{(A)} + \boldsymbol{\mu}_{0a}^{(A)} \mathbf{m}_{k0}^{(A)} \} +$$

$$+ \sum_b 2 \frac{\langle \Psi_k^{(A)} \Psi_b^{(B)} \mid \hat{V}_{AB} \mid \Psi_0^{(A)} \Psi_0^{(B)} \rangle}{E_k^2 - E_b^2} [E_k \{ \boldsymbol{\mu}_{0k}^{(A)} \mathbf{m}_{b0}^{(B)} \} + E_b \{ \boldsymbol{\mu}_{0b}^{(B)} \mathbf{m}_{k0}^{(A)} \}] +$$

$$+ \sum_b \frac{\langle \Psi_k^{(A)} \Psi_b^{(B)} \mid \hat{V}_{AB} \mid \Psi_0^{(A)} \Psi_0^{(B)} \rangle}{E_k^2 - E_b^2} \cdot E_k E_b \left\{ \frac{1}{\hbar c} \mathbf{R}_{AB} \cdot \boldsymbol{\mu}_{0b}^{(B)} \times \boldsymbol{\mu}_{0k}^{(A)} \right\}. \tag{3.204}$$

In the above expression the terms in curly brackets, which are the scalar products of two transition moments,* are the *optical factors*. The other dimensionless factors depending on the interaction matrix elements are the *geometric factors*, since their values are determined mainly by the relative geometry of the interacting groups [1235].

The interaction integrals can be calculated from the Coulomb interaction of ground state and transition charge densities. Usually these integrals are expanded in multipole series and only the leading terms are retained [1235]. It is the symmetry of the chromophores that determines which multipole moments of the various transition densities are different from zero, and on this basis useful symmetry rules can be derived [1235]. For example in the case of dipole-allowed transitions dipolar interactions dominate, while for magnetically allowed transitions the first nonvanishing multipole moment is the quadrupole.

Equation (3.204) forms the basis of the derivation of the different *models of optical activity* [174]. For an achiral chromophore, which has either electrically or magnetically allowed transitions (if both, the two moments are perpendicular), there are various possibilities for acquiring the missing magnetic or electric transition moment component. These possibilities are also referred to as the various mechanisms of optical activity.

The first term of Eq. (3.204) describes the mixing of electronic states of the same chromophore A due to the perturbing effect of the static field of ground state charge distribution of the chiral environment B. This is the one-electron model of optical activity, first derived by Condon, Altar and Eyring [237]. On the basis of the symmetry of the chromophore, various sector rules can be derived. The well-known octant rule can be obtained in this way [1296] as it is illustrated on Fig. 3.54.

* In Eq. (3.204) the electric transition dipole moment is denoted by $\boldsymbol{\mu}_{0k}$, while the magnetic transition dipole is abbreviated as $\mathbf{m}_{0k}$.

The second term includes the coupling of the electric and magnetic moments on different chromophores, this is the electric-magnetic coupling mechanism [1435] which is of great importance in the interpretation of the CD spectra of chiral diamides [72].

Finally, optical activity may arise from the coupling of two electrically allowed transitions, if the respective transition dipole moments are dissymmetrically arranged.

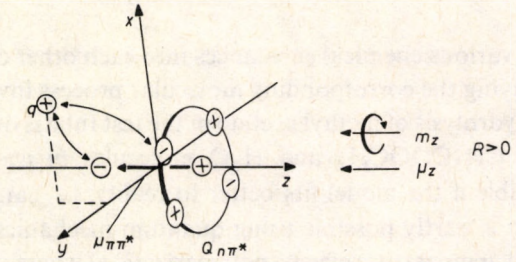


Fig. 3.54 Pictorial illustration for the derivation of the carbonyl octant rule with the one-electron mechanism. The interactions of the extrachromophoric partial point charge with the transition quadrupole moment of the (n, π^*) and with the transition dipole of the (π, π^*) excitations determine the relative direction of the electric and magnetic dipole moments. As it can be seen, the presence of a perturber in the left upper back octant induces positive Cotton effect in the carbonyl (n, π^*) transition

This is the coupled oscillator mechanism [695, 1296]. The formula in Eq. (3.204) is valid only if the transitions of the two chromophores are of different energy. For degenerate transitions (identical chromophores) analogous relations can be derived by degenerate perturbation theory [922]. This is the exciton model, which is an extremely successful way of relating the sign of observed Cotton effects to the absolute geometry of organic molecules [509].

Solvent effects on the optical rotational strength were calculated for carbonyl (n, π^*) transitions within a continuum model using the CNDO/S method [1209].

Rapidly developing fields in optical activity are magnetic optical activity [455, 906] and vibrational optical activity [411, 961, 1111].

4. CHEMICAL REACTIONS

Transformation of various chemical substances into each other can be understood, in most cases, by studying the corresponding molecular process involving a few number of particles only. Hydrolysis of methyl acetate in the test tube is quite well modelled by the interaction of CH_3COOCH_3 and H_2O molecules *in vacuo*. A more precise description is possible if the model fits better to reality, *i.e.* catalytic effects are also accounted for. This is partly possible using quantum mechanics alone but there are chemical events (*e.g.* temperature effects, polymerization) where statistical mechanical considerations have to be applied. Statistical methods will not be discussed here. In the first sections we treat exclusively *in vacuo* models containing only a few molecules. This approach is best for gas-phase processes and for reactions in apolar solvents. Environmental effects in polar solvents and catalysis will be discussed in the last section.

4.1 CHEMICAL EQUILIBRIA

It is known that in the course of a reaction reactants and products are in equilibrium with each other

$$\mu_1 A_1 + \ldots + \mu_k A_k \rightleftharpoons \nu_1 B_1 \ldots \nu_m B_m . \tag{4.1}$$

$A_1, \ldots, A_k$ stand for reactants, $B_1, \ldots, B_m$ for products $\mu_1, \ldots, \mu_k$ and $\nu_1, \ldots, \nu_k$ are stochiometric coefficients. The *equilibrium constant* of an isomolar reaction can be given as follows [276, 452]

$$K_T = \frac{[B_1]^{\nu_1} \ldots [B_m]^{\nu_m}}{[A_1]^{\mu_1} \ldots [A_k]^{\mu_k}} = f \exp(-\Delta E/kT) \tag{4.2a}$$

$$f = \frac{f_{A_1}^{\mu_1} \ldots f_{A_k}^{\mu_k}}{f_{B_1}^{\nu_1} \ldots f_{B_m}^{\nu_m}} . \tag{4.2b}$$

Square brackets stand for concentration; $f_{A_1}, \ldots, f_{B_m}$ are the *partition functions* of compounds $A_1, \ldots, B_m$; ΔE is the difference between the sums of the ground-state energies of the products and of the reactants, respectively (the *reaction heat* at the absolute zero of temperature); k is the Boltzmann constant; T is the absolute temperature. The change in Gibbs free energy, governing the reaction is expressed in

terms of enthalpy and entropy changes

$$\Delta G_T = -RT\ln K_T = \Delta H_T - T\Delta S_T . \tag{4.3}$$

The partition function for compound M is defined as

$$f_M = \sum_i p_{iM} \exp\left[-(E_{iM} - E_{0M})/kT\right] . \tag{4.4}$$

Summation runs over all possible states of M with energies E_{iM} starting from the lowest, E_{0M}. p_{iM} is the statistical weight of the state iM. Thermodynamic quantities (enthalpy and entropy changes, ΔH_T and ΔS_T) can be written in terms ΔE and partition function [276, 452]

$$\Delta H_T = RT\frac{2\mathrm{d}\ln f}{\mathrm{d}T} + N\,\Delta E \tag{4.5}$$

$$\Delta S_T = R\ln f + RT\frac{\mathrm{d}\ln f}{\mathrm{d}T} . \tag{4.6}$$

N is Avogadro's number; $R = Nk$, the gas constant.

The partition function of a free molecule can be written approximately as a simple product of translational (tr), rotational (r), vibrational (v) and electronic (el) terms

$$f_{A_i} \approx f^{tr}_{A_i} \cdot f^{r}_{A_i} \cdot f^{v}_{A_i} \cdot f^{el}_{A_i} . \tag{4.7}$$

Simple analytical expressions, depending on molecular mass, moments of inertia and normal frequencies may be given for the translational, rotational and vibrational partition functions (see *e.g.* [182, 556]). Owing to the high value of electronic excitation energies, as compared to thermal energies, at moderate temperatures the electronic term is approximately equal to unity and is practically independent of the temperature, therefore it can be omitted from consideration in comparative calculations [1284]. Other terms can be calculated by quantum chemical methods with a sufficient accuracy. Since ΔS depends on the partition function alone reaction entropies are reproduced very accurately. This is illustrated for the $C_2H_2 + OH^- \rightleftharpoons C_2H^- + H_2O$ reaction in Table 4.1 [801]. The calculated entropy change is $\Delta S_{296} = 18.4$ J/mol K; this reproduces the experimental value, 15.1 ± 4.2 J/mol K, excellently.

The ratio in Eq. (4.2b) is close to unity for a number of isomolar reactions. This is due to the fact that mass, moment of inertia and normal frequencies do not change very much during the process. However, there are cases like solvation reactions where the size (moment of inertia) of the product supermolecule gets considerably larger compared to that of the reactant. Therefore, the entropy change may be especially important in determining the Gibbs free energy of the reaction. A change in vibration entropy terms is decisive, for example, for the $H_2NCHO \ldots HNHCOH + CCl_3H \rightleftharpoons H_2NCHO \ldots HCCl_3 + H_2NCOH$ reaction, where normal frequencies, corresponding to intermolecular interactions (*e.g.* hydrogen bonds) alter considerably. Thus for

$T = 298$ K, $\Delta H = 0.5$ kJ/mol, $T\Delta S = 7.8$ kJ/mol and the Gibbs free energy (7—7.3 kJ/mol) is determined almost by the entropy term alone [571]. Reactions where the energy increase is overcompensated by the decrease of $T\Delta S$, resulting in a negative ΔG and a shift of equilibrium towards the products, are called *entropy driven* and they play an especially important role in biology [1340].

While it is relatively easy to obtain accurate reaction entropies by theoretical methods serious difficulties may arise if relative energies of reacting species are desired. Effect of electron correlation is in most cases very important therefore reliable figures are obtained only if this is also taken into account. Fortunately, there are cases where

TABLE 4.1

Calculated (upper row) and experimental (lower row) values of S_T/R of molecules for participating in the $C_2H_2 + OH^- \rightleftharpoons C_2H^- + H_2O$ reaction [801]

Molecule	500 K	1000 K	2000 K
C_2H_2	26.54	31.38	37.40
	27.25	32.37	38.64
C_2H^-	26.19	29.86	34.33
	—	—	—
H_2O	24.79	27.89	31.62
	24.83	27.98	31.82
OH^-	22.52	24.97	27.61
	22.56	25.03	27.75

the correlation energy, though large in absolute value, is approximately conserved for the reacting molecules. This is observed for *homodesmic reactions* where the number of bonds and atoms of a particular type (*e.g.* C_4—C_4, C_4—C_3, C_3—C_3, etc. and C_4, C_3, etc., the subscripts refer to coordination numbers) remain conserved, so only their mutual arrangement changes

$$CH_3CH_2CH_2CH_3 + CH_3CH_3 \rightleftharpoons 2CH_3CH_2CH_3$$

$$C_2H_5O^- + CH_3OH \rightleftharpoons CH_3O^- + C_2H_5OH\,.$$

In *isodesmic reactions* [528] the number of bonds is conserved but their types may change, for example,

$$CH_3CHO + CH_4 \rightleftharpoons CH_3CH_3 + H_2CO$$

$$CH_3OCH_3 + H_2O \rightleftharpoons 2CH_3OH\,.$$

For the above reactions relatively small basis set (DZ or minimal) Hartree–Fock calculations reproduce experimental reaction heats within 5–20 kJ/mol [434, 528]. The relative constancy of the correlation energy is due to the fact that both the number and

neighbourhood of electron pairs is conserved. In other reactions where the second requirement is not fulfilled (reactions between closed-shell species) the correlation energy change may be as large as 70 kJ/mol [182]. Most problematic are bond fission reactions where electron correlation plays a decisive role even in a qualitative characterization of the reaction potential curve. Some examples are given in Table 4.2 [567]. There are cases where even a limited configuration interaction calculation is insufficient if quantitative agreement with experiment is to be achieved. However, for most reactions sign and order of magnitude of reaction heats is correctly predicted by the Hartree–Fock method, too [393].

Experimental reaction heats, extrapolated to absolute zero temperature, are calculated from the vibrational ground states of the reacting systems. The energies of these lie slightly higher than the local minima on the potential surfaces (*cf.* Section 3.3). The difference is due to the zero-point energy which is, in general, small but non-negligible if quantitative agreement with experiment is desired (*cf.* Table 4.3).

Owing to the difficulties in calculating reaction heats, equilibrium constants of Eq. (4.2a) which depend exponentially on ΔE can be estimated quantitatively only in exceptional cases. The calculated Gibbs free energy of the $C_2H_2 + OH^- \rightleftharpoons C_2H^- + H_2O$ reaction is -62.4 kJ/mol; the experimental value is only -26 ± 2 kJ/mol. This means that equilibrium constants differ by more than 6 orders of magnitude (the pK is 11.9 instead of 5.4) [801]. The situation is better for the $Li + H_2O \rightleftharpoons LiOH + H$ reaction where the calculated equilibrium constant at 2370 K is 0.13 while experiment yields 0.27 [801].

While a quantitative theoretical description of chemical equilibrium is not practicable at present, qualitative trends are in most cases correctly reproduced even for more complicated reactions for which semiempirical methods have to be applied. Some examples can be seen in Table 4.4. If reaction heats are classified only as "small" or "large" positive or negative values, predictions are satisfactory, only the MINDO/3

TABLE 4.2

Role of electron correlation in the enthalpies of some hydrogenation reactions (for 298 K in kJ/mol) [567]

Reaction	Hartree–Fock	HF + CI	Exp.
$C_2H_6 + H_2 \rightleftharpoons 2CH_4$	−53.2	−63.8	−84.3
$C_2H_5N + H_2 \rightleftharpoons CH_4 + NH_3$	−1.7	−8.4	−23.1
$CH_4O + H_2 \rightleftharpoons CH_4 + H_2O$	−184	−194	−202
$C_2H_4 + 2H_2 \rightleftharpoons 2CH_4$	+84.1	+53.5	+52.5
$CH_3N + 2H_2 \rightleftharpoons CH_4 + NH_3$	+126	+90.5	+83.8
$CH_2O + 2H_2 \rightleftharpoons CH_4 + H_2O$	−79.0	−111	−116
$C_2H_2 + 3H_2 \rightleftharpoons 2CH_4$	+252	+202	+226
$HCN + 3H_2 \rightleftharpoons CH_4 + NH_3$	+134	+71.2	+131
$N_2 + 3H_2 \rightleftharpoons 2NH_3$	+39.9	−44.5	0.0

TABLE 4.3

Theoretical and experimental heats of hydration of monovalent ions (in kJ/mol) [182, 705]

Complex	ΔE_{SCF}	ΔE_{corr}	ΔE_{zp}^{a}	$\Delta H_{298}{}^{b} - \Delta H_0$	ΔH_{298}	
					Calc.	Exp.
$Li^+ \ldots H_2O$	−147.3	−1.1	8.5	−4.4	−144.3	−142
$Na^+ \ldots H_2O$	−100.2	−1.1	6.3	−3.5	−98.5	−100
$K^+ \ldots H_2O$	−69.6	−1.4	5.5	−3.1	−68.6	−70.7
$F^- \ldots H_2O$	−99.2	−3.1	13.3	−4.7	−93.7	−97.5
$Cl^- \ldots H_2O$	−49.6	−2.4	6.6	−3.2	−48.6	−54.8

[a] Zero-point energy from equilibrium geometries and vibrational normal frequencies
[b] Calculated from Eq. (4.5)

results for the methylacetylene⇌allene and propene⇌cyclopropane reactions can be criticized. However, even to describe qualitative trends in reaction heats correctly, careful optimization of reactant and product geometries is imperative since energy effects due to geometry distortions may be very large. Keeping all computational difficulties in mind, the best way to apply quantum chemistry to reaction equilibria is to combine theory and experiment; this may lead to a better understanding of a given process. It does not seem probable in the near future that theoretical calculations will

TABLE 4.4

Reaction heats as calculated by the *ab initio* and MINDO/3 methods (in kJ/mol)

Reaction	Hartree–Fock 4-31G basis set	MINDO/3[a]	Exp.[a]
$EtNH_2 \rightleftharpoons Me_2NH$	35.6[b]	–	28.5
$EtOH \rightleftharpoons Me_2O$	48.5[b]	–	51.0
$MeC{\equiv}CH \rightleftharpoons CH_2{=}C{=}CH_2$	7.9[b]	29.4	6.7
$CH_2{=}C{=}CH_2 \rightleftharpoons \triangle$	146[c]	72.6	84.2
$Me{-}CH{=}CH_2 \rightleftharpoons \triangle$	52.2[c]	8.8	32.6
$3C_2H_2 \rightleftharpoons C_6H_6$	−639[a]	−605	−599
$C_2H_4 + H_2 \rightleftharpoons C_2H_6$	–	164	137
$C_2H_2 + 2H_2 \rightleftharpoons C_2H_6$	–	323	313
$\triangle + H_2 \rightleftharpoons \triangle$	–	213	225
$\square + H_2 \rightleftharpoons \square$	–	160	129
Butadiene $+ 2H_2 \rightleftharpoons$ butane	–	261	237
$CH_3 + H \rightleftharpoons CH_4$	355	–	431
$2H \rightleftharpoons H_2$	335	–	435

[a] Ref. [318]
[b] Ref. [1150a]
[c] Ref. [528]

compete with experiment, as in the case of molecular geometries or vibrational frequencies.

An important class of reactions where quantum chemistry yields very good results is protonation. Protonation energies of small neutral species can be calculated with chemical accuracy. For example, the proton affinity of ketene, $CH_2{=}C{=}O$, is 848, 883 and 882 kJ/mol when calculated respectively by the Hartree–Fock method with a 4-31G or 6-31G** basis set or if electron correlation is also considered [1023]. Taking the zero-point vibrational energy change into account, 849 kJ/mol is obtained which is in excellent agreement with the experimental value of 842 kJ/mol. The small change in correlation energy is not surprising since protonation is an isodesmic process (see above). Furthermore, since mass and vibrational frequencies of a molecule change little upon protonation, zero-point energy and entropy remain approximately constant. Unfortunately, theoretical investigation of anionic species possess special problems [196], since the extra electron in the anion is weakly bound. Therefore, *ab initio* methods using common basis sets (even 6-31G*) severely overestimate protonation energies (by about 130–150 kJ/mol) even if electron correlation is considered, too. Accurate calculations need diffuse functions to be included into the basis set. In this case good agreement with experiment is achieved [196]. Some numerical examples are given in Table 4.5. The satisfactory agreement of MNDO results with experiment is noticeable.

While absolute values of protonation energies cannot be reproduced, experimental trends are well reflected by *ab initio* STO-3G calculations [848]. For such purposes even the simple CNDO/2 method can be applied with success (*cf.* Fig. 4.1) [1055].

Since the proton is a pointlike charge, protonation can be described qualitatively correctly by means of electrostatic models. A pictorial, yet reliable, way to reproduce

TABLE 4.5

Comparison of calculated and experimental proton affinities of anions (kJ/mol) [196]. Geometries of all species were optimized

Anion	MNDO	STO-3G// //STO-3G[a]	4-31G*// //4-31G[a]	MP2/4-31+G// //4-31+G[a,b]	Exp.
CH_3^-	1824	2343	1914	1780	1744
NH_2^-	1761	2290	1862	1711	1689
OH^-	1767	2366	1797	1595	1638
F^-	1722	2520	1714	1471	1555
CN^-	1620	1937	1548	1481	1478
CH_3NH^-	1666	2214	–	1719	1688
CH_3O^-	1610	2214	–	1597	1587
CH_2CHO^-	1563	2106	1661	1545	1534
$HCOO^-$	1499	–	–	1412	1445

[a] Upper row: basis set for the anion, lower row: basis set for the neutral form

[b] MP2: second-order Møller–Plesset correlation correction, 4-31+G: diffuse function augmented 4-31G basis set

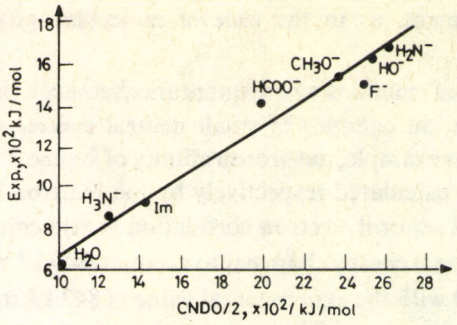


Fig. 4.1 Correlation between experimental and CNDO/2 calculated gas-phase protonation energies

trends is offered by the molecular electrostatic potential maps (*cf.* Section 4.4.1). This potential has a minimum in the vicinity of proton-binding atoms (N, O, F) which is produced by their lone pairs. Other minima (above aromatic rings or near strained bonds) indicate also the possibility of protonation at a given site. It has been shown that for a number of three-membered rings a fair correlation exists between minimal values of electrostatic potentials and protonation energies [441].

Further simplification is possible if solely atomic (Mulliken) net charges are used to characterize relative ease of protonation (*cf. e.g.* Ref. [589]). An almost quantitative correlation between charge shifts and proton transfer energies is achieved for substituted amines (Fig. 4.2) [1167]. Net charges are especially useful for special cases,

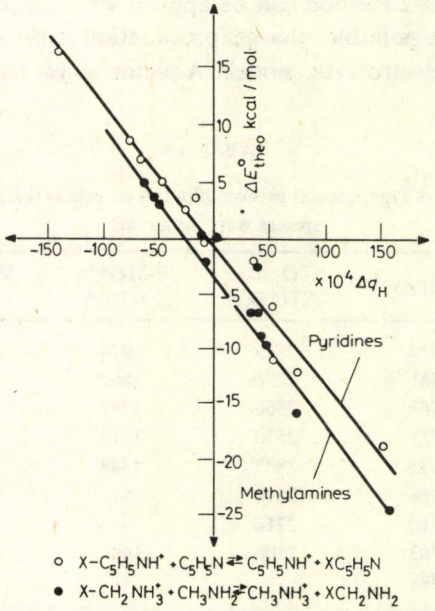


Fig. 4.2 Plot of proton transfer energies vs. proton net charges. Correlation coefficients for substituted pyridinium ions (open circles), and methylammonium ions (closed circles) are 0.982 and 0.969, respectively

like interpretation of changes in CH acidity. CNDO/2 calculations yield 63 millielectrons for the hydrogen net charge in acetylene [970] indicating its moderate acidity. On the other hand, hydrogen charges in ethylene and ethane are 18 and 3 millielectrons, respectively: proton dissociation is practically impossible here. Net charges of hydrogens on α, β and γ carbons in butyric acid are 40, 9 and -3 millielectrons, respectively, showing the rapid decrease of the inductive effect of the carboxyl group. This is in accord with classical chemical experience: dissociation of hydrogen atoms from the α-position is easier than from others. The charges on the dissociable hydrogens in malonic ester and cyclopentadiene are 74 and 31 millielectrons indicating their slight acidity.

Besides inductive effects through-space field effects may also affect acidity especially in charged molecules. This can be modelled theoretically, too [1359]. The distant, charged groups produce a Coulombic field around the protonating atom and this may strongly influence protonation energies. For the gas-phase protonation of molecules substituted by carboxylate and/or ammonium groups, the following simple relation holds [1055]

$$E_p^{\text{subst}} = E_p^{\text{unsubst}} + 156 r_{CO_2}^{-1} - 95.7 r_{NH_3}^{-1} \text{ kJ/mol} \tag{4.8}$$

where r_{CO_2} and r_{NH_3} are distances (put equal to zero if the substituent is absent) of the centroids of carboxylate and ammonium groups from the protonation site (in nm). Through-space field effects on the protonation energies of α, ω-diaminocarboxylic acids may be as large as 400 kJ/mol [1055]

4.2 MOLECULAR COLLISIONS

The first step in an understanding of real chemical reactions in the gas phase is to describe *elementary processes*, that is, to study the collision of isolated molecular species. Since powerful experimental methods like molecular beam techniques [861] are at hand, theoretical calculations can be compared directly to empirical data. Owing to the fruitful interplay between theory and experiment, our knowledge about elementary processes has increased considerably in the past decade. A series of exhaustive reviews on theoretical methods can be found in the first two volumes of Modern Theoretical Chemistry published by Plenum Press [914].

Elementary processes follow, in general one of the undermentioned schemes

$$A \rightarrow B_1 + B_2 \tag{4.9}$$

$$A_1 + A_2 \rightarrow B_1 + B_2 \,. \tag{4.10}$$

Equation (4.9) corresponds to a *unimolecular reaction* where molecule A decomposes to yield B_1 and B_2. In *bimolecular processes*, described by Eq. (4.10), two molecules, A_1 and A_2, collide to yield new products B_1 and B_2. Strictly speaking, unimolecular reactions are not collision processes but we discuss them here since several features are

common with bimolecular reactions. Simultaneous collisions of three molecules is of very low probability; therefore, we do not consider this case.

The first stage of a unimolecular reaction (dissociation, isomerization, conformational change) is that the energy of molecule A in Eq. (4.9) increases (*e.g.* by collision or by electronic excitation). The excess energy is shared among various vibration modes of the molecule (*cf.* Section 3.3). As a result, a state may arise where the energy of one or more vibration modes gets so large that the geometry changes irreversibly: the molecule dissociates or transforms to an isomer. A characteristic example is bond fission: if the vibration energy of a diatomic, AB, reaches a given threshold atoms A and B get far apart from each other and dissociation occurs. It is obvious that the theories of molecular vibrations and unimolecular reactions are closely linked. For further details see some standard references [398, 756, 1184].

In a bimolecular reaction, ground-state or excited molecules collide as indicated in Eq. (4.10). Products can be in their ground states or in excited states, as well. The rigorous quantum mechanical treatment of bimolecular reactions is possible on the basis of scattering theory [204]. The principal aim of this theory is to derive the experimentally observable *cross section* at a particular angle, χ, and energy, E. The cross section is defined by the following equation

$$\sigma(\chi)=\frac{j_s(\chi, E)}{j_i(\chi, E)} \tag{4.11}$$

where the fluxes j_s and j_i represent the number of scattered and incident particles per unit time, referred to unit solid angle and unit area, respectively. In the scattering theory the collision of two particles is described by dealing formally with a single "particle" exhibiting the relative motion of the original pair of particles in the coordinate system of their centre of mass. Their wave functions, corresponding to a uniform plane wave of incident and an angular-dependent spherical wave of scattered particles is considered. (In agreement with the above definition, σ has the dimension of area.) If both the nature and the energy of the incident and scattered particles is the same, one deals with *elastic scattering* in which only the direction of the motion is changed. If the kinetic energy of the particles is also changed during the process one has *inelastic scattering*. If a reaction takes place the scattering is called *reactive*.

Equation (4.11) defines the so-called *differential cross section*, integrating which for all angles one gets the total (overall) cross section. Note that the existence of several internal degrees of freedom for molecular species introduces severe complications in the theory of their scattering. A simple thermically averaged quantity, the *rate constant*, can be directly related to the reactive cross section [756, 861] by integrating over a Boltzmann distribution. The macroscopic rate constant, k measures the concentration loss of the reactants per unit time, assuming unit concentration for all of them. For most chemical reactions it is the k constant which is measurable experimentally; therefore, it is especially important. To obtain the cross section is rather complicated and exact numerical calculations are very difficult to carry out [1020]. A simplification

can be made if it is supposed that the system moves on the same energy hypersurface throughout the course of the reaction *(adiabatic approximation)*. This means that no electronic excitation occurs and electronic and nuclear coordinates are separable (*cf.* Section 1.2.2). If a reaction can be modelled as an adiabatic process the quantum mechanical treatment gets considerably simpler. To describe an elementary process means to solve the kinetic equations of the nuclei moving on the potential surface. A simple example is the anharmonic oscillator (*cf.* Section 3.3) which models the dissociating diatomic molecule. The use of the potential surface in the calculations allows us to give a pictorial interpretation to the mathematical results. Reactants and products correspond to states which oscillate around local minima of the energy hypersurface, and reaction means a transition from the reactant minimum to the product one. Since potential surfaces are of special importance in the theory of chemical reactions we discuss them in more detail in Section 4.3.

The motion of the nuclei on the potential surface can be treated quantum mechanically or classically. The quantum treatment gets extremely laborious for even relatively simple systems but it is manageable for some cases (collinear $F+H_2 \rightarrow HF+H$ [41, 1234, 1416], collinear $H+Cl_2 \rightarrow HCl+Cl$ [51], etc.). Truhlar and coworkers [1370] compared quantum and various classical calculations on the collinear $H+Cl_2 \rightarrow HCl+Cl$ reaction and they have found that the quasi-classical calculations of total rate constants for reaction in a given initial vibration state agree with the quantum calculations within 30% for the 300–1000 K temperature range. However, classically calculated state-to-state rate constants, describing processes where initial and final vibrational states are settled, may be in error by a factor of 2 or more.

One of the potential sources of discrepancies between quantum and classical calculations of reaction rates is the *tunnel effect*. In contrast to classical mechanics a moving particle (affected nucleus in a chemical reaction) can cross an energy barrier of height E even if its energy is lower than E, or can be reflected even if its energy is higher than E. Owing to the sharp decrease of the Boltzmann factor this latter type of reflection influences the rate of a thermal reaction to a much smaller extent than the possibility of crossing the barrier with an energy beyond the barrier height. The tunnel effect is important only for light nuclei, especially for hydrogen. Another condition is that the energy barrier be relatively small and narrow [756]. The effect of tunnelling may be followed on Fig. 4.3 for the calculated transition probability of the unimolecular reaction $H_2CO \rightarrow H_2+CO$ as a function of the total energy [915]. For comparison the classical rate constant is also shown. While this latter vanishes at the energy V_0 which is the sum of the barrier height and the zero-point energy of the transition state, tunnelling allows a significant rate somewhat below this threshold energy. This rate falls quickly but has a value of $10^6\ s^{-1}$ even at an energy 35 kJ/mol below V_0. The most important reaction type where the tunnel effect may play a decisive role is proton or deuteron transfer. Since the tunnel effect is the smaller the smaller the mass of the moving nucleus is, transfer of a proton is much easier than that of a deuteron. This explains the experimentally observable *kinetic isotope effect* which may

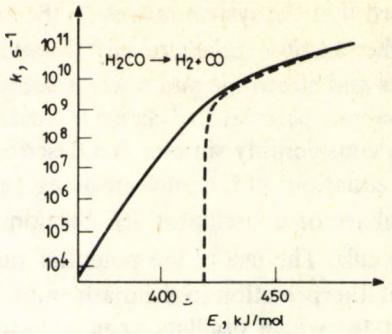


Fig. 4.3 Unimolecular rate constant for the $H_2CO \rightarrow H_2 + CO$ reaction as a function of total energy for total angular momentum $J = 0$. The full line includes tunneling effects, the dashed line is the classical rate. (With permission from Ref. [915])

play a role in other reactions, too. Classical theory is not able to distinguish between the transfer rate of a proton and of a deuteron *i.e.* it predicts $k_H/k_D = 1$. However, it has been found experimentally that this ratio may range between 10 and 100 [786]. The considerable discrepancy can be understood partly in terms of the tunnel effect.

A significant isotope effect is observed for the $H_2CO \rightarrow H_2 + CO$ and $HCOH \rightarrow H_2CO$ unimolecular reactions [915]. Figure 4.4 shows the ratio of the hydrogen to the deuterium transition probabilities for the two reactions, as a function of the total energy (relative to the minimum of the potential energy surface of H_2CO). The classical energy independent limit ($\log k_H/k_D = 0$) is approached for energies above the saddle point of the H_2CO potential surface (classical threshold). However, in the threshold region and below, the isotope ratio is strongly dependent on energy. Pronounced minima are observed on the $\log(k_H/k_D)$ *vs.* E plots indicating that the deuterium versions of the reactions are actually faster than the hydrogen versions. It is worthwile to note, however, that in most practical cases the reactions involving the lighter isotope are faster.

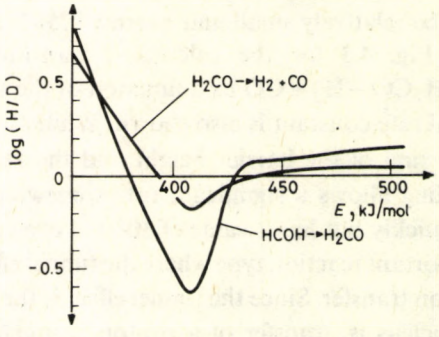


Fig. 4.4 Plot of the logarithm of the ratio of hydrogen to deuterium rate constants for the reactions indicated *vs.* the total energy (with permission from Ref. [915])

If quantum effects are not important displacement of nuclei on the potential surface can be discussed on the basis of classical equations of motion. Nuclei follow trajectories on the surface depending on the initial conditions; therefore, this type of approach is called classical *trajectory analysis* [914]. Initial conditions for the nuclear motion (relative velocity, vibrational and rotational state) are selected at random and the classical equations of motion are solved numerically for each case. The initial conditions are usually restricted so that the energy should coincide with one of the quantized levels of reactant vibrations and, possibly rotations (*cf.* Section 3.3), but afterwards the motion of the system is described by classical mechanics. This approach

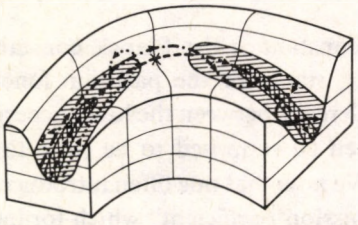


Fig. 4.5 Characteristic trajectories for the AB + C → A + BC reaction. Dashed line: minimum energy path, dash-dotted line: successful collision, dotted line: unsuccessful collision

is often called quasi-classical. Tens or even hundreds of thousands of trajectories are obtained which are used to calculate the reaction cross section. Depending on the initial conditions various trajectories are realized (Fig. 4.5). If the initial energy is sufficiently large, the system passes the col and reaction takes place. In the opposite case where the collision is unsuccessful the trajectory goes back in the direction of the initial state. It is not necessary that the trajectory of the successful reaction consists the saddle point for energies higher than the threshold. Various energy paths are possible which run to a greater or less extent above the col *(bob-sledge effect)*.

The quasiclassical trajectory method may be inaccurate due to the lack of knowledge of the correct potential energy surface, to statistical errors because of the insufficient number of trajectories and to inadequacy of classical mechanics for certain aspects of chemical dynamics (see below). An important defect may be the neglect of the quantized nature of the product vibrational states which is not reflected by the classical equations of motion. Several methods offer a solution to this problem sometimes with good results but often without sufficient theoretical background [1397].

Since quasiclassical trajectory calculations are extremely laborious and costly they can be applied only to the simplest systems. These calculations would reproduce fine details for more complicated reactions which are not even detectable experimentally. For complex processes in the gas phase and especially in condensed phases a simple model was proposed by Wigner, Polanyi, Evans and particularly by Eyring [380, 381, 756, 1423]. This is the *transition-state* theory or the *theory of activated complexes.*

The theory postulates that reaction takes place in two successive hypothetical steps

$$A_1 + A_2 \rightleftharpoons C^* \rightarrow B_1 + B_2 \tag{4.12}$$

C* denotes the so-called *activated complex* which is supposed to be in thermal equilibrium with the reactants. Let us suppose that C* cannot decompose to yield the reactants A_1 and A_2 again, *i.e.* the first step in Eq. (4.12) is irreversible. If we introduce further simplifications, the following expression was postulated for the rate constant [756]

$$k_R = \frac{kT}{h} \frac{f_{C^*}}{f_{A_1} f_{A_2}} \exp(-\Delta\varepsilon/kT). \tag{4.13}$$

Here k is the Boltzmann constant, h the Planck constant, T denotes the absolute temperature, f_{C^*}, f_{A_1} and f_{A_2} stand for the partition function of the corresponding systems. $\Delta\varepsilon$ is the energy difference between the lowest energy levels of C* and $A_1 + A_2$ respectively, which can often be supposed to be close to the barrier height on the reaction surface (Fig. 4.6). We note that one often introduces an additional factor $x < 1$ in Eq. (4.13) called "transmission coefficient" which formally takes into account the reversibility of the process.

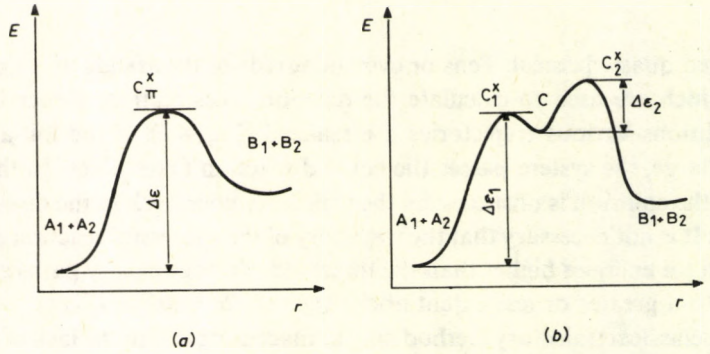


Fig. 4.6 Potential curves for some typical reactions. (*a*) One-step process C* denotes the transition-state complex, (*b*) two-step process C_1^* and C_2^* denote transition-state complexes, C is the short-lived intermediate

Equation (4.13) may be related to the empirical Arrhenius equation

$$k = A \exp(-E_a/RT) \tag{4.14}$$

where E_a is called *activation energy*, A is the universal pre-exponential factor and R is the gas constant. For most reactions A and E_a are independent of the temperature within the experimental accuracy. It can be shown that if $\Delta\varepsilon$ is not too small it is close but strictly speaking never equal to the activation energy per molecule [756]. Since $Nk = R$, $\Delta\varepsilon/kT = -E_a/NkT = -E_a/RT$. The activation parameters in Eq. (4.14) exhibit significant temperature dependence if the experimentally observable reaction is the

superposition of several elementary processes having considerably different activation energies. If this is the case one often encounters also the so-called "compensation phenomenon" in series of closely related reactions (differing *e.g.* only by some substituent in one of the reactants). The activation parameters A and E_a change in the same direction, so their effect on the rate constant is compensated to a great extent [879a]. We have pointed out above that the reaction does not necessarily take place if the initial energy just reaches the activation barrier. There are cases where an energy is needed which is larger than $\Delta\varepsilon$. Therefore it is better to call $\Delta\varepsilon$ a threshold energy which has to be surpassed during reaction. It is possible to introduce a tunneling correction, Γ, into Eq. (4.13) which accounts for this effect. Thus $k_R^{\text{tunnel}} = \Gamma k_R^{\text{classical}}$.

The derivation of the rate constant using Eq. (4.12) is completely formal. It cannot be otherwise, since the C* "activated complex" is physically nonexisting, its lifetime is postulated zero (*cf.* Fig. 4.6 *a*). A stable intermediate product corresponds to a local minimum on the potential surface (*cf.* Fig. 4.6*b*) which involves a two-step mechanism, $A_1 + A_2 \rightarrow C$ and $C \rightarrow B_1 + B_2$. Activated complexes are different for both steps. On the other hand, the transition-state theory can be derived on the basis of a rigorous model, too [913]. The principal but by far unrealistic assumption is that the motion along a reaction coordinate is separable, that is, changes along various degrees of translational, vibrational or rotational degrees of freedom are independent of each other. This is true for reactions considerably above the threshold region. Figure 4.7 depicts the variation of rate constant with temperature as calculated by quantum mechanical scattering theory and transition-state theory, respectively, for the collinear $H + H_2 \rightarrow H_2 + H$ reaction. Though the error at $T = 200$ K is more than an order of magnitude, the separated transition-state theory reproduces trends correctly even in this region.

One can conclude that it is most reasonable to consider Eq. (4.13) provided by the transition-state theory as a (semi)-empirical formula for estimating rate constants. It

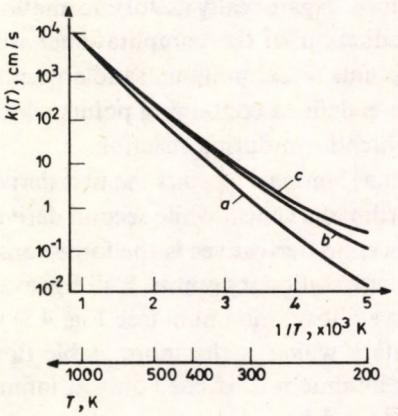


Fig. 4.7 Rate constant as a function of temperature for the collinear $H + H_2 \rightarrow H_2 + H$ reaction *(a)* Separated transition-state theory, *(b)* nonseparated transition-state theory, *(c)* quantum mechanical scattering calculation (with permission from Ref. [917])

can be shown by a detailed analysis that for a model of balls without internal structure Eq. (4.13) essentially reduces to the result given by the elementary classical collision theory of reactions; for more complicated systems, therefore, transition-state theory provides an empirical formula to make qualitative or semiquantitative estimations on the role of internal degrees of freedom in influencing reaction rate constants [1279a].

4.3 REACTION PATHS

In this section we shall discuss the possibility of characterizing a chemical reaction through the potential hypersurface. Quantum chemical calculation of potential surfaces became much easier with the rapid development of high-speed computers and efficient programs. This is the reason why the number of applications to a wide variety of chemical reactions increased considerably.

The potential surface gives the energy of the reacting molecules as a function of their shape and relative position. Reaction rates can be compared using barrier heights, while the stabilities of species may be ordered according to the relative energies of local minima. However, not only barrier heights determine the outcome of a chemical reaction: it may be controlled in two ways. In the case of *thermodynamic control*, the reaction proceeds to the product with the lowest total energy, while *kinetic control* means that the reaction path with the lowest energy barrier is preferred.

A potential surface is calculated within the Born–Oppenheimer approximation by use of the variation principle. If N atoms are involved, this surface has $3N$-6 dimensions (internal coordinates). This indicates that its complete calculation for all, but the simplest systems is a formidable task. This is why one or multi-dimensional cuts are considered, even though they may be prejudical *i.e.* experimental or other informations may be put in the calculation which, in turn, may yield just the same information as a "theoretical result". Therefore, to gain really useful information on chemical reactions a practical but adequate reduction of the computational work is necessary. This is possible if characteristic points (local minima, saddle points, etc.) are found and an appropriate reaction path is defined containing points which correspond to various intermediate structures which form during reaction.

At characteristic or (better) *stationary points* the first derivatives of the energy with respect to all internal coordinates vanish while second derivatives may have different values. The matrix of all second derivatives is the force constant matrix (or Hessian) and this is used to characterize stationary points. If all eigenvalues of the force constant matrix are positive we have a local minimum (see Fig. 4.8) which corresponds to an equilibrium, observable state which is the more stable (longer-lived) the lower its energy. In some cases this minimum is reached only at infinite values of one or more internal coordinates, *cf.* Fig. 4.8 *b*.

Among local minima, *saddle points* or *cols* are distributed on potential surfaces. The simplest ones have just one negative canonical second derivative eigenvalue of the force

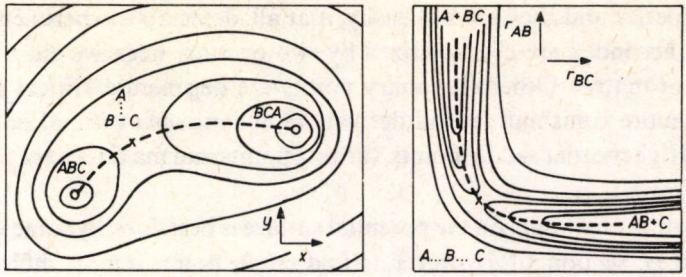


Fig. 4.8 Typical potential surfaces *(a)* isomerization, *(b)* bimolecular reaction. Minimum energy paths are indicated by dashed lines

constant matrix all others are positive (Fig. 4.8). Such saddle points are often called "transition states" though they do not correspond to any physically observable entity. There may exist several saddle points between reactant and product and one or more *intermediates* are formed which need only a small amount of energy to transform them into a more stable form (Fig. 4.9). Owing to their high energy content, intermediates are

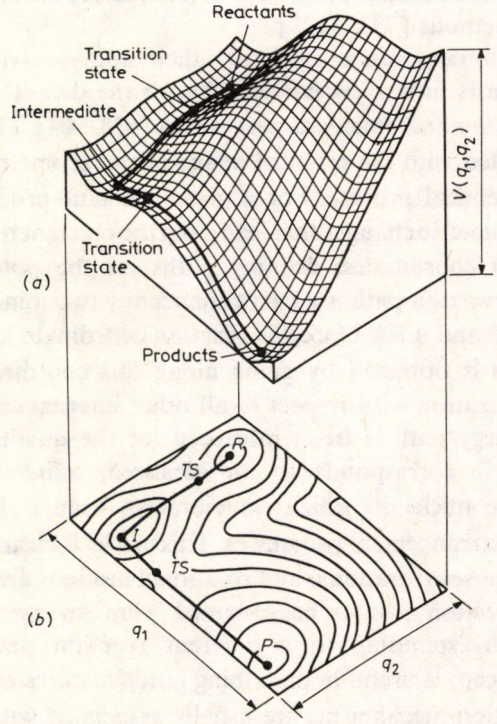


Fig. 4.9 Graphic representation of potential surfaces. *(a)* Pseudo-three-dimensional plot, *(b)* contour map. Pseudo-minimum energy path is indicated by heavy dark line (with permission from Ref. [856])

short-lived species and they are not easily, if at all, detectable experimentally. Saddle points of higher index are characterized by two or more negative eigenvalues of the force constant matrix. Other stationary points are degenerate critical points which have one or more vanishing second derivatives and *maxima* with all positive second derivatives. Higher order saddle points, turning points and maxima have little chemical importance.

Determination of minima on the potential surface is best done by some version of the force method, *cf.* Section 3.1. However, to find saddle points is more difficult and none of the several methods proposed till now is generally efficient. For recent reviews see Refs 658 and 904. Maybe the most practical approach has been proposed by McIver and Komornicki [847] and modified by Poppinger [1127]. These authors calculate the scalar square of the gradient norm

$$\sigma(\mathbf{R}) = \sum_i \frac{\partial E(\mathbf{R})}{\partial R_i} \cdot \frac{\partial E(\mathbf{R})}{\partial R_i} . \tag{4.15}$$

Function $\sigma(\mathbf{R})$ is zero at every stationary point of the energy hypersurface $E(\mathbf{R})$ but no distinction between minima, maxima and various order saddle points can be made. To do this, a subsequent analysis of the force constant matrix is necessary. σ is minimized by an iterative procedure which is programmed for several semiempirical and *ab initio* single determinant methods [733, 1128].

To determine stationary points efficiently their approximate location must be known. This problem is intimately connected with the definition of *reaction paths* which depend on *reaction coordinates* as parameters [658, 904]. The notion of reaction coordinate is associated with the classical image of the geometric rearrangement of nuclei during the chemical process. For a given reactant–product pair of nuclear configurations, all geometric changes that lead from the reactant to the product may be regarded as reaction coordinates, defining paths on the potential hypersurface. Mathematically, the reaction path is a curve connecting two minima on the potential hypersurface (Figs 4.3 and 4.10). Once the reaction coordinate has been defined, the *minimum energy path* is obtained by going along this coordinate for appropriate increments by minimization with respect to all other internal coordinates.

The minimum energy path is frequently used for the qualitative description of chemical reactions. It corresponds to an idealized, infinitely slow (adiabatic) rearrangement of the nuclei in which no vibration occurs. The energy changes continuously as the rearrangement progresses. This model is clearly an oversimplification since in real processes vibrational and rotational motions are always present and the reaction cross section should be obtained from an averaging over several trajectories, each corresponding to a different reaction path, *cf.* Section 4.2. Nevertheless, the concept is useful in describing crude features of reaction processes, because distinct reaction mechanisms are usually associated with distinct minimum energy paths.

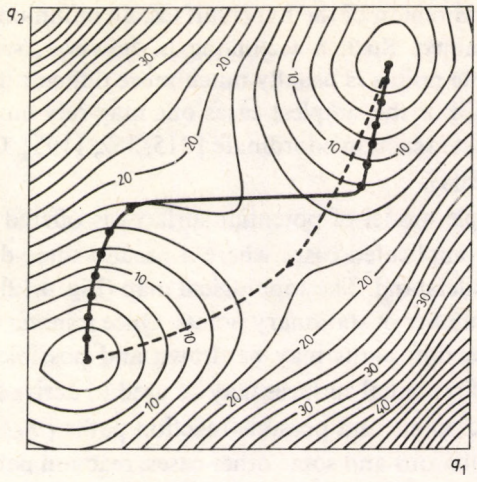


Fig. 4.10 Example of the difference between two reaction paths. Full line with dots: constrained minimization procedure, dashed line: minimum energy path. The col (arrow) lies on the minimum energy path but not on the path determined by constrained minimization. (With permission from Ref. [856])

There are several problems connected with minimum energy paths since the choice of the reaction coordinate is not unique. This is illustrated in Fig. 4.10 where the full line represents the minimum energy path if q_2 is the independently varying reaction coordinate and q_1 is optimized for all points [856]. The curve does not even pass over the saddle point and it suggests that the reaction follows in three subsequent steps: in the first and last ones q_2 is changing while q_1 remains constant, and in the vicinity of the saddle point q_1 is the strongly changing variable. The proper definition of the reaction coordinate is important since due to an oversimplification "kinks" may be predicted in the minimum energy path at the saddle point [845, 1060a]. This means that the energy derivatives are discontinuous here, which contradicts the concept of the reaction path. Furthermore, the minimal ascent to the saddle point may be different from the steepest descent if the path is reversed. The situation is more complicated if several saddle points exist between reactant and product: often it is impossible to predict the reaction path with the lowest barrier, starting from the reactant.

A precise definition of the reaction coordinate called *intrinsic reaction coordinate* was given by Fukui [417, 1337]. Going along this coordinate a reaction path is obtained which connects reactant and product minima, passes through the saddle point and is orthogonal to any equipotential contours crossed, *cf.* Fig. 4.10. Though even this definition suffers from some problems [658, 904] it is put on a more physical footing than others.

Ideally, a method for minimum energy path determination would start with the location of first-order saddle points and simple relaxation methods could be used to find the two steepest descent path portions leading to the two minima. By locating all

saddle points in a given region of the hypersurface, all minimum energy paths in this region can be determined. Such a technique is, however, seldom used since the determination of saddle points is usually much more difficult than that of minimum energy configurations. For the simplest cases one may rely on chemical intuition in selecting the appropriate reaction coordinate [315, 362, 1195]. Other possibilities are surveyed by Mezey [904].

An apparently simple model of potential surfaces is offered by topology. This is especially useful for complicated cases where a pseudo three-dimensional plot (Fig. 4.11) is not easy to understand. The topological map (Fig. 4.12) offers a technique to survey location and number of stationary points. Once minima and saddle points are located, schematic reaction paths may be drawn and possible mechanisms can be analyzed. Topology of potential surfaces may be used to derive some simple relations between characteristic points and possible reaction paths [902, 903].

For trajectory calculations and some other cases, reaction paths and critical points alone are insufficient; the whole potential surface is needed. Since quantum chemical calculations yield discrete points on the surface it is imperative in these cases that an analytic expression be fitted to the computed points. This expression allows us to do rapid calculations and to draw pseudo three-dimensional contour plots which are especially useful to study the overall surface topology by visualization (Fig. 4.11). A further application of fitting analytic equations to *ab initio* energy values is the determination of force constants. The advantage of this approach is that both the

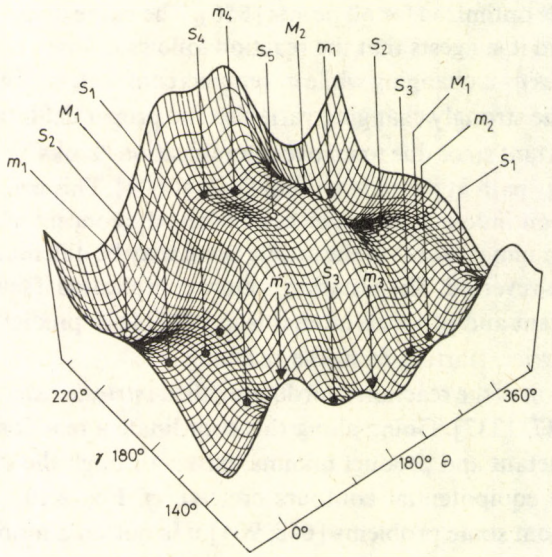


Fig. 4.11 Pseudo-three-dimensional plot of the $PH_2(OH)NH_2^+$ rotation-inversion energy surface. Minima are shown as m_1 through m_6 while saddle points are labeled s_1 through s_5. M_1 and M_2 denote low maxima Θ = HOPN torsional angle, γ = out-of-plane deformation angle of the PNH_2 pyramid. (With permission from Ref. [1087])

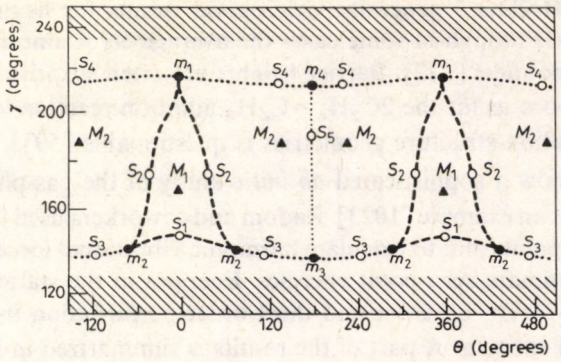


Fig. 4.12 Topological map of the energy surface of Fig. 4.11. Shaded areas represent rapidly increasing energy. (With permission from Ref. [1087])

harmonic and higher order anharmonic force constants are simply related to the linear coefficients of the analytic equation. Hypersurface fitting is best made by an automatic stepwise regression technique. This selects the best subset containing a given number of terms (polynomial, trigonometric or exponential) from a large number of candidate terms. A survey on fitting techniques together with numerous illustrative examples was given recently by Peterson and Csizmadia [1087].

Let us turn now to the problem of how various quantum chemical methods are capable of giving reliable potential surfaces. In contrast to equilibrium states, electron correlation is in most cases important in determining geometries and relative energies of "transition-state" structures. The classical bond concept is not applicable to these strange formations; therefore, transferability of bond correlation energies breaks down. Table 4.6 includes some examples which give information on correlation effects. For the transformation of cyclobutane into two ethylene molecules the configuration interaction calculation drastically reduces the barrier height as compared to the SCF value, which, however, remains considerably higher than the experimental value [1252, 1440]. On the other hand, for the $Cl^- + CH_3Cl \rightarrow ClCH_3 + Cl^-$ substitution reaction the barrier height increases if correlation is partly considered in the calculations [680].

An important problem is the choice of the basis set. Some impressions may be obtained from Table 4.6. Minimal basis sets often considerably overestimate barrier heights; the error gets much smaller if double-zeta quality sets are used. The quality of the basis set is especially important if correlation effects are estimated. For the $F^- + CH_3F \rightarrow FCH_3 + F^-$ reaction the correlation energy for the "transition state" is zero if a small basis set is used [284]. This becomes +19.4 kJ/mol with a large basis set [680].

The formidable amount of computational work using *ab initio* programs may be drastically reduced by semiempirical methods (*cf.* Section 1.3.2). To estimate barrier heights to chemical reactions the MINDO methods are the only reasonable tools. They may be considered as some kind of interpolation techniques based on the use of

empirical data. MINDO/3 generally yields good results for heats of formation of hydrocarbons [102] though in some cases the average error amounts to 100 kJ/mol (*e.g.* fluorine compounds) [322]. Barrier heights are often surprisingly good, though sometimes quite poor as for the $2C_2H_4 \rightarrow C_4H_8$ addition reaction (*cf.* Table 4.6). The reliability of transition-structure geometries is questionable [59].

Let us discuss now a sophisticated *ab initio* study of the gas-phase $C_2H_3O^+$ ion potential surface as an example [1023]. Radom and coworkers used the 4-31G basis set to find stationary points and to calculate harmonic vibrational force constants for the Hessian and to estimate zero-point energies. Energies in the stationary points were calculated by a 6-31G** basis set and third-order perturbation theory was used to obtain correlation energies. A part of the results is summarized in Figs 4.13–15. The

TABLE 4.6

Theoretical activation energies (in kJ/mol) for some selected reactions as obtained by various quantum chemical methods. Experimental values, if available, are given in parentheses

Reactant	Product	Activation energy	Method or basis set	Ref.
Rearrangement reactions				
		187 (169)	STO-3G	[534]
		150	4-31G	[534]
		159 (63)	STO-3G	[526]
		84	4-31G	[526]
		203 (208)	MINDO/3+CI	[311]
CH_3NC	CH_3CN	146 (161)	MINDO/2	[317]
		253	DZ	[802]
		358 (239)	STO-3G+CI	[99]
Addition reactions				
		77 (186)	MINDO/3	[316]
		118 (125)	MINDO/3	[313, 320]
		178; 87	STO-3G+CI	[1361]
Elimination reactions				
		653 (262)	min STO	[1440]
		325	STO-3G+CI	[1252]
		473 (251)	STO-3G	[562]
		291	4-31G	[562]
Substitution reactions				
$H^- + H_2$	$H_2 + H^-$	68	DZ+P	[680]
		49	DZ+P+CI	[680]
$F + H_2$	$FH + H$	7.1 (7.1)	DZ+P+CI	[84]
$H + F_2$	$HF + F$	4.2 (10.0)	DZ+P+CI	[989]
$CH_3 + CH_4$	$CH_4 + CH_3$	17 (6)	MINDO/2	[1160]
		109	STO-3G	[1160]
		125	4-31G	[1160]
$Cl^- +$	$ClCH_3 +$	9.2	DZ+P	[680]
CH_3Cl	Cl^-	40.5	DZ+P+CI	[680]

most stable species is the acetyl cation (**1**) which is an important fragment ion in the mass spectra of many oxygen-containing organic molecules. Another stable species is 1-hydroxyl vinyl cation (**2**). Recent experimental estimates of the heats of formation of **1** and **2** yield an energy difference of 180 kJ/mol which is in excellent agreement with the calculated result, 181 kJ/mol. It is noteworthy that previous measurements gave only 75 ± 30 kJ/mol for the energy difference, that is in this case the accuracy of quantum chemical calculations competes with experiment. This means that other energy differences, obtained by the calculation, can be used as substitutes for missing experimental data.

It is interesting to study saddle-point structures [**5**], [**6**] and [**7**], given in Fig. 4.15. These are "transition states" in rearrangements involving the formylmethyl cation, **3** (*cf.* Fig. 4.13). At the 4-31G level the transition structure [**6**] was located involving a barrier of 44 kJ/mol for the **3**→**1** rearrangement. However, the higher level calculations

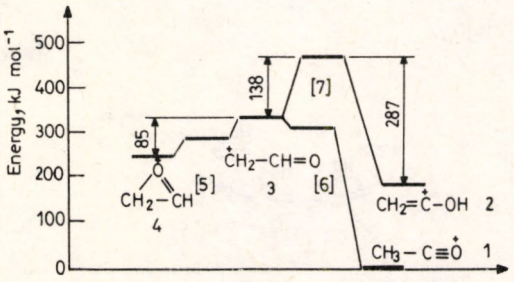


Fig. 4.13 Schematic energy profile for rearrangements involving the formylmethyl cation (**3**). Transition state structures are indicated by square brackets (cf. Figs 4.14 and 4.15 for structures of stable intermediates and transition states). (With permission from Ref. [1023])

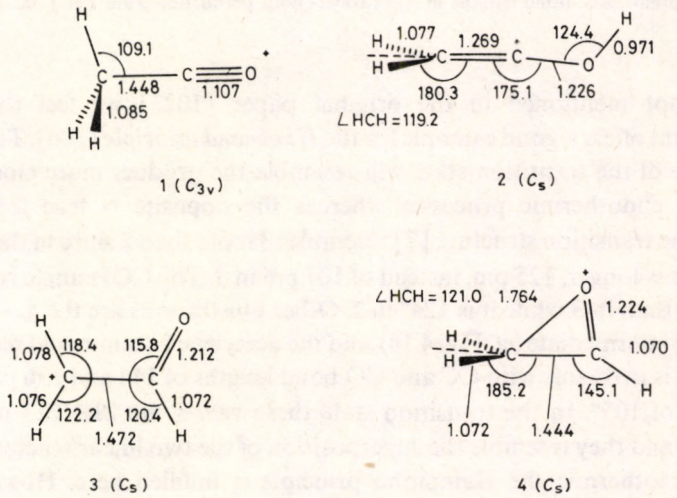


Fig. 4.14 Structures of stable intermediates in the $C_2H_3O^+$ rearrangements. Symmetry classes are indicated in parentheses. Bond lengths in Ångstroms (With permission from Ref. [1023])

(6-31G with correlation) indicate that [**6**] actually lies lower in energy than [**3**]; therefore, it is probable that the 1,2-hydrogen shift **3**→**1** occurs without activation energy. No transition structure for a 3,1-hydrogen shift (**2**→**1**) was found, indicating that this pathway would have **3** as an intermediate. However, the activation energy for the **2**→**3**→**1** process is quite high, 287 kJ/mol. Ring closure of **3** to **4** needs no activation energy since the transition structure [**5**] which was found by the 4-31G basis set calculation proved to be lower in energy than **3**.

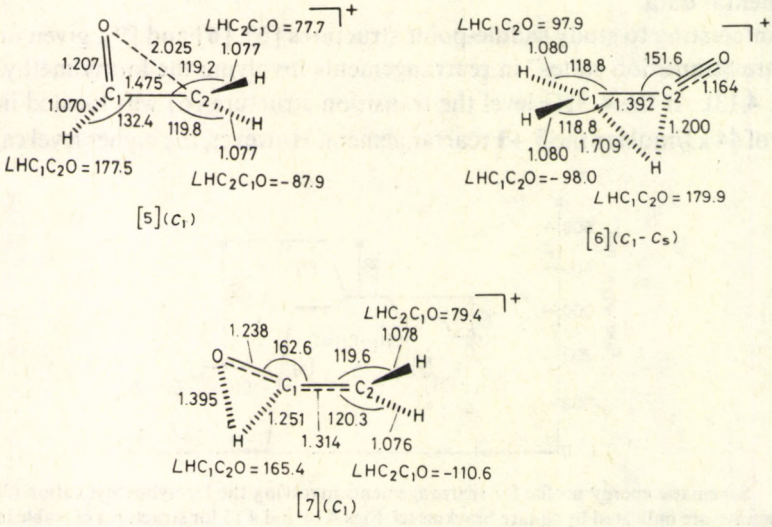


Fig. 4.15 Transition-state structures in the $C_2H_3O^+$ rearrangements. Symmetry classes are indicated in parentheses. Bond lengths in Ångstroms (With permission from Ref. [1023])

Though not mentioned in the original paper [1023] we feel that the **3**→**2** rearrangement offers a good example for the *Hammond principle* [506]. This states that the structure of the transition state will resemble the product more closely than the reactant for endothermic processes whereas the opposite is true for exothermic reactions. The transition structure [**7**] resembles **3** more than **2** since in the former only the CH bond is longer, 125 pm, instead of 107 pm in **3**. The COH angle is only slightly larger in [**7**] than in **3** while it is 124° in **2**. Other illustrations are the **4**→**3**→**1** process where **3** is an intermediate (*cf.* Fig. 4.14), and the acetylene fulminic acid reaction [731]. The product is isoxazole with CC and CO bond lengths of 144 and 136 pm and with a CNO angle of 105°. In the transition state these values are 218, 223 pm and 137°, respectively, and they resemble the superposition of the two linear reactants. Since the reaction is exothermic the Hammond principle is fulfilled here. However, for the silanediyl insertion reaction Grew and Schaefer stated that no definite conclusions can be drawn about the validity (or exception) to the Hammond postulate [484].

TABLE 4.7

Relative potential energies (ΔU), Gibbs free energies (ΔG) and entropies (ΔS) for the concerted reaction paths of the $NH_3 + HCOOH$ and $NH_3 + NH_2CH_2COOH$ reactions (in kJ/mol). The transition state is denoted by a double cross [1040]

Reaction and method[a] for single-point energy	$\Delta U\dagger$	$\Delta G\dagger$	$-T\Delta S\dagger$	ΔU	ΔG	$-T\Delta S$
$NH_3 + HCOOH$						
HF/3-21G	181[b]	228[b]	46[b]	23[b]	21[b]	0[c]
HF/6-31G	229[b]	273[b]	–	−5[b]	−7[b]	–
MP4/6-31G**	196[c]	241[c]	–	2[c]	0[c]	–
$NH_3 + NH_2CH_2COOH$						
HF/3-21G	185[b]	237[b]	52[d]	28[b]	24[b]	0[d]
HF/6-31G	237[b]	288[b]	–	3[b]	−1[b]	–

[a] HF/$m-n$1G: Hartree–Fock calculation with $m-n$1G basis set, MP4/6-31G**: Hartree–Fock calculation with 6-31G** basis set and fourth-order Møller–Plesset perturbation expression for the valence electron correlation energy

[b] Geometry optimization with HF/STO-3G basis set

[c] Geometry optimization with HF/3-21G basis set

[d] Single-point energy and geometry optimization with HF/STO-3G

Few calculations have been published on the role of entropy in determining reaction rates. A recent example is the *ab initio* study of the following reactions [1040]

$$NH_3 + HCOOH \rightarrow NH_2CHO + H_2O$$

$$NH_3 + NH_2CH_2COOH \rightarrow NH_2CH_2CONH_2 + H_2O.$$

Some results are given in Table 4.7. The Gibbs free energy was calculated as a sum of potential energy (ΔU), zero-point vibrational energy (ΔV) and entropy ($T\Delta S$) contributions, $\Delta G = \Delta U + \Delta V - T\Delta S$. It is seen that ΔV is very small, almost negligible, for the transition-state and equilibrium species. The entropy contribution is larger for the transition state but it is not decisive. The main conclusion that the parameters for the two reactions are very similar remains true even if the entropy term is neglected. It is an interesting feature of the reaction that the entropy difference between initial and final states is zero.

Further recent examples of application are found in Refs [89, 674, 960 and 1005].

4.4 REACTIVITY OF MOLECULES

Numerical calculation of potential surfaces and reaction paths for bimolecular reactions is very costly due to the large number of degrees of freedom in reacting systems. To overcome this difficulty simple models were introduced which use only one of the reacting molecules (as a rule the larger) to characterize the process. The other reacting species is not explicitly considered or is treated only as a pointlike perturbing

centre. A useful molecular property, the *reactivity*, can be defined which allows that molecule A alone provide important information concerning a series of related A + B →C or A + B→C + D reactions. Reactivity can characterize one or more atoms or it can be given for several points around the molecule. In this latter case we have *reactivity maps* which yield more detailed pieces of information on the process. In the following we treat reactivity maps and reactivity indices separately.

4.4.1 REACTION POTENTIAL MAPS

If one of the reacting molecules is treated as rigid and the other as a pointlike perturbing centre the interaction energy, essentially governing the reaction, can be calculated relatively simply. Therefore it becomes possible to do these calculations for a large number of points around the molecule *i.e.* to construct *reaction potential maps.* These maps give a pictorial representation of possible reaction channels and their relative importance. Regions where the interaction energy is negative, represent reactive domains and it is probable that the attack of the smaller reacting agent occurs here. On the other hand, positive regions are avoided; no reaction takes place here. It is important to notice that, apart from some special cases, interaction energy maps yield only qualitative information on a reaction. This is why relatively crude methods are sometimes appropriate to calculate these maps or, in other words, application of a sophisticated method brings nothing very new.

We have mentioned in Section 2.1 that the interaction energy between two molecules can be written as a sum of physically interpretable terms. Klopman and coworkers [718] modelled a nucleophile (N)—electrophile (E) system by a rigid, structured part (the nucleophile) and a unit positive charge with an empty 1*s* orbital (which models the electrophile). With this simplification of E the interaction energy can be approximated as a sum of Coulombic, inductive and charge transfer terms

$$E_{\text{int}} = E_{\text{C}} + E_{\text{I}} + E_{\text{CT}} \tag{4.16}$$

with

$$E_{\text{C}} = 2\sum_i V_{ii}^{\text{E}} + \sum_{\text{A}} \frac{Z_{\text{A}}}{r_{\text{AE}}} \tag{4.17}$$

$$E_{\text{I}} = 2\sum_{ik} \frac{(V_{ik}^{\text{E}})^2}{\varepsilon_k - \varepsilon_i - (ii|kk) + 2(ik|ik)} \tag{4.18}$$

$$E_{\text{CT}} = 2\sum_i \frac{(V_{ie}^{\text{E}} - S_{ie} V_{ii}^{\text{E}})^2}{\varepsilon_e - \varepsilon_i}. \tag{4.19}$$

V_{pq}^{E} is the core attraction energy between the positive charge of the model electrophile and the overlap density $\psi_p \psi_q$, i and k are occupied and empty orbitals of N, respectively. Z_{A} is the nuclear charge of the A'th atom of N being at a distance of r_{AE}

from E. The ε_p is the orbital energy, S_{pq}, $(ii|kk)$ and $(ik|ik)$ are the overlap, Coulomb repulsion and exchange integrals, respectively. The subscript e refers to the empty 1*s* orbital of E.

Equations (4.16–19) may be used to estimate interaction energies at sufficiently large distances. It is difficult to say which distance is "sufficiently large" however; it seems that the model works well outside the van der Waals volume of the molecule. Since summation includes only orbitals in N the computational work considerably reduces. Using a semiempirical method, like CNDO/2, E_{int} can be calculated for a large number of points and the reaction potential map can be constructed easily [931].

A further considerable simplification is possible if E_{int} is approximated in Eq. (4.16) by E_C only. In this case E_{int} is just the molecular electrostatic potential (MEP) which is given at a point $\mathbf{r}$ as [1250, 1251]

$$E_C(\mathbf{r}) = V(\mathbf{r}) = -\int \rho(\mathbf{r}')|\mathbf{r}-\mathbf{r}'|^{-1}\,d\mathbf{r} + \sum_A Z_A|\mathbf{r}_A-\mathbf{r}|^{-1}. \tag{4.20}$$

ρ is the electronic density, $\mathbf{r}_A$ is the position vector of nucleus A with a charge of Z_A. Clearly $|\mathbf{r}_A-\mathbf{r}|$ is identical to r_{AE} in Eq. (4.17). Within the Hartree–Fock approximation for a closed-shell molecule

$$\rho(\mathbf{r}) = 2\sum_p^{\text{occ}} |\psi_p(\mathbf{r})|^2 \tag{4.21}$$

i.e. ρ equals the sum of the squares of occupied orbitals. The MEP, defined in Eq. (4.20) is an observable quantity, *e.g.* by X-ray diffraction [940] or by electron diffraction [388].

It is the electronic charge distribution, ρ, and the position of the nuclei which are needed to calculate the MEP. The ρ can be obtained by any standard quantum chemical method, preferably by an *ab initio* one. It was observed that the numerical value of the MEP is at least moderately and sometimes strongly dependent on the basis set [354, 920, 1090]. However, qualitative features do not alter considerably; therefore, minimal basis set calculations are appropriate if chemical reactivity is studied. Semiempirical methods often yield erroneous results, for example the negative region above and under aromatic rings is predicted to be positive. However, an appropriate version of the CNDO/2 method may be applied with sufficient care [354, 443, 444, 1090].

All MO methods suffer from the problem that the computational work is proportional to a higher (at least third if not fourth) power of the number of basis orbitals. Therefore, especially if the molecule is larger, the construction of the MEP becomes very expensive in spite of the simple calculation of V from the charge distribution. One possible way to overcome this difficulty is the bond-increment method which uses strictly localized MOs (SLMOs, φ_i) which are considered to be fully transferable (*cf.* Section 1.4) [28, 973, 981]. SLMOs are only approximately orthogonal but, due to their relatively strong spatial separation, nonorthogonality terms can be

neglected and Eq. (4.21) can be used. Since φ_i's are transferable their coefficients need not be determined by a laborious SCF procedure and the computation of V in Eq. (4.20) is drastically reduced. The numerical work becomes proportional to the first power of the number of SLMOs. This allows us to write efficient and fast programs which calculate the MEP for very large molecules [975], even for proteins [26].

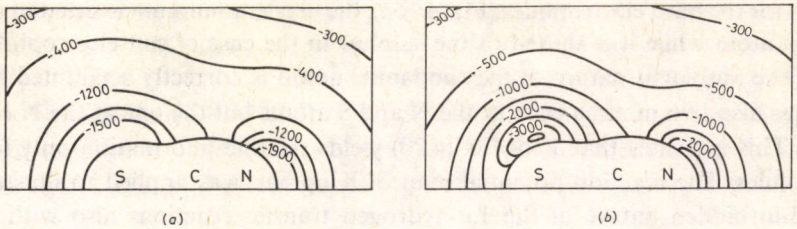
Some authors use a multipole expansion to calculate MEPs [262, 523, 1165]. This approximates the exact potential with point charges, point dipoles and higher point multipoles which are positioned at the atomic nuclei and, in some cases, along the bonds. To be economic, very high multipoles should not be considered and this results in the breakdown of the approximation at distances smaller than about 200 pm from the nuclei. This may be especially important in lone-pair regions of the molecule. The principal problem with multipole expansions is that the atomic parameters are, in general, nontransferable [262, 379]. If appropriate fragments are considered, transferability gets much better but the problem arises as to how we define molecular constituents. A straightforward fragmentation is at hand for proteins and the rapid calculation of the MEP becomes possible [523].

The transferability problem may best be overcome by combination of the multipole expansion technique with localized molecular orbitals [123, 262, 768]. These are well transferable for σ-bonds, somewhat less for lone pairs, but if the MEP is calculated, nontransferability is unimportant since tails and inductive effects play a minor role in this case. Using LMOs certain conformational changes can be followed in the molecule and a more elegant superposition of small subunits to form macromolecules may be achieved [379].

In its original form, the MEP can be used only for electrophilic reactions since it gives the interaction energy of a reacting molecule with the simplest model electrophile: a positive point charge. For nucleophilic reactions the situation is a bit more complicated. If the nucleophile is a negative point charge positive regions of the MEP around the nuclei should be considered as strongly attractive but these do not necessarily indicate a corresponding affinity for nucleophiles. For example, hydrogen atoms usually have positive regions around them but are not sites for nucleophilic attack. Politzer and coworkers proposed a procedure which uses electrostatic potentials to interpret nucleophilic processes [1116]. They calculate the MEP for appropriately distorted molecules which are already amenable to the approach of the nucleophile. Examples like nucleophilic attack on acrolein, methyl chloride and fluorbenzene, illustrate that this approach is promising. A simple, heuristic solution of the problem is offered by the inclusion of a 6–12 pair potential [976].

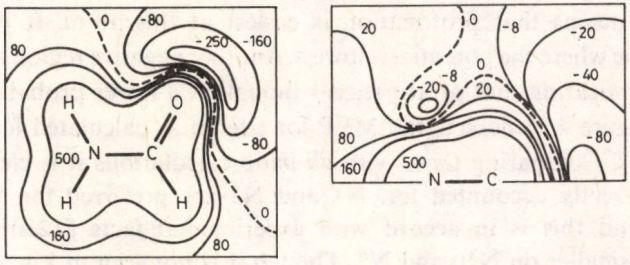
$$E_{\text{int}} = q_X V(\mathbf{r}_X) + \sum_A (-B_A r_{XA}^{-6} + C_A r_{XA}^{-12}) \tag{4.22}$$

where $q_X = \pm 1$ if X = E or N, respectively. V is given in Eq. (4.20), r_{XA} is the distance of the attacking pointlike agent from atom A of the reactant. B_A and C_A are empirical constants. Their proposed values are



(a) (b)

Fig. 4.16 Reaction potential maps for the attack of the SCN^- ion by *(a)* hard and *(b)* soft electrophiles. Contour values are in kJ/mol. (With permission from Ref. [718])



(a) (b)

Fig. 4.17 MEP for formamide as calculated by the *ab initio* SCF procedure *(a)* in the molecular plane *(b)* in a perpendicular plane containing the NC bond. Contour values are in kJ/mol

$$B_H = 1.7 \times 10^{-4} \text{ kJ nm}^6/\text{mol}$$

$$C_H = 1.3 \times 10^{-9} \text{ kJ nm}^{12}/\text{mol}$$

$$B_Z = 5.2 \times 10^{-4} \text{ kJ nm}^6/\text{mol}$$

$$C_Z = 6.3 \times 10^{-9} \text{ kJ nm}^{12}/\text{mol}. \qquad (4.23)$$

Subscripts H and Z denote hydrogen and one of the C, N, O and F atoms respectively. Equation (4.22) may be considered as a 6–12 type empirical potential where the Coulombic potential of a point charge is replaced by a somewhat more sophisticated expression: Eq. (4.20). If V in Eq. (4.22) is calculated by the bond-increment method [973, 981] nucleophilic and electrophilic reaction potential maps can be constructed at a very low cost. These reflect general trends, like orientation effects of first- and second-order substituents, correctly [976].

Let us now discuss some examples on the application of reaction potential maps. Klopman and coworkers used Eqs (4.16–19) to study the ambient nature of the SCN^- ion as a nucleophile [718]. It reacts with soft electrophiles (*e.g.* Ag^+, Zn^{2+}, CH_3I) on the sulphur while with hard electrophiles (*e.g.* Ti^{4+}, Mg^{2+}, carbonyl derivatives, saturated carbon-fluorine bonds) on the nitrogen atom. ε_e of Eq. (4.19) was put equal to 0 and 6 eV (580 kJ/mol) for soft and hard electrophiles, respectively. Based on the CNDO/2 method two reaction potential maps were calculated (Fig. 4.16). On

the map for the hard electrophiles (Fig. 4.16*a*), the deeper minimum is situated near the nitrogen atom while it is shifted to the sulphur in the case of soft electrophiles (Fig. 4.16*b*). The ambident nature of the rhodanide anion is correctly accounted for. The MEP has also two minima each at the N and S atoms but the one at the N region is deeper. This indicates that V of Eq. (4.20) yields reliable information only for hard electrophiles. The reaction potential map of Klopman was applied to illustrate the allowed/forbidden nature of the 1,*n*-hydrogen transfer reactions also with success [717].

The applicability of MEPs to reactivity problems is illustrated with formamide (Fig. 4.17) [1250]. The lone pairs of the carbonyl oxygen atom produce an extended negative region which means that protonation is easiest at this atom. It proceeds in the molecular plane where the potential is lowest. Another negative region is observed near the nitrogen indicating that protonation—though at a lower probability—may also occur here. Figure 4.18 depicts the MEP for adenin as calculated for the CNDO/2 method [1142]. Comparing these with *ab initio* calculations it is clear that general trends are correctly accounted for. N1 and N3 are preferred for an electrophilic substitution and this is in accord with experimental facts [1250]. The reaction probability is smaller on N10 and N7. Though it is not seen in Fig. 4.18, a negative region is formed above and under N10 which means that the direction of eventual protonation on this atom should be perpendicular to the molecular plane. Substituent effects are also discussed using MEPs [1114].

An interesting application of MEPs is the study of through-space electrostatic field effect of distant substituents on certain reactions [977, 979, 1055, 1258]. This is especially important in serine proteases which enzymes hydrolyze peptide or ester bonds by making use of an active serine hydroxyl group, *cf.* Fig. 4.19. It is seen on Fig. 4.20 that the buried aspartate, hydrogen-bonded to an imidazole side chain (Im), considerably lowers the potential around the active serine hydroxyl group. The nucleophilicity of this group can be measured by the minimum value of the potential. The lower this is the higher is the probability of the serine hydroxyl attack on the

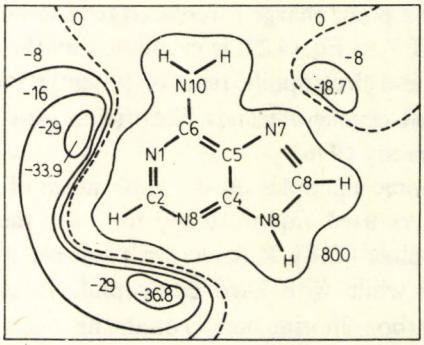


Fig. 4.18 MEP for adenine in the molecular plane as calculated by the CNDO/2 method. Contour values are in kJ/mol

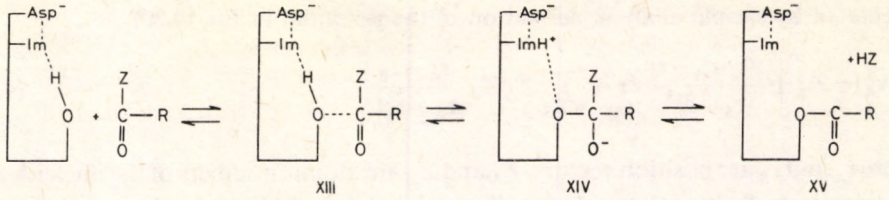


Fig. 4.19 Scheme for the hydrolytic reactions catalyzed by serine proteinases. Z = R'NH or R'O. XIII: Michaelis complex, XIV: tetrahedral intermediate, XV: acyl enzyme

carbon atom. If the negatively charged aspartate were replaced by a neutral asparagine the potential would become considerably less negative and the nucleophilicity would decrease. This is why it is thought that the buried aspartate side chain has an essential accelerating effect on the enzymatic reaction.

Other applications of MEP to problems of chemical reactivity are given in an interesting review by Tomasi [1357].

Another quantity which can be applied to interpret chemical reactions is the electrostatic force acting on atoms in reacting systems [966, 967]. This is easily

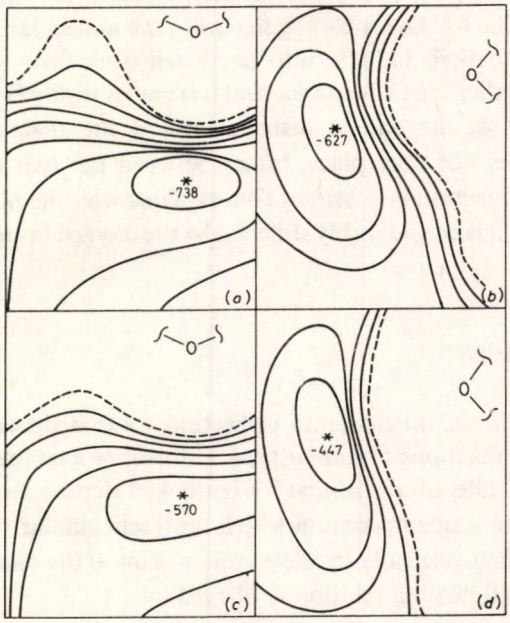


Fig. 4.20 Electrostatic potential around the active serine side chain in *(a)* α-chymotrypsin and *(b)* subtilisin. Corresponding MEPs where the buried aspartate is replaced by a neutral asparagine are given in *(c)* and in *(d)*. Contour values outside from the oxygen atom correspond to −100, −200, −300, −400, −500 and −600 kJ/mol, respectively

calculated by simple analytic derivation of the potential in Eq. (4.20)

$$\mathbf{F}_A(\mathbf{r}_A) = Z_A \int \frac{\rho(\mathbf{r})(\mathbf{r}_A - \mathbf{r})}{|\mathbf{r}_A - \mathbf{r}|^3} d\mathbf{r} - \sum_{B \neq A} Z_A Z_B \frac{\mathbf{r}_A - \mathbf{r}_B}{|\mathbf{r}_A - \mathbf{r}_B|^3} \tag{4.24}$$

where $\mathbf{r}_A$ and $\mathbf{r}_B$ are position vectors, Z_A and Z_B are atomic numbers of the nuclei A and B, respectively. Summation includes all nuclei, but A and $\rho(\mathbf{r})$ is the electron density of the whole reacting system. In actual calculations, results, obtained by using Eq. (4.24)

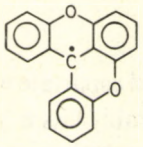


Fig. 4.21 The 5,9-dioxa-9,14-dihydrocoeranthryl radical

are only of qualitative value because usual quantum chemical methods violate the Hellmann—Feynman theorem (*cf.* Section 1.2.2.). Also, the real forces, acting on nuclei are determined by Eq. (1.20) which accounts also for "wave function forces". The analysis of forces acting on nuclei during a reaction yields important pieces of information. For example, if two planar methyl radicals are approaching from an infinite distance and the CC line is perpendicular to the molecular planes, electrostatic forces distort the methyl moiety into a tetrahedral form [967]. The larger the distortion, the smaller the CC distance and it is energetically favoured since methyl radicals mutually repel the charge distributions of the reacting partner. If this pyramidalization does not take place, forces between the two radicals are always repulsive, that is, no reaction is possible. This explains why the planar radical of Fig. 4.21 cannot dimerize: it is considerably stiffened by the oxygen bridges and distortion is impossible.

4.4.2 REACTIVITY INDICES

We have mentioned in the introduction to Section 4.3 that the concept of reactivity may be used only for reactions of similar type. Let us now examine in which case two reactions may be considered as "similar". Figure 4.22 depicts two minimum energy paths each having one single maximum which represent similar reactions. Note that the curves can be shifted vertically to allow comparison. If the reaction paths **1** and **2'** do not cross and the following relation is obeyed

$$\frac{E_p^1}{E_p^2} \approx \frac{E_a^1}{E_a^2} \approx \frac{\Delta E^1}{\Delta E^2} \tag{4.25}$$

the reactions are called similar, *cf. e.g.* [713]. E_a is the activation energy, ΔE the reaction

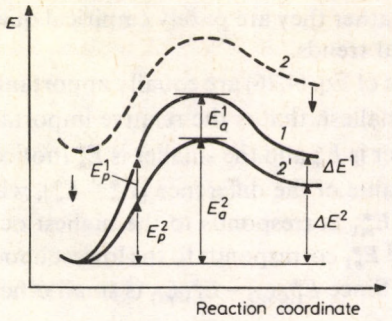


Fig. 4.22 Schematic minimum energy paths for similar reactions (1 and 2). 2′ denotes the shifted path. E_p, E_a and E stand for polarization, activation and reaction energy, respectively

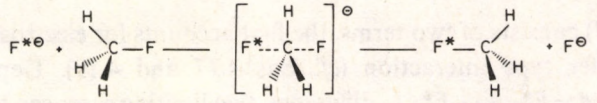


Fig. 4.23 Scheme of the Walden inversion. Transition-state structure is indicated in a square bracket

enthalpy and E_p is called polarization energy. This is the energy gain of the system in some intermediate, nonstationary point with respect to the reactant. A rationalization of the relationship in Eq. (4.25) was given on the basis of perturbation theory by Hudson [606].

A straightforward derivation of the reactivity concept is based on the comparison of the energy content of polarized states. The polarization energy, E_p, has to be estimated and this is best done by perturbation theory applied to an adequate model reaction [608, 712, 714, 716]. For single-site donor–acceptor interactions (*e.g.* Walden inversion, Fig. 4.23) where the rate-determining step involves a formal transfer of electrons from one of the reagents to the other and the interaction of only one atom of each of the reagents (A*D* and B*A*), the polarization energy is written as follows, *cf.* Section 1.3.3.

$$E_p = -\frac{q_A q_B}{R_{AB}\varepsilon} + 2\sum_{m(D)}^{occ}\sum_{n(A)}\frac{(c_{AD}^m c_{BA}^n \Delta\beta_{AB})^2}{E_m^* - E_n^*}. \tag{4.26}$$

Here q_A and q_B are the net charges on atoms A and B belonging to the reagent *D* (donor) and *A* (acceptor) and lying at a distance of R_{AB}; ε is the dielectric constant of the solvent; c_{AD}^m and c_{BA}^n are the atomic orbital coefficients of atoms A and B in molecular orbitals *m* of *D* and *n* of *A*; $\Delta\beta_{AB}$ is the change in resonance integral (which is proportional to the overlap integral) between the interacting orbitals of atoms A and B; E_m^* and E_n^* are quantities related to the energy of the molecular orbitals *m* and *n* of the isolated *D* and *A* molecules. Summation runs over occupied orbitals of *D* and unoccupied orbitals of *A*. Note that E_m^* and E_n^* cannot be calculated using *e.g.* the Hartree–Fock approximation

for some model system. Rather they are purely empirical quantities which are selected to reproduce experimental trends.

Not all terms in the sum of Eq. (4.26) are equally important. The energy difference in the denominator is the smallest, that is the relative importance of the corresponding term is the larger, the larger is E_m^* and the smaller is E_n^* (notice that these quantities are negative). The absolute value of the difference $|E_m^* - E_n^*|$, will be the smallest for $E_{m1}^* - E_{n1}^*$ pair (*cf.* Fig. 4.24). E_{m1}^* corresponds to the highest occupied molecular orbital (HOMO) of the donor and E_{n1}^* corresponds to the lowest unoccupied molecular orbital (LUMO) of the acceptor. Since $E_{\text{HOMO}}^* - E_{\text{LUMO}}^*$ is small other terms in the sum of Eq. (4.26) can be neglected:

$$E_p \approx -\frac{q_A q_B}{R_{AB}\varepsilon} + \frac{2\Delta\beta_{AB}^2}{E_{\text{HOMO}}^* - E_{\text{LUMO}}^*}(c_{AD}^{\text{HOMO}} c_{BA}^{\text{LUMO}})^2 . \tag{4.27}$$

Equation (4.27) consists of two terms, the first accounts for electrostatic the second for charge-transfer type interaction (*cf.* Eqs 4.17 and 4.19). Depending on the magnitude of the $\Delta = E_{\text{HOMO}}^* - E_{\text{LUMO}}^*$ difference, two limiting cases can be defined. If Δ is large the second term is negligible and the outcome depends only on the first electrostatic term. This type of reaction is called *charge controlled:* the interaction is favoured on those atoms which carry the largest opposite charges. As we have pointed out in Section 4.3.1 molecular electrostatic potential maps yield informations on charge controlled reactions. If Δ is small the second term gets more important and the reaction is called *orbital controlled.* The reaction outcome will be determined by the magnitude of AO coefficients in the HOMO and LUMO, c_{AD}^{HOMO} and c_{BA}^{LUMO}. These orbitals are often called *frontier orbitals* and the synonym for orbital controlled reactions is *frontier controlled.* $(c_{AD}^{\text{HOMO}})^2$ and $(c_{BA}^{\text{LUMO}})^2$ are *frontier electron densities* [421, 422]. Frontier orbitals play a key role in many molecular phenomena (*cf.* Sections 2.7–8) especially in chemical reactions [394, 419].

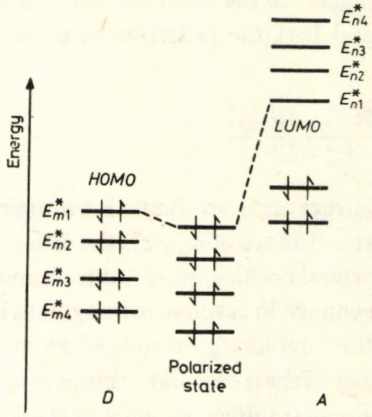


Fig. 4.24 HOMO-LUMO interaction for the polarized state

TABLE 4.8

Classification of acceptor and donor-type reagents after Klopman [714]. E^*_{LUMO} for acids and E^*_{HOMO} for bases is given in parentheses (in kJ/mol)

Character	Acids	Bases
Hard	Al^{3+} (580)	F^- (−1180)
	Mg^{2+} (233)	H_2O (−1030)
	Ca^{2+} (225)	HO^- (−1010)
	Fe^{3+} (214)	Cl^- (−960)
	Fe^{2+} (67)	Br^- (−890)
	Mn^{2+} (64)	
Intermediate	H^+ (41)	
	Cu^+ (−222)	CN^- (−850)
Soft	Ag^+ (−272)	HS^- (−830)
	Au^+ (−417)	I^- (−800)
	Hg^{2+} (−448)	H^- (−710)

TABLE 4.9

Reactivity sequence of donor molecules based on Eq. (4.27) and experimental evidence, respectively. k is the reaction rate constant in relative units.

Attack at peroxide oxygen		Attack at carbonyl carbon (acylation)	
Theoretical	Exp. $10^4 k$	Theoretical	Exp. k
HS^-	Very-fast	HO^-	890
I^-	6900	NC^-	10.8
NC^-	10	HS^-	–
Br^-	0.23	F^-	0.001
Cl^-	0.0011	Cl^-	Not reactive
HO^-	–	Br^-	
F^-	–	I^-	

TABLE 4.10

Substituent groups for electrophilic aromatic substitution

Ortho- or *para*-orienting	*Meta*-orienting
O^-, NR_2, NHR, NH_2, OH, OR, NHCOR, SR, OCOR, F, Cl, Br, I, SH	NR_3^+, NO_2, CN, CHO, COR, COOH, COOR, SO_3H, $CONH_2$, CCl_3, NH_3^+

Let us now discuss practical applications of Eq. (4.27). The concept of hard and soft acids and bases [1074] is well understood on the basis of the Klopman model. The hardness or softness of an acid or a base is determined by the magnitude and sign of E^*_{LUMO} and E^*_{HOMO}. These quantities were determined for a number of reagents by Klopman who applied some approximations [712]. Some selected values are given in Table 4.8. The theoretical classification corresponds, with some exceptions which are underlined, to the empirical one given by Pearson [1074]. According to the Klopman model reactions between hard acids and hard bases (large Δ) are charge controlled while interaction between soft acids and soft bases (small Δ) is frontier controlled. This theorem can be applied to some other reaction types, like electrophilic aromatic substitution, too.

A typical question which can be answered by the Klopman model, is the following: what are the relative rates of the reactions where different reagents attack the same atom in a molecule [714]. Table 4.9 gives rate constants for two prototype reactions. In the first the centre of attack is the oxygen atom of the peroxy moiety in peroxides which is a very soft acid ($E^*_{HOMO} = -670$ kJ/mol, *cf.* Table 4.8). Using Eq. (4.27) the nucleophilic order of various bases can be estimated [712]. As may be seen from Table 4.9 this nucleophilic order which decreases from above ($HS^- > I^- > NC^-$, etc.) runs parallel to the experimental rate constants. Soft bases (HS^-, I^-, etc. in Table 4.8) react most readily, while for hard bases the attack is unsuccessful. The second example in Table 4.9 is the attack on a carbonyl carbon atom (acylation). The corresponding compound is a hard acid ($E^*_{HOMO} = 96$ kJ/mol) therefore, the nucleophilic order changes essentially comparable with the attack on the soft peroxide oxygen. Hydroxyl and cyanide anions react readily while attack by the other bases is virtually unsuccessful.

The soft-soft and hard-hard acid-base affinity, first recognized by Pearson [1074], is also reflected in Table 4.9. HS^-, I^- and CN^- are soft bases and they react readily with the soft peroxide oxygen. Similarly, HO^- is a hard base; its attack on the hard carbonyl carbon is easy ($k = 890$). However, exceptions are also observed: the soft cyanide ion reacts much better than the hard F^- and Cl^- ions.

Another problem which can be handled by the Klopman model is the selection of preferred sites of attack by a given reagent in a given molecule. This selection is made by an appropriate reactivity index which is the atomic net charge for charge-controlled reactions and the frontier electron density for orbital-controlled reactions, respectively.

Let us discuss first charge-controlled electrophilic aromatic substitution (*e.g.* nitration of substituted benzene derivatives) [714]. Empirical orientation rules for this reaction have been known for a long time [871]. Substituents can be classified roughly in two groups (Table 4.10). Substituents of the first group are π-electron donating and they activate the benzene ring in the *o*- and *p*-positions. Substituents of group **2** are electron withdrawing and they inactivate the ring, the *m*-position the least. Therefore, nitration occurs primarily at *o*- and *p*-positions for group **1** substituents and at *m*-position for group **2** substituents. This observation is explained by the molecular charge distribution (Fig. 4.25). NH_2 which is a group **1** substituent deforms the charge

distribution of the benzene ring. *o*- and *p*-positions will be more negative and this means that these are activated with respect to an electrophilic attack. On the other hand, the least positive site in nitrobenzene is the *m*-carbon atom; here the reaction is least hindered.

The charge distribution on Fig. 4.25 was obtained by the simple Hückel method illustrating that this works also for some simple cases. However, it is advisable to consider the σ-skeleton, too. Therefore it is best to calculate the charge distribution by an all-valence semiempirical method (CNDO/2) or even by the *ab initio* method. In the latter case a minimal basis set (STO-3G) can also be applied. The simple model which is used to derive the above orientation rules works, in principle, only for *kinetically controlled* reactions where the reaction rate is determined by the barrier height. However, the case of *thermodynamic control* is also known where the reaction outcome

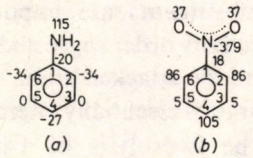


Fig. 4.25 Net π-charges for aniline and nitrobenzene (in millielectrons) as obtained by the simple Hückel method

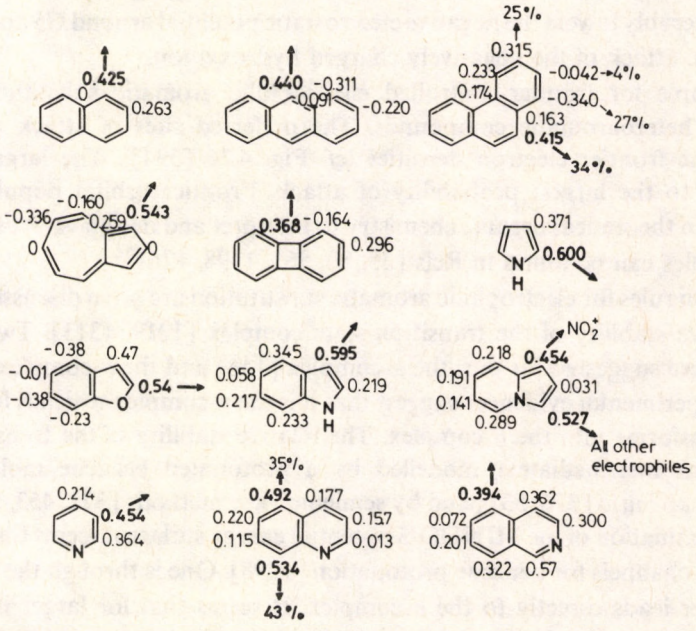


Fig. 4.26 Frontier electron populations of some aromatic compounds. Preferred sites of nitration are indicated by an arrow. (With permission from Ref. [394])

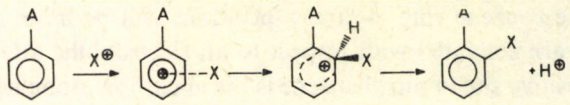


Fig. 4.27 Scheme of an electrophilic aromatic substitution reaction

depends on the relative energy content of the products [871]. For such reactions the orientation rules, inherent in the molecular charge distribution, are not necessarily correct. Therefore, if using net charges to obtain orientation rules, it is advisable to consider only atoms of the same type. Such types are, for example, unsubstituted sp^2 hybridized carbon atoms or unsubstituted sp^2 hybridized nitrogen atoms. This means that in Fig. 4.25 only the reactivity of C2, C3, C4, C5 and C6 can be compared.

Another type of exception is observed for compounds where through-space electrostatic field effects of substituents are important, *cf.* Section 4.3.1. These substituents may reverse the reactivity order suggested by the charge distribution since the electrostatic potential around the attacked atom, which is a more refined measure of the reactivity than the net charge, is essentially altered by the direct effect of a distant substituent. An example is the hydrolysis of 1-ethoxycarbonyl-3-phenylamino-maleimide [1258] where the net charges at carbonyl reaction centres 2 and 5 are 323 and 364 millielectrons, respectively. In spite of the smaller positive charge, hydroxyl attack takes place exclusively at C2. The breakdown of the charge distribution model is due to the through-space electrostatic effect of the carbonyl group at the 1 position which considerably lowers the negative electrostatic potential around C5 and therefore it hinders the attack of the negatively charged hydroxyl ion.

Our example for frontier-controlled electrophilic aromatic substitution is the nitration of heteroaromatic compounds. The preferred sites of attack are closely related to the frontier electron densities (*cf.* Fig. 4.26 [394]). The largest density corresponds to the largest probability of attack. Frontier orbital populations are widely used in theoretical organic chemistry to interpret and design various reactions. Some examples can be found in Refs [35, 80, 561, 1198, 1261].

Orientation rules for electrophilic aromatic substitution are often discussed in terms of the relative stability of the transition-state complex [1219, 1313]. Two types of structures were suggested for this: the π-complex [146] and the σ-complex [1414] *cf.* Fig. 4.27. Experimental evidences suggest that it is the π-complex which is formed first and this transforms into the σ-complex. The relative stability of the transition state complexes (or intermediates), modelled by a protonated benzene molecule, was estimated by *ab initio* [376, 531] and by semiempirical methods [321, 453, 538, 1298]. From an examination of the MINDO/3 potential energy surface it seems that there are two different channels for benzene protonation [1298]. One is through the π-complex and the other leads directly to the σ-complex. It seems that for larger interatomic distances the π-complex is the more stable; thus, the reaction course in Fig. 4.27 is confirmed. There are controversies as to whether the π-complex is a true intermediate

(corresponding to a local minimum on the potential surface) or it is a transition state (saddle point) for the intramolecular isomerization of the σ-complex.

The aromaticity of the σ-complex decreases if compared to the unperturbed benzene ring since, due to the extra ligand on the attacked carbon atom, sp^3 hybridization occurs and the delocalization is disturbed. The energy effect accompanying desaromatization can be estimated using the so-called atomic localization energy. This runs parallel to the energy content of the σ-complex which represents the polarized state in this case and consequently, parallel to the reactivity [1219, 1313]. Using localization energies, orientation rules can be derived for example, for condensed aromatic systems [276]. Unfortunately, this index can be used only for the discussion of aromatic reactivity.

As may be seen from Eq. (4.25), for a series of closely related reactions reactivity can be compared to thermodynamic stability. This is exploited in the *linear free energy relationships* (LFERs) which are widely used in organic chemistry and in medicinal chemistry [607]. The classical example is the *Brönsted equation* which relates the rate constants (k) and acid dissociation exponents (pK_a) of proton-transfer reactions [145].

$$\log \frac{k}{k_0} = \beta(pK_0 - pK_{a0}) \tag{4.28}$$

k_0 and pK_{a0} correspond to an appropriate reference reaction. Equation (4.28) can be applied, for example, to acid dissociation processes where its meaning is that strong acids dissociate fast while weak acids dissociate slowly.

A very important example for LFERs is the Hammett equation [841] which has several variants [871, 1358]. For the case of *m*- and *p*-disubstituted benzene derivatives, XC_6H_4Y, the following relationship holds for a reaction taking place at the Y group.

$$\log \frac{k}{k_0} = \rho\sigma_X . \tag{4.29}$$

Here k_0 and k are the rate constants for the unsubstituted case (X = H) and for the substituted case, respectively, σ_X characterizes the substituent; its value is different for the *meta*- and *para*-positions (*cf.* Table 4.11). ρ is equal, by definition, to unity for the dissociation of benzoic acids (Y = COOH). In other cases it is a parameter which is specific to the reaction under investigation. Relationships of the type of Eq. (4.29) are useful in predicting relative rates for a class of related processes. Some examples are

$$XC_6H_4COOMe + OH^- \rightarrow XC_6H_4COO^-$$

$$H_4CH_2Cl + I^- \rightarrow XC_6H_4CH_2I$$

$$XC_6H_4NH_2 + PhCOCl \rightarrow XC_6H_4NHCOPh$$

$$XC_6H_5 + NO_2^+ \rightarrow XC_6H_4NO_2 .$$

TABLE 4.11

Hammett σ parameters for some common groups [871] (Me = methyl, Ph = phenyl)

Group	*Para*	*Meta*
NH_2	−0.66	−0.16
NMe_2	−0.60	−0.21
O^-	−0.52	−0.71
OH	−0.36	−0.002
OMe	−0.27	0.12
CMe_3	−0.20	−0.12
Me	−0.17	−0.07
Ph	0.01	0.22
F	0.06	0.34
COO^-	0.13	0.10
Cl	0.23	0.37
Br	0.23	0.39
COOH	0.27	0.36
I	0.28	0.35
CHO	0.45	0.36
COMe	0.52	0.31
CN	0.63	0.68
NO_2	0.78	0.71
NMe_3^+	0.86	0.90
N_2^+	1.8	1.7

The original assumption in the Hammett equation that substituent effects are approximately independent of the reaction type has been confirmed by *ab initio* MO calculations, too [1390].

An especially important field of LFERs is in medicinal chemistry where quantitative relationships can be derived between chemical structure and biological activity [408, 507].

4.5 CONSERVATION OF ORBITAL SYMMETRY

Reactivity indices, as discussed in the previous section, yield informations primarily for reactions where the first elementary step is a single-site attack of a small reagent. Several processes are known, however, where this is certainly not the case. An example is the Diels–Alder reaction between a diene (butadiene) and a dienophile (ethylene) (Fig. 4.28). Here a synchronous attack of two reaction centres occur and it leads to the formation of two bonds simultaneously. Such reactions are called *concerted.* Fortunately, the Klopman equation (4.26) is applicable to these cases, too, and again frontier orbitals have an important role in determining the reaction outcome. It may be

seen in Fig. 4.29 that the HOMO of the diene and the LUMO of the dienophile match each other [419]. The same is true for the LUMO of the diene and the HOMO of the dienophile.

Woodward and Hoffmann [1436] and at the same time Longuet-Higgins and Abrahamson [810] derived simple rules which are based on the analysis of nodal properties of orbitals and which can be used to predict the outcome of a wide variety of concerted reactions (see Refs [394] and [1438] for reviews). The rules are derived from a simple postulate: *the conservation of orbital symmetry*. This was found by the analysis of a great number of organic reactions and by making use of quantum chemical concepts. Some other conditions which have to be fulfilled are postulated as follows [1438].

(1) The reaction course is determined by the frontier orbitals.

(2) Arrangement of atoms participating directly in the rearrangement is symmetric and at least one element (mirror plane or twofold axis) of this local symmetry is conserved during reaction.

(3) The magnitude of the barrier height is roughly determined by correlation diagrams which can be constructed on the basis of symmetry properties (*cf.* Section 1.3.3). The following rules have to be considered

— the bisector plane of the forming or scissile bond contains the conserving symmetry element;
— useful information can be obtained only if not all frontier MOs are symmetric or antisymmetric with respect to the symmetry operation in question;
— diagrams connecting energy levels of MOs of the same symmetry must not cross *(noncrossing rule)*.

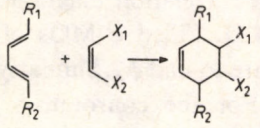


Fig. 4.28 Scheme of a Diels–Alder reaction

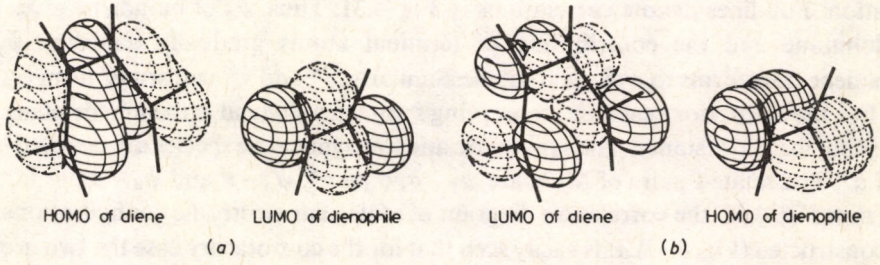


Fig. 4.29 The significance of orbital symmetry in the HOMO–LUMO overlap in Diels–Alder reactions. (With permission from Ref. [419])

Point 1 can be verified by the Klopman theory (Section 4.3.2). The symmetry requirement is rarely fulfilled exactly but the distortion is, in general, small; therefore, the conclusions are not essentially modified. More precisely: the real quasisymmetric case can be adequately represented by a fully symmetric model which reflects most important features correctly. Applicability of correlation diagrams will be illustrated on some examples.

Let us treat first the butadiene-cyclobutene transformation. This is a prototype of *electrocyclic reactions* [1436] where a σ bond is formed or broken between the ends of a

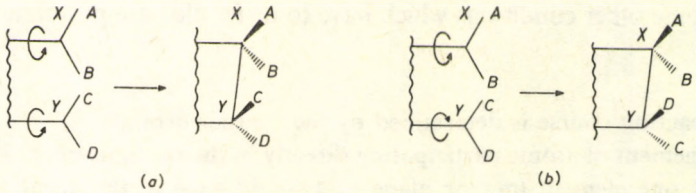


Fig. 4.30 Scheme of electrocyclic reaction paths. *(a)* Conrotatory *(b)* disrotatory

linear conjugated system. In our case (Fig. 4.30), the π-bond shifts to the central atoms of butadiene while the planes determined by the terminal atoms and attached substituents, A, B, C and D, rotate. It is supposed that formation of the σ-bond and rotation of the terminal planes take place synchronously. Two cases are possible. If the two planes, ABX and ABY, rotate in the same direction the reaction is called *conrotatory* (Fig. 4.30 *a*); in the opposite case it is called *disrotatory*, *cf.* Fig. 4.30 *b*. If substituents *A*, *B*, *C* and *D* are different the two reaction paths lead to different products (steroisomers).

Let us construct the orbital correlation diagrams. Schematic drawings and MO sequences are given in Fig. 4.31. Filled π MOs of butadiene are ψ_1 and ψ_2; the corresponding empty orbitals are ψ_3 and ψ_4. Similarly, for cyclobutene σ and π, σ^* and π^* orbitals are considered. For the conrotatory reaction path, the conserving symmetry element is a twofold rotation axis, C_2, which bisects the XY distance. MOs can be symmetric (species *a*) or antisymmetric (species *b*) with respect to twofold rotation. Full lines denote correlations in Fig. 4.31. Thus, ψ_2 of butadiene gives σ in cyclobutane and the contribution of terminal atoms gradually vanishes: ψ_1 of butadiene transforms to π of cyclobutene. Similarly, σ^* and π^* are formed from ψ_3 and ψ_4. For the disrotatory case, the conserving symmetry element is the mirror plane, C_v, bisecting the XY distance. The symmetric and antisymmetric species are denoted by a' and a''. The related pairs of MOs are $\psi_1-\sigma$, $\psi_2-\pi^*$, $\psi_3-\pi$ and $\psi_4-\sigma^*$.

From Fig. 4.31, the correlation diagram of molecular electronic configurations can be constructed (Fig. 4.32). It is easily seen that for the conrotatory case the two ground states are related, since ψ_1 and ψ_2 transform to π and σ, respectively. The $\psi_1^2\psi_2\psi_3$ configuration of butadiene corresponds to $\sigma\pi^2\sigma^*$ configuration of cyclobutene since ψ_3

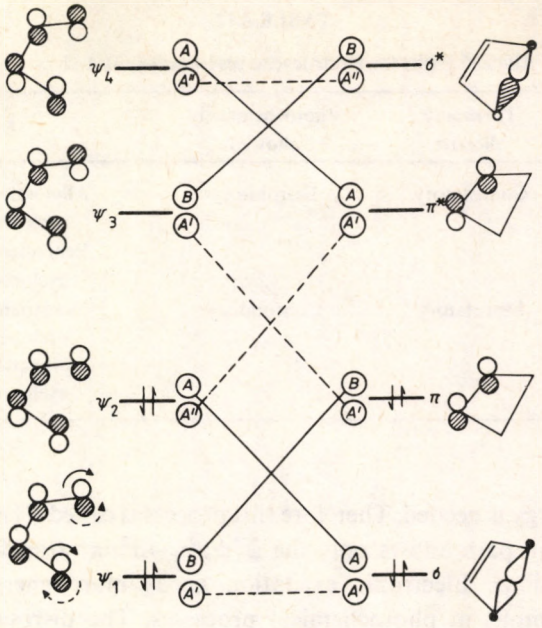


Fig. 4.31 Correlation diagram for the MOs of butadiene and cyclobutene. Full and dashed lines correspond to conrotatory and disrotatory reaction paths, respectively. Negative MO regions are shaded

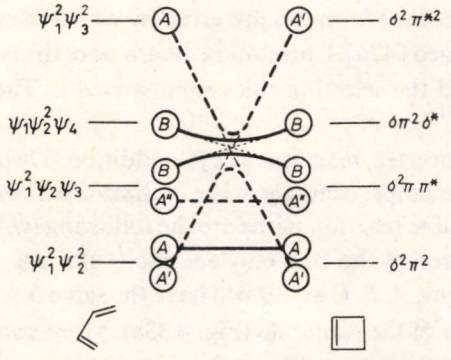


Fig. 4.32 Correlation diagram for the ground and some lower excited states of butadiene and cyclobutene. Full and dashed lines correspond to conrotatory and disrotatory reaction paths, respectively

gives σ^* during the change of geometry of the system. Similarly, configurations $\psi_1\psi_2^2\psi_4$ and $\sigma^2\pi\pi^*$ correspond to each other. According to the noncrossing rule only transformations $\psi_1^2\psi_2\psi_3 \rightarrow \sigma^2\pi\pi^*$ and $\psi_1\psi_2^2\psi_4 \rightarrow \sigma\pi^2\sigma^*$ are possible. In these cases so-called "avoided crossings" take place for which activation energies are large so the probability of the transformation is low (symmetry forbidden case). No avoided crossing is present for the $\psi_1^2\psi_2^2 \rightarrow \sigma^2\pi^2$ transformation, so its activation energy is considerably smaller (symmetry allowed case). Activation can take place by heat where

TABLE 4.12

Allowed paths for electrocyclic reactions ($n=0, 1, 2, \ldots$)

Number of π-electrons	Thermally allowed	Photochemically allowed	Examples
$4n$	Conrotatory	Disrotatory	Allyl anion→ cyclopropyl anion Pentadiene cation→ cyclopentene cation
$4n+2$	Disrotatory	Conrotatory	Hexatriene→ cyclohexadiene Allyl cation→ cyclopropyl cation

relatively little energy is needed. Therefore this process is called *thermally allowed*. The disrotatory reaction path allows only the $\psi_1^2\psi_2\psi_3 \rightarrow \sigma^2\pi\pi^*$ transformation between excited configurations. Electronic excitation needs more energy which can be absorbed, for example, in photochemical processes. The disrotatory path is thus *photochemically allowed* in the present case.

The above rules which allow us to select probable reaction paths for the butadiene →cyclobutene reaction can be derived for the general case, too. Based on the simple Hückel theory mathematical formulas are given by which the symmetry properties of π-orbitals can be analyzed [476]. Correlation diagrams of the type of Figs 4.31 and 4.32 can be constructed and the selection rules summarized in Table 4.12 can be derived [1438].

Another class of concerted reactions is cycloaddition (Diels–Alder reaction). This will be discussed on the simple example of the cyclization of two ethylene molecules to give cyclobutane. Possible reaction paths are the following (*cf.* Fig. 4.33). The simplest case is where the planes of the two ethylene molecules are parallel to each other; therefore, all substituents, *A*, *B*, *C* and *D* will have the same orientation in cyclobutane: all lie on the same side of the molecule (Fig. 4.33*a*). More complicated, but possible, reaction paths are where one or more substituents get to the opposite side of the molecular plane (Figs 4.33 *b* and 4.33 *c*). The reaction path where the two points of concerted attack lie on the same side of the molecular plane is called *suprafacial* (*s*). If the attack takes place from opposite sides the path is called *antarafacial* (*a*). Various reaction paths are denoted by giving the number of π-electrons participating in the process and the type of approach. Thus the paths of Fig. 4.33 *a*, *b* and *c* are called $[2_s+2_s]$, $[2_s+2_a]$ and $[2_a+2_a]$ processes, respectively being suprafacial (*s*) and antarafacial (*a*) with respect to the two reactant molecules.

Correlation diagrams can be constructed or cycloaddition reactions, too. The procedure may be similar to that discussed for electrocyclic reactions (*cf.* Figs 4.31 and 4.32) but now we present a simplified version (Figs 4.34–4.36). We are going from the

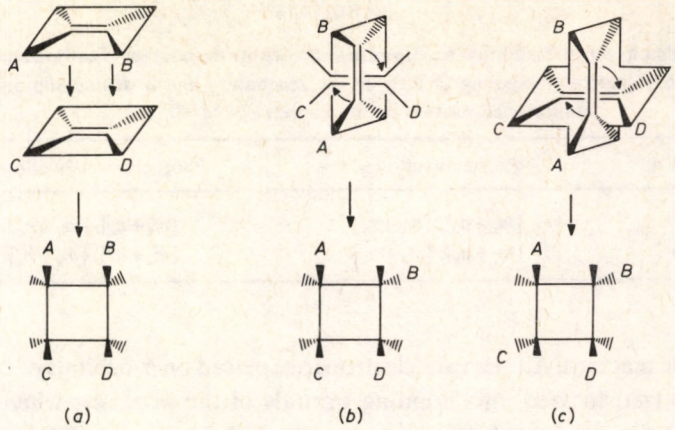


Fig. 4.33 Possible reaction paths for ethylene dimerization. *(a)* Suprafacial-suprafacial, *(b)* suprafacial-antarafacial, *(c)* antarafacial-antarafacial

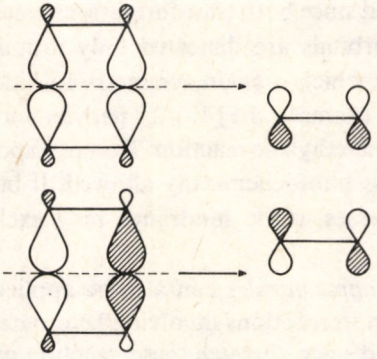


Fig. 4.34 Orbital pattern for the $[2_s+2_s]$ reaction

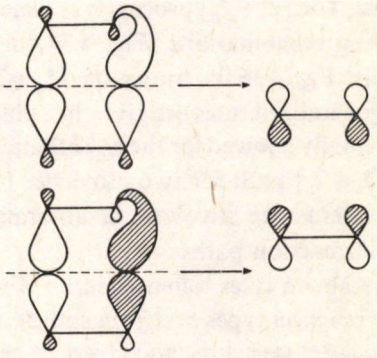


Fig. 4.35 Orbital pattern for the $[2_s+2_a]$ reaction

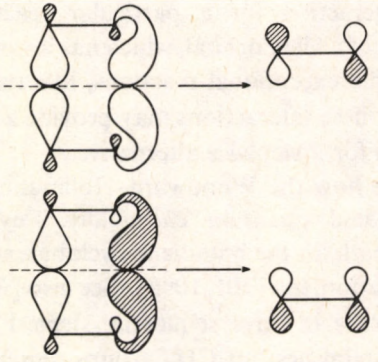


Fig. 4.36 Orbital pattern for the $[2_a+2_a]$ reaction

TABLE 4.13

Allowed paths for cycloaddition reactions. m and n denote the number of carbon atoms in the conjugated chain participating directly in the reaction. s and a denote suprafacial and antarafacial reaction paths, respectively. ($q=0, 1, 2, \ldots$)

$m+n$	Thermally allowed	Photochemically allowed
$4q$	$[m_s+n_a]$, $[m_a+n_s]$	$[m_s+n_s]$, $[m_a+n_a]$
$4q+2$	$[m_s+n_s]$, $[m_a+n_a]$	$[m_s+n_a]$, $[m_a+n_s]$

product to the reactant. All relevant electrons are placed on σ-orbitals of cyclobutane; if these can be transformed into bonding orbitals of the products when σ-bonds are broken with conservation of the symmetry the path is allowed. This transformation corresponds to the vanishing of the upper or lower half of the σ-orbital pattern in the figures to yield pure π-orbitals. The $[2_s+2_s]$ process is symmetry-forbidden (Fig. 4.34) because one transformation yields a bonding but the other an antibonding ethylene orbital. The $[2_s+2_a]$ process is symmetry-allowed since both transformations result in bonding combinations (Fig. 4.35 the atomic orbitals are distorted only formally). Finally, Fig. 4.36 illustrates the $[2_a+2_a]$ process which is again symmetry-forbidden. The generalized rules are given in Table 4.13. For example, the $[4_s+2_s]$ path ($m+n=6$) is thermally allowed for the hypothetical butadiene-ethylene reaction. The corresponding $[2_s+2_s]$ path for two ethylenes ($m+n=4$) is photochemically allowed. If bulky substituents are involved in antarafacial processes, steric hindrance may exclude certain reaction paths.

The above rules, often cited as *Woodward–Hoffmann rules* can also be applied to other reaction types and with sufficient care even to reactions involving heteroatoms. In the latter case, lone pairs have to be considered since, through these, reaction paths may be realized which cannot be derived from symmetry properties of the orbitals [1438]. An interesting exception to these rules is *subjacent orbital control* [92] where not only frontier orbitals are decisive in determining the allowed reaction path. Though the HOMO–LUMO interaction for a particular reaction is antibonding, the corresponding interaction of a filled orbital, which has lower energy than the HOMO, may be bonding. For some exceptional reactions, like rearrangement of *trans*-1,2-dipropenyl-cyclobutanes, these interactions may provide a lower energy path for the "forbidden" reaction than for a stepwise alternative.

The question may arise how the Woodward–Hoffmann rules are reflected in the potential surfaces calculated quantum chemically. Peyerimhoff and coworkers investigated the reaction path for the butadiene-cyclobutene transformation and they considered electron correlation, too [601, 1092]. (See also [Ref. 143]) They have found that the reaction takes place in three sequential steps. First the distance between terminal carbon atoms diminishes but CH_2 groups remain in the molecular plane. Second, the CH_2 planes rotate synchronously while the CC distance remains

practically constant. "Synchronous" means here that C_2 or C_v symmetry is conserved during the process. In the last stage of the reaction the bonding carbon atoms approach each other till the cyclobutene molecule has its final shape. Distinction between conrotatory and disrotatory paths has a meaning only in the second step of the reaction. Theoretical results are in accord with the Woodward–Hoffmann rules: the activation energy along the conrotatory path is lower by 59 kJ/mol than along the disrotatory one. The experimentally estimated difference is 42–63 kJ/mol.

The calculations of Peyerimhoff and coworkers indicate that the asynchronous reaction path is unfavoured. If the CH_2 planes are perpendicular to each other in the transition state, that is, the symmetry is distorted, the energy of the system gets considerably higher therefore this arrangement is improbable. Similarly, a concerted reaction path was predicted for the addition of water to formaldehyde [1426] and hydrogen fluoride to ethylene [677]. On the other hand, for the addition of BH_4^- on formaldehyde a mechanism with a nonsynchronous four-centre transition state is predicted [357]. This indicates that the reaction is a superposition of two steps, a hydride transfer from BH_4^- to formaldehyde and a BH_3 shift from this hydride to the carbonyl oxygen atom. It is interesting to note that the orbital symmetry rules predict the concerted process to be forbidden [1438]. Recently, Dewar stated that multibond reactions cannot normally be synchronous [308]. However, the idea is based on MNDO semiempirical calculations, so it needs further support.

4.6 ENVIRONMENTAL EFFECTS

In the previous sections we discussed chemical reactions by neglecting all interactions with the environment. This is permissible for gas-phase processes, but most reactions take place in solution. The effect of an apolar medium is sometimes negligible; but polar solvents, especially water, often play a key role in chemical reactions. In the last decade, several quantum chemical methods were developed which include environmental effects in a more-or-less approximate fashion, *cf.* Section 1.5. Using these techniques a considerable amount of work was done and our knowledge on more realistic models of chemical processes became deeper.

Before treating solvent effects explicitly some words should be devoted to the theoretical description of the liquid state, especially water [225, 1434]. Liquids are complicated systems which, in most cases, cannot be described solely in terms of isolated molecular species or associations. A "first principles" description is based on some adequate microscopic model which is introduced in one of the numerical approximation methods of statistical mechanics. The more complicated and computer-time consuming *molecular dynamics* method accounts, among other things for the time-dependent properties while the *Monte Carlo* method is a numerical scheme to evaluate averages of physical quantities.

Owing to the formidable mathematical complexity of the computational methods the approximation is introduced that the total intermolecular potential energy function of a liquid can be written as a sum of paired additive atomic terms [1434]. This assumption was extensively studied by quantum chemical calculations and it was found that three and four-body contributions to the potential energy are of about 10 % [704]. This is often negligible but there are cases where the error is of thermodynamic importance.

A useful quantity, the *pair correlation function*, can be defined which reflects the averaged and inhomogeneous structure of $N-1$ molecules in the external field of a fixed molecule. Note that this pair correlation function has no direct relation to the electron correlation (*cf.* Section 1.2). To discuss the equilibrium structure of a liquid it is often more useful to define a set of internuclear pair correlation functions, $g_{AB}(r)$, where r is the distance between nuclear species A on one molecule and B on another molecule. $\rho_A \rho_B g_{AB}(r)\, d\mathbf{r}_A\, d\mathbf{r}_B$ is the probability that different volume elements $d\mathbf{r}_A$ and $d\mathbf{r}_B$, separated by a distance r, simultaneously and respectively contain nuclear species of A and B for distinct molecules. ρ_A and ρ_B are the densities of the respective species in the whole assembly.

Clementi and his coworkers did extensive Hartree–Fock calculations at the *ab initio* level to find a reliable interaction potential for water [255]. In an attempt to improve the fidelity of the model Lie and Clementi applied dispersion force corrections. Using their improved potential they performed a Monte Carlo calculation on 343 water molecules [788]. The pair correlation functions, obtained by them are depicted in Fig. 4.37. The theoretical result is compared with data obtained from X-ray scattering and it is seen that good agreement is achieved.

Internuclear pair correlation functions of Fig. 4.37 have maxima. These correspond to partly ordered hydrogen-bonded domains in the liquid. The first sharp maximum on the g_{OO} curve is at 270 pm. This is close to the O...O distance in hydrogen-bonded water dimers indicating that a *hydration shell* is formed around each water molecule in the liquid phase (*cf.* Fig. 4.38). The hydrogen-bonded ensemble is ordered in a

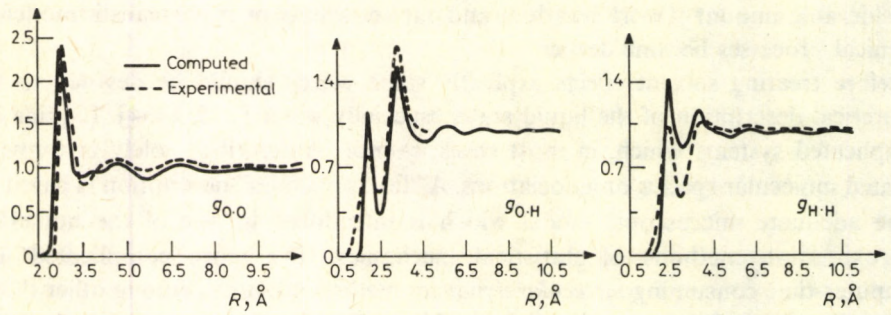


Fig. 4.37 The pair correlation functions obtained in a Monte Carlo calculation on 343 water molecules using an improved Hartree–Fock potential and the dispersion interaction. $T=25\,°C$, $\rho=1$ gcm^{-3}. Experimental results are obtained from X-ray scattering. (With permission from Ref. [788])

quasitetrahedral structure. The validity of the model of Fig. 4.38 is reflected in the calculated average number of neighbouring oxygens within the distance corresponding to the first peak of the g_{OO} curve which is about four. If we go farther from the central molecule the ordered structure is destroyed, the second hydration shell is much less recognizable than the first one. This is reflected on g_{OO} in Fig. 4.37. Further maxima are much smaller, indicating that ordering occurs only in small domains.

Now that we have some impression of the structure of water in the liquid phase let us turn to the solvation phenomena. The simplest systems where this can be studied are dilute aqueous solutions of Li^+, Na^+, K^+, F^-, Cl^-, etc. [226, 705, 901, 1153]. The environment of a solvated ion is divided into three regions labelled *A*, *B* and *C* [406].

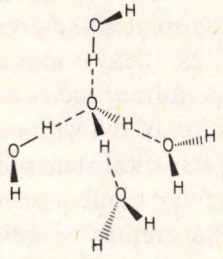


Fig. 4.38 First hydration shell of a water molecule

Region *A* is generally identified with the first hydration shell while region *C* is bulk water which is the same as in the pure liquid. The nature and extent of region *B* is not well understood yet; this interfaces regions *A* and *C*. Informations concerning region *B* may be obtained by Monte Carlo or molecular dynamics calculations.

Mezei and Beveridge used *ab initio* potential functions obtained by Clementi and coworkers [226, 705] in their Monte Carlo studies on ion hydration [901]. They could compare their results with experiment and overall a fair agreement was achieved. The calculations yielded hydration numbers (number of water molecules within the first hydration shell). These are 5.97 ± 0.02, 5.96 ± 0.02 and 6.27 ± 0.25 for Li^+, Na^+ and K^+, respectively. This means that region *A* contains about 6 water molecules independently of the atomic number of the positive ion. In contrast, drastic changes are observed for F^- and Cl^- where hydration numbers are 4.09 ± 0.10 and 8.36 ± 0.17, respectively. Mezei and Beveridge defined effective ionic radii, which are obtained as the difference between the position of the first maximum of the ion-water pair distribution function and the effective water radius 138 pm. The values (in pm, experimental crystal radii in parentheses [1070]) are the following: Li^+ : 72 (60), Na^+ : 97 (95), K^+ : 133 (133), F^- : 122 (138), Cl^- : 187 (181). Based on the above studies it was possible to extract certain molecular structures which significantly contribute to the statistical ensemble, that is these can be used in nonstatistical calculations to estimate hydration energies. Of course, none of these structures are of exclusive importance but they are quite useful if considered with sufficient care.

Monte Carlo calculations yield useful information on the structure of hydration region *B* [198, 901]. For hydrated ions this region is less structured than bulk water (region *B* is structure breaking). However, apolar solutes, like methane, induce an ordered cage structure in the solvent: region *A* and region *B* gets also more structured [1328, 1329]. This phenomenon gives rise to the *hydrophobic effect*. Owing to the higher structuration, the entropy increases and the corresponding loss in the Gibbs free energy of solvation is not exceeded by the gain in solvation energy which is very small for polar-apolar interactions. As a result, apolar solutes readily associate in aqueous solution since the overall size of the standard hydration region decreases; this results in a relative entropy decrease which will be the decisive term in the Gibbs free energy expression. This is why such association processes are called *entropy-driven.*

Hydration of more complicated solutes like organic molecules [91, 248, 273, 835, 1146] and biomacromolecules [228, 1068] is also studied by Monte Carlo methods. Beveridge and coworkers [895] performed such a calculation for glyoxal $(HCO)_2$ and they characterized the coordination of the various atoms. For oxygen, the average coordination number is 2.3. The statistical state solvation sites are localized into two specific regions which correspond to the solute-solvent hydrogen bonds involving the carbonyl oxygen lone pairs. The average coordination numbers for carbon and hydrogen are 0.73 and 5.78, respectively. In the first case, the solvation sites are localized above and below the molecular plane and correspond to the interaction of

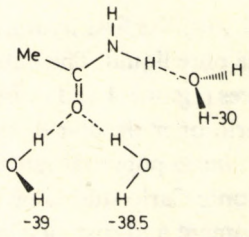


Fig. 4.39 First hydration shell of acetamide. Binding energies are given in kJ/mol

water molecules with the π-system of the carbonyl group. For the hydrogen atom the hydration is of hydrophobic nature: the statistical state solvation site is broad and diffuse in character.

Owing to the formidable numerical difficulties hydration is mostly studied at a nonstatistical level using *ab initio* or semiempirical methods [273, 581, 983]. An example for such calculations, hydration of acetamide, is depicted in Fig. 4.39. Three water molecules belong to the first hydration shell: two lie in the plane of the solute, while the third is twisted. It is interesting that the amino group is able to bind only one water molecule. Its second hydrogen atom binds water so loosely that this is not depicted in the Figure. The possible reason for this is the unfavourable steric effect of the methyl group.

It is a puzzling fact that in polar liquids separation of positively and negatively charged pointlike ions from 400 pm to infinity costs practically no energy. This problem was studied by Warshel using his "surface constrained soft sphere dipoles" model for the treatment of solvation effects [1401]. He has found that the forces created by a small increase of charge separation can be compensated by a small reorientation and compression of the solvent molecules without significant change in the total energy of the system. Furthermore, it seems that the reason that the dielectric constant in Coulomb's law works on a microscopic scale is not that the solvent molecules can be considered a continuum but rather the solvent has sufficient degrees of freedom to compensate for any change in charge–charge interactions by rearrangement.

Hydration considerably influences the acidity and basicity of different species as compared to the gas phase. This is illustrated by the protonation of carboxylate and imidazole [983]. Protonation energies of $HCOO^-$ and $C_3H_4N_2$ as calculated by the *ab initio* SCF method with a 4-31G basis set are 1487 and 1028 kJ/mol, respectively, that is, formic acid is much less "acidic" in the gas phase than the imidazolium cation. Experimentally measured and estimated values are 1430 and 920 kJ/mol, respectively. On the other hand, in aqueous solution formic acid is more acidic than imidazolium cation, tne pK of the former being smaller. The drastic change in the proton binding ability is due to hydration. The protonation process is modeled by the following equations (*cf.* Fig. 4.40)

$$HCOO^- . 3H_2O + H^+ . nH_2O \rightleftharpoons HCOOH . 3H_2O + nH_2O$$

$$C_3H_4N_2 . 5H_2O + H^+ . nH_2O \rightleftharpoons C_3H_5N_2^+ . 5H_2O + nH_2O .$$

Water-solute interaction energies were calculated using a point-charge model of the solute and the electrostatic potential of the solvation shell of Fig. 4.40. Hydration stabilizes formate and imidazolium much more than the neutral forms; thus, the difference in protonation energy becomes 53 kJ/mol, considerably less than the value found *in vacuo* (459 kJ/mol). Owing to the crude method of estimation of hydration energies the sign of the protonation energy difference does not change (this would correspond to the stronger acidity of formic acid in water) but the trend is unequivocal.

Similar dramatic effect of hydration on proton transfer equilibria was found by gas-phase studies on primary amines [1046]. The first hydration shell was built up of three water molecules for the protonated form and three (model *A*), one (model *B*) or no (model *C*) water molecules for the neutral species. Using the *ab initio* SCF method with STO-3G minimal basis set the interaction energies were calculated and for all models a good agreement with experimental values was achieved. This supports the power of the present model to predict hydration effects. Furthermore, it seems that the number of water molecules in the first hydration shell of neutral amines is irrelevant in determining hydration energies. The maximum and mean differences between models *A*, *B* and *C* and experiment are only 10 kJ/mol and 3 kJ/mol for the investigated species, respectively.

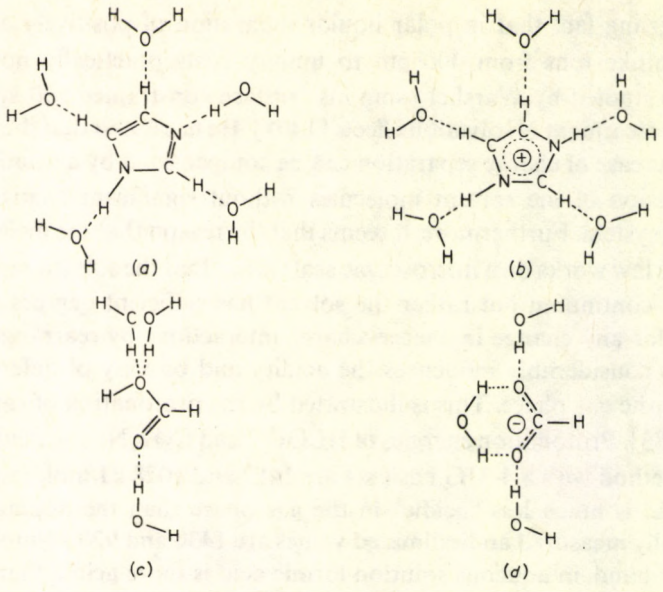


Fig. 4.40 Molecular model of hydrated *(a)* imidazole, *(b)* imidazolium ion, *(c)* formic acid, *(d)* formate ion

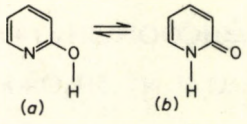


Fig. 4.41 The lactim (A)⇌lactam (B) tautomerization for 2-oxopyridine

Tautomeric equilibria, like that of 2-oxopyridine are often strongly solvent dependent [248, 273]. For the reaction shown on Fig. 4.41 the tautomeric ratio, K_{AB} = [concentration of species A]/[concentration of species B] changes by about three orders of magnitude and the stabilization energy of the lactam (B) form upon solvation is estimated to be higher than that of the lactim (A) form by about 17 kJ/mol. Monte Carlo studies using an empirical atom-atom potential function could reproduce this trend correctly even if a relatively crude model of hydration was used. To go further, an even simpler approach using semiempirically calculated electrostatic potentials predicted the same trend [581] indicating that hydration effects, in the present case, are primarily of electrostatic nature. It seems that the estimation of the influence of the solvent on the tautomeric equilibrium is less approximate in the present case than the direct prediction of the tautomeric constants in the vapour phase. We have pointed out in Section 4.1 that this latter is a tricky task.

Polar solvents, especially water, often play a key role in determining chemical reaction rates. In the simplest cases, the solvent as a polarizable dielectrics stabilizes the

(polar) transition state relative to the initial and final products of the reaction. Such an effect was found by Tomasi and coworkers who investigated the mechanism of carbonyl reduction by $LiBH_4$ *in vacuo* [120] and with inclusion of solvent (diethylether) [118]. The reduction of the barrier height was calculated to be 91 kJ/mol.

An extensively studied case is the proton transfer reaction between ammonia and hydrogen fluoride [27, 726, 907, 1024]

$$NH_3 + HF \rightarrow NH_4^+ + F^- .$$

In the gas phase, only the neutral form exists; the ion pair is marked on the proton transfer potential curve solely by a shoulder. On the other hand, in aqueous solution

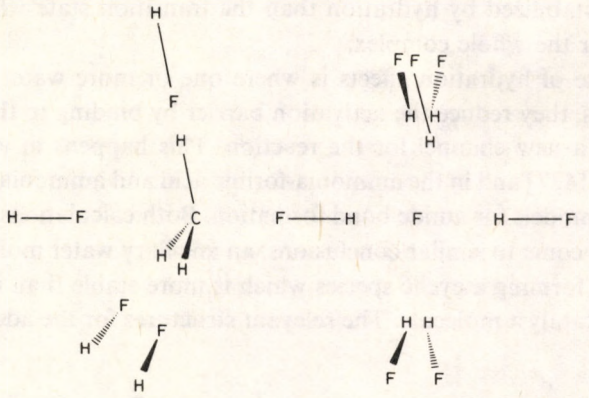


Fig. 4.42 Geometry of the solvated ion-molecule pair for the dissociation of fluormethane

both neutral and ion-pair forms may be present as stable species. This prediction is virtually independent of the method applied to consider the effect of hydration. However, a more refined method (*ab initio* SCF with 4-31G basis set) is needed if the experimentally observed stabilization of the ion-pair form is to be reproduced [726].

Kollman and Kuntz have found in the same study that solvent separated ion pairs become competitive with the contact ion pairs as more water molecules than four are added to the system. Existence of solvent (water and hydrogen fluoride) separated ion pairs for the dissociation of fluormethane was pointed out by Simonetta and coworkers [264, 302] using CNDO/2 supermolecule calculations. The structure where just one HF molecule separates the solvated CH^+ and F^- ions is depicted in Fig. 4.42. Comparing the solvents, it was found that the structure of dissociated ions and molecules is more affected by water than by hydrogen fluoride though their dielectric constants are about the same. On the other hand, the dissociation proceeding through single-solvent and double-solvent separated ion pairs as stable intermediates is quite similar in both solvents. Dissociation in methane, a solvent with very low dielectric constant, goes without the formation of intermediates [303].

There are cases where the effect of solvent is not to decrease but to increase the reaction barrier height. It was found experimentally that the S_N2 nucleophilic substitution reaction proceeds up to 20 orders of magnitude faster in the gas phase than in solution. Morokuma studied this phenomenon theoretically on the following model [932]

$$Cl^-(H_2O)_n + CH_3Cl \rightarrow ClCH_3 + Cl^-(H_2O)_n .$$

Using the *ab initio* SCF method with a 3-21G basis set he optimized relevant equilibrium and transition state geometries. Theory was able to give an explanation to the experimental finding: the energy barrier along the reaction path considerably increases upon hydration. The reason for this is that the ionic reactant and product are more strongly stabilized by hydration than the transition state where the charge is delocalized over the whole complex.

A special case of hydration effects is where one or more water molecules act as catalysts, that is, they reduce the activation barrier by binding to the transition state and thus open a new channel for the reaction. This happens in water addition on formaldehyde [1427] and in the ammonia-formic acid and ammonia-glycine reactions [1040], simple models for amide bond formation. Both calculations consider entropy effects and they come to similar conclusions: an ancillary water molecule binds to the transition state forming a cyclic species which is more stable than it would be in the absence of the catalyst molecule. The relevant structures for the addition of water on

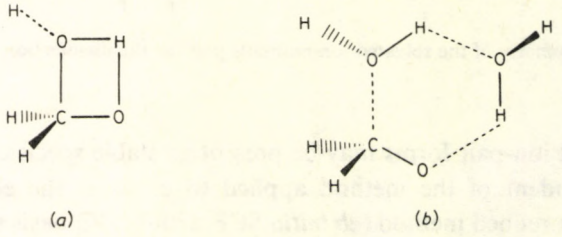


Fig. 4.43 Monohydrated *(a)* and dihydrated *(b)* transition-state structures for the addition of water on formaldehyde

formaldehyde are depicted in Fig. 4.43. Formation of structure *b* is entropically unfavourable but the extremely favourable enthalpy change leads to an overall reduction of the Gibbs free energy of the transition state by 113 kJ/mol.

A special case of environmental effects is observed in biomacromolecules (proteins, ribonucleic acids, etc.). Their function is often modelled by small systems which mimic the most important region (*e.g.* catalytic machinery in enzymes) of the whole system. An example is given in Section 4.4.1 and in Fig. 4.19 showing that most important features of amide or ester hydrolysis by serine proteinases can be understood using a model constructed of some small molecules. However, often important and sometimes

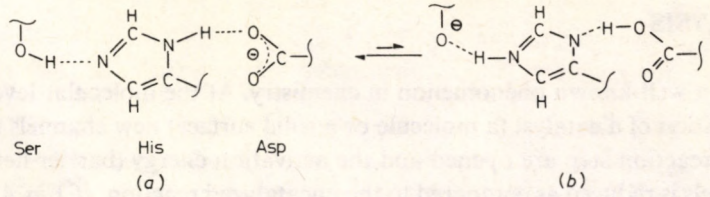


Fig. 4.44 Schematic representation of the catalytic triad in serine proteases. *(a)* unperturbed form, *(b)* hypothetical activated form

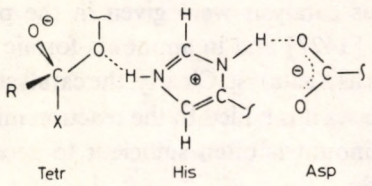


Fig. 4.45 Schematic representation of the tetrahedral intermediate (Tetr) in serine proteinases. X = NHR′ or OR′

decisive, effects are observed which originate from the macromolecular environment. These effects are mostly electrostatic in nature so they can be studied relatively easily by theoretical methods [980]. The first calculations were published by Warshel and Levitt [1403] and by Hayes and Kollman [524]; these were followed by several other studies [339, 983, 1345].

Let us discuss now the Asp-His proton transfer in serine proteinases (Fig. 4.44). Based on X-ray crystallographic, nuclear magnetic resonance and other experimental studies it was thought for a long time that upon perturbation by the substrate the Ser-His-Asp catalytic triad of these enzymes undergoes a double proton-transfer (charge relay) and the aspartate side chain is the ultimate proton acceptor. Later experiments, followed by theoretical calculations, have shown that the proton does not transfer from His to Asp during the reaction instead a $(- + -)$ pattern is formed, *cf.* Fig. 4.45. This contradicts classical chemical evidence suggesting that in an apolar medium a neutral diad would be favoured over an ion pair. However, the protein environment cannot be considered in the present case as an apolar medium. In contrast, a strong electrostatic field exists, both inside and in the vicinity of proteins, which is produced by α-helices [339] or by charged or polar side chains. The theoretically estimated His-Asp proton transfer energy is 15–101 kJ/mol in the gas phase but this is drastically lowered (by -116 kJ/mol) to a value between -101 and -15 kJ/mol in the protein [983], *i.e.* the proton is located on the His side chain. The special importance of theoretical studies on such problems [339, 983, 1345] is to call attention to the limitations of biomimetic chemistry, the discipline where biomacromulecular processes are studied on small models.

4.7 CATALYSIS

Catalysis is a well-known phenomenon in chemistry. At the molecular level it means that on addition of a catalyst (a molecule or a solid surface) new channels for a given elementary reaction step are opened and the activation energy (barrier height) along these channels is reduced as compared to the uncatalyzed reaction, *cf.* Fig. 4.46 [1448]. In *homogeneous catalysis* the catalyst, reactants and products are in the same (commonly liquid) phase while in *heterogeneous catalysis* the catalytic process takes place at boundary surfaces (commonly gas/solid or liquid/solid). Some preliminary examples for homogeneous catalysis were given in the previous section. In water addition on formaldehyde [1427] and in ammonia-formic acid reactions [1040] the solvent water molecule acts as a catalyst. Clearly, the catalyst does not necessarily come from the solvent; in most cases it is added to the reaction mixture. Since it regenerates during reaction a small amount is often sufficient to accelerate some reactions by several orders of magnitude.

Activation of carbon dioxide towards hydration by binding ammonium cations has been discussed by Jean and Volatron [639]. The process with a single NH_4^+ ion as a catalyst yielding H_2CO_3 is schematically depicted in Fig. 4.47. The barrier height of the

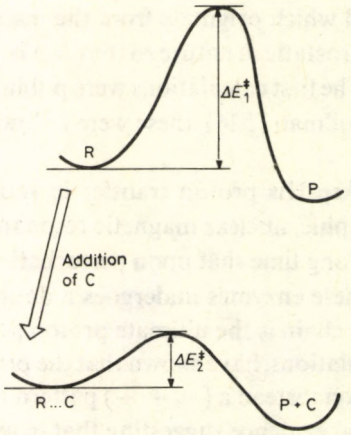


Fig. 4.46 Schematic plot of a catalytic pathway. R = reactant, P = product, C = catalyst. $\Delta E_2^{\ddagger} < \Delta E_1^{\ddagger}$

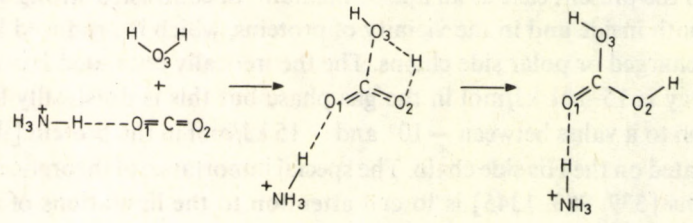


Fig. 4.47 Schematic representation of the reaction path for the $[CO_2, NH_4^+] + H_2O \rightarrow [H_2CO_3, NH_4^+]$ reaction

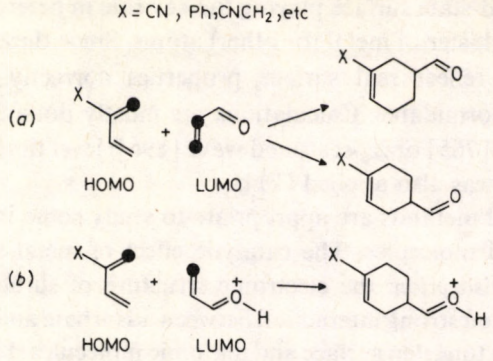


Fig. 4.48 Possible reactions between 2-substituted butadiene and acrolein. *(a)* without catalyst, *(b)* in the presence of a Lewis acid (*e.g.* proton). Area of full squares is proportional to the frontier electron density

reaction as calculated by the *ab initio* SCF method using an STO-3G basis set decreases from 222 kJ/mol to 194 kJ/mol and to 146 kJ/mol upon binding one and two ammonium cations, respectively. Further examples of quantum chemical studies on homogeneous catalysis are found in Refs [93] and [1004].

Investigating catalytic stabilization of transition states it is not always imperative to calculate the whole reaction path quantitatively. This is shown on the Diels–Alder reaction between 2-substituted butadiene and acrolein as discussed by Houk and Strozier [595, 596]. Under ordinary conditions two products may be formed (*cf.* Fig. 4.48). However, in the presence of Lewis acids (modelled here by a bare proton) almost exclusively the *para* isomer is formed. Houk [595] applied the frontier orbital theory (*cf.* Section 4.4.2) and postulated that the stability of the transition-state complex is determined by the interaction between the diene HOMO and dienophile LUMO. Stronger interaction means a stabilization of the transition state relative to the reactants and products. Furthermore, it is predicted that bonds are formed between atoms having the largest frontier electron densities. In the uncatalyzed case, LUMO coefficients of reacting carbon atoms in acrolein are about the same: both isomers are formed with the same probability. However, if acrolein is protonated at the only possible site, the oxygen atom, the LUMO coefficient on the terminal carbon atom gets much larger than on the neighbouring one. Consequently, almost exclusively the *para* isomer is formed. The qualitative considerations of Houk were also confirmed by numerical calculations [622].

It is known that transition-metal complexes act as good catalysts. They form loose bonds with several molecules and the arising structures may serve as reactive intermediates in various reactions. Thus, a theoretical treatment of specific transition-metal complex structures provides useful information on a variety of catalytic processes, too [78, 283, 1031, 1208, 1217].

To understand heterogeneous catalysis in detail, methods of solid-state physics are needed. Though these are beyond the scope of our book some simple results are

presented here. A solid-state surface playing the key role in heterogeneous catalysis is often modelled by a cluster of metal (or other) atoms. Since these clusters have to be sufficiently large to reflect real surface properties correctly the computational difficulties are often formidable. Calculations are mostly done at the semiempirical (EHT [21], CNDO/2 [765] or X_α-scattered wave [896]) level though for simpler cases the *ab initio* method was also applied [71].

Even semiempirical methods are appropriate to study some important features of clusters and attached molecules. The catalytic effect of metal surfaces is mostly a consequence of *chemisorption*: the electronic structure of surface-bound molecules considerably changes on strong interaction between adsorbate and adsorbent (surface). Interaction between a tungsten surface and diatomic molecules (Li_2, B_2, C_2, N_2, O_2, F_2, CO, NO) was studied by Anderson and Hoffmann using the EHT method [21]. They have detected a charge transfer from the adsorbate to the surface for Li_2 and in the reverse direction for B_2, C_2, N_2, O_2 and F_2. The overlap populations in the bonds of Li_2 and F_2 are negative, indicating that the bonds break on the surface. Bonds get weaker for C_2, N_2, CO and O_2 molecules while the bond order becomes larger for B_2. This means that the BB link becomes stronger upon adsorption, that is, the catalytic activity is absent. Simultaneously with bond weakening, a relatively strong interaction occurs between B_2, C_2, N_2 and O_2 and the surface. On the other hand, the interaction with Li_2 and F_2 is negligible it is slightly repulsive.

Anderson and Hoffmann did calculations on the homogeneity of the surface, too. Owing to the close packing (*cf.* Fig. 4.49), *d*-orbitals of tungsten atoms almost completely fill the surface. Therefore, interaction between the surface and the adsorbate

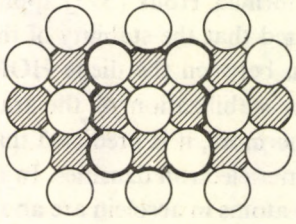


Fig. 4.49 Model of the surface of tungsten metal. Shaded atoms lie under the uppermost plane of empty atoms. The cluster treated in the theoretical study is indicated by a heavy line

is almost independent of the orientation of the latter. Calculations on various cluster models have shown that steps and corners of the surface are considerably more active in chemisorption than other parts of the surface since here a large amount of negative charge is concentrated. This is why these special sites attract electrophilic molecules like N_2 strongly.

The Fischer–Tropsch reaction between CO and H_2 was studied by an extended muffin–tin orbital theory [676]. Analyzing bond strengths, Kasowski and Caruthers pointed out that CO molecules disproportionate at the surface and one of the following

processes take place

$$CO(adsorbed)+CO(gas)\rightarrow CO_2+C$$

$$2CO(adsorbed)\rightarrow CO_2+C.$$

The carbon atom reacts with two hydrogen molecules to yield methane. Another possible reaction path is the formation of formaldehyde from H_2+CO and a subsequent decomposition of H_2CO into H_2C+O. H_2C gives methane with an additional hydrogen molecule

$$2H+CO\rightarrow H_2CO$$

$$H_2CO\rightarrow H_2C+O$$

$$H_2C+H_2\rightarrow CH_4.$$

The theoretical propositions are in accord with experimental facts.

Based on theoretical calculations, Lundqvist gave a scenario for the catalytic decomposition of H_2 on a magnesium surface (*cf.* Fig. 4.50) [836]. When a slow hydrogen molecule hits the surface it meets a repulsive potential barrier and no reaction occurs. However, for hot molecules with large incident kinetic energy the

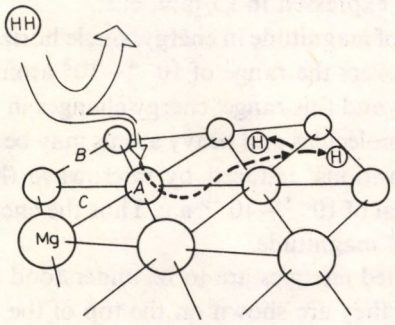


Fig. 4.50 Schematic plot of the approach of a hydrogen molecule to a magnesium surface. Atop *(A)*, bridge *(B)* and centre *(C)* sites are indicated. The dashed curve represents a possible path of the molecule for the dissociation

barrier is surmountable and the molecule penetrates a few hundreds of pm deeper into the surface. A trapped molecule may perform oscillations on the surface though vibrations are effectively damped. At the same time the adsorbed molecule is almost free to slide along the surface in a shallow potential well. The bound molecule dissociates into two hydrogen atoms which remain adsorbed on the surface. The individual hydrogen atoms are almost free to migrate along the surface, however, avoiding atom (*A* in Fig. 4.50) sites and sites earlier occupied by hydrogen atoms.

Further theoretical studies on chemisorption are summarized in Refs [1215, 1276 and 1377].

APPENDIX

A.1 ENERGETICS IN THE WORLD OF MOLECULES

This appendix gives a quantum chemical view of energetic relations of different physical quantities, some important molecular properties and related experimental methods in atomic and molecular physics. For this purpose, Table A1 presents selected sample molecules, ordered vertically in a logarithmic energy scale. Different columns correspond to different molecular or atomic properties. At the left-hand side there is a nomogram comparing the most frequent energy scales. An energy unit represents the "natural unit" of the phenomenon under study if the values of the corresponding physical quantities have the order of magnitude of 1. For example, the energies of light atoms and small molecules are a few atomic units, thus the *hartree* is an appropriate energy unit for total energies. The lowest electronic excitation energies are in the order of magnitude of 1 eV, which serves as the usual unit in spectroscopy. The rotational barriers are conveniently expressed in kJ/mol, etc.

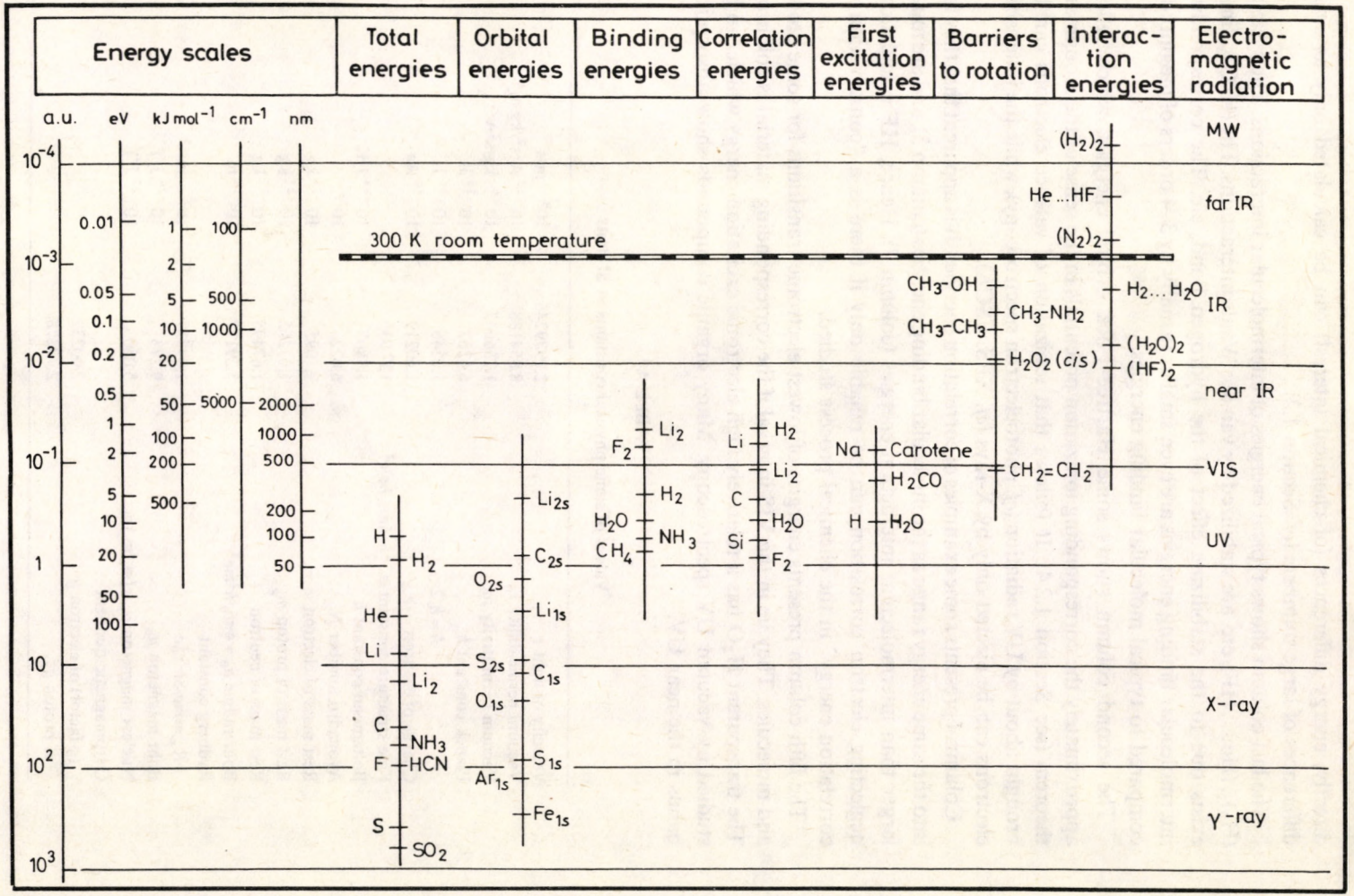
To separate the orders of magnitude in energy, single horizontal lines are used in the table. The energy scale covers the range of $10^{-4} - 10^{3}$ atomic units. There are some characteristic energies beyond this range: energy changes in Mössbauer spectroscopy or total energies of large molecules and heavy atoms may be as large as 10^{4} a.u., while the energies of spin transitions, induced by microwave (MW) or radio-frequency radiation, lie in the interval of $10^{-5} - 10^{-9}$ a.u. Thus the energetic world of molecules covers about 13 orders of magnitude.

The signs of the indicated energies are to be understood as follows. Free particles possess positive energies, they are shown on the top of the table. Bound states have negative energies (columns 1 and 2). Energy differences (columns 3, 5, 6, 7) are positive numbers according to the usual definition. The correlation energy (4th column) is always negative.

The usual classification of electromagnetic radiations which may interact with molecules is presented on the right hand side of the table. Here IR, VIS and UV stand for infrared, visible and ultraviolet radiations, respectively.

Let us now discuss briefly the different columns of Table A1. The first column shows the total energies of atoms (on the left) and molecules (on the right). The simplest is the hydrogen atom having the energy -0.5 a.u. Two H atoms form the H_2 molecule which possesses an energy slightly lower than -1.0 a.u. The difference is the binding energy which is shown in the third column. It is fortuitous that the molecular binding energies are less by at least one (and usually several) orders of magnitude than the corresponding total energies. Since in quantum chemistry total energies are computed

TABLE A1


Energy scales
Total energies
Orbital energies
Binding energies
Correlation energies
First excitation energies
Barriers to rotation
Interaction energies
Electromagnetic radiation
a.u.
eV
kJ mol⁻¹
cm⁻¹
nm
10⁻⁴
10⁻³
10⁻²
10⁻¹
1
10
10²
10³
0.01
0.05
0.1
0.2
0.5
1
2
5
10
20
50
100
200
500
1
2
5
10
20
50
100
500
1000
5000
100
500
1000
2000
1000
500
200
100
50
300 K room temperature
MW
far IR
IR
near IR
VIS
UV
X-ray
γ-ray
(H2)2
He...HF
(N2)2
CH3-OH
CH3-CH3
CH3-NH2
H2...H2O
H2O2 (cis)
(H2O)2
(HF)2
CH2=CH2
Na
Carotene
H2CO
H
H2O
F2
Li2
H2
H2O
NH3
CH4
Li
H2
Li2
C
H2O
Si
F2
H
H2
He
Li
Li2
F
HCN
S
SO2
O2s
Li2s
C2s
Li1s
S2s
C1s
O1s
S1s
Ar1s
Fe1s

directly, energy differences (of chemical interest) can be calculated only as small differences of large numbers (*cf.* Section 1.2).

The last column shows typical energies of intermolecular interactions. The systems $(H_2)_2$, (He. . . HF), etc. are stabilized by van der Waals interactions. The $(H_2O)_2$ dimer exists due to the stabilizing effect of the hydrogen bond, etc. The corresponding intermolecular binding energies are even smaller (usually by 3–4 orders of magnitude) compared to typical molecular binding energies.

The second column shows some Hartree–Fock orbital energies, which reflect approximately the corresponding ionization potentials in the sense of the Koopmans theorem (see Section 1.2.4). It follows that ionization of valence electrons can be brought about by UV radiation (*cf.* photoelectron spectroscopy), while the inner shell electrons can be ejected only by X-rays (*cf.* XPS, ESCA).

Column 4 presents some examples of correlation energies. It is apparent that they fall into the same energy range as the molecular binding energies (column 3), and are much larger than intermolecular interaction energies (column 7). Hence, HF calculations neglecting electron correlation can be reliable only if there is a "conservation of correlation energy" in the chemical process studied.

The fifth column presents energies of lowest electronic transitions for some atoms and molecules. They lie in the VIS interval if the corresponding material is coloured. The transparent H_2O has a relatively high electronic excitation energy which can be studied by vacuum UV spectroscopy. Many organic compounds show absorption bands in the near UV.

TABLE A2

Values of some physical constants in SI units

Velocity of light c	2.9979246	10^8 m/s
Vacuum permeability ε_0	8.854188	10^{-12} $A^2s^2/kg\,m^3$
Vacuum permittivity μ_0	1.256637	10^{-6} kg/s^2A^2
Planck constant h	6.6262	10^{-34} Js
$\hbar = h/2\pi$	1.0546	10^{-34} Js
Charge of electron $-e$	1.60219	10^{-19} As
Fine structure constant $\alpha^{-1} = 4\pi\varepsilon_0 \hbar c/e^2$	137.036	
Boltzmann constant k	1.3807	10^{-23} J/K
Avogadro number N_A	6.022	10^{23}
Rest mass of electron m_e	9.1095	10^{-31} kg
Rest mass of proton m_p	1.67265	10^{-27} kg
Rest mass of neutron	1.67495	10^{-27} kg
Bohr radius $a_0 = 4\pi\varepsilon_0 \hbar^2 me^2$	5.29177	10^{-11} m
Rydberg constant		
$R_\infty = me/8h^3\varepsilon_0^2 c$	1.09737	10^7 m^{-1}
Bohr magneton μ_B	9.273	10^{-24} J/T
Nuclear magneton $\mu_n = (m_e/m_p)\mu_B$	5.050	10^{-27} J/T
Gyromagnetic quotient		
(g-factor) of electron g	2.00232	
of proton g_p	2.79278	

In the last but one column some typical values of rotational barriers are indicated. Barriers to rotations around single bonds are smaller by an order of magnitude than around double bonds. It seems that, for example, the ethylene ($H_2C{=}CH_2$) molecule cannot be rotated around the C=C axis without a significant change in its electronic structure, since the corresponding energy barrier is comparable with the typical electronic excitation energies.

Table A1 indicates also the energy kT at room temperature, 300 °K (the dashed horizontal line). Bound states having stabilization energies less than kT disappear due to thermal excitations (*cf.* the equipartition theorem of statistical physics). This means, in particular, that weak intermolecular interactions (last column) cannot be studied experimentally at room temperature. Degrees of freedom corresponding to rotations around single bonds (see column 6) can easily be activated at room temperature, since the energies of the relevant barriers are close to kT at 300 K. Under such conditions, methyl groups in molecules can rotate almost freely.

A.2 PHYSICAL CONSTANTS AND CONVERSION FACTORS

The values of the most important physical constants in SI units are presented in Table A2. Then Table A3 offers some help in converting physical quantities from the atomic units widely used in quantum chemistry (see Section 1.1) to SI or some conventional units. For the different units, the standard notations are used (K: kelvin, D: debye, T: tesla, G: gauss, etc.).

TABLE A3

Conversion factors between atomic and SI units. Some of the conventional units are also indicated

Quantity (one atomic unit)	SI unit	Conventional unit
Length (bohr, a_0)	$5.29177\ 10^{-11}$ m	0.529177 Å
Mass (m_e)	$9.1095\ 10^{-31}$ kg	
Time	$2.4189\ 10^{-17}$ s	
Charge (e)	$1.60219\ 10^{-19}$ C	
Energy (hartree	$4.559828\ 10^{-18}$ J	27.21165 eV
or rydberg)	2625.56 kJ/mol	627.104 kcal/mol
		$3.15787\ 10^5$ K
Linear momentum	$1.9929\ 10^{-24}$ kgm/s	
Angular momentum	$1.0546\ 10^{-34}$ kgm^2/s	
Force	$8.2389\ 10^{-8}$ N	$8.2389\ 10^{-3}$ dyn
Force constant	1.5569 N/m	15.5692 mdyn/Å
Electric field	$5.14226\ 10^{11}$ V/m	
Magnetic induction	$1.71527\ 10^3$ T	$1.71527\ 10^7$ G
Dipole moment	$8.4784\ 10^{-30}$ Cm	2.54177 D
Quadrupole moment	$4.4866\ 10^{-40}$ Cm^2	
Magnetic dipole moment	$2.5417\ 10^{-21}$ J/T	
Electric dipole polarizability	$1.48184\ 10^{-31}$ m^3	0.148184 Å^3

REFERENCES

1. D. B. Adams, *J. Electron Spectry.*, **9,** 251 (1976).
2. W. H. Adams, *J. Chem. Phys.*, **34,** 89 (1961); **37,** 2009 (1962); **42,** 4030 (1965).
3. W. H. Adams, *Chem. Phys. Lett.*, **11,** 71 (1971); **12,** 295 (1971).
4. W. H. Adams, *Phys. Rev. Lett.*, **32,** 1093 (1974).
5. W. H. Adams, *Int. J. Quant. Chem.*, **S9,** 367 (1975).
6. R. Ahlrichs and W. Kutzelnigg, *J. Chem. Phys.*, **48,** 1819 (1968).
7. K. Akagi, T. Yamabe, H. Kato, A Imamura and K. Fukui, *J. Am. Chem. Soc.*, **102,** 5157 (1980).

7a N. S. Akhmetov, *General and Inorganic Chemistry*, MIR, Moscow, 1983.

8. P. Albertsen, P. Jorgensen and D. L. Yeager, *Int. J. Quant. Chem. Symp.*, **14,** 249 (1980).
9. T. A. Albright and R. Hoffmann, *J. Am. Chem. Soc.*, **100,** 7736 (1978).
10. L. C. Allen, *J. Am. Chem. Soc.*, **97,** 6921 (1975).
11. N. L. Allinger, *Adv. Phys. Org. Chem.*, **13,** 1 (1976).
12. J. Almlöf and U. Wahlgren, *Theoret. Chim. Acta.* **28,** 161 (1973).
13. A. T. Amos and R. J. Crispin, *J. Chem. Phys.*, **63,** 1890 (1975).
14. A. T. Amos and R. J. Crispin in, *Theoretical Chemistry*, Vol. 2: *Advances and Perspectives* (Eds: H. Eyring and D. Henderson), Academic, New York, 1976.
15. A. T. Amos and H. G. F. Roberts, *J. Chem. Phys.*, **50,** 2376 (1969).
16. R. D. Amos, *Chem. Phys. Lett.*, **68,** 536 (1979).
17. R. D. Amos, *Mol. Phys.*, **35,** 1765 (1978).
18. R. D. Amos, *Mol. Phys.*, **38,** 33 (1979).
19. R. D. Amos, *Chem. Phys. Lett.*, **88,** 89 (1982).
20. R. D. Amos and J. H. Williams, *Chem. Phys. Lett.*, **66,** 471 (1979).
21. A. B. Anderson and R. Hoffmann, *J. Chem. Phys.*, **61,** 4545 (1974).
22. I. Ando, M. Jallali-Heravi, M. Kondo, S. Watanabe and G. A. Webb, *Bull. Chem. Soc. Jpn.*, **52,** 2240 (1979).
23. F. A. L. Anet and X. H. Ji, *Tetrahedron Lett.*, **25,** 1419 (1984).
24. J. Ángyán, unpublished results.
25. J. Ángyán, M. Allavena, M. Picard, A. Potier and O. Tapia, *J. Chem. Phys.*, **77,** 4723 (1982).
26. J. Ángyán and G. Náray–Szabó, *Program PROTPOT*, Budapest, 1981.
27. J. Ángyán and G. Náray–Szabó, *Theoret. Chim. Acta.*, **64,** 27 (1983).
28. J. Ángyán, G. Náray–Szabó, P. Nagy and G. Peinel, *Int. J. Quant. Chem.*, **31,** 927 (1987).
29. J. Ángyán R. A. Poirier, Á. Kucsman and I. G. Csizmadia, *J. Am. Chem. Soc.*, **109,** 2237 (1987).
30. J. Angyán and P. R. Surján, *Theoret. Chim. Acta*, **63,** 43 (1983).
31. T. Anno, *J. Chem. Phys.*, **72,** 782 (1980).
32. T. Aoyama and H. Yamakawa, *Chem. Phys. Lett.*, **51,** 508 (1977).
33. J. Applequist, *Acc. Chem. Res.*, **10,** 79 (1977).
34. T. Arai, *Rev. Mod. Phys.*, **32,** 370 (1960).
35. R. Arnaud, J. Court, J. M. Bonnier and J. Fossey, *Nouv. J. Chim.*, **4,** 299 (1980).
36. L. Åsbrink, C. Fridh and E. Lindholm, *J. Am. Chem. Soc.*, **94,** 5501 (1972).
37. L. Åsbrink, C. Fridh and E. Lindholm, *Chem. Phys. Lett.*, **52,** 63, 69, 72 (1977).

37a L. Åsbrink, C. Fridh, E. Lindholm, S. deBruijn and D. P. Chong, *Physica Scripta*, **22,** 475 (1980).

38. C. Aslangul, R. Constanciel, R. Daudel and P. Kottis, *Adv. Quant. Chem.*, **6,** 93 (1972).
39. J. Avery, *Creation and Annihilation Operators*, McGraw Hill, Toronto, 1976.
40. R. C. Axtmann, Y. Hazony and J. W. Hurley, *Chem. Phys. Lett.*, **2,** 673 (1968).
41. V. K. Babamov and A. Kupperman, *J. Chem. Phys.*, **77,** 1891 (1982).
42. G. G. Bácskay, *J. Chem. Phys.*, **79,** 2090 (1983).

43. G. B. Bácskay and N. S. Hush, *Theoret. Chim. Acta*, **32,** 311 (1974).
44. R. F. W. Bader, *Can. J. Chem.*, **40,** 1164 (1962).
45. R. F. W. Bader, *J. Am. Chem. Soc.*, **86,** 5070 (1964).
46. R. F. W. Bader, W. H. Henneker and P. E. Cade, *J. Chem. Phys.*, **46,** 3341 (1967).
47. R. F. W. Bader and T. T. Nguyen-Dang, *Adv. Quant. Chem.*, **14,** 63 (1981).
48. R. F. W. Bader, T. T. Nguyen and Y. Tal, *J. Chem. Phys.*, **70,** 4316 (1979).
49. R. F. W. Bader and R. R. Messer, *Can. J. Chem.*, **52,** 2268 (1974).
50. R. M. Badger, *J. Chem. Phys. Rev.*, **2,** 128 (1934).
51. M. Baer, *J. Chem. Phys.* **60,** 1057 (1974).
52. E. J. Baerends and P. Roos, *Mol. Phys.*, **30,** 1735 (1975).
53. P. S. Bagus, *Phys.. A*, **139,** 619 (1965).
54. P. S. Bagus and H. F. Schaefer III, *J. Chem. Phys.*, **56,** 224 (1972).
55. P. S. Bagus, B. Liu, D. H. Liskow and H. F. Schaefer III, *J. Am. Chem. Soc.*, **97,** 7216 (1975).
56. A. D. Baker, D. Betteridge, M. R. Kemp and R. E. Kirby, *J. Mol. Struct.*, **8,** 75 (1971).
57. C. J. Ballhausen and A. E. Hansen, *Annu. Rev. Phys. Chem.* **23,** 15 (1972).
58. A. S. Banzai and B. M. Deb, *Rev. Mod. Phys.*, **53,** 95 (1981).
59. S. Bantle and R. Ahlrichs, *Chem. Phys. Lett.* **53,** 148 (1978).
60. Z. Barandiarán, L. Pueyo and F. Gómez Beltrán, *J. Chem. Phys.*, **78,** 4612 (1983).
60a G. Barbier, H. Faucher and G. Berthier, *Theoret. Chim. Acta*, **21,** 105 (1971).
61. M. Barfeld and M. D. Johnston, jr., *Chem. Rev.*, **73,** 53 (1973).
62. A. J. Barnes and W. J. Orville–Thomas, Eds, *Vibrational Spectroscopy–Modern Trends*, Chapter 13., Elsevier, Amsterdam, 1977.
63. R. J. Bartlett, *Ann. Rev. Phys. Chem.*, **32,** 359 (1981).
64. R. J. Bartlett and G. D. Purvis, *Int. J. Quant. Chem.*, **14,** 561 (1978).
65. R. J. Bartlett and G. D. Purvis III, *Phys. Rev.*, **A20,** 1313 (1979).
66. R. J. Bartlett, H. Sekino and G. D. Purvis III, *Chem. Phys. Lett.*, **98,** 66 (1983).
67. R. J. Bartlett, I. Shavitt and G. D. Purvis III, *J. Chem. Phys.*, **71,** 281 (1979).
68. H. Basch, *J. Electron Spectry. and Rel. Phen.*, **5,** 463 (1974).
69. D. R. Bates, K. Ledsham and A. L. Stewart, *Phil. Trans. Roy. Soc. London*, **A246,** 215 (1953).
70. G. E. W. Bauer and C. Huiszoon, *Mol. Phys.*, **47**, 565 (1982).
71. G. W. Bauschlicher, Jr., O. H. Liskow, C. F. Bender and H. F. Schaefer III, *J. Chem. Phys.*, **62,** 4818 (1975).
72. P. M. Bayley, E. G. Nielsen and J. A. Schellman, *J. Phys. Chem.*, **73,** 228 (1969).
73. D. B. Beach, C. J. Eyermann, S. P. Smit, S. F. Xiang and W. L. Jolly, *J. Am. Chem. Soc.*, **106,** 536 (1984).
74. P. Becker, *Phys. Scripta*, **15,** 119 (1977).
75. P. Becker in, *Electron and Magnetization Densities in Molecules and Crystals*, (Ed: P. Becker), Plenum, New York (1980).
76. P. Becker, P. Coppens and F. K. Ross, *J. Am. Chem. Soc.*, **95,** 7604 (1973).
77. H. D. Beckey, *Field Ionization Mass Spectrometry*, Akademie-Verlag, Berlin, 1971.
78. C. I. Belchenko and P. V. Schastnev, *Inorg. Chim. Acta*, **37,** 187 (1979).
79. D. J. Bellville and N. L. Bauld, *J. Am. Chem. Soc.*, **104,** 294 (1982).
80. D. J. Bellville, N. L. Bauld, R. Pabon and S. A. Gardner, *J. Am. Chem. Soc.*, **105,** 3584 (1983).
81. M. Benard, P. Coppens, M. L. DeLucia and E. D. Stevens, *Inorg. Chem.*, **19,** 1924 (1980).
82. M. Benard, *Theoret. Chim. Acta*, **61,** 379 (1982).
83. G. Bendazzoli, P. Biscarini, P. Palmieri and G. Gottarelli, *J. Chem. Soc. Faraday Trans. II*, **77,** 503 (1981).
84. C. F. Bender, P. K. Pearson, S. V. O'Neill and H. F. Schaefer III, *J. Chem. Phys.*, **56,** 4626 (1972).
85. E. D. Bergmann and B. Pullman (Eds), *The Jerusalem Symposia on Quantum Chemistry and Biochemistry*, Vol. III: *Aromaticity, Pseudoaromaticity, Homoaromaticity*. The Israel Academy of Sciences, Jerusalem, 1971.
86. Z. Berkovitch Yellin and L. Leiserowitz, *J. Am. Chem. Soc.*, **97,** 5627 (1975).
87. F. Bernardi and A. Bottoni, *Theoret. Chim. Acta*, **58,** 245 (1981).
88. F. Bernardi and A. Bottoni, *Prog. Theoret. Org. Chem.*, **3,** 65 (1982).
89. F. Bernardi, M. A. Robb, H. B. Schlegel and G. Tonachini, *J. Am. Chem. Soc.*, **106,** 1198 (1984).
90. F. Bernardi, M. A. Robb and G. Tonachini, *Chem. Phys. Lett.*, **66,** 195 (1979).
91. M. Berndt and J. S. Kwiatkowski, *Theoret. Chim. Acta*, **50,** 223 (1978).
92. J. A. Berson, *Acc. Chem. Res.*, **5,** 406 (1972).
93. J. Bertrán, V. Branchadell, M. Duran and A. Oliva, *J. Mol. Struct. THEOCHEM*, **16,** 191 (1984).

94. H. A. Bethe and E. E. Salpeter, *Quantum Mechanics of One- and Two-electron Systems*, Springer, Berlin, 1957.
95. D. Bethell in, *Comprehensive Organic Chemistry* (Eds: D. Barton and W. D. Ollis), Vol. 1 (Ed: J. F. Stoddart), Pergamon, Oxford, 1979, p. 411.
96. D. L.Beveridge in, *Modern Theoretical Chemistry*, Vol. 8 (Ed: G. A. Segal), Plenum, New York, 1977, p. 163.
97. A. A. Bhattacharyya, A. Bhattacharyya, R. R. Adkins and A. G. Turner, *J. Am. Chem. Soc.*, **103,** 7458 (1981).
98. J. F. Birge, J. Herranz and J. Morcillo, *Anales R. Soc. Esp. Fis. Quim. A*, **57,** 81 (1961).
99. B. Bigot, A. Sevin and A. Devaquet, *J. Am. Chem. Soc.*, **101,** 1095, 1101 (1979).
100. J. L. Bills and R. L. Snow, *J. Am. Chem. Soc.*, **97,** 6340 (1975).
101. W. A. Bingel and W. Lüttke, *Angew. Chem. Int. Ed. Engl.*, **20,** 899 (1981).
102. R. C. Bingham, M. J. S. Dewar and P. H. Lo, *J. Am. Chem. Soc.*, **97,** 1294, 1302, 1307 (1971).
103. J. S. Binkley, R. A. Whitehead, P. C. Hariharan, R. Seeger and J. A. Pople, *Quantum Chemistry Program Exchange*, **11,** 368 (1978).
104. J. S. Binkley, R. A. Whiteside, R. Krishnan, R. Seeger, D. J. DeFrees, H. B. Schlegel, S. Topiol, L. R. Kahn and J. A. Pople, *Quantum Chemistry Program Exchange*, **13,** 406 (1981).
105. P. Birner, H. J. Köhler and C. Weiss, *Chem. Phys. Lett.* **27,** 347 (1974).
106. P. Birner, S. Kugler, K. Simon and G. Náray–Szabó, *Mol. Cryst. Liq. Cryst.*, **80,** 11 (1982).
107. D. M. Bishop, *Adv. Quant. Chem.*, **3,** 25 (1967).
108. B. Blaive and J. Metzger, *Nouv. J. Chim.*, **7,** 361 (1983).
109. C. E. Blom and C. Altona, *Mol. Phys.*, **31,** 1377 (1976).
110. C. E. Blom and C. Altona, *Mol. Phys.* **33,** 875 (1977).
111. J. Blomquist, B. Roos and M. Sundbom. *J. Chem. Phys.*, **55,** 141 (1971).
112. R. Boča, private communication.
113. R. Boča, *Coll. Czech. Chem. Comm.*, **44,** 3041 (1979).
114. R. Boča, *Theoret. Chim. Acta*, **61,** 179 (1982).
115. R. Boča, P. Pelikán, L. Valko and S. Miertuš, *Chem. Phys.* **11,** 229 (1975).
116. R. Bonaccorsi, R. Cimiraglia and J. Tomasi, *J. Comp. Chem.*, **4,** 567 (1983).
117. R. Bonaccorsi, R. Cimiraglia and J. Tomasi, *J. Mol. Struct. THEOCHEM*, **16,** 197 (1984).
118. R. Bonaccorsi, R. Cimiraglia, J. Tomasi and S. Miertuš, *J. Mol. Struct. THEOCHEM*, **94,** 11 (1983).
119. R. Bonaccorsi, G. Ghio, E. Scrocco and J. Tomasi, *Isr. J. Chem.*, **19,** 109 (1980).
120. R. Bonaccorsi, D. Palla and J. Tomasi, *J. Mol. Struct. THEOCHEM*, **87,** 181 (1982).
121. R. Bonaccorsi, P. Palla and J. Tomasi, *J. Am. Chem. Soc.*, **106,** 1945 (1984).
122. R. Bonaccorsi, C. Petrongolo, E. Scrocco and J. Tomasi, *Theoret. Chim. Acta*, **20,** 331 (1971).
123. R. Bonaccorsi, E. Scrocco and J. Tomasi, *J. Am. Chem. Soc.*, **98,** 4049 (1976); **99,** 4545 (1977).
124. V. Bonačič–Koutecky, P. Bruckmann, P. Hiberty, J. Koutecky, C. Leforestier and L. Salem, *Angew. Chem. Int. Ed. Engl.*, **14,** 575 (1975).
125. A. Bondi, *J. Phys. Chem.*, **68,** 441 (1964).
126. W. T. Borden, E. R. Davidson and D. Feller, *J. Am. Chem. Soc.*, **102,** 5302 (1980).
127. M. Boring, J. H. Wood, J. W. Moskowitz and J. W. D. Connolly, *J. Chem. Phys.*, **58,** 5163 (1973).
128. M. Born, *Z. Phys.*, **1,** 45 (1920).
129. M. Born and J. R. Oppenheimer, *Ann. Phys.*, **87,** 457 (1927).
130. A. Botrel, F. Corre and A. Le Beuze, *Chem. Phys.*, **74,** 383 (1983).
131. T. D. Bouman and A. E. Hansen, *Chem. Phys. Lett.*, **45,** 326 (1977).
132. T. D. Bouman and A. E. Hansen, *J. Chem. Phys.*, **66,** 3460 (1977).
133. T. D. Bouman, A. E. Hansen, B. Voigt and S. Rettrup, *Int. J. Quant. Chem.*, **23,** 595 (1983).
134. T. D. Bouman and D. A. Lightner, *J. Am. Chem. Soc.*, **98,** 3145 (1976).
135. T. D. Bouman, B. Voigt and A. E. Hansen, *J. Am. Chem. Soc.*, **101,** 550 (1979).
136. P. J. Bounds, *Chem. Phys. Lett.*, **70,** 143 (1980).
137. S. F. Boys, *Proc. Roy. Soc. (London)*, **A200,** 542 (1950).
138. S. F. Boys in, *Quantum Theory of Atoms, Molecules and the Solid State*, (Ed. P.–O. Löwdin), Academic, New York, 1966.
139. S. F. Boys and F. Bernardi, *Mol. Phys.*, **19,** 553 (1970).
140. M. C. Böhm, *Theoret. Chim. Acta*, **59,** 609 (1981).
141. M. C. Böhm, *Theoret. Chim. Acta*, **61,** 539 (1982).

141a F. Brailsford, *Magnetic Materials*, Methuen, London, 1960.
142. J. V. Brencic and F. A. Cotton, *Inorg. Chem.*, **9**, 346 (1970).
143. J. Breulet and H. F. Schaefer III, *J. Am. Chem. Soc.* **106**, 1221 (1984).
144. M. Brillouin, *Actual. Sci. Ind*, **71**, (1933).
145. J. N. Brönsted, *Z. Phys.Chem.*, **102**, 169 (1922).
146. R. D. Brown, *Quart. Rev. (London)*, **6**, 63 (1952).
147. K. A. Bruckner, *Phys. Rev.*, **97**, 1353 (1955); **100**, 36 (1955).
147a S. deBruijn, *Chem. Phys. Letters*, **52**, 76 (1977).
148. T. K. Brunck and F. Weinhold, *J. Am. Chem. Soc.*, **101**, 1700 (1979).
149. C. R. Brundle, M. B. Robin and H. Basch, *J. Chem. Phys.*, **53**, 2169 (1972).
150. R. E. Bruns and W. B. Person, *J. Chem. Phys.*, **53**, 1413 (1970); 324 (1972); **61**, 1779 (1974).
151. R. E. Bruns, A. B. M. S. Bassi and P. M. Kuznesof, *J. Am. Chem. Soc.*, **98**, 3432 (1970).
152. A. D. Buckingham, *Quart. Rev.*, **13**, 183 (1959).
153. A. D. Buckingham, *Adv. Chem. Phys.*, **12**, 107 (1967).
154. A. D. Buckingham in, *Intermolecular Interactions: From Diatomics to Biopolymers* (Ed.: B. Pullman), Wiley, New York, 1978, p. 2.
155. A. D. Buckingham, R. L. Dish and D. A. Dunmur, *J. Am. Chem. Soc.*, **90**, 3104 (1968).
155a A. D. Buckingham and S. M. Mahn, *Mol. Phys.*, **22**, 1127 (1971).
156. R. J. Buenker, *Gazz. Chim. Ital.*, **108**, 245 (1978).
157. R. J. Buenker and S. D. Peyerimhoff, *J. Chem. Phys.*, **53**, 1368 (1970).
158. R. J. Buenker and S. D. Peyerimhoff, *Chem. Rev.*, **74**, 127 (1974).
159. R. J. Buenker and S. D. Peyerimhoff, *Chem. Phys. Lett.*, **29**, 253 (1974).
160. R. J. Buenker and S. D. Peyerimhoff, *Chem. Phys.*, **8**, 56 (1975).
161. R. J. Buenker and S. D. Peyerimhoff, *Theoret. Chim. Acta*, **35**, 33 (1974); **39**, 217 (1975).
162. R. J. Buenker and S. D. Peyerimhoff, *Chem. Phys. Lett.*, **36**, 415 (1975).
163. R. J. Buenker and S. D. Peyerimhoff in, *Excited States in Quantum Chemistry*. (Eds: A. Nicolaides and D. R. Beck), Reidel, Dordrecht, 1978.
164. R. J. Buenker, S. D. Peyerimhoff and W. Butscher, *Mol. Phys.*, **35**, 771 (1978).
165. R. J. Buenker, S. Shih and S. D. Peyerimhoff, *Chem. Phys. Lett.*, **44**, 385 (1976).
166. J. K. Burdett, *Structure and Bonding*, **31**, 67 (1976).
166a J. Burns, *J. Chem. Phys.*, **41**, 1521 (1964).
167. B. E. Bursten, F. A. Cotton, J. C. Green, E. A. Seddon and G. G. Stanley, *J. Am. Chem. Soc.*, **102**, 4579 (1980).
168. B. E. Bursten, F. A. Cotton and M. B. Hall, *J. Am. Chem. Soc.* **102**, 6348 (1980).
169. B. E. Bursten and M. G. Gatter, *J. Am. Chem. Soc.*, **106**, 2554 (1984).
170. L. G. Butler and T. L. Brown, *J. Am. Chem. Soc.*, **103**, 6541 (1981).
171. P. E. Cade, *Trans. Am. Cryst. Ass.*, **8**, 1 (1972).
172. P. E. Cade, K. D. Sales and A. C. Wahl, *J. Chem. Phys.*, **44**, 1973 (1966).
173. D. J. Caldwell and H. Eyring, *The Theory of Optical Activity*, Wiley, New York, 1971.
174. D. J. Caldwell and H. Eyring, *Theor. Chem. Adv. Perspect.*, **1**, 53 (1975).
175. D. J. Caldwell and H. Eyring, *Adv. Quant. Chem.*, **11**, 93 (1978).
176. D. J. Caldwell, P. Redington and H. Eyring, *Proc. Natl. Acad. Sci. USA*. **76**, 3042 (1979).
177. S. Califano, *Vibrational States*, Wiley, London, 1976.
178. R. Carbo and C. Arnau, *Gazz. Chim. Ital.*, **108**, 171 (1978).
179. N. R. Carlsen, *Chem. Phys. Lett.*, **47**, 203 (1977).
180. T. A. Carlson, *Photoelectron and Auger Spectroscopy*, Plenum, New York, 1975.
181. P. Čársky, B. A. Hess and L. J. Schaad, *J. Am. Chem. Soc.*, **105**, 396 (1983).
182. P. Čársky and M. Urban, *Ab Initio Calculations*, Lecture Notes in Chemistry, No. 16, Springer, Berlin, 1980.
183. A. Cartier, *Theoret. Chim. Acta*, **59**, 181 (1981).
184. L. S. Cederbaum, *Chem. Phys. Lett.*, **25**, 562 (1974).
185. L. S. Cederbaum and W. Domcke, *J. Chem. Phys.*, **60**, 2878 (1974).
186. L. S. Cederbaum and W. Domcke, *Adv. Chem. Phys.*, **36**, 205 (1977).
187. L. S. Cederbaum and W. Domcke, *J. Chem. Phys.*, **66**, 5084 (1977).
188. L. S. Cederbaum, W. Domcke, H. Köppel and W. von Niessen, *Chem. Phys.*, **26**, 169 (1977).
189. L. S. Cederbaum, W. Domcke and W. von Niessen, *Mol. Phys.*, **33**, 1399 (1977).

190. L. S. Cederbaum and H. Köppel, *Chem. Phys*, **87,** 14 (1982).
191. L. S. Cederbaum and W. von Niessen, *J. Chem. Phys.*, **62,** 3824 (1975).
192. P. R. Certain and J. O. Hirschfelder, *Chem. Phys. Lett.*, **2,** 274 (1968).
193. O. Chalvet, R. Daudel, S. Diner and J. P. Malrieu (Eds), *Localization and Delocalization in Quantum Chemistry*, Vol. I, Reidel, Dordrecht, 1975.
194. D. Chandler, *Ann. Rev. Phys. Chem.*, **29,** 441 (1978).
195. D. Chandler, J. D. Weeks and H. C. Andersen, *Science*, **220,** 787 (1983).
196. J. Chandrasekhar, J. C. Andrade and P. v. R. Schleyer, *J. Am. Chem. Soc.*, **103,** 5609 (1981).
197. J. Chandrasekhar, E. D. Jemmis and P. v. R. Schleyer, *Tetrahedron Lett.*, 3707 (1979).
198. J. Chandrasekhar, D. C. Spellmeyer and W. L. Jorgensen, *J.Am.Chem.Soc.*, **106,** 903 (1984).
199. E. Charney, *Tetrahedron*, **21,** 3127 (1965).
200. E. Charney, *The Molecular Basis of Optical Activity*, Wiley, New York, 1979.
201. J. C. Y. Chen, *J.Chem.Phys.*, **40,** 615 (1964).
202. C. P. Cheng and T. L. Brown, *J.Am.Chem.Soc.*, **101,** 2327 (1979).
203. L. M. Cheung, K. R. Sundberg and K. Ruedenberg, *Int.J.Quant.Chem.*, **16,** 1103 (1979).
204. M. S. Child, *Molecular Collision Theory*, Academic, London, 1974.
205. D. M. Chipman, *J.Chem.Phys.*, **78,** 3112 (1983).
206. H. Chojnacki, *private communication.*
207. D. P. Chong, T. Minato and P. K. Mukherjee, *Int.J.Quant.Chem.*, **23,** 1903 (1983).
208. P. C. Christiansen, Y. S. Lee and K. S. Pitzer, *J.Chem.Phys.*, **71,** 4445 (1979).
209. P. A. Christiansen and W. E. Palke, *Chem.Phys.Lett.*, **31,** 462 (1975).
210. R. E. Christoffersen, *Adv. Quant.Chem.*, **6,** 333 (1972).
211. S. V. Chu and A. A. Frost, *J.Chem.Phys.*, **54,** 760 (1971).
212. W. A. Chupka, J. Berkowitz and D. Gutman, *J.Chem.Phys.*, **55,** 2724 (1971).
213. F. Ciardelli and P. Salvadori (Eds), *Fundamental Aspects and Recent Developments in Optical Rotatory Dispersion and Circular Dichroism*, NATO Adv. Stud. Ser., Heyden, London, (1973).
214. J. Cipriani and B. Silvi, *Mol.Phys.*, **45,** 259 (1982).
215. R. Cimiraglia, T. K. Ha, R. Meyer and H. H. Günthard, *Chem.Phys.*, **66,** 209 (1982).
216. R. Cimiraglia, S. Miertuš and J. Tomasi, *Chem.Phys.Lett.*, **80,** 286 (1981).
217. J. Čižek, *Mol.Phys.*, **6,** 20 (1963); **10,** 83 (1965).
218. J. Čižek, *J.Chem.Phys.*, **45,** 4256 (1966).
219. R. J. H. Clark and R. E. Hester (Eds), *Advances in Infrared and Raman Spectroscopy*, Vols 1–2, Heyden, London, 1975–76.
220. C. R. Claydon, G. A. Segal and H. S. Taylor, *J.Chem.Phys.*, **52,** 3387 (1971).
221. C. R. Claydon, G. A. Segal and H. S. Taylor, *J.Chem.Phys.*, **54,** 3799 (1971).
222. P. Claverie in, *Intermolecular Interactions: From Diatomics to Bipolymers*, (Ed: B. Pullman), Wiley, New York, 1978, p. 69.
223. E. Clementi, *J.Chem.Phys.*, **46,** 3842 (1967).
224. E. Clementi, *J.Chem.Phys.*, **46,** 3851 (1967).
225. E. Clementi, *Lecture Notes in Chemistry*, **2,** Springer-Verlag, Berlin, 1976.
226. E. Clementi, and R. Barsotti, *Chem.Phys.Lett.*, **59,** 21 (1978).
227. E. Clementi, F. Cavallone and R. Scordamaglia, *J.Am.Chem.Soc.*, **99,** 5531 (1977).
228. E. Clementi and G. Corongiu, *Ann.N.Y.Acad.Sci.*, **367,** 83 (1981).
229. E. Clementi and D. R. Davis, *J.Comput.Phys.*, **1,** 223 (1966).
230. E. Clementi, W. Kołos, G. C. Lie and G. Ranghino, *Int.J.Quant.Chem.*, **17,** 377 (1980).
230a. E. Clementi and D. L. Raimondi, *J.Chem.Phys.*, **38,** 2686 (1963).
231. E. Clementi, and C. Roetti, *Atomic Data and Nuclear Data Tables*, **14,** 177 (1974).
232. W. L. Clinton and L. J. Massa, *Phys.Rev.Lett.*, **29,** 1363 (1972).
233. F. Colapietro, A. Domenicano, G. Portalone, G. Schultz and I. Hargittai, *J.Mol.Struct.*, **112,** 141 (1984).
234. N. B. Colthup, L. H. Daly and S. E. Wiberley, *Introduction to Infrared and Raman Spectroscopy*, 2nd Ed., Academic, New York, 1975.
235. E. U. Condon, *Phys.Rev.*, **32,** 858 (1928).
236. E. U. Condon, *Rev.Mod.Phys.*, **9,** 432 (1937).
237. E. U. Condon, W. Altar and H. Eyring, *J.Chem.Phys.*, **5,** 753 (1937).
238. E. U. Condon and G. H. Shortley, *The Theory of Atomic Spectra*, Cambridge University Press, London, 1935.

239. J. W. D. Connolly in, *Modern Theoretical Chemistry*, Vol. VII (Ed: G. A. Segal), Plenum, New York, 1977, p. 105.
240. J. W. D. Connolly and K. H. Johnson, *Chem.Phys.Lett.*, **10,** 616 (1971).
241. J. W. D. Connolly and J. D. Sabin, *Chem.Phys.*, **56,** 5529 (1972).
242. J. W. D. Connolly, H. Siegbahn. U. Gelius and C. Nordling, *J.Chem.Phys.*, **58,** 4265 (1973).
243. J. A. Connor, I. H. Hillier, V. R. Saunders and M. H. Wood, *Mol.Phys.*, **24,** 497 (1972).
244. J. A. Connor, G. Pilcher, H. A. Skinner, M. H. Chisholm and F. A. Cotton, *J.Am.Chem.Soc.*, **100,** 7738 (1978).
245. R. Constanciel and R. C. Ramos, *Comp.Rend.Acad.Sci. (Paris)*, **296,** 333 (1983).
246. R. Constanciel and O. Tapia, *Theoret.Chim.Acta*, **48,** 75 (1978).
247. C. T. Corcoran and F. Weinhold, *J.Chem.Phys.*, **72,** 2866 (1980).
248. G. Corongiu, E. Clementi, M. Dagnino and L. Paoloni, *Chem.Phys.*, **40,** 439 (1979).
249. F. A. Cotton, *Chemical Applications of Group Theory*, Wiley, New York, 1963.
250. F. A. Cotton, *Inorg,Chem.*, **4,** 334 (1965).
251. F. A. Cotton, *Acc.Chem.Res.*, **11,** 225 (1978).
252. F. A. Cotton and M. H. Chisholm, *Chem.Eng.News*, **60,** 40 (1982).
253. F. A. Cotton and R. A. Walton, *Multiple Bonds Between Metal Atoms*, Wiley, New York, 1982.
254. C. A. Coulson, *Proc.Roy.Soc.(London)*, **A169,** 413 (1939).
255. C. A. Coulson, *Valence*, Clarendon, Oxford, 1952.
256. C. A. Coulson in, *Physical Chemistry*, Vol. V: *Valency* (Ed: H. Eyring), Academic, New York, 1970, p. 287.
257. C. A. Coulson in, *Physical Chemistry*, Vol. V: *Valency* (Ed: H. Eyring), Academic, New York, 1970, p. 402.
258. C. A. Coulson and G. S. Rushbrooke, *Proc.Camb.Phil.Soc.*, **36,** 193 (1940).
259. C. A. Coulson and G. S. Rushbrooke, *Proc.Cambridge Phil.Soc.*, **44,** 272 (1948).
260. C. A. Coulson and A. Streitwieser Jr., *Dictionary of π-Electron Calculations*, Pergamon, Oxford, 1965.
261. W. Coughram, J. Rose, T. Shibuya and V. McKoy, *J.Chem.Phys.*, **58,** 2699 (1973).
262. S. R. Cox and D. E. Williams, *J.Comput.Chem.*, **2,** 304 (1981).
263. D. P. Craig, P. J. Stiles, P. Palmieri and C. Zauli, *J.Chem.Soc.Faraday Trans.* II, **75,** 97 (1979).
264. P. Cremaschi, A. Gamba and M. Simonetta, *J.C.S.Perkin II*, 162 (1972).
265. D. Cremer. and J. A. Pople, *J.Am.Chem.Soc.*, **97,** 1354 (1975).
266. I. G. Csizmadia in, *Localization and Delocalization in Quantum Chemistry* (Eds: O. Chalvet, R. Daudel, S. Diner and J. P. Malrieu), Vol. I, Reidel, Dordrecht, 1972, p. 349.
267. I. G. Csizmadia, M. C. Harrison, J. W. Moscowitz, S. Seung, B. T. Sutcliffe and M. P. Barnett, *Quantum Chemistry Program Exchange*, **11,** 47 (1964).
268. D. P. Craig and T. Thirunamachandran, *Adv.Quant.Chem.*, **16,** 97 (1982).
269. J. M. Cullen, M. C. Zerner, *Int.J.Quant.Chem.*, **22,** 497 (1983).
270. L. A. Curtiss, S. R. Langhoff and G. D. Carney, *J.Chem.Phys.*, **71,** 5016 (1979).
271. E. Dalgaard and J. Linderberg, *J.Chem.Phys.* **65,** 692 (1976).
272. A. Dalgarno, *Adv.Phys.*, **11,** 281 (1962).
273. V. I. Danilov, J. S. Kwiatkowski, B. Lesyng and V. I. Poltev, *Int.J.Quant.Chem.Quantum Biol.Symp.*, **8** 359 (1981).
274. T. P. Das and E. L. Hahn, *Nuclear Quadrupole Resonance Spectroscopy*, Academic Press, New York, 1958.
275. R. Daudel, *Quantum Theory of the Chemical Bond*, Reidel, Dordrecht, 1974.
276. R. Daudel, *Quantum Theory of Chemical Reactivity*, Reidel, Dordrecht, 1973.
277. R. Daudel, G. Leroy, D. Peeters and M. Sana, *Quantum Chemistry*, Wiley, New York, 1983.
278. J. P. Daudey, *Chem.Phys.Lett.*, **24,** 574 (1974).
279. J. P. Daudey, J. Langlet and J. P. Malrieu, *J.Am.Chem.Soc.*, **96,** 3393 (1974).
280. E. R. Davidson, *Int.J.Quant.Chem.Symp.*, **15,** 65 (1981).
280a D. W. Davies, *The Theory of the Electric and Magnetic Properties of Molecules*, Wiley, London, 1967.
280b D. W. Davies, *Chem. Commun.*, 258 (1965).
281. A. S. Davydov, *Theory of Molecular Excitons*, McGraw-Hill, New York, 1973.
282. J. C. Decius, *J.Mol.Spectry.*, **57,** 348 (1975).
283. A. Dedieu, *Inorg.Chem.*, **19,** 375 (1980).

284. A. Dedieu, A. Veillard and B. Roos in, *The Jerusalem Symposia on Quantum Chemistry and Biochemistry*, Vol. VI: *Chemical and Biochemical Reactivity* (Eds: E. D. Bergman and B. Pullman), The Israel Academy of Sciences, Jerusalem, 1974, p. 374.
284a M. Defranceschi, M. Suard and G. Berthier, *Int.J.Quant.Chem.*, **25**, 863 (1984).
285. D. J. DeFrees, K. Raghavachari, H. B. Schlegel and J. A. Pople, *J.Am.Chem.Soc.*, **104**, 5576 (1982).
286. D. Dehareng, *Chem.Phys.*, **84**, 393 (1984).
287. J. E. Del Bene, *J.Chem.Phys.*, **55**, 4633 (1971).
288. J. E. Del Bene, *J.Chem.Phys.*, **57**, 1899 (1972).
289. J. E. Del Bene, *J.Am.Chem.Soc.*, **95**, 6517 (1973).
290. J. E. Del Bene, *Chem.Phys.Lett.*, **24**, 203 (1974).
291. J. E. Del Bene, *J. Chem.Phys.*, **62**, 666 (1975).
292. J. E. Del Bene, *J.Am.Chem.Soc.*, **95**, 6517 (1973).
293. J. E. Del Bene and H. H. Jaffé, *J.Chem.Phys.*, **48**, 1807, 4050 (1968); **49**, 1221 (1968).
294. J. E. Del Bene and H. H. Jaffé, *J.Chem.Phys.*, **48**, 1807, 4050 (1968).
295. J. E. Del Bene and H. H. Jaffé, *J.Chem.Phys.*, **49**, 1221 (1968).
296. J. E. Del Bene and W. L. Kochenour, *Chem.Phys.Lett.*, **81**, 293 (1981).
297. J. E. Del Bene and J. A. Pople, *J.Chem.Phys.*, **52**, 4858 (1970).
298. G. Del Re, *J.Chem.Soc.*, 4031 (1958).
299. G. Del Re, *Theoret.Chim.Acta*, **1**, 188 (1963).
300. G. Del Re, *Croat.Chem.Acta*, **57**, 787 (1984).
301. G. Del Re, G. Berthier and J. Serre, *Electronic States of Molecules and Atom Clusters*, Lecture Notes in Chemistry, No. 13, Springer, Berlin, 1980.
302. P. Demontis, E. Fois, A. Gamba, B. Manunza, G. B. Suffritti and M. Simonetta, *J.C.S. Perkin II*, 783 (1982).
303. P. Demontis, A. Gamba, G. Suffritti and M. Simonetta, *J.C.S. Perkin II*, 997 (1983).
304. D. Demoulin and M. Jungen, *Theoret.Chim.Acta*, **34**, 1 (1974).
305. A. Denis, J. Langlet and J-P. Malrieu, *Theoret.Chim.Acta*, **29**, 117 (1973).
306. A. Denis, J. Langlet and J-P. Malrieu, *Theoret.Chim.Acta*, **38**, 49 (1975).
307. M. J. S. Dewar, *The Molecular Orbital Theory of Organic Chemistry*, McGraw-Hill, New York, 1969.
308. M. J. S. Dewar, *J.Am.Chem.Soc.*, **106**, 209 (1984).
309. M. J. S. Dewar, *J.Am.Chem.Soc.*, **106**, 669 (1984).
310. M. J. S. Dewar and R. C. Dougherty, *The PMO Theory of Organic Chemistry*, Plenum, New York, 1975.
311. M. J. S. Dewar, G. J. Fonken, S. Kirschner and P. E. Minter, *J.Am.Chem.Soc.*, **96**, 7579 (1974).
312. M. J. S. Dewar and G. P. Ford, *J.Am.Chem.Soc.*, **99**, 1685 (1977).
313. M. J. S. Dewar, A. C. Griffin and S. Kirschner, *J.Am.Chem.Soc.*, **96**, 6225 (1974).
314. M. J. S. Dewar, R. C. Haddon and S. H. Suck, *J.C.S.Chem.Commun.*, 611 (1974).
315. M. J. S. Dewar and S. Kirschner, *J.Am.Chem.Soc.*, **93**, 4290 (1971).
316. M. J. S. Dewar and S. Kirschner, *J.Am.Chem.Soc.*, **96**, 5246 (1974).
317. M. J. S. Dewar and M. C. Kohn, *J.Am.Chem.Soc.*, **94**, 2705 (1972).
318. M. J. S. Dewar, D. H. Lo and C. A. Ramsden, *J.Am.Chem.Soc.*, **97**, 1311 (1975).
319. M. J. S. Dewar and H. C. Longuet-Higgins, *Proc.Phys. Soc.(London) A*, **67**, 795 (1954).
320. M. J. S. Dewar, S. Olivella and H. S. Rzepa, *J.Am.Chem.Soc.*, **100**, 5650 (1978).
321. M. J. S. Dewar and C. H. Reynolds, *J.Am.Chem.Soc.*, **106**, 1744 (1984).
322. M. J. S. Dewar and H. S. Rzepa, *J.Am.Chem.Soc.*, **100**, 58, 777, 784 (1978).
323. M. J. S. Dewar and W. Thiel, *J.Am.Chem.Soc.*, **99**, 4899, 4907 (1977).
324. G. H. F. Diercksen, V. Kellő and A. J. Sadlej, *Chem.Phys.Lett.*, **95**, 226 (1983).
325. S. Diner, J. P. Malrieu and P. Claverie, *Theoret.Chim.Acta*, **13**, 1 (1969).
326. S. Diner, J. P. Malrieu, F. Jordan and P. Claverie, *Theoret.Chim.Acta*, **18**, 86 (1970).
327. P. A. M. Dirac, *Proc.Roy.Soc.*, **123**, 714 (1929).
327a R. Ditchfield, *Mol.Phys.*, **27**, 789 (1974).
327b R. Ditchfield in, *Progress in Theoretical Organic Chemistry*, Vol. II (Ed.: I. G. Csizmadia), Elsevier, Amsterdam, 1977, p. 503.
328. R. Ditchfield, W. J. Hehre and J. A. Pople, *J.Chem.Phys.*, **54**, 724 (1971).
328a R. Ditchfield, D. P. Miller and J. A. Pople, *J.Chem.Phys.*, **53**, 613 (1970).
328b R. Ditchfield and R. C. Snyder, *J.Chem.Phys.*, **56**, 5823 (1972).
329. D. A. Dixon, D. A. Kleier and W. N. Lipscomb, *J. Am. Chem. Soc.*, **100**, 5681 (1978).

330. C. Djerassi, *Optical Rotatory Dispersion*, McGraw Hill, New York, 1960.
330a P. A. Dobosh, *Quantum Chemistry Program Exchange*, No. 141, Indiana University, Bloomington, USA
331. R. J. Doedens, *Progr. Inorg. Chem.*, **21,** 209 (1976).
332. W. Domcke and L. S. Cederbaum, *Chem.Phys.*, **25,** 189 (1977).
333. W. Domcke, L. S. Cederbaum, H. Köppel and W. von Niessen, *Mol.Phys.*, **27,** 789 (1974).
334. J. Douady, V. Barone, Y. Ellinger and R. Subra, *Int.J.Quant.Chem.*, **17,** 211 (1980).
335. F. Driessler and W. Kutzelnigg, *Theoret.Chim.Acta*, **43,** 1 (1976).
336. P. K. L. Drude, *The Theory of Optics*, Longman, London, 1933.
337. L. Ducasse, J. Hoarau and M. Pesquer, *J.Mol.Struct. THEOCHEM*, **88,** 61 (1982).
338. P. T. van Duijnen and B. T. Thole in, *Steric Effects in Biomolecules* (Ed: G. Náray-Szabó), Elsevier, Amsterdam, 1982, p. 347.
339. P. T. van Duijnen, B. T. Thole and W. G. J. Hol, *Biophys. Chem.*, **9,** 273 (1979).
340. B. J. Duke and B. O'Leary, *J.Chem.Phys.*, **79,** 3424 (1983).
341. B. J. Duke and B. O' Leary, *Theoret.Chim.Acta*, **62,** 223 (1983).
342. A. F. B. Duncan, *Rydberg Series in Atoms, and Molecules*, Academic, New York, 1971.
343. J. D. Dunitz, *X-Ray Analysis and the Structure of Organic Molecules*, Cornell, Ithaca, 1979.
344. T. M. Dunn in, *Physical Chemistry*, Vol V: *Valency* (Ed: H. Eyring), Academic, New York, 1970, p. 205.
345. T. H. Dunning and V. McKoy, *J.Chem.Phys.*, **47,** 1735 (1967).
346. T. H. Dunning, Jr., *J.Chem.Phys.*, **53,** 2823 (1970).
347. T. H. Dunning, Jr., *J.Chem.Phys.*, **55,** 3958 (1971).
348. T. H. Dunning, Jr. and P. J. Hay, in, *Modern Theoretical Chemistry*, Vol. III (Ed: H. F. Schaefer III), Plenum, New York, 1977.
349. M. Dupuis, J. Rys and H. F. King, *Quantum Chemistry Program Exchange* **11,** 336 (1977); **11,** 338 (1977); **13,** 401 (1981).
349a P. Dvortsák, G. Náray-Szabó and L. Vasvári-Debreczy, *Z. Naturforsch.*, **30b,** 784 (1975).
350. C. Eckart, *Phys.Rev.*, **47,** 552 (1935).
351. C. Edmiston and K. Ruedenberg, *Rev.Mod.Phys.*, **35,** 457 (1963).
352. C. Edmiston and K. Ruedenberg, *J.Chem.Phys.*, **43,** S97 (1965).
353. T. G. Edwards, *Theoret.Chim.Acta*, **27,** 1 (1972).
354. W. D. Edwards and H. Weinstein, *Chem.Phys.Lett.*, **56,** 582 (1978).
355. Y. M. Efremov, A. N. Samoilova, V. B. Kozhukhovsky and L. V. Gurvich, *J.Mol.Spectry.*, **73,** 430 (1978).
355a G. Ege and H. Vogler, *Z. Naturforsch.*, **27b,** 1164 (1974).
356. J. Eilers and E. Whitman, *J.Am.Chem.Soc.*, **95,** 2067 (1973).
357. O. Eisenstein, H. B. Schlegel and M. M. Kayser, *J.Org.Chem.*, **47,** 2886 (1982).
358. R. L. Ellis and H. H. Jaffé in, *Modern Theoretical Chemistry*, Vol. VIII (Ed: G. A. Segal), Plenum, New York, 1977, p. 81.
359. R. L. Ellis, G. Kuehnlenz and H. H. Jaffé, *Theoret.Chim.Acta*, **26,** 131 (1972).
360. R. L. Ellis, R. Squire, H. H. Jaffé, *J.Chem.Phys.*, **55,** 3500 (1971).
361. F. O. Ellison, *J.Am.Chem.Soc.*, **85,** 3540 (1963).
362. P. Empedocles, *Theoret.Chim.Acta*, **13,** 139 (1969).
363. P. B. Empedocles and J. W. Linnett, *Proc.Roy.Soc.London*, **A282,** 166 (1964).
364. J. W. Emsley, *Chem.Soc.Rev.*, **9,** 91 (1980).
364a I. W. Emsley, J. Feeney and L. H. Sutcliffe, *High Resolution Organic Magnetic Resonance Spectroscopy*, Pergamon, Oxford, 1965.
365. W. B. England, *Chem.Phys.Lett.*, **78,** 607 (1981).
366. W. England and M. S. Gordon, *J.Am.Chem.Soc.*, **91,** 6864 (1969).
367. W. England and M. S. Gordon, *J.Am.Chem.Soc.*, **93,** 4649 (1971).
368. W. England and M. S. Gordon, *J.Am.Chem.Soc.*, **94,** 4818 (1972).
369. W. England and K. Ruedenberg, *Theoret.Chim.Acta*, **22,** 196 (1971).
370. W. England and K. Ruedenberg, *J.Am.Chem.Soc.*, **95,** 8769 (1973).
371. W. England, L. S. Salmon and K. Ruedenberg, *Topics Curr.Chem.*, **23,** 31 (1971).
372. R. Englman, *The Jahn–Teller Effect in Molecules and Crystals*, Wiley, New York, 1972.
373. S. Engström, H. Wennerström, B. Jönsson and G. Karlström, *Mol.Phys.*, **34,** 813 (1977).
374. N. D. Epiotis, J. R. Larson and H. L. Eaton, *Unified Valence Bond Theory of Electronic Structure.* Lecture Notes in Chemistry, No. 29, Springer, Berlin, 1982.

375. P. S. Epstein, *Phys.Rev.*, **28,** 695 (1926).
376. W. C. Ermler, R. S. Mulliken and E. Clementi, *J.Am.Chem.Soc.*, **98,** 388 (1978).
377. N. P. Ernsting, J. Pfab, J. C. Green and J. Römelt, *J. C. S. Faraday Trans.*, **2,** 844 (1980).
378. L. Espinoza, A. Toro and P. Fuentealba, *Int.J.Quant.Chem.*, **16,** 939 (1979).
379. C. Etchebest, R. Lavery and A. Pullman, *Theoret.Chim.Acta*, **62,** 17 (1982).
380. M. C. Evans and M. Polanyi, *Trans.Faraday Soc.*, **31,** 875 (1935).
381. H. Eyring, *J.Chem.Phys.*, **8,** 107 (1935).
382. H. Eyring, J. Walter and G. E. Kimball, *Quantum Chemistry*, Wiley, New York, 1944.
382a J. C. Facelli, C. G. Giribet and R. H. Contreras, *Int.J.Quant.Chem.*, **25,** 515 (1984).
383. K. Fajans and G. Joos, *Z.Phys.*, **23,** 1 (1924).
384. T. R. Faulkner and F. S. Richardson, *J.Chem.Phys.*, **70,** 1201 (1979).
385. D. Feil and G. deWith, *private communication to* V. H. Smith, Jr., cited in Ref. 1294.
386. D. F. Feller, M. W. Schmiedt and K. Ruedenberg, *J.Am.Chem.Soc.*, **104,** 960 (1982).
387. R. P. Feynman, *Phys.Rev.*, **56,** 340 (1939).
388. M. Fink and R. A. Bonham in, *Chemical Applications of Atomic and Molecular Electrostatic Potentials* (Eds: P. Politzer and D. G. Truhlar), Plenum, New York, 1980, p. 93.
389. M. Fink, D. Gregory and P. G Moore, *Phys.Rev.Lett.*, **37,** 15 (1976).
390. I. Fischer-Hjalmars, *Adv.Quant.Chem.*, **2,** 25 (1965).
391. I. Fischer-Hjalmars, *J.Chem.Phys.*, **42,** 1962 (1965).
392. I. Fischer-Hjalmars, A. Henriksson-Enflo and C. Herrmann, *Chem.Phys.*, **24,** 167 (1977).
393. M. C. Flanigan, A. Komornicki and J. W. McIver, Jr. in, *Modern Theoretical Chemistry*, Vol. VIII (Ed: G. A. Segal), Plenum, New York, 1977, p. 1.
394. I. Fleming, *Frontier Orbitals and Organic Chemical Reactions*, Wiley, London, 1976.
395. R. Fletcher and M. J. D. Powell, *Comput. J.*, **6,** 163 (1963).
396. W. H Flygare and R. C. Benson, *Mol. Phys.*, **20,** 225 (1971).
397. V. Fock, *Z. Physik*, **61,** 126 (1930).
398. W. Forst, *Theory of Unimolecular Reactions*, Academic, New York, 1973.
399. S. Forster, S. Felps, L. C. Cusachs and S. P. McGlynn, *J. Am. Chem. Soc.*, **95,** 5521 (1973).
400. J. M. Foster and S. F. Boys, *Rev. Mod. Phys.*, **32,** 300 (1960).
401. J. P. Foster and F. Weinhold, *J. Am. Chem. Soc.*, **102,** 7211 (1980).
402. P. W. Fowler, *Mol. Phys.*, **47,** 355 (1982).
403. W. Förner, P. Otto, J. Bernhardt and J. Ladik, *Theoret. Chim. Acta*, **60,** 269 (1981).
404. J. Franck, *Trans. Faraday Soc.*, **21,** 536 (1926); E.U. Condon, *Phys. Rev.*, **28,** 1182 (1926).
405. M. M. Francl, R. F. Hout, and W. J. Hehre, *J. Am. Chem. Soc.*, **106,** 563 (1984).
406. H. S. Frank and M. Y. Wen, *Discuss. Faraday Soc.* **24,** 133 (1957).
407. L. Fredin and B. Nelander, *J. Mol. Struct.*, **16,** 217 (1973).
408. S. M. Free and J. W. Wilson, *J. Med. Chem.*, **7,** 395 (1964).
409. K. F. Freed in, *Modern Theoretical Chemistry*, Vol. VII, (Ed: G. A. Segal), Plenum, New York, 1977, p. 201.
410. K. F. Freed and D. L. Yeager, *Chem. Phys.*, **22,** 401 (1977).
411. T. B. Freedman, M. Diem, P. L. Polavarapu and L. A. Nafie, *J. Am. Chem. Soc.*, **104,** 3343 (1982).
412. H. Frei and H. H. Günthard, *Chem. Phys.*, **15,** 155 (1976).
413. H. J. Freund and E. W. Plummer, *Phys. Rev. B*, **23,** 4859 (1981).
414. A. A. Frost, *J. Chem. Phys.*, **47,** 3707, 3714 (1967).
415. A. A. Frost and R. A. Rouse, *J. Am. Chem. Soc.*, **90,** 1965 (1968).
416. H. Fukui, H. Yoshida and K. Miura, *J. Chem. Phys.*, **74,** 6988 (1981).
417. K. Fukui, *J. Phys. Chem.*, **74,** 4161 (1970).
418. K. Fukui, *Acc. Chem. Res.*, **4,** 57 (1961).
419. K. Fukui, *Angew. Chem. Int. Ed. Engl.*, **21,** 801 (1982).
420. K. Fukui, *Int. J. Quant. Chem.*, **23,** 633 (1983).
421. K. Fukui, T. Yonezawa and C. Nagata, *J. Chem. Phys.*, **26,** 831 (1957).
422. K. Fukui, T. Yonezawa and H. Shingu, *J. Chem. Phys.* **20,** 722 (1952).
423. V. Galasso and G. C. Pappalardo, *J. Chem. Soc. Perkin* II, 547 (1976).
424. R. Gáspár, *Acta Phys. Hung.*, **3,** 263 (1954).
425. R. Gáspár, *Acta Phys. Hung.*, **35,** 213 (1974).
426. R. Gáspár Jr. and R. Gáspár, *Int. J. Quant, Chem.*, **16,** 57 (1979).

427. R. Gáspár and R. Gáspár Jr., *Int. J. Quant. Chem.*, **22,** 415, 421 (1982).
427a A. H. Gawer and B. P. Dailey, *J. Chem. Phys.*, **42,** 2658 (1965).
428. A. Gedanken, N. A. Kuebler and M. B. Robin, *J. Chem. Phys.*, **76,** 46 (1982).
429. R. E. Geiger and G. H. Wagnière, *Helv. Chim. Acta*, **58,** 738 (1975).
430. W. M. Gelbart, *Adv. Chem. Phys.*, **26,** 1 (1974).
431. U. Gelius, *Phys. Scripta*, **9,** 33 (1974).
432. U. Gelius, B. Roos and P. Siegbahn, *Chem. Phys. Lett.*, **4,** 471 (1970).
433. M. Genest and M. Ptak, *Int. J. Peptide Protein Res.*, **19,** 420 (1982).
434. P. George, M. Trachtman, A. M. Brett and C. W. Bock, *J. C. S. Perkin II*, 1036 (1977).
435. J. Gerhards, T. K. Ha and X. Perlia, *Helv. Chim. Acta*, **65,** 105 (1982).
436. M. Gerloch, J. H. Harding and G. Wooley, *Structure and Bonding*, **46,** 1 (1981).
437. H. A. Germer, Jr., *Theoret. Chim Acta*, **34,** 145 (1974); **35,** 273 (1974).
438. J. Gerratt and M. Raimondi, *Proc. Roy. Soc., London*, **A371,** 525 (1980).
439. P. J. M. Geurts, J. W. Gosselink, A. van der Avoird, E. J. Baerends and J. G. Snijders, *Chem. Phys.*, **46,** 133 (1980).
440. C. Ghio, E. Scrocco and J. Tomasi, *Theoret. Chim. Acta*, **56,** 61, 75 (1980).
441. C. Ghio and J. Tomasi, *Theoret. Chim. Acta*, **30,** 151 (1973).
442. C. Giessner-Prettre and A. Pullman, *Theoret. Chim. Acta*, **13,** 265 (1969).
443. C. Giessner-Prettre and A. Pullman, *Theoret. Chim. Acta*, **25,** 83 (1972).
444. G. Giessner-Prettre and A. Pullman, *Theoret. Chim. Acta*, **33,** 91 (1974); **37,** 335 (1975).
445. T. L. Gilbert in, *Molecular Orbitals in Chemistry, Physics and Biology*, (Ed: P.-O. Löwdin and B. Pullman), Academic, New York, 1964, p. 405.
446. T. L. Gilbert, *Phys. Rev.*, **A6,** 580 (1972).
447. T. L. Gilbert, *J. Chem. Phys.*, **60,** 3835 (1974).
448. R. J. Gillespie, *Molecular Geometry*, Van Nostrand, London, 1972.
449. B. M. Gimarc, *Qualitative Molecular Orbital Theory*, Academic, New York, 1979.
450. B. M. Gimarc and N. Trinajstić, *Pure Appl. Chem.*, **52,** 1443 (1980).
451. B. M. Gimarc and N. Trinajstić, *Inorg. Chem.*, **21,** 21 (1982).
452. S. Glasstone, K. J. Laidler and H. Eyring, *The Theory of Rate Processes*, McGraw Hill New York, 1941.
453. J. T. Gleghorn and F. W. McConkey, *J. C. S. Perkin II*, 1079 (1976).
454. W. A. Goddard III, T. H. Dunning Jr., W. J. Hunt and P. J. Hay, *Acc. Chem. Res.*, **6,** 368 (1973).
455. E. Goldstein, S. Vijaya and G. A. Segal, *J. Am. Chem. Soc.*, **102,** 6198 (1980).
456. J. Goldstone, *Proc. Roy. Soc.*, **A239,** 267 (1957).
457. P. Gombás, *Z. Phys.*, **94,** 473 (1935).
458. P. Gombás, *Die statistische Theorie des Atoms und ihre Anwendungen*, Springer, Wien, 1949.
459. J. A. N. F. Gomes, *J. Chem. Phys.*, **78,** 3133 (1983).
460. J. Goodisman, *Diatomic Interaction Potential Theory*, Vol. II: *Applications*, Academic, New York, 1973.
461. J. Goodisman and W. Klemperer, *J. Chem. Phys.*, **38,** 721 (1963).
462. L. Goodman and B. J. Laurenzi, *Adv. Quant. Chem.*, **4,** 153 (1968).
462a M. S. Gopinathan and P. T. Narasimhan, *Mol. Phys.*, **21,** 943 (1971).
462b C. T. Goralski and W. B. Neely, *Theoret. Chim. Acta*, **20,** 41 (1971).
463. M. S. Gordon and W. England, *J. Am. Chem. Soc.*, **94,** 5168 (1972).
464. M. S. Gordon and W. England, *J. Am. Chem. Soc.*, **95,** 1753 (1973).
465. M. S. Gordon, D. E. Tallman, C. Monroe, M. Steinbach and J. Armbrust, *J. Am. Chem. Soc.*, **97,** 1326 (1975).
466. R. C. Gordon and Y. S. Kim, *J. Chem. Phys.*, **56,** 3122 (1972).
467. W. Gordy, *J. Chem. Phys.*, **19,** 792 (1950).
468. W. Gordy, *Theory and Application of Electron Spin Resonance*, Wiley, New York, 1980.
469. W. Gordy and R. L. Cook, *Microwave Molecular Spectra*, Wiley, New York, 1970.
470. O. Goscinski, B. T. Pickup and G. Purvis, *Chem. Phys. Lett.*, **22,** 167 (1973).
471. O. Goscinski and H. Siegbahn, *Chem. Phys. Lett.*, **48,** 568 (1977).
472. G. Gottarelli, B. Samori, G. L. Bendazzoli, P. Palmieri and A. F. Drake, *Chem. Phys. Lett.*, **45,** 318 (1977).
473. M. Göppert-Mayer, *Ann. Phys.*, **9,** 273 (1931).
474. M. Göppert-Mayer and A. L. Sklar, *J. Chem. Phys.*, **6,** 645 (1938).
475. I. P. Grant, *Comput. Phys. Commun.*, **17,** 149 (1979).

476. A. Graovac, I. Gutman and N. Trinajstić, *Topological Approach to the Chemistry of Conjugated Molecules*, Lecture Notes in Chemistry, Vol. 4, Springer, Berlin, 1977.
477. A. Graovac, K. Kovaćević, Z. B. Maksić and A. Veseli, *Int. J. Quant. Chem.*, **17,** 757 (1980).
478. G. Graovac, H. J. Monkhorst and T. Živković, *Int. J. Quant. Chem.*, **7,** 233 (1973).
479. A. Graovac and N. Trinajstić (Eds), *Proceedings of the Symposium on Aromaticity, Dubrovnik 1979, Pure Appl. Chem.*, **52,** 1397 (1980).
480. C. G. Gray and B. W. N. Lo, *Chem. Phys.*, **14,** 73 (1976).
481. S. J. Green, *J. Chem. Phys.*, **54,** 827 (1971).
482. S. J. Green, *Adv. Chem. Phys.*, **25,** 179 (1974).
483. N. N. Greenwood and T. C. Gibb, *Mössbauer Spectroscopy*, Chapman Hill, London, 1971.
484. R. S. Grew and H. F. Schaefer III, *J. C. S. Chem. Comm.*, 785 (1983).
485. L. A. Gribov, *Intensity Theory for Infrared Spectra of Polyatomic Molecules*, Consultants Bureau, New York, 1964, (original, Academy of Sciences Press, Moscow, 1963).
486. K. M. Griffing and J. Simons, *J. Chem. Phys.*, **64,** 3610.
487. D. Guenzburger and E. M. Baggio Saitovitsh, *Phys. Rev. B.*, **24,** 2368 (1981).
488. M. F. Guest, M. B. Hall and I. H. Hillier, *Mol. Phys.*, **25,** 629 (1973).
489. M. F. Guest, I. H. Hillier, V. R. Saunders and M. H. Wood, *Proc. Roy. Soc.*, **A333,** 201 (1973).
490. M. F. Guest, I. H. Hillier, B. R. Higginson and D. R. Lloyd, *Mol. Phys.*, **29,** 113 (1975).
491. M. F. Guest and V. R. Saunders, *Mol. Phys.*, **28,** 819 (1974).
492. M. Gussoni, C. Castiglione and G. Zerbi, *Chem. Phys. Lett.*, **95,** 483 (1983).
493. I. Gutman, M. Milun and N. Trinajstić, *J. Am. Chem. Soc.*, **99,** 1692 (1977).
494. I. Gutman and N. Trinajstić, *Topics Curr. Chem.*, **42,** 49 (1973).
495. T. K. Ha, C. E. Blom and H. H. Günthard, *Chem. Phys. Lett.*, **70,** 473 (1980).
496. A. Haaland, *Acc. Chem. Res.* **12,** 415 (1979).
497. R. C. Haddon, *J. Am. Chem. Soc.*, **101,** 1722 (1979).
498. R. C. Haddon, *J. Org. Chem.*, **44,** 3608 (1979).
499. G. G. Hall, *Proc. Roy. Soc.*, **A202,** 336 (1950); **A205** 541 (1951).
500. G. G. Hall, *Int. J. Quant. Chem.*, **7,** 15 (1973).
501. G. G. Hall and J. E. Lennard–Jones, *Proc. Roy. Soc.*, **A202,** 155 (1950); **A205,** 357 (1951).
502. G. G. Hall and D. Martin, *Isr. J. Chem.*, **19,** 255 (1980).
503. M. B. Hall, *J. Am. Chem. Soc.*, **100,** 6333 (1978).
504. T. A. Halgren and W. N. Lipscomb, *Proc. Natl. Acad. Sci. USA*, **69,** 652 (1972).
505. T. A. Halgren and W. N. Lipscomb, *J. Chem. Phys.*, **58,** 1569 (1973).
506. G. S. Hammond, *J. Am. Chem. Soc.*, **77,** 334 (1955).
507. C. Hansch in, *Drug Design* (Ed: E. J. Ariëns), Academic, New York, 1971, p. 271.
507a A. E. Hansen and T. D. Bouman, *Chem. Phys. Lett.*, **45,** 326 (1977).
508. A. E. Hansen and T. D. Bouman, *Adv. Chem. Phys.*, **64,** 545 (1980).
509. N. Harada, S–M. Lai Chen and K. Nakanishi, *J. Am. Chem. Soc.*, **97,** 5354 (1975).
510. R. D. Harcourt, *Lecture Notes in Chemistry*, **30,** Springer, Berlin, 1982.
511. L. B. Harding and W. A. Goddard III, *J. Am. Chem. Soc.*, **97,** 6293 (1975).
512. L. B. Harding and W. A. Goddard III, *J. Am. Chem. Soc.*, **97,** 6300 (1975).
513. L. B. Harding and W. A. Goddard III, *J. Chem. Phys.*, **67,** 1777 (1977).
514. M. D. Harmony, *Chem. Soc. Rev.*, **1,** 211 (1972).
515. R. J. Harrison and N. C. Handy, *Chem. Phys. Lett.*, **98,** 97 (1983).
516. S. L. Hartford, W. C. Allen, C. L. Norris, E. F. Pearson and W. H. Flygare, *Chem. Phys. Lett.*, **18,** 153 (1973).
517. H. Hartmann, *Adv. Chem. Phys.*, **5,** 1 (1963).
518. P. J. Hay, *J. Chem. Phys.*, **66,** 4377 (1977).
519. P. J. Hay, *J. Am. Chem. Soc.*, **100,** 2897 (1978).
520. P. J. Hay, *J. Am. Chem. Soc.*, **104,** 7007 (1982).
521. P. J. Hay, T. H. Dunning, Jr. and W. A. Goddard III., *J. Chem. Phys.*, **62,** 3912 (1975).
522. P. J. Hay and I. Shavitt, *J. Chem. Phys.*, **60,** 2865 (1974).
523. D. M. Hayes and P. A. Kollman, *J. Am. Chem. Soc.*, **98,** 3335 (1976).
524. D. M. Hayes and P. A. Kollman, *J. Am. Chem. Soc.*, **98,** 7811 (1976).
525. D. M. Hayes and P. A. Kollman, *J. Am. Chem. Soc.*, **103,** 2955 (1981).
526. W. J. Hehre, *J. Am. Chem. Soc.*, **96,** 5207 (1974).

527. W. J. Hehre, R. Ditchfield and J. A. Pople, *J. Chem. Phys.*, **56,** 2257 (1972).
528. W. J. Hehre, R. Ditchfield, L. Radom and J. A. Pople, *J. Am. Chem. Soc.*, **92,** 4796 (1970).
529. W. J. Hehre, R. Ditchfield, R. F. Stewart and J. A. Pople, *J. Chem. Phys.*, **52,** 2769 (1970).
530. W. J. Hehre, W. A. Lathan, R. Ditchfield, M. D. Newton, L. I. Upon and J. A. Pople, *Quantum Chemistry Program Exchange*, **11,** 236 (1973).
531. W. J. Hehre and J. A. Pople, *J. Am. Chem. Soc.*, **94,** 6901 (1972).
532. W. J. Hehre and J. A. Pople, *J. Chem. Phys.*, **56,** 4233 (1972).
533. W. J. Hehre, L. Radom and J. A. Pople, *J. Am. Chem. Soc.*, **94,** 1496 (1972).
534. W. J. Hehre, L. Salem and M. R. Wilcott, *J. Am. Chem. Soc.*, **96,** 4329 (1974).
535. W. J. Hehre, R. F. Stewart and J. A. Pople, *Symp. Far. Soc.*, **2,** 15 (1968); *J. Chem. Phys.*, **51,** 2657 (1969).
536. W. J. Hehre, M. Taagepera, R. W. Taft and R. D. Topsom, *J. Am. Chem. Soc.*, **103,** 1344 (1981).
537. W. J. Hehre, R. W. Taft and R. D. Topsom, *Prog. Phys. Org. Chem.*, **12,** 159 (1975).
538. D. Heidrich and M. Grimmer, *Int. J. Quant. Chem.*, **9,** 923 (1975).
539. E. Heilbronner, *Tetrahedron Lett.*, 1923 (1964).
540. E. Heilbronner and A. Schmelzer, *Helv. Chim. Acta*, **58,** 936 (1975).
541. E. Heilbronner and P. A. Straub, *Table of Hückel Molecular Orbitals*, Springer, Berlin, 1966.
542. W. Heitler and F. London, *Z. Physik*, **44,** 455 (1927).
543. E. J. Heller, *J. Chem. Phys.*, **68,** 2066, 3891 (1978).
544. E. J. Heller, *Acc. Chem. Res.*, **14,** 368 (1981).
545. H. Hellmann, *Einführung in die Quantumchemie*, Deuticke, Leipzig, 1937.
546. M. C. van Hemert and C. E. Blom, *Mol. Phys.*, **43,** 229 (1981).
547. G. Henderson, *J. Chem. Educ.*, **56,** 631 (1979).
548. D. N. Hendrickson, J. M. Hollander and W. L. Jolly, *Inorg. Chem.*, **8,** 2642 (1969).
549. M. F. Herman, K. F. Freed and D. L. Yeager, *Adv. Chem. Phys.*, **48,** 1 (1981).
550. M. F. Herman, D. L. Yeager, K. F. Freed and V. McKoy, *Chem. Phys. Lett.*, **46,** 1 (1977).
551. Z. S. Herman, *Int. J. Quant. Chem.*, **23,** 929 (1983).
552. K. Hermansson and S. Lunell, *Acta Cryst.*, **B38,** 2563 (1982).
553. K. Hermansson and J. O. T. Thomas, *Acta Cryst.*, **B38,** 2555 (1982).
554. I. Hermecz, P. R. Surján, T. Breining, K. Simon, G. Horváth, Z. Mészáros, M. Kajtár and G. Tóth, *J. Chem. Soc. Perkin Trans.* II, 1413 (1983).
555. G. Herzberg, *Molecular Spectra and Molecular Structure*, Vol. I, *Spectra of Diatomic Molecules*, Van Nostrand, New York, 1950.
556. G. Herzberg, *Molecular Spectra and Molecular Structure*, Vol. II, *Infrared and Raman Spectra of Polyatomic Molecules*, Van Nostrand New York, 1955.
557. G. Herzberg, *Molecular Spectra and Molecular Structure*, Vol. III, *Electronic Spectra and Electronic Structure of Polyatomic Molecules*, Van Nostrand, New York, 1966.
558. G. Herzberg and E. Teller, *Z. Phys. Chem. B*, **21,** 410 (1933).
559. B. A. Hess and L. J. Schaad, *J. Am. Chem. Soc.*, **93,** 305 (1971).
560. B. A. Hess, L. J. Schaad and C. W. Holyoke, *Tetrahedron*, **28,** 3657 (1972); **31,** 295 (1975).
561. C. J. M. van der Heuvel, J. W. Verhoeven and T. J. De Boer, *Recl. Trav. Chim. Pays-Bas*, **99,** 280 (1980).
562. P. C. Hiberty, *J. Am. Chem. Soc.*, **97,** 5975 (1975).
563. R. L. Hilderbrandt, *J. Chem. Phys.*, **51,** 1654 (1969).
564. A. Hinchcliffe and I. F. Kidd, *J. Chem. Soc. Faraday Trans. II*, **76,** 172 (1980).
565. J. Hinze, *Topics Curr. Chem.*, **9,** 465 (1968).
566. K. Hirao, *J. Chem. Phys.*, **79,** 5000 (1983).
567. H. von Hirschhausen and K. Wenzel, *Theoret. Chim. Acta*, **35,** 293 (1974).
568. F. L. Hirshfeld, *Theoret. Chim. Acta*, **44,** 129 (1977).
569. F. L. Hirshfeld and S. Rzotkiewicz, *Mol. Phys.*, **27,** 1319 (1974).
570. D. M. Hirst, *Adv. Chem. Phys.*, **50,** 517 (1982).
570a J. Hoarau in, *Localization and Delocalization in Quantum Chemistry* (Eds: O. Chalvet, R. Daudel, S. Diner and J. P. Malrieu), Reidel, Dordrecht, 1975, p. 265.
571. P. Hobza, F. Mulder and C. Sandorfy, *J. Am. Chem. Soc.*, **104,** 925 (1982).
572. P. Hobza and R. Zahradník, *Weak Intermolecular Interactions in Chemistry and Biology*, Elsevier, Amsterdam, 1980.
573. A. J. Hoefnagel, M. A. Hoefnagel and B. M. Wepster, *J. Org. Chem.*, **43,** 4720 (1978).
574. D. K. Hoffman, K. Ruedenberg and J. G. Verkade, *Structure and Bonding*, **33,** 57 (1977).

575. R. Hoffmann, *J. Chem. Phys.*, **39,** 1379 (1963).
576. R. Hoffmann, *Acc. Chem. Res.*, **4,** 1 (1971).
577. R. Hoffmann, *Angew. Chem. Int. Ed. Engl.*, **21,** 711 (1982).
578. R. Hoffmann, E. Heilbronner and R. Gleiter, *J. Am. Chem. Soc.*, **92,** 706 (1970).
579. R. Hoffmann, A. Imamura and W. J. Hehre, *J. Am. Chem. Soc.*, **90,** 1499 (1968).
580. R. Hoffmann, P. D. Mollere and E. Heilbronner, *J. Am. Chem. Soc.*, **95,** 4860 (1975).
581. H. J. Hofmann, G. Peinel, C. Krebs and C. Weiss, *Int. J. Quant. Chem.*, **20,** 785 (1981).
582. H. J. Hofmann, G. Peinel and T. Weller, *Int. J. Quant. Chem.*, **16,** 379 (1979).
583. C. Hoheisel and W. Kutzelnigg, *J. Am. Chem. Soc.*, **97,** 6970 (1975).
584. P. Hohenberg and W. Kohn, *Phys. Rev.* B, **136,** 864 (1964).
585. G. J. Hoijtink, E. de Boer, P. H. van der Meij and W. P. Weijland, *Rec. Trav. Chim. Pays-Bas*, **75,** 487 (1956).
586. J. M. Holder and D. Peters, *J. Mol. Struct.*, **56,** 221, 233 (1979).
587. J. M. Hollander, D. N. Hendrickson and W. L. Jolly, *J. Chem. Phys.*, **49,** 3315 (1968).
588. J. M. Hollander and W. L. Jolly, *Acc. Chem. Res.*, **3,** 193 (1970).
589. A. C. Hopkinson in, *Progress in Theoretical Organic* Chemistry, Vol. II (Ed: I. G. Csizmadia), Elsevier, Amsterdam, 1977, p. 230.
590. M. Horák, S. Hilgard and P. Hobza, *Coll. Czech. Chem. Commun.*, **40,** 1801 (1975).
591. J. F. Hornig and J. O. Hirschfelder, *J. Chem. Phys.*, **20,** 1812 (1952).
592. G. Horváth, M. Pongor–Csákvári, A. I. Kiss, G. Fogarasi and P. Pulay, *Tetrahedron*, **33,** 2293 (1977).
593. R. P. Hosteny, T. H. Dunning, Jr., R. R. Gilman, A. Pipano and I. Shavitt, *J. Chem. Phys.*, **62,** 4764 (1975).
594. C. Hosticka, T. K. Bose and J. S. Sochanski, *J. Chem. Phys.*, **61,** 2575 (1974).
595. K. N. Houk, *J. Am. Chem. Soc.*, **95,** 4092 (1973).
596. K. N. Houk and R. W. Strozier, *J. Am. Chem. Soc.*, **95,** 4094 (1973).
597. J. R. Hoyland, *J. Am. Chem. Soc.*, **90,** 2227 (1968).
598. J. R. Hoyland, *J. Chem. Phys.*, **50,** 473 (1969).
599. E. G. Höhn and O. E. Weigang, *J. Chem. Phys.*, **48,** 1127 (1968).
600. R. Höller and H. Lischka, *Mol. Phys.*, **41,** 1041 (1980).
601. K. Hsu, R. J. Buenker and S. D. Peyerimhoff, *J. Am. Chem. Soc.*, **93,** 2117, 5005, 5693 (1971).
602. I. Hubač V. Kvasnička and A. Holubec, *Chem. Phys. Lett.*, **23,** 381 (1973).
603. I. Hubač and V. Kvasnička, *Croat. Chem. Acta*, **49,** 677 (1977).
604. I. Hubač and M. Urban, *Theoret. Chim. Acta*, **45,** 185 (1977).
605. J. A. Hudis and R. Ditchfield, *Chem. Phys. Lett.*, **77,** 202 (1981).
606. R. F. Hudson, *Angew. Chem.*, **85,** 63 (1973).
607. R. F. Hudson in *Chemical Reactivity and Reaction Paths* (Ed: G. Klopman), Wiley, New York, 1974, p. 167.
608. R. F. Hudson and G. Klopman, *Tetrahedron Lett.*, **12,** 1103 (1967).
609. W. Hug and G. Wagnière, *Tetrahedron*, **28,** 1241 (1972).
610. W. F. Hunt and W. A. Goddard III, *Chem. Phys. Lett.*, **3,** 414 (1969).
611. A. C. Hurley, J. E. Lennard–Jones and J. A. Pople, *Proc. Roy. Soc.*, **A220,** 446 (1953).
612. M. J. Huron and P. Claverie, *J. Phys. Chem.*, **78,** 1853 (1974).
613. A. T. Hutton, H. M. N. H. Irving, K. R. Koch, L. Nassimbeni and G. Gafner, *J. C. S. Chem. Commun.*, 57, (1979).
614. S. Huzinaga, *J. Chem. Phys.*, **42,** 1293 (1965).
615. S. Huzinaga and C. Arnau, *J. Chem. Phys.*, **54,** 1948 (1971); *Phys. Rev. A*, **1,** 1285 (1970).
616. S. Huzinaga and A. A. Cantu, *J. Chem. Phys.* **55,** 5543 (1971).
617. E. A. Hylleras, *Adv. Quant. Chem.*, **1,** 1 (1964).
618. J. Hylton, R. E. Christoffersen and G. G. Hall, *Chem. Phys. Lett.*, **24,** 501 (1974).
619. H. H. Hyman in, *Physical Chemistry*, Vol. V: *Valency* (Ed: H. Eyring), Academic, New York, 1970, p. 590.
620. D. Ilić and N. Trinajstić, *Pure Appl. Chem.*, **52,** 1495 (1980).
621. A. Imamura, *Mol. Phys.*, **15,** 225 (1968).
622. A. Imamura and T. Hirano, *J. Am. Chem. Soc.*, **97,** 4192 (1975).
623. A. Imamura and K. Hirao, *Tetrahedron*, **35,** 2243 (1979).
624. A. Imamura, T. Hirano, C. Nagata and T. Tsurata, *Bull. Chem. Soc. Jpn*, **45,** 396 (1972).
625. A. Imamura and M. Ohsaku, *Tetrahedron*, **37,** 2195 (1981).
626. A. Imamura, M. Ohsaku and K. Akagi, *Tetrahedron*, **39,** 1291 (1983).

627. A. Imamura, A. Tachibana and M. Ohsaku, *Tetrahedron*, **37,** 2793 (1981).
628. S. Inagaki and Y. Hirabayashi, *Chemistry Lett.*, 709 (1982).
629. A. D. Isaacson and K. Morokuma, *J. Am. Chem. Soc.*, **97,** 4453 (1975).
630. S. Iwata and K. Morokuma, *Theoret. Chim. Acta*, **33,** 285 (1974).
631. S. Iwata and K. Morokuma, *Theoret. Chim. Acta*, **44,** 323 (1977).
631a L. M. Jackman and S. Sternhell, *Application of Nuclear Magnetic Resonance Spectroscopy in Organic Chemistry*, Pergamon, Oxford, 1969.
632. H. H. Jaffé and M. Orchin, *Theory and Application of Ultraviolet Spectroscopy*, Wiley, New York, 1962.
633. H. J. Jahn and E. Teller, *Proc. Roy. Soc.*, **A161,** 220 (1937).
634. G. Jalsovszky and P. Pulay, *J. Mol. Struct.*, **26,** 277 (1975).
635. C. J. Jameson, *Nucl. Magn. Res.*, **10,** 1 (1981).
636. J. W. Janis, P. Kaiser, J. R. Sabin and V. H. Smith, Jr., *Mol. Phys.*, **37,** 463 (1979).
637. I. Jano, *Compt. Rend. Acad. Sci. (Paris)*, **261,** 103 (1965).
638. R. Janoschek, E. G. Weidemann, H. Pfeiffer and G. Zundel, *J. Am. Chem. Soc.*, **94,** 2387 (1972).
639. Y. Jean and F. Volatron, *Chem. Phys.*, **65,** 107 (1982).
640. J. A. Jaecker, W. R. Robinson and R. A. Walton, *J. C. S. Chem. Commun.*, 306 (1974).
641. R. J. Jerrard, A. T. Amos and P. A. Brook, *Theoret. Chim. Acta*, **61,** 163 (1982).
642. G. H. Jeung, J. P. Malrieu and J. P. Daudey, *J. Chem. Phys.*, **77,** 3571 (1982).
643. M. D. Joesten and L. J. Schaad, *Hydrogen Bonding*, Dekker, New York, 1974.
644. G. Johannin and K. Kellersohn, *Biochem. Biophys. Res. Commun.*, **49,** 321 (1972).
645. K. H. Johnson, *Adv. Quant. Chem.*, **7,** 143 (1973).
646. K. H. Johnson, *Ann. Rev. Phys. Chem.*, **26,** 39 (1975).
647. R. P. Johnson and M. W. Schmiedt, *J. Am. Chem. Soc.*, **103,** 3244 (1981).
648. H. W. Jones, *Int. J. Quant. Chem.*, **23,** 953 (1983).
648a R. G. Jones and R. Partington, *J. Chem. Soc. Faraday Trans. 2*, **68,** 2087 (1972).
649. G. Jonkers, W. J. van der Meer, C. A. de Lange, B. J. Baerends, J. Stapersma and G. W. Klupp, *J. Am. Chem. Soc.*, **106,** 587 (1984).
650. C. K. Jorgensen, *Modern Aspects of Ligand Field Theory*, North Holland, Amsterdam, 1979.
651. P. Jorgensen, *Annu. Rev. Phys. Chem.*, **26,** 359 (1975).
652. P. Jorgensen and J. Oddershede, *J. Chem. Phys.*, **78,** 1898 (1983).
653. P. Jorgensen and J. Simons, *Second Quantization Based Methods in Quantum Chemistry*, Academic, New York, 1981.
654. W. L. Jorgensen and L. Salem, *The Organic Chemist's Book of Orbitals*, Academic, New York, 1973.
655. B. Jönsson, S. Romano and G. Karlström, *Int. J. Quant. Chem.*, **25,** 503 (1984).
656. K. Jug, *Theoret. Chim. Acta*, **31,** 63 (1973).
657. K. Jug, *J. Am. Chem. Soc.*, **100,** 6581 (1978).
658. K. Jug, *Theoret. Chim. Acta*, **54,** 263 (1980).
659. A. Julg, *Top. Curr. Chem.*, **58,** 1 (1975).
660. A. Julg and F. François, *Theoret. Chim. Acta*, **22,** 196 (1971).
661. M. Jungen and R. Ahlrichs, *Theoret. Chim. Acta*, **17,** 339 (1970).
662. L. R. Kahn, P. Baybutt and D. G. Truhlar, *J. Chem. Phys.*, **65,** 3826 (1976).
663. L. R. Kahn, P. J. Hay and R. D. Cowan, *J. Chem. Phys.*, **68,** 2368 (1978).
664. H. C. Kalinowski and H. Kessler, *Top. Stereochemistry*, **7,** 316 (1973).
665. E. Kapuy, *J. Chem. Phys.*, **44,** 956 (1966); *Theoret. Chim. Acta*, **6,** 281 (1966).
666. E. Kapuy, *Acta Phys. Acad. Sci. Hung.*, **27,** 179 (1969).
667. E. Kapuy, *Acta Phys. Acad. Sci. Hung.*, **51,** 21 (1981).
668. E. Kapuy, Z. Csépes and C. Kozmutza, *Int. J. Quant. Chem.*, **23,** 981 (1983).
669. E. Kapuy and C. Kozmutza, *Theoret. Chim. Acta*, **56,** 259 (1980).
670. E. Kapuy, C. Kozmutza and R. Daudel, *Theoret. Chim. Acta*, **56,** 259 (1980).
671. E. Kapuy, C. Kozmutza and M. E. Stephens, *Theoret. Chim. Acta*, **43,** 175 (1976).
672. J. Karle, *Electron Diffraction, Determination of Organic Structure by Physical Methods*, Vol. V, Academic, New York, 1973.
673. G. Karlström, B. Jönsson, B. O. Roos and H. Wennerström, *J. Am. Chem. Soc.*, **98,** 6851 (1976).
674. G. Karlström, B. O. Roos and L. Carlsen, *J. Am. Chem. Soc.*, **106,** 1557 (1984).
675. G. Karlström, H. Wennerström, B. Jönsson, S. Forsén, J. Almlöf and B. Roos, *J. Am. Chem. Soc.*, **97,** 4188 (1975).

675a M. Karplus and H. J. Kolker, *J. Chem. Phys.*, **35,** 2235 (1961); **38,** 1263 (1963).
676. R. V. Kasowski and E. Caruthers, *Phys. Rev. B*, **21,** 3200 (1980).
677. S. Kato and K. Morokuma, *J. Chem. Phys.*, **73,** 3900 (1980).
678. W. Kauzmann, *Quantum Chemistry*, Academic, New York, 1957.
679. Z. Kecki, J. Sadlej and A. J. Sadlej, *J. Mol. Struct. THEOCHEM*, **5,** 71 (1982).
680. F. Keil and R. Ahlrichs, *J. Am. Chem. Soc.*, **98,** 4787 (1976).
681. F. Keil and W. Kutzelnigg, *J. Am. Chem. Soc.*, **97,** 3623 (1976).
682. M. J. H. Kemper, L. Lemmens and H. M. Buck, *Chem. Phys.*, **57,** 245 (1981).
683. J. Kenney and J. Simons, *J. Chem. Phys.*, **62,** 592 (1975).
684. C. W. Kern and M. Karplus, *J. Chem. Phys.*, **40,** 1374 (1964).
685. C. W. Kern, R. M. Pitzer and O. J. Sovers, *J. Chem. Phys.*, **60,** 3583 (1974).
686. M. Kertész, *Adv. Quant. Chem.*, **15,** 161 (1982).
687. M. Kertész, J. Koller and A. Ažman, *J. Chem. Phys.*, **69,** 2937 (1978).
688. M. Kertész and P. R. Surján, *Solid State Commun.*, **39,** 611 (1981).
689. M. Kertész, P. R. Surján and K. Holzer, *Mol. Cryst. Liq. Cryst.*, **77,** 341 (1981).
690. L. B. Kier and L. H. Hall, *Molecular Connectivity in Chemistry and Drug Research*, Academic, New York, 1976.
691. T. Kihara, in *Physical Chemistry*, Vol. V., *Valency*, (Ed: H. Eyring), Academic, New York, 1970.
692. K. Kim and W. T. King, *J. Chem. Phys.*, **80,** 969, 974, 978, 983 (1984).
693. J. G. Kirkwood, *Phys. Z.*, **33,** 57 (1932).
694. J. G. Kirkwood, *J. Chem. Phys.*, **2,** 351 (1934).
695. J. G. Kirkwood, *J. Chem. Phys.*, **5,** 479 (1937).
696. B. Kirtman, *J. Phys. Chem.*, **86,** 1059 (1982).
697. B. Kirtman, and C. de Melo, *J. Chem. Phys.*, **75,** 4592 (1981).
698. B. Kirtman, W. E. Palke, and D. M. Chipman, *Isr. J. Chem.*, **19,** 82 (1980)
699. S. Kishner, M. A. Whitehead and M. S. Gopinathan, *J. Am. Chem. Soc.*, **100,** 1365 (1978).
700. Á. I. Kiss and I. Lukovits, *Chem. Phys. Lett.*, **65,** 169 (1979).
701. Á. I. Kiss and J. Szőke, *Acta Chim. Acad. Sci. Hung.*, **74,** 59 (1972).
702. Á. I. Kiss and J. Szőke, *J. Mol. Struct.*, **18,** 457 (1973).
703. Á. I. Kiss and J. Szőke, *Acta Chim. Acad. Sci. Hung.*, **89,** 337 (1976).
704. H. Kistenmacher, G. C. Lie, H. Popkie and E. Clementi, *J. Chem. Phys.*, **61,** 546 (1974).
705. H. Kistenmacher, H. Popkie and E. Clementi, *J. Chem. Phys.*, **59,** 5842 (1973); **61,** 799, 2550 (1974); **62,** 1388 (1975).
706. K. Kitaura and K. Morokuma, *Int. J. Quantum Chem.*, **10,** 325 (1976).
707. D. A. Kleier, R. L. Martin, W. R. Wadt and W. R. Moomaw, *J. Am. Chem. Soc.*, **104,** 60 (1982).
708. M. Klessinger, *Theoret. Chim. Acta*, **49,** 77 (1978).
709. M. Klessinger, *Int. J. Quant. Chem.*, **23,** 535 (1983).
710. M. Klessinger and R. McWeeny, *J. Chem. Phys.*, **42,** 3343 (1965).
711. G. Klopman, *Chem. Phys. Lett.*, **1,** 200 (1967).
712. G. Klopman, *J. Am. Chem. Soc.*, **90,** 223 (1968).
713. G. Klopman in, *Chemical Reactivity and Reaction Paths* (Ed: G. Klopman), Wiley, 1974, p. 1.
714. G. Klopman in, *Chemical Reactivity and Reaction Paths* (Ed: G. Klopman), Wiley, 1974. p. 55.
715. G. Klopman and P. Andreozzi, *Theoret. Chim. Acta*, **55,** 77 (1980).
716. G. Klopman and R. F. Hudson, *Theoret. Chim. Acta*, **8,** 165 (1967).
717. G. Klopman, O. Kikuchi, H. Moriishi and K. Suzuki, *Tetrahedron Lett.*, **23,** 3447 (1982).
718. G. Klopman, H. Moriishi, O. Kikuchi and K. Suzuki, *Tetrahedron Lett.*, **23,** 1027 (1982).
719. E. Kochanski, *J. Mol. Struct. THEOCHEM*, **16,** 49 (1984).
720. T. Koga and M. Morita, *Theoret. Chim. Acta*, **59,** 639 (1981).
720a T. Koga and M. Sasaki, *J. Chem. Phys.*, **81,** 1947 (1984).
721. T. Koga, K. Shimokawa, I. Inagawa and M. Morita, *Theoret. Chim. Acta*, **62,** 39 (1982).
722. T. Koga, M. Sugawara and M. Morita, *Theoret. Chim. Acta*, **61,** 87 (1982).
723. P. Kollman, *J. Am. Chem. Soc.*, **99,** 4875 (1977).
724. P. Kollman in *Modern Theoretical Chemistry*, Vol. IV. (Ed: H. F. Schaefer III), Plenum, New York, 1977, p. 109.
725. P. A. Kollman in, *Chemical Applications of Atomic and Molecular Electrostatic Potentials* (Ed: P. Politzer and D. G. Truhlar), Plenum, New York, 1981, p. 243.

726. P. Kollman and I. Kuntz, *J. Am. Chem. Soc.*, **98,** 6820 (1976).
727. P. A. Kollman, J. McKelvey, A. Johansson and S. Rothenberg, *J. Am Chem. Soc.*, **97,** 955 (1975).
728. W. Kołos, *Adv. Quant. Chem.*, **5,** 99 (1970).
729. W. Kołos and C. C. J. Roothaan, *Rev. Mod. Phys.*, **32,** 219 (1960).
730. W. Kołos and L. Wolniewicz, *J. Chem. Phys.*, **49,** 404 (1968).
731. A. Komornicki, J. O. Goddard and H. F. Schaefer III, *J. Am. Chem. Soc.*, **102,** 1765 (1980).
732. A. Komornicki and R. L. Jaffé, *J. Chem. Phys.*, **71,** 2150 (1979).
733. A. Komornicki and J. W. McIver, *J. Am. Chem. Soc.*, **95,** 4512 (1973); **96,** 5798 (1974); **98,** 4553 (1976).
734. A. Komornicki and J. W. McIver, Jr., *J. Chem. Phys.*, **70,** 2014 (1979).
735. T. Koopmans, *Physica*, **1,** 104 (1933).
736. C. Kozmutza and P. Pulay, *Theoret. Chim. Acta*, **37,** 67 (1975).
737. H. J. Köhler, T. Weller and D. Klöpper, *Z. Chem.*, **15,** 224 (1975).
738. H. Köppel, L. S. Cederbaum and W. Domcke, *J. Chem. Phys.*, **77,** 2014 (1982).
739. H. Köppel, L. S. Cederbaum, W. Domcke and S. S. Shaik, *Angew. Chem. Int. Ed. Engl.*, **22,** 210 (1983).
740. H. Köppel, W. Domcke, L. S. Cederbaum and W. von Niessen, *J. Chem. Phys.*, **69,** 4252 (1978).
741. S. Kubota and Y. Ikegami, *J. Phys. Chem.*, **82,** 2739 (1978).
742. G. Kuehnlenz and H. H. Jaffé, *J. Chem. Phys.*, **58,** 2238 (1973).
742a S. G. Kukolich, *J. Chem. Phys.*, **58,** 2238 (1973).
743. A. Kuppermann, W. M. Flicker and O. A. Mosher, *Chem. Rev.*, **79,** 77 (1979).
744. W. Kutzelnigg, *Theoret. Chim. Acta*, **1,** 327 (1963); *J. Chem. Phys.*, **40,** 3640 (1964).
745. W. Kutzelnigg, *Angew. Chem.*, **85,** 551 (1973).
746. W. Kutzelnigg in, *Localization and Delocalization in Quantum Chemistry*, (Ed: O. Chalvet, R. Daudel, S. Diner and J.–P. Malrieu), Reidel, Dordrecht, 1975, p. 143.
747. W. Kutzelnigg in, *Modern Theoretical Chemistry*, Vol. III, (Ed: H. F. Schaefer III), Plenum, New York, 1977.
748. W. Kutzelnigg, *Isr. J. Chem.*, **19,** 193 (1980).
749. W. Kutzelnigg, *Angew. Chem. Int. Ed. Engl.*, **23,** 272 (1984).
750. S. Kuwajima, *J. Chem. Phys.*, **74,** 6342 (1981).
751. H. Kuzmany, P. R. Surján and M. Kertész, *Solid State Commun.*, **48,** 243 (1983).
752. V. Kvasnička, *Theoret. Chim. Acta*, **34,** 61 (1974).
753. V. Kvasnička and I. Hubač, *J. Chem. Phys.*, **60,** 4483 (1974).
754. H. Kwart and K. G. King in, *Concepts in Organic Chemistry* (Ed: K. Hafner, J. M. Lehn, C. W. Rees, P. v. R. Schleyer, B. M. Trost and R. Zahradnik), Springer, Berlin, 1971.
755. L. Laaksonen, P. Pyykkö and D. Sundholm, *Chem. Phys. Lett.*, **96,** 1 (1983).
756. K. J. Laidler, *Theories of Chemical Reaction Rates*, McGraw Hill, New York, 1972.
757. A. Laforgue, *Int. J. Quant. Chem.*, **19,** 989 (1981).
758. P. Lallemand, D. J. David and B. Bigot, *Mol. Phys.*, **27,** 1029 (1974).
759. L. D. Landau and E. M. Lifschitz, *Lehrbuch der Theoretischen Physik*, Vol. III, Akademie-Verlag, Berlin, 1965.
760. L. Láng (Ed), *Absorption Spectra in the Ultraviolet and Visible Region*, Akadémiai Kiadó, Budapest, published since 1960 continuously.
761. S. R. Langhoff and E. R. Davidson, *Int. J. Quant. Chem.*, **8,** 61 (1974).
762. S. R. Langhoff and E. R. Davidson, *J. Chem. Phys.*, **64,** 4699 (1976).
763. P. W. Langhoff, M. Karplus and R. P. Hurst, *J. Chem. Phys.*, **44,** 505 (1966).
764. J. Langlet and J.–P. Malrieu in, *Localization and Delocalizitaion in Quantum Chemistry*, Vol. II, (Ed: O. Chalvet, R. Daudel, S. Diner and J.–P. Malrieu), Reidel, Dordrecht, 1976, pp. 15.
765. I. László, . *Int. J. Quant. Chem. Symp.*, **12,** 105 (1977); *Int. J. Quant. Chem.*, **21,** 813 (1982).
766. W. A. Lathan and K. Morokuma, *J. Am. Chem. Soc.*, **97,** 3615 (1975).
767. W. A. Lathan, G. R. Pack and K. Morokuma, *J. Am. Chem. Soc.*, **97,** 6624 (1975).
768. R. Lavery, C. Etchebest and A. Pullman, *Chem. Phys. Lett.*, **85,** 266 (1982).
769. P. Lazzeretti, *Mol. Phys.*, **28,** 1389 (1974).
770. P. Lazzeretti, B. Cadioli and U. Pincelli, *Int. J. Quant. Chem.*, **10,** 771 (1976).
771. P. Lazzeretti, R. Rossi and R. Zanasi, *J. Chem. Phys.*, **77,** 3129 (1982).
772. P. Lazzeretti and R. Zanasi, *Chem. Phys. Lett.*, **100,** 67 (1983).
773. D. Lee and A. C. Albrecht, *J. Chem. Phys.*, **78,** 3382 (1983).
774. F. H. de Leeuw and A. Dymanus, *J. Mol. Spectry.*, **48,** 427 (1973).

775. R. Lefebre, *Cah. Phys.*, **13,** 369 (1959).
776. H. Lefebre–Brion, *J. Mol. Struct.*, **19,** 103 (1974).
777. R. J. W. Le Fevre, *Adv. Phys. Org. Chem.*, **3,** 1 (1965).
778. R. J. W. Le Fevre, B. J. Orr and G. L. D. Ritchie, *J. Chem. Soc. B.*, 273 (1966).
779. J. E. Lennard–Jones, *Proc. Roy. Soc.*, **A106,** 441, 463.
780. J. E. Lennard–Jones, *Proc. Roy. Soc.*, **A198,** 1, 14 (1949).
781. J. H. van Lenthe and G. G. Balint–Kürti, *Chem. Phys. Lett.*, **76,** 138 (1980).
782. G. Leroy, *J. Mol. Struct. THEOCHEM*, **12,** 45 (1983).
783. J. H. Letcher, *J. Chem. Phys.*, **54,** 3215 (1971).
784. J. H. Letcher, I. Absar and J. R. Van Wazer, *Int. J. Quant. Chem.*, **86,** 451 (1972).
785. B. Levy and J. Riddard, *Mol. Phys.*, **44,** 1099 (1981).
786. E. S. Lewis in, *Proton Transfer Reactions* (Eds: E. Caldin and V. Gold), Chapman and Hall, London, 1975. p. 317.
787. D. R. Lide and M. A. Paul (Eds), *Critical Evaluation of Chemical and Physical Structural Information*, Natl. Acad. Sci., Washington, 1974.
788. G. C. Lie and E. Clementi, *J. Chem. Phys.*, **62,** 2195 (1976).
789. G. C. Lie, S. D. Peyerimhoff, and R. J. Buenker, *J. Chem. Phys.* **75,** 2892 (1981).
790. C–M. Liegener, *Chem. Phys.*, **76,** 397 (1983).
791. C–M. Liegener, *Chem. Phys. Lett.*, **90,** 188 (1982).
792. D. A. Lightner, T. D. Bouman, J. K. Gawronski, K. Gawronska, J. L. Chappuis, B. V. Crist and A. E. Hansen, *J. Am. Chem. Soc.*, **103,** 5314 (1981).
793. D. A. Lightner, T. D. Bouman, W. M. D. Wijekoon and A. E. Hansen, *J.Am.Chem.Soc.*, **106,** 934 (1984).
794. B. Linder and D. A. Rabenold, *Adv.Quant.Chem.*, **6,** 203 (1972).
795. J. Linderberg and J. Michl, *J.Am.Chem.Soc.*, **92,** 2619 (1970).
796. J. Linderberg and Y. Öhrn, *Propagators in Quantum Chemistry*, Academic, London, 1973.
797. J. Linderberg and L. Seamans, *Int.J.Quant.Chem.*, **8,** 925 (1974).
798. J. W. Linnett, *J.Am.Chem.Soc.*, **83,** 2643 (1961).
799. J. L. Lippert, M. W. Hanna and P. J. Trotter, *J.Am.Chem.Soc.*, **91,** 4035 (1969).
800. H. Lischka, *Pure Appl.Chem.*, **51,** 1627 (1979).
801. H. Lischka, P. Čársky and R. Zahradník, *Chem.Phys.*, **25,** 19 (1977).
802. D. H. Liskow, C. F. Bender and H. F. Schaefer III, *J.Chem.Phys.*, **57,** 4509 (1972).
803. D. H. Liskow and G. A. Segal, *J.Am.Chem.Soc.*, **100,** 2945 (1978).
804. K. B. Lipkowitz, *Tetrahedron Lett.*, **25,** 2297 (1984).
805. B. Liu, K. M. Sando, C. S. North, H. B. Friedrich and D. M. Chipman, *J.Chem.Phys.*, **69,** 1425 (1978).
806. R. Lochmann and H. J. Hoffmann, *Int.J.Quant.Chem.*, **11,** 427 (1977).
806a F. London, *J.Phys.Rad.*, **8,** 397 (1937).
806b F. London, *Rev.Mod.Phys.*, **17,** 310 (1945).
807. H. C. Longuet-Higgins, *J.Chem.Phys.*, **18,** 265 (1950).
808. H. C. Longuet-Higgins, *Adv.Spectry.*, **2,** 249 (1961).
809. H. C. Longuet-Higgins, *Proc.Roy.Soc.*, **A344,** 147 (1975).
810. H. C. Longuet-Higgins, and E. W. Abrahamson, *J.Am.Chem.Soc.*, **87,** 2045 (1965).
811. H. C. Longuet-Higgins, and J. N. Murrell, *Proc.Roy.Soc.*, **A68,** 601 (1955).
812. H. C. Longuet-Higgins, and L. Salem, *Proc.Roy.Soc., London*, **A251,** 172 (1959).
813. A. Lopata and Á. I. Kiss, *Comput.Chem.*, **3,** 107 (1979).
814. R. L. Lozes, O. Goscinski and U. I. Wahlgren, *Chem.Phys.Lett.*, **63,** 77 (1970).
815. J. P. Lowe, *J.Am.Chem.Soc.*, **99,** 5557 (1977).
816. J. P. Lowe, *Quantum Chemistry*, Academic, New York, 1978, Chapter 14.
817. P.-O. Löwdin, *J.Chem.Phys.*, **18,** 365 (1950).
818. P.-O. Löwdin, *J.Chem.Phys.*, **21,** 374 (1953).
819. P.-O. Löwdin, *Phys.Rev.*, **97,** 1474 (1955).
820. P.-O. Löwdin, *Phys.Rev.*, **97,** 1490 (1955).
821. P.-O. Löwdin, *Phys.Rev.*, **97,** 1509 (1955).
822. P.-O. Löwdin, *Adv.Chem.Phys.*, **2,** 207 (1959).
823. P.-O. Löwdin, *Rev.Mod.Phys.*, **34,** 520 (1962).
824. P.-O. Löwdin, *J. Math.Phys.*, **3,** 969, 1171 (1962); **6,** 1341 (1965).
825. P.-O. Löwdin, *J.Mol.Spectry.*, **10,** 12 (1963); **13,** 326 (1964); **14,** 112, 119, 131 (1964).

826. P.-O. Löwdin, *Phys.Rev.*, **139,** A357 (1965).
827. P.-O. Löwdin in, *Quantum Theory of Atoms, Molecules and the Solid State*, (Ed: P.-O. Löwdin), Academic, New York, 1966.
828. P.-O. Löwdin, *Adv.Quant.Chem.*, **3,** 323 (1967).
829. P.-O. Löwdin, *Int.J.Quant.Chem.*, **12,** 8197 (1977).
830. P.-O. Löwdin, *Int.J.Quant.Chem.*, **21,** 275 (1982).
831. R. R. Lucchese, K. Haber and H. F. Schaefer III, *J.Am.Chem.Soc.*, **98,** 7617 (1976).
832. R. E. Lucchese and H. F. Schaefer III, *J.Am.Chem.Soc.*, **97,** 7205 (1975).
833. E. A. C. Lucken, *Nuclear Quadrupole Coupling Constants*, Academic, London, 1969.
834. W. L. Luken and O. Sinanoğlu, *J.Chem.Phys.*, **64,** 1495 (1976).
835. I. Lukovits, A. Karpfen, H. Lischka and P. Schuster, *Chem.Phys.Lett.*, **63,** 151 (1979).
836. B. I. Lundqvist in, *Vibrations at Surfaces* (Eds: R. Caudano, J. M. Gilles and A. A. Lucas), Plenum, New York, 1982, p. 541.
837. S. Lunell, *Int.J.Quant.Chem.*, **15,** 97 (1979).
838. T. Luty, *Chem.Phys.Lett.*, **44,** 335 (1976).
839. P. G. Lykos and R. G. Parr, *J.Chem.Phys.*, **24,** 1166 (1956).
840. D. Lynch, M.-T. Lee, R. R. Lucchese and V. McKoy, *J.Chem.Phys.*, **80,** 1907 (1984).
841. H. R. McCleary and L. P. Hammett, *J.Am.Chem.Soc.*, **63,** 2254 (1941).
842. A. L. McClellan, *Tables of Experimental Dipole Moments*, Vol. I, Freeman, San Francisco 1963; Vol. II. Rahara, El Cerrito, California 1974.
842a H. M. McConnell, *J.Chem.Phys.* **24,** 764 (1956).
842b H. M. McConnell, *J.Chem.Phys.* **30,** 126 (1959).
842c H. M. McConnell, *J.Chem.Phys.* **27,** 226 (1957).
843. H. M. McConnell, C. Heller, T. Cole and R. W. Fessenden, *J.Am.Chem.Soc.*, **82,** 766 (1960).
844. E. A. McCullough, *Mol.Phys.*, **42,** 943 (1981).
845. E. A. McCullough and D. M. Silver, *J.Chem.Phys.*, **62,** 4050 (1975).
846. J. W. McIver and A. Komornicki, *Chem.Phys.Lett.*, **10,** 303 (1971).
847. J. W. McIver and A. Komornicki, *J.Am.Chem.Soc.*, **94,** 2625 (1972).
848. J. M. McKelvey, S. Alexandratos, A. Streitwieser, J. L. M. Abboud and W. J. Hehre, *J.Am.Chem. Soc.*, **98,** 244 (1976).
848a A. D. McLachlan, *Mol.Phys.*, **1,** 233 (1958).
849. A. D. McLachlan and M. A. Ball, *Rev.Mod.Phys.*, **36,** 844 (1964); *Mol.Phys.*, **7,** 507 (1964).
850. A. D. McLean and M. Yoshimine, *Int.J.Quant.Chem.Symp.*, **1,** 313 (1967).
851. J. D. Macomber, *The Dynamics of Spectroscopic Transitions*, Wiley, New York, 1976.
851a R. McWeeny, *Mol.Phys.*, **1,** 311 (1958)
852. R. McWeeny, *Proc.Roy.Soc.*, **A253,** 242 (1959).
853. R. McWeeny, *Rev.Mod.Phys.*, **32,** 335 (1960).
854. R. McWeeny and G. Del Re, *Theoret.Chim.Acta*, **10,** 13 (1968).
855. B. Maessen and P.C. Schmidt., *Theoret.Chim.Acta*, **59,** 299 (1981).
856. G. M. Maggiora and R. E. Christoffersen in, *Transition States of Biochemical Processes* (Eds: R. D. Gandour and R. L. Schowen), Plenum, New York, 1978, p. 119.
857. V. Magnasco and G. F. Musso, *Chem.Phys.Lett.*, **87,** 447 (1982).
858. V. Magnasco and A. Perico, *J.Chem.Phys.*, **47,** 971 (1967).
859. E. Magnusson, *J.Am.Chem.Soc.*, **106,** 1177, 1185 (1984).
860. D. Maillard and B. Silvi, *Mol.Phys.*, **40,** 933 (1980).
861. G. C. Maitland, M. Righby, E. B. Smith and W. A. Wakeham, *Intermolecular Forces*, Clarendon, Oxford, 1981.
862. Z. B. Maksić, and N. Mikać, *Mol.Phys.*, **40,** 455 (1980).
863. Z. B. Maksić and A. Rubćić, *J.Am.Chem.Soc.*, **99,** 4233 (1977).
864. Z. B. Maksić and K. Rupnik, *Theoret.Chim.Acta*, **62,** 219 (1983).
864a. G. Malli, *J. Chem. Phys.*, **80,** 2060 (1984).
865. P. Maloń and K. Bláha, *Coll.Czech.Chem.Commun.*, **42,** 687 (1977).
866. J. P. Malrieu in, *Modern Theoretical Chemistry*, Vol. VII, (Ed: G. A. Segal), Plenum, New York, 1977.
866a J. P. Malrieu in, *Localization and Delocalization in Quantum Chemistry*, Vol. I, (Eds: O. Chalvet, R. Daudel, S. Diner and J. P. Malrieu), Reidel, Dordrecht, 1975, p. 335.
867. J. P. Malrieu, *Theoret.Chim.Acta*, **59,** 251 (1981).

868. J. P. Malrieu, P. Claverie and S. Diner, *Theoret.Chim.Acta*, **13,** 18 (1969).
869. R. Manne and T. Aberg, *Chem.Phys.Lett.*, **7,** 282 (1972).
870. R. Manne, K. Wittel and B. S. Mohanty, *Mol.Phys.*, **29,** 485 (1975).
871. J. March, *Advanced Organic Chemistry*, 2nd ed., McGraw Hill, Tokyo, 1977.
872. F. T. Marchese and H. H. Jaffé, *J.Mol.Struct.THEOCHEM*, **3,** 97 (1981).
873. S. Marriott and R. D. Topsom, *J.Mol.Struct.THEOCHEM*, **6,** 83 (1982).
874. C. J. Marsden, *J.C.S.Chem.Commun.*, 401 (1984).
875. F. J. Marsh and M. S. Gordon, *J.Mol.Struct.*, **31,** 345 (1976).
876. H. D. Martin and B. Mayer, *Angew.Chem.Int.Ed.Engl.* **22,** 283 (1983).
877. R. L. Martin and W. R. Wadt, *J.Phys.Chem.*, **86,** 2382 (1982).
878. F. A. Matsen, *J.Am.Chem.Soc.*, **92,** 3525 (1970).
879. O. Matsuoka, *Int.J.Quant. Chem.*, **5,** 1 (1971).
879a I. Mayer quoted in M. Simonyi and F. Tüdős, *Adv.Phys.Org.Chem.*, **9,** 127 (1971).
880. I. Mayer, *Acta Phys.Acad.Sci.Hung.* **30,** 373 (1971); **31,** 403 (1972).
881. I. Mayer, *Acta Phys.Acad.Sci.Hung.*, **36,** 11 (1974).
882. I. Mayer, *Adv.Quant.Chem.*, **12,** 189 (1980).
883. I. Mayer, *Chem.Phys.Lett.*, **89,** 390 (1982).
884. I. Mayer, *Chem.Phys.Lett.*, **97,** 270 (1983).
885. I. Mayer, *Inorg.Chim.Acta*, **77,** L205 (1983).
886. I. Mayer, *Int.J.Quant.Chem.*, **23,** 341 (1983).
887. I. Mayer, *Int.J.Quant.Chem.*, **26,** 151 (1984).
888. I. Mayer, and S. A. Angelov, *Int.J.Quant.Chem.*, **18,** 783 (1980).
889. I. Mayer and P. R. Surján, *Acta Chim.Acad.Sci.Hung.*, **117,** 85 (1984).
890. I. Mayer and P. R. Surján, *J.Chem.Phys.*, **80,** 5649 (1984).
891. F. D. Mayer in, *New Directions in Atomic Physics*, Vol. I., (Eds: E. H. Condon and O. Sinanoğlu), University Press, New Haven, 1972, p. 139.
892. C. A. Mead and A. Moscowitz, *Int.J.Quant.Chem.*, **1,** 243 (1967).
893. E. L. Mehler, *J.Chem.Phys.*, **67,** 2728 (1977).
894. E. L. Mehler, *J.Chem.Phys.*, **74,** 6298 (1981).
895. P. K. Mehrotra, F. T. Marchese and D. L. Beveridge, *J.Am.Chem.Soc.*, **103,** 672 (1981).
896. R. P. Messmer in, *Modern Theoretical Chemistry*, Vol. VIII (Ed: G. A. Segal), Plenum, New York, 1977, p. 215.
897. R. M. Metzger, *J.Chem.Phys.*, **74,** 3444, 3458 (1981).
898. W. Meyer in, *Modern Theoretical Chemistry*, Vol. III, (Ed: H. F. Schaefer III), Plenum, New York, 1977.
899. W. Meyer and P. Pulay, *J.Chem.Phys.*, **56,** 2109 (1972).
900. W. Meyer and P. Rosmus, *J.Chem.Phys.*, **63,** 2356 (1975).
901. M. Mezei and D. L. Beveridge. *J.Chem.Phys.*, **74,** 6902 (1981).
902. P. G. Mezey, *Theoret.Chim.Acta*, **54,** 95 (1980); **58,** 309 (1981); **59,** 321 (1981); **60,** 97, 409 (1982); *J.Chem.Phys.*, **78,** 6182 (1983).
903. P. G. Mezey, *Chem.Phys.Lett.*, **82,** 100 (1981).
904. P. G. Mezey in, *Computational Theoretical Organic Chemistry* (Eds: I. G. Csizmadia and R. Daudel), Reidel, Dordrecht, 1981, p. 101.
905. P. G. Mezey and W. F. Reynolds, *Can.J.Chem.*, **55,** 1567 (1977).
906. J. Michl, *J.Am.Chem.Soc.*,**100,** 6801, 6812 6819 (1978).
907. S. Miertuš and J. Bartos, *Coll.Czech.Chem.Commun.*, **45,** 2308 (1980).
908. S. Miertuš, R. Boča, P. Pelikán and L. Valko, *Chem.Phys.*, **11,** 237 (1976).
909. S. Miertuš and O. Kysel, *Chem.Phys.*, **21,** 33 (1977).
910. S. Miertuš and O. Kysel, *Chem.Phys.*, **21,** 43 (1977).
911. S. Miertuš and O. Kysel, *Chem.Phys.Lett.*, **65,** 395 (1979).
912. S. Miertuš, E. Scrocco and J. Tomasi, *Chem.Phys.*, **55,** 117 (1981).
913. W. H. Miller, *Acc.Chem.Res.*, **9,** 306 (1976).
914. W. H. Miller (Ed), *Modern Theoretical Chemistry*, Vols. I–II, Plenum, New York, 1976.
915. W. H. Miller, *J.Am.Chem.Soc.*, **101,** 6810 (1979).
916. D. M. P. Mingos in, *Comprehensive Organometallic Chemistry* (Eds: G. Wilkinson, F. G. A. Stone and E. W. Abel), Pergamon, Oxford, 1982. Vol. 3, p. 1.

917. V. I. Minkin and R. M. Minyaev in, *Progress in Theoretical Organic Chemistry. Vol. III*, (Ed: I. G. Csizmadia), Elsevier, Amsterdam, 1982, p. 121.
918. V. I. Minkin, O. A. Osipov and Yu. A. Zhdanov, *Dipole Moments in Organic Chemistry*, Plenum, New York, 1970.
919. P. C. Mishra and K. Jug. *Theoret.Chim.Acta*, **61**, 559 (1982).
920. O. Mo and M. Yanez, *Theoret.Chim.Acta*, **47**, 263 (1978).
921. W. Moffitt, *Proc. Roy.Soc.*, **A210**, 245 (1951).
922. W. Moffitt, *Proc. U.S.Natl.Acad.Sci.*, **42**, 736 (1956).
923. W. Moffit, R. B. Woodward, A. Moscowitz, W. Klyne and C. Djerassi, *J.Am.Chem.Soc.*, **83**, 4013 (1961).
924. F. A. Momany, R. F. McGuire, A. W. Burgess and H. A. Scheraga, *J.Phys.Chem.*, **79**, 2361 (1975).
925. C. Møller and M. S. Plesset, *Phys.Rev.*, **46**, 618 (1934).
926. H. J. Monkhorst and B. Jeziorski, *J.Chem.Phys.*, **71**, 5268 (1979).
927. H. J. Monkhorst and M. Kertész, *Phys.Rev.*, **B24**, 3015 (1981).
928. H. J. Monkhorst and K. Salevicz, *J.Chem.Phys.*, **75**, 5782 (1981).
929. S. Montero and G. del Rio, *Mol.Phys.*, **31**, 357 (1976).
930. P. de Montgolfier and A. Hoareau, *J.Chem.Phys.*, **65**, 2477 (1976).
931. H. Moriishi, O. Kikuchi, K. Suzuki and G. Klopman, *Theoret.Chim.Acta*, **64**, 319 (1984).
932. K. Morokuma, *J.Am.Chem.Soc.*, **104**, 3732 (1982).
933. K. Morokuma and S. Iwata, *Chem.Phys.Lett.*, **16**, 192 (1972).
934. K. Morokuma, S. Iwata and W. A. Lathan in, *The World of Quantum Chemistry* (Eds: R. Daudel and B. Pullman), Reidel, Dordrecht, 1973, p. 277.
935. K. Morokuma and K. Kitaura in, *Chemical Application of Atomic and Molecular Electrostatic Potentials* (Eds: P. Politzer and D. G. Truhlar), Plenum, New York, 1980, p. 215.
936. K. Morokuma and H. Umeyama, *Chem.Phys.Lett.*, **49**, 333 (1977).
937. M. Morse, *Phys.Rev.*, **34**, 57 (1929).
938. A. Moscowitz in, *Modern Quantum Chemistry*, Vol. III, (Ed: O. Sinanoğlu), Academic, New York, 1962.
939. A. Moscowitz, K. Mislow, M. A. W. Glass and C. Djerassi, *J.Am.Chem.Soc.*, **84**, 1945 (1962).
940. G. Moss and P. Coppens in, *Chemical Application of Atomic and Molecular Electrostatic Potentials* (Eds: P. Politzer and D. G. Truhlar), Plenum, New York, 1980, p. 427.
941. D. C. Moule and A. D. Walsh, *Chem.Rev.*, **75**, 67 (1975).
942. C. Møller and M. S. Plesset, *Phys.Rev.*, **46**, 618 (1934).
943. P. K. Mukherjee, T. Minato and D. P. Chong, *Int.J.Quant.Chem.*, **23**, 447 (1983).
944. F. Mulder, G. van Dijk and C. Huiszoon, *Mol.Phys.*, **38**, 577 (1979), *erratum*: **40**, 247 (1980).
945. R. S. Mulliken, *J.Chem.Phys.*, **2**, 782 (1934); **3**, 573 (1935).
946. R. S. Mulliken, *J.Chim.Phys.*, **46**, 497, 675 (1949).
947. R. S. Mulliken, *J.Am.Chem.Soc.*, **72**, 600 (1950).
948. R. S. Mulliken, *J.Am.Chem.Soc.*, **72**, 4493 (1950).
949. R. S. Mulliken, *Tetrahedron*, **5**, 253 (1953).
950. R. S. Mulliken, *J.Chem.Phys.* **23**, 1833 (1955).
951. R. S. Mulliken, *Acc.Chem.Res.*, **9**, 7 (1976).
952. R. S. Mulliken and W. C. Ermler, *Diatomic Molecules; Results of ab initio Calculations*, Academic, New York, 1977.
953. R. S. Mulliken and W. C. Ermler, *Polyatomic Molecules*, Academic, New York, 1981.
954. P. Murray-Rust and S. Motherwell, *Acta Cryst.*, **B34**, 2518 (1978).
955. J. N. Murrell and G. Shaw, *Mol.Phys.*, **15**, 325 (1968).
956. J. N. Murrell and J. J. Teixeira-Dias, *Mol.Phys.*, **19**, 329 (1970).
957. B. A. Murtagh and R. W. H. Sargent, *Comput.J.*, **13**, 185 (1970).
958. G. F. Musso and V. Magnasco, *J.Chem.Phys.*, **60**, 3754 (1974).
959. J. N. Murrell and J. A. Pople, *Proc.Phys.Soc. London A*, **69**, 245 (1956).
960. P. L. Müller-Remmers, P. C. Mishra and K. Jug, *J.Am.Chem.Soc.*, **106**, 2518 (1984).
960a L. A. Nafie, *J.Chem.Phys.*, **79**, 4950 (1983).
961. L. A. Nafie and M. Diem, *Acc.Chem.Res.*, **12**, 296 (1979).
962. L. A. Nafie and T. B. Freedman, *J.Chem.Phys.*, **78**, 7108 (1983).
963. H. M. Nagarathna, P. A. Montano and V. M. Naik, *J.Am.Chem.Soc.*, **105**, 2938 (1983).
964. H. Nakatsuji, *J.Chem.Phys.*, **80**, 3703 (1984).
965. H. Nakatsuji, T. Hayakawa and T. Yonezawa, *J.Am.Chem.Soc.*, **103**, 7426 (1981).

966. H. Nakatsuji, T. Koga, K. Kondo and T.Yonezawa, *J.Am.Chem.Soc.*, **100,** 1029 (1978).
967. H. Nakatsuji, T. Kuwata and A. Yoshida, *J.Am.Chem.Soc.*, **95,** 6894 (1973).
968. H. Nakatsuji, K. Ohta and K. Hirao, *J.Chem.Phys.*, **75,** 2952 (1981).
969. R. F. Nalewajski, *J.Mol.Struct.*, **40,** 247 (1977).
970. G. Náray-Szabó, unpublished.
971. G. Náray-Szabó, *Int.J.Quant.Chem.*, **16,** 265 (1969).
972. G. Náray-Szabó, *Acta Phys.Acad.Sci.Hung.*, **40,** 261 (1976).
973. G. Náray-Szabó, *Int.J.Quant.Chem.*, **16,** 265 (1979).
974. G. Náray-Szabó, *Pure Appl.Chem.*, **52,** 1565 (1980).
975. G. Náray-Szabó, *Quantum Chemistry Program Exchange*, **13,** 396 (1980).
976. G. Náray-Szabó, *Acta Phys.Acad.Sci.Hung.*, **51,** 65 (1981).
977. G. Náray-Szabó, *Int.J.Quant.Chem.*, **23,** 723 (1983).
978. G. Náray-Szabó, *Croat.Chem.Acta*, **57,** 901 (1984).
979. G. Náray-Szabó, J. Ángyán and P. R. Surján in, *Steric Effects in Biomolecules* (Ed: G. Náray-Szabó), Elsevier, Amsterdam, 1982, p. 291.
980. G. Náray-Szabó and T. Bleha in, *Progress in Theoretical Organic Chemistry*, Vol. III (Ed: I. G. Csizmadia), Elsevier, Amsterdam, 1982, p. 267.
981. G. Náray-Szabó, A. Grofcsik, K. Kósa, M. Kubinyi and A. Martin, *J.Comput.Chem.*, **2,** 58 (1981).
982. G. Náray-Szabó, and K. Horváth, *Croat.Chem.Acta*, **49,** 461 (1977).
983. G. Náray-Szabó, A. Kapur, P. G. Mezey and L. Polgár, *J.Mol.Struct.THEOCHEM*, **90,** 137 (1982).
984. G. Náray-Szabó and A. Kucsman, *J.Chem.Soc.Dalton*, 891 (1979).
985. G. Náray-Szabó and M. R. Peterson, *J.Mol.Struct.THEOCHEM*, **85,** 249 (1981).
986. G. Náray-Szabó and P. R. Surján, *Chem.Phys.Lett.*, **96,** 499 (1983).
987. M. A. C. Nascimento and W. A. Goddard III, *Chem.Phys.*, **36,** 147 (1979).
988. J. Navaza and G. Tsoucaris, *Phys.Rev.*, **A24,** 683 (1981).
989. S. V. O'Neill, P. K. Pearson, H. F. Schaefer III and C. F. Bender, *J.Chem.Phys.*, **58,** 1126 (1973).
990. D. Neisius and G. Verhangen, *Chem.Phys.Lett.*, **66,** 358 (1979).
991. D. Neisius and G. Verhangen, *Chem.Phys.Lett.*, **78,** 147 (1981).
992. B. Nelander and G. Del Re, *J.Chem.Phys.*, **52,** 5225 (1970).
993. J. L. Nelson and A. A. Frost, *Theoret.Chim.Acta*, **29,** 75 (1973).
994. R. D. Nelson, D. R. Lide and A. A. Maryott, *Natl.Stand.Ref.Data Ser., Natl.Bur.Stand. No.* **10,** (1967).
995. G. Némethy and H. A. Scheraga, *Quart.Rev.Biophys.*, **10,** 239 (1977).
996. P. O. Nerbrant, B. Roos and A. J. Sadlej, *Int.J.Quant.Chem.*, **15,** 135 (1979).
997. R. K. Nesbet, *Proc.Roy.Soc.*, **A230,** 312 (1955).
998. R. K. Nesbet, *Adv.Chem.Phys.*, **9,** 321 (1965).
999. R. K. Nesbet, *Adv.Chem.Phys.*, **14,** 1 (1969).
1000. D. Neuman, and J. W. Moscowitz, *J. Chem. Phys.*, **49,** 2056 (1968).
1001. M. D. Newton, *J. Chem. Phys.*, **58,** 5833 (1973).
1002. M. D. Newton, *J. Phys. Chem.*, **79,** 2795 (1975).
1003. M. D. Newton, W. A. Lathan, W. J. Hehre and J. A. Pople, *J. Am. Chem. Soc.*, **52,** 4064 (1970).
1004. M. T. Nguyen and T. K. Ha, *J. Am. Chem. Soc.*, **106,** 599 (1984).
1005. M. T. Nguyen and A. F. Hegarty, *J. Am. Chem. Soc.*, **106,** 1552 (1984).
1006. J. A. Nichols, D. L. Yeager and P. Jorgensen, *J. Chem. Phys.*, **80,** 293 (1984).
1007. C. A. Nicolaides, M. Papadopoulos and J. Waite, *Theoret. Chim. Acta*, **61,** 427 (1982).
1008. C. A. Nicolaides and G. Theodorakopoulos, *Int. J. Quant. Chem. Symp.*, **14,** 315 (1980).
1009. W. von Niessen, *J. Chem. Phys.*, **56,** 4290 (1970).
1010. W. von Niessen, *Theoret. Chim. Acta*, **27,** 9 (1972).
1011. W. von Niessen, *Theoret. Chim. Acta*, **33,** 185 (1974).
1012. W. von Niessen, *Theoret. Chim. Acta*, **38,** 9 (1975).
1013. W. von Niessen, *Chem. Phys.*, **45,** 47 (1980).
1014. W. von Niessen, G. Bieri and L. Åsbrink, *J. Electron Spectry. Rel. Phen.*, **21,** 175 (1980).
1015. W. von Niessen, L. S. Cederbaum and W. Domcke in, *Excited States in Quantum Chemistry* (Eds: A. Nicolaides and D. R. Beck), Reidel, Dordrecht, 1978, p. 183.
1016. W. von Niessen, L. S. Cederbaum and W. P. Kraemer, *Theoret. Chim. Acta*, **44,** 85 (1977).
1017. W. von Niessen, G. H. F. Diercksen and L. S. Cederbaum, *J. Am. Chem. Soc.*, **100,** 6347 (1978).
1018. W. von Niessen, W. P. Kraemer and J. Schirmer, *J. Chem. Soc. Faraday II*, **77,** 1461 (1981).

1019. E. E. Nikitin, *Adv. Quant. Chem.*, **5,** 135 (1970).
1020. E. E. Nikitin, *Theory of Elementary Atomic and Molecular Processes in Gases*, Clarendon. Oxford, 1974.
1021. K. Nishimoto and N. Mataga, *Z. Phys. Chem.*, **12,** 335 (1957).
1022. L. E. Nitzsche and E. R. Davidson, *Chem. Phys. Lett.*, **58,** 171 (1978).
1023. R. H. Nobes, W. J. Bouma and L. Radom, *J. Am. Chem. Soc.*, **105,** 309 (1983).
1024. J. Noell and K. Morokuma, *Chem. Phys. Lett.*, **36,** 465 (1975).
1025. J. O. Noell and K. Morokuma, *J. Phys. Chem.*, **80,** 2675 (1976).
1026. J. M. Norbeck and R. McWeeny, *Chem. Phys. Lett.*, **34,** 206 (1975).
1027. J. G. Norman and H. J. Kolari, *J. Am. Chem. Soc.*, **97,** 33 (1975).
1028. J. G. Norman, H. J. Kolari, H. B. Gray and W. C. Trogler, *Inorg. Chem.* **16,** 987 (1977).
1029. T. Nozawa, M. Hatano, U. Nagashima, S. Obara, and H. Kashiwagi, *Bull. Chem. Soc. Jpn*, **56,** 1721 (1983).
1030. B. K. Novosadov, A. I. Pogonin, *Theoret. Chim. Acta*, **60,** 495 (1982).
1031. R. Noyori, M. Yamakawa and H. Takaya, *J. Am. Chem. Soc.*, **98,** 1471 (1976).
1032. J. Oddershede, *Adv. Quant. Chem.*, **11,** 275 (1978).
1033. J. Oddershede, *Int. J. Quant. Chem., Symp.* **16,** 583 (1982).
1034. K. Ohno, *Theoret. Chim. Acta*, **2,** 219 (1964).
1035. K. Ohno and K. Morokuma, *Quantum Chemistry Literature Data Base Bibliography of ab initio Calculations for 1978–80*, Elsevier, New York, 1982.
1036. M. Ohsaku, A. Imamura, and K. Hirao, *Bull. Chem. Soc. Japan*, **51,** 3443 (1978).
1037. M. Ohsaku, A. Imamura, K. Hirao and T. Kowamura, *Tetrahedron*, **35,** 701 (1979).
1038. M. Ohsaku, H. Murata, A. Imamura and K. Hirao, *Tetrahedron*, **35,** 1595 (1979).
1039. M. Ohsaku, H. Murata, A. Imamura and K. Hirao, *Tetrahedron*, **36,** 177 (1980).
1040. T. Oie, G. Loew, S. K. Burt, J. S. Binkley and R. D. MacElroy, *Int. J. Quant. Chem. Quant. Biol. Symp.* **9,** 223 (1982).
1041. C. T. O'Konski and J. W. Jost, *J. Mol. Struct.*, **58,** 475 (1980).
1042. B. O'Leary, J. E. Eilers and B. J. Duke, *Quantum Chemistry Program Exchange*, **11,** 263 (1974).
1043. L. Onsager, *J. Am. Chem. Soc.*, **58,** 1486 (1936).
1044. K. O-ohata, H. Taketa and S. Huzinaga, *J. Phys. Soc. Jpn*, **21,** 2306 (1966).
1045. M. Orchin and H. H. Jaffé, *Symmetry, Orbitals and Spectra*, Wiley, New York, 1971.
1046. Y. Orita and A. Pullman, *Theoret. Chim. Acta*, **46,** 251 (1977).
1047. J. V. Ortiz and Y. Öhrn, *Chem. Phys. Lett.*, **77,** 548 (1981).
1048. W. J. Orville–Thomas (Ed), *Internal Rotation in Molecules*, Wiley, London, 1974.
1049. P. Otto and J. Ladik, *Chem. Phys.*, **8,** 192 (1975); *Chem. Phys.*, **19,** 209 (1977).
1050. P. Otto and J. Ladik, *Int. J. Quant. Chem.*, **22,** 169 (1982).
1051. J. Overend, in *Infrared Spectroscopy and Molecular Structure*, (Ed: M. Davies), Elsevier, Amsterdam, 1963.
1052. D. W. Oxtoby, *J. Chem. Phys.*, **69,** 1184 (1978).
1053. D. W. Oxtoby, *J. Chem. Phys.*, **72,** 5171 (1980).
1054. K. Ősapay and G. Náray–Szabó, *Adv. Mol. Relaxation Int. Proc.*, **12,** 97 (1978).
1055. K. Ősapay and G. Náray–Szabó, *J. Mol. Struct. THEOCHEM*, **92,** 57 (1983).
1056. I. Özken and L. Goodman, *Chem. Rev.*, **79,** 275 (1979).
1056a K. G. R. Pachler, *Nucl. Magn. Resonance*, **9,** 49 (1980).
1057. J. Pacansky, U. Wahlgren and P. S. Bagus, *J. Chem. Phys.*, **62,** 2740 (1975).
1058. J. Paldus in, *Theoretical Chemistry: Advances and Perspectives*, Vol II, (Eds: H. Eyring and D. J. Henderson), Academic, New York, 1976.
1059. J. Paldus, J. Čizek and I. Shavitt, *Phys. Rev.*, **A5,** 50 (1972).
1060. J. Paldus, J. Čizek, M. Saute and A. Laforgue, *Phys. Rev. A*, **17,** 805 (1978).
1060a J. Pančíř and R. Zahradník, *Helv. Chim. Acta*, **61,** 59 (1978).
1062. R. Pariser and R. G. Parr, *J. Chem. Phys.*, **21,** 466, 767 (1953).
1063. J. M. Parks and R. G. Parr, *J. Chem. Phys.*, **28,** 335 (1958).
1064. R. G. Parr, *J. Chem. Phys.*, **20,** 1499 (1952).
1065. R. G. Parr, *J. Chem. Phys.*, **33,** 1184 (1960).
1066. R. G. Parr, *The Quantum Theory of Molecular Electronic Structure*, Benjamin, New York, 1964.
1067. R. G. Parr, F. O. Ellison and P. G. Lykos, *J. Chem. Phys.*, **24,** 1106 (1956).

1068. Y. Paterson, G. Némethy and H. A. Scheraga, *Ann. N. Y. Acad. Sci.*, **367,** 132 (1981).
1069. R. Paul, *Field Theoretical Methods in Chemical Physics*, Elsevier, Amsterdam, 1982.
1069a L. Pauling, *J. Chem. Phys.*, **4,** 673 (1936).
1070. L. Pauling, *The Nature of the Chemical Bond*, Cornell, Ithaca, New York, 1960.
1071. R. Pauncz, *Alternant Molecular Orbital Method*, Saunders, Philadelphia, 1967.
1072. R. Pauncz, *Spin Eigenfunctions–Construction and Use*, Plenum, New York, 1979.
1073. F. Pauzat, B. Levy and Y. Ellinger, *Nouv. J. Chim.*, **4,** 147 (1980).
1074. R. G. Pearson, *J. Chem. Ed.*, **45,** 581, 643 (1968).
1075. R. G. Pearson, *Acc. Chem. Res.*, **4,** 152 (1971).
1076. R. G. Pearson, *Symmetry Rules for Chemical Reactions: Orbital Topology and Elementary Processes*, Wiley New York, 1976.
1077. J. B. Peel, *Int. J. Quant. Chem.*, **23,** 653 (1983).
1078. C. L. Pekeris, *Phys. Rev.*, **112,** 1649 (1958).
1079. C. L. Pekeris, *Phys. Rev.*, **115,** 1216 (1959).
1080. A. Pelter and K. Smith in, *Comprehensive Organic Chemistry* (Eds: D. Barton and W. D. Ollis), Vol. III, (Ed: D. Neville Jones), Pergamon, Oxford, 1979, p. 695.
1081. I. Pepperberg, T. A. Halgren and W. N. Lipscomb, *J. Am. Chem. Soc.*, **98,** 3442 (1976).
1082. M. Peric, R. J. Buenker and S. D. Peyerimhoff, *Can. J. Chem.*, **55,** 1533 (1977).
1083. H. Perrin, A. Cosse–Barbi, N. Brigot and S. Odiot, *Mol. Phys.*, **29,** 1261 (1975).
1084. W. B. Person and J. H. Newton, *J. Chem. Phys.*, **61,** 1040 (1974).
1085. D. Peters, *J. Chem. Phys.*, **46,** 4427 (1967).
1086. D. Peters, *J. Am. Chem. Soc.*, **94,** 707 (1972).
1087. M. R. Peterson and I. G. Csizmadia, in *Progress in Theoretical Organic Chemistry*, Vol. III (Ed.: I. G. Csizmadia) Elsevier, Amsterdam, 1983, p. 190.
1088. M. R. Peterson and R. A. Poirier, *Program MONSTERGAUSS*, University of Toronto, 1981.
1089. M. I. Petrashen, L. V. Abarenkov and N. N. Kristofel, *Opt. Spectrosc.*, **9,** 276 (1960).
1090. C. Petrongolo, *Gazz. Chim. Ital.*, **108,** 445 (1978).
1091. C. Petrongolo, R. J. Buenker and S. D. Peyerimhoff, *J. Chem. Phys.*, **76,** 3635 (1982).
1092. S. D. Peyerimhoff in, *The Jerusalem Symposia on Quantum Chemistry and Biochemistry*, Vol. VI: *Chemical and Biochemical Reactivity* (Eds: E. D. Bergmann and B. Pullman), The Israel Academy of Sciences, Jerusalem, 1974, p. 359.
1093. S. D. Peyerimhoff, *Gazz. Chim. Ital*, **108,** 411 (1978).
1094. S. D. Peyerimhoff and R. J. Buenker, *Adv. Quant. Chem.*, **9,** 69 (1975).
1095. S. D. Peyerimhoff and R. J. Buenker, *Theoret. Chim. Acta*, **27,** 243 (1972).
1096. S. D. Peyerimhoff, R. J. Buenker, W. E. Kammer and H. Hsu, *Chem. Phys. Lett.*, **8,** 129 (1971).
1097. J. C. Phillips and L. Kleinman, *Phys. Rev.*, **116,** 287 (1959).
1098. P. Phillips and E. R. Davidson, *Chem. Phys. Lett.*, **78,** 230 (1981).
1099. R. A. Phillips, R. J. Buenker, P. J. Bruna and S. D. Peyerimhoff, *Chem. Phys.*, **84,** 11 (1984).
1100. B. T. Pickup and O. Goscinski, *Mol. Phys.*, **26,** 1013 (1973).
1101. M. R. Pincus, S. S. Zimmerman and H. A. Scheraga, *Proc. Natl. Acad. Sci. USA*. **74,** 4261 (1977).
1102. K. S. Pitzer, *Adv. Chem. Phys.*, **2,** 59 (1959).
1103. K. S. Pitzer, *Acc. Chem. Res.*, **12,** 271 (1979).
1104. J. R. Platt, in *Handbuch der Physik*, **371c,** 188 (1967).
1105. J. R. Platt, K. Ruedenberg, C. W. Scherr, N. S. Ham, H. Labhart and W. Lichten, *Free-Electron Theory of Conjugated Molecules: A Source Book*, New York, 1964.
1106. R. Polák, *Theoret. Chim. Acta*, **14,** 163 (1969).
1107. R. Polák, *Int. J. Quant. Chem.*, **4.** 271 (1970).
1108. R. Polák, *Int. J. Quant. Chem.*, **6,** 10 (1972).
1109. R. Polák, *Coll. Czech. Chem. Commun.*, **38,** 1450 (1973).
1110. R. Polák, *Coll. Czech. Chem. Commun.*, **39,** 2877 (1974).
1111. P. L. Polavarapu and L. A. Nafie, *J. Chem. Phys.*, **73,** 1567 (1980).
1112. P. Politzer, *Theoret. Chim. Acta*, **23,** 203 (1971).
1113. P. Politzer, *J. Chem. Phys.*, **64,** 4239 (1976); **69,** 491 (1978); **70,** 1067 (1979).
1114. P. Politzer, L. Abrahamsen and P. Sjoberg, *J. Am. Chem. Soc.*, **106,** 855 (1984).
1115. P. Politzer and R. R. Harris, *J. Am. Chem. Soc.*, **92,** 6451 (1970).
1116. P. Politzer, S. J. Landry and T. Wärnheim, *J. Phys. Chem.*, **86,** 4767 (1982).

1117. P. Politzer and R. S. Mulliken, *J. Chem. Phys.*, **55,** 5135 (1971).
1118. P. Politzer and R. G. Parr, *J. Chem. Phys.*, **61,** 4258 (1974).
1118a J. A. Pople, *Mol. Phys.*, **1,** 216 (1958).
1119. J. A. Pople, *Trans, Faraday Soc.*, **49,** 1375 (1953).
1120. J. A. Pople in, *Modern Theoretical Chemistry*, Vol. IV (Ed: H. F. Schaefer III), Plenum, New York, 1977, p. 1.
1121. J. A. Pople and D. L. Beveridge, *Approximate Molecular Orbital Theory*, McGraw Hill, New York, 1970.
1121a J. A. Pople, D. L. Beveridge and P. A. Dobosh, *J. Am. Chem. Soc.*, **90,** 4201 (1968).
1122. J. A. Pople and M. Gordon, *J. Am. Chem. Soc.*, **89,** 4253 (1967).
1123. J. A. Pople, R. Krishnan, H. B. Schlegel and J. S. Binkley, *Int. J. Quant. Chem.*, **14,** 545 (1978).
1124. J. A. Pople, J. W. McIver, jr. and N. S. Ostlund, *J. Chem. Phys.*, **49,** 2960 (1968).
1125. J. A. Pople and P. Schofield, *Phil. Mag.*, **2,** 591 (1957).
1126. J. A. Pople and G. A. Segal, *J. Chem. Phys.*, **43,** 5136 (1965).
1127. D. Poppinger, *Chem. Phys. Lett.*, **35,** 550 (1975).
1128. D. Poppinger, L. Radom and J. A. Pople, *J. Am. Chem. Soc.*, **99,** 7806 (1977).
1129. R. E. Powell, *J. Chem. Educ.*, **45,** 558, 790 (1968).
1130. E. A. Power, *Introductory Quantum Electrodynamics*, Longmans, London, 1964.
1131. E. A. Power and T. Tirunamachandran, *J. Chem. Phys.*, **55,** 5322 (1971); **60,** 3695 (1974).
1132. P. L. Prasad, *J. Chem. Phys.*, **69,** 4403 (1978).
1133. H. Preuss, *Z. Naturforsch.*, **19a,** 1335 (1964); **20a,** 17, 21 (1965).
1134. P. Pulay, *Mol. Phys.*, **17,** 197 (1969).
1135. P. Pulay in, *Modern Theoretical Chemistry*, Vol. IV (Ed: H. F. Schaefer III), Plenum, New York, 1977, p. 153.
1135a P. Pulay, *Theoret. Chim. Acta*, **50,** 229 (1979).
1136. P. Pulay, G. Fogarasi, F. Pang and J. E. Boggs, *J. Am. Chem. Soc.*, **101,** 2550 (1979).
1137. P. Pulay, G. Fogarasi, G. Pongor, J. E. Boggs and A. Vargha, *J. Am. Chem. Soc.*, **105,** 7037 (1983).
1138. P. Pulay and W. Meyer, *J. Mol. Spectry.*, **40,** 59 (1971).
1139. P. Pulay and W. Meyer, *J. Chem. Phys.*, **57,** 3337 (1972).
1140. P. Pulay and W. Meyer, *Mol. Phys.*, **27,** 473 (1974).
1141. P. Pulay and F. Török, *Mol. Phys.*, **25,** 1153 (1973).
1142. A. Pullman, *Top. Curr. Chem.*, **31,** 45 (1972).
1143. A. Pullman in, *The New World of Quantum Chemistry*, (Eds: B. Pullmann and R. G. Parr), Reidel, Dordrecht, 1976, p. 149.
1144. B. Pullman in, *Quantum Mechanics of Molecular Conformations* (Ed: B. Pullman), Wiley, London, 1976, p. 295.
1145. B. Pullman and A. Pullman, *Quantum Biochemistry*, Wiley, New York, 1963.
1146. B. Pullman, S. Miertuš and D. Perahia, *Theoret. Chim. Acta*, **50,** 317 (1979).
1147. P. Pyykkö, *Adv. Quant. Chem.*, **11,** 353 (1978).
1148. *Quantum Chemistry Program Exchange*, Programs No. 135, 250 and 332, Indiana University, Bloomington, USA.
1149. J. Rabinowitz and R. Rein, *Int. J. Quant. Chem.*, **6,** 669 (1972).
1150. L. Radom, in *Progress in Theoretical Organic Chemistry*, Vol. III (Ed. I. G. Csizmadia), Elsevier, Amsterdam, 1982, p. 1.
1150a L. Radom, W. J. Hehre and J. A. Pople, *J. Am. Chem. Soc.*, **93,** 289 (1971).
1151. K. Raghavachari and J. A. Pople, *Int. J. Quant. Chem.*, **20,** 1067 (1981).
1151a N. F. Ramsey, *Phys. Rev.*, **91,** 303 (1953).
1152. C. N. R. Rao, P. K. Baso and M. S. Hedge, *Appl. Spectrosc. Rev.*, **15,** 1 (1979).
1153. M. Rao and B. J. Berne, *J. Phys. Chem.*, **85,** 1498 (1981).
1154. A. Rauk, *J. Am. Chem. Soc.*, **103,** 1023 (1981).
1155. A. Rauk, L. C. Allen and E. Clementi, *J. Chem. Phys.* **52,** 4133 (1970).
1156. A. Rauk and J. M. Barriel, *Chem. Phys.*, **25,** 409 (1977).
1157. A. Rauk, J. M. Barriel and T. Ziegler, in, *Progress in Theoretical Organic Chemistry*, Vol. II: *Application of MO Theory in Organic Chemistry*, (Ed.: I. G. Csizmadia), Elsevier, Amsterdam, 1977, p. 467.
1158. A. Rauk, J. O. Jarvie. H. Ichimura and J. M. Barriel, *J. Am. Chem. Soc.*, **97,** 5656 (1975).

1159. G. Ravishanker, M. Mezei and D. L. Beveridge, *Chem. Soc. Symp. Faraday*, **17,** (1983).
1160. M. T. Rayez-Meaune, J. J. Danneberg and J. L. Whitten, *J. Am. Chem. Soc.*, **100,** 747 (1978).
1161. K. Razi Naqvi and W. Byers Brown, *Int. J. Quant. Chem.*, **6,** 271 (1972).
1162. M. Redshaw and W. J. Orville–Thomas, *J. Chem. Soc. Faraday Trans.* II, **75,** 1103 (1979).
1163. A. E. Reed and F. Weinhold, *J. Chem. Phys.*, **78,** 4066 (1983).
1164. C. M. Reeves and R. Fletcher, *J. Chem. Phys.*, **42,** 4073 (1965).
1165. R. Rein, *Adv. Quant. Chem.*, **7,** 325 (1973).
1166. R. Rein, G. Clarke and F. E. Harris in, *The Jerusalem Symposia on Quantum Chemistry and Biochemistry*, Vol. II: *Quantum Aspects of Heterocyclic Compounds in Chemistry and Biochemistry*, (Eds: E. D. Bergmann and B. Pullman), The Israel Academy of Sciences Jerusalem, 1970, p. 86.
1167. W. F. Reynolds, P. G. Mezey, W. J. Hehre, R. D. Topsom and R. W. Taft, *J. Am. Chem. Soc.*, **99,** 5821 (1977).
1168. W. F. Reynolds, R. W. Taft, S. Marriott and R. D. Topsom, *Tetrahedron Lett.*, **23,** 1055 (1982).
1169. C. H. Rhee, R. M. Metzger and F. M. Wiygul, *J. Chem. Phys.*, **77,** 899 (1982).
1170. W. G. Richards and V. Sackwild, *Chem. Ber.*, **18,** 636 (1982).
1171. W. G. Richards, T. E. H. Walker, L. Farnell and P. R. Scott, *Bibliography of ab initio Molecular Wawe Functions*, Clarendon, Oxford, 1974.
1172. W. G. Richards, T. E. H. Walker and R. K. Hinkley, *Bibliography of ab initio Molecular Wave Functions.* Oxford. Univ. Press, London, 1971.
1173. W. G. Richards, T. E. H. Walker and P. R. Scott, *Bibliography of ab initio Molecular Wave Functions, Supplement for 1974–1977*, Oxford Univ. Press, London, 1978.
1174. F. S. Richardson, D. D. Shillady and J. E. Bloor, *J. Phys. Chem.*, **75,** 2466 (1971).
1175. F. S. Richardson, R. Strickland and D. D. Shillady, *J. Phys. Chem.*, **77,** 248 (1973).
1176. J. E. Ridley and M. C. Zerner, *Theoret. Chim. Acta*, **32,** 111 (1973); **42,** 223 (1976).
1177. D. Rinaldi and J. L. Rivail, *Theoret. Chim. Acta*, **32,** 57 (1973).
1178. D. Rinaldi, M. F. Ruiz–Lopez and J. L. Rivail, *J. Chem. Phys.*, **78,** 834 (1983).
1179. J. L. Rivail and A. Cartier, *Mol. Phys.*, **36,**1085 (1978).
1180. J. L. Rivail and D. Rinaldi, *Chem. Phys.*, **18,** 233 (1976).
1181. A. B. Rives and F. Weinhold, *Int. J. Quant. Chem., Symp.*,**14,** 201 (1980).
1181a M. A. Robb, R. Eade, I. G. Csizmadia, R. K. Gosawi and O. P. Strausz, in: *Progress in Theoretical Organic Chemistry*, Vol. II.: *Application of MO Theory in Organic Chemistry*, (Ed. I. G. Csizmadia), Elsevier, Amsterdam, 1977, p. 248.
1182. D. A. Roberts and G. L. Geoffroy in, *Comprehensive Organometallic Chemistry*, Vol. VI (Eds: G. Wilkinson, F. G. A. Stone and E. W. Abel), Pergamon, Oxford, 1982, p. 763.
1183. M. B. Robin, *Higher Excited States of Molecules*, Vols. I–II, Academic, New York, 1975.
1184. P. J. Robinson and K. A. Holbrook, Unimolecular Reactions, Wiley, New York, 1972.
1185. H. W. Roesky, *Angew. Chem.*, **91,** 112 (1979).
1186. J. D. Rogers and J. J. Hillman, *J. Chem. Phys.*, **77,** 3615 (1982).
1187. B. O. Roos, *Int. J. Quant. Chem. Symp.*, **14,** 175 (1980).
1188. R. O. Roos and P. E. M. Siegbahn in, *Modern Theoretical Chemistry*, Vol. III (Ed.: H. F. Schaefer III), Plenum, New York, 1977.
1188a K. D. J. Root, M. C. R. Symons and B. C. Weatherley, *Mol. Phys.*, **11,** 161 (1966).
1189. C. C. J. Roothaan, *Rev. Mod. Phys.*, **23,** 69 (1951).
1190. C. C. J. Roothaan and P. S. Bagus in, *Methods in Computational Physics*, Vol. II (Ed: B. Alder, S. Fernbach and M. Rothenberg), Academic, New York, 1963.
1191. J. B. Rose, T. I. Shibuya and V. McKoy, *J. Chem. Phys.*, **60,** 2700 (1974).
1192. A. Rosén and I. Lindgren, *Phys. Rev.*, **176,** 114 (1968).
1193. L. Rosenfeld, *Z. Phys.*, **52,** 161 (1928).
1194. J. S. Rosenfield and E. Charney, *J. Am. Chem. Soc.*, **99,** 3209 (1977).
1195. M. J. Rothman and L. L. Lohr, Jr., *Chem. Phys. Lett.*, **70,** 405 (1980).
1196. M. Roux, S. Besnainou and R. Daudel, *J. Chim. Phys.*, **54,** 218, 939 (1956).
1197. D. J. Rowe, *Rev. Mod. Phys.*, **40,** 153 (1968).
1198. M. D. Rozeboom, I. M. Tegmo–Larsson and K. N. Houk, *J. Org. Chem.*, **46,** 2338 (1981).
1199. N. Rösch, R. P. Messmer and K. H. Johnson, *J. Am. Chem. Soc.*, **96,** 3855 (1974).
1200. N. Rösch and A. Streitwieser, Jr., *J. Organomet. Chem.*, **145,** 195 (1978).
1201. K. Ruedenberg, *J. Chem. Phys.* **19,** 1433 (1951).

1202. K. Ruedenberg, *Rev. Mod. Phys.*, **34,** 326 (1962).
1203. K. Ruedenberg in *Localization and Delocalization in Quantum Chemistry*, Vol. I (Eds: O. Chalvet, R. Daudel, S. Diner and J. P. Malrieu), Reidel, Dordrecht, 1975, p. 223.
1204. K. Ruedenberg, *J. Chem. Phys.*, **66,** 374 (1977).
1205. K. Ruedenberg, M. W. Schmidt, M. M. Gilbert and S. T. Elbert, *Chem. Phys.*, **71,** 41 (1982).
1206. K. Ruedenberg and K. R. Sundberg in, *Quantum Science*, (Eds: J. L. Calais, O. Goscinski, J. Linderberg and Y. Öhrn), Plenum, New York, 1976.
1207. P. Ruelle and C. Sandorfy, *Theoret. Chim. Acta*, **61,** 11 (1982).
1208. M. E. Ruiz, A. Flores–Riveros and C. Novaro, *J. Catal.*, **64,** 1 (1980).
1209. M. F. Ruiz–Lopez and D. Rinaldi, *J. Mol. Struct. THEOCHEM*, **10,** 265 (1983).
1210. M. Ruiz–Lopez, D. Rinaldi, J. L. Rivail and A. Oliva, *J. Chem. Res. S*, 329 (1982).
1211. P. Rusegger, H. Lischka and P. Schuster, *Chem. Phys. Lett.*, **12,** 392 (1971).
1212. A. J. Sadlej, *Chem. Phys. Lett.*, **47,** 50 (1977).
1213. A. J. Sadlej, *Mol. Phys.*, **40,** 509 (1980).
1214. A. J. Sadlej, *J. Chem. Phys.*, **75,** 320 (1981).
1215. J. Y. Saillard and R. Hoffmann, *J. Am. Chem. Soc.*, **106,** 2006 (1984).
1216. Y. Sakai and S. Huzinaga, *J. Chem. Phys.*, **76,** 2552, 2537 (1982).
1217. S. Sakaki, M. Nishikawa and A. Ohyoshi, *J. Am. Chem. Soc.*, **102,** 4062 (1980).
1218. D. R. Salahub and C. Sandorfy, *Theoret. Chim. Acta*, **20,** 227 (1971).
1219. L. Salem, *The Molecular Orbital Theory of Conjugated Systems*, Benjamin, New York, 1966.
1220. L. Salem, *Acc. Chem. Res.*, **12,** 67 (1979).
1221. C. Sandorfy, in, *Progress in Theoretical Organic Chemistry, Vol. II: Application of MO Theory in Organic Chemistry*, (Ed.: I. G. Csizmadia), Elsevier, Amsterdam, 1977, p. 384.
1222. J. E. Sanhueza, *Theoret. Chim. Acta*, **60,** 143 (1981).
1223. J. E. Sanhueza, O. Tapia, W. G. Laidlaw and M. Trsic, *J. Chem. Phys.*, **70,** 3096 (1979).
1224. A. B. Sannigrahi, D. C. Mukherjee and B. R. De, *Int. J. Quant. Chem.*, **23,** 1695 (1983).
1225. D. P. Santry, *Theoret. Chim. Acta*, **42,** 67 (1977).
1226. V. R. Saunders in, *Computational Techniques in Quantum Chemistry and Molecular Physics*, (Eds: G. H. F. Diercksen, B. T. Sutcliffe and A. Veillard), Reidel, Dordrecht, 1965.
1227. V. R. Saunders and I. H. Hillier, *Int. J. Quant. Chem.*, **7,** 699 (1973).
1228. P. Saxe, H. F. Schaefer III and N. C. Handy, *Chem. Phys. Lett.*, **79,** 202 (1982).
1229. H. F. Schaefer III, *J. Chem. Phys.*, **54,** 2207 (1971).
1230. H. F. Schaefer III, *The Electronic Structure of Atoms and Molecules: A Survey of Rigorous Quantum Mechanical Results*, Addison–Wesley, Reading, 1972.
1231. H. F. Schaefer III, *Ann. Rev. Phys. Chem.*, **27,** 261 (1977).
1232. L. Schäfer, *J. Mol. Struct.*, **100,** 59 (1983).
1233. P. Scharfenberg, *Theoret. Chim. Acta*, **49,** 123 (1978).
1234. C. C. Schatz, J. M. Bowman and A. Kupperman, *Chem. Phys.*, **63,** 674, 685 (1975).
1235. J. A. Schellman, *Acc. Chem. Res.*, **1,** 144 (1968).
1236. J. A. Schellman, *Chem. Rev.*, **75,** 323 (1975).
1237. L. I. Schiff, *Quantum Mechanics*, 3rd Ed., McGraw Hill, New York, 1968.
1238. M. Schindler and W. Kutzelnigg, *J. Chem. Phys.*, **76,** 1919 (1982).
1239. M. Schindler and W. Kutzelnigg, *J. Am. Chem. Soc.*, **105,** 1360 (1983).
1240. M. Schindler and W. Kutzelnigg, *Mol. Phys.*, **88,** 781 (1983).
1241. B. Schneider, H. S. Taylor and R. Yaris, *Phys. Rev. A*, **1,** 855 (1970).
1242. V. Schomaker and D. P. Stevenson, *J. Am. Chem. Soc.*, **63,** 37 (1941).
1243. J. Schirmer, L. S. Cederbaum, W. Domcke and W. von Niessen, *Chem. Phys.*, **26,** 149 (1977).
1244. J. M. Schulman, J. W. Moscowitz and C. Hollister, *J. Chem. Phys.*, **46,** 2759 (1967).
1245. P. Schuster in, *Intermolecular Interactions: From Diatomics to Biopolymers*, (Ed: B. Pullman), Wiley, London, 1978, p. 363.
1246. P. Schuster, *Angew. Chem. Int. Ed. Engl.*, **20,** 546 (1981).
1247. P. Schuster, A. Karpfen and A. Beyer in, *Molecular Interactions*, (Eds: W. J. Orville–Thomas and H. Ratajczak), Wiley, London, 1979.
1248. A. Schweig, *Chem. Phys. Lett.*, **1,** 163, 195 (1967).
1249. A. Schweig and W. Thiel, *J. Am. Chem. Soc.*, **103,** 1425 (1981).
1250. E. Scrocco and J. Tomasi, *Top. Curr. Chem.*, **42,** 95 (1973).

1251. E. Scrocco and J. Tomasi, *Adv. Quant. Chem.*, **11,** 115 (1978).
1252. G. A. Segal, *J. Am. Chem. Soc.*, **96,** 7892 (1974).
1253. G. A. Segal (Ed), *Semiempirical Methods of Electronic Structure Calculation, Modern Theoretical Chemistry*, Vol. VII, Plenum, New York, 1977.
1254. G. Seger and E. Kochanski, *Int. J. Quant. Chem.*, **17,** 955 (1980).
1255. A. M. Senkow and J. W. Linnett, *J. Chem. Soc. Faraday II*, **72,** 1503 (1976).
1256. K. D. Sen, *Int. J. Quant. Chem.*, **18,** 907 (1980).
1257. K. D. Sen, *J. Chem. Phys.*, **74,** 1500 (1981).
1258. J. Seres, G. Náray–Szabó, K. Simon, K. Daróczi–Csuka, I. Szilágyi and L. Párkányi, *Tetrahedron*, **37,** 1565 (1981).
1259. J. Serre, *Int. J. Quant. Chem.*, **19,** 1171 (1981).
1260. L. M. Sesé and M. Fernández, *J. Mol. Struct. THEOCHEM*, **16,** 101 (1984).
1261. A. Sevin and P. Chaguin, *J. Org. Chem.*, **47,** 4145 (1982).
1262. S. Shaik, R. Hoffmann, C. R. Fisel and R. H. Summerville, *J. Am. Chem. Soc.*, **102,** 4555 (1980).
1263. I. Shavitt in, *Methods of Computational Physics*, Vol. II, Academic, New York, 1963, p. 30.
1264. I. Shavitt, *Int. J. Quant. Chem., Symp.*, **11,** 131 (1977); **12,** 5 (1978).
1265. I. Shavitt, *Chem. Phys. Lett.*, **63,** 421 (1979).
1266. I. Shavitt and M. Karplus, *J. Chem. Phys.*, **36,** 550 (1962); **43,** 398 (1965).
1267. T. I. Shibuya and V. McKoy, *Phys. Rev. A*, **2,** 2208 (1970).
1268. T. I. Shibuya, J. Rose and D. McKoy, *J. Chem. Phys.*, **58,** 500 (1973).
1269. L. L. Shipman and R. E. Christoffersen, *Chem. Phys. Lett.*, **15,** 469 (1972).
1270. D. A. Shirley, *Rev. Mod. Phys.*, **36,** 339 (1964).
1271. D. A. Shirley, *Chem. Phys. Lett.*, **15,** 325 (1972).
1272. R. G. Shulman and S. Sugano, *J. Chem. Phys.*, **42,** 39 (1965).
1273. K. Siegbahn, C. Nordling, G. Johansson, J. Hedman, P. F. Hedén, K. Hamrin, U. Gelius, T. Bergmark, L. O. Werme, R. Manne and Y. Baer, *ESCA Applied to Free Molecules*, North Holland, Amsterdam, 1969.
1274. C. Sieiro, P. Gonzalez–Diaz and Y. G. Smeyers, *J. Mol. Struct.*, **24,** 345 (1975).
1275. A. M. Simas, A. J. Thakkar and V. H. Smith, *Int. J. Quant. Chem.*, **21,** 419 (1982).
1275a A. M. Simas, W. M. Westgate and V. H. Smith, *J. Chem. Phys.*, **80,** 2636 (1984).
1276. M. Simonetta and A. Gavezzotti, *J. Mol. Struct. THEOCHEM*, **16,** 75 (1984).
1277. M. Simonetta, M. Raimondi and G. F. Tantardini, *Int. J. Quant. Chem., Symp.*, **15,** 225 (1981).
1278. J. Simons, *Ann. Rev. Phys. Chem.*, **28,** 15 (1977).
1279. J. Simons and W. D. Smith, *J. Chem. Phys.*, **58,** 4899 (1973).
1279a M. Simonyi and I. Mayer, *Acta Chim. Acad. Sci. Hung.*, **87,** 15 (1975).
1280. W. T. Simpson, *J. Am. Chem. Soc.*, **73,** 5363 (1951); **77,** 6164 (1955).
1281. O. Sinanoğlu, *J. Chem. Phys.*, **36,** 706 (1962).
1282. O. Sinanoğlu, *Adv. Chem. Phys.*, **6,** 315 (1964).
1283. A. L. Sklar, *J. Chem. Phys.*, **7,** 987 (1939).
1284. Z. Slanina and R. Zahradník, *Coll. Czech. Chem. Commun.*, **39,** 729 (1974).
1285. J. C. Slater, *Phys. Rev.*, **36,** 57 (1930).
1286. J. C. Slater, *Phys. Rev.*, **38,** 1109 (1931).
1287. J. C. Slater, *Quantum Theory of Atomic Structure*, McGraw Hill, New York, 1960.
1288. J. C. Slater, *Adv. Quantum Chem.*, **6,** 1 (1972).
1289. C. P. Slichter, *Principles of Magnetic Resonance*, 2nd ed., Springer-Verlag, Berlin, 1978.
1290. W. M. A. Smit and T. van Dam, *J. Mol. Struct. THEOCHEM*, **5,** 273 (1982).
1291. W. M. A. Smit and T. van Dam, *J. Chem. Phys.*, **72,** 3658 (1980).
1292. D. W. Smith, *Structure and Bonding*, **35,** 87 (1978).
1293. J. W. Smith, *Electric Dipole Moments*, Butterworth, London, 1955.
1294. V. H. Smith, Jr., *Phys., Scripta*, **15,** 147 (1977).
1295. W. L. Smith, *Mol. Phys.*, **26,** 361 (1973).
1296. G. Snatzke, *Angew. Chem. Int. Ed. Engl.*, **18,** 363 (1979).
1297. L. C. Snyder, *Chem. Phys.*, **55,** 95 (1971).
1297a P. Sohár, *Nuclear Magnetic Resonance Spectroscopy*, Vols I–III, CRC, Boca Raton, 1983.
1298. T. Sordo, J. Bertrán and E. Canadell, *J. C. S. Perkin II*, 1486 (1979).
1299. O. J. Sovers, C. W. Kern, R. M. Pitzer and M. Karplus, *J. Chem. Phys.*, **49,** 259 (1968).

1300. K. Spartalian and C. J. Carrano, *J. Chim. Phys.*, **78.** 4811 (1983).
1301. H. Sponer and E. Teller, *Rev. Mod. Phys.*, **13,** 75 (1961).
1302. H. A. Staab, *Einführung in die theoretische Organische Chemie*, 4. Aufl., Verlag Chemie, Weinheim, 1964.
1303. V. Staemmler, *Theoret. Chim. Acta*, **62,** 69 (1982).
1304. V. Staemmler, R. Jaquet and M. Jungen, *J. Chem. Phys.*, **74,** 1285 (1981).
1305. R. E. Stanton, *J. Chem. Phys.*, **75,** 3426, 5416 (1981).
1306. D. Steele in, *Advances in Infrared and Raman Spectroscopy*, (Eds: R. J. H. Clark and R. E. Hester), Vol. I, Heyden, London, 1976, pp. 232.
1307. P. J. Stephens, *J. Chem. Phys.*, **52,** 2489 (1970); *Annu. Rev. Phys. Chem.*, **25,** 201 (1974).
1308. R. M. Sternheimer, *Phys. Rev.*, **84,** 244 (1951); **93,** 734 (1954); **102,** 731 (1956); **130,** 1423 (1963).
1309. R. M. Stevens, *J. Chem. Phys.*, **52,** 1397 (1970); **55,** 1725 (1971).
1310. R. M. Stevens, R. M. Pitzer and W. N. Lipscomb, *J. Chem. Phys.*, **38,** 550 (1963).
1311. R. F. Stewart, *Isr. J. Chem.*, **16,** 124 (1977).
1312. F. G. A. Stone, *Angew. Chem. Int. Ed. Engl.*, **23,** 89 (1984).
1313. A. Streitwieser, *Molecular Orbital Theory for Organic Chemists*, Wiley, New York, 1961.
1314. H. A. Stuart, *Molekülstruktur*, 3. Aufl., Springer-Verlag, Berlin, 1967.
1315. P. R. Surján, unpublished.
1316. P. R. Surján, *Chem.Phys.Lett.*, **92,** 483 (1982).
1317. P. R. Surján, *Croat.Chem.Acta*, **56,** 289 (1983).
1318. P. R. Surján and J. Ángyán, *Phys.Rev.A.*, **28,** 45 (1983).
1319. P. R. Surján and M. Kertész, *Theoret.Chim.Acta*, **55,** 103 (1980).
1320. P. R. Surján, M. Kertész, A. Karpfen and J. Koller, *Phys.Rev.*, **B27,** 7583 (1983).
1321. P. R. Surján and I. Mayer, *Theoret.Chim.Acta*, **59,** 603 (1981).
1322. P. R. Surján, I. Mayer and M. Kertész, *J.Chem.Phys.*, **77,** 2454 (1982).
1323. P. R. Surján, G. Náray-Szabó and I. Mayer, *Int.J.Quant.Chem.*, **22,** 929 (1982).
1324. P. R. Surján, M. Révész and I. Mayer, *J.Chem.Soc.Faraday* II, **77,** 1129 (1981).
1325. B. Sustman, J. E. Williams, M. J. S. Dewar, L. C. Allen and P. v. R. Schleyer, *J.Am.Chem.Soc.*, **91,** 5350 (1969).
1326. B. T. Sutcliffe in, *Proc.Seminar on Computational Problems in Quantum Chemistry*, (Eds: A. Veillard and G. H. F. Diercksen), Strassbourg, 1969.
1327. E. Sutton (Ed), *Tables of Interatomic Distances*, Chem.Soc.Per.Publ., **21,** London, 1968.
1328. S. W. Swaminathan and D. L. Beveridge, *J.Am.Chem.Soc.*, **101,** 5832 (1979).
1329. S. Swaminathan, S. W. Harrison and D. L. Beveridge, *J.Am.Chem.Soc.*, **100,** 5705 (1978).
1330. P. Swanstrom, W. P. Kraemer and G. H. F. Diercksen, *Theoret.Chim.Acta*, **44,** 109 (1977).
1330a A. Szabó and N. S. Ostlund, *Modern Quantum Chemistry: Introduction to Advanced Electronic Structure Theory*, MacMillan, New York, 1982.
1331. K. Szalewicz and B. Jeziorski, *Mol.Phys.*, **38,** 191 (1979).
1332. K. Szalewicz, B. Jeziorski, H. J. Monkhorst and J. G. Zabolitzky, *J.Chem.Phys.*, **78,** 1420 (1983).
1333. M. M. Szczesniak and S. Scheiner, *J.Chem.Phys.*, **80,** 1535 (1984).
1334. L. von Szentpály, *Chem.Phys.Lett*, **67,** 63 (1979), **77,** 352 (1981); *J.Mol.Struct.*, **60,** 891 (1980).
1335. L. Szepes, G. Náray-Szabó, F. P. Colonna and G. Distefano, *J.Organomet.Chem.*, **117,** 141 (1976).
1336. M. Taagepera, K. D. Summerhays, W. J. Hehre, R. D. Topsom, A. Pross, L. Radom, and R. W. Taft, *J.Org.Chem.*, **46,** 891 (1981).
1337. A. Tachibana and K. Fukui, *Theoret.Chim.Acta*, **51,** 189 (1979).
1337a H. Tai, *J. Phys. B.*, **12,** 177 (1979).
1338. A. D. Tait and G. G. Hall, *Theoret.Chim.Acta*, **31,** 311 (1973).
1339. H. Taketa, S. Huzinaga and K. O-ohata, *J.Phys.Soc. Jpn*, **21,** 2313 (1966).
1340. C. Tanford, *The Hydrophobic Effect*, Wiley, New York, (1973).
1341. O. Tapia in, *Quantum Theory of Chemical Reactions*, Vol. II (Eds: R. Daudel, A. Pullman, L. Salem and A. Veillard), 1980, p. 25.
1342. O. Tapia in, *Intermolecular Interactions*, Vol. II. Chapter 2, (Eds: H. Ratajczak and W. J. Orville-Thomas), Wiley, Chichester, 1982.
1343. O. Tapia and O. Goscinski, *Mol.Phys.*, **29,** 1653 (1975).
1344. O. Tapia and G. Johannin, *J.Chem.Phys.*, **75,** 3624 (1981).
1345. O. Tapia C. Lamborelle and G. Johannin, *Chem.Phys.Lett.*, **72,** 334 (1980).

1346. T. E. Taylor and M. B. Hall, *J.Am.Chem.Soc.*, **106,** 1576 (1984).
1347. J. J. C. Teixeira-Dias and P. J. Serre, *J.Chem.Soc.Faraday Trans.II*, 906 (1975).
1348. B. T. Thole, *Chem.Phys.*, **59,** 341 (1981).
1349. B. T. Thole and P. T. van Duijnen, *Theoret.Chim.Acta*, **55,** 307 (1980).
1350. B. T. Thole and P. T. van Duijnen, *Chem.Phys.*, **71,** 211 (1982).
1351. B. T. Thole and P. T. van Duijnen, *Theoret.Chim.Acta*, **63,** 209 (1983).
1352. H. B. Thompson, *Inorg.Chem.*, **7,** 604 (1968).
1352a C. Thomson, *Electron Spin Resonance*, Vol. I., *Chem.Soc.Spec.Rep.*, London, 1973.
1353. D. J. Thouless, *Quantum Mechanics of Many-Body Systems*, Academic Press, New York, 1960.
1354. J. Tiňo and V. Klimo, *Chem.Phys.Lett.*, **25,** 427 (1974).
1355. I. Tinoco, Jr., *Adv.Chem.Phys.*, **4,** 113 (1962).
1356. I. Tinoco, Jr., *Int.J.Quant.Chem.*, **16,** 111 (1979).
1356a T. Tokuhiro, B. R. Appelman, G. Fraenkel, P. K. Pearson and C. W. Kern, *J.Chem.Phys.*, **57,** 20 (1972).
1357. J. Tomasi in, *Quantum Theory of Chemical Reactivity* (Eds: R. Daudel, A. Pullman, L. Salem and A. Veillard), Reidel, Dordrecht, 1980, p. 191.
1358. R. D. Topsom, *Prog.Phys.Org.Chem.*, **12,** 1 (1976).
1359. R. D. Topsom, *J.Am.Chem.Soc.*, **103,** 39 (1981).
1360. C. H. Townes and B. P. Dailey, *J.Chem.Phys.*, **17,** 782 (1949).
1361. R. E. Townshend, G. Ramunni, G. Segal, W. J. Hehre and L. Salem, *J.Am.Chem.Soc.*, **98,** 2190 (1976).
1362. C. Trindle and O. Sinanoğlu, *J.Chem.Phys.*, **49,** 65 (1968).
1363. H. P. Trivedi and E. O. Steinborn, *Phys.Rev.*, **A27,** 670 (1983).
1364. F. Török, Á. Hegedüs and P. Pulay, *Theoret.Chim.Acta*, **32,** 145 (1973).
1365. S. Trajmar, J. K. Rice and A. Kuppermann, *Adv.Chem.Phys.*, **18,** 15 (1970).
1366. A. Trautwein and F. E. Harris, *Theoret.Chim.Acta*, **30,** 45 (1973).
1367. G. Trinquier, J. P. Malrieu and P. Riviers, *J.Am.Chem.Soc.*, **104,** 4529 (1982).
1368. W. C. Trogler, *J.Chem.Educ.*, **57,** 424 (1980).
1369. M. Trsic, T. Ziegler and W. C. Laidlaw, *Chem.Phys.*, **15,** 383 (1976).
1370. D. C. Truhlar, J. A. Merrick and J. W. Duff, *J.Am.Chem.Soc.*, **98,** 6771 (1976).
1371. J. C. Tully in, *Modern Theoretical Chemistry*, Vol. VIIA, (Ed: G. A. Segal), Plenum, New York, 1977, p. 173.
1372. D. W. Turner, C. Baker, A. D. Baker and C. R. Brundle, *Molecular Photoelectron Spectroscopy*, Wiley, New York, 1970.
1373. I. Tvaroška and T. Kozár, *J.Am.Chem.Soc.*, **102,** 6929 (1980).
1374. I. I. Ukrainskii, *Theoret.Chim.Acta*, **38,** 139 (1965).
1375. H. Umeyama and K. Morokuma, *J.Am.Chem.Soc.*, **98,** 7208 (1976).
1376. H. Umeyama and K. Morokuma, *J.Am.Chem.Soc.*, **99,** 1316 (1977).
1377. T. R. Upton, *J.Am.Chem.Soc.*, **106,** 1561 (1984).
1378. M. Urban, J. Noga and V. Kellő, *Theoret.Chim.Acta*, **62,** 549 (1963).
1379. H. Vahrenkamp, *Angew.Chem.Int.Ed.Engl.*, **17,** 379 (1978).
1380. A. Veillard, *IBMOL-4 Computer Program*, IBM Research Laboratory, San Jose, 1968.
1381. A. Veillard, *Theoret.Chim.Acta*, **18,** 21 (1970).
1382. A. Veillard in, *Computational Techniques in Quantum Chemistry and Molecular Physics*, (Eds: G. H. F. Diercksen, B. T. Sutcliffe and A. Veillard), Reidel, Dordrecht, 1975.
1383. A. Veillard in, *Quantum Mechanics of Molecular Conformations* (Ed: B. Pullman), Wiley, London 1976. p. 1.
1384. A. Veillard and E. Clementi, *Theoret.Chim.Acta*, **7,** 133 (1967).
1385. C. Verhaegen, J. J. Berger, J. P. Desclaux and C. M. Moser, *Chem.Phys.Lett.*, **9,** 479 (1971).
1386. J. Verhoeven and A. Dymanus, *J.Chem.Phys.*, **52,** 3222 (1970).
1387. J. H. van Vleck and D. L. Huber. *Rev.Mod.Phys.*, **49,** 939 (1977).
1388. A. P. Volosov and V. A. Zubkov, *Theoret.Chim.Acta*, **44,** 375 (1977).
1389. A. P. Volosov, V. A. Zubkov and T. M. Birshtein, *Tetrahedron*, **31,** 1259 (1975).
1390. E. R. Vorpagel, A. Streitwieser Jr. and S. D. Alexandratos, *J.Am.Chem.Soc.*, **103,** 3777 (1981).
1391. A. F. Voter and W. A. Goddard III, *Chem.Phys.*, **57,** 253 (1981).
1392. K. Wade, *Adv.Inorg.Chem.Radiochem.*, **18,** 1 (1976).
1393. W. R. Wadt and W. A. Goddard, *J.Am.Chem.Soc.*, **97,** 2034 (1975).
1394. A. C. Wahl and G. Das, *Adv.Quant.Chem.*, **5,** 261 (1970).

1395. A. C. Wahl and G. Das in, *Modern Theoretical Chemistry*, Vol. III. (Ed: H. F. Schaeffer III), Plenum, New York, 1977.
1396. L. R. Walker, G. K. Wertheim and V. Jaccarino, *Phys.Rev.Lett.*, **6,** 98 (1961).
1397. R. B. Walker and J. C. Light, *Ann.Rev.Phys.Chem.*, **31,** 401 (1980).
1398. T. H. Walnut and L. A. Nafie, *J.Chem.Phys.*, **67,** 1491 (1977).
1399. A. D. Walsh, *J.Chem.Soc.*, 2260 (1953), and following articles.
1400. A. Warshel in, *Modern Theoretical Chemistry*, Vol. VI (Ed: G. A. Segal), Plenum, New York, 1977, p. 133.
1401. A. Warshel, *J.Phys.Chem.*, **83,** 1640 (1979).
1402. A. Warshel and A. Lappicirella, *J.Am.Chem.Soc.*, **103,** 4664 (1981).
1403. A. Warshel and M. Levitt, *J.Mol.Biol.*, **103,** 227 (1976).
1404. R. E. Watson, *Phys.Rev.*, **118,** 1036 (1960); **119,** 1934 (1960).
1405. J. R. van Wazer and I. Absar, *Electron Densities in Molecules and Molecular Orbitals*, Academic, New York, 1975.
1406. J. D. Weeks, A. Hazi and S. T. Rice, *Adv.Chem.Phys.*, **16,** 283 (1969).
1407. E. Weigold, *Aust.J.Phys.*, **35,** 571 (1982).
1408. F. Weinhold, *J.Chem.Phys.*, **54,** 1874 (1971); *Adv.Quant.Chem.*, **6,** 299 (1972).
1409. T. Weller, W. Meiler, H. J. Köhler, H. Lischka and R. Höller, *Chem.Phys.Lett.*, **98,** 541 (1983).
1410. H. J. Werner, *Mol.Phys.*, **44,** 111 (1981).
1411. H. J. Werner and W. Meyer, *Mol.Phys.*, **31,** 855 (1976).
1412. H. J. Werner and W. Meyer, *Phys.Rev.*, **A13,** 13 (1976).
1412a J. E. Wertz and J. P. Bolton, *Electron Spin Resonance, Elementary Theory and Practical Applications*, McGraw Hill, New York, 1972.
1413. M-H. Whangbo, H. B. Schlegel and S. Wolfe, *J.Am.Chem.Soc.*, **99,** 1296 (1977).
1414. G. W. Wheland, *J.Am.Chem.Soc.*, **64,** 900 (1942).
1415. G. W. Wheland, *Resonance in Organic Chemistry*, Wiley, New York, 1955.
1416. P. A. Whitlock and J. T. Muckerman, *J.Chem.Phys.*, **61,** 4618 (1974).
1417. J. L. Whitten, *J.Chem.Phys.*, **44,** 359 (1966).
1418. K. B. Wiberg, *Tetrahedron*, **24,** 1083 (1968).
1419. K. B. Wiberg, *J.Am.Chem.Soc.*, **101,** 1718 (1979).
1420. K. B. Wiberg, *J.Am.Chem.Soc.*, **102,** 1229 (1980).
1421. K. B. Wiberg, *J.Am.Chem.Soc.*, **105,** 1227 (1983).
1422. K. B. Wiberg and J. J. Wendoloski, *J.Am.Chem.Soc.*, **98,** 5465 (1976); **100,** 723 (1978).
1423. E. Wigner, *Trans.Faraday Soc.*, **34,** 29 (1938).
1424. D. L. Wilhite and J. C. Whitten, *J.Chem.Phys.*, **58,** 948 (1973).
1425. G. Wilkinson, F. G. A. Stone and E. W. Abel (Eds), *Comprehensive Orgometallic Chemistry*, Pergamon, Oxford, 1982.
1426. I. H. Williams, G. M. Maggiora and R. L. Schowen, *J.Am.Chem.Soc.*, **102,** 7831 (1980).
1427. I. H. Williams, D. Spangler, D. A. Femec, G. M. Maggiora and R. L. Schowen, *J.Am.Chem.Soc.*, **105,** 31 (1983).
1428. E. B. Wilson Jr., J. C. Decius and P. C. Cross, *Molecular Vibrations*, McGraw Hill, Toronto, 1955.
1429. H. Wind, *J.Chem.Phys.*, **42,** 2371 (1965).
1430. S. Winstein, *Q.Rev.Chem.Soc.*, **23,** 141 (1969).
1431. N. W. Winter, W. A. Goddard III and F. W. Bobrowitz, *J.Chem.Phys.*, **62,** 4325 (1975).
1432. K. Wittel and S. P. McGlynn, *Chem.Rev.*, **77,** 745 (1977).
1433. M. Wolfsberg and L. Helmholtz, *J.Chem.Phys.*, **20,** 837 (1962).
1434. R. D. Wood in, *Water: A Comprehensive Treatise*, Vol VI (Ed: F. Franks), Plenum, New York, 1979, p. 279.
1435. R. W. Woody and I. Tinoco, Jr., *J.Chem.Phys.*, **46,** 4927 (1967).
1436. R. B. Woodward and R. Hoffmann, *J.Am.Chem.Soc.*, **87,** 395 (1965).
1437. R. B. Woodward and H. Hoffmann, *Angew.Chem.Int.Ed.Engl.*, **8,** 781 (1969).
1438. R. B. Woodward and R. Hoffmann, *The Conservation of Orbital Symmetry*, Verlag Chemie, Weinheim, 1971.
1439. R. G. Wooley, *Isr.J.Chem.*, **19,** 30 (1980).
1440. J. S. Wright and L. Salem, *J.Am.Chem.Soc.*, **94,** 322 (1972).
1440a J. S. Wright, D. J. Donaldson and R. J. Williams, *J.Chem.Phys.*, **81,** 397 (1984).

1440b J. S. Wright and R. J. Williams, *J.Chem.Phys.*, **79,** 2893 (1983).
1441. S. Yamabe, S. Kato, H. Fujimoto and K. Fukui, *Theoret.Chim.Acta*, **30,** 327 (1973).
1442. S. Yamamoto and A. Saika, *Chem.Phys.Lett.*, **78,** 316 (1981).
1443. D. L. Yeager and V. McKoy, *J.Chem.Phys.*, **60,** 2714 (1974).
1444. D. L. Yeager, V. McKoy and G. A. Segal, *J.Chem.Phys.*, **61,** 755 (1974).
1445. C. Y. Yeh and F. S. Richardson, *J.Chem.Soc.Faraday Trans. II.*, **72,** 331 (1976).
1446. S. Yomosa, *J.Phys.Soc.Jpn.*, **44,** 602 (1978).
1447. J. M. Younkin, L. J. Smith and R. N. Compton, *Theoret.Chim.Acta*, **41,** 157 (1975).
1448. R. Zahradník, P. Hobza and J. Sauer in, *Steric Effects in Biomolecules* (Ed.: G. Náray-Szabó), Elsevier, Amsterdam, 1982, p. 327.
1449. R. Zahradník and R. Polák, *Elements of Quantum Chemistry*, Plenum, New York, 1980.
1450. M. Žaucer and A. Ažman, *Phys.Rev.A.*, **16,** 475 (1977).
1451. G. D. Zeiss, W. R. Scott, N. Suzuki, D. P. Chong and S. R. Langhoff, *Mol.Phys.*, **37,** 1543 (1979).
1451a G. M. Zhidomirov and N. D. Chuvylkin, *Theor.Chim.Acta*, **30,** 197, (1973).
1452. J. K. Zhu, D. Li, J. Li and Y. K. Pan, *Theoret.Chim.Acta*, **63,** 223 (1983).
1453. B. A. Zilles and W. B. Person, *J.Chem.Phys.*, **79,** 65 (1983).
1454. F. Zuccarello, A. Raudino and G. Buemi, *J.Mol.Struct.THEOCHEM*, **10,** 265 (1983).
1455. F. Zuccarello, A. Raudino and G. Buemi, *J.Mol.Struct.THEOCHEM*, **16,** 215 (1984).
1456. B. Żurawski and W. Kutzelnigg, *Bull.Acad.Sci.Pol.Sci.Ser.Chim.*, **22,** 361 (1974).

SELECTED RECENT REFERENCES

1 MODELS AND METHODS OF QUANTUM CHEMISTRY

1.2 Basic physical methods in quantum chemistry

— Why is there a molecular relativistic effect
J. Katriel, D. Feller and E. R. Davidson
Int. J. Quant. Chem. **26,** 489 (1984).

— Diagrammatic valence bond theory for finite-model Hamiltonians
S. Ramasesha and Z. G. Soos
Int. J. Quant. Chem. **25,** 1003 (1984).

— Pseudopotential calculations including core valence correlation: Alkali and noble-metal compounds
H. Stoll, L. von Szentpáli, P. Fuentealba, J. Flad, M. Dolg, F.–X. Fraschio, P. Schwerdtfeger, G. Igel and H. Preuss
Int. J. Quant. Chem. **26,** 725 (1984).

— Model potential calculations for second-row transition metal molecules within the local-spin-density method
J. Andzelm, E. Radzio and D. R. Salahub
J. Chem. Phys. **83,** 4573 (1985).

— Relativistic configuration interaction of low lying states of PbF
K. Balasubramanian
J. Chem. Phys. **83,** 2311 (1985).

— The convergence of CI calculations for atomic and molecular electronic bound states in a basis of floating Gauss orbitals
B. Klahn
J. Chem. Phys. **83,** 5754 (1985).

— A strategy for time dependent quantum mechanical calculations using a Gaussian wave packet representation of the wave function.
S. I. Sawada, R. Heather, B. Jackson and H. Metiu
J. Chem. Phys. **83,** 3009 (1985).

— The diagonal correction to the Born-Oppenheimer approximation: Its effect on the singlet-triplet splitting of CH_2 and other molecular effects
N. C. Handy, Y. Yamaguchi and H. F. Schaefer III
J. Chem. Phys. **84,** 4481 (1986).

— Gaussian basis sets and the nuclear cusp problem
W. Klopper and W. Kutzelnigg
J. Mol. Struct. THEOCHEM **28,** 339 (1986).

— The atom in a molecule: A density matrix approach
L. Li and R. G. Parr
J. Chem. Phys. **84,** 1704 (1986).

1.3 Computational methods

— MNDO calculations for compounds containing tin
M. J. S. Dewar, G. L. Grady and J. J. P. Stewart
J. Am. Chem. Soc. **106,** 6771 (1984).

— Unitary group approach to the many-electron problem
M. D. Gould and G. S. Chandler
Int. J. Quant. Chem. **25,** 553, 603 (1984).
— Application of cluster expansion techniques to open shells: Calculation of difference energies
M. A. Haque and D. Mukherjee
J. Chem. Phys. **80,** 5058 (1984).
— Correlation effects and bond-correlation energies in the series of molecules including C_1 to C_4 hydrocarbons. Fourth order MB-RSPT calculations
V. Kellő, M. Urban, J. Noga and G. H. F. Diercksen
J. Am. Chem. Soc. **106,** 5864 (1984).
— Simple models for large-molecule calculations
R. McWeeny
Int. J. Quant. Chem. **26,** 693 (1984).
— An efficient reformulation of the closed-shell self-consistent electron pair theory
P. Pulay, S. Saebø and W. Meyer
J. Chem. Phys. **84,** 3320 (1986).
— All-electron and valence-electron calculations on AgH, Ag_2 an AgO
P. J. Hay and R. L. Martin
J. Chem. Phys. **83,** 5274 (1985).
— Exact Hückel molecular orbitals of the finite square-cut FCC crystal
L. Salem and C. Leforestier
J. Am. Chem. Soc. **107,** 2527 (1985).
— The local approach: Electronic correlations in small hydrocarbon molecules
G. Stoelhoff and D. Vasilopoulos
J. Chem. Phys. **84,** 2744 (1986).
— Analysis of the kinetic energy functional in density functional theory
W. Yang and J. E. Harriman
J. Chem. Phys. **84,** 3320 (1986).

1.4 The framework of localized molecular orbitals

— Localized orbitals based on the Fermi hole
W. L. Luken and J. C. Culberson
Theoret. Chim. Acta **66,** 279 (1984).
— Conceptual quantum chemistry
Z. B. Maksić (Ed.)
Croat. Chem. Acta **57,** (1984).
— Localized molecular orbitals for multiple bonds in the ZDO approximation: The σ-π vs. banana bonds dilemma
J. C. Paniagua, A. Moyano and L. M. Tel
Int. J. Quant. Chem. **26,** 383 (1984).
— Interactions of chemical bonds: Strictly localized wave functions in orthogonal basis
P. R. Surján
Phys. Rev. A **30,** 43 (1984).
— Natural localized molecular orbitals
A. E. Reed and F. Weinhold
J. Chem. Phys. **83,** 1736 (1985).
— Calculation and properties of non-orthogonal, strictly local molecular orbitals
G. F. Smiths and C. Altona
Theoret. Chim. Acta **67,** 461 (1985).

— The interaction of chemical bonds. II. Ab initio theory for overlap, delocalization and dispersion interactions
P. R. Surján, I. Mayer and I. Lukovits
Phys. Rev. A **32,** 748 (1985).

1.5 Representation of environmental effects in quantum chemical calculations

— Quantum theory of solvation
D. Chandler
J. Phys. Chem. **88,** 3400 (1984).

— Theoretical study on the hydrogen bonding and solvation of ammonium and pyridinium ions
S. Ikuta and M. Imamura
Chem. Phys. **90,** 37 (1984).

— Thermodynamic and structural aspects on liquid and solid benzene. Monte Carlo study
P. Linse
J. Am. Chem. Soc. **106,** 5425 (1984).

— Pattern recognition approach to the analysis of geometrical features of solvation: Application to the aqueous hydratation of Li^+, Na^+, K^+, F^- and Cl^- ions.
F. T. Marchese and D. L. Beveridge
J. Am. Chem. Soc. **106,** 3713 (1984).

— Monte Carlo simulations of the solvation of the dimethyl phosphate anion
G. Alagona, C. Ghio and P. A. Kollman
J. Am. Chem. Soc. **107,** 2229 (1985).

— Role of electrostatics in the structure, energy and dynamics of biomolecules: A model study of N-methylalanylacetamide
B. M. Pettitt and M. Karplus
J. Am. Chem. Soc. **107,** 1166 (1985).

— Hartree–Fock–Slater–LCAO implementation of the moderately large-embedded-cluster approach to chemisorption. Calculations for hydrogen on lithium (100)
W. Ravenek and F. M. M. Geurts
J. Chem. Phys. **84,** 1613 (1986).

2 THE CHEMICAL BONDS

2.1 Definitions and origin of bonding

— Electronegativities and hardnesses of open-shell atoms
J. Gazquez and E. Ortiz
J. Chem. Phys. **81,** 2741 (1984).

— Electronegativities, electron affinites, ionization potentials and hardnesses of the elements within spin polarized density functional theory
J. Robles and L. J. Bartolotti
J. Am. Chem. Soc. **106,** 3723 (1984).

— Quantum chemical interpretation of oxidation number as applied to carbon and oxygen compounds. Numerical analysis of the electron distribution with ab initio molecular orbital wave functions
K. Takano, H. Hosoya and S. Iwata
J. Am. Chem. Soc. **106,** 2787 (1984).

— Electronegativity equalization: Application and parametrization
W. J. Mortier, K. van Genechten and J. Gasteiger
J. Am. Chem. Soc. **107,** 829 (1985).

— Theoretical studies of the polar effect. 5. The use of the isolated molecule approach
S. Marriott and R. D. Topsom
J. Am. Chem. Soc. **107,** 2253 (1985).

— Absolute electronegativity and absolute hardness of Lewis acids and bases
R. G. Pearson
J. Am. Chem. Soc. **107,** 6801 (1985).

— Electron difference densities and chemical bonding
P. Valtazanos, W. H. E. Schwarz and K. Ruedenberg
Theoret. Chim. Acta **68,** 471 (1985).

— Semiclassical models in theoretical chemistry. Some results and future prospects
G. Alagona, R. Bonaccorsi, C. Ghio and J. Tomasi
J. Mol. Struct. THEOCHEM **28,** 39 (1986).

— Counterpoise corrections to the evaluation of the bimolecular interaction energy components. On the decoupling of the E_{MIX} term
R. Cammi and J. Tomasi
Theoret. Chim. Acta **69,** 11 (1986).

2.2 The sigma bond

— Long bonds in cation radicals of vicinally difunctional molecules
D. J. Belville, R. A. Pabon and N. L. Bauld
J. Am. Chem. Soc. **107,** 4978 (1985).

— Theoretical determination of molecular structure and conformation. 16. Substituted cyclopropanes. An electron density model of substituent-ring interactions
D. Cremer and E. Kraka
J. Am. Chem. Soc. **107,** 3811 (1985).

— Studies of silicon-phosphorus binding
K. J. Dykema, T. N. Truong and M. S. Gordon
J. Am. Chem. Soc. **107,** 4535 (1985).

— A systematic approach to calculate molecular properties of organosulfur compounds containing the $C(sp^2)$-S bond
J. Kao, C. Eyermann, E. Southwick and D. Leister
J. Am. Chem. Soc. **107,** 5323 (1985).

— Some effects of amine substituent in strained hydrocarbons
P. Politzer, K. Jayasuriya and B. A. Zilles
J. Am. Chem. Soc. **107,** 121 (1985).

— Theoretical study of the bonding in CuH and Cu_2
K. Raghavachari, K. K. Sunil and D. K. Jordan
J. Chem. Phys. **83,** 4633 (1985).

— Methylene: A paradigm for computational quantum chemistry
H. F. Schaefer III
Science **231,** 1100 (1986).

— Relativistic and correlation effects in pseudopotential calculations for Br, I, HBr, HI, Br_2 and I_2
P. Schwerdtfeger, L. v. Szentpály, K. Vogel, H. Silberbach, H. Stoll and H. Preuss
J. Chem. Phys. **84,** 1606 (1986).

2.3 The pi bond

— Phosphorus-nitrogen multiple bonds. A theoretical investigation of structure and bonding in $(NH)_2PNH_2$, $(NH_2)_2PN$ and the (cyclic) dimer $P_2N_6H_8$
R. Ahlrichs and H. Schiffer
J. Am. Chem. Soc. **107,** 6494 (1985).

— Hybridization and the orientation and alignment of π-orbitals in nonplanar conjugated organic molecules: π-orbital axis vector analysis (POAV2)
R. C. Haddon
J. Am. Chem. Soc. **108,** 2837 (1986).

2.6 Aromaticity

Valence bond description of conjugated molecules 3. The through-resonance concept in para-substituted nitrobenzenes
P. C. Hiberty and G. Ohanessian
J. Am. Chem. Soc. **106,** 6963 (1984).

— Aromaticity of unusual heteropolar monocyclic rings with $(4n+2)$ π-electrons
K. Jug
J. Org. Chem. **49,** 4475 (1984).

— Valence bond theory of aromaticity
S. Kuwajima
J. Am. Chem. Soc. **106,** 6496 (1984).

— Conjugation and aromaticity of corannulenes
M. Randić and N. Trinajstić
J. Am. Chem. Soc. **106,** 4428 (1984).

— Comparative molecular orbital study of [6]-, [10]- and [8] annulenes and the bridged [10] annulenes
R. C. Haddon and K. Raghavachari
J. Am. Chem. Soc. **107,** 289 (1985).

— Hartree–Fock MO theoretical approach to aromaticity. Interpretation of Hückel resonance energy in terms of kinetic energy of π-electrons
H. Ichikava and Y. Ebisawa
J. Am. Chem. Soc. **107,** 1161 (1985).

— Aromatic stability of heterocyclic conjugated systems
M. Randić, N. Trinajstić, J. V. Knop and Z. Jericević
J. Am. Chem. Soc. **107,** 849 (1985).

— The generalized resonating valence-bond description of cyclobutadiene
A. F. Voter and W. A. Goddard III
J. Am. Chem. Soc. **108,** 2830 (1986).

— The silicon analog of benzene — hexasilabenzene (Si_6H_6)
D. A. Clabo, Jr. and H. F. Schaefer III.
J. Chem. Phys. **84,** 1664 (1986).

2.7 Metal-metal bonds

— Theoretical study of multiple metal-metal bonds in binuclear complexes of group-6*d* and group-7*d* transition-elements with the general formula $M_2Cl_4(PH_3)_n$ $(n=0, 1, 2)$ by the Hartree–Fock–Slater transition-state method
T. Ziegler
J. Am. Chem. Soc. **106,** 5901 (1984).

— Metal-metal bonding and antibonding molecular orbitals in triangular skeletons of the type L_6M_3
C. Mealli
J. Am. Chem. Soc. **107,** 2245 (1985).

— Theoretical study on the quadruple metal bond in d^4-d^4 binuclear tetracarboxylate complexes of chromium, molybdenum and tungsten by the Hartree–Fock–Slater transition-state method
T. Ziegler
J. Am. Chem. Soc. **107,** 4453 (1085).

— On the bonding in $Fe_2(CO)_9$
C. W. Bauschlicher, Jr.
J. Chem. Phys. **84,** 872 (1986).

2.8 Transition-metal complexes

— Reactivity of coordinated nucleophiles towards *cis* migration in (π-olefin)palladium complexes
J.-E. Bäckvall, E. E. Björkman, L. Pettersson and P. Siegbahn
J. Am. Chem. Soc. **106,** 4369 (1984).

— Electronic structure and bonding of $Hg(CH_3)_2$
R. L. DeKock, E. J. Baerends, P. M. Boerrigter and R. Hengelmolen
J. Am. Chem Soc. **106,** 3387 (1984).
— Theoretical electron deformation density studies on chromium benzene tricarbonyl
R. A. Kok and M. B. Hall
J. Am. Chem. Soc. **107,** 2581 (1985).
— *Ab initio* MO study of the coordination modes and bonding nature of Rh^I-N_2 complexes
S. Sakaki, K. Morokuma and K. Ohkubo
J. Am. Chem. Soc. **107,** 2686 (1985).
— Transition metal-ligand bonding
C. W. Bauschlicher, Jr.
J. Chem. Phys. **84,** 260 (1986).
— Structure of Pt-DNA complexes in solution: Bidentate models
K. Jankowski, N. Turkhan and W. Brostow
J. Mol. Struct. THEOCHEM **30,** 299 (1986).

2.9 The hydrogen bond

— Water-water interaction potential — an aproximation of the electron correlation contribution by a functional of the SCF density matrix
V. Carravet and E. Clementi
J. Chem. Phys. **81,** 2646 (1984).
— Effects of molecular charge and methyl substitution on proton transfer between oxygen atoms
E. A. Hillenbrand and S. Scheiner
J. Am. Chem. Soc. **106,** 6266 (1984).
— A quantum chemical study of the effect of Na^+ on the hydrogen bonds in the adenine-thymine base-pair
P. Hobza and C. Sandorfy
Biophys. Chem. **19,** 201 (1984).
— Theoretical studies on the interaction of proteins with base pairs. I. *Ab initio* calculation for the effect of H-bonding interaction of proteins on the stability of adenine-uracil pair
A. Sarai and M. Saito
Int. J. Quant. Chem. **25,** 527 (1984).
— Cation binding effect on hydrogen bonding
H. Basch, M. Krauss and W. J. Stevens
J. Am. Chem. Soc. **107,** 7267 (1985).
— Theoretical studies of proton transfers
S. Scheiner
Acc. Chem. Res. **18,** 174 (1985).
— *Ab initio* study of the hydrogen-bonded complexes $NH_3 \ldots HCN$, $PH_3 \ldots HCN$, $AsH_3 \ldots HCN$, $H_2O \ldots HCN$, $H_2S \ldots HCN$ and $H_2Se \ldots HCN$
A. Hinchcliffe
J. Mol. Struct. THEOCHEM **29,** 193 (1986).

2.10 Electron donor-acceptor complexes

— Energies of interactions between purine and pyrimidine-bases in B-DNA and Z-DNA
W. Förner, P. Otto and J. Ladik
Chem. Phys. **86,** 49 (1984).
— Electron donor-acceptor orbital correlations 3. *syn* and *anti* correlation schemes for cofacial complexes of 1,2,4,5-benzenetetracarbonitrile with some aromatic hydrocarbons
B. Stevens
Chem. Phys. **90,** 1 (1984).

— Geometrical structures of four conformers of the phosphocenium ion, $P(C_5H_5)^+$. A phosphorus sandwich
T. J. Lee, H. F. Schaefer III and E. A. Magnusson
J. Am. Chem. Soc. **107,** 7239 (1985).

— A molecular orbital study of the bonding in complexes of lithium with polynuclear aromatic hydrocarbons
D. A. Morton-Blake, J. Corish and F. Beniere
Theoret. Chim. Acta **68,** 407 (1985).

— Nature and location of excited charge-transfer states in porphyrin dimers: Development of preliminary design characteristics for biomimetics solar energy conversion systems
J. D. Petke and G. M. Maggiora
J. Chem. Phys. **84,** 1640 (1986).

2.11 van der Waals molecules

— Structure and internal rotation of HDO-CO_2 and D_2O-CO_2 van der Waals complexes
I. I. Peterson and W. Klemperer
J. Chem. Phys. **80,** 2439 (1984).

— The secular equation/perturbation theory method for calculating spectra of van der Waals complexes
J. M. Hutson and R. J. Le Roy
J. Chem. Phys. **83,** 1197 (1985).

— An improved intermolecular potential for nitrogen
A. van der Avoird, P. E. S. Worner and A. P. J. Jansen
J. Chem. Phys. **84,** 1629 (1986).

— The He_2 potential at small distances
D. M. Ceperley and H. Patridge
J. Chem. Phys. **84,** 820 (1986).

— Determination of polarizabilities and van der Waals constants
S. H. Patil
J. Chem. Phys. **84,** 5067 (1986).

3 MOLECULAR STRUCTURE

3.1 Geometry

— Valence-shell electron-pair repulsions: A quantum test of a naive mechanical model
L. S. Bartell and Y. Z. Barshad
J. Am. Chem. Soc. **106,** 7700 (1984).

— Substituent effects on the geometries and energies of cyclopropanes and the corresponding 2-propyl derivatives
T. Clark, G. W. Spitznagel, R. Klose and P. v. R. Schleyer
J. Am. Chem. Soc. **106,** 4412 (1984).

— Influence of *d*-orbital occupancy on the geometry of pentacoordinated molecules
R. R. Holmes
J. Am. Chem. Soc. **106,** 3745 (1984).

— Equilibrium geometries for triplet trimethylene, $CH_2CH_2CH_2$
Y. Yamaguchi and H. F. Schaefer III
J. Am. Chem. Soc. **106,** 5115 (1984).

— The malonaldehyde equilibrium geometry. A major structural shift due to the effects of electron correlation
M. J. Frisch, A. C. Scheiner and H. F. Schaefer III
J. Chem. Phys. **82,** 4194 (1985).

— Factors determining bond angles from a classical valence bond perspective. Covalent structure of H_2O
R. G. A. R. Maclagan and B. Kirtman
Theoret. Chim. Acta **68,** 407 (1985).

3.2 Conformation

— Comparison between the *s-cis* and *gauche* conformers of 1,3-butadiene
J. Breulet, T. J. Lee and H. F. Schaefer III
J. Am. Chem. Soc. **106,** 6250 (1984).
— Quantum-mechanical and statistical mechanical studies of the torsional barrier of H_2O_2 in aqueous solution
B. Jonsson and S. Romano
Int. J. Quant. Chem. **25,** 503 (1984).
— *Ab initio* calculations of rotational barriers for the diselenide bridge in dimethyl diselenide
V. Renugopalakrishnan and R. Walter
J. Am. Chem. Soc. **106,** 3413 (1984).
— Quantum and molecular mechanical studies on alanyl dipeptide
S. J. Weiner, U. C. Singh, T. J. O'Donnell and P. A. Kollman
J. Am. Chem. Soc. **106,** 6243 (1984).
— Geometric structure and pseudorotational potential of pyrimidine. An *ab initio* and electron diffraction study
G. Pfafferott, H. Oberhammer, J. E. Boggs and W. Caminati
J. Am. Chem. Soc. **107,** 2305 (1985).
— Monte Carlo study of the conformation dependent hydration of the 18-crown-6-macrocycle
G. Ranghino, S. Romano, J. M. Lehn and G. Wipff
J. Am. Chem. Soc. **107,** 7873 (1985).
— The intrinsic reaction coordinate and the rotational barrier in silaethylene
M. W. Schmidt, M. S. Gordon and M. Dupuis
J. Am. Chem. Soc. **107,** 2581 (1985).
— Barriers to rotation adjacent to double bonds
K. B. Wilberg and E. Martin
J. Am. Chem. Soc. **107,** 5035 (1985).
— The influence of the basis set on the evaluation of conformational energies for small organic solutes in aqueous solutions
G. Alagona, R. Bonaccorsi, C. Ghio and J. Tomasi
J. Mol. Struct. THEOCHEM **30,** 263 (1986).
— A molecular orbital study on nitrogen inversion in aniline with extensive geometry optimization
C. W. Bock, P. George and M. Trachtman
Theoret. Chim. Acta **69,** 235 (1986).

3.3 Molecular vibrations

— Theoretical prediction of vibrational spectra 1. The in-plane force field and vibrational spectra of pyridine
G. Pongor, P. Pulay, G. Fogarasi and J. E. Boggs
J. Am. Chem. Soc. **106,** 2765 (1984).
— Theoretical study of substituent effects on CH stretching frequencies
K. Raghavacharya
J. Chem. Phys. **81,** 2718, (1984).
— Molecular structure rotational constants and vibrational frequencies for ethynamine (NH_2—CCH): A possible interstellar molecule
S. Saebø, L. Farnell, N. V. Riggs and L. Radom
J. Am. Chem. Soc. **106,** 5047 (1984).

— *Ab initio* second-order Møller–Plesset calculation of the vibrational spectrum of tetrahedrane
B. A. Hess and L. J. Schaad
J. Am. Chem. Soc. **107,** 865 (1985).

— Quantum and semiclassical vibrational transition frequencies for a Hamiltonian with stretch-bend potential energy coupling
K. N. Swamy and W. L. Hase
J. Chem. Phys. **84,** 361 (1986).

— Dynamic perturbation theory of vibrational energy transfer in a nonrigid molecular system
A. Tachibana, M. Nagaoka and T. Yamabe
J. Chem. Phys. **84,** 2247 (1986).

3.4 Electric properties

— A new form of electric-field-dependent basis functions for the calculation of eletric polarizabilities and dipole moments
J. A. Hudis and R. Ditchfield
Chem. Phys. **86,** 455 (1984).

— An approach to computing electrostatic charges for molecules
U. C. Singh and P. A. Kollman
J. Comput. Chem. **5,** 129 (1984).

— Basis set effects on the electron density and spectroscopic properties of CO
E. J. Baerends, P. Vernooijs, A. Rozendaal, P. M. Boerrigter, M. Kvijn, D. Feiland and D. Sundholm
J. Mol. Struct. THEOCHEM **26,** 147 (1985).

— Electron density distribution analysis for nitromethane, nitromethide and nitranide
J. P. Ritchie
J. Am. Chem. Soc. **107,** 1829 (1985).

— Electron density and response theory
R. McWeeny
J. Mol. Struct. THEOCHEM **24,** 231 (1985).

— The hydrogen bonding influence on polarizability and hyperpolarizability. A derivate Hartree–Fock study of the electrical properties of hydrogen fluoride and the hydrogen fluoride dimer
C. E. Dykstra, S. Y. Liu and D. J. Malik
J. Mol. Struct. THEOCHEM **28,** 357 (1986).

3.5 Magnetic properties

— Charge-carbon-13 empirical relationships in organic ions: An improvement extending the access to experimental charge maps
S. Bradamente and G. A. Pagani
J. Org. Chem. **49,** 2863 (1984).

— Relativistic effects on hf interactions: Applications to ytterbium fluorides
D. A. Case and J. P. Lopez
J. Chem. Phys. **80,** 3270 (1984).

— Importance of multicenter integrals in semiempirical calculations of nuclear spin-spin coupling constants 1. Isotropic coupling
J. C. Facelli and M. Barfield
J. Am. Chem. Soc. **106,** 3407 (1984).

— A theoretical study of medium effects on the transmission mechanisms of the Fermi-contact term of spin-spin coupling constants in the acetamide molecule
J. C. Facelli, C. A. Airibet and R. H. Conteras
Int. J. Quant. Chem. **25,** 515 (1984).

— 2nd-order polarization propagator calculations of indirect nuclear spin-spin coupling tensors in the water molecule
J. Geertsen and J. Oddershede
Chem. Phys. **90,** 301 (1984).
— Semiempirical calculation of diamagnetic susceptibilities of alkyl ω-aminovinyl ketones
R. R. Gupta, R. Swaroop, M. Kumar and Kishan
J. Am. Chem. Soc. **106,** 4378 (1984).
— Theoretical study of the metal chemical shift in nuclear magnetic resonance. Ag, Cd, Cu and Zn complexes
H. Nakatsuji, K. Kanda, K. Endo and T. Yonezawa
J. Am. Chem. Soc. **106,** 4653 (1984).
— ^{13}C chemical shifts in series of adamantane and norbornane derivaties. INDO calculations
R. Pachter and P. L. Wessels
J. Mol. Struct. THEOCHEM **30,** 143 (1986).
— *Ab initio* calculations of ^{29}Si NMR chemical shifts for some gas phase and solid state silicon fluorides and oxides
J. A. Tossell and P. Lazzeretti
J. Chem. Phys. **84,** 369 (1986).

3.6 Excited and ionized electronic states

— A theoretical investigation of the complete valence ionization spectra of cynamide, isocyanamide, diazirine and diazomethane
R. Cambi, W. Vonniess and J. Schirmer
Chem. Phys. **86,** 389 (1984).
— An *ab initio* study of the satellite structure in the heteroatom core ionization of furan, pyrrole and thiophene
G. Dealti, P. Decleva and A. Lisini
Chem. Phys. **90,** 231 (1984).
— Vibronic coupling in polyenes: High-resolution optical spectroscopy of a simple Schiff-base
M. Girard, E. Arvidson and R. Christen
J. Chem. Phys. **80,** 2265 (1984).
— Bending in low-lying states of N_2O^+: A qualitative and *ab initio* molecular orbital study
A. R. Gregory
Chem. Phys. **90,** 63 (1984).
— *Ab initio* CI study of the ground and excited states of *p*-quinodimethane
T. K. Ha
Theoret. Chim. Acta **66,** 111 (1984).
— SAC-CI calculations for Rydberg levels of the ammonium radical
K. Hirao
J. Am. Chem. Soc. **106,** 6283 (1984).
— Rydberg transitions in the ammonium radical: Scattered-wave local-spin-density calculations
J. Kaspar and V. H. Smith
Chem. Phys. **90,** 47 (1984).
— Where to look for the electronic-spectrum of hydrogen isocyanide, HNC
W. D. Laidig, Y. Aamaguchi and H. F. Schaefer III
J. Chem. Phys. **80,** 3069 (1984).
— Photoelectron spectra and molecular orbital calculations on *bis*(cyclopentadienyldicarbonyl-chromium-molybdenum and -tungsten): Nature of the bonding of linear semibridging carbonyls
B. J. Morris-Sherwood, C. B. Powell and M. B. Hall
J. Am. Chem. Soc. **106,** 5079 (1984).

— Cluster-expansion of the wave-function: Valence and Rydberg excitations and ionizations of ethylene
H. Nakatsuji
J. Chem. Phys. **80,** 3703 (1984).

— Theoretical study of the ground and excited states of styrene
R. J. Hemley, U. Dinur, V. Vaide and M. Karplus
J. Am. Chem. Soc. **107,** 836 (1985).

— Perturbation theoretical calculation of optical effects in polypeptides
S. Suhai
J. Mol. Struct. THEOCHEM **24,** 97 (1985).

— A Møller–Plesset study of the electron affinities of the diatomic hydrides XH (X = Li, B, Be, C, N, O)
G. Frenking and W. Koch
J. Chem. Phys. **84,** 3224 (1986).

— Electron affinity of fluorine: A quantum Monte Carlo study
R. N. Barnett, P. J. Reynolds and W. A. Lester, jr.
J. Chem. Phys. **84,** 4993 (1986).

— Discrete variational Xα studies of core excitation photoemission and inverse photoemission for CO and NiCO clusters
I. Kojima, A. K. Srivastava, E. Miyazaki and H. Adachi
J. Chem. Phys. **84,** 4455 (1986).

— *Ab initio* band structure calculations of organic polymers with large unit cells and treatment of aperiodicity caused by dopants
P. Otto, A. K. Bakshi and J. Ladik
J. Mol. Struct. THEOCHEM **28,** 209 (1986).

3.7 Interaction of molecules with electromagnetic radiation

— Vibrational circular dichroism of *trans*-1,2-dideuteroxycyclobutane. A comparison of fixed partial charge and localized molecular orbital theories with different force fields
A. Annamalai, T. A. Keiderling and J. S. Chickos
J. Am. Chem. Soc. **106,** 6254 (1984).

— *Ab initio* dipole surfaces, vibrationally averaged dipole moments, and infrared transition intensities for KCN and LiCN
G. Brocks, J. Tennyson and A. van der Avoird
J. Chem. Phys. **80,** 3223 (1984).

— Photoionisation cross-section calculations for H_2O and NH_3 by one-center expansion and Stieltjes technique
I. Cacelli, R. Moccia and V. Carravet
Chem. Phys. **90,** 313 (1984).

— Dipole-moment and hyperfine properties of the ground-state and the C-H excited vibrational state of HCN
W. L. Ebenstein and J. S. Muenter
J. Chem. Phys. **80,** 3989 (1984).

— *Ab initio* calculations of infrared transition probabilities in the electronic ground states of F and AlF^+
R. Klein and P. Rosmus
Theoret. Chim. Acta **66,** 21 (1984).

— Mid infrared vibrational circular dichroism in (*S*)-(-)-epoxypropane: Bond moment model predictions and comparison to the experimental results
P. L. Polavara and D. F. Michalski
Molec. Phys. **52,** 1225 (1984).

— Chiroptical properties of disulfides. *Ab initio* studies of dihydrogen disulfide and dimethyl disulfide
A. Rauk
J. Am. Chem. Soc. **106,** 6517 (1984).

— Theoretical study of the circular dichroism of (+)-(*S*)-2-butanol in the vacuum ultraviolet
G. A. Segal, K. Wolf and J. J. Diamond
J. Am. Chem. Soc. **106,** 3175 (1984).

— Molecular properties from MCSF-SCEP wave functions 2. Calculation of electronic transition moments
H. J. Werner
J. Chem. Phys. **80,** 5080 (1984).

— Investigation of *ab initio* HF-SCF-CI methods for calculating rotatory strengths in (*R*)-3-methylcyclobutene
C. F. Chabalowski, G. M. Maggiora and R. E. Christoffersen
J. Am. Chem. Soc. **107,** 1632 (1985).

— Origin of the conical intersection between the singlet ionic excited surfaces of twisted ethylene
P. Karafiloglou and J. P. Malrieu
Theoret. Chim. Acta **67,** 275 (1985).

— Infrared intensities: Cyclohexane. A molecular force field and dipole moment derivatives
K. B. Wiberg, V. A. Walters and W. P. Dailey
J. Am. Chem. Soc. **107,** 4860 (1985).

— Radiation-molecule and molecule-molecule interactions. A unified viewpoint from quantum electrodynamics
D. P. Craig and T. Thirunamachandran
Acc. Chem. Res. **19,** 10 (1986).

— Quantum chemical (MNDO SCFI/CI) calculations of the chiroptical properties of twisted conjugated diene and dione chromophores
M. C. A. Donkersloot and H. M. Buck
J. Mol. Struct. THEOCHEM **30,** 347 (1986).

— MCSCF-CI calculations of infrared transition probabilities in the CH^- and NH^- ions
U. Manz, A. Zilch, P. Rosmus and H. J. Werner
J. Chem. Phys. **84,** 5037 (1986).

4 CHEMICAL REACTIONS

4.1 Chemical equilibria

— Relationship between substituent-induced energy and charge effects in proton-transfer equilibria involving heteroaromatic nitrogen systems. The "lone pair charge" approach
J. Catalàn, J. L. G. de Paz, M. Yànez and J. E: Elguero
J. Am. Chem. Soc. **106,** 6552 (1984).

— *Ab initio* calculation of reaction energies. III. Basis set dependence of relative energies on the FH_2 and H_2CO potential energy surfaces
M. J. Frisch, J. S. Binkley and H. F. Schaefer III
J. Chem. Phys. **81,** 1882 (1984).

— An *ab initio* study of tautomerism of uracil, thymine, 5-fluorouracil and cytosine
M. J. Scanlan and I. H. Hillier
J. Am. Chem. Soc. **106,** 3737 (1984).

— *Ab initio* heats of formation of medium-sized hydrocarbons. 2. Use of second-order correlation energies
R. L. Disch, J. M. Schulman and M. L. Sabio
J. Am. Chem. Soc. **107,** 1904 (1985).

— Does fluoroformic acid exist
Z. Havlas, T. Kovar and R. Zahradník
J. Am. Chem. Soc. **107,** 7243 (1985).

— Theoretical study of the tautomeric equilibrium of (1*H*)-pyridone in solution
J. A. Sordo, M. Klobukowski and S. Fraga
J. Am. Chem. Soc. **107,** 7569 (1985).

— MINDO/3 computed proton affinities
J. J. Novoa
J. Mol. Struct. THEOCHEM **29,** 361 (1986).

4.2 Molecular collisions

— Reaction Hamiltonian and the adiabatic approach to the dynamics of chemical reactions
V. Z. Kresin and W. A. Lester, jr.
Chem. Phys. **90,** 335 (1984).

— Monte Carlo simulation of RRKM unimolecular decomposition in molecular-beam experiments 3. Application to angular-distributions and branching fractions for the system K + CsF
K. Rynefors, P. A. Elofson and L. Holmlid
Chem. Phys. **90,** 347 (1984).

— Quasiclassical trajectory study of H_2/LiF (001) corrugated surface scattering: Comparison with other theoretical results
S. Saini, D. A. Dows and H. S. Taylor
Chem. Phys. **90,** 87 (1984).

— Trajectories through an intermediate at a fourfold branch point. Implications for the stereochemistry of biradical reactions
B. K. Carpenter
J. Am. Chem. Soc. **107,** 5730 (1985).

— Evaluation of microcanonical rate constants for bimolecular reactions by path integral techniques
D. Thirumalai, B. C. Garrett and B. J. Berne
J. Chem. Phys. **83,** 2972 (1985).

— Test of variational transition state theory and multidimensional semiclassical transmission coefficient methods against accurate quantal rate constants for $H + H_2$/HD, $D + H_2$ and $O + H_2/D_2$/HD including intra- and intermolecular kinetic isotope effects
B. C. Garrett, D. G. Truhlar and G. C. Schatz
J. Am. Chem. Soc. **108,** 2876 (1986).

4.3 Reaction paths

— Quantum mechanical and molecular mechanical studies on a model for dihydroxyacetone phosphate-glyceraldehyde phosphate isomerization catalyzed by triosephosphate isomerase (TIM)
G. Alagona, P. Desmeules, C. Ghio and P. A. Kollman
J. Am. Chem. Soc. **106,** 3623 (1984).

— A procedure for determining reaction paths and saddle points
I. Bálint and M. I. Bán
Int. J. Quant. Chem. **25,** 667 (1984).

— Photolysis of methanol at 185 nm. Quantum mechanical calculations and product study
R. J. Buenker, G. Olbrich H.-P. Schuchmann, B. L. Schurmann and C. von Sonntag
J. Am. Chem. Soc. **106,** 4362 (1984).

— Origin of negative activation energies and entropy control of halocarbone cycloadditions and related fast reactions
K. N. Houk and N. G. Rondan
J. Am. Chem. Soc. **106,** 4293 (1984).

— Rearrangement and fragmentation processes in the methanethiol and dimethyl sulfide radical cations
R. H. Nobes, W. J. Bauma and L. Radom
J. Am. Chem. Soc. **106,** 2774 (1984).

— Theoretical study of the photochemistry of carbonyl compounds: Potential-energy surface for the photodissociation of propynal
P. Russegger and H. Lischka
Chem. Phys. **86,** 31 (1984).
— Comparative tests of theoretical procedures for studying chemical reactions
M. J. S. Dewar and D. M. Storch
J. Am. Chem. Soc. **107,** 3898 (1985).
— Quantum chemical studies of model cytochrome P450 oxidations of amines. 1. MNDO pathways for alkylamine reactions with singlet and triplet oxygen
A. Goldblum and G. H. Loew
J. Am. Chem. Soc. **107,** 4265 (1985).
— Theoretical studies of [1,*n*]-sigmatropic rearrangements involving hydrogen transfer in simple methyl-substituted conjugated polyenes
B. A. Hess, L. J. Schaad and J. Pancíř
J. Am. Chem. Soc. **107,** 149 (1985).
— A simple relation between nuclear charges and potential surfaces
P. G. Mezey
J. Am. Chem. Soc. **107,** 3100 (1985).
— Theoretical studies on gas-phase reactions of F^- with fluorethane: E_2 and S_N2 reactions
T. Minato and S. Yamabe
J. Am. Chem. Soc. **107,** 4621 (1985).
— Electronic aspects of the hydride transfer mechanism. *Ab initio* analytical gradient studies of the cyclopropenyl-cation/lithium hydride model reactant system
O. Tapia, J. Andres, J. M. Aullo and C. I. Brändén
J. Chem. Phys. **83,** 4673 (1985).

4.4 Reactivity of molecules

— An analysis of the hard-soft Lewis acid-base concept and the Drago equation employing *ab initio* molecular orbital theory
J. Douglas and P. Kollman
J. Phys. Chem. **85,** 2717 (1981).
— Quantum chemical calculation of the enzyme-ligand interaction energy for trypsin inhibition by benzamidines
G. Náray-Szabó
J. Am. Chem. Soc. **106,** 4584 (1984).
— Toward a theory of chemical reactivity based on the charge density
R. F. W. Bader and P. J. McDougall
J. Am. Chem. Soc. **107,** 6788 (1985).
— Electrostatic lock-and-key model for the analysis of inhibitor recognition by dihydrofolate reductase
P. Nagy and G. Náray-Szabó
Canad. J. Chem. **63,** 1694 (1985).
— Reaction potential map analysis of electrophilic aromatic substitution reactions
O. Kikuchi
J. Mol. Struct. THEOCHEM **31,** 121 (1986).

4.5 Conservation of orbital symmetry

— Trajectory analysis. 1. Theoretical model for nucleophilic attack at π-systems. The stabilizing and destabilizing orbital terms
C. L. Liotta, E. M. Burgess and W. H. Eberhardt
J. Am. Chem. Soc. **106,** 4849 (1984).

— The origin of barriers to thermally allowed six electron pericyclic reactions. The effect of HOMO–LUMO interaction on the trimerization of acetylene
R. D. Bach, G. J. Wolter and H. B. Schlegel
J. Am. Chem. Soc. **107,** 2837 (1985).
— MNDO calculations for dehydrocyclooctatetraenes
M. J. S. Dewar and K. M. Merz, Jr.
J. Am. Chem. Soc. **107,** 6175 (1985).
— A theoretical study of olefin insertions into Ti-C and Ti-H bonds. An analysis by paired interacting orbitals
H. Fujimoto, T. Yamasaki, H. Mizutani and N. Koga
J. Am. Chem. Soc. **107,** 6175 (1985).
— Theory and modelling of stereoselective organic reactions
K. N. Houk, M. N. Paddon-Row, N. G. Rondan, Y. D. Wu, F. K. Brown, D. C. Spellmeyer, J. T. Metz, Y. Li and R. J. Loncharich
Science **231,** 1108 (1986).

4.6 Environmental effects

— Extended Hückel study of the metallic growth of small platinum clusters: Structure and energetics
B. Bigot and C. Minot
J. Am. Chem. Sos. **106,** 6601 (1984).
— Monte Carlo studies of a dilute aqueous solution of benzene
P. Linse, G. Karlstrom and B. Johnsson
J. Am. Chem. Soc. **106,** 4096 (1984).
— Aqueous hydration of benzene
G. Ravishanker, P. K. Mehrotra, M. Mezei and D. L. Beveridge
J. Am. Chem. Soc. **106,** 4105 (1984).
— Quantum chemical studies on zeolites and silica
J. Sauer and R. Zahradník
Int. J. Quant. Chem. **26,** 793 (1984).
— Activation barrier for adsorbate surface diffusion, heat of chemisorption and adsorbate registry: Theoretical interrelations
E. Shustorovich
J. Am. Chem. Soc. **106,** 6479 (1984).
— The dissociation of H_2 on the Ni (100) surface
P. E. M. Siegbahn, M. R. A. Blomerg and C. W. Bauschlicher, Jr.
J. Chem. Phys. **81,** 4 (1984).
— Factors determining CO adsorption sites on Pd and Pt (100) and (111) surfaces. Theoretical study
A. B. Anderson and M. K. Awad
J. Am. Chem. Soc. **107,** 7854 (1985).
— Theoretical examination of the S_N2 reaction involving chloride ion and methyl chloride in the gas phase and aqueous solution
J. Chandrasekhar, S. F. Smith and W. L. Jorgensen
J. Am. Chem. Soc. **107,** 154 (1985).
— Theoretical studies of the system $H_3O^+(H_2O)_n$ for $n = 1$-9
E. Kochanski
J. Am. Chem. Soc. **107,** 7869 (1985).
— Noncovalent structural models for the Asp-His dyad in the active site of serine proteases and for solid-state switching of protonation states: Crystal structure of the associates of 1,1′-bi-naphtyl-2,2′-dicarboxylic acid with imidazole in dihydrate and in anhydrous forms
M. Czugler, J. G. Ángyán, G. Náray-Szabó and E. Weber
J. Am. Chem. Soc. **108,** 1275 (1986).

SUBJECT INDEX

Ab initio method 37, 58, 127, 182, 300, 308, 315, 322, 324, 340, 360, 386, 405, 418
— simulated 76
Absorption 333
— electronic 100
Acid
— hard and soft 404
Acidity 377, 419
Acoustic relaxation 182, 205
Additivity, bond 147, 259
Adiabatic approximation 13, 344, 379
Adsorption 477
All valence electron methods 81
Alternant hydrocarbons *cf.* Hydrocarbons, alternant
Alternant molecular orbital method 88
Anharmonicity 182, 216, 337
Annulenes 164, 467
Antisymmetry 18
AO
— *d*- 51, 62, 96, 153, 159, 174, 176, 182, 223, 301, 426, 467
— Gaussian 40, 59, 241
— hybrid 48, 57, 122, 342
— hydrogenic 7, 38, 94
— London-type 278
— Rydberg 375
— Slater-type 38, 59, 82
Aromaticity 98, 127, 161, 182, 188, 407, 467
— "acyclic" 166
— anti 163
— homo 165, 231, 234, 260
Arrhenius equation 382
Association, entropy-driven 418
Atom 6, 10, 463
— first-row 10, 39, 61, 144
— hydrogen 6
— united 38, 283
Atomic number 6
Atomic orbital *cf.* AO
Atomic units 428
Aufbau principle 9, 32, 282
Back-donation 182, 246
Badger's rule 183, 221
Barrier 384, 389, 421, 424
— inversion 65, 183, 210
— rotational 65, 87, 106, 122, 152, 156, 183, 205, 428, 431, 470
— torsional 325
Base
— hard and soft 404
Basicity 419
Basis set 37, 59, 184, 298, 315, 318, 339, 470, 471, 474
— balanced 63
— double zeta 60, 227
— extended 61
— LCAO 42
— linearly dependent 64
— minimal 61
— nonorthogonal 86, 314
— polarized 65
— split-shell 63, 65
— STO-*n*G 63, 65
— subminimal 60
— superposition error 43, 133, 134, 183, 226
Benzene 327
Biomolecules 129, 184, 207, 214, 465
Biopolymers 418
Biradical 264, 475
Bob-sledge effect 381
Bohr frequency 335
Bond
— angle 65, 87, 184, 190, 196, 200, 202
— banana 154, 464
— chemical 47, 112, 142, 186, 226, 238, 465, 466
— conjugated double 154
— cumulated double 154
— $(d\text{-}p)\pi$ 153, 176
— d^3-d^3 triple 171
— d^5-d^5 triple 171
— delta 169
— double 171
— energy 148, 153
— Fe–Fe 173

— function 62
— hydrogen 148, 184, 216, 224, 371, 465, 468, 471
— — cooperativity in 188, 216
— isolated double 154
— length 65, 87, 152, 156, 167, 170, 173, 184, 199, 216
— many-centre 147
— metal–metal 168, 467
— order 44, 90, 101, 104, 184, 188, 201, 221
— phosphorus–nitrogen 466
— phosphorus–silicon 466
— π 153, 172, 178, 466
— polarity 150, 242, 243
— quadruple 168, 170
— sextuple 168, 172
— σ 172, 268, 466
— three-centre 157, 186, 190
— triple 154
Bonding
— back 178
Born model 140, 141
Born–Oppenheimer approximation 13, 40, 58, 131, 143, 186, 188, 190, 196, 214, 222, 288, 304, 310, 325, 337, 346, 384, 463
Brillouin theorem 22, 70, 72, 188, 228
— local 23, 109, 124
Brönsted equation 407
Bulk solvent 132, 188, 195, 417
Butadiene 111, 325

Carbonium ions 160
Catalysis 424
Cavity 140
Charge
— core 54
— density 476
— density function 41, 239
— density, partitioning 186, 236
— distribution 188, 192, 222, 342, 395
— effective 141
— net atomic 41, 104, 136, 189, 236, 239, 279, 295, 340, 376, 404
— transfer 87, 126, 133, 146, 179, 188, 190, 426
Charge-bond order matris 90
Chemical formula 92
Chemical reaction *cf.* Reaction, chemical
Chemical shift
— NMR 190, 240, 276, 472
— XPS 190, 194, 239, 240, 243, 295
Chemisorption 426, 477
Chiroptical phenomena 355
Chromophore 328
— chirally perturbed 359, 364
— inherently chiral 359
Circular dichroism 355
— vibrational 473
CI 19, 22, 59, 70, 169, 297, 362, 463
— all-single 84
— brute force 71
— direct 71
— full 71, 114
— multireference single-double 314
— single-double 72, 229, 313
— single excitation 313
Closed shell system 27
Cluster expansion 75, 292, 308
Cluster, metal 168, 426
CNDO method 81, 91, 126, 190, 236, 340
CNDO/S method 83, 316
Col 384
Collision, molecular 192, 224, 377, 475
Complete neglect of differential overlap *cf.* CNDO
Complex
— activated 382
— binuclear 170
— charge transfer 168
— donor–acceptor 190, 193, 205, 468
— high spin 183, 192, 197, 205
— low spin 183, 192, 197, 205
— π 406
— σ 406
— transition metal 425, 463, 467
— transition-state 406, 425
— van der Waals 134
Computer programs, *ab initio* 67
Condon approximation 344
Configuration 18
— core-ionized 286
— electron 193, 197, 245, 282
— interaction *cf.* CI
— Koopmans 286
— nuclear 197
— space 2, 14
Conformation 193, 205, 470
Conjugated compounds 98, 325
Conjugation 194, 198, 219
Continuum dielectric theory 252
Continuum models 140
Contour plot, electron density 155, 223, 237, 388

Conversion factors 431
Cooperative effects 135
Coordinate
— chemical 198, 214, 217
— internal 196, 200, 217, 339, 384
— normal 196, 200, 216
— puckering 196, 205
— reaction 386, 470
— relative electronic 68
— symmetry 197, 201, 205, 217
Core 54
Correlation diagram 107, 197, 202, 205, 302, 409
Correlation table 281
Cotton compounds 170
Cotton effect 356
Coulomb hole 29, 31, 56
Counterpoise correction 134, 466
Coupled electron pair approximation 318
Coupled oscillator mechanism 369
Coupling constant
— hyperfine 144
— quadrupole 248
Coupling
— Coriolis 197, 205, 214
— hyperfine 265, 267, 271
— nuclear spin-spin 264, 270, 471
— spin-orbit 2, 351
— spin-spin 2, 204
— through bond 275
— through space 275
— vibronic 205, 306, 321, 347, 472
Cross section 378
— differential 378
— photoionization 344, 473
Crystal field theory 96, 182, 197, 205
Crystalline state 205, 255
Cusp 39, 59, 228, 463
Cybotactic region 132

Davidson correction 72
Degeneracy 7, 182, 197, 205, 264, 290, 305
Del Re method 91, 123, 198, 236
Delocalization 127, 145, 158, 162, 178, 198, 207, 210
— electron 133, 136, 329
— exciton 330
— through bond 198, 214
— through space 198, 214
Density
— charge *cf.* Charge density
— deformation 199, 226, 228, 468
— difference 154, 200, 466
— electron 16, 201, 205, 223, 243, 471
— frontier electron 402, 404, 425
— functional method 198, 207, 214, 226, 256, 299, 464
— map, electronic difference 144, 186, 190, 199, 227
— matrix 20, 29, 36, 66, 113, 200, 202, 233, 236
— — asymptotics 126
— — spin 46
— π-electron 101
— polarization 138
— probability 3
— spin 46, 84, 266, 269
Dewar structures 56
Diatomics in molecules method 331
Diborane 159
Dielectric parameter 201, 209
Diffraction
— electron 197, 201, 205
— neutron 201, 213, 226
— X-ray 197, 201, 205, 222, 226
Dipole length formalism 336, 338, 343
Dipole moment, *cf.* Moment, dipole
Dipole velocity formalism 336, 338
Dirac equation 263
Dispersion forces 133, 135, 136, 141
Dispersion, optical rotatory 355
Dissociation catastrophe 31
Dissociation curve 74
DNA 468

Eckart conditions 339
Electric field gradient 217, 246, 247
Electron,
— core 52
— inner shell 84, 248
— solvated 134
— valence 52
Electron affinity 34, 79, 82, 288, 292, 307, 473
Electron correlation 56, 64, 68, 88, 114, 133, 146, 184, 199, 202, 204, 206, 210, 234, 253, 273, 277, 289, 291, 297, 307, 312, 331, 373, 389, 414, 428, 464, 466, 469
Electron pair approximation
— coupled 74
— independent 74
Electronegativity 122, 151, 201, 205, 216, 240, 242, 246, 280, 465
Electron-gas model 194, 205

Electron-hole potential method 312
Electron propagator method 75, 292
Electro-optical parameters 342
Electrophile 394
— hard and soft 397
Enantiomer 15, 358
Energy
— activation 382, 401
— binding 287
— bond 174
— correlation 30, 126
— — conservation 30, 68, 372
— decomposition 205, 211, 220
— delocalization 91, 163, 167
— dissociation 308
— electronic 14
— electronic excitation 167, 326, 428
— empirical resonance 163
— expression, Hartree-Fock 28
— free 131, 140
— interaction 132
— — dispersion 133, 135
— — electrostatic 133, 135
— — exchange repulsion 133
— — pair-wise additivity 134
— — partitioning 132
— — polarization 133, 135
— ionization 206, 240, 287, 297
— isomerization 87, 218, 220
— localization 407
— one-electron 26
— orbital 86, 89, 99, 104, 289, 298, 430
— pair correlation 71
— partitioning 43, 178, 186, 205
— path, minimum 205, 210, 401
— proton transfer 376
— reaction *cf.* Reaction heat
— resonance per electron 164
— surface 144, 379
— three-body contribution 416
— total 15, 28
— transfer, vibrational 471
— transition 312
— units 428
— virtual orbital 309
— zero-point 207, 216, 373, 375, 379, 390, 393
Enthalpy 371
Entropy 371, 393, 422
Environmental effects 130, 415, 465, 477
Enzyme, catalytic site 136
Enzyme field 136
Equation of motion method 292, 308, 315
Equilibrium
— constant 370
— chemical 474
Ethylene 94, 249, 325, 346
Exchange 207, 213
— repulsion 133, 136, 224
Excitation 87
— core 287
— double 34
— electronic 152, 169, 188, 207, 287, 378
— Rydberg 62, 473
— singlet 315
— triplet 315
— valence *cf.* Transition, intravalence
Excited state 32, 34, 126, 310
Exciton 256, 330, 369
Expectation value 3
Extended Hückel theory 85, 91, 109, 169, 202, 208, 212, 299, 302
Extinction coefficient, molar 343

Fermi hole 4, 29, 268, 464
Field effect 152, 377, 398, 406
Field, electrostatic 209, 221, 243, 249, 423
— gradient *cf.* Electric field gradient
Fine structure
— rotational 288
— vibrational 288, 304, 350, 359
Fluorescence 222
Force,
— electrostatic 399
— wave function 17
Force constant 65, 156, 198, 210, 216, 388
— bending 211, 218, 220
— coupling 211, 218, 220
— stretching 152, 174, 212, 218, 220
Force field, empirical 208, 212
Force method 198, 212, 218, 386
Formaldehyde 284, 323
Formamide 398
Fragment methods 129
Franck–Condon principle 288, 310, 345, 351
Free energy, Gibbs 131, 140, 370, 371, 393, 418
Free-electron gas 76
Free electron molecular orbital theory 99, 103
— perimeter model 100
Frequency, vibrational group 213, 219

Frontier orbital method 106, 180, 402, 410
Frozen core approximation 317

Gas constant 382
Gas imperfection 196
Gauge 277, 335
Gaussian orbital *cf.* AO, Gaussian
GAUSSIAN program family 67
Geminal 75
Generator orbital method 94, 102
Geometry 197, 249, 469
Geometry, excited state 332
Geometry optimization 67
Graphical unitary group approach 71
Graph theory 90
Green's function method 292, 297, 308, 314
Group function method 128, 135
Gyromagnetic coefficient 271

Hammett equation 407
Hammond principle 392
HAM/3 method 85, 226, 299
Hardness, of acids and bases 465, 476
Harmonic approximation 214, 216
Hartree–Fock instability 294
Hartree–Fock limit 37, 228
Hartree–Fock method 22, 214, 226, 234
— coupled 254
— extended 31, 69
— restricted 26
— time-dependent 315, 354
— uncoupled 254
— unrestricted 30
Hartree–Fock–Roothaan method 36, 40, 59
Hartree–Fock–Slater method 76, 315, 467
Hartree product *cf.* Wave function, Hartree product
Heisenberg's equation of motion 314
Heisenberg uncertainty principle 214, 216, 347
Helicity 364
Helix, α- 189, 214
Hellman–Feynman theorem 4, 76, 225, 250, 400
Hessian 198, 384
Hexasilabenzene 467
Hohenberg–Kohn theorem 226
Hole state 24
HONDO program 67
Hückel method 28, 85, 89, 98, 120, 123, 162, 201, 214, 311, 326, 405, 464
Hückel $4n+2$ rule 98, 163
Hückel systems 98
Hund's rule 11, 183, 215, 233, 236, 268, 275, 322
Hybridization 48, 50, 150, 466
— dipole *cf.* Moment, hybridization dipole
Hydration 470, 477
— shell 416, 419
Hydride transfer 476
Hydrocarbons
— alternant 100, 167, 275
— conjugated 329
— polycondensed 167
— saturated 152
Hydrogen bond *cf.* Bond, hydrogen
Hydrophobic effect 418
Hyperconjugation 149, 155, 216, 219
Hyperfine structure 264
Hyperpolarizability 250
Hypervirial theorem, off-diagonal 4, 336, 343, 352, 354, 357

IBMOL program 67
INDO method 91, 127, 472
— modified *cf.* MINDO
Inductive effect 122, 152, 216, 219, 377
Integral
— core 79
— Coulomb 25, 83, 89, 311
— exchange 25, 34, 84, 311
— one-centre 83
— overlap 86
— resonance 82, 89
— two-centre 83
— two-electron 67, 71, 79
Intensity
— absorption 335
— infrared 216, 239, 474
— integrated 337
— Raman 339
— vibronic 344
Interaction
— bimolecular 466
— charge-transfer 149, 402
— cooperative 135
— Coulomb 136, 149
— dispersion 68, 133, 141, 149, 193, 216
— electrostatic 193, 216, 233, 241, 402
— enzyme-ligand 476
— exchange repulsion 136, 149, 211, 217
— HOMO–LUMO 192, 217, 243
— hyperfine 236
— induction 193, 217

— molecule–molecule 474
— polarization 149, 401
— radiation–matter 335, 474
— solute–solvent 131
— spin–orbit 272
— through bond 125, 240, 301
— through space 125, 240, 301
— van der Waals 430
— vibronic 214, 217
— water–water 468
Intermediate neglect of differential overlap *cf.* INDO
Inversion 205, 209, 217
Ion 6
Ionization
— adiabatic 288
— Auger 296
— core 293, 472
— potential 79, 82, 297
— valence 297, 472
— vertical 288
Isolated molecule approach 12
Isolobal analogy 179
Isomeric shift, Mössbauer 153, 244
Isomerization 385
Isomers 198, 217
Isotope effect, kinetic 379, 475

Jahn–Teller effect 258, 283, 305, 363
— second order 107

Kekulé structure 56, 91, 127, 163
Kinetic control 384
Kirkwood model
— solvation 140
Klopman equation 408
Krönig–Kramers transformation 357
Koopmans theorem 27, 111, 289, 298, 311

Lattice, crystal 137
LCAO 37, 93, 238
Level shift technique 67
Lewis octet rule 92, 169
Lewis structure 92, 118
Librational motion 131
Ligand field theory 96, 182, 217, 246
Linear combination of atomic orbitals *cf.* LCAO
Linear free energy relationships 407
Localizability 110, 148, 154, 157, 162, 165, 185, 218
Localization
— *a posteriori* 115
— Edmiston–Ruedenberg 115
— Foster–Boys 117
— Magnasco–Perico 117
— von Niessen 116
Loges 238
Longuet–Higgins' rule 103, 104

Magnetic hyperfine parameters 246
Mataga–Nishimoto approximation 83, 88
Matching rule 107
Maximum overlap criterion 123
McConnel relation 269
Metal alkyls 161
Metallic growth 477
MINDO method 85, 91, 127
MNDO method 463
MO 29, 35
— canonical 25, 95, 109, 284, 311, 330
— canonical lone pair 157
— contour map 171, 178
— core 47, 52, 283
— diffuse 252, 307
— expansion of
— frontier 106, 180, 402, 408
— highest occupied 106, 402, 425
— improved ground state 311
— improved virtual 311
— localized 55, 57, 96, 109, 111, 143, 203, 212, 221, 242, 259, 274, 330, 364, 464
— lone pair 50, 96, 157, 255, 302
— lowest unoccupied 106, 309, 402, 425
— model 57, 93
— — qualitative 86, 93
— natural localized 464
— nonbonding 101
— one-electron 112
— parent configuration 313
— π 47
— Rydberg 283, 316
— σ 47, 54
— strictly localized 66, 119, 147, 395, 464
— tail 112, 124
— theory, qualitative 108, 247, 301, 309, 355, 366
— valence 283
— virtual 32
Möbius systems 98
Molecular beam technique 377
Molecular dynamics 134, 415

Molecular graphics 225
Molecular mechanics 208, 470
Molecular orbital *cf.* MO
Molecule 11, 143
Molecule
— chiral 357
— classical 145
— electron-deficient 159
— nonclassical 159
— nonrigid 471
— open shell 146
— sandwich 148, 181
— saturated 146, 149
— super 12, 132, 184
— van der Waals 144, 193, 469
Møller–Plesset theorem 227
Momentum, orbital 249, 258
Moment
— bond dipole 221, 242, 340
— dipole 42, 65, 137, 153, 157, 159, 192, 205, 231, 234
— — derivative 217, 337, 339, 341
— electronic transition 347, 351, 358
— hybridization dipole 236, 241
— magnetic 257, 262
— magnetic dipole 257, 357
— magnetic transition dipole 357, 358, 365, 367, 369
— —atomic
— multipole 42, 229, 231, 232, 235
— quadrupole 231, 233, 236
— second 231, 317
— transition dipole 336
MONSTERGAUSS program 67
Monte Carlo method 134, 415, 417, 420, 465, 470, 471, 475, 477
Mulliken approximation 77
Multiplicity 32
— spin 31, 33, 311
Mutually consistent field method 136

Nodal plane 153, 162
Nonadiabatic effects 325, 350
Noncrossing rule 107, 409
Nonempirical methods 75
Normal modes 217, 222
Normalization 4
— intermediate 69
Nucleic acids 422
Nucleophile 394
Nucleophilic order 404
Nucleophilicity 398

Octant rule 365
Octet rule 92, 146
Ohno approximation 88
One-electron approximation 21
One-electron function
Onsager model 140
Open shell systems 45
Operator 3
— Coulomb 27
— effective one-electron 86
— electrostatic 222, 226
— exchange 27, 135
— Fock 23, 59, 64, 66, 82, 121, 124, 311
— Hamilton 3, 89, 94, 97, 131, 137, 250, 334
— — chemical 77
— — core 27, 78, 81
— — effective 137
— — Hückel 90
— — model 66
— transition moment 336
Optical activity 358, 368
Optical factor 368
Optical rotatory strength 336
Orbital
— atomic 29, 37
— bonding 96
— control, subjacent 414
— equivalent 113
— exponent 60
— floating 60, 62
— generator 94, 102
— Löwdin orthogonalized 80
— natural 71
— nonorthogonal 123, 128
— spin 18
— symmetry 95
— — conservation of 107, 408, 476
— valence shell 47, 282
Orientation rules 407
Orthogonality 312
— strong 129
Orthogonalization
— Löwdin 80
— Schmidt 81
Oscillator
— anharmonic 379
— dipole 335

— strength 325, 336, 347, 351
Overlap 170
— differential 77
— matrix 36
— repulsion 212, 223
— zero differential *cf.* ZDO
Oxidation number 465

Pair correlation function 416
Pairing theorem 101
Pariser–Parr–Pople method 87, 91, 201, 223, 327
Partition
— Epstein–Nesbet 126
— function 370
— Møller–Plesset 126, 219, 228
Partitioning
— charge density 236
— energy 43
— — Clementi 42
— — Morokuma 131
Pauli exclusion principle 4, 110, 145, 204, 213, 224, 268
PCILO method 87, 114, 126
Perfect pairing 69
Periodicity 11
Permeability, magnetic 257
Perturbation molecular orbital theory 104
— quantitative 106
Perturbation theory 5, 73, 103, 347, 351, 390, 401, 471
— finite 251, 253, 339
— many-body Rayleigh–Schrödinger 261, 266, 292, 297, 308
— partitioning 73
— Rayleigh–Schrödinger 6, 73, 138, 251, 253, 368
— time-dependent 334
Phase transitions 224
Phosphorescence 287
Photochemistry 476
Photoionization 263
Physical constants 430
π-electron methods 87
Point group, molecular 94
Polar effect 465
Polar tensor, atomic 340
Polarity, bond 122
Polarizability 139, 194, 224, 255, 339, 469, 471
— anisotropy 252
— atom–atom 269
— atomic 256
— bond 256, 264, 343
— — derivative 343
— dipole 250, 343
— multipole 225, 232
— octupole 252
— π-electron 90
— pair 255
— quadrupole 252
Polarization 179, 184, 225, 269
— atom 249
— density 138
— electron 249
— function 61, 228, 253
— orientational 139
— potential 137, 139
— σ–π 328
— solvent 137, 142
— spin 268
— "sudden" 326
POLYATOM program 67
Polyene 326
— conjugated 118
— cyclic 101
— free electron MO model 99, 103
— linear 99, 101
Polymers 473
Polypeptides 473
Population
— analysis 45, 67, 137, 240
— gross atomic 45, 240
— gross orbital 42
— net atomic 45, 240
— overlap 44
Porphyrin 469
Potential
— atom–atom 135
— Coulomb 2, 136
— curve 331
— double-well 188, 226
— electrostatic 136, 137, 141, 192, 205, 236, 241, 268, 295, 304, 376, 395, 402
— — multipole expansion 230
— exchange 136
— function, empirical atom–atom 420
— hard-sphere 195, 224, 226
— intermolecular 469
— Lennard–Jones 196, 226, 275
— Madelung 137, 256
— Morse 215, 226

— muffin-tin 76
— polarization 137
— surface 14, 197, 226, 304, 373, 384, 476
— — adiabatic 131, 304
Promolecule 226, 237
Promotion 144
Propagator
— electron 292, 314
— polarization 314
Proteins 249, 396, 422, 468
— iron–sulphur 173
Proton
— affinity 270, 296, 375, 475
— migration 189, 226
— transfer 189, 240, 226, 379, 468, 474
Protonation 375, 398
Pseudopotential 53, 75, 129, 463, 466
Pseudorotation 205, 226, 470
p-Character 49

Quantum
— chemistry, spin-free 4
— defect 316
— electrodynamics 333, 474
— jump 334
— mechanics 1
— — matrix representation 19
— number
— — azimuthal 7
— — magnetic 7
— — principal 7

Radiation
— absorption 333
— electromagnetic 333
— emission 333
Radical
— free 261, 266
— organic 268
Radius
— covalent 200, 227
— van der Waals 196, 224, 228
Random phase approximation 315, 354
Rate constant 378, 383, 475
Reaction
— addition 390, 422
— adiabatic 15
— bimolecular 377, 385
— charge controlled 41, 402
— chemical 370, 474
— concerted 105, 108, 408
— cycloaddition 475
— Diels–Alder 408, 412, 425
— dynamics 475
— electrocyclic 410
— electrophilic 396, 403
— elimination 390
— enthalpy 401
— entropy controlled 475
— entropy driven 372
— Fischer–Tropsch 426
— heat 64, 370, 371
— homodesmic 372
— hydrogen transfer 398
— intermediate 15, 385
— isodesmic 372
— kinetically controlled 405
— nitration 405
— nucleophilic 396, 476
— orbital controlled 402
— path 105, 384, 386, 475
— — antarafacial 412
— — conrotatory 410
— — disrotatory 410
— — suprafacial 412
— — symmetry forbidden 411
— photochemically allowed 412
— potential map 394
— proton transfer 407, 419, 421, 423
— rate 520
— rearrangement 390
— S_N2 477
— substitution 390, 476
— symmetry allowed 411
— thermally allowed 412
— thermodynamically controlled 405
— unimolecular 377
Reaction field 139, 141
Reactivity 150, 259, 163, 393, 476
— index 89, 400
Recognition 476
Relativistic effects 2, 64, 168, 206, 228, 244, 265, 289, 352, 463, 466, 471
Relaxation effects 290, 292, 313
Representation
— coordinate 3
— momentum 3
Resonance 93
Ridig rotor approximation 207, 229
Ring current 167, 261, 281

Ring strain 164
Rotational constant 470
Rotatory strength, optical 126, 357, 474
Ruedenberg approximation 239
Rydberg formula 316
Rydberg state 229, 231, 235, 284, 315, 320, 472

Saddle point 15, 205, 231, 234, 384
Sandwich compounds 231, 282
Sanibel coefficients 31
Satellite peaks 296
Scattering
— elastic 378
— inelastic 378
— Raman 216, 232
— surface 475
— theory 378, 383
SCF method 25, 64
— fragment 129
— linearized 124
— multiconfiguration 69, 340
s-character 49, 150, 158, 201, 239, 243, 268, 274, 342
Schrödinger equation 3, 13, 17, 334
— for H atom 6
— nonlinear 137, 139
— time-dependent 346, 463
Screening, magnetic 276
Secular equation 19
Selection rules 108, 335, 338, 343, 351
Self-consistent electron pair theory 464
Self-consistent field method *cf.* SCF
Self-consistent reaction field method 139, 333
Semiempirical methods 77, 284, 299, 307, 316, 322, 360, 386, 405, 418
Separability
— electron 55
—σ–π 52, 54, 87, 268, 325
Serine proteases 398, 423, 477
Shake-off process 286, 289
Shake-up process 286, 289, 296
Shape, molecular 202, 223, 233, 236
Shielding
— Sternheimer 247
— tensor 276
Singlet–triplet separation *cf* Splitting, singlet–triplet
Single-transition approximation 310, 322
Size-consistency 72
Slater determinant 22
Slater–Condon parameter 84
Slater rules 21, 313
Solvation 417, 419, 465
— ionic 140
— shell 136
Solvaton model 141, 142, 333
Solvent effects 130, 196, 210, 219, 233, 236, 256, 270, 332, 415
Spectrochemical series 183, 236
Spectroscopy 11
— Auger 287
— circular dichroism 355
— electron beam 310
— electron paramagnetic resonance 261
— electron spin resonance 85, 257, 261
— emission 287
— infrared 214, 216, 236, 238, 337, 428
— magnetic circular dichroism 358
— mass 287
— microwave 197, 222, 236, 248, 257
— Mössbauer 236, 241, 243, 428
— nuclear magnetic resonance 188, 248, 270, 276, 281
— nuclear quadrupole resonance 247, 236, 287
— optical rotatory dispersion 355
— photoelectron 287, 304, 344, 349, 430
— Raman 214, 236
— ultraviolet 287, 310, 343, 428
— visible 287, 428
— X-ray absorption 287
— X-ray emission 287
— X-ray photoelectron 287, 295
Spectrum, electronic 100, 192, 264
Spherical harmonics 8, 232, 238
Spin 262
— function 27
— orbital 19, 22, 32
Splitting
— crystal field 96
— quadrupole 238, 246
— singlet–triplet 311, 322, 324
— zero-field 264
Stark effect 7
State
— core hole 293
— nonstationary 334
Stationary point 384
Statistical mechanics 131, 134, 139, 370, 415
Steric hindrance 414
Strain 202, 219, 238
Structural formula 146

Substituent
— effect 105, 149, 239, 469, 470
— electron donating 404
— electron withdrawing 404
Sum rule 358
— Thomas–Kuhn 344
Supermolecule *cf.* Molecule, super
— method 132, 255, 421
Superposition function 334
Susceptibility
— bond contribution 297
— diamagnetic 257, 260, 277, 472
— paramagnetic 258
Symmetry 94, 233, 359
— breaking 294
— dilemma 32, 294
— lowering 304

Tail, of localized MO 112, 119
Tamm–Dancoff approximation 84, 313, 352, 354
Tautomerism 219, 240, 297, 420, 474
TEXAS program 67
Thermodynamic control 384
Three-body effects 135
Topology 90, 388
Trajectory analysis 381
Transferability 48, 114, 128, 135, 155, 157, 162, 198, 201, 219, 221, 240, 242, 256, 281, 389, 395
Transformation, unitary 23
Transition
— allowed 351
— electronic 346
— forbidden 347, 349, 351
— intravalence 321
— π/π^* 89
— Rydberg 316
— vertical 310, 346
Transition metal compounds 96, 151, 159, 174, 299, 316
Transition operator method 292
Transition probability
— — electronic 343
— — infrared 473
— — vibrational 337
Transition state 15
— theory 381
Transmission coefficient 382
Trans-cyclooctene 360
Tunnel effect 189, 241, 379, 383

Unitary group approach 71, 464
Unitary transformation 21, 48, 110
United atom approximation 38
Units, atomic 5

Vahrenkamp compounds 170
Valence 44, 51, 112
— bond method 55, 69, 92, 463, 467, 470
— — generalized 69, 326, 331
— — qualitative 92
— bond structure 93, 118
— free 47, 90
— state 144
Valence-shell electron repulsion theory 157, 159, 202, 241, 302, 469
van der Waals radius *cf.* Radius, van der Waals
Variation principle 5, 137
Vibrational borrowing model 348
Vibration
— bending 217, 243
— deformation 217, 243
— molecular 470
— rocking 218, 243
— scissoring 218, 244
— stretching 217, 219, 242, 244, 300
— torsional 217, 245
— twisting 218, 246
— wagging 218, 246
Virial theorem 4, 76, 238, 246
Virtual charge method 333

Walden inversion 401
Walsh rule 108, 202, 246, 268, 324
Walton compounds 170
Water 319, 353
Wave function 2
— dynamical 304
— Hartree product 18, 133, 204, 246
— Heitler–London 55, 58
— many electron 21
— nonstationary 346
Wiberg index 44
Wolfsberg–Helmholtz formula 86, 107
Woodward–Hoffmann rule 107, 414

X_α method 76, 169

ZDO approximation 77, 79, 87, 120, 236
Zeeman effect 7, 262
Zeise's anion 178
Zeolites 477

UNDERSTANDING CHEMICAL REACTIVITY

APPLIED QUANTUM CHEMISTRY

by

Gábor Náray-Szabó, Péter R. Surján and János G. Ángyán

Scientific Information Department, CHINOIN Pharmaceutical Works, Budapest, Hungary

Applied Quantum Chemistry is written for theoretical and structural chemists, spectroscopists and biochemists who wish to gain insight into methods and applications of quantum chemistry. Graduate students, having some experience in quantum chemical methods, may also use the book as a general overview. Part One deals with the methods and most important concepts of quantum chemistry emphasizing the chemical aspect. Part Two is devoted to the chemical bond while molecular structure (geometry, spectroscopy, electric and magnetic properties) is treated in Part Three. Chemical reactions are discussed in Part Four. Numerous tables help the reader in forming an opinion on the reliability of various quantum chemical methods while illustrative figures are included to make the text more readable. The interested reader may find 1500 references to recent and classical works for further information.

AKADÉMIAI KIADÓ, BUDAPEST